Acta Chimica Hungarica

VOLUME 121, NUMBERS 1–2, JANUARY–FEBRUARY 1986

Akadémiai Kiadó, Budapest
ACTA CHIM. HUNG. ACHUDC 121 (1–2) 1–231 (1986) HU ISSN 0231–3146

ACTA CHIMICA HUNGARICA

A JOURNAL OF THE HUNGARIAN ACADEMY OF SCIENCES

Acta Chimica publishes original reports on all aspects of chemistry in English.

Acta Chimica is published in three bolumes per year, each volume consisting of four issues, by

AKADÉMIAI KIADÓ

Publiching House of the Hungarian Academy of Sciences
H-1054 Budapest, Alkotmány u. 21.

Manuscripts and editorial correspondence should be addressed to

Acta Chimica
H-1450 Budapest P.O. Box 67

Subscription information

Orders should be addressed to

KULTURA Foreign Trading Company
H-1389 Budapest P.O. Box 149

or to its representatives abroad

Acta Chimica is indexed in Current Contents.

NOTICE TO AUTHORS

Acta Chimica publishes original papers on all aspects of chemistry in English. Before preparing a manuscript for submission to this journal authors are advised to consult recent issues.

Form of manuscript

Manuscripts, tables and illustrations should be submitted in triplicate. Manuscripts should be typewritten double spaced (25 lines, 50 characters per line including spaces). The *title page* should include (1) the title of the paper, (2) the full names of the author(s) in the sequence to be published; apply an asterisk to designate the name of the author to whom correspondence should be addressed, (3) name and address of the institution where the work was done. If the paper is part of a series, reference to the previous communication must be given as a footnote.

Abstract

A summary is printed at the head of each paper. This should not exceed 200 words and should state briefly the principal results and major conclusions of the work. It should be suitable for use by abstracting services.

ACTA CHIMICA HUNGARICA

VOLUME 121

AKADÉMIAI KIADÓ, BUDAPEST
1985

THIS ISSUE COMPRISES THE INVITED LECTURES PRESENTED DURING THE

SYMPOSIUM
on the
STRUCTURE
of
LIQUIDS AND SOLUTIONS
in commemoration of
Tibor Erdey-Grúz

which was held at Veszprém, Hungary
August 27—30, 1984

CONTENTS

Acta Chimica Hungarica 121 (1—2), pp. 5—6 (1986)

SYMPOSIUM ON THE STRUCTURE OF LIQUIDS AND SOLUTIONS

Erika KÁLMÁN

(Central Research Institute for Chemistry of the Hungarian Academy of Sciences, H-1025 Budapest, Pusztaszeri u. 59/67)

Under the auspieces of The Chemistry Section of the Hungarian Academy of Sciences (HAS), The Hungarian Chemical Society, The Faculty of Natural Sciences of the L. Eötvös University, The University of Veszprém and the Veszprém Commission of the HAS, a symposium on the Structure of Liquids and Solutions was held in commemoration of Professor Tibor Erdey-Grúz through 26—30 August, 1984.

The number of participants attending the Symposium from 16 various countries amounted to 112.

The site of the Symposium was at the Headquarters of Veszprém Commission of the HAS. Papers presented at the symposium numbered altogether 90 lectures, 37 of which covered theoretical aspects of liquids and solutions and 53 dealt with experimental topics, including 11 plenary lectures and 40 posters.

The scientific sections were opened by plenary lectures under the following titles:

F. Márta:
Opening Lecture
M. Abraham:
Continuum Approach to Ionic Solvation
E. Berecz:
Relations between the Structure and Transport Properties of Solutions
J. S. Høye:
Statistical Theory of Tense Molecular Systems
K. Heinzinger:
Molecular Dynamics Simulation of Ionic Hydration
G. Krestov:
Thermodynamics of Electrolyte Solutions
W. A. P, Luck:
Role of Hydrogen Bonding in the Structure of Liquids
S. Mørup:
Mössbauer Spectroscopy as applied to Solution Chemistry

A. H. Narten:
Diffractions Studies of Liquids
G. Pálinkás:
Order and Disorder in Liquids
I. Ruff:
Nonlinear Dielectric Effects in Liquids
I. R. Yukhnovskii:
Statistical Technical Description of Ion-Solvent Interaction

Titles of Scientific Sections:
— *Applications of Spectroscopic Methods*
— *Liquid Diffraction Methods*
— *Theoretical Aspects of Liquids and Solutions, Computer Simulations*
— *Thermodynamical Investigations*

The Opening Lecture of the Symposium was presented by Professor F. Márta, Head of the Organizing Committee, in appreciation of the valuable activities of Professor T. Erdey-Grúz in the field of electrochemistry.

Acta Chimica Hungarica 121 (1—2), pp. 7—10 (1986)

OPENING LECTURE+

FERENC MÁRTA

(Central Research Institute for Chemistry of the Hungarian Academy of Sciences, H-1025 Budapest, Pusztaszeri u. 59/67.)

It is my great pleasure to welcome you on behalf of the Organizing Committee and sponsoring Institutions at this meeting dedicated in honour of Erdey-Grúz whose name is closely linked with the school of liquid phase research, in Hungary.

In the field of structure investigations of liquids and solutions a great amount of empirical knowledge has been accumulated on the properties of molecular liquids however, no uniform theory for systematic arrangement of these molecular parameters has been elaborated so far.

In the various fields of physics and chemistry dealing with macroscopic material structure, the most challenging questions confronting researchers today are the problems of liquid phase structure. One explanation of this may be that in the case of liquids there is no system of reference qualifying ideal state, represented in the case of gases by ideal gas and in the case of solids by the perfect crystal. Another reason may be the diversity of liquids, considering e.g., pure liquids, mixtures, and specific interactions between solutions and particles.

The complexity of liquid structure, the wide range of controversial problems and our vague knowledge on the subject seem to justify a detailed theoretical study and extensive experimental investigations in the field.

Tibor Erdey-Grúz was born in Budapest in 1902, he became interested in chemistry as early as in his secondary school years and soon decided to take up the subject as his career. After completing his university studies, he obtained his Ph. D. degree from the University in Budapest in 1924. In the same year he started investigations in electrochemistry as an associate to Professor Buchböck, pursuing studies on the topic of his thesis. The period of one year between 1928 and 1931 he worked with Professor Fajans in Münich and the two years in the institute of Professor Volmer in Berlin had a decisive effect on his scientific career. He was appointed honorary lecturer in 1934, titular associate professor in 1941 and full professor at the University of

+ This paper was presented at the Symposium on Structure of Liquids and Solutions at Veszprém, August 27—30, 1984.

Sciences, Budapest in 1946. In 1949 he was assigned head of the Institute of Physical Chemistry and Radiology.

In 1943 he was nominated corresponding member and in 1948 elected full member of the Hungarian Academy of Sciences. With this he joined to work, and with the highly responsible posts assigned to him he soon gained a leading role in scientific life and activities in Hungary. He was appointed Minister of Higher Education, then Minister of Education in 1952—56 and filled the post of General Secretary of the Hungarian Academy of Sciences during the periods of 1950—53, 1956—57 and 1964—70. From 1959 to 1964 he acted as Secretary of the Department of Chemistry and from 1970 to the day of his death on 16th August, 1976, he officiated as President of the Hungarian Academy of Sciences. In addition to fulfilling his tasks in science- and education-policy with full responsibility, he was also engaged in teaching and research, carrying out activities with full energy and zealous ambition.

The main achievements and results of his scientific work may be summarized as follows. Erdey-Grúz and Vollmer made significant contribution to elucidation of the mechanism of electrode processes. They set up their theory of hydrogen overpotential based on the recognition that the charge transfer should be treated according to the laws of reaction kinetics and that the activation energy of charge transfer is dependent on the overpotential. It has soon become evident that the correlations derived for the hydrogen overpotential and the theoretical conclusions drawn therefrom are valid also for electrode reactions where charge transfer is the rate-determining process. The theory developed by Erdey-Grúz and Vollmer thus offered the first generalization of the reactions on electrode process.

The scientific activities of Erdey-Grúz also had a significant part in laying the foundations of our current knowledge of electrolytic metal deposition. Together with Vollmer he elaborated the fundamental laws of the theory of electro-crystallization. In addition he tried to find an answer to the difference in potentials at metal-electrolyte interphase and studied the potential-determining processes.

From the early 1950-s he and his coworkers started extensive experimental investigations with AC methods. During the past decade his activities in the investigation of electrode processes covered mainly the study of oxygen overpotential. Significant results were attained in the study of various parameters (temperature, electrolyte concentration) determining the overpotential and there is practically no monography today, which does not make reference to the work of Erdey-Grúz in the field.

His study of the correlation between solution structure and oxygen overpotential and treatment of the problem from this aspect can be considered by no means a coincidence, if we take into account another field of his activities, the study of transport processes in electrolyte solutions. It is not possible to

give in this brief review all the details of his many-sided activities, the results of which contributed to a better understanding of phenomena related to transport processes in electrolytes and to the elucidation of important aspects of solution structure. He and his coworkers thoroughly studied the effect of organic compounds with and without hydroxyl radicals upon the conductivity of aqueous solutions of electrolytes and the transfer number of ions. Within this, a predominant problem in many of his papers was the anomalous conductivity of hydrogen and hydroxide ions. Based on experimental results on conductivity and the number of ion transfers he offered an interpretation to numerous phenomena.

By studying the self-diffusion of organic components and dissolved electrolytes in water-dioxane and water-methanol he has greatly extended our knowledge also in this field. His wide range of activities and extensive knowledge is reflected by the number of publications, approximately 100 papers and two comprehensive monographies, "The Kinetics of Electrode Processes" published in Hungarian in 1969, and later also in English and German, and "Transport Processes in Aqueous Solutions" published in 1971 and subsequently in English translation.

The activities and ideas of Professor Erdey-Grúz gained a large number of disciples and through them, directly or indirectly, liquid structure investigations in Hungary are associated with his name up to this day. These researches are conducted mainly in University laboratories and Research Institutes of the Hungarian Academy.

At the Eötvös Loránd University in Budapest the structure of quenched solutions is studied by Mössbauer spectroscopy and the ESCA method. Positron annihilation technics is used for study of the coordination spheres complexes in solutions. The structure of molten salts and concentrated electrolyte solutions is investigated by the Monte Carlo method. Theoretical studies are made on the nonlinear dielectric behaviour of liquids in strong electric field.

Investigations at the University of Chemistry in Veszprém concern ion-solvation and nonlinear dielectric behaviour of the solvent and the properties of concentrated electrolytes.

At the Central Research Institute for Chemistry of the Hungarian Academy of Sciences the structure of H-bonded solvents and aqueous and non-aqueous solutions as well as complex formation is studied by means of X-ray and electron diffraction methods.

Researches at the Central Research Institute of Physics of the Hungarian Academy of Sciences concern the correlation between the isotope effect and structure and the thermodynamic properties of solutions. Mössbauer spectroscopy is used for the study of complex formation in aqueous solutions.

Researches at the József Attila University in Szeged are engaged with the relationship between equilibrium constants and the structure of solutions.

At the Technical University of Heavy Industry in Miskolc the structure of solutions is studied based on transport properties, microwave dielectric properties and isotherm evaporation measurements.

The above investigations will be presented at this Symposium in various lectures and posters to give a general review of recent activities in this field.

The aim of the Symposium is to convene interested experts and discuss problems and present new ideas and results in the structure investigations of liquids and solutions.

Acta Chimica Hungarica 121 (1—2), pp. 11—25 (1986)

A CONTINUUM APPROACH TO IONIC SOLVATION+

Michael H. ABRAHAM

(Department of Chemistry, University of Surrey, Guildford, Surrey GU2 5XH, U.K.)

Received January 18, 1985

An account is given of the calculation of thermodynamic parameters for the solvation of gaseous ions using the recent continuum approach of Abraham and Liszi. With a simple "one-layer" or "one-step" model, in which an ion in solution is surrounded by a solvent layer of low dielectric constant, followed by the bulk solvent, values of ΔG_s°, ΔH_s°, ΔS_s° and probably also ΔCp_s° for solvation of the alkali halide series of univalent ions in aprotic solvents can be calculated in very good agreement with experiment, at 298 K. For solvation in hydrogen-bonded solvents at 298 K only values of ΔG_s° are in agreement with experiment, due, it is suggested, to the presence of a second, disordered, solvent layer.

Calculations of solvation in water over the range 273—573 K show that above about 420 K all four thermodynamic functions are in agreement with experiment. It is suggested that above this temperature water behaves as a simple, comparatively unstructured, liquid; this is illustrated also by a comparison of structure-making and -breaking effects of ions in water at various temperatures with effects in aprotic solvents at 298 K.

Introduction

The continuum approach to ionic solvation was first introduced by Born [1] who calculated the work of charging a sphere in vacuum and in a dielectric continuum of bulk dielectric constant ε_0, and derived eq. (1) as the electrostatic contribution to the Gibbs energy of solvation of a gaseous ion of radius a and charge z. Corresponding equations for

$$\Delta G_E = \frac{z^2}{2}\left(\frac{1}{\varepsilon_0} - 1\right)\frac{1}{a} \tag{1}$$

$$\Delta S_E = \frac{z^2}{2}\left(\frac{1}{\varepsilon_0^2}\right)\left(\frac{\partial \varepsilon_0}{\delta T}\right)\frac{1}{a} \tag{2}$$

$$\Delta Cp_E = \frac{z^2 T}{2}\left[\left(\frac{-2}{\varepsilon_0^3}\right)\left(\frac{\partial \varepsilon_0}{\partial T}\right)^2 + \frac{1}{\varepsilon_0^2}\left(\frac{\partial^2 \varepsilon_0}{\partial T^2}\right)\right]\frac{1}{a} \tag{3}$$

the electrostatic contribution to the entropy and heat capacity of solvation can easily be derived, eq. (2) and eq. (3). In order to compare Gibbs energies

+ This paper was presented at the Symposium on Structure of Liquids and Solutions at Veszprém, August 27—30, 1984.

calculated via eq. (1) with observed solvation energies of gaseous ions, ΔG°_{S}, several factors must be considered , not all of which have always been taken into account. Firstly, eq. (1) yields only the electrostatic component of ΔG°_{S}; nonelectrostatic effects such as the work of creating a cavity in the solvent and loss of translational entropy on transferring a particle from the gas phase to solution are not included. Secondly, it is not clear what standard states should be adopted for the observed ΔG°_{S} values. The stratagem of using the standard state of 1 mol dm^{-3} for both the gas phase and solution, in order to circumvent the difficulty over loss of translational entropy, is not effective because a particle in solution is not free to occupy the nominal volume [2]. Thirdly, although eq. (1) yields values for single ions, there is as yet no thermodynamically rigorous method of obtaining experimental single-ion solvation energies; either calculations must be carried out for a neutral combination of cation and anion, or some arbitrary procedure must be used to deduce the experimental single-ion quantities.

However, the Born equation is still used as a guide to the order of magnitude of solvation energies [3], although it is now well known that eq. (1) considerably overestimates the Gibbs energy of solvation. Various modification of eq. (1), or of the corresponding equations in enthalpy or entropy, have been suggested. Thus the ionic radius a may be replaced by the term $(a + \Delta)$, in which Δ is an adjustable parameter [4, 5], or an "effective" dielectric constant can be introduced [6]. These modifications considerably reduce the predictive power of eq. (1—3) but do point to the reason for the failure of the Born model, namely that the variation of local dielectric constant with distance from a charge is not taken into account [7—12]. In Fig. 1 is shown

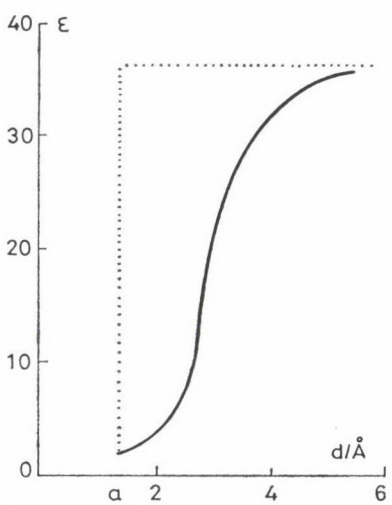

Fig. 1. Plot of ε against d for a univalent ion in acetonitrile. Born model: . . .

the dielectric constant/distance profile around a univalent ion of radius a in acetonitrile, as calculated by Abraham and Liszi [13]. The Born profile, in which the dielectric constant takes the value ε_0 at all distances from the surface of the ion, overestimates ε, and hence the calculated value of ΔG_E is always far too negative. Many attempts [8—12] have been made to incorporate the variation of ε with distance into solvation energy calculations, and in this paper an account is given of the method due to Abraham and Liszi [14, 15], together with some recent applications of the method.

Calculation of solvation energies at 298 K

Beveridge and Schnuelle [16] had derived an equation for the electrostatic Gibbs energy of an ion of radius a and dielectric constant ε_{ion} surrounded by a solvent layer of thickness $b - a$ and dielectric constant ε_l, and immersed in a bulk solvent of dielectric constant ε_0. Abraham and Liszi [14, 15] used the Beveridge-Schnuelle equation with $\varepsilon_{\text{ion}} = 1$, but later Abraham, Liszi and Mészáros [17] solved the equations for the electrostatic Gibbs energy of an ion surrounded by any number of concentric spherical layers, each with a different dielectric constant, immersed in the bulk solvent. The form of the one-layer equation was much simpler than that of the Beveridge—Schnuelle equation, although the two equations were proved to be algebraically identical, and so only the Abraham—Liszi—Mészáros equation will be considered. The one-layer equation for ΔG_E, and the corresponding equations for ΔS_E and ΔCp_E are given in eq. (4—6); when $a = b$ and $\varepsilon_l = \varepsilon_0$ these equations reduce to the Born eq. (1—3). In all three eq. (4—6), the terms in $(1/a - 1/b)$

$$\Delta G_E = \frac{z^2}{2}\left(\frac{1}{\varepsilon_l} - 1\right)\left(\frac{1}{a} - \frac{1}{b}\right) + \frac{z^2}{2}\left(\frac{1}{\varepsilon_0} - 1\right)\frac{1}{b} \tag{4}$$

$$\Delta S_E = \frac{z^2}{2}\left(\frac{1}{\varepsilon_l^2}\right)\left(\frac{\partial \varepsilon_l}{\partial T}\right)\left(\frac{1}{a} - \frac{1}{b}\right) + \frac{z^2}{2}\left(\frac{1}{\varepsilon_0^2}\right)\left(\frac{\partial \varepsilon_0}{\partial T}\right)\frac{1}{b} \tag{5}$$

$$\Delta Cp_E = \frac{z^2 T}{2}\left[\left(\frac{-2}{\varepsilon_l^3}\right)\left(\frac{\partial \varepsilon_l}{\partial T}\right)^2 + \left(\frac{1}{\varepsilon_l^2}\right)\left(\frac{\partial^2 \varepsilon_l}{\partial T^2}\right)\right]\frac{1}{a} - \frac{1}{b}$$
$$+ \frac{z^2 T}{2}\left[\left(\frac{-2}{\varepsilon_0^3}\right)\left(\frac{\partial \varepsilon_0}{\partial T}\right)^2 + \frac{1}{\varepsilon_0^2}\left(\frac{\partial^2 \varepsilon_0}{\partial T^2}\right)\right]\frac{1}{b} \tag{6}$$

give the contribution of the local layer, and the terms in $(1/b)$ give the contribution of the bulk solution outside the local layer. Abraham and Liszi [14] first took a value for ε_l as 2.0, but later showed that the expression $1.05\ n^2$, where n is the solvent refractive index, yielded comparable results. For most liquids $1.05\ n^2 \simeq 2.0$, this being taken as ε_∞, the dielectric constant when the

solvent orientation polarisation is zero. In the particular case of water, it has proved difficult to establish the value of ε below which dipole reorientation ceases: it seems as though ε_∞ cannot be higher than 5.0 and could be as low as 1.8 [see 18, 19]. Since for nonpolar liquids which have ε_0 about 2.0, the value of $\partial\varepsilon_0/\partial T$ is about -1.6×10^{-3} K^{-1}, the latter value was adopted for $\partial\varepsilon_l/\partial T$, leaving only the thickness of the local layer, $(b - a)$ to be fixed in order to apply eq. (4) and eq. (5). The latter was taken as the radius of a solvent molecule, calculated from solvent bulk molar volumes at 298 K using the Stearn-Eyring formula, $r = (\overline{V}/8N)^{1/3}$.

In order to deal with the cavity term and loss of translational entropy, Abraham and Liszi regarded the total solvation term as consisting of an electrostatic contribution, calculated as above, and a nonelectrostatic contribution, obtained from parameters for solution of the gaseous rare gases; eq. (6) where $Q = G, H, S, Cp$, etc. Use of eq. (6) also removes all difficulties over the gaseous and solution

$$\Delta Q_S^\circ = \Delta Q_E + \Delta Q_N \tag{7}$$

standard states. Provided that the same set of standard states are adopted for ΔQ_S° and ΔQ_N, the value of ΔQ_E will not depend on the actual standard states used. In this work standard states of 1 atm (gas) and unit mol fraction (solution) will be employed.

In Table I are given parameters for a number of solvents at 298 K [14, 15] and in Table II are listed the ionic radii used on the calculations [14]. Values of ΔG_N and ΔS_N are obtained from expressions given by Abraham

Table I

Solvent properties used in the calculations at 298 K [13, 14]

Solvent	ε_0	$-\partial\varepsilon_0/\partial T$	r/Å
water	78.36	0.3595	1.553
methanol	32.64	0.197	2.037
ethanol	24.33	0.147	2.300
1-propanol	20.45	0.142	2.498
formamide	109.5	0.72	2.023
N-methylformamide	182.4	1.62	2.307
propylene carbonate	64.92	0.234	2.599
dimethylsulphoxide	46.68	0.106	2.456
dimethylformamide	36.71	0.178	2.524
acetonitrile	36.02	0.160	2.222
acetone	20.49	0.0967	2.485
ammonia	16.90	0.0780	1.796
1,2-dichloroethane	10.23	0.0560	2.546
1,1-dichloroethane	9.90	0.0480	2.600
tetrahydrofuran	7.40	0.0299	2.569
1,2-dimethoxyethane	7.30	0.0410	2.789

Table II

Values of ionic radii used in the calculations [13, 21]

Ion	a/Å	Ion	a/Å
Li^+	0.90	F^-	1.33
Na^+	1.05	Cl^-	1.81
K^+	1.33	Br^-	1.95
Rb^+	1.43	I^-	2.20
Cs^+	1.66	ClO_4^-	2.45
Ag^+	1.13		

and Liszi [14, 15], so that if ε_l is taken as 2.0 and $\partial\varepsilon_l/\partial T$ as -1.6×10^{-3} K^{-1} there are no adjustable parameters left at all in eq. (4), eq. (5), and eq. (7). Experimental values of ΔG_S° were available for several ions in 16 solvents, there being invariably good agreement between the observed and calculated ΔG_S° values; typical results are shown in Table III. A measure of any systematic deviation is τ, defined as the average of the calculated values minus the average of the observed values, whereas σ is defined as $\{[\Delta Q_S^\circ(\text{calc}) - \Delta Q_S^\circ(\text{obs})]^2/(n-1)\}^{1/2}$ where n is the number of ions studied. For the 16 solvents, including hydroxylic solvents and water, no general trends in either τ or σ were observed in the case of Gibbs energies of solvation. Since τ itself averages about ±0.8 kcal mol^{-1} and σ about 1.9 kcal mol^{-1} across the 16 solvents, and since these values will also include a contribution from experimental error, it is clear that a very simple calculation based on eq. (4) can be used to predict solvation Gibbs energies of ions to within about 2 kcal mol^{-1} for each ion. The improvement over the Born equation is impressive; for $(K^+ + Br^-)$ in acetonitrile a calculation via eq. (4) and eq. (7) yields $\Delta G_S^\circ = -135.7$ kcal

Table III

Calculation of Gibbs energy of solvation of ions, using $\varepsilon_l = 2.0$ *and the constants in Table I,* kcal mol^{-1} *at* 298 K [13]

Ion	1,2-dichloroethane		acetonitrile		methanol	
	calc.	obs.	calc.	obs.	calc.	obs.
Na^+	−91.1	−92.2	−96.3	−93.7	−102.8	−98.0
K^+	−74.0	−74.2	−78.6	−77.6	−79.9	−79.9
Rb^+	−69.6	−69.4	−73.9	−73.0	−75.1	−74.8
Cs^+	−61.4	−61.9	−65.2	−65.6	−66.3	−67.3
Cl^-	−57.2	−57.9	−60.7	−60.6	−61.7	−64.7
Br^-	−53.9	−54.4	−57.1	−56.6	−58.0	−58.4
I^-	−49.1	−48.9	−52.0	−50.9	−52.6	−50.5
ClO_4^-	−45.3	−45.2	−48.0	−48.4	−48.3	−45.0
σ	0.6		1.2		2.6	
τ	0.3		−0.7		−0.8	

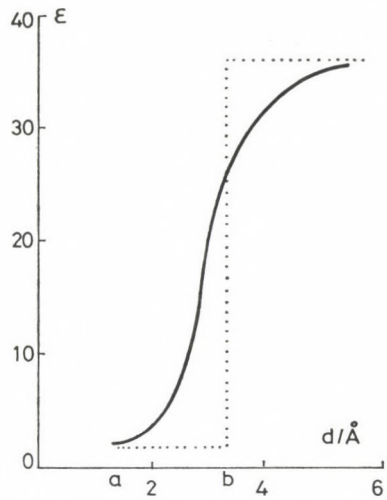

Fig. 2. Plot of ε against d for a univalent ion in acetonitrile. One-step profile: . . .

mol^{-1} and the Born eq. (1) with eq. (7) gives a value of —194.0 kcal mol^{-1}, as compared to the experimental value of —134.4 kcal mol^{-1}. The reason for the improvement can be seen from the dielectric profiles in Fig. 1 and Fig. 2: the "one-layer" or "one-step"profile in Fig. 2 underestimates ε at low values of d, but overestimates ε at high values of d, there being apparently almost complete cancellation.

Application of eq. (5) and eq. (7) to the calculation of entropies of solvation is quite straightforward, provided that ΔS_N values can be obtained from solution of the rare gases in the solvents concerned. Fortunately, the latter are available [20] and taking $\varepsilon_l = 2.0$ and $\partial\varepsilon_l/\partial T = 1.6\times10^{-3}$ K^{-1}, ΔS_S° values may be calculated; results for three solvents are in Table IV. The good agreement found for the aprotic solvents is quite general; Abraham and Liszi [15] showed that for 9 aprotic solvents, ΔS_S° values could be calculated to within about 2 cal K^{-1} mol^{-1} for each ion. This is not so for hydrogen-bonded solvents, where there is always a systematic discrepancy, see Tables IV and V. This arises because of a disordered second-layer, interposed between the ordered first-layer and the relatively ordered hydrogen-bonded bulk solvent, which contributes between about 7 cal K^{-1} mol^{-1} to 30 cal K^{-1} mol^{-1} per ion depending on the solvent.

The use of different numerical values for ε_l (taken also as 1.05 n^2) and for the thickness of the layer (b — a) was later investigated [21], as well as the use of a two-layer (i.e. a two-step) or a continuous dielectric profile [22]. These refinements lead only to marginal improvements in the calculation of ΔG_S° and ΔS_S°, and do not materially affect the difficulty over the calculation of ΔS_S° in hydrogen-bonded solvents. For both aprotic and hydrogen-bonded

Table IV

Calculation of entropies of solvation of ions, using $\varepsilon_l = 2.0$ *and* $\partial\varepsilon_l/\partial T = -1.6\times10^{-3}$ K^{-1} *and the constants in Table I,* cal K^{-1} mol^{-1} *at* 298 K [14]

Ion	1,2-dichloroethane		acetonitrile		methanol	
	calc.	obs.	calc.	obs.	calc.	obs.
Na^+	−78	−69	−58	−55	−64	−47
K^+	−66	−64	−48	−50	−54	−42
Rb^+	−63	−60	−45	−46	−51	−38
Cs^+	−58	−58	−41	−44	−47	−36
Cl^-	−56	−55	−39	−41	−45	−33
Br^-	−54	−53	−38	−39	−44	−31
I^-	−51	−49	−36	−35	−43	−27
ClO_4^-	−50	−48	−35	−34	−41	−26
σ	4		2		15	
τ	−2		0.5		−17	

Table V

Entropies of solvation of $(K^+ + Br^-)$ *in hydrogen-bonded and aprotic solvents,* cal K^{-1} mol^{-1} *at* 298 K [14]

Solvent	calc.	obs.	τ^a
water	−107	−48	−30
methanol	−98	−73	−12
ethanol	−102	−79	−11
propanol	−110	−87	−11
formamide	−84	−63	−11
N-methylformamide	−84	−69	7
propylene carbonate	−82	−77	−2
dimethylsulphoxide	−81	−79	−1
dimethylformamide	−88	−93	+2
acetonitrile	−85	−89	+2
acetone	−96	−99	+1
ammonia	−97	−99	+1
1,2-dichloroethane	−120	−117	−1
1,1-dichloroethane	−116	−119	+1

[a] Value per ion.

solvents, it is possible to interpret entropy terms with respect to ion-solvent interactions. The overall ΔS_S° values can be broken down into ΔS_E and ΔS_N through eq. (7), and the former then divided into contributions from the first-layer, the disordered second-layer, and the bulk solvent, as in eq. (8) and eq. (9). Either ΔS_E or ΔS_I plus ΔS_{II} can be taken as

$$\Delta S_E = \Delta S_I + \Delta S_{II} + \Delta S_B \tag{8}$$

$$\Delta S_S^\circ = \Delta S_I + \Delta S_{II} + \Delta S_B + \Delta S_N \tag{9}$$

Table VI

Comparison of ΔS_E with B- and B'-coefficients for ions in water and in methanol at 298 K [21]

Ion	water			methanol		
	ΔS_E	B	B'	ΔS_E	B	B'
H^+		0.096	0.09			
Li^+	−33	0.174	0.17	−40	0.63	0.25
Na^+	−20	0.110	0.09	−34	0.59	0.14
K^+	−4	0.017	0.02	−27	0.56	0.11
Rb^+	1	−0.006	−0.01	−23	0.44	0.08
Cs^+	5	−0.021	−0.02	−19	0.36	0.07
F^-	−12	0.072	0.11	−26		
Cl^-	9	−0.031	−0.04	−15	0.20	0.05
Br^-	14	−0.066	−0.07	−12	0.18	0.03
I^-	22	−0.092	−0.11	−6	0.11	0.00
ClO_4^-	26	−0.089	−0.12	−4		−0.01

ameasure of ion-solvent interactions. In Table VI are listed values of ΔS_E for ions in water and in methanol at 298 K, together with viscosity B-coefficients and B'-coefficients of Engel and Hertz [23]. There are excellent linear correlations of either ΔS_E or $\Delta S_{I,II}$ against B or B' for all solvents studied, see the examples in Fig. 3, with ΔS_E or $\Delta S_{I,II}$ negative and B or B' positive for ions that are structure-makers and ΔS_E or $\Delta S_{I,II}$ positive and B and B' negative for ions that are structure-breakers [21].

It seems therefore that the "one-layer" or "one-step" equations, eq. (4) an d eq. (5) in conjunction with eq. (7) can be used to predict Gibbs energies of solvation of ions in solvents generally, and entropies of solvation of ions in aprotic solvents. Even when predictions cannot be made that is for solvation entropies in hydrogen-bonded solvents, where the continuum approach fails, useful interpretations of solvation entropies in terms of ion-solvent interactions can still be made.

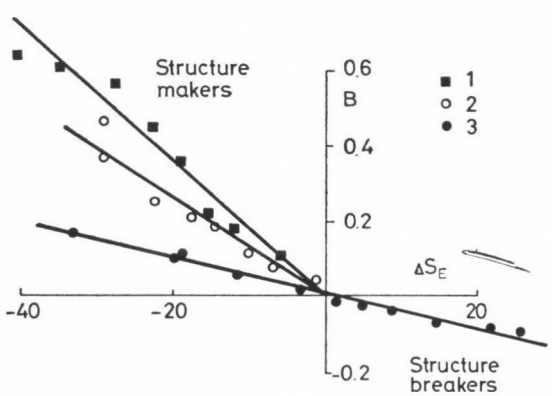

Fig. 3. Plot of B coefficients against ΔS_E at 298 K; (1) methanol, (2) formamide (3) water

Calculations of solvation energies at various temperatures

In principle, the application of the above continuum approach to the calculation of solvation energies at any given temperature is no different to a calculation at 298 K. There are, however, a number of practical difficulties. Firstly, a knowledge of the temperature variation of ε_0 is required over the temperature range to be considered; for many nonaqueous solvents values of ε_0 are known only at around room temperature. Secondly, thermodynamic parameters for solution of the rare gases in the solvent concerned must also be available over the temperature range in order that the nonelectrostic contribution can be determined. Thirdly, some estimate of $\partial\varepsilon_l/\partial T$ and $\partial^2\varepsilon_l/\partial T^2$ is necessary.

If the above three factors are known accurately, it is possible to calculate ΔC_p° for solvation of ions via eq. (6) and eq. (7), where $Q = Cp$. Results are very limited for nonaqueous solvents, but from the known value of $\bar{C}_p^\circ$ for KBr in acetonitrile [24], the heat capacity of solvation at 298 K is about —10 cal K^{-1} mol^{-1}. The corresponding ΔCp_N value for the two ions is probably around 20 cal K^{-1} mol^{-1}, so that if $\partial\varepsilon_l/\partial T$ is taken as -1.6×10^{-3} K^{-1} and $\partial^2\varepsilon_l/\partial T^2$ as zero (since nothing is known about this quantity), the only remaining required parameters are these of the bulk dielectric constant, $\partial\varepsilon_0/\partial T$ and $\partial^2\varepsilon_0/\partial T^2$. Values of ε_0 have recently been obtained [25] over the range 233 to 298 K and may be fitted to eq. (10) or to eq. (11). In Table VII are given

$$\varepsilon_0 = 94.378 - 0.1958\,T \quad r = 0.99993 \tag{10}$$

$$\varepsilon_0 = 103.598 - 0.2656\,T + 0.000131\,T^2 \quad r = 0.99999 \tag{11}$$

ΔC_p° values using constants derived from eq. (10) and eq. (11), together with results based on the earlier value of —0.160 K^{-1} for $\partial\varepsilon_0/\partial T$, with $\partial^2\varepsilon_0/\partial T^2$ taken as either zero or as an assumed value of 1×10^{-4} K^{-1}. It can be seen

Table VII

Calculation of ΔC_p° for solvation of $K^+ + Br^-$ *in acetonitrile at* 298 K

ε_0	$\partial\varepsilon_0/\partial T$	$\partial^2\varepsilon_0/\partial T^2$	ΔG_S°	ΔS_S°	ΔCp_S
36.01[a]	—0.196	0	—135.7	—88	—45
36.09[b]	—0.187	2.6×10^{-4}	—135.7	—87	—40
36.02[c]	—0.160	0	—135.7	—85	—30
36.02[d]	—0.160	1.0×10^{-4}	—135.7	—85	—10
		observed values	—134.2	—89	—10

[a] Values from eq. (10).
[b] Values from eq. (11).
[c] Table I assuming $\partial^2\varepsilon_0/\partial T^2 = 0$.
[d] Table I assuming $\partial^2\varepsilon_0/\partial T^2 = 1.0\times10^{-4}$ K^{-1}.

that the numerical value of $\partial^2\varepsilon_0/\partial T^2$ is crucial, but also that there is the possibility of reasonable calculations of ΔC_p° for solvation through a continuum approach.

Some of the above difficulties are not present for water as the solvent, thus the variation of ε_0 with temperature is well known and parameters for solution of the rare gases are also available. An attempt was therefore made to calculate ΔG°, ΔS°, and ΔC_p° for solvation of gaseous ions in water over a wide range of temperature [26]. If ε_l is taken as either 2.0 or as 1.05 n^2 at 298 K (the latter is 1.87 for water), $\partial\varepsilon_l/\partial T$ as -1.6×10^{-3} K and $\partial^2\varepsilon_l/\partial T^2$ as zero, then apparently there are left no adjustable or variable constants in eq. (4—6). However the value of b, or of $(b - a)$, is not necessarily a fixed constant. Previously, $(b - a)$ was taken as a constant for all ions in a given solvent but for more precise calculations different values of $(b - a)$ could be used for the different ions studied. Furthermore, in the derivation of eq. (5) and eq. (6) from eq. (4) it is assumed that values of a and b are independent of temperature. Even if a is taken as a constant, there is no reason why $(b - a)$ and hence b should be constant. There are, however, considerable difficulties if b is allowed to vary with temperature, because it then becomes impossible to calculate ΔS_E at any given temperature unless a value for $\partial b/\partial T$ can be deduced; if b varies with temperature an additional term in eq. (5) is required:

$$\Delta S_E = \Delta S_E \text{ calc. via eq. (5)} + \frac{z^2}{2}\left(\frac{1}{\varepsilon_l} - \frac{1}{\varepsilon_0}\right)\frac{1}{b^2}\left(\frac{\partial b}{\partial T}\right)$$

It seemed more useful to attempt calculations using b values that are invariant with temperature, but which are allowed to differ from ion to ion [26]. Two extreme cases can be considered, (i) b values can be assigned to ions so that ΔG_S° (calc) and ΔG_S° (obs) are identical at 298 K, or (ii) b values can be obtained so that ΔG_S° (calc) and ΔG_S° (obs) become identical at high temperature [26]. Thermodynamic parameters for solvation of ions over a wide range of temperature can be obtained from equations given by Tremaine and Goldman [27], although it should be noted that such parameters are based on experimental quantities at lower temperatures and Tremaine and Goldman's extrapolation procedures at higher temperatures. Using ΔG_S° (obs) values at 298 K, and ΔG_S° values from Tremaine and Goldman's procedure at high temperatures, b values were assigned to various ions as shown in Table VIII. Then using eq. (4) and eq. (5) together with eq. (7), values of ΔG_S° and ΔS_S° could be calculated at various temperatures (in these calculations ε_l at 298 K was taken as 1.87). In Fig. 4 are shown results of calculations using both b (298) and b (573) values for $(Na^+ + Cl^-)$. There is not much difference in ΔS_S° (calc) using the two sets of b values. As found before, the calculated entropies of solvation at 298 K are far too negative, due to the disordered second-layer that is not taken into account by the calculations. But as the temperature increases, bulk

Table VIII

Assignment of b values to ions in water, in Å [26]

Ion	$b(298)$	$b(573)$
Na^+	2.65	2.24
K^+	2.91	2.56
Rb^+	3.03	2.75
Cs^+	3.11	2.79
Cl^-	2.73	2.43
Br^-	3.14	2.67
I^-	3.82	3.05

water becomes itself more disordered and more like an aprotic solvent, and the disordered second-layer effect becomes smaller. Indeed, at around 450 K there is good agreement between calculated and observed ΔS°_S values, so that at this temperature and above, water seems to behave as a dielectric continuum.

If structural effects in water decrease markedly with temperature, then this should be reflected in structure-making and -breaking properties of ions.

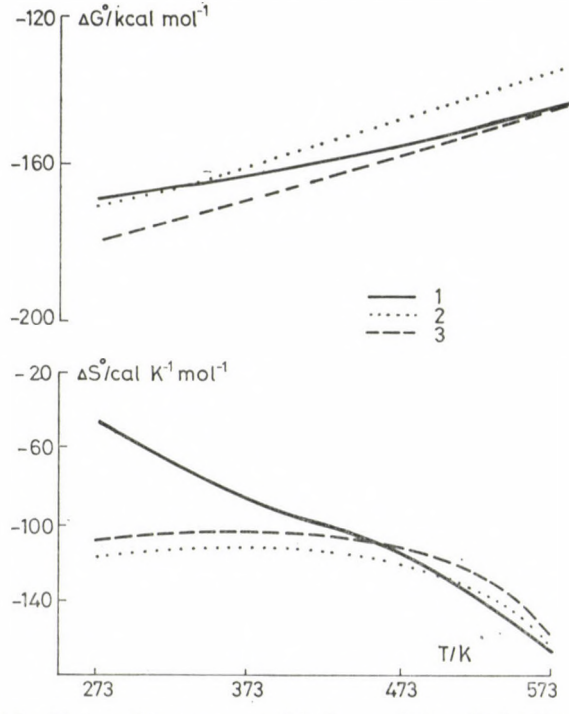

Fig. 4. ΔG^0 and ΔS^0 for $Na^+ + Cl^-$ gas → aq; (1) observed from Ref. [27], (2) calculated with b (298), (3) calculated with b (573)

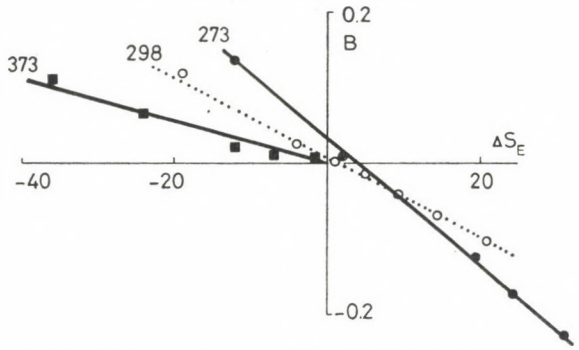

Fig. 5. Plot of B-coefficients against ΔS_E in water at 273, 298, and 373 K

Values of ΔS_E or $\Delta S_{I,II}$ can be calculated for ions in water at different temperatures, and then correlated with viscosity B-coefficients in exactly the same way as for solvents at 298 K. Results for the alkali halide ions in water at 273, 298, and 373 K are shown in Fig. 5. With one or two minor exceptions when ΔS_E or B are close to zero, ions may again be characterised as structure-makers or structure-breakers. But at 273 K, only Li^+ and Na^+ are net structure-making ions, with K^+ and F^- borderline cases. At 298 K, Li^+, Na^+ and F^- are structure-making ions and K^+ and Rb^+ borderline cases, whereas at 373 K all the ions Li^+ to Cs^+ and F^- to Br^- are structure-makers with only I^- as a borderline case. At 423 K even I^- is now quite a strong structure-making ion; so that as the temperature increases all ions become structure-makers, just as for nonaqueous solvents at 298 K. Thus ΔS_E values for the alkali halide ions in water at 373 K are quite comparable to ΔS_E values in formamide at 298 K, and ΔS_E values in water at 423 K are almost identical with S_E values for the alkali halide ions in acetonitrile at 298 K [21, 26], see Table IX.

Table IX

Comparison of ΔS_E values for ions in water with values for ions in other solvents, in cal K^{-1} mol^{-1}

Ion	water 373 K	formamide 298 K	water 423 K	acetonitrile 298 K	water 523 K	1,2-dichloro-ethane 298 K
Na^+	−36	−29	−45	−46	−66	−67
K^+	−24	−22	−35	−40	−56	−54
Rb^+	−23	−18	−36	−35	−60	−50
Cs^+	−19	−14	−32	−31	−57	−44
Cl^-	−12	−10	−29	−27	−34	−40
Br^-	−7	−7	−18	−24	−39	−37
I^-	−1	−1	−16	−18	−31	−33

These structural effects should also be reflected in heat capacities of solvation, and, indeed, observed ΔCp°_S values could be analysed in terms of contributions from an ordered first-layer, a disordered second-layer, and a relatively ordered bulk solvent at 298 K [26]. Experimental $\overline{C}p^\circ$ values are available for sodium chloride in water up to 573 K; from these, experimental ΔCp°_S values may be obtained again up to 573 K. As expected, the calculated ΔCp°_S values for ($Na^+ + Cl^-$) via eq. (6) and eq. (7) were much too positive than the observed values at ambient temperatures, due to a contribution (negative) from the disordered layer that is not included in the calculations. Again, just as for the entropy calculations, observed and calculated ΔCp°_S values were in good agreement above about 423 K. Interestingly, the calculated ΔCp°_S values did not depend very much on the actual values of b for Na^+ or Cl^- used in the calculations. In Fig. 6 are shown ΔCp°_S (obs) for ($Na^+ + Cl^-$) in water from 273 to 573 K, together with calculated values using the b (298) values in Table VIII. There is very good agreement between the two sets at temperatures above about 423 K. Now in the calculation of $\Delta C\overline{p}^\circ$ via eq. (6) and eq. (7), the values for the dielectric constant of water are known, ε_l is taken as 1.87 at 298 K and $\partial\varepsilon_l/\partial T$ as -1.6×10^{-3} K^{-1} with $\partial^2\varepsilon_l/\partial T^2$ as zero. Thus if b is obtained by matching ΔG°_S (calc) with ΔG°_S (obs) at 298 K, a knowledge of ΔG°_S at 298 K is all that is required in order to be able to predict ΔCp°_S at high temperature. Values of ΔCp°_S at ambient temperatures are not too difficult to obtain, via values of $\overline{C}p^\circ$, so that a combination of observed values at low temperatures with predicted values at high temperatures will enable the ΔCp°_S vs T profile to be obtained over a wide temperature range. The ΔCp°_S values can be fitted to a function of temperature, and integration will yield values of ΔS°_S, ΔH°_S, and ΔG°_S over the entire range. In Fig. 7 is shown such a ΔCp°_S vs T profile for the case of ($K^+ + Br^-$) constructed from recently obtained experimental values at ambient temperature [28] and predicted values at high temperature using the b (298) parameters in Table VIII. It seems quite possible that a combination of experimental and calculated heat capacities of solvation will provide predictions of other thermodynamic functions for solvation of ions from 273 K up to around 550 K, and it is hoped to report on such predictions in the future. It might be noted that although the Born eq. (3) has been shown to reproduce heat capacities for sodium chloride over a wide temperature range [29], this equation cannot be used as the basis for any predictive calculation because the ionic radius, a, is used as an adjustable parameter in order to obtain the required fit of calculated and observed heat capacities over the temperature range considered.

Although continuum theories of solvation can provide a surprising amount of information on ion-solvent interactions, as well as being of predictive capability, other theories of solvation should not be overlooked. Jorgensen and co-workers [30] have recently calculated ΔH°_S values at 298 K for various

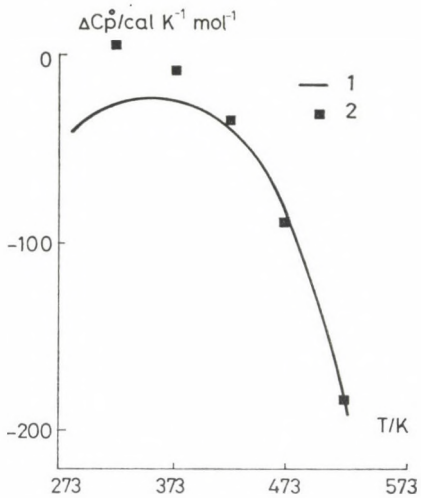

Fig. 6. ΔC_p° for $Na^+ + Cl^-$ gas → aq; (1) observed, (2) calculated with *b* (298)

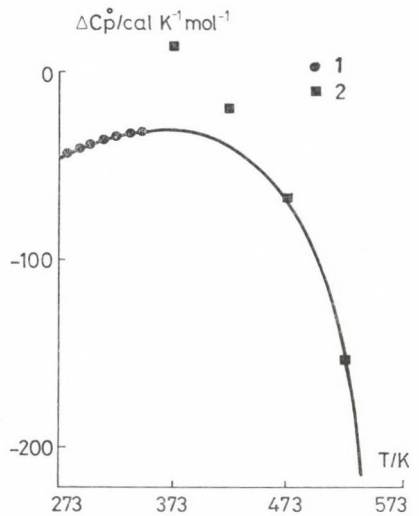

Fig. 7. ΔC_p° for $K^+ + Br^-$ gas → aq; (1) observed, (2) calculated with *b* (298)

ions in water using Monte Carlo simulations. Their calculated values are in fair agreement with experiment, for example ΔH_S° (calc) for $(Na^+ + Cl^-)$ is —205 kcal mol^{-1} as compared with the observed value of —187 kcal mol^{-1} [31], and particularly useful information on ion-solvent and solvent-solvent interactions is obtained. Thus both recent continuum theories and discrete theories of ionic solvation will continue to provide valuable results.

REFERENCES

[1] Born, M.: Z. Physik., **1,** 45 (1920)
[2] Friedman, H. L., Krishnan, C. V.: in Water, Vol. 7 (Ed. F. Franks), Plenum Press, London 1973
[3] Popvych, O., Tomkins, R. P. T.: Nonaqueous Solution Chemistry, Wiley, New York 1981
[4] Voet, A.: Trans. Faraday Soc., **32,** 1301 (1936)
[5] Latimer, W. W., Pitzer, K. S., Slansky, C. M.: J. Chem. Phys., **7,** 108 (1939)
[6] Noyes, R. M.: J. Am. Chem. Soc., **84,** 513 (1962)
[7] Hasted, J. B., Riston, D. M., Collie, C. H.: J. Chem. Phys., **16,** 1, 11 (1948)
[8] Glueckauf, E.: in Chemical Physics of Ionic Solutions (Eds. B. E. Conway and R. G. Barrados), Wiley, New York 1966
[9] Muirhead-Gould, J. S., Laidler, K. J.: Trans. Faraday Soc., **63,** 953 (1967)
[10] Hepler, L. G.: Aust. J. Chem., **17,** 587 (1964)
[11] Stiles, P. J.: Aust. J. Chem., **33,** 1389 (1980)
[12] Padova, J.: J. Chem. Phys., **39,** 1552 (1968); J. Chem. Phys., **56,** 1606 (1972)
[13] Abraham, M. H., Liszi, J.: J. Chem. Soc., Faraday Trans. 1, **76,** 1219 (1980)
[14] Abraham, M. H., Liszi, J.: J. Chem. Soc., Faraday Trans. 1, **74,** 1604 (1978)
[15] Abraham, M. H., Liszi, J.: J. Chem. Soc., Faraday Trans. 1, **74,** 2858 (1978)
[16] Beveridge, D. L., Schunelle,, G. W.: J. Phys. Chem., **79,** 2562 (1975)
[17] Abraham, M. H., Liszi, J., Mészáros, L.: J. Chem. Phys., **70,** 2491 (1979)
[18] Davies, M.: Annual Rep. Chem. Soc., **67A,** 65 (1970)
[19] Hasted, J. B.: in Dielectric and Related Molecular Processes, Chem. Specialist Periodical Reports, **1,** 121 (1972)
[20] Abraham, M. H.: J. Am. Chem. Soc., **104,** 2085 (1982)
[21] Abraham, M. H., Liszi, J., Papp, E.: J. Chem. Soc., Faraday Trans. 1, **78,** 197 (1982)
[22] Abraham, M. H., Liszi, J., Kristof, E.: Aust. J. Chem., **35,** 1273 (1982)
[23] Engel, G., Hertz, H. G.: Ber. Bunsenges. Phys. Chem., **72,** 808 (1968)
[24] Zana, R., Perron, G., Desnoyers, J. E.: J. Soln. Chem., **8,** 729 (1979)
[25] Würflinger, A.: Ber. Bunsenges. Phys. Chem., **84,** 653 (1980)
[26] Abraham, M. H., Liszi, J., Matteoli, E.: J. Chem. Soc. Faraday Trans. 1, **79,** 2781 (1983)
[27] Tremaine, P. R., Goldman, S.: J. Phys. Chem., **82,** 2317 (1978)
[28] Abraham, M. H., Date, R. F., Schultz, R. A., Bawden, R. J., Turner, D. J.: Tenth Experimental Thermodynamics Conference, Sheffield, April 1984
[29] Smith-Magowan, D., Wood, R. H.: J. Chem. Thermodyn., **13,** 1047 (1981)
[30] Chandrasekhar, J., Spellmeyer, D. C., Jorgensen, W. L.: J. Am. Chem. Soc., **106,** 903 (1984)
[31] Morris, D. F. C.: Electrochim. Acta, **27,** 1481 (1982)

Acta Chimica Hungarica 121 (1—2), pp. 27—53 (1986)

MOLECULAR DYNAMICS SIMULATION OF IONIC HYDRATION+

Karl HEINZINGER, Philippe BOPP* and Gábor JANCSÓ**

(Max-Planck-Institut für Chemie (Otto-Hahn-Institut), D-6500 Mainz, Federal Republic of Germany)

Received January 18, 1985

The hydration of some monovalent and divalent ions in aqueous solutions of moderate concentration has been studied by Molecular Dynamics simulations using both rigid and flexible models for water. The ion-water and ion-ion potentials were determined either from isoelectronic noble gases and Pauling radii or from quantum mechnical ab initio calculations.

The structural arrangement of the water molecules in the vicinity of the ions is discussed in terms of radial distribution functions, average molecule orientations and symmetries of the hydration complex. Among the dynamical properties studied are the diffusion coefficients, the hindered translations of the solvent molecule and of the solute particles and the shifts in inter- and intramolecular vibrational frequencies of the solvent molecules due to the solute. Single ion values of these quantities are easily obtained and discussed in comparison with experimental values.

Introduction

It is the purpose of this contribution to give a brief overview of the Molecular Dynamics (MD) simulations which have been performed on aqueous electrolyte solutions. The attention will focus on the phenomenon of ionic hydration and we shall attempt to elucidate some of its structural and dynamical aspects.

In a Molecular Dynamics simulation, the Newtonian equations of motion for a number of particles (typically several hundred) under the influence of their mutual interactions are solved numerically under (mostly) periodic boundary conditions. The interactions are described by sums of atom-atom (or site-site) pair potentials, such sets of pair potentials for different chemical species are often referred to as the "model" for that species. The interaction potentials, the masses (or moments of inertia in case of molecules) and the density are the only input to an MD simulation, i.e. there are no adjustable parameters.

* Present address: Institut Physikalische Chemie I, Technische Hochschule, D-6100 Darmstadt, Federal Republic of Germany.

** Address for correspondence: Central Research Institute for Physics of the Hungarian Academy of Sciences, H-1121 Budapest. Konkoly Thege út, Hungary.

+ This paper was presented at the Symposium on Structure of Liquids and Solutions at Veszprém, August 27—30, 1984.

Of course, the results of such a simulation depend critically on the pair potentials employed. For instance, high accuracy ab initio calculations are not necessarily a guarantee for proper pair potentials as in complicated liquids, such as water, the pair potentials used need to be effective ones, which means that many-body interactions must be incorporated. In this contribution the fact is stressed that the best test of the reliability of the pair potentials is the agreement of calculated quantities with experimental results as far as they can be deduced unambiguously from measurements.

In the following section some models employed in the simulation of aqueous electrolyte solutions are introduced and details of the calculations are given. Structural properties of the solution are discussed in a later section on the basis of radial distribution functions, the orientation of the water molecules in the hydration shell of the ions and their geometrical arrangement. In the last section dynamical properties of the solution, such as self-diffusion coefficients, and the spectral densities of hindered translations, librations and internal vibrations are discussed — derived from simulation with the help of various autocorrelation functions.

Models

A number of models for liquid water have been developed in the past 15 years, the most successful and most widely used ones being the ST2 [1], the MCY [2] and the central force (CF) models [3, 4]. While the ST2 and MCY models considered the water molecule as a rigid unit, the CF model consists of oxygen and hydrogen atoms — bearing partial charges — where the water molecule geometry is solely preserved by an appropriate set of oxygen-hydrogen and hydrogen-hydrogen pair potentials. Thus, the CF model has the advantage that the influence of ions on the intramolecular geometries and frequencies can be studied.

In the work presented here, both the ST2 and CF models were used. MC simulations of ionic hydration using the MCY model have been reported by Beveridge and Mezei [5] and MD simulations with this model have been carried out by McDonald et al. [6].

The ST2 water model (Fig. 1) developed by Stillinger and Rahman [1] is a four point charge model with the charges arranged tetrahedrally around the oxygen atom. The positive charges are located at the hydrogen atom positions at a distance of 1 Å from the oxygen atom, approximately the real distance in the water molecule. The negative charges are located at the other two vertices of the tetrahedron but at a distance of only 0.8 Å from the oxygen atom. The charges have been chosen to be 0.23 elementary charges, leading to an enhanced (compared to the gas phase) dipole moment of the water

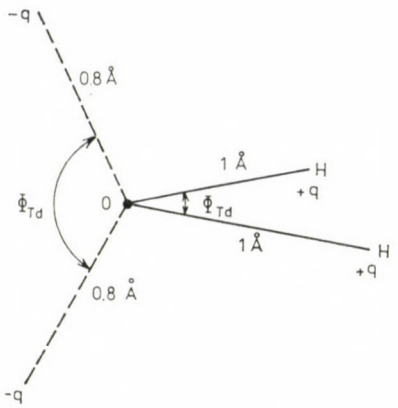

Fig. 1. The ST2 point charge model for water. The tetrahedral angle $\Phi_{Td} = 109° 28'$ and $q = 0.23\ e$

molecule. The tetrahedrally arranged point charges render possible the formation of hydrogen bonds in the right directions. A switching function depending on the interoxygen distances prevents the unlimited increase of the Coulomb energy for close approach of two water molecules. The ST2 model is completed by adding a (12; 6) Lennard—Jones (LJ) potential, the center of which is located at the oxygen atom. In the simulations where the ST2 model is employed, the alkali and halide ions are modelled as LJ spheres with a point charge at the center. With these models for the two kinds of particles — water and ions — it is easy to formulate the effective pair potentials for the six different kinds of interactions: cation-cation, anion-anion, cation-anion, cation-water, anion-water, and water-water.

All six pair potentials consists of an LJ term:

$$V_{ij}^{LJ}(r) = 4\varepsilon_{ij}[(\sigma_{ij}/r)^{12} - (\sigma_{ij}/r)^{6}], \tag{1}$$

where i and j refer either to ions or water molecules, and a Coulomb term, different for water-water, ion-water, and ion-ion interactions, given by:

$$V_{ww}^{C}(r, d_{11}, d_{12}, \ldots) = S_{ww}(r) \cdot q^2 \sum_{\alpha,\beta=1}^{4} (-1)^{\alpha+\beta}/d_{\alpha\beta} \tag{2a}$$

$$\underset{(-w)}{V_{+w}^{C}}(\underset{(-1)}{d_{+1}}, \underset{(-2)}{d_{+2}}, \ldots) = -\sum_{(+)\alpha=1}^{4} (-1)^{\alpha}\, q \cdot \underset{(+)}{e}/\underset{(-\alpha)}{d_{+\alpha}} \tag{2b}$$

$$\underset{(+-)}{V_{\pm\pm}}(r) = \underset{(-)}{+e^2}/r. \tag{2c}$$

d and r denote distances between point charges and LJ centers, respectively, q the charge in the ST2 model. The sign of the Coulomb term is correct if

α and β are chosen to be odd for positive and even for negative charges. The switching function $S_{ww}(r)$ is given by

$$S_{ww}(r) = \begin{cases} 0 & r < R^{L} \\ (r - R^{L})^2 (3R^{U} - R^{L} - 2r)/(R^{U} - R^{L})^3 & R^{L} \leq r \leq R^{U} \\ 1 & r > R^{U} \end{cases} \quad (3)$$

with

$$R^{L} = 2.016 \text{ Å}, \quad R^{U} = 3.1287 \text{ Å}$$

The LJ parameters for the cations are taken from the isoelectronic noble gases [7]. Comparing e.g. Pauling radii it is obvious that halide ions have a larger ionic radius than the isoelectronic alkali ions. In order to describe all interactions consistently, new LJ parameters had to be determined for the halide ions on the basis of the Pauling radii. As there exist no direct relationships between Pauling radii and the ε and σ of the LJ potential, a fitting procedure was used.

Knowing the parameters for cation-cation and anion-anion interactions the parameters for cation-anion and ion-water interactions have been determined by applying Kong's combination rules [8]. The values are given in Table I.

Table I

Lennard–Jones parameters in the pair potentials for cation-cation, anion-anion, cation-water and anion-water interactions
In the ST2 model: $\sigma_{WW} = 3.10$ Å and $\varepsilon_{WW} = 0.317$ kJ/mol

Ion	Pauling radius (Å)	σ_{II} (Å)	ε_{II} (kJ mol^{-1})	σ_{IW} (Å)	ε_{IW} (kJ mol^{-1})
Li^+	0.60	2.37	0.149	2.77	0.224
Na^+	0.95	2.37	0.358	2.92	0.330
F^-	1.36	4.00	0.050	3.53	0.123
K^+	1.33	3.36	1.120	3.25	0.568
Cl^-	1.81	4.86	0.168	4.02	0.185
Rb^+	1.48	3.57	1.602	3.39	0.641
Br^-	1.95	5.04	0.270	4.16	0.215
Cs^+	1.69	3.92	2.132	3.61	0.662
I^-	2.16	5.40	0.408	4.41	0.228

In the CF models the water molecule consists of oxygen and hydrogen ions and its geometry is solely preserved by an appropriate choice of oxygen-hydrogen and hydrogen-hydrogen potentials. In contrast to the rigid ST2 model, the CF model has internal degrees of freedom and differences, for example in geometry or vibrational frequencies, between hydration water of ions and bulk water can be calculated. The CF model was originally developed

by Lemberg and Stillinger [3]: [V in units of kcal/mol, r in units of Å]

$$V_{OO}(r) = \frac{144.538}{r} + \frac{26758.2}{r^{8.8591}} - 0.25 \exp\left[-4(r - 3.4)^2\right] \qquad (4a)$$

$$- 0.25 \exp\left[-1.5(r - 4.5)^2\right].$$

$$V_{OH}(r) = -\frac{72.269}{r} + \frac{6.23403}{r^{9.19912}} - \frac{10}{1 + \exp[40(r - 1.05)]} \qquad (4b)$$

$$- \frac{4}{1 + \exp\left[5.49305(r - 2.2)\right]}$$

$$V_{HH}(r) = \frac{36.1345}{r} + \frac{100.04}{1 + \exp\left[29.9(r - 1.968)\right]} \qquad (4c)$$

With this water model, MD simulations have been performed for a 13.9 molal LiCl [9], a 2.2 molal NaCl [10] and a 1.1 molal $MgCl_2$ [11] solution. In these cases the ion-oxygen and ion-hydrogen potentials were determined from ab initio calculations [12] by suitable fitting procedures [10, 11]. Figure 2 shows the potentials for Na^+-water and Cl^--water as a function of ion-oxygen distance for the water molecule orientations shown in the insertion; the dots

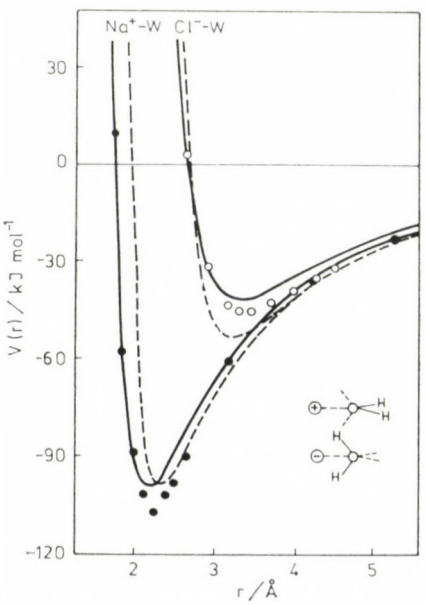

Fig. 2. Na^+-water and Cl^--water pair potentials as a function of ion-oxygen distance for the water molecule orientations shown in the insertion. Solid line: potential used in conjunction with CF water; dashed line: potential used in conjunction with ST2 water; dots and circles: binding energies from the ab initio calculations [12]

and circles indicate the binding energies for the ion-water complexes resulting directly from the ab initio calculations [12], the solid line the above mentioned fits with the CF water model, and the dashed lines the potentials obtained from the simple LJ-ST2 model [7]. The rather poor agreement of the fit with the CF model for the specific orientations shown here is a consequence of the fact that the best fit has to be achieved for all possible water molecule orientations [11]. It is also interesting to note that the combination of the ST2 model with the simple model for Na^+ and Cl^- (LJ spheres with an elementary charge in the center) leads to pair potentials not too different from the ones obtained from the ab initio calculations.

In the course of the above mentioned investigations using the CF model, a number of shortcomings became apparent, especially with respect to the vibrational motions of the water molecule [10, 13]. The vibrational motions in the gas phase cannot be adequately described within the harmonic approximation with only two independent quadratic force constants, as yielded by a central force field approximation. Secondly, the experimentally observed gas--liquid frequency shifts are not well reproduced due to inadequate anharmonicities in these models. A further shortcoming is the insufficient height of the barrier to molecular dissociation or to non-physical deformation of the molecule, which prohibits the simulation of water and aqueous systems at elevated temperature or pressure.

A convenient way to overcome these shortcomings is the separation of the potential into an intramolecular part, which can no longer be of central force type, i.e. depending only on the distances between two interacting centers, and an intermolecular part, similar to a water model proposed by Watts [14]. Because of its well-established high quality, the intermolecular parts of the interaction potential were taken from the CF potential. The intramolecular potential was written as a series expansion [15]

$$V_{\text{intra}} = \Sigma L_{ij}\varrho_i\varrho_j + \Sigma L_{ijk}\varrho_i\varrho_j\varrho_k + \Sigma L_{ijkl}\varrho_i\varrho_j\varrho_k\varrho_l. \tag{5}$$

with

$$\varrho_1 = (r_1 - r_e)/r_1,\ \varrho_2 = (r_2 - r_e)/r_2 \text{ and } \varrho_3 = (\alpha - \alpha_e) = \Delta\alpha,$$

where r_1, r_2 and α are the instantaneous O—H bond lengths and H—O—H angle; the quantities r_e and α_e are the corresponding equilibrium values ($r_e = 0.9572$ Å, $\alpha_e = 104.52°$).

The harmonic constants L_{ij} were taken as the accepted gas phase values [15] and the higher order constants were adapted [4]. Simulations carried out with this model yielded more realistic results [4] which will be discussed in a subsequent chapter. This model has also been used [19, 36] for simulations of a 1.1 molal $CaCl_2$ solution and of 2.2 molal NaCl solutions at high pressure [21].

Details of the simulations

In all simulations discussed here, the "basic box" contains 200 water molecules, 8 anions and 8 monovalent or 4 divalent cations. The edge of the cube is determined from the experimental density and amounts to about 18 to 19 Å. The classical equations of motion are integrated in time steps of about 2×10^{-16} s; the simulations, carried out at room temperature, extended over about 10 ps. Ewald summation [17] is used for all Coulomb interactions in the simulations using CF water models and for the ion-ion interactions in simulations with the ST2 model. Other interactions were modified according to the "shifted force potential" method of Streett et al. [18]. With this procedure, the total energy of the system remains stable and no rescaling of the velocities has to be performed which is very important for the reliability of the dynamical properties calculated from velocity autocorrelation functions. The slight modification of the pair potentials seems to be acceptable in view of all the other uncertainties in the choice of the potentials.

Structural properties

Radial distribution functions

The first properties derived from an MD simulation as far as the structure of an aqueous electrolyte solution is concerned are the various radial distribution function (RDF), $g_{xy}(r)$. In Fig. 3 the ion-oxygen and ion-hydrogen RDFs are shown for various monovalent alkali and halide ions. In addition the corresponding running integration numbers, $n_{xy}(r)$, are drawn. They are defined as:

$$n_{xy}(r) = 4\pi\varrho_0 \int_0^r g_{xy}(r')\, r'^2\, \mathrm{d}r', \tag{6}$$

where ϱ_0 is the number density of the water molecules.

Figure 3 shows that with increasing ion size the first hydration shell becomes less and less pronounced, as expected. The height of the first peak in the ion-oxygen RDF decreases and the first minimum gets filled up. Accordingly, the plateau in $n(r)$ disappears and the end of the first hydration shell becomes less well defined. The existence of a second hydration shell around Li^+, with about twelve water molecules, is well established and has been confirmed by x-ray diffraction studies as discussed below. Even in the case of Na^+ and F^- the formation of a second shell is indicated in Fig. 3. It should be mentioned that the positions of the first maxima in the ion-oxygen RDFs almost coincide with the minima of the ion-water pair potentials for the energetically most favourable orientations. The positions of the first maxima in the ion-oxygen and ion-hydrogen RDFs agree within the limits of uncer-

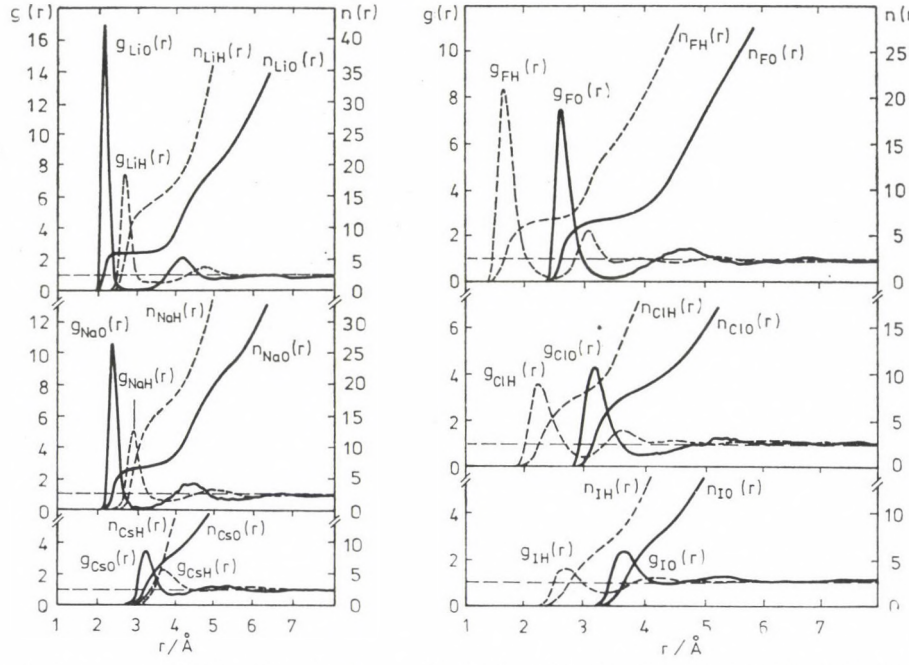

Fig. 3. Ion-oxygen (full) and ion-hydrogen (dashed) radial distribution functions and running integration numbers from MD simulations of 2.2 molal LiI [22], $NaClO_4$ [30], NH_4Cl [31] and CsF [32] solutions

tainty with the values reported by Mezei and Beveridge [5] from their MC work and with the values from MD simulations with the MCY model [6] (see Table II). The largest discrepancies seem to arise for the Cl^- ion, where a dependence on counterion and concentration cannot be excluded [19]. RDFs

Table II

Comparison of characteristic values of the radial distribution functions shown in Fig. 3 with the ones from Monte Carlo calculations by Mezei and Beveridge [5] *and* MD *simulations by Impey et al.* [6]

$r_{IO}^{(M)}$ and $r_{IH}^{(M)}$ denote the position of the first maxima in the ion-oxygen and ion-hydrogen RDF, respectively, $r_{IO}^{(m)}$ gives the position of the first minimum and n the hydration number according to Eq. (6)

	$r_{IO}^{(M)}$			$r_{IO}^{(m)}$		$n(r_{IO}^{(m)})$			$r_{IH}^{(M)}$		
	MD this work	[6]	MC [5]	MD this work	MC [5]	MD this work	[6]	MC [5]	MD this work	[6]	MC [5]
Li^+	2.13	1.98	2.10	2.90	2.65	6.1	5.3	6.0	2.68	2.57	2.70
Na^+	2.36	2.29	2.35	3.12	3.00	6.5	6.0	6.0	2.90	2.95	2.89
Cs^+	3.22	—	—	3.90	—	7.9	—	—	3.72	—	—
F^-	2.64	2.67	2.60	3.36	3.30	6.8	5.8	4.1	1.65	1.73	1.68
Cl^-	3.22	3.29	3.25	3.87	4.1	8.2	7.2	8.4	2.24	2.35	2.25
I^-	3.68	—	—	4.4	—	8.7	—	—	3.40	—	—

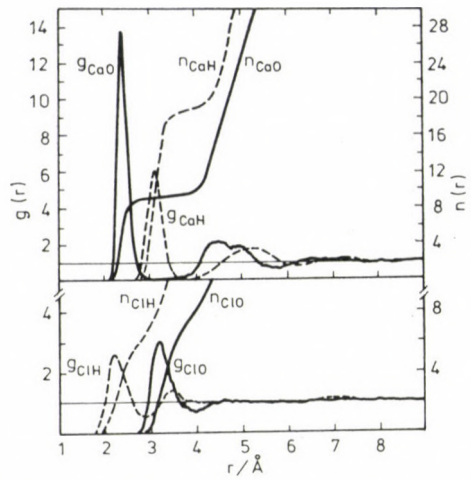

Fig. 4. Ca^{2+}-oxygen, Ca^{2+}-hydrogen, Cl^--oxygen and Cl^--hydrogen radial distribution functions and running integration numbers from the MD simulation of a 1.1 molal $CaCl_2$ solution using the modified CF model [19]. The Cl—O and Cl—H RDFs can be usefully compared with the ones in Fig. 3 obtained from simulations with the ST2 model

obtained for Na^+—O and Cl^-—O from the simulations using the CF model or modified CF model also look very similar to the ones presented here [10].

The agreement between the MD simulations with the ST2 model for water and the ions described as charged LJ spheres, simulations with the CF model for water and other potentials fitted from ab initio data and the MC and MD calculations, where all the pair potentials are derived from ab initio calculations, is quite satisfying. This can be considered as a strong indication of the reliability of both kinds of pair potentials employed as far as the RDFs discussed here are concerned. Some differences between properties calculated from different models will be discussed later. Figure 4 shows the Ca^{2+}-oxygen and Ca^{2+}-hydrogen RDF as an example of the hydration of a divalent ion [19]. Note the very narrow peak in g_{CaO}, containing 9 oxygens, the corresponding peak in g_{CaH} with 18 hydrogens and the pronounced second hydration sphere. A more detailed discussion of the structure of the hydration layer of this ion follows below.

The effect of elevated temperature at constant density on the ion-oxygen RDFs has been investigated for a 0.55 molal LiI solution (only two ions of each kind in the box) [20]. It can be seen from Fig. 5 that the increase in temperature reduces significantly the height of the first peak in $g_{LiO}(r)$ and broadens it (full line). At the same time the gap between first and second hydration shell begins to get filled up. In this way the number of water molecules (six) in the first hydration shell of Li^+ remains constant, as can be seen from $n_{LiO}(r)$ at $r = 3$ Å. The second hydration shell of Li^+ almost disappears at high temperature and pressure. Accordingly, there is a significant difference

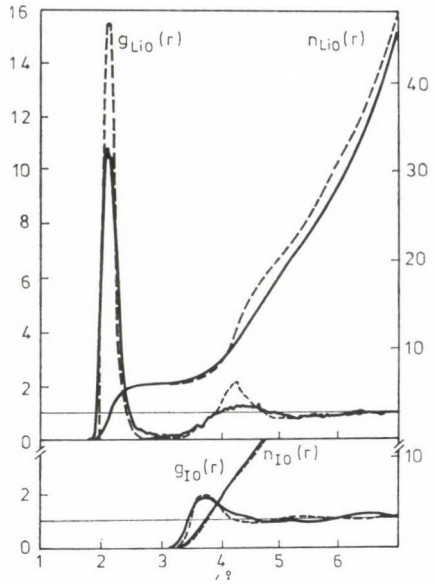

Fig. 5. Ion-oxygen radial distribution functions and running integration numbers for a 0.55 molal LiI solution at 508 K (full) and 308 K (dashed) with the same density of 1.05 g/cm³. At the high temperature the pressure is about 3 kbar [20]

between the two curves for $n_{LiO}(r)$ at $r = 4.5$ Å which slowly disappears with increasing distance. In the case of the iodide ion the first hydration shell is, even at normal temperature and pressure, not well pronounced (lower part of Fig. 5). Consequently not much change can be observed. Only a slight smearing out of the first peak results from the temperature (and pressure) increase.

Pressure increase can also be simulated by increasing the density of the system, that is by reducing the size of the basic box. This has been studied with simulations of a 2.2 molal NaCl solution at densities of 1.0792 g/cm³ and 1.3067 g/cm³ [21], corresponding to normal pressure and a pressure of 10 kbar at room temperature, respectively. The relevant RDFs are presented in Figure 6. The changes brought about by the density increase will be discussed briefly. The position and width of the first peak in g_{NaO} is unchanged, while its height decreases with increasing pressure. Similarly, the second peak flattens. The coordination number increases slightly by about 0.5. This small increase in the coordination number (the density is 21% higher) as well as the decrease in peak height seem to indicate a certain loss of structure of the Na-hydration sphere with increasing pressure. From a comparison between g_{NaO} and g_{NaH}, one sees that there is penetration of hydrogens belonging to the second hydrogen layer into the region of the first.

The chloride hydration seems to undergo larger changes with pressure increase, suggesting that the hydration layer of this ion is even less developed

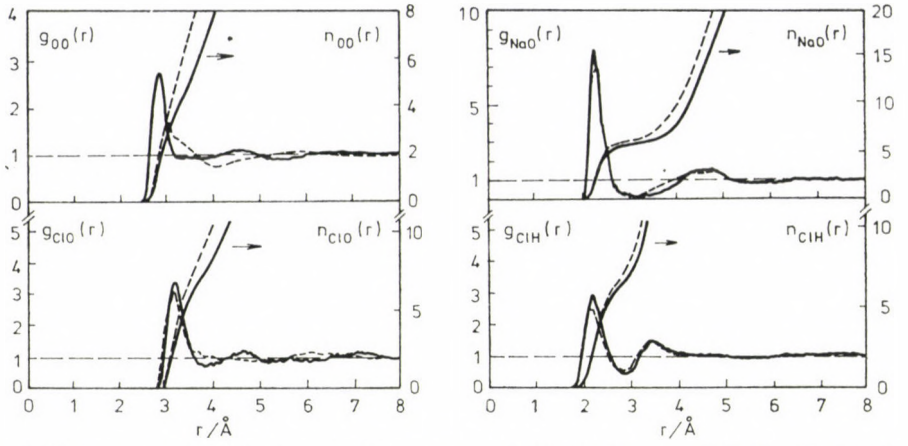

Fig. 6. Na$^+$-oxygen, Na$^+$-hydrogen, Cl$^-$-oxygen and Cl$^-$-hydrogen radial distribution functions and running integration numbers from MD simulations of 2.2 molal NaCl solutions using the modified CF model [21]. Solid lines: density 1.0792 g/cm^3, dashed lines: density 1.3067 g/cm^3

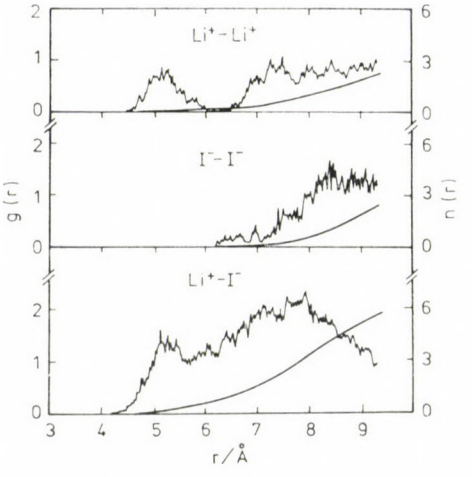

Fig. 7. Li$^+$—Li$^+$, Li$^+$—I$^-$ and I$^-$—I$^-$ radial distribution functions and running integration numbers from the simulation of a 2.2 molal LiI solution using the ST2 model [22]

under pressure than it is normally, though the preference for forming hydrogen bonds (vide infra) between Cl$^-$ and water seems not to be affected.

Ion-ion RDFs are of course also available, though because of the small number of ions present in the sample they are of lower statistical reliability, as is apparent from the noise on the curves for a LiI solution presented in Fig. 7 [22]. From the peak in the g_{LiI} function at $r_{LiI} \approx 5.2$ Å a preference for so-called "solvent separated ion pairs" may be inferred. This finding seems to be in keeping with similar observations obtained from other methods.

As has already been stressed, the only reliable way to check the pair potentials employed in the simulations is the comparison of the results with data resulting unambiguously from experiments. As far as the structure of solutions is concerned, the comparison may be carried out both on the level of the total structure function (x-ray or neutron) or on the level of total or partial RDFs, both methods having their advantages and disadvantages. As an example for such a comparison and for the kind of agreement that may be reached, Fig. 8 shows the comparison between the neutron weighted Cl^--water RDF from an MD-simulation and from several neutron diffraction studies with isotopic substitution. The experimental curves have been rescaled for concentration, while the influence of counterions and concentrations on $g_{ClO}(r)$ and $g_{ClH}(r)$ is not known. Part of the deviations from the overall good agreement has, therefore, to be attributed to this effect. Several detailed comparative studies between data from MD simulations and x-ray scattering studies have also been conducted [23]. An overall good agreement between experiment and MD simulation has been found. By this comparison not only the reliability of the pair potentials employed in the simulation could be checked, but also the models used in the analysis of the x-ray scattering data could be improved and limitations shown [7]. In addition, the combination of both methods has led to the experimental confirmation of properties — like the existence of a second hydration shell around Li^+ and the shortening of the hydrogen bonds between first and second hydration shell — which had been predicted from the simulation (ref. [23b]). Detailed comparison of structural data with scattering results for pure water under pressure [16] had also been carried out [38].

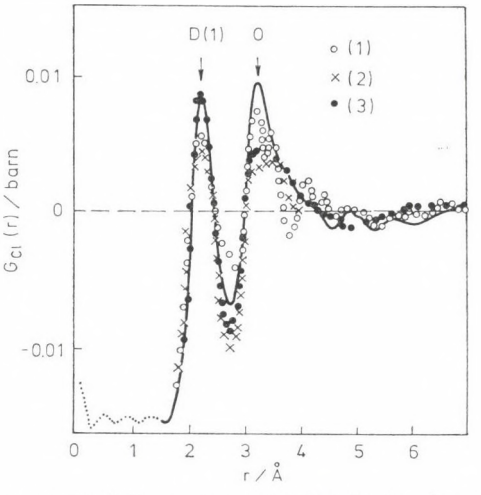

Fig. 8. Comparison of the weighted Cl^--water radial distribution function from an MD simulation of a 1.1 molal $MgCl_2$ solution with results from neutron diffraction studies of a 5.32 molal NaCl (1), a 3.0 molal $NiCl_2$ (2) and a 9.95 molal LiCl (3) solution [24]

Orientation of the water molecules

The orientation of the water molecules in the hydration shells of the ions could be calculated from the distances of the first maxima in the ion-oxygen and ion-hydrogen RDFs. Only in this way can information on the orientation of the water molecules be deduced from diffraction studies. The difficulties connected with this approach have been discussed in detail in ref. [24]. For the MD simulations these difficulties do not arise since the orientations can be calculated directly from the data produced. In Fig. 9 the probability distribution of cos (Θ) — where Θ is the angle between water dipole moment and the vector connecting the oxygen and the ion, as illustrated in the insertion — is shown for various monovalent cations and anions from simulations with the ST2 water model. Only water molecules in the first hydration shells of the ions are taken into account. It is seen that in all cases

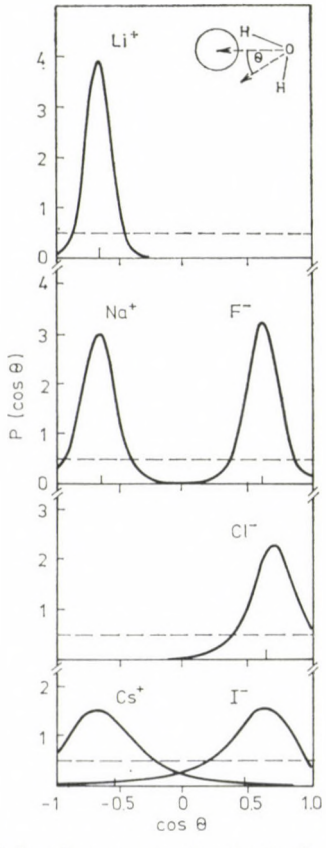

Fig. 9. Distribution of cos (Θ) for the water molecules in the first hydration shells of various alkali and halide ions, calculated from MD simulations of 2.2 molal LiI [22], $NaClO_4$ [30], CsF [32] and NH_4Cl [31] solutions. The dashed lines indicate uniform distributions

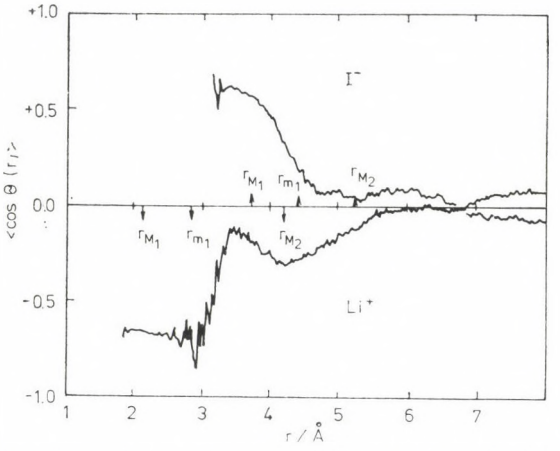

Fig. 10. Average value of cos (Θ) as a function of distance from the iodide and the lithium ion from an MD simulation of a 2.2 molal LiI solution [22]. Θ is defined in the insertion of Fig. 9. r_{M1}, r_{M2} and r_{m_1} indicate the position of the first and second maximum and the first minimum in the ion-oxygen RDF, respectively

the maximum probability corresponds to the formation of a hydrogen bond between anions and water and that "lone pair orbitals" tend to be oriented towards cations. But these distributions have a sizable width, which increases with increasing ion size. Figure 10 shows the average value of cos (Θ) as a function of the ion-oxygen distance. Note the almost constant value for Li^+ across the range of the first hydration layer (r_{m_1} is indicated, cf. Table II) and the pronounced second hydration layer also visible here. In contrast, a much faster decrease of preferred orientation of the water molecules is observed for I^-.

The orientation of the water molecules in the first hydration shells of the ions is one of the rare cases where the results of the simulations depend upon the water model employed [10]. This is demonstrated in Fig. 11 where the distribution of cos Θ is shown for the water molecules in the first hydration shells of Na^+ and Cl^-. The result of the simulation with the ST2 model of water and ion-water interaction as described above are presented as full lines, while the dashed lines result from simulations with the CF model and ion-water pair potential derived from ab initio calculations. In both cases 2.2 molal solutions have been simulated at room temperature. In the case of the chloride ion both simulations agree in showing a preference for a linear hydrogen bond formation. For Na^+ the simulation with the CF model results in a preferentially trigonal orientation of the water molecules while in the ST2 case a preference exists for a lone pair orbital directed towards the cation. The reason for this discrepancy might be that in the ST2 model the directionality of the lone pair orbital is exaggerated by the negative point charges.

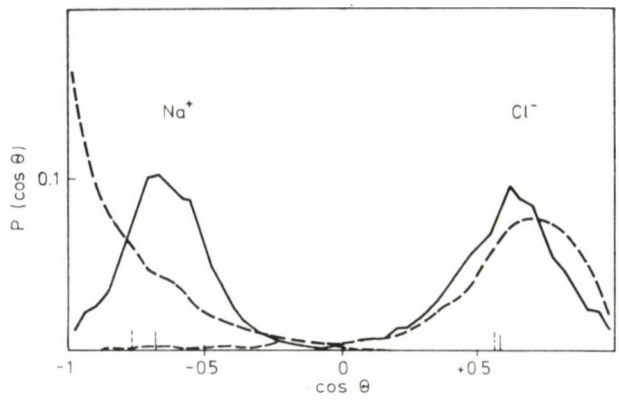

Fig. 11. Distribution of cos (Θ) for the water molecules in the first hydration shells of Na^+ and Cl^-, by analogy to Fig. 9. Solid line: simulation with the ST2 model, dashed line: simulation with the CF model [10]

Hydration shell symmetries

The registration of the water positions in an ion centered coordinate system at several hundred different times spread over the whole simulation run provides the average spatial distribution of the water molecules in the hydration shells. For the monovalent ions, the symmetries (or lack thereof) have already been discussed in another contribution to this symposium [25]; this will therefore not be reported here. We will only briefly discuss some interesting features found in the hydration layer of divalent ions [19, 23a].

Figure 12 shows the projection of the positions of the 6 water molecules found in the first hydration layer of Mg^{2+} and of the 9 water molecules of the Ca^{2+} ion onto the 3 planes of an ion-fixed coordinate system, after suitable averaging over the possible choices of such systems. It can be seen that in the case of Mg^{2+}, the six corners of an octahedron are strongly preferred. In the case of Ca^{2+}, there is also preference for certain sites, yet they do not correspond to any symmetric regular body. The attempt to explain the hydration layer of this ion by means of two subshells or by strongly distorted symmetric arrangements and additional disordered molecules also fails; the crosses in the plot show as an example the expected positions for a hexahedron. One may thus conclude that the Ca^{2+} ion is capable of coordinating a large number of water molecules, which show (in contrast, eg., to monovalent ions with the same hydration number) a high degree of lateral spatial correlation among each other, probably due to their mutual steric hindrance, but no symmetry.

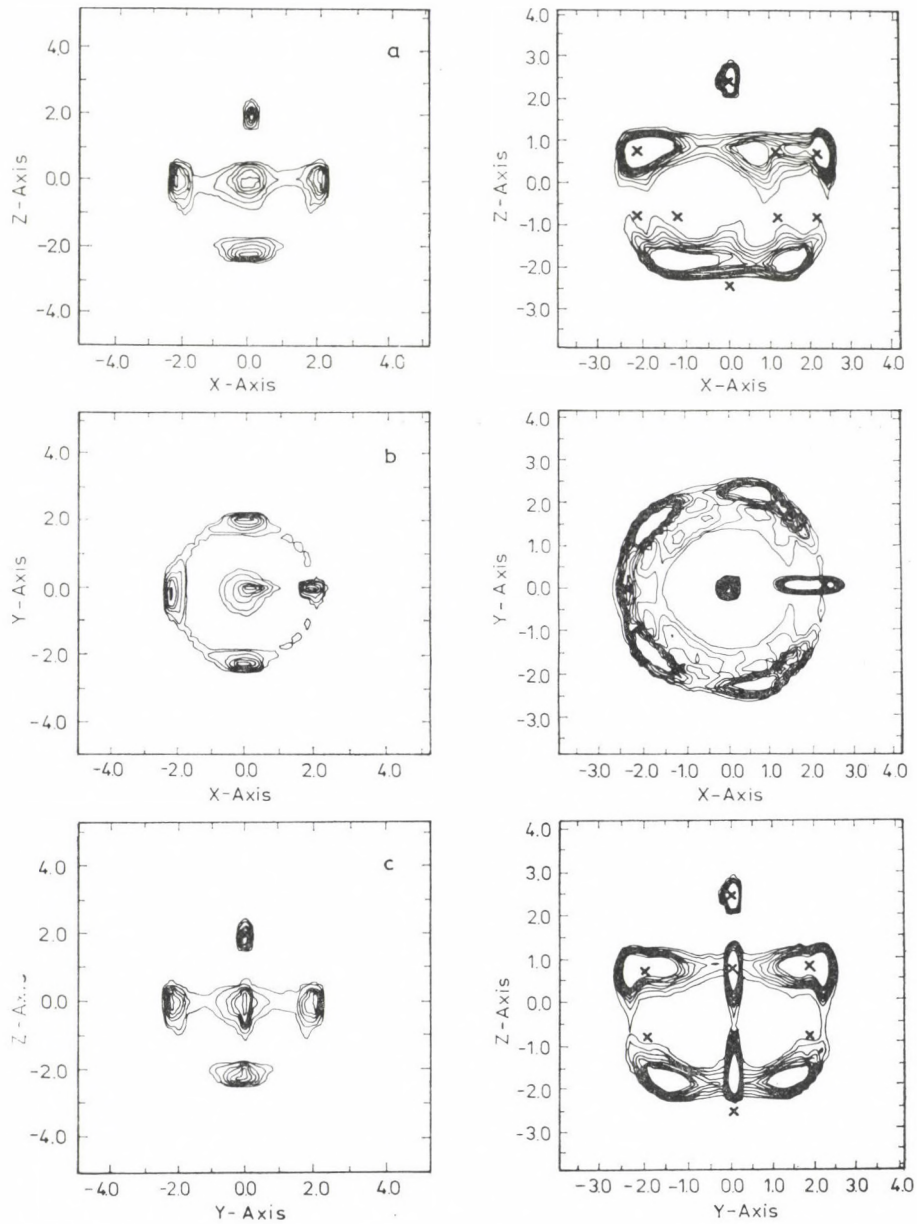

Fig. 12. Density maps of the projections of the oxygen atom positions of the 6 (9) nearest neighbour water molecules around a Mg^{2+} (left) and Ca^{2+} (right) onto the three planes of an ion-centered coordinate system, calculated from the MD simulation. The crosses indicate the positions of the spots expected in the case of a hexahedral arrangement around the Ca^{2+}

Dynamical properties

Self-diffusion coefficients

The self-diffusion coefficients can be determined from the simulation either by the mean square displacement

$$D = \lim_{t \to \infty} < [\vec{R}(t) - \vec{R}(0)]^2 > /6\,t \tag{7}$$

or — as done here — through the velocity autocorrelation functions with the help of the Green—Kubo relation:

$$D = \lim_{t \to \infty} \frac{1}{3} \int_0^t \langle \vec{v}(0) \cdot \vec{v}(t') \rangle \, \mathrm{d}t'. \tag{8}$$

The averages have been calculated according to

$$\langle \vec{v}(0) \cdot \vec{v}(t) \rangle = \frac{1}{N_T \, N} \sum_{i=1}^{N_T} \sum_{j=1}^{N} \vec{v}_j(t_i) \cdot \vec{v}_j(t_i + t) \tag{9}$$

where N denotes the number of particles, N_T the number of time averages and $\vec{v}_j(t)$ the velocity of particle j at time t.

As an example, the normalized velocity autocorrelation functions for the ions and the (total) water of the LiI solution are shown in Fig. 13 [26]. For a better comparison of their different time dependences they are drawn only up to 0.5 ps. The strongly different curves for I^- and Li^+ reflect the translational motions of the heavy iodide ion, slowly changing its velocity, and the practically vibrational motion of the lithium ion in the cage of the six firmly attached water molecules of its first hydration shell. Obviously, the decay times are different for the water molecules and the two ions. Therefore, the upper limit of integral (8) has been chosen differently to be 1.5 ps for water, 0.6 ps for Li^+ and 2.2 ps for I^-, times above which the correlation functions vanish, apart from statistical noise [26]. The statistical quality of the results depends on the length of the correlation time. The shorter the correlation time the more time averages can be employed for a given simulation length.

The results are compared in Table III with the experimentally determined self-diffusion coefficients [27]. The errors are estimated from the variations of the integrals at the upper integration limit, while the uncertainties of the experimental values should be about 10%. There is good agreement within the limits of error.

Having shown that the pair potentials employed in the simulation lead to good agreement with the experimental results, it can be expected that the properties which are not directly accessible by the experiment can be calculated

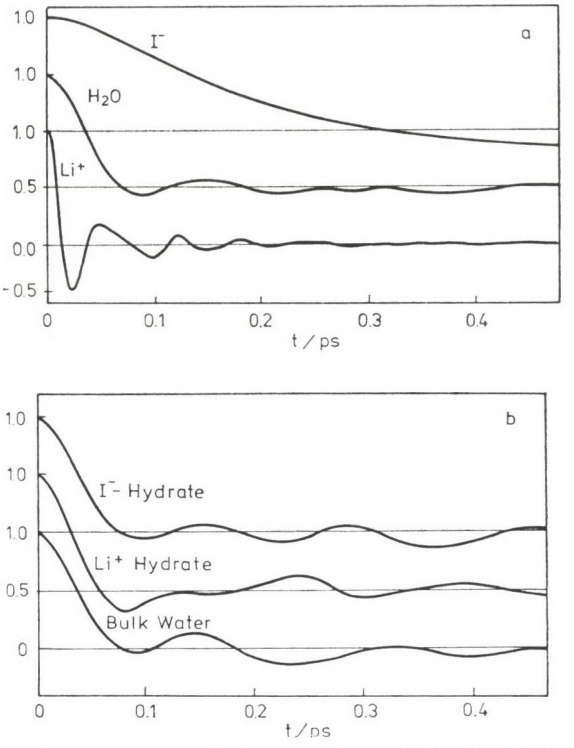

Fig. 13. Normalized velocity autocorrelation functions $\langle \vec{v}(0) \cdot \vec{v}(t) \rangle / \langle \vec{v}(0)^2 \rangle$ for water molecules, lithium ions, and iodide ions (top) and separately for bulk water, hydration water of Li^+ and I^- (bottom) in a 2.2 molal LiI solution [26]

from the simulation with a high degree of reliability. In order to investigate how the single ions contribute to the difference in the self-diffusion coefficients between pure water and solvent water, the velocity autocorrelation functions have been calculated separately for the three water subsystems — water in the first hydration layer of Li^+, I^-, and not in any first hydration layer (called "bulk" water) — and are shown also in Fig. 13. The resulting self-diffusion coefficients are given in Table IV. The following conclusions can be drawn:

1. In all three water subsystems the diffusional motion is reduced relative to pure water.

Table III

Self-diffusion coefficients of the ions and solvent water (D_w) in 2.2 *molal* LiI *solution from the* MD *simulation and from experiments at* 305 K *in units of* 10^{-5} cm^2/s [26]

	D_w	D_{Li^+}	D_{I^-}
MD	2.48 ± 0.06	0.7 ± 0.3	1.40 ± 0.15
exp.	2.35	1.0	1.47

2. The difference in the self-diffusion coefficients between bulk water and pure water contributes more than half to the change which occurs on going from pure water to the 2.2 molal LiI solution.

3. The self-diffusion coefficient of Li^+ and its hydration water is smaller by more than a factor of two than that of bulk water.

4. The self-diffusion coefficient of I^- is much smaller than that of its hydration water and of bulk water, which are approximately equal.

The difference in the self-diffusion coefficients between bulk water in the 2.2 molal LiI solution and pure water can easily be explained on the basis of the structure of the solution as discussed above. All water molecules outside the first hydration shells ($n^+ = 6$; $n^- = 8$) are counted as bulk water but it can be seen from Fig. 3 that twelve additional water molecules form a second hydration shell around Li^+. Therefore, the dynamical properties of all water molecules in the solution are influenced by the ions and are expected to differ from pure water significantly even at this concentration. Occasionally, models are developed to explain experimental data which use the assumption that bulk water has the same properties as pure water [28]. This example shows that even at moderate concentrations, this models may lead to erroneous conclusions.

One would expect in the hydration shell of I^- a larger self-diffusion coefficient than in pure water. However, just the opposite has been found (Table IV). As some of these water molecules belong to the second and some even to the first hydration shell of Li^+, it is easy to understand that the simulation leads to very similar results for the water molecules in the hydration shell of I^- and bulk water. Actually, bulk water should be written with quotation marks, as most of the water molecules belong to the second hydration sphere of Li^+. It is important to note that the ST2 model employed in the simulation is not responsible for the above reversed effect. From an MD simulation where a single ion is surrounded by 215 ST2 water molecules, it has been shown by Geiger [29] that for the hydration sphere of a negatively charged ion the self-diffusion coefficient is increased.

The self-diffusion coefficient for the water molecules in the first hydration shell of Li^+ is somewhat larger than for the ion itself but smaller than for

Table IV

Self-diffusion coefficients in units of 10^{-5} cm^2/s *for bulk water* (D^b), *hydration water of* Li^+ (D^+) *and of* I^- (D^-) *from an* MD *simulation of a* 2.2 *molal* LiI *solution at* 305 K, ° *denotes pure water* [26]

i	D^i	D^i/D°
b	2.85 ± 0.08	0.84
$+$	1.33 ± 0.10	0.39
$-$	2.67 ± 0.10	0.78

pure water by a factor of 2.5 (Table IV). This results from the long residence time of the water molecules in the hydration shell. The simulation shows that more than 50% of the water molecules remain in the first hydration sphere of Li^+ over the whole simulation time of 10 ps.

The residence time of water molecules in the hydration spheres of ions may also be determined by a correlation function technique [10, 6]. As expected, the residence time is found to increase with decreasing radii of cations and anions. For Cl^-, values of 3.8 ps at 290 K [10] and 4.5 ps at 287 K [6] have been determined, in good agreement with each other. This residence time of a water molecule in the first hydration layer of Cl^- is quite similar to the residence time of a water molecule in the neighbourhood of another water molecule [6].

Molecular reorientation, librations and hindered translations

Characteristic times for various molecular reorientations, typical frequencies for librational or translational oscillations of the particles or molecules can of course also be determined from MD simulations. The comparison of such data with spectroscopic experimental results (NMR, IR or Raman) leads to further insight into the dynamics of the ionic hydration.

Typically, such quantities are studied by calculating correlation functions (by analogy to the velocity autocorrelation function in Eq. (9)) and their Fourier transform. Some approximations may have to be introduced in certain cases where the correlation function does not reach its long time limiting value during the simulation time. Only a few examples can be presented here.

We will thus not discuss the various molecular reorientation times and their comparison with (mostly) NMR data, which is quite complicated [26, 33]. We will instead briefly review some results obtained for the hindered translational and librational motion of water molecules in the hydration layers of the Li^+ and I^- ion.

The spectral densities $f(\omega)$ of the hindered translational motions in the 2.2 molal LiI solution have been calculated by Fourier transformation

$$f(\omega) = \int_0^\infty \frac{\langle \vec{v}(0) \cdot \vec{v}(t) \rangle}{\langle \vec{v}(0)^2 \rangle} \cos(\omega t)\, \mathrm{d}t \tag{10}$$

from the normalized velocity autocorrelation functions for the two ions and the total water of the solution as well as separately for the three water subsystems as shown in Fig. 13. The results are presented in Figs. 14—16.

In Fig. 14, $f(\omega)$ is shown for the lithium ion. There is a main peak at 560 cm^{-1} and a second one at 760 cm^{-1}. The high frequencies of the hindered translations are expected from the velocity autocorrelation function (Fig. 13)

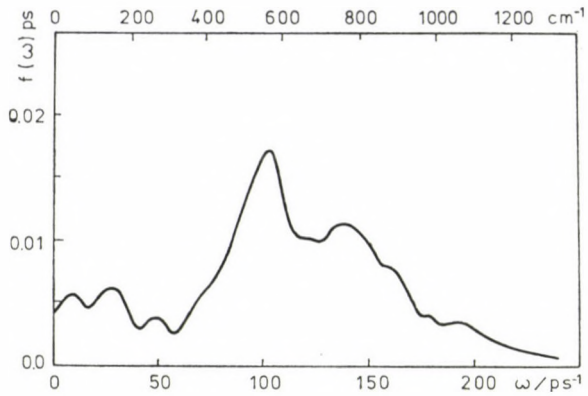

Fig. 14. Spectral density of the hindered translations of the lithium ion from an MD simulation of a 2.2 molal LiI solution [33]

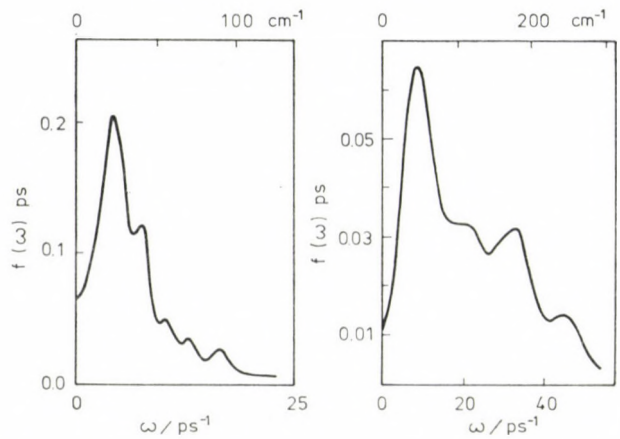

Fig. 15. Spectral densities of the hindered translations of the iodide ion (left) in a 2.2 molal LiI solution and the chloride ion in a 2.2 molal NH_4Cl solution [33, 34]

and fall in the range of the librational band of the water molecules in the first hydration shell of Li^+. It should be noted that the spectral densities of the librations around the dipole moment direction (z in Fig. 17) are similar to those of the hindered translations. From this similarity it can be inferred that the translational motion of the Li^+ is coupled with the librational motions of the strongly attached six water molecules in its first hydration shell.

The spectral densities of the hindered translations of I^- (Fig. 15) are very different from those of Li^+. There is a main peak at 23 cm^{-1} followed by a strong decrease, with $f(\omega)$ being practically zero beyond 100 cm^{-1}. This is in accordance with the picture of the heavy iodide ion moving without its hydration shell and being hindered occasionally by collisions with neighbouring water molecules. It is interesting to compare $f(\omega)$ for I^- with that for Cl^-

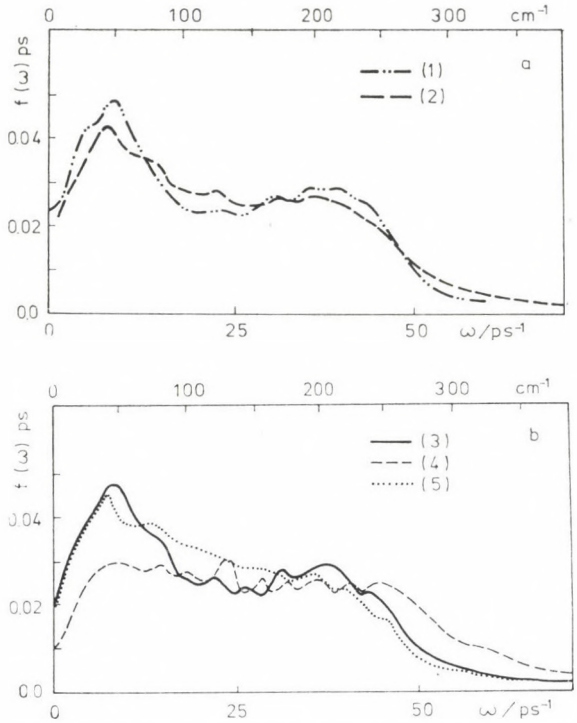

Fig. 16. Spectral densities of the hindered translations of the water molecules from MD simulations of pure water and of a 2.2 molal LiI solution. Top: pure water (1) and total water of the solution (2). Bottom: bulk water (3) hydration water of Li^+ (4) and of I^- (5) [33]

as calculated from an MD simulation of a 2.2 molal NH_4Cl solution [34]. The main peak (Fig. 15) is positioned at 50 cm^{-1} with a shoulder in the range 100—200 cm^{-1} and furthermore $f(\omega)$ for Cl^- is similar to that for pure water as shown in Fig. 16. The ratio of the main hindered translational frequencies of Cl^- and I^- is about two and reflects mainly the difference in the masses of the ions. The additional shoulder at higher frequencies in the case of Cl^- indicates the interactions with its hydration shell water molecules. The structural properties of the solutions support this conclusion.

The hindered translational motions of the water molecules are shown in Fig. 16 for pure water and the total water in the 2.2 molal LiI solution. The curve for pure water roughly resembles that obtained from spectroscopic investigations, where the first peak at 50 cm^{-1} has been assigned to hydrogen bond bending (O—O—O flexing) motions and the broad peak around 175 cm^{-1} to O—O streching motions. The curve for the total water of the solution shows a slight decrease around 50 and 200 cm^{-1} and a slight increase around 100 cm^{-1}, a tendency similar to the changes observed by Stillinger and Rahman for an increase in temperature of pure water [1].

In order to understand the difference between pure water and total water of the solution in more detail, the spectral densities of the hindered translations have been calculated separately for hydration water of Li^+ and I^- and for bulk water and are shown in Fig. 16. The result for bulk water is very similar to that for pure water and needs no further discussion. The effect of the Li^+ on its hydration shell water molecules is twofold. The water molecules in the first hydration shell are strongly attached to the ion and the O—O distances between the water molecules in the first and second hydration shell (2.72 Å, ref. [23b]) are strongly reduced relative to pure water (2.85 Å.) Both effects lead to higher frequencies for the hydrogen bond bending motion (strong reduction of the peak around 50 cm^{-1}) and the O—O stretching frequencies (extension beyond 250 cm^{-1}) and result in an overall shift in $f(\omega)$ to higher frequencies relative to pure water, as can be seen from Fig. 16. The figure shows also that the hydration water of I^- is responsible for the enhancement of $f(\omega)$ in the range 75—150 cm^{-1}. The interaction of I^- with its neighbouring water molecules leads to a loosening of their hydrogen bonds and results, therefore, in a displacement of the O—O stretching motions toward the low frequency range.

A similarly detailed discussion can be conducted with respect to the librational motions of the water molecules. Figure 17 will suffice here to demonstrate the kind of information that can be obtained. Only the spectral densities of the librations of the hydration water of Li^+ are significantly different from those for the other kinds of water. The main feature is a shift or at least a broadening by about 200 cm^{-1} to higher frequencies for all three components. The librations around the y-axis (the axis in the plane of the water molecule and perpendicular to the dipole moment direction) are most strongly affected by the Li^+, as a strong preference exists for a lone pair orientation of the water molecules in the first hydration shell towards the Li^+ (Fig. 9). The librational motions of the first hydration shell water molecules are influenced not only by strong interactions with the cation but also by interactions with other octahedrally arranged water molecules belonging to the same hydration shell and with molecules in the second hydration shell. Because of these complicated interactions a more detailed analysis does not seem warranted.

We will finish this discussion of the dynamics by looking at results obtained for the frequency shifts of intramolecular vibrations. These data were obtained with the improved CF model [4] in a simulation of a 1.1 molal $CaCl_2$ solution [36].

From the normalized velocity autocorrelation functions of the hydrogen atoms the spectral densities of the intramolecular vibrations have been calculated separately for bulk water, hydration water of Ca^{2+} and Cl^- by Fourier transformation. In Fig. 18 the spectral densities in the range of the O—H stretching frequencies are shown for the different water subsystems together

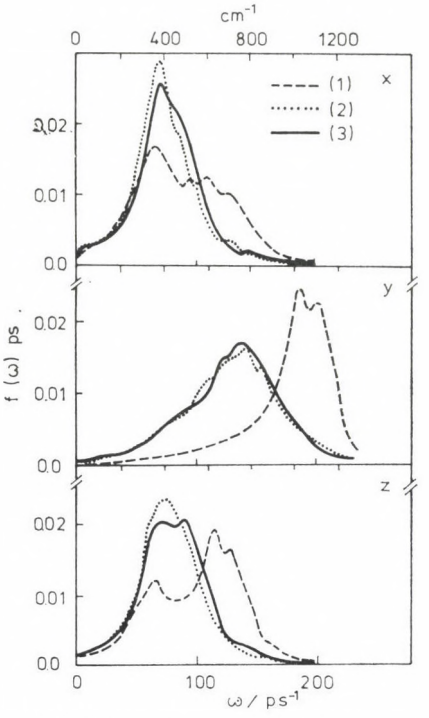

Fig. 17. Spectral densities of the libration around the three main axes of the water molecule calculated separately for the hydration water of the lithium ion (1), the iodide ion (2) and bulk water (3) from an MD simulation of a 2.2 molal LiI solution [33]

with the one resulting from a simulation of pure water [36]. The shift in the position of the maxima between pure water and the total water of the solution (Fig. 18a) is within the limits of error, which is estimated to be ± 10 cm^{-1}.

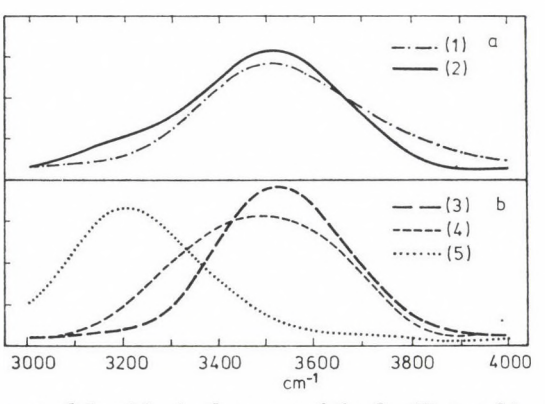

Fig. 18. Normalized spectral densities in the range of the O—H stretching frequencies of water in arbitrary units from an MD simulation of pure water and of a 1.1 molal $CaCl_2$ solution. Pure water (1), total water of the solution (2), bulk water (3), hydration water of Cl^- (4) and of Ca^{2+} (5) [36]

This result is in agreement with Raman-spectroscopic investigations [37]. The spectral densities for the three water subsystems in the $CaCl_2$ solution are given in Figure 18b and show the single ion effects. They are normalized and therefore do not reflect the number of water molecules in the subsystems. (In the 1.1 molal solution their ratio is roughly 1 : 2 : 3 for hydration water

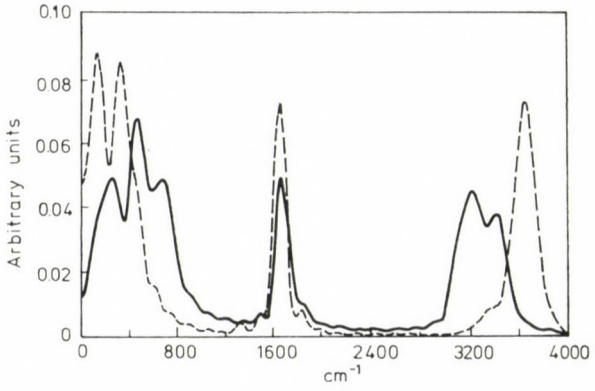

Fig. 19. Fourier transform of the velocity autocorrelation function of the hydrogens in a cluster consisting of one Ca^{2+} ion and 18 water molecules (length of the correlation: 0.225×10^{-12} s). Solid line: The 9 water molecules closest to the ion; dashed line: the other 9 water molecules

of Ca^{2+}, of Cl^- and bulk water). Their maxima are shifted by —17 cm^{-1} for bulk water, —15 cm^{-1} for hydration water of Cl^- and —302 cm^{-1} for hydration water of Ca^{2+} relative to pure water. Small effects are also observed in the H—O—H bending region; we will not discuss them here. A detailed comparison of these findings with experiment has been given in [36].

To further illustrate and summarize what has been said above, Fig. 19 shows the spectral density of the hydrogen motions over the entire frequency range from 0 to 4000 cm^{-1}. This plot has been obtained, contrary to all preceding ones, from the simulation of a small cluster consisting of one Ca^{2+} ion and 18 water molecules in vacuum. The correlation and Fourier transform has again been taken separately for the 9 water molecules closest to the ion, and for the other 9 ones. Three characteristic regions appear in the plot: translations and librations in the region between 0 and 1000 cm^{-1}, the H—O—H bend at about 1675 cm^{-1} and the O—H stretching motions above 2900 cm^{-1}. A brief discussion of this figure also recapitulates some of what has been said above. We note the higher librational frequencies of water molecules close to the cation (cf. Fig. 17), some change in the bending region and finally three bands in the O—H stretching region: one corresponding to O—H oscillators strongly disturbed by the ion at low frequency (cf. Fig. 18), one at high frequency obviously belonging to undisturbed O—H oscillators not engaged in

bonds on the outside of the cluster, and an intermediate one appearing in the spectra of both water subspecies and indicating the onset of a bulk band in spite of the small number of molecules present.

*

Financial support of Deutsche Forschungsgemeinschaft is gratefully acknowledged. One of us (G.J.) thanks the Max-Planck-Gesellschaft for a fellowship. The authors also thank Dipl. Chem. E. Spohr for useful discussions.

REFERENCES

[1] Stillinger, F. H., Rahman, A.: J. Chem. Phys., **60,** 1545 (1974)
[2] Matsuoka, O., Clementi, E., Yoshimine, M.: J. Chem. Phys., **64,** 1351 (1976)
[3] Lemberg, H. L., Stillinger, F. H.: J. Chem. Phys., **62,** 1677 (1975); Stillinger, F. H., Rahman, A.: J. Chem. Phys., **68,** 666 (1978)
[4] Bopp, P., Jancsó, G., Heinzinger, K.: Chem. Phys. Lett., **98,** 129 (1983)
[5] Beveridge, D. L., Mezei, M., Mehrota, P. K., Marchese, F. T., Shanker, G. R., Vasu, T., Swaminathan, S.: in Molecular-Based Study of Fluids (J. M. Haile and G. A. Mansoori, eds.), The American Chemical Society, Washington, D. C. 1983; Mezei, M., Beveridge, D. L.: J. Chem. Phys., **74,** 6902 (1981)
[6] Impey, R. W., Madden, P. A., McDonald, I. R.: J. Phys. Chem., **87,** 5071 (1983); Böhm, J. H., McDonald, I. R.: J. Chem. Soc., Faraday Trans., 2, **1984,** 887
[7] Pálinkás, G., Riede, W. O., Heinzinger, K.: Z. Naturforsch., **32a,** 1137 (1977)
[8] Kong, C. L.: J. Chem. Phys., **59,** 2464 (1973)
[9] Okada, I., Kitsuno, Y., Lee, H. G., Ohtaki, H.: in Ions and Molecules in Solution. Studies in Physical and Theoretical Chemistry, Vol. **27** (N. Tanaka, H. Ohtaki, and R. Tamamushi, eds.), Elsevier, Amsterdam 1983
[10] Bopp, P., Dietz, W., Heinzinger, K.: Z. Naturforsch., **34a,** 1424 (1979)
[11] Dietz, W., Riede, W. O., Heinzinger, K.: Z. Naturforsch., **37a,** 1038 (1982)
[12] Clementi, E., Popkie, H.: J. Chem. Phys., **57,** 1077 (1972); Kistenmacher, H., Popkie, H., Clementi, E.: J. Chem. Phys., **58,** 1689 (1973); **58,** 5627 (1973); **59,** 5842 (1973)
[13] Jancsó, G., Bopp, P.: Z. Naturforsch., **38a,** 206 (1983)
[14] Reimers, J. R., Watts, R. O., Klein, M. L.: Chem. Phys., **64,** 95 (1982)
[15] Carney, G. D., Curtiss, L. A., Langhoff, S. R.: J. Mol. Spectry., **61,** 371 (1976)
[16] Soper, A. K., Silver, R. N.: Phys. Rev. Lett., **49,** 471 (1982); Wu, A. Y., Whalley, E., Dolling, G.: Mol. Phys., **47,** 603 (1982)
[17] Ewald, P. P.: Ann. Phys., **64,** 253 (1921)
[18] Streett, W. B., Tildesley, D. J., Saville, G.: in Computer Modeling of Matter (P. Lykos, ed.), ACS Symp. Series Vol. **86** (1978)
[19] Probst, M. M., Radnai, T., Heinzinger, K., Bopp, P., Rode, B. M.: J. Phys. Chem., **89,** 753 (1985)
[20] Szász, Gy. I., Heinzinger, K.: Earth Planet. Sci. Lett., **64,** 163 (1983)
[21] Jancsó, G., Heinzinger, K., Radnai, T.: Chem. Phys. Lett., **110,** 196 (1984); Jancsó, G., Bopp, P., Heinzinger, K.: in press
[22] Szász, Gy. I., Heinzinger, K., Riede, W. O.: Z. Naturforsch., **36a,** 1067 (1981)
[23] a) Pálinkás, G., Radnai, T., Dietz, W., Szász, Gy. I., Heinzinger, K.: Z. Naturforsch., **37a,** 1042 (1982); b) Radnai, T., Pálinkás, G., Szász, Gy. I., Heinzinger, K.: Z. Naturforsch., **36a,** 1076 (1981)
[24] Szász, Gy. I., Dietz, W., Heinzinger, K., Pálinkás, G., Radnai, T.: Chem. Phys. Lett., **92,** 388 (1982)
[25] Pálinkás, G.: Order and Disorder in Liquids, Plenary Lecture, Symposium on the Structure of Liquids and Solutions, Veszprém, Hungary 1984
[26] Szász, Gy. I., Heinzinger, K., Riede, W. O.: Ber. Bunsenges. Phys. Chem., **85,** 1056 (1981)
[27] Endom, L., Hertz, H. G., Thül, B., Zeidler, M. D.: Ber. Bunsenges. Phys. Chem., **71,** 1008 (1967); Emelyanov, M. I.: Zhurn. Struct. Khim., **6,** 295 (1965); McCall, D. W., Douglas, D. C.: J. Phys., Chem., **69,** 2001 (1965)
[28] Hertz, H. G.: in Water — A Comprehensive Treatise, Vol. **3** (Franks, F., ed.). Plenum Press, New York and London 1973

[29] Geiger, A.: Ber. Bunsenges. Phys. Chem., **85,** 52 (1981)
[30] Heinje, G., Luck, W. A. P., Heinzinger, K.: to be published
[31] Szász, Gy. I., Heinzinger, K.: Z. Naturforsch., **34a,** 840 (1979)
[32] Szász, Gy. I., Heinzinger, K.: Z. Naturforsch., **38a,** 214 (1983)
[33] Szász, Gy. I., Heinzinger, K.: J. Chem. Phys., **79,** 3467 (1983)
[34] Szász, Gy. I., Riede, W. O., Heinzinger, K.: Z. Naturforsch., **34a,** 1083 (1979)
[35] Sceats, M. G., Rice, S. A.: J. Chem. Phys., **72,** 3236 (1980)
[36] Probst, M. M., Bopp, P., Heinzinger, K., Rode, B. M.: Chem. Phys. Lett., **106,** 317 (1984)
[37] Kanno, H., Hiraishi, J.: J. Phys. Chem., **87,** 3664 (1983)
[38] Jancsó, G., Bopp, P., Heinzinger, K.: Chem. Phys., **85,** 377 (1984)

Acta Chimica Hungarica 121 (1—2), pp. 55—69 (1986)

STATISTICAL THEORY OF MOLECULAR SYSTEMS: DIELECTRIC PROPERTIES OF FLUIDS+

Johan S. HØYE

(Institutt for teoretisk fysikk Universitetet i Trondheim, N-7034 Trondheim-NTH, Norway)

Received January 18, 1985

A review of the statistical mechanical theory of polar and polarizable fluids in zero electric field according to considerations by Høye and Stell is presented. Exact limiting results and general relations are found, and basic approximations (MSA) are discussed.

Introduction

The task of statistical mechanics is to evaluate the properties of many particle systems at thermal equilibrium, i.e. from the knowledge of interactions between particles on the microscopic level one wants to compute macroscopic properties like thermodynamic quantities, or one wants to determine structural properties that may be expressed via correlation functions. In principle the basic formulas of statistical mechanics should give exact answers to such questions. However, as is well known, it does not seem possible to obtain explicit exact solutions for more realistic systems with interacting particles. So far only certain one-dimensional systems and a limited number of two-dimensional systems (like the Ising model for a magnet in zero field) can be solved exactly. Thus in other situations one has to rely on approximations which one hopes will work reasonably for the problem considered. Even this is usually a formidable task. To make the problem less formidable, one can make simplified models of the real system whose details may not be so well known either. The discrepancy between real systems and models that are treated theoretically may make comparison between experiments and theory uncertain. However, with computers this difficulty may to a certain extent be overcome as systems with something like a few hundred particles in a box may be modelled and simulated (Monte-Carlo methods or Molecular Dynamics). Thus the computer may act as some kind of an apparatus that yields experimental results for the theoretical model itself.

+ This paper was presented at the Symposium on Structure of Liquids and Solutions at Veszprém, August 27—30, 1984.

In this review we will consider molecular fluids in 3 dimensions, and we will mainly limit ourselves to the effect of dipolar interaction between particles. This interaction is due to electric dipole moments that often are permanently present in molecules due to asymmetry with respect to location of positive and negative charges. In addition, some dipole moment is induced when an electric field acts on composite molecules and single atoms (polarizable particles). The dipolar interactions influence the thermodynamic and structural properties of a fluid. However, the property most closely attributed to this interaction is the dielectric behaviour that results, and we will mostly focus here upon the connection between the dielectric constant and the structure of a fluid.

First we will consider the straightforward situation at low density when the dipole-dipole interaction can be neglected. In other cases when this is not so, it must be taken into account. As is well known this raises various problems. A special problem with dipolar forces is their long-range nature. Upon applying an external electric field to a dielectric fluid, the dipolar forces will induce an electric field such that the resulting field will depend upon the shape of the system. Computations may then depend upon shape too, and to make the situation as simple as possible spherical samples have usually been chosen. By that a homogeneous applied electric field gives rise to a homogeneous resulting field in the sample, and it can be computed in a straightforward way with a known dielectric constant. However, we shall here see that it is possible to make statistical theory on the microscopic level such that dielectric properties can be evaluated in a shape independent way. This we will do next, and it will be shown how the dielectric constant is related to the pair correlation function for a polar fluid with rigid dipole moment (i.e. non-polarizable). Thereafter we will consider the MSA (Mean Spherical Approximation) for a simple polar fluid. Its solution will be explained briefly, and the result for the dielectric constant will be given. We will also explain how the formalism and the MSA solution developed for polar fluids may be extended to polarizable fluids and to polar/polarizable fluids. To do so, we introduce particles with fluctuating polarizability, where the induced dipole moment due to an electric field is not fixed as is the case of a non-fluctuating model, but it performs thermal fluctuations around its average value.

This model of interacting particles has also been solved quantum mechanically for a case where the fluctuating dipole moments and their mutual dipole-dipole interactions are quantized. A generalization of the MSA for classical systems was then applied to the path integral formulation of the quantum partition function (Refs. [20] and [21]).

A more comprehensive presentation of dielectric constants of fluid models with respect to statistical mechanical theory and its quantitative implementation may be found in the review article by Stell, Patey and Høye [1].

Low density limit and earlier theories

Consider a polar nonpolarizable particle with dipole moment $\vec{m}$. Its energy in an electric field $\vec{E}$ is $-\vec{m}\vec{E}$. The probability distribution for the direction of $\vec{m}$ is proportional to the Boltzmann factor $\exp(-\beta\vec{m}\vec{E})$ with $\beta = (k_B T)^{-1}$, where k_B is Boltzmann's constant, and T is temperature. Integrating over the directions of $\vec{m}$ one finds the partition function for this single dipole

$$Z = \int e^{-\beta\vec{m}\vec{E}} \frac{\mathrm{d}\Omega}{4\pi} = \frac{\sinh x}{x} \tag{1}$$

with

$$x = \beta m E$$

The average dipole moment will be ($\hat{E} = \vec{E}/E$)

$$\vec{p} = \langle\vec{m}\rangle = \frac{\int \vec{m} e^{-\beta\vec{m}\vec{E}}\,\mathrm{d}\Omega}{\int e^{-\beta\vec{m}\vec{E}}\,\mathrm{d}\Omega} = \frac{1}{\beta}\frac{\partial}{\partial E}(\ln Z)\,\hat{E}$$

$$= m\left(\operatorname{cotgh} x - \frac{1}{x}\right)\hat{E} = \left(\frac{1}{3}mx + \ldots\right)\hat{E} = \frac{1}{3}\beta m^2\,\vec{E} + \ldots \tag{2}$$

With a number density ϱ of particles per volume unit the polarization $\vec{P}$ becomes (for small $\vec{E}$)

$$\vec{P} = \varrho\vec{p} = \frac{1}{3}\varrho\beta m^2\,\vec{E} \tag{3}$$

The dielectric constant ε is defined by (Gaussian units)

$$4\pi\vec{P} = (\varepsilon - 1)\,\vec{E} \tag{4}$$

So the low density result, which may be used whenever ε is close to one, is

$$\varepsilon - 1 = 3y \tag{5}$$

where

$$y = \frac{4\pi}{3}\varrho\beta m^2 \tag{6}$$

For a nonpolar but polarizable particle the induced dipole moment is given by

$$\vec{p} = \alpha\vec{E} \tag{7}$$

where α is the polarizability. Like Eqs. (2)—(6) the dielectric constant now becomes

$$\varepsilon - 1 = 4\pi\varrho\alpha \tag{8}$$

For a polar/polarizable fluid the low density result likewise becomes

$$\varepsilon - 1 = 3y + 4\pi\varrho\alpha \tag{9}$$

For higher densities the dipolar interaction between the particles becomes more important, and it can no longer be neglected as it will induce an electric field that adds to the applied field. Attempts have been made to include this induced field to compute ε for arbitrary density. The best known result in this connection is the Clausius—Mosotti relation

$$\frac{\varepsilon - 1}{\varepsilon + 2} = \frac{4\pi}{3}\varrho\alpha \tag{10}$$

This is in fact exact for regular cubic crystals with linear polarizability as in Eq. (7), and it can be derived by purely macroscopic considerations. One may consider a spherical sample in given external field. The local electric field $\vec{E}_{\text{loc}}$ at a particle can be computed and then used in Eq. (7). The resulting (average) field $\vec{E}$ in the medium to be used in (4) can also be found by which expression (10) is obtained.

On comparing (2) and (7) it is seen that a single polar molecule in a not too strong electric field may be regarded as a polarizable particle with polarizability $\alpha = 1/3\,\beta m^2$. The corresponding Clausius—Mosotti relation would be

$$\frac{\varepsilon - 1}{\varepsilon + 2} = y \tag{11}$$

It turns out that the Clausius—Mosotti relation works fairly well for polarizable fluids with no permanent dipole moment, but deviations can be measured experimentally. However, for polar fluids it fails drastically. On the other hand, polar fluids usually have a large ε, while nonpolar ones have a small ε, which may partly explain why Eq. (10) works fairly well for this latter case.

Onsager [2] reconsidered the derivation of ε for a polar fluid. By his considerations, instead of (11), he obtained

$$\frac{(\varepsilon - 1)\ (2\varepsilon + 1)}{9\varepsilon} = y \tag{12}$$

when no polarizability is present.

The theories above may be compared with experiments. For example, for water at room temperature one has $\varepsilon \approx 80$. The measured permanent dipole moment of water is 1.85 Debye (in e.s.u.) which means $y \approx 4$. From

this it is clear that the Clausius—Mosotti relation (11) fails completely in this case as it tells that $\varepsilon \to \infty$ when $y \to 1$. Onsager's result (12) is somewhat low as it only yields $\varepsilon \approx 19$ in the present case. However, for other polar fluids it seems to work better, and adding the effect of polarizability will increase ε. So Onsager's theory obviously works better for polar fluids than the Clausius—Mosotti theory.

In a study of the theory of polar fluids Kirkwood [3] derived an expression for ε for a spherical sample. He found

$$\frac{(\varepsilon - 1)\,(2\varepsilon + 1)}{9\varepsilon} = yg \tag{13}$$

which is the same as expression (12) except for the Kirkwood g-factor. This factor reflects the coordination of the dipole moments of particles surrounding a molecule.

Pair correlation function of a polar fluid and its relation to the dielectric constant

Kirkwood's expression (13) suggests that knowledge of the pair correlation will yield g and by that ε. We shall now consider this in the formalism used by Høye and Stell for systems in zero electric field. There derivations are done in a way that does not depend upon the shape of the sample.

Consider the dipole-dipole interaction

$$\psi_{DD}(12) = -\frac{m^2}{r^3} D(12) \tag{14}$$

between two dipoles 1 and 2. They are separated by a distance $\vec{r}$, and m is the magnitude of their dipole moments. Further

$$D(12) = 3(\hat{s}_1\hat{r})(\hat{s}_2\hat{r}) - \hat{s}_1\hat{s}_2 \tag{15}$$

where $\hat{s}_1$ and $\hat{s}_2$ are unit vectors along the dipole moments of the two particles, while $\hat{r}$ is the unit vector along the relative distance. Besides this dipole interaction, molecules will have other types of interaction that affect the properties of the system. Unless the molecules have a net charge, these interactions will be of a more short-ranged nature. (Molecules with net charge, i.e. ionic systems will not be considered here). Real molecules have a strongly repulsive core, and they will have attractive dispersion forces too. However, composite molecules are not shperical, but as an approximate model one may say they are. If this other type of interaction is the Lennard—Jones interaction

$\Phi(r) = 4\varepsilon[(\sigma/r)^{12} - (\sigma/r)^6]$, then the resulting interaction will be the Stockmayer potential. An even more simple model will be to let $\Phi(r)$ be a simple hard core potential of range R.

Now let $\Phi(r)$ be the potential of a reference system whose properties are considered known. This system we perturb by the dipolar interaction $\psi_{DD}(12)$ whose effect we want to evaluate. By perturbation we will consider the γ-ordering scheme invented for weak long-range interactions of spherical shape [4]. (In the long-range limit $\gamma \to 0$ a Van der Waals like equation of state was obtained.) The γ-parametrization means that the potential can be written as

$$\psi_{DD}(12) = \gamma^3 F(\gamma r) \tag{16}$$

Obviously the potential (14) does not define an inverse range parameter γ as it will drop out. Trying to remedy this by modifying $\psi_{DD}(12)$ for large r cannot be done since then the dielectric behaviour will be lost. But the $\psi_{DD}(12)$ can be modified for small r. In fact for real systems the $\psi(12)$ can be chosen rather freely inside the hard core, e.g. we may cut $\psi_{DD}(12)$ inside a certain radius $1/\gamma$ to obtain [5].

$$\psi(12) = H(\gamma r - 1)\psi_{DD}(12) \tag{17}$$

where $H(x)$ is a step function

$$H(x) = \begin{cases} 0 & \text{if} \quad x < 0 \\ 1 & \text{if} \quad x > 0 \end{cases}$$

Fourier transforming (17) with respect to $\vec{r}$ one obtains [5]

$$\tilde{\psi}(12) = \frac{4\pi}{3} m^2 \tilde{f}(k/\gamma)\, \tilde{D}(12) \tag{18}$$

where

$$\tilde{D}(12) = 3(\hat{s}_1 \hat{k})(\hat{s}_2 \hat{k}) - \hat{s}_1 \hat{s}_2 \tag{19}$$

The $\hat{k}$ is the unit vector along the Fourier variable k. Generally

$$\tilde{f}(k/\gamma) \to 1 \quad \text{as} \quad k \to 0 \tag{20}$$

With the sharp cut-off in (17) the explicit form of $\tilde{f}(z)$ will be

$$\tilde{f}(z) = 3\left(\frac{\sin z}{z^3} - \frac{\cos z}{z^2}\right) \tag{21}$$

It is interesting to note here that $\tilde{f}(k/\gamma)$ will be the Fourier transform of a potential of spherical symmetry of range $1/\gamma$ in accordance with the idea of γ-ordering. In fact, (21) is the transform of a square well potential. This is consistent with the idea that the cut dipole-dipole interaction (17) can be

considered as a perturbation, and by that we are in a situation that exact results may be obtained for a model where the limit $\gamma \to 0$ is taken.

Computations may be done in terms of graphs. These originate from the well known Mayer graph fugacity expansion, where the fugacity is eliminated in favour of density with the result that only irreducible graphs remain. Furthermore, the Mayer f-bonds may be expanded in potential bonds

$$v(12) = -\beta\psi(12) \tag{22}$$

and the resulting graphs may be ordered in orders of γ. The lowest order contribution to the pair correlation function beyond the reference system piece then turns out to be given by the sum of simple chain graphs in terms of v-bonds. The vertices of these graphs will be hypervertices that consist of graphs from the references system pair correlation function [4]. However, in the present situation these hypervertices will reduce to simple ϱ-vertices since averaging over orientations of the dipole moments requires the v-bonds to be directly connected to give a nonzero contribution. So the lowest order contribution becomes

$$\varrho h(12) = \varrho v(12) + \int \varrho v(13)\ \varrho v(32)\, d\vec{r}_3 \frac{d\Omega_3}{4\pi} + \ldots \tag{23}$$

Thelse integrals will be integrals of convolution, so Fourier transformation yields

$$\varrho\tilde{h}(12) = \varrho\tilde{v}(12) + \int \varrho\tilde{v}(13)\ \varrho\tilde{v}(32) \frac{d\Omega_3}{4\pi} + \ldots \tag{24}$$

Performing the angular integration once, one finds that the $\tilde{D}(12)$ piece is kept and a $\Delta(12)$ term is created where

$$\Delta(12) = \hat{s}_1\hat{s}_2 \tag{25}$$

By repeated integrations no more terms are created, and expression (24) can be evaluated in various ways. The simplest is perhaps to note that introduction of $J_1 = \Delta + D$ and $J_2 = 2\Delta - D$ ($\Delta = \Delta(12)$ and $D = \tilde{D}(12)$) will create 2 independent geometric series that can be easily summed. From (18), (20) and (22)

$$\tilde{v}(12) = -3y\, \tilde{f}(k/\gamma)\ \tilde{D}(12) \underset{k\to 0}{\to} -3y\tilde{D}(12) \tag{26}$$

So we find when $k \to 0$

$$\varrho\tilde{h}(12) = a\tilde{D}(12) + b\Delta(12)$$

$$a = \frac{-3y}{(1+2y)\,(1-y)}; \quad b = -2ya \tag{27}$$

where $y = 4\pi/9\ \varrho\beta m^2$ as given by (6).

The dielectric constant ε can now be found by putting two test charges q_1 and q_2 into the fluid and find how they are correlated for large distances. This gives their effective interaction which from electrostatics is given by

$$\Phi^e_{CC}(r) = \frac{q_1 q_2}{\varepsilon r} \tag{28}$$

whose Fourier transform is

$$\tilde{\Phi}^e_{CC}(k) = \frac{4\pi q_1 q_2}{\varepsilon k^2} \tag{29}$$

This will be shape independent as the system can be large compared to the separation of charges by which the effect of the surface upon the electric field can be neglected.

From the microscopic viewpoint the correlation between the test charges arises from their direct interaction $q_1 q_2/r$ plus an interaction via one dipole plus an interaction via 2 dipoles that are correlated (which includes the effect of interaction via more particles). For this computation we need the charge-dipole interaction

$$\Phi_{CD}(12) = \pm \frac{q_1 m(\hat{r}\hat{s}_2)}{r^2} \tag{30}$$

whose Fourier transform is [5]

$$\tilde{\Phi}_{CD}(12) = \pm \frac{4\pi i q_1 m(\hat{k}\hat{s}_2)}{k} \tag{31}$$

The $\pm$sign will depend upon whether $\hat{r}$ is pointing towards or away from the charge. Note that both signs will be needed since we start at the charge q_1 and finish at the charge q_2. Computing these three contributions and performing integrations like the ones in (24) the result becomes ($k \to 0$) [5]

$$\tilde{\Phi}^e_{CC}(k) = \frac{4\pi q_1 q_2}{k^2}[1 - 3y - 2ya - yb] = \frac{1-y}{1+2y}\frac{4\pi q_1 q_2}{k^2} \tag{32}$$

with a and b given by (27). Comparing this with (29) one can conclude that the dielectric constant is given by

$$\varepsilon = \frac{1+2y}{1-y} \tag{33}$$

or

$$\frac{\varepsilon - 1}{\varepsilon + 2} = y \tag{34}$$

This is precisely the Clausius—Mosotti result (11) which here has been obtained as an exact limiting result when $\gamma \to 0$.

Although we are not able to compute the pair correlation function exactly in other situations, we can still evaluate its general structure and find its relation to the dielectric constant. This is done by consideration of the graph structure. Result (27) was found by summation of chains of v-bonds with simple ϱ-vertices. Now a chain may be cut at ϱ-vertices, and all kinds of allowed graphs may fill the gap at the cut. These graphs cannot be singly connected by v-bonds since this is already included in the chain structure. Thus these inserted graphs will be of short range compared to the dipolar v-bond itself and can be regarded as a δ-function when large r (or small k) behaviour is considered. When $k \to 0$, this inserted piece can in principle be expanded in Legendre polynomials with respect to $\hat{s}_1\hat{s}_2$. By integration of this expansion over orientations together with the v-bond, only the $\Delta(12)$ term will contribute [5]. Adding this contribution to the ϱ-vertex an effective density ϱ_e that can be written as

$$\varrho_e = \varrho \frac{z}{y} \tag{35}$$

is obtained. From that, the general form of $\tilde{h}(12)$ is found by some modification of (27) [5].

$$\varrho\tilde{h}(12) = 3\left(\frac{z}{y} - 1\right)\Delta(12) + \frac{z}{y}(a\tilde{D}(12) + b\Delta(12)) + (\text{terms that will not contribute to } \varepsilon) \tag{36}$$

where now

$$a = \frac{-3z}{(1+2z)\ (1-z)}; \quad b = -2za \tag{37}$$

The first term in (36) represents the above mentioned inserted piece alone which also is part of the full $\tilde{h}(12)$.

With (36) the effective charge interaction, instead of (32), becomes

$$\tilde{\Phi}^e_{CC}(k) = \frac{4\pi q_1 q_2}{k^2}\left\{1 - 3y - 2y\frac{z}{y}a - y\left[3\left(\frac{z}{y} - 1\right) + \frac{z}{y}b\right]\right\} = \frac{1-z}{1+2z}\frac{4\pi q_1 q_2}{k^2} \tag{38}$$

Accordingly

$$\varepsilon = \frac{1+2z}{1-z} \tag{39}$$

or

$$\frac{\varepsilon - 1}{\varepsilon + 2} = z \tag{40}$$

This gives a formally exact relation between the pair correlation function and the dielectric constant. The problem is to determine z in Eq. (35). In the mean field limit $\gamma \to 0$, $z \to y$.

In (36) the z may be eliminated in favour of ε from Eq. (40) ($k \to 0$). So the general structure in terms of ε is [6].

$$\varrho\tilde{h}(12) = \varrho\tilde{h}_D(0)\,\tilde{D}(12) + \varrho\tilde{h}_\Delta(0)\;\Delta(12)$$

$$\varrho h_D(0) = -3y\frac{1}{\varepsilon}\left(\frac{\varepsilon-1}{3y}\right)^2\;;\quad \varrho\tilde{h}_\Delta(0) = 3\left(\frac{(\varepsilon-1)\;(2\varepsilon+1)}{9\varepsilon y}-1\right) \tag{41}$$

From the $D(12)$ term it is seen that the effective interaction between a pair of the dipolar particles is not merely a modification of the direct interaction by a factor $1/\varepsilon$ as must be the case for net charges. Furthermore, the two terms in (41) are not independent of each other. This has the consequence that ε can be related to $\tilde{h}(12)$ in various ways of which Eq. (40) represents one [5, 7].

Equation (41) yields the relation ;

$$\frac{(\varepsilon-1)\;(2\varepsilon+1)}{9\varepsilon} = yg$$

with

$$g = 1 + \frac{1}{3}\varrho\tilde{h}_\Delta(0),\;\tilde{h}_\Delta(0) = \int h_\Delta(r)\,\mathrm{d}\vec{r} \tag{42}$$

This is just Kirkwood's result (13) with g specified.

Finally in this part we note that for real systems the perturbing potential can be chosen rather freely inside hard cores without changing the resulting physics. This, however, will change perturbing computations. So to (17) a $\Delta(12)$ term of range $1/\gamma$ may be added. This modifies (18) and (26) correspondingly such that one can write ($k \to 0$)

$$\tilde{v}(12) = -3y[\tilde{D}(12) + \Theta\Delta(12)] \tag{43}$$

where the magnitude of this term has entered as a parameter Θ. With (43) expression (24) may again be evaluated. Instead of (34) this will yield the following for ε [6]

$$\frac{\varepsilon-1}{(1-\Theta)\;\varepsilon+2+\Theta} = y \tag{44}$$

Thus, varying Θ, one can have a continuous family of mean field results, not just (34) ($\gamma \to 0$).

The MSA solution

For a polar fluid the OZ (Ornstein—Zernike) equation is [8]

$$h(12) = c(12) + \varrho \int c(13)\, h(32)\, \mathrm{d}\vec{r}_3 \frac{\mathrm{d}\Omega_3}{4\pi} \tag{45}$$

Its Fourier transform will be

$$\tilde{h}(12) = \tilde{c}(12) + \varrho \int \tilde{c}(13)\, \tilde{h}(32) \frac{\mathrm{d}\Omega_3}{4\pi} \tag{46}$$

Here $c(12)$ is the direct correlation function.

Let the system consist of particles that have spherical hard cores of diameter R and in addition interact with the dipole-dipole interaction (14). The MSA of this problem is defined by the condition [9]

$$\begin{aligned} h(12) &= -1 \qquad \text{for} \quad r < R \\ c(12) &= -\beta\psi_{DD}(12) \qquad \text{for} \quad r > R \end{aligned} \tag{47}$$

which together with (45) will determine $h(12)$ and $c(12)$ for all r. The first condition in (47) is the exact core condition for hard spheres, while the second one is an approximation.

One may now note that Eqs. (24) and (46) are in fact the same except that $\tilde{v}(12)$ is replaced by $\tilde{c}(12)$. With condition (47) the $v(12)$ and $c(12)$ will also be the same for $r > R$. The determination of $c(12)$ for $r < R$ may further be considered as a preferred choice for $v(12)$ for $r < R$ by which they will be equal for all r. Thus the MSA may be considered as a mean field approximation that will specify a Θ-parameter in (43) dictated by the core condition (47). In this way it represents a lowest perturbation in γ-ordering, and the implicit specification of Θ may be regarded as some kind of optimized choice.

Without the dipolar interaction the MSA problem reduces to the well known PY (Percus—Yevick) solution for hard spheres. Adding the dipolar interaction this solution can be separated out and like (41) and (43) one finds that the total $h(12)$ will have the form

$$h(12) = h_0(r) + h_D(r)\, D(12) + h_\Delta(r)\, \Delta(12) \tag{48}$$

with similar form for $c(12)$. The $h_0(r)$ is the hard sphere solution. The boundary conditions on the different terms will follow from (47). As was the case for computation of (24) to obtain (27) the D- and Δ-terms will couple. However, as noted under (24), it all decouples into two parts by introduction of $J_1 = \Delta + D$ and $J_2 = 2\Delta - \mathrm{D}$. The same happens in the MSA problem [10].

In (46) the orientation dependent factors J_1 and J_2 can then be erased, and the resulting two equations can be regarded as Fourier transformed OZ--equations of spherically symmetrical functions. With (21) we noted that when disregarding angular dependence, the cut dipole interaction (17) had the same Fourier transform as a square well. Likewise the conditions (47) make the two new direct correlation functions equal to zero for $r > R$ while the two correlation functions will be constants $-2K$ and K respectively for $r < R$ with K to be determined later. By this all is reduced to two additional hard sphere problems, and the known result can simply be taken over [10]. The MSA solution then leads to the following result for the dielectric constant

$$\varepsilon = \frac{q(2\xi)}{q(-\xi)} \tag{49}$$

where

$$q(x) = \frac{[(1+2x)^2}{(1-x)^4} .$$

The parameter $\xi = \pi/6\, K\varrho R^3$ is determined by

$$3y = q(2\xi) - q(-\xi) \tag{50}$$

with y given by (6). The MSA solution was first performed by Wertheim [10].

As a numerical example $y \approx 4$ yields $\varepsilon \approx 48$ which compares more favourably with $\varepsilon \approx 80$ for water than Onsager's result considered under Eq. (12)

To go beyond the MSA various ideas have been proposed [1]. When doing so the pair correlation function of the reference system will also enter and affect dielectric properties.

Polarizable fluids

For a polarizable fluid, the induced polarization varies with the local electric field and like Eq. (7), this relation is usually considered to be linear. This model was employed, for example, in the pioneering studies of the dielectric properties of polarizable systems by Kirkwood [11] and by Yvon [12] and in a more recent work by Wertheim [13] who considers particles that carry a permanent dipole moment as well.

Here we want to consider a somewhat different model, earlier considered by Van Vleck [14], in which the polarization carried by a particle is regarded as the amplitude of a classically oscillating quantity. Due to thermal motion the dipole moment will fluctuate so that a relation like (7) will only hold for the average dipole moment rather then for the instantaneous one. The advan-

tage of the latter model is that the methods developed for polar fluids can be readily applied to it by some generalization. To do so, we use a trick which was used by Onsager in a different context [15]. The trick is to regard molecules that have different instantaneous dipole moments as being different species of a polar fluid mixture [16, 17]. The extension to mixtures has been considered in Ref. [18]. For instance, the relevant mixture problem related to the polarizable fluid is easily solved in the MSA as the different species all have the same hard core diameter. In fact the solution is simply the one for the one component case with ε given by (49) and (50) except that the y given by (6) now has to be replaced by an effective y_e given by

$$y_e = \frac{4\pi}{9}\beta \sum_i \varrho_i m_i^2 \tag{51}$$

where ϱ_i and m_i are number densities and dipole moments respectively, of the species. However, this alone does not solve the MSA polarizable fluid problem as the ϱ_i so far are unknown. To determine the density distribution, which will become continuous, one must specify some potential that governs the fluctuations. As the simplest choice one can choose a harmonic potential [16, 17]

$$\Phi(s) = \frac{1}{2\alpha} s^2 \tag{52}$$

where s is the amplitude of the fluctuating dipole moment while α will be the polarizability. When a single particle is placed in an electric field, the average polarization will follow the linear relation (7). For a single particle the density distribution will be

$$\varrho_{os} = Ce^{-\beta\Phi(s)} \tag{53}$$

where C is such that $\varrho = \int \varrho_{os} d\vec{s}$.

With this distribution one will easily find

$$y_e = \frac{4\pi}{9}\beta\varrho\langle s^2\rangle = \frac{4\pi}{3}\varrho\alpha \tag{54}$$

However, this is not correct when the particles interact since the interactions will affect the density distribution ϱ_s. So the additional problem is to determine this distribution. In principle, this can be done by relating it to the distribution of chemical potentials via the corresponding equation of state. The chemical potentials will be some constant to which the potential $\Phi(s)$ is added. With MSA this latter problem can be solved explicitly to yield [16, 17]

$$\varrho_s = C_e^{-\beta\Phi(s) - \frac{1}{2}(s^2/\langle s^2\rangle)c_A^{(0)}} \tag{55}$$

$$\varrho = \int \varrho_s \, d\vec{s}$$

where

$$c_{\Delta}(0)/\langle s^2\rangle = -16\xi\beta$$

which yields

$$y_e = \frac{4\pi}{3}\beta\varrho\langle s^2\rangle = \frac{4\pi}{3}\varrho\alpha'. \tag{56}$$

$$\alpha' = \alpha a; \quad a = \frac{1}{1-16\alpha\xi} \quad \text{(with } R = 1\text{)}$$

to replace y in (50).

If a permanent dipole moment m is added then the result becomes [16]

$$y_e = \frac{4\pi}{3}\varrho\alpha' + y\left(\frac{m'}{m}\right)^2 \tag{57}$$

with y given by (6) and

$$m' = ma$$

The quantities α' and m' may be regarded as renormalized polarizability and dipole moment respectively due to the fluid surrounding a particle. These MSA results were also previously obtained by Wertheim [13] using the model with nonfluctuating polarization.

It may be interesting to note that if the MSA method outlined here is applied to polarizable particles located on a regular close-packed cubic lattice, it will yield the exact answer which is known to be the Clausius—Mosotti relation (10) [16].

The fluctuating model for polarizable particles will create attractive dispersion forces between the particles due to the fluctuation of dipole moments. In this respect, it may be considered a more realistic model than the nonfluctuating model. As mentioned in the introduction a quantum mechanical computation of this many-body system of oscillating dipoles has also been performed generalizing the MSA method [19, 20]. Not surprisingly, as the oscillators and dipolar interactions are harmonic, the result for ε becomes the same as the one found here.

REFERENCES

[1] Stell, G., Patey, G. N., Høye, J. S.: Adv. Chem. Phys., **48,** 183 (1981)
[2] Onsager, L.: J. Am. Chem. Soc., **58,** 1486 (1936)
[3] Kirkwood, J. G.: J. Chem. Phys., **7,** 911 (1939)
[4] Hemmer, P. C.: J. Math. Phys., **5,** 75 (1964); Lebowitz, J. L., Stell, G., Baer, S.: J. Math. Phys., **6,** 1282 (1965)
[5] Høye, J. S., Stell, G.: J. Chem. Phys., **61,** 562 (1974)
[6] Høye, J. S., Stell, G.: J. Chem. Phys., **64,** 1952 (1976)
[7] Nienhuis, G., Deutch, J. M.: J. Chem. Phys., **55,** 4213 (1971); **56,** 5511 (1972); Ramshaw, J. D.: J. Chem. Phys., **57,** 2684 (1972)
[8] Ornstein, L. S., Zernike, F.: Proc. Acad. Sci., Amsterdam, **17,** 793 (1914)

[9] Percus, J. K., Yevick, G.: Phys. Rev., **136,** B290 (1964); Lebowitz, J. L., Percus, J. K.: Phys. Rev., **144,** 251 (1966); Brout, R.: Phys. Rev., **122,** 469 (1961)
[10] Wertheim, M. S.: J. Chem. Phys., **55,** 4291 (1971); Høye, J. S., Lebowitz, J. L., Stell, G.: J. Chem. Phys., **61,** 3253 (1974)
[11] Kirkwood, J. G.: J. Chem. Phys., **4,** 592 (1936)
[12] Yvon, J.: Actualités Scientifique et Industrielles, Nos. 542 and 543. Herman & Cie, Paris 1937
[13] Wertheim, M. S.: Mol. Phys., **25,** 211 (1973); **26,** 1425 (1973); **33,** 95 (1977); **34,** 1109 (1977); **36,** 1217 (1978)
[14] Van Vleck, H. J.: J. Chem. Phys., **5,** 556, 991 (1937)
[15] Onsager, L.: Ann. N. Y. Acad. Sci., **51,** 627 (1949)
[16] Høye, J. S., Stell, G.: J. Chem. Phys., **73,** 461 (1980)
[17] Pratt, L.: Mol. Phys., **40,** 347 (1980)
[18] Høye, J. S., Stell, G.: J. Chem. Phys., **70,** 2894, (1979)
[19] Chandler, D., Wolynes, P. G.: J. Chem. Phys., **76,** 1128 (1982); Chandler, D., Schweizer, K., Wolynes, P. G.: Phys. Rev. Lett., **49,** 1100 (1982)
[20] Høye, J. S., Stell, G.: J. Chem. Phys., **75,** 5133 (1982); Høye, J. S., Olaussen, K.: J. Chem. Phys., **77,** 2533 (1982)

Acta Chimica Hungarica 121 (1—2), pp. 71—89 (1986)

THE DESCRIPTION OF ION MOLECULAR INTERACTIONS IN STATISTICAL MECHANICS+

Igor Rafatiovich YUKHNOVS'KII

(Institute for Theoret. Physics of the Academy of Sciences of the Ukrainian SSR, Division "Statistical Physics", Lvov 5. Dragomanova Str. 14/16.)

Received January 18, 1985

In the theory of electrolyte solutions a semiphenomenological ion approach has been substituted by the ion-molecular one, which is grounded on the explicit allowance for ions and solvent molecules. The latter is based on the calculations of the binary distribution function which define structural properties as well as thermodynamical and dielectronic ones.

In the description of the interactions in the statistical physics three levels can be distinguished.

The first is the quantum one, which is characterised by the Hamiltonian of the system.

The second one is the classical level — when the energy of the system is considered as a sum of classical kinetic and potential energies, and finally the third — macroscopic, when we speek about the experimentally observed interaction energy between a pair of particles. This is the so-called 'mean force potential" (MFP).

Let our system consists of atoms. Each atom consists of nucleus and electrons. In the atom (for example in the atom of a metal) the electrons may be grouped into external and internal ones. Internal electrons as a rule do not leave the nucleus while external ones may belong to different nuclei. Let us consider the question how the classical interaction potentials appear and what is their behaviour.

We shall use here results obtained by Vavrukh and Kokhmalsky in [1, 2]. The initial Hamiltonian of the system is equal to

$$H = -\frac{\hbar^2}{2}\sum_i \frac{1}{M}\Delta_i - \frac{\hbar^2}{2m}\sum_i \Delta_i + \frac{1}{2}\sum \frac{e^2}{r_{ij}} + \frac{1}{2}\sum_{i,j}\frac{z^2 e^2}{R_{ij}} - \sum_{i,j}\frac{z\,e^2}{(\vec{r}_i - \vec{R}_j)}$$

where Z_e — is the nucleus charge, N_n — nucleus number, N — number of electrons, $ZN_n = N$. Let there be Q valent (free) electrons and $Z - Q$ — bounded ones. Let us consider the interaction energy of the valent (free) electrons with the nucleus.

+ This paper was presented at the Symposium on Structure of Liquids and Solutions at Veszprém, August 27—30, 1984.

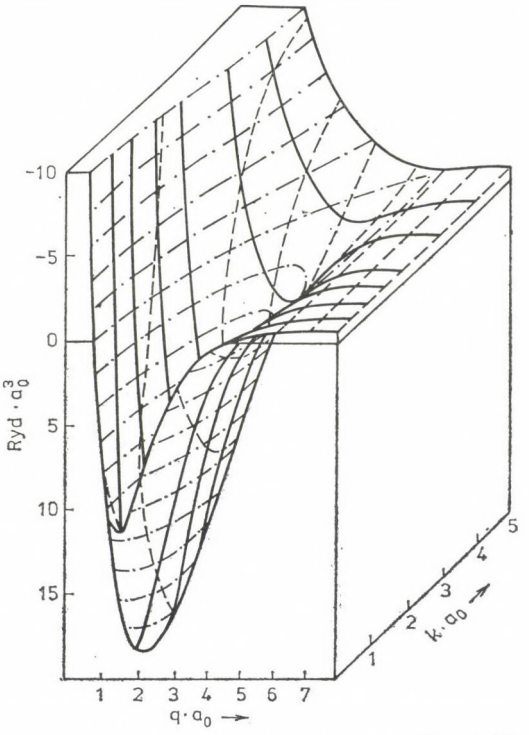

Fig. 1. Pair non-local potential of electron-ion interaction $a_2(\vec{k} + \vec{q}, \vec{k})$ for lithium for angle $\widehat{(\vec{q}, \vec{k})} = \pi$

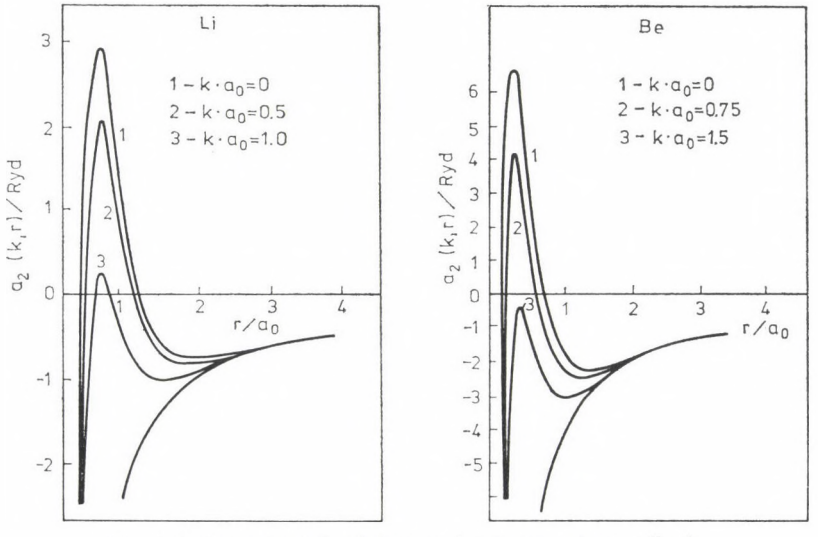

Fig. 2. Pair potentials of electron-ion interactions $a_2(k, r)$

In order to find it it is necessary to take the sum over all bounded states in the statistical operator $\exp(-\beta H_{\text{eff}}) = Sp_\lambda (\exp -\beta H)$. The most difficult problem is to create a suitable complete set of orthonormal eigenfunctions. Usually the atomic eigenfunctions are taken as the initial ones. They may be orthonormalized by the Bogoliubov procedure. Such procedure was applied in the above mentioned works. As a result the energy H_{eff} can be obtained

$$H_{\text{eff}} = H_n + T + V_{ee} + V_{ei}$$

where

H_n — is the Hamiltonian of the nuclei,

T — is the kinetic energy operator of valent (free) electrons,

V_{ee} — the energy of the Coulomb interactions between these electrons,

V_{ei} — is a new Hamiltonian which appears as a result of the summing over the bounded states.

$$V_{ei} = \sum_{n\geq 1} \frac{1}{n!} V^{-n} \sum_{q_1,\ldots,q_n} \sum_{\substack{k_1,\ldots,k_n \\ S_1\ldots,S_n}} a_{2n}(k_1 + q_1, \ldots; \; k_n + q_n; k_n, \ldots, k_1) \cdot \qquad (1)$$

$$\cdot C^+_{k_1-q_1,\, s_1} \ldots C^+_{k_n-q_n,\, s_n} C_{k_n,\, s_n} \ldots C_{k_1,s_1}$$

where $C^+_{k_1S}$, C_{k_1S} are the creation and annihilation electron operators, k — momentum, S — spin of the electron.

We shall regard the term $a_2(k_1 + q, k_1)$ for $n = 1$. The other components of a_{2n} are small and are not taken into consideration. $a_2(k_1 + q_1\, k_1)$ — is the Fourier transform of the effective interaction potential between the valent electron and the ion. It is non-local and depends upon the electron momentum k_1.

Figure 1 gives the curves of this potential when the angle between k and q vectors equals π, i.e. in the result of the interaction with ion the free electron moves back awards. The curves are plotted for Li, Be.

Figure 2 represents electron-ion interaction potential averaged over all directions of the electron movement towards the ion:

$$a_s\,(r,\; k) = \frac{1}{4\pi} \int \left(\frac{1}{V} \sum_q a_s(k + q_1\, k)\, e^{iqz} \right) d\text{—}\varrho_k$$

Its characteristic feature is the dependence upon the electron velocity. We have attraction region, corresponding to Hartree model, and repulsion region. The slower the electron moves the stronger is the repulsion.

Potential $a_2(r)$ averaged over the electron momentum inside the Fermi sphere is represented in Fig. 3.

We have two attraction regions and a repulsion one. The outer attraction region corresponds to Coulomb attraction between the positive charge e

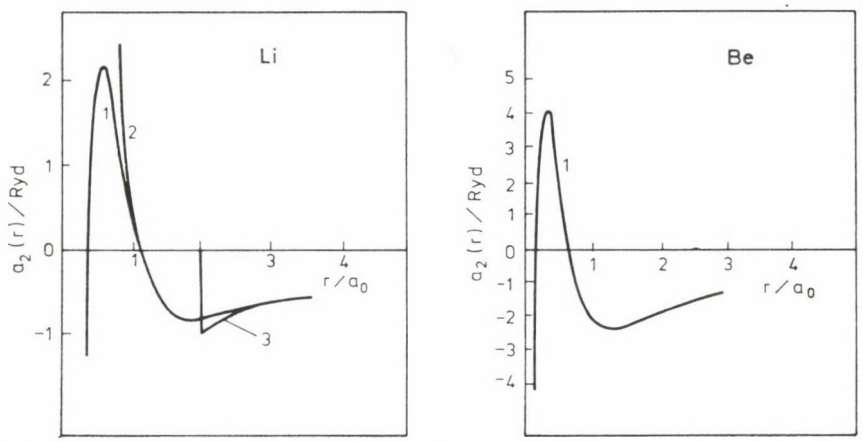

Fig. 3. 1-pair potential of electron-ion interaction averaged over the Fermi sphere; 2-model potential of Krasko and Gurski; 3-model potential of Ashcroft

(value for Li) and the electron. In the inner attraction region the value of the positive charge is equal to $3e$ for Li and $4e$ for Be. The curves for the known pseudopotentials are also plotted in the same figure.

Fig. 4 illustrates the interaction between two protons, obtained after averaging over all electron states. The sharp decrease of the curve in the repulsion region can be attributed to interactions via electrons.

So we see that in the electron-ion interaction there appears a region of repulsion. Consequently, in the interaction between two atoms, molecules or ions there appears a repulsion on short distances. That is why, all classical interaction potentials must have attraction at long distances and repulsion at short ones.

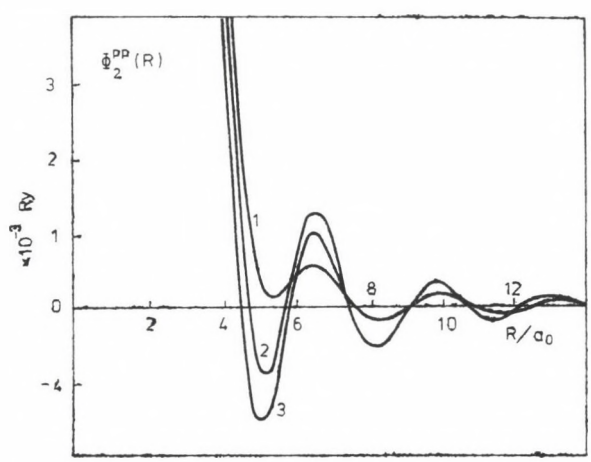

Fig. 4. The proton-proton effective potential in the electron-proton system. The different approximations the dielectric function: 1 — RPA; 2 — second virial coefficient; 3 — Geldart—Taylor approximation

In general, the potentials are divided into short-range and long-range ones. The electrostatic potentials belong to long-range ones. They may be written in the following form:

$$\Phi_{ab}^{(el)}(|R_1 - R_2|) = Q_a(\nabla_1)\, Q_b(\nabla_2) \frac{1}{|R_1 - R_2|}$$

where

$$Q_a(\nabla_1) = e_a z_a + p_a^{(1)} \nabla_1 + \frac{1}{3} p_a^{(2)} : \nabla_1 \nabla_1 + \ldots$$

The first form stands for the charge, the second — for dipole, the third — for quadrupole momentum etc. of the particle of a'th sort. The electrostatic interaction possesses an infinite effective radius.

The short-range interaction may have different forms. The most popular forms of it are the Lennard—Jones (L—J) potential, the Morse potential and others.

$$\psi_{LJ}(|r_1 - r_2|) = A\left[\left(\frac{R_0}{R}\right)^{12} - \left(\frac{R_0}{R}\right)^{6}\right]$$

$$\psi_M(|r_1 - r_2|) = \varepsilon[e^{-2\left(\frac{R-R_0}{\sigma}\right)} - 2e^{-\left(\frac{R-R_0}{\sigma}\right)}]$$

Both potentials display similar behaviour in the well region. They differ distinctively at very short or long distances. The L—J potential contains the well known Van der Waals term: proportional to $1/R^6$. The $\sim 1/R^6$ potential characterises the energy of dispersive interactions at long distances. Besides these forces, there exist inductive ones proportional to $1/R^4$ for the particles with non-zero electrostatic charge Qa.

For particles with non-zero charge there is no distinct difference between the so called short- and long-range interactions. Nevertheless, we attribute to the short-range interactions the potential, which models the interaction between two hard cores.

$$\varphi_{HC}(R) = \begin{cases} \infty & R \leq \sigma \\ 0 & R > \sigma \end{cases}$$

This potential is a particular one, it is positive, and has no Fourier transform. At present, the sum of hard-core potential, some attractive potential and electrostatic potential is regarded as an initial potential of the interaction between two particles.

$$\Phi_{ab} = \varphi_{ab}^{(HC)}(R) + \varphi_{ab}^{(attr)}(R) + \Phi_{ab}^{(el)}(R)$$

In general, the potential Φab has a very week temperature dependence [3].

We obtain as when averaging the partition functions over all electron states we obtain:

$$\exp(-\beta \Phi ab) = \sum_{n_{e\alpha}} \langle n_{e_\alpha} | \exp -\beta H | n_{e_\alpha} \rangle$$

Let us regard the sum

$$\psi_{ab} = \varphi_{ab}^{(\mathrm{HC})}(R) + \varphi_{ab}^{(\mathrm{attr})}(R)$$

as the short-range part and the term $\Phi_{ab}^{(el)}(R)$ as the long-range part of the initial potential Φ_{ab}. Let us see what comes out of it in statistical physics. It appears that the description of these two types of interactions cannot be performed in the same phase space.

The average potential energy of the interaction of the regarded particle with all the others is proportional to the density in case with short-range forces and to the inverse density for Coulomb forces. Indeed, for the short-range potential we have:

$$\langle E\rangle_{\mathrm{sh}} = \sum_b \frac{N_b}{V}\frac{1}{kT}\int \psi_{ab}\, F_{ab}(R)\, dR =$$

$$= \sum_b \frac{N_b}{V}\sigma^3 \int \psi_{ab}(x)\, F_{ab}(x)\, \mathrm{d}x = \frac{N}{V}\sigma^3\langle\psi\rangle;\ x = \frac{R}{\sigma}$$

where the angular brackets denote the average values. For the Coulomb systems, involving the electroneutrality conditions, we have

$$\langle E\rangle_L = \sum_\sigma \frac{N_b}{V}\frac{1}{kT}\int \Phi_{ab}^{(\mathrm{el})}(R)\,(F_{ab} - 1)\,\mathrm{d}R \simeq$$

$$\simeq \sum_b \frac{N_b}{V}\frac{1}{kT}\int \Phi_{ab}^{(el)}(R)\, g_{ab}(R)\,\mathrm{d}R = \sum_b \frac{N_b}{V}\varkappa^{-1}\int \Phi^{(el)}(x)\, g_{ab}(x)\,\mathrm{d}(x)$$

$$= \sum_b \frac{N_b}{V} e_a^2 e_b^2 \frac{1}{(kT)^2}\varkappa^{-1}\int \Phi^{(el)}(x)\, g(x)\,\mathrm{d}x = \lambda_a^2 \frac{V}{N}\varkappa^3\langle\psi\rangle$$

where $g_{ab}(R)$ is a screened potential, which for the charged particles is of the form

$$g_{ab}(R) = e_a\, e_b\, g(R) = e_a\, e_b \frac{e^{-\varkappa R}}{R};$$

$$\lambda_a^2 = e_a^2 \Big/ \sum_b e_b^2 \frac{N_b}{N}$$

So for the short-range interactions $\langle E\rangle \underset{sh}{\sim} \frac{N}{V}\sigma^3$ and for the Coulomb forces

$$\langle E\rangle_L \sim \frac{V}{N}\ r_{\mathrm{D}}^{-3}\ r_D = \varkappa^{-1} = (kTV/4\pi \sum_a e_a^2 N_a)^{1/2}$$

Therefore there is no unique way to describe these two types of forces. The problem was successfully solved with the help of the collective variables method [4].

The idea of the method is the following. As the Coulomb forces are long-range ones, the neutral system of charged particles is analogous to the stressed

medium: the displacement of arbitrary particle from its origin leads to the propagating of the charge density waves. So the Coulomb effects, or in general electrostatic interactions, can be described by means of a set of charge-density waves, instead of the usual Cartesian coordinates.

Let us introduce the charge density function

$$\hat{\varrho}(R) = \sum_{a,i} \delta(R - R_i)\, Q_a(\nabla_i)$$

The charge in the volume Ω is equal to

$$\int_{\Omega} \hat{\varrho}(R)\, \mathrm{d}R$$

The Fourier transform of $\hat{\varrho}(R)$ is $\hat{\varrho}(R) = \sum_k N/V \hat{\varrho}_k \exp(ikR)$;

$$\tilde{\varrho}_k = \frac{1}{\sqrt{N}} \sum_{a,i} \tilde{Q}_a(k) \exp(i_K R);$$

represents the charge-density wave mode.

The electrostatic interaction may be written in the form:

$$\sum_{ab} Q_a(\nabla_i) Q_b(\nabla_j) \frac{1}{|R_i - R_j|} = \int \varrho(R)\ \varrho(R') \frac{1}{|R - R'|}\, \mathrm{d}R\, \mathrm{d}R' =$$
$$= \frac{N}{V} \sum_k \tilde{\Phi}(k)\, \tilde{\varrho}_k \tilde{\varrho}_k - \sum_{k,a} \tilde{\Phi}(k) \frac{N}{V} |\tilde{Q}_a(k)|^2; \quad \tilde{\Phi}(k) = \frac{4\pi}{k^2}$$

$\tilde{Q}(V)$ is a Fourier transform of $\hat{Q}(R)$. Now we can write for the partition function the following:

$$Z = \int \exp = \beta[\Sigma \psi_{ab}(R_{ij}) + \Phi^{\mathrm{el}}_{ab}(R_{ij})]\ (\mathrm{d}R)^N =$$
$$= \int \exp - \beta \Bigg[\Sigma \psi_{ab}(R_{ij}) + \sum_k \tilde{\Phi}(k)\ \varrho_k\ \varrho_k -$$
$$- \sum_{k,a} \tilde{\Phi}(k) \frac{N}{V} |\tilde{Q}_a(k)|^2 \Bigg] \prod_k \delta(\varrho_k - \tilde{\varrho}_k)\ (\mathrm{d}\varrho)\ (\mathrm{d}R)^N \qquad (2)$$

We have here an extended phase space, the Dirac functions $\delta(\varrho_k - \varrho_k)$ prevent its overfilling. It involves the space of individual coordinates for describing of short-range interactions and the space of generalised charge density waves for long-range forces.

Let us integrate over the individual coordinates of the particles. The integration may be performed in two ways. In the first case we consider non-dense systems. In expression (2) we write a product of Mayer functions for the short-range interaction exponent:

$$\exp\left(-\beta \sum_{\substack{a,b \\ i,j}} \psi_{ab}(R_{ij})\right) = \prod_{\substack{ab \\ ij}} (1 + f_{ab}(R_{i,j}))$$

where

$$f_{ab}(R) = \exp\left[-\beta\psi_{ab}(R)\right] - 1$$

Then we expand the partition function into functional Taylor series [4]

$$Z = \int exp^{-\beta} \sum_k \tilde{\Phi}(k) \left[\varrho_k\, \varrho_{-k} - \frac{N}{V} \sum_a \tilde{Q}|_a|^2\right]$$

$$\left\{1 + \sum_{\substack{ab\\ij}} f_{ab}(R_{ij}) + \sum_{\substack{abe\\ije}} f_{ab} f_{ac} + \ldots\right\}$$

$$\prod_k \delta(\varrho_k - \tilde{\varrho}_k)\, (\mathrm{d}R)^N\, (d\varrho)$$

To have the explicit expression for the whole series it is sufficient to calculate the first term. The integration $(\mathrm{d}R)^N$ within it corresponds to the product $\prod_k \delta(\varrho_k - \hat{\varrho}_k)$ only, and leads to the Jacobian:

$$J(\varrho) = \int \prod_k \delta(\varrho_k - \hat{\varrho}_k)\ (\mathrm{d}R)^N$$

of the transition from the Cartesian coordinates to the set of collective variables (CV). In the second case the reference system (RS) is introduced. In this system particles are interacting by means of the short-range potential

$$\Sigma\psi_{ab}(R_{ij})$$

It is supposed that the partition function and the distribution functions of the reference system are known.

Then the partition function may be represented as follows [4]

$$Z = Z_{RS} \int \exp - \beta \sum_k \tilde{\Phi}(k) \left(\varrho_k\, \varrho_{-k} - \frac{N}{V}\, |\tilde{Q}|^2\right) J_{RS}(\varrho)\ (\mathrm{d}\varrho)$$

where

$$Z_{RS} = \int \exp\left[-\beta\Sigma\psi_{ab}(R_{ij})\right]\ (\mathrm{d}R)^N$$

is the partition function of the RS, $J_{RS}(\varrho)$ — the Jacobian of transition to the CV, modulated by short-range interaction.

$$J_{RS}(\varrho) = Z_{RS}^{-1} \int - \beta \sum_{ab} \psi_{ab}(R_{ij}) \prod_k \delta(\varrho_k - \hat{\varrho}_k)\, (\mathrm{d}R)^N$$

The first approach is known better and is considered in many papers [4].

Here we shall represent some results for the binary distribution function.

By taking the logarithm of the partition function we obtain the free energy. The functional derivative of the free energy with respect to pair interaction potential leads to binary distribution function: $F_{ab}(R) = \delta F/(\delta\psi_{ba}(R)$

The logarithm of binary function is called mean force potential (MFP).

$$W_{ab}(R) = -\vartheta \ln F_{ab}(R)$$

The one-particle distribution function for the spatially homogeneous systems is equal to unity.

The MFP characterises an effective interaction which takes place between two arbitrary particles in thermodynamic system.

The general form of MFP is:

$$W_{ab}(R) = \psi_{ab}(R) - \Theta g_{ab}\ (R) - \Theta \Big[$$

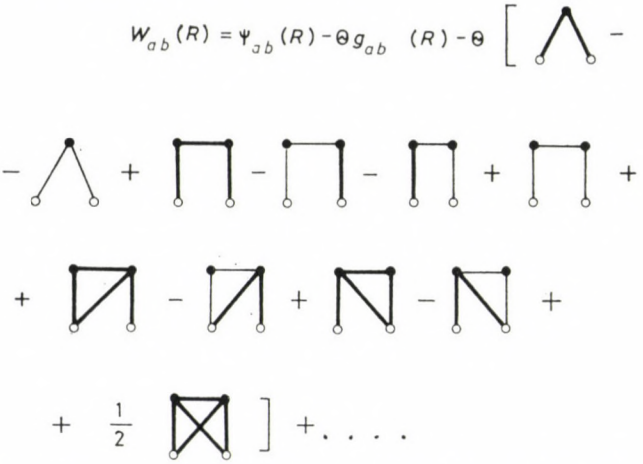

where $\psi_{ab}(R)$ is the initial short-range potential, is the screened potential. The thin line denoted screened potential: —— $= g_{ab}$ the thick line represents the function —— $= \exp(-\beta\psi_{ab} + g_{ab})^{-1}$ the full circle denotes the sum

$$\bullet = \sum_a \frac{N_a}{V} \int \ldots dR$$

the open circle ○ — fixed coordinate of the chosen particle.

In this way the first term describes a direct short-range interaction, the second one — a screened electrostatic interaction, the first two graphs — the indirect interaction via the third one, the rest of the graphs — the indirect interactions via two arbitrary particles etc. The expression for the potential $W_{ab}(e)$ is considered in detail in our book [4]. Here we give some important facts:

1. All electrostatic interactions are being screened. The ions screen all electrostatic interactions: instead of the initial potential $Q_a(\nabla)Q_b(\nabla)^1/R$ there appears $Q_a(\nabla)Q_b(\nabla)e^{-\varkappa_0/R}/R$
where

$$\varkappa_0 = (r_D^{(O)})^{-1}$$

$$\varkappa_0^2 = \frac{4\pi}{kT} \sum_a \frac{N_a}{V} e_a^2$$

r_D Debye's radius

The dipole screening consists in that the form of initial potential does not change, while the strength of the interaction changes: instead of $Q_a(\nabla_1)Q_b(\nabla_2)^1/R$ we have $Q_a'(\nabla)Q_b'(\nabla)/\varepsilon_0 R$ where ε_0 — is a part of the dielectric

constant of the system initiated by the screening:

$$\varepsilon_0 = 1 + \frac{4\pi}{V} \sum_J p_J^2 < (\cos^2 \vartheta) > \beta = 1 + 3y; \quad y = \frac{4\pi}{9} p_S^2 \beta$$

for example, for water $\varepsilon_0 \sim 15$ (More exact calculations for the orientation motion of molecules leads to $\varepsilon = \left.\frac{1+2y}{1-y}\right)$. Simultaneously, the Debye radius changes and becomes equal to $r_D = r_D^0 \sqrt{\varepsilon_0}$.

The guadrupole (L) and higher multipole screening forms packet:

$$Q_a Q_b \frac{1}{R} \to Q_a Q_b \frac{1}{R} (e^{-\varkappa' R} - e^{-\alpha R})$$

and at $R = 0$ the curve of the electrostatic potential has a finite ordinate. When in expression for W_{ab} we take the first two terms only we have MFP as a sum of two curves. The first one $-\psi_{ab}(R)$ — runs close to the axis, and the second — the curve of g_{ab} is considerably greater.

The resulting curve describes a wide range of possible mutual arrangement of the two chosen particles.

2. Consideration of the cluster integrals changes essentially the form of this curve. Consideration of integrals with one field vertex involves indirect interaction between the two particles via the arbitrary third one, in particular, via the solvent particle. And graphs with two field vertices involve indirect interaction via two arbitrary particles. Here, interasection between two arbitrary particles of the solvent is already taken into account. This corresponds to the fourth virial coefficient in free energy of the system.

MFP in the fourth virial coefficient approximation has three minima, and a minimum point corresponding to the sum $\psi_{ab} - \Theta g_{ab}$ is considerably educed. We can conclude that the involvement of graphs with greater number of field vertices will lead to the appearance of the corresponding number of minimum on the MFP curve.

In such a way the involvement of graphs of the virial series brings us to a real macroscopic potential of interaction between two particles in a thermodynamic system.

The probability of mutual ion arrangement depends essentially on the depth of the potential well which, in its turn, corresponds to the form of the short-range potential.

Fig. 5 displays the influence of the solvent molecule dipole momentum on the energy of the interaction between two oppositely charged and two identically charged ions calculated up to the graphs with one field vertex. It is evident that with the increase of the dipole moment of the molecule of

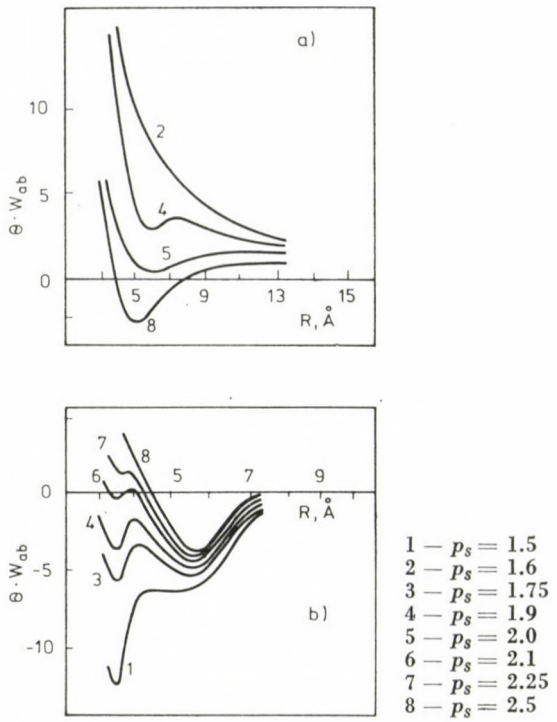

Fig. 5. The mean force potential between a pair of ions in an ion-dipole system with account for the third virial coefficient. a) — + + ions; b) — - - ions. p_s — denotes the dipole moment value

the solvent, the minimum which corresponds to the function $\psi_{+-}(R/a)$ — — $\Theta g_{+-}(R)$ vanishes. It is replaced by the new minimum at a distance of $\sim$5 Å. This corresponds to the formation of solvated pair of ions (the curves are plotted for the dipole molecules density equal to 0.5). Asymptotic value of the complete MFP corresponds to the total value of the dielectric constant of the system.

Up till now we considered spatially homogeneous systems. Now we shall regard the influence of surfaces.

Let us take the two-phase system with a flat separation surface. The first phase is situated in the upper semispace. Let us denote its volume by V_+. The second phase is situated in the lower semispace, its volume is V_-. Let, as previously, $Q_a(\nabla)$ be the generalised electrostatic charge of the a sort. In calculations it is supposed that particles of the a sort may have a charge ea, dipole moment $p_a^{(1)}$ and quadrupole moment $p_a^{(2)}$. The potential of external field is introduced. It forbids particles belonging to phase 1 to be present in phase two and vice versa. Problems of mathematical description remain the same as in the regarded case with spatially homogeneous system. But the

influence of surface and violation of translation-invariance should be accounted for. Here are the results of investigations performed in our laboratory by Soviak [5], see also [6].

The logarithm of one-particle distribution functions is the MFP with respect to the separation surface. It is also expressed in terms of one particle screened potential and of cluster integrals $W_a(Z) = \psi_a(Z) - \vartheta g_a(Z) + \vartheta$ (cluster integrals). The one particle MFP behaviour is mainly defined by the form of the one particle screening potential $-\vartheta g_a(Z)$. Its form depends on the form of the system considered, and in general may be represented in the following way:

$$g_a(\bar{R}) = |\hat{Q}_a|^2 \cdot g_+(Z) \qquad \bar{R} \in V_+$$

where

$$\hat{Q}_a = e_a + p_a^{(1)} \nabla + p_a^{(2)} : \nabla \nabla + \ldots$$

For the ion-dipole system $V_+ \oplus V_-$, in the "+" phase there are ions and dipoles, and in the "—" phase — dipoles only.

$$g_+(z) = -\frac{1}{\varepsilon_+ \vartheta} \int_0^\infty \frac{p \, \mathrm{d}p}{\sqrt{p^2 + \varkappa_+^2/\varepsilon_+}} \varepsilon(p) \; e^{-2\sqrt{p^2 + \varkappa_+/\varepsilon_+}\, z}$$

$$g_-(z) = -\frac{1}{\varepsilon_- \vartheta} \int_0^\infty \varepsilon(p) \, e^{2pz} \, \mathrm{d}p$$

$$\varepsilon(p) = \frac{\varepsilon_+ \sqrt{p^2 + \varkappa_+^2/\varepsilon_+} - \varepsilon_- p}{\varepsilon_+ \sqrt{p^2 + \varkappa_+^2/\varepsilon_+} + \varepsilon_- p}$$

the factor $\varepsilon(p)$ shows the influence of one medium on the distribution of the particles in the other one.

$$\varepsilon_+ = 1 + 3y_+ \quad \varkappa_+^2 = \frac{4\pi \sum_a e_a^2 N_a^+}{V_+ \vartheta}$$

$$\varepsilon_- = 1 + 3y_- \quad \vartheta = kT, \; y_+ = \frac{4\pi}{9} (p_+^{(1)})^2 \frac{N_+}{V_+}$$

$\psi_a(Z)$ — short-range potential of external field

$$\psi_a(z) = \begin{cases} \infty & z \leq \frac{1}{2}\sigma_a \\ 0 & z > \frac{1}{2}\sigma_a \end{cases}$$

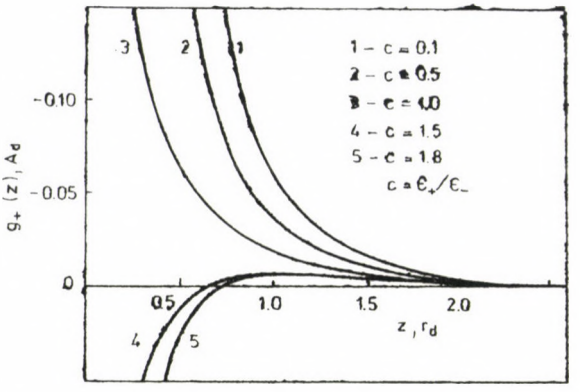

Fig. 6. The non-uniform ion-dipole system. The one-particle screened potential.

$$g_\alpha(z) = Q^2(\Omega) \cdot \begin{cases} g_+(z) & \text{for } z > 0, \ (\alpha\, \varepsilon\, V^+), \\ g_-(z) & \text{for } z < 0, \ (\alpha\, \varepsilon\, V^-). \end{cases}$$

$$g_+(z) = -\frac{1}{\varepsilon_+ \cdot T} \cdot \int_0^\infty \frac{p \cdot \mathrm{d}p}{a(p)} \cdot \frac{\varepsilon_+ \cdot a(p) - \varepsilon_- \cdot p}{\varepsilon_+ \cdot a(p) + \varepsilon_- \cdot p} \cdot \exp(-2 \cdot a(p) \cdot z),$$

$$g_-(z) = \frac{1}{\varepsilon_- \cdot T} \cdot \int_0^\infty \mathrm{d}p \cdot \frac{\varepsilon_+ \cdot a(p) - \varepsilon_- \cdot p}{\varepsilon_+ \cdot a(p) + \varepsilon_- \cdot p} \cdot \exp(-p \cdot z),$$

$$a(p) = (p^2 + r_d^{-2})^{1/2}.$$

The dependence of $g_+(z)$ — function on the distance to the surface:

$$A_d = 1/\varepsilon_+ \cdot T \cdot r_d, \quad r_d^{-2} = \varkappa_+^2 + /\varepsilon_+$$

We denote $C = \varepsilon_-/\varepsilon_+$, and for $g_+(\bar{\bar{Z}})$ we have curves plotted in Fig. 5. The behaviour of g_+ on short distances $\bar{\bar{Z}}$ is different depending on whether C is greater or less than unity. But on long distances $\bar{\bar{Z}}$ the asymptotic behaviour remains the same, and does not depend on the value of C (Fig. 6).

Function g_- behaves similarly. When quadrupole moments of the particles are taken into consideration the potentials g_+ and g_- display similar behaviour, though depend on the greater number of parameters. Let us consider now the interaction between particles in a non-homogeneous system. It is defined by the logarithm of the binary distribution function:

$$W_{ab} = -\vartheta \ln [F_a(\bar{R}_1)\ F_b(R_2)\ F_{ab}(R_{12})] \simeq$$
$$\simeq \psi(z_1) + \psi_b(z_2) + \psi_{ab}(R_{12}) —$$
$$— \vartheta(g_a(\bar{R}_1) + g_b(\bar{R}_2)) + g_{ab}(\bar{R}_1\bar{R}_2) + \ldots)$$

$g_a(\bar{R}_1), g_b(\bar{R}_2)$ have been already introduced above. We shall speak about the potential $g_{ab}(\bar{R}_1\bar{R}_2)$. It consists of two parts: the first one is quite the

same as in the spatially homogeneous case, and the second is connected with the presence of the surface and leads to the form close to the image potential. So we have:

$$g_{ab}(R_1\, R_2) = Q_a(\nabla_1)\, Q_b(\nabla_2) \cdot \begin{cases} g_{++} \\ g_{+-} \\ g_{--} \end{cases}$$

where

$$g_{++} = f_1(z_1 - z_2, s) + f_2(z_1 + z_2, s)$$

$g_{+-} = f(z_1, z_2, s)$ here we have neither $z_1 - z_2$ nor $z_1 + z_2$ $g_{--} = f_1'(z_1 - z_2, s) + + f_2'(z_1 + z_2, s)$.

The explicit expressions for functions f_1, f_2, f_1, f_2' is in Fig. 7. The case when quadrupoles are present was investigated for the first time by E. Soviak. Here we have the essential difference from the ion-dipole system for g_{++} and for g_{--}; besides the terms $f_1(z_1 - z_2)$, $f_2(z_1 + z_2)$ there appear functions $\varphi(z_1, z_2)$.

In general the potentials g_{++} decrease proportionally to $e^{-\varkappa S}/s$ on short distances where s is the distance between two particles situated in a plane

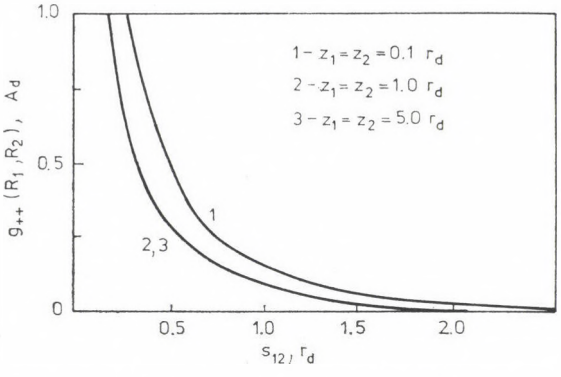

Fig. 7. The non-uniform ion-dipole system. The two-particle screened potential

$$g_{\alpha\beta}(R_1, R_2) = Q_\alpha(\Omega_1) \cdot Q_\beta(\Omega_2) \cdot \begin{cases} g_{++}(R_1, R_2) \text{ for } z_1, z_2 > 0, \\ g_{+-}(R_1, R_2) \text{ for } z_1 > 0,\ z_2 < 0, \\ g_{--}(R_1, R_2) \text{ for } z_1, z_2 < 0. \end{cases}$$

$$g_{++}(R_1, R_2) = -\frac{1}{\varepsilon_+ \cdot T} \cdot \int_0^\infty p \cdot \mathrm{d}p \cdot J_0(p \cdot s_{12}) \cdot (1/a(p) \cdot \exp(-a(p) \cdot |z_1 - z_2|) +$$

$$+ \frac{1}{a(p)} \cdot \frac{\varepsilon_+ \cdot a(p) - \varepsilon_- \cdot p}{\varepsilon_+ \cdot a(p) + \varepsilon_- \cdot p} \cdot \exp(-a(p) \cdot (z_1 + z_2))),$$

$$g_{+-}(R_1, R_2) = -\frac{2}{T} \cdot \int_0^\infty \frac{p \cdot \mathrm{d}p \cdot J_0(p \cdot s_{12})}{\varepsilon_+ \cdot a(p) + \varepsilon_- \cdot p} \cdot \exp(-a(p) \cdot z_1 + p \cdot z_2),$$

Here $J_0(x)$ is the zeroth Bessel function

upon xy plane to the height z (see Fig. 7). But asymptotically $g_{\pm\mp}^{\pm\pm} \sim 1/S^3\tilde{f}(z_1, z_2)$ which seems to be quite unexpected. Asymptotics is achieved at distances of fifty-sixty particle size.

From the above considerations we see how important it is the suitable choice of the short-range potential form. We have seen also that all electrostatic interactions are being screened. The influence of charges leads to that the initial potential is multiplied by factor exp $(-\varkappa R)$.

Now we are concerned with the question: which states have been spoken about — gas or liquid states. We dealt with gases. In problems considered we had two effective radii: short-range interaction radius and an electrostatic one which coincides with the Debye radius r_D. Both of them do not tend to infinity at any finite temperature. When integrating the partition function we have discovered no variable the mean value of which is a macroscopic quantity connected with an order parameter. Consequently, no phenomenon connected with the phase transition has been found.

Though the equation of state has an instability region.

The gas-liquid phase transition is a collective phenomenon.

The short-range interaction, in the form of Morse potential for example may be expanded into Fourier series. Lennard—Jones-type potentials may be an approximation consisting of two curves: the first one is the generalized function simulating the elastic wall, the second is a negative regular function describing the attraction:

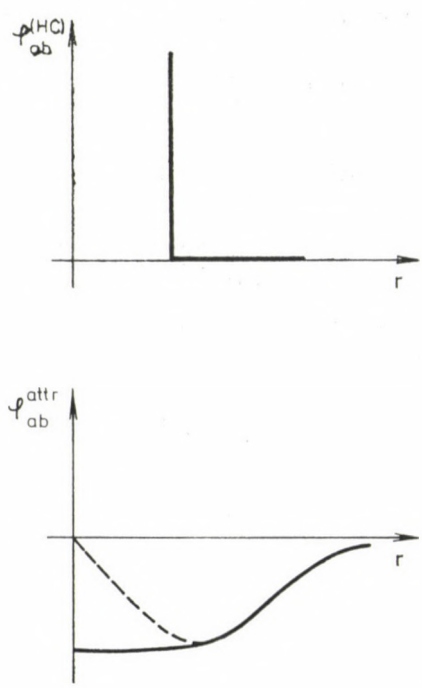

For example,

$$\varphi_{ab}^{hc}(R) = \begin{cases} \infty & R \leq \sigma \\ 0 & R > \sigma \end{cases}$$

$$\varphi_{ab}^{\text{attr}}(R) = -Ae^{-r/b}$$

where b is the radius of the effective interaction.

The potential $\varphi_{ab}^{\text{attr}}$ possesses a Fourier transform and from this point of view is as suitable as any long-range electrostatic potential. Moreover, the function $e^{-r/b}$ appears to be more regular than any other electrostatic potential.

It seems to be true that the $\varphi_{ab}^{\text{attr}}$ plays the main role in the process of aggregation of the system. Let us consider the simple example of the one-sort system, with the potential energy:

$$V = V_{hc} + V_{\text{attr}} \quad V_{hc} = \frac{1}{2}\sum_{ij} \varphi^{hc}(R_{ij}); \quad V_{\text{attr}} = \frac{1}{2}\sum_{ij} \varphi^{\text{attr}}(R_{ij})$$

The electrostatic potentials are excluded from the consideration (they do not change the results qualitatively).

The partition functions is

$$\mathbf{Z} = \int \exp -\beta(V_{hc} + V_{\text{attr}})\,(\mathrm{d}R)^N$$

We introduce the density operators for the number of particles

$$p(R) = \sum_i \delta(R - R_i)\,,$$

$$p_1(R) = \frac{N}{V}\sum_k p_k\, e^{ikR}\,,$$

$$\hat{p}_k = \frac{1}{\sqrt{N}}\sum_i \exp\,(i_k R_i),$$

and an additional phase space of density oscillation modes, i.e. the collective variable (CV) space. Then

$$Z = \int \exp\,(-\beta\ V_{hc}) \exp\left(-\beta\,\frac{1}{2}\sum_k \varphi^{\text{attr}}(k)\ p_k\, p_{-k}\right) \cdot$$

$$\cdot \prod_k \delta(p_k - \hat{p}_k)\,(\mathrm{d}p)\,(\mathrm{d}R)^N.$$

Let us integrate over all particle coordinates. For the partition function we obtain:

$$Z = Z_{RS} \int \exp\,(-\beta \tilde{V}_{\text{attr}}(p) < J(p) > (\mathrm{d}p) \tag{4}$$

where

$$Z_{RS} = \int \exp\left(-\beta V_{hc}\right) (\mathrm{d}R)^N$$

is the partition function of the system of hard cores,

$$\widetilde{V}_{\mathrm{attr}}(p) = \frac{1}{2} \sum \widetilde{\varphi}_{\mathrm{attr}}(k)\, p_k\, p_{-k}$$

and

$$\langle J(p) \rangle = Z_{RS}^{-1} \int e^{-\beta V^{hc}} \prod_k \delta(p_k - \hat{p}_k)\ (\mathrm{d}R)^N.$$

Expression (4) has been integrated in [7]. As a result the partition function is represented in the form

$$Z = \exp - \beta \{ F_{\mathrm{HC}} + F_{\mathrm{mean}} + F_{\mathrm{RPA}} + F_{\mathrm{VIR}} + F_{\mathrm{corr}} \}$$

where

F_{HC} — the free energy of the system of hard core particles

$$F_{\mathrm{mean}} = \frac{N(N-1)}{2V} \int \varphi_{\mathrm{attr}}(k)\ F_2^{\mathrm{HC}}(R)\, \mathrm{d}R$$

$$F_{\mathrm{RPa}} = \frac{\vartheta}{2} \sum_k \alpha(k)\, [1 + \mu_2^0(k)] - \ln\, [1 + \alpha(k)\, (1 + \mu_2^0(k))]$$

$$\alpha(k) = \frac{N}{V} \beta \widetilde{\varphi}_{\mathrm{attr}}(k) < 0;\ \mu_2^0(k) = \frac{N}{V} \int (F_2^{\mathrm{HC}}(R) - 1)\, e^{ikR}\, \mathrm{d}R$$

$$F_{\mathrm{corr}} = -\vartheta \left\{ \frac{N(N-1)\,(N-2)}{3!\ V^2} \int g(R_{12}) g(R_{13}) g(R_{32}) \cdot \right.$$

$$\left. \cdot\, [F_3^{\mathrm{HC}}(R_{12}R_{13}) - 3F_2^{\mathrm{HC}}(R_{12}) + 2]\, \mathrm{d}R_{12}\, \mathrm{d}R_{13} \right.$$

and

$$F_{\mathrm{vir}} = B_2 + B_3 + B_4 + \ldots$$

$$B_2 = -\vartheta \frac{N(N-1)}{2V} \int F_2^{\mathrm{HC}}(R) \left(e^{g(R)} - 1 - g(R) - \frac{g^2(R)}{2} \right) \mathrm{d}R$$

$$B_3 = -\vartheta \frac{N(N-1)\,(N-2)}{3!\ V^2} \int F_3^{\mathrm{HC}}(R_{12}R_{13})\, [e^{g(R_{13})} - 1 - g(R_{12})) \cdot$$

$$\cdot\, (e^{g(R_{13})} - 1 - g(R_{13}) \cdot (e^{g(R_{23})} - 1 - g(R_{23})) + 3g(R_{12}) \cdot$$

$$\cdot\, (e^{g(R_{13})} - 1 - g(R_{13}) \cdot (e^{g(R_{23})} - 1 - g(R_{23})]\, \mathrm{d}R_{12}\, \mathrm{d}R_{13}$$

F_{corr} is convergent at all temperatures. F_S^{HC} is the S^{th} distribution function for the system of hard core particles $g(R)$ is the screened potential for $\varphi_{\mathrm{attr}}(R)$

equal to

$$g(R) = \sum_k \frac{1}{V} \tilde{g}(k) \exp(ikR)$$

$$g(k) = \frac{-\beta \tilde{\varphi}_{\text{att}}(k)}{1 + (1 + \mu_2^0(k)) \frac{N}{V} \frac{1}{kT} \varphi_{\text{attr}}(k)}$$

We see that F_{vir} is quite similar to the free energy of the system with an electrostatic interaction. The difference is that the cluster integrals contain the hard core distribution functions, which results in the vanishing of divergences at short distances. Besides, a new screened potential arises. In order to have the asymptotic value of $g(R)$ it is quite enough to consider $\hat{g}(k)$ for small values of k. As far as $\mu_2^{(0)}(k)$ and $\tilde{\varphi}_{\text{attr}}(k)$ remain finite at $k = 0$ for $\hat{g}(k)$ we have

$$g(k) = \frac{\text{const}}{k^2 + \varkappa^2_{\text{attr}}}$$

where

$$\varkappa_{\text{attr}} = b^{-1} \sqrt{|\tau|}$$

and

$$\tau = \frac{T - T_{cr}}{T_{cr}}$$

$$T_{cr} = -\frac{N}{V} \tilde{\varphi}_{\text{attr}}(0) (1 + \mu_2^0(0))$$

$$1 + \mu_2^0(0) = \frac{N}{V} \vartheta \chi_T^{(0)}$$

$\chi_T^{(0)}$ is — the hard core compressibility. Inverse Fourier transformation gives the following

$$g(R) \sim \text{cost} \exp(-\varkappa_{\text{attr}} R)/R$$

There exists a temperature T_{cr} and a density N_{cr}/V at which $\varkappa_{\text{attr}} = 0$ and $g(R) \sim 1/R$ i.e. the correlation radius tends to infinity. This is the critical point. In virial expansions, the cluster integrals become divergent. The dispersion of the Gauss distribution function for the density fluctuation becomes infinite. It is necessary to find the point T_c, N_c/V. Below it non-zero values exist for the order parameter: one is for the liquid phase and another for the corresponding gas phase. They must be found. Then we shall be able to speak whether we have a liquid or a gas.

The principal difference between the screened potential of charged particle system and the screened potential for Van der Waalls like forces in the

vicinity of $T = T_{cr}$ should be stressed. For the charges we have: the long-range initial potential $\sim 1/r$ the screened one $g \sim \exp(-\varkappa r)/r$, where $\varkappa^2 = 4\pi \sum_a e_a^2 N_a / V\Theta$ is always positive g — is of the short-range.

For short-range forces the initial potential is

$$\varphi_{\text{attr}} \simeq -Ae^{-r/b}$$

but the screened one near $T = T_{cr}$, $N/V = N_{cr}/V$ is

$$\sim e^{-\varkappa_{\text{attr}} R}/R \; \widetilde{H}_{\; attr \to 0}^{\; 1/R}$$

Here is a good example how sharply the effective interaction changes depending on the density and temperature of the system.

At present the solution for the critical point is not available yet. Nevertheless, we have obtained a good solution fo the three-dimensional Ising model.

Besides, we have the explicit expression for free energy. We expect that in future we shall be able to suggest a model for liquids.

REFERENCES

[1] Vavzukh, M. V., Kzokhmalsky, T. E.: The Effective Potentials of Interaction in the Subsystem of Collectivized Electrons in the Simple Metals Preprint I TP-83-176P Kiev 1984. 26 p.
[2] Vavzukh, M. V., Kzokhmalsky, T. E.: Theor. Math. Fiz., **50,** 438 (1983)
[3] Golovashkin, A. I., Shelekhov, A. L.: Journ. Teor. Experim. Fiz., **84,** 2141 (1983)
[4] Yukhnovskij, I. R., Golovko, M. E.: The Statistical Theory of the Classical Equilibrium Systems, Kiev, Naukova Dumka. 1980. 372 p.
[5] Yukhnovskij, I. P., Soviak, E. N.: Physics of Many-Particle Systems, **3,** 3 (1983)
[6] Yuzylyak, I. I., Yukhnovsky, J. R.: Theoret. Math. Fiz., **52,** 114 (1982)
[7] Yukhnovsky, I. R., Idzyk, I. M.: Fiz. of Many-Particle Systems, **3,** 3 (1983)

Acta Chimica Hungarica 121 (1—2), pp. 91—105 (1986)

THERMODYNAMICS OF ELECTROLYTE SOLUTIONS+

Gennady A. KRESTOV

(Institute of Chemistry of Non-Aqueous Solutions of the Academy of Sciences of the USSR, 1 Acadamicheskaya Str., Ivanovo 153018, USSR)

Received January 18, 1985

General ideas of the structure of solvents and solutions have been considered. A conclusion has been drawn to the effect that there is a need for rejecting concrete models of the liquid structure and a need for its statistical interpretation.

The thermodynamic method of investigating solutions is being adopted on an ever wider scale [1—2]. It is the most universal and fruitful for both the determination of the role of the solvent in chemical reactions and the investigation of changes in solvent structure with changes in external factors (changes of temperature and pressure), and changes in the nature of admixtures, solvent composition and so on. The peculiarity of the method is in the fact that it characterizes the structural changes of solutions, considering both energy and entropy factors. This makes it superior overy many other methods of investigation [1—2].

When considering processes in solutions, the double nature of the solvent — i.e. that it is a medium and a chemical reagent should be considered. Its latter property is the more important one [2—3].

A variety of different thermodynamic approaches are described in the literature, e.g. [2]:

1. A comparative thermodynamic characteristic of reactions in solutions and in the gaseous phase (in two different solvents, one of which is considered as standards);

2. Singling out the contributions to the thermodynamic characteristics in solutions under the influence of the solvent;

3. Determination of the functional dependences of the thermodynamic characteristics of the processes in solutions on the properties of the solutions and their components;

4. Comparison of the parameters which are derived from the thermodynamic characteristics of solvents and solutions (donor-acceptor numbers, solvent polarity, etc.).

+ This paper was presented at the Symposium on Structure of Liquids and Solutions at Veszprém, August 27—30, 1984.

The wide use of the thermodynamic method is provided for by the presence of reliable thermodynamic data on various solution properties for a possible greater number of systems and a greater range of external conditions, including standard conditions.

The study of non-aqueous solutions has called forth new theoretical and experimental approaches for the investigation of their properties, estimation of reagent purity and so on. This situation is complicated by the limited number of complex investigations, by considerable methodical difficulties in obtaining high purity reagents and working with degassed and dehydrated (absolutized) solvents, the great need for new experimental techniques allowing for such solvent properties as volatility, hygroscopity, toxicality, chemical reactivity, limited electrolyte solubility in the solvents, etc. In addition, many experimental and theoretical results obtained for aqueous solutions can not be used directly.

When working with non-aqueous electrolyte solutions, special attention must be paid to the processing and interpreting of the results obtained: to the correct comparison of temperature and concentration properties of solutions, the separation of summary values into ionic components, the solving of standardization problems, and the working out of standards, and many other things.

The most urgent problems of electrolytic thermodynamics are discussed in the present communication regarding for the above considerations and on the basis of theoretical and experimental results.

The novel results of calorimetric investigations of the thermal effects of dissolution of number of electrolytes in non-aqueous and mixed solvents within a wide range of external conditions have been considered. The most interesting of them were obtained during the investigation of the thermal effects of salt dissolution at lower temperatures (below 273 K) [4—5]. It has been found that alkaline iodides and tetrabutylammonium iodide, behave anonalously: the heat of dissolution is greater at lower temperatures (Fig. 1).

The temperature limits of the effect as regards the nature of solvents and electrolytes have been established. It has been found that one and the same electrolyte can yield various types of isotherms at different temperatures.

The results obtained can be interpreted in terms of local solvation. The desctruction of the solvent structure by electrolyte ions occurs, not in the whole volume of the solvent, but in definite local regions around the ions. The size of the regions decreases with a decrease in temperature. Local solvation has been proved by our NMR investigations of NaI solution in alcohols at lower temperatures (Fig. 2) [6].

Figure 2 shows the dependence of the chemical shift of the hydroxyl proton on the temperature. The shift of the signal to the stronger field proves the breaking of H-bonds in the solvent. For NaI solution in the three alcohols

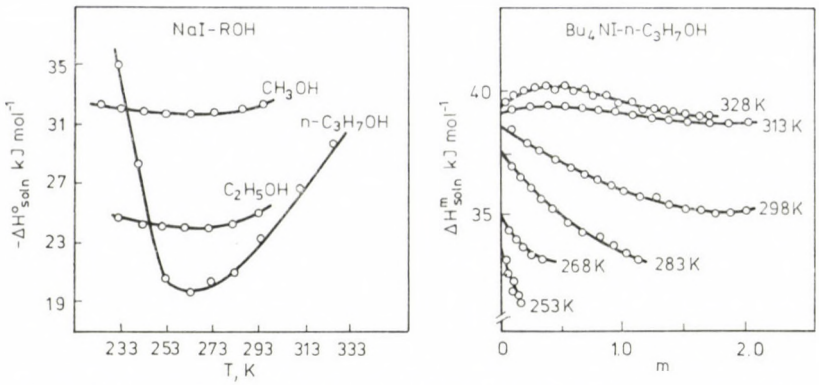

Fig. 1. Dependences of H°_{soln} for NaI and of H^{m}_{soln} for $(C_2H_5)_4NI$ in monohydric alcohols

Alcohol	CH_3OH		C_2H_5OH			C_3H_+OH		
T, K	253	313	233	253	313	233	253	313
association degree	90	31	68	42	14.7	50	33	12.5

studied the signal is also shifted to the stronger field, at 223 K its value being twice as much as at 323 K. The temperature dependence of the mean association degree of alcohols found on the basis of dielectric measurements is shown in the Table [7].

It can be seen in the Fig. 2 that the association degree of an alcohol decreases more than three times at transition from 223 K to 323 K. Thus, the concentration of bonds is three times as great in alcohols at 223 K, and they are broken about twice as much as at 323 K. From this we can conclude that at 223 K, H-bonds in the solvent are broken in a lesser volume with the introduction of the electrolyte into it.

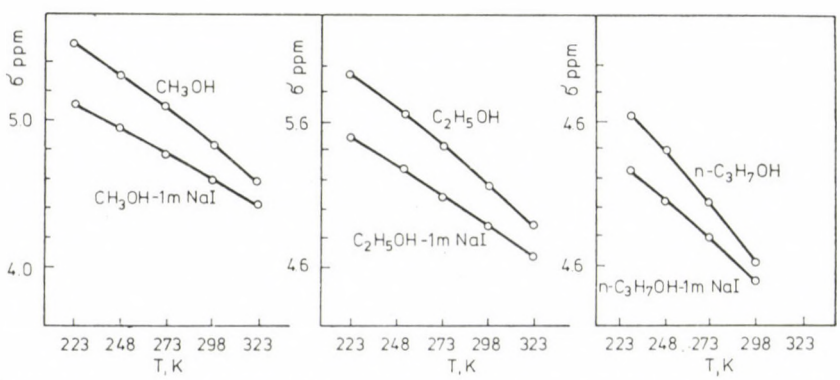

Fig. 2. Temperature dependences of the chemical shift of the hydroxyl proton of alcohols in individual solvents and their electrolyte solutions

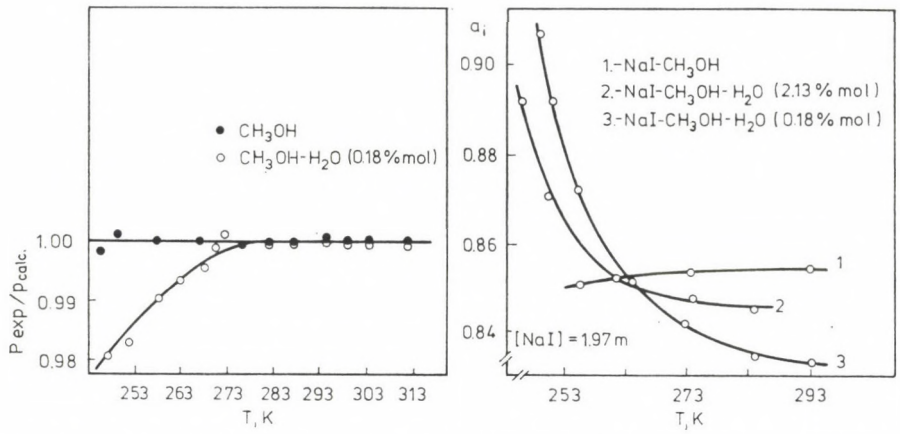

Fig. 3. Influence of contaminant water on the solvent activity in solutions at various temperatures

It has been found that contaminant water has considerable influence on the thermodynamic properties of non-aqueous solutions, this influence being the greatest at temperatures below 273 K. This can be seen in Fig. 3.

Interesting results have been obtained in the investigation of the thermal effects of other electrolyte solutions in mixed organic-aqueous solvents characterized by a spatial network of H-bonds at temperatures above 273 K, as these results reflect the peculiarities of both the structure of solvent molecules and the solvation of lithium ions [8].

Figure 4 shows H°_{soln} of LiCl, NaCl and KCl in aqueous diethyleneglycol (1), glycerine (2), ethylene glycol (3), 1,2-propylene glycol (4), 1,4-butylene glycol (5) versus the mixed solvent composition at 298.15 K.

According to their influence on water structure, the polyhydric alcohols studied are divided into two groups: stabilizing and breaking water structure. The first group contains 1,2-propylene glycol and 1,4-butylene glycol with molecules, the hydrocarbon fragments of which are not bonded with functional OH-groups and have an ordering effect on the structure of water. Polyhydric alcohols, such as ethylene glycol diethylene glycol, glycerine, the molecules of which have a functional OH-group for each C-atom belong to the second group. The results obtained illustrate the arrangement of solvents into these groups. The grouping of the solvents studied is not observed in lithium salt solutions. This is a manifestation of the specific behaviour of lithium ions in aqueous polyhydric alcohols, which is associated with the presence of a stable ion-molecular particle (Li—R) in the solution. Derivatographic results confirm this fact.

The dependences of H°_{soln} for LiCl solutions in aqueous ethylene glycol, glycerine and diethylene glycol at various temperatures are given in Fig. 5.

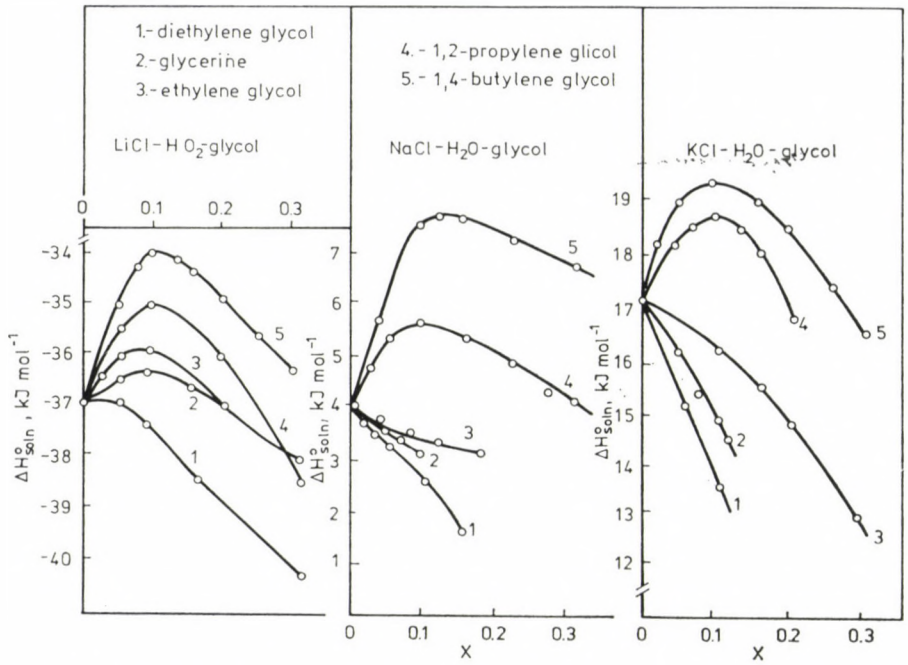

Fig. 4. Composition dependences of H°_{soln} for LiCl, NaCl, KCl in aqueous glycols T — 298.15 K,

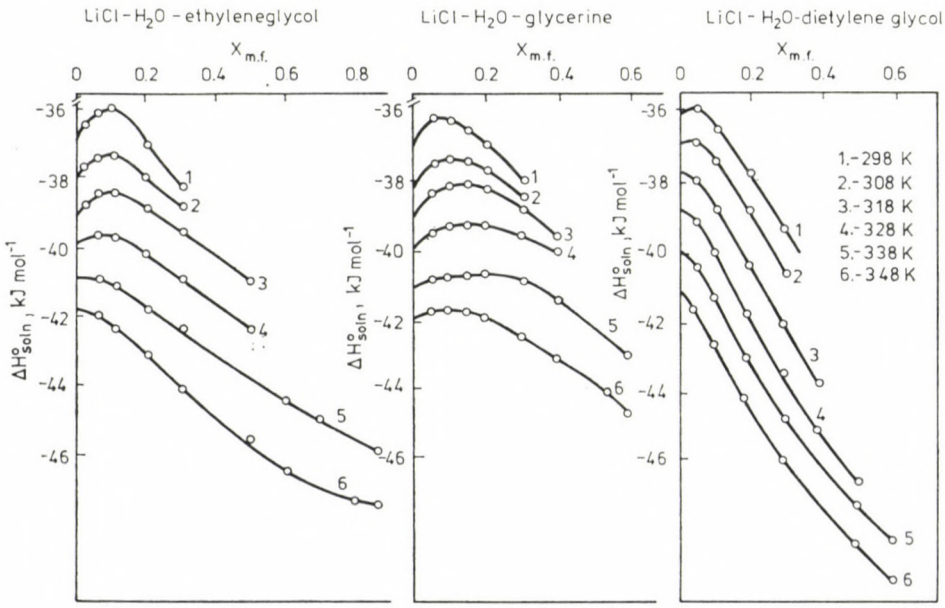

Fig. 5. Composition dependences of H°_{soln} for LiCl solution in aqueous glycols at various temperatures

As follows from Fig. 5, the magnitudes of H°_{soln} in aqueous polyhydric alcohols of any composition and at all temperatures studied are exothermic and increase with an increase in temperature. In that case, the specific behaviour of lithium salts is levelled with increasing temperature.

Along with the thermal effects of solution we have studied the heat capacity characteristics of aprotic solvents (formamide, methylformamide, hexamethylphosphortriamide, dimethylformamide, dimethylsulphoxide, propylene carbonate) and their aqueous solution, including their D_2O solutions [9—10]. The excess heat capacities of a number of systems are given in Figs. 6 and 7. As follows from the Figs. 6 and 7, there are positive and negative devia-

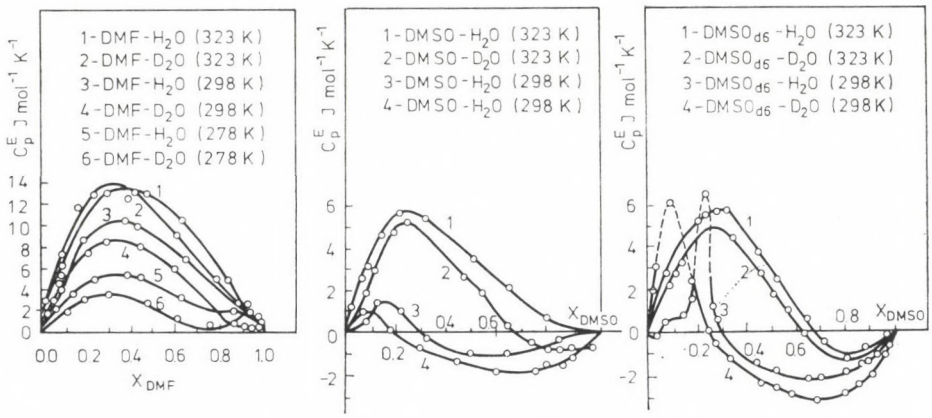

Fig. 6. Heat capacity characteristics of aqueous DMF and DMSO at various temperatures

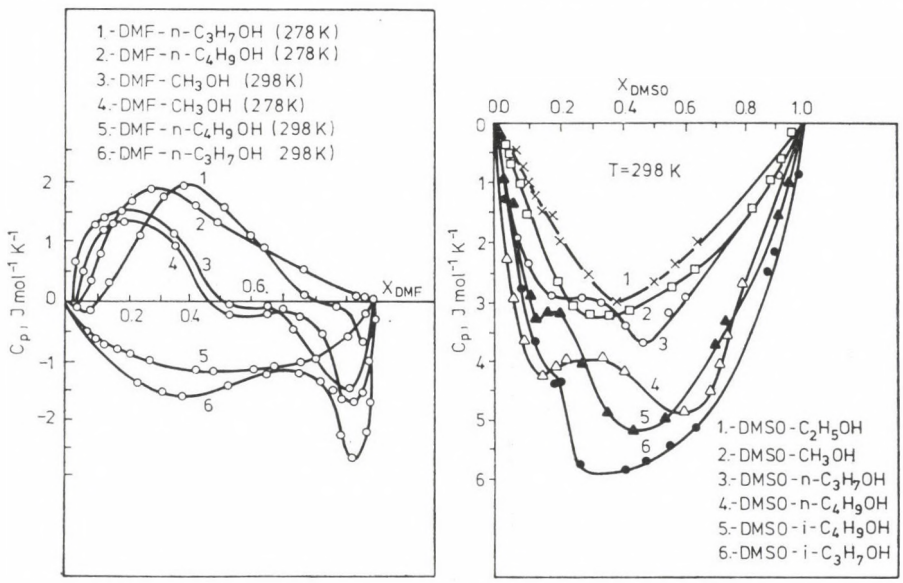

Fig. 7. Heat capacity characteristics of DMF and DMSO in alcohol solutions at 298 K

tions of C_p from additivity for the system studied, which testify to the intermolecular interaction among the solution components. At the same time, the character of the changes of $C_p^E = f(X)$ is tangibly influenced by temperature. For the binary systems we studied, the replacement of the functional groups (—NCOH, —SO) does not change the dependence $C_p^E = f(X)$, in principle. It can be noted that there is a regular change of C_p^E with composition and with an increase in the number of carbon atoms in alcohols of normal structure and certain influence of isomery and isotopy of the solvents on the dependences of $C_p^E = f(X)$.

The use of extensive thermodynamic data allows for consideration of some common problems of the chemistry of non-aqueous solutions.

It is very interesting to discover the structural peculiarities of non-aqueous solutions A new effect similar to the hydrophobic effect in aqueous solutions has been found for solvents with a spatial network of H-bonds by means of the noble gas solubility method (Fig. 8) [11—12].

In this case, the hydrophobic effect occurs with the additions of electrolytes containing no hydrophobic groups, e.g. $[Co(NH_3)_5Cl]Cl_2$. The data obtained made it possible to draw the conclusion that there are no reasons to single out water as a specific solvent of the general system of solvents.

It is rather interesting to compare the composition and temperature dependences of C_{Sm} and ΔS_A and their dependences on other factors (Fig. 9) [13]. This comparison makes it possible to determine the role of energy and structure changes in gas solutions in liquid systems, thus giving the thermodynamic interpretation of their solubility. When comparing $\Delta S_A = f(X)$ and

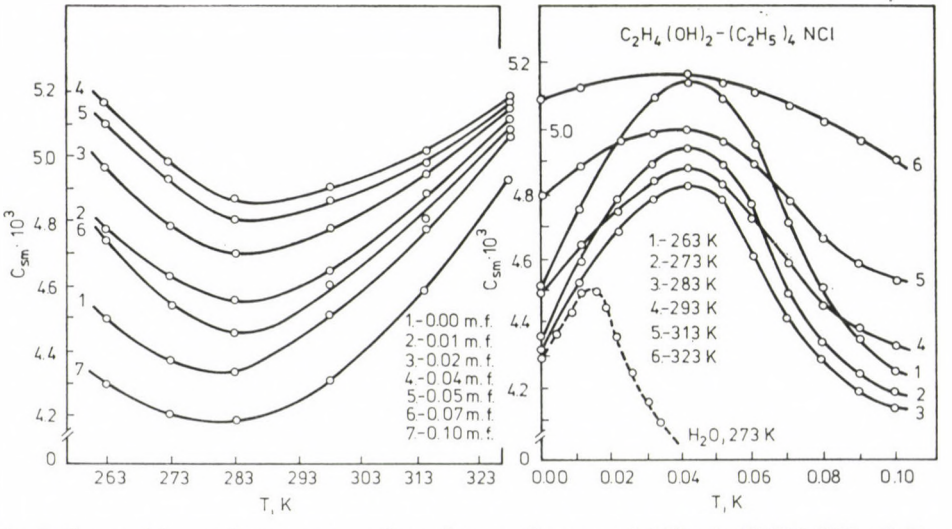

Fig. 8. Composition and temperature dependences of argon solubility in $(C_2H_5)_4NCl$ solutions in $C_2H_4(OH)_2$

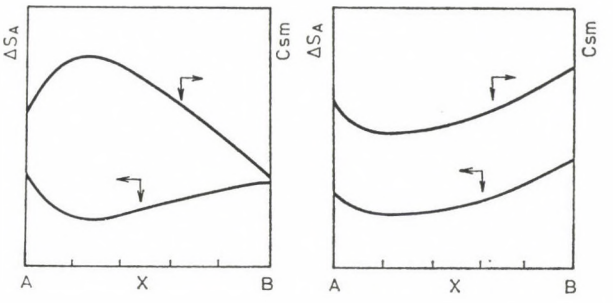

Fig. 9. Interconnection of dependences $S_A = f(X)$ and $C_{Sm} = f(X)$; the opposite and the simbatic nature of the curves

$C_{Sm} = f(X)$ two extreme cases are encountered (Fig. 9). One of them corresponds to the opposite, and the other corresponds to the simbatic nature of these dependences. In the first case, the solutions process is determined by the structural changes of the solvent, and in the second case, it is determined by the energy changes. The predominancy of the structural changes is peculiar to the systems, one component of which has a structure with a spatial network of hydrogen bonds. Such dependences are observed for aqueous monohydric and aqueous polyhydric alcohols, and the mixtures of monohydric and polyhydric alcohols [14]. The energy changes play a predominant role in solution processes for binary non-aqueous mixtures of monohydric alcohols [15].

A series of works concerning the thermodynamic characteristics of the reactions of basic-acidic interaction and complex formation in non-aqueous media have been analyzed [16—18].

The main conclusion following the investigations is that the solvation characteristics of every reactant must be known in order to state the role of a solvent in chemical reactions. The most fruitful proved to be the use of the thermodynamic characteristics of transfer of a reactant from water to a solvent of a given composition (ΔY_{tr}), the algebraic sum of which is equal to the thermodynamic characteristics of the reactions mentioned. Some examples have been brought forth to illustrate this approach (Figs 10—12).

A number of general problems of the thermodynamics of solutions have been discussed.

Methods of solving the Gibbs—Duhem equation for determining the electrolyte activity coefficients in binary system on the basis of solvent activity data have been suggested [15, 19]. They are based on either a description of the general dependence on the basis of individual part regularities, or on the use of polynomials followed by the exclusion of separate members based on standardization conditions or other chemical factors.

A great number of various experimental methods for determination of the standard thermodynamic characteristics of electrolyte solutions based on

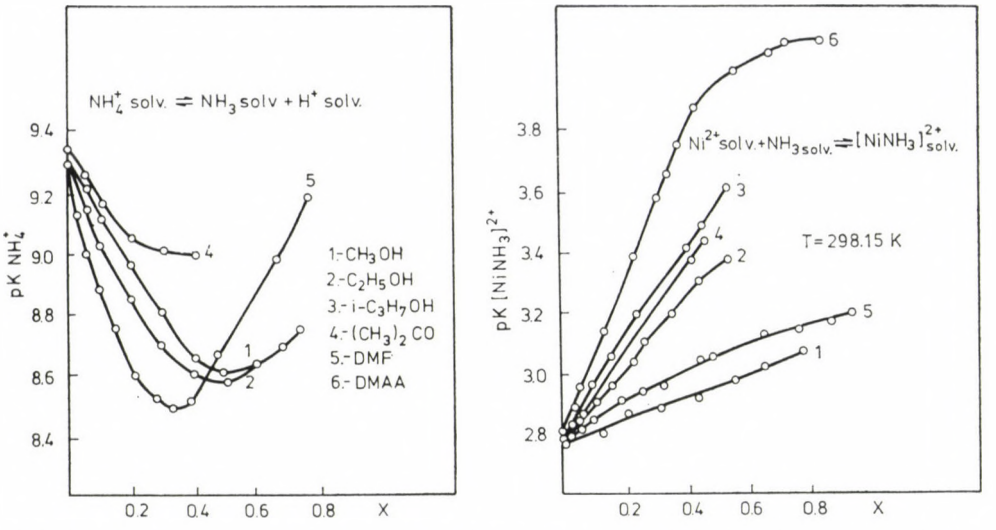

Fig. 10. Composition dependences of equilibrium constants of the reactions of dissociation of $NH_{4\,solv}^{+}$ and of complex formation of $(NiNH_3)_{solv}^{2+}$ in mixed solvents at 298.15 K

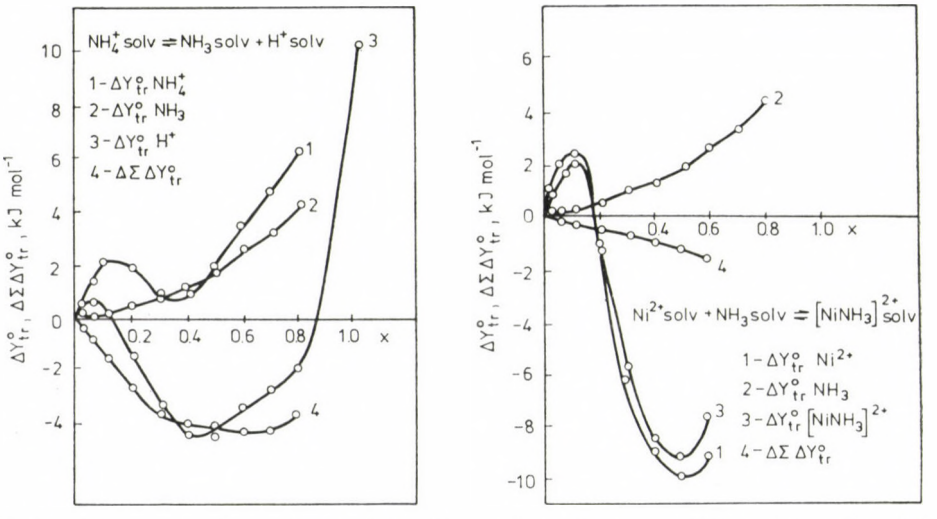

Fig. 11. Composition dependences of the thermodynamic characteristics of transfer of the reactions of dissociation of $NH_{4\,solv}^{+}$ and of complex formation of $(NiNH_3)_{solv}^{2+}$ in mixed solvents

both the Debye—Hückel theory and various semiempirical equations, are described in the literature on the subject. However, in many cases their use does not have sufficient justification. Therefore, it is very interesting to use non-extrapolation methods for the determination of the standard thermodynamic characteristics of solution [20]. The following equations can serve as examples.

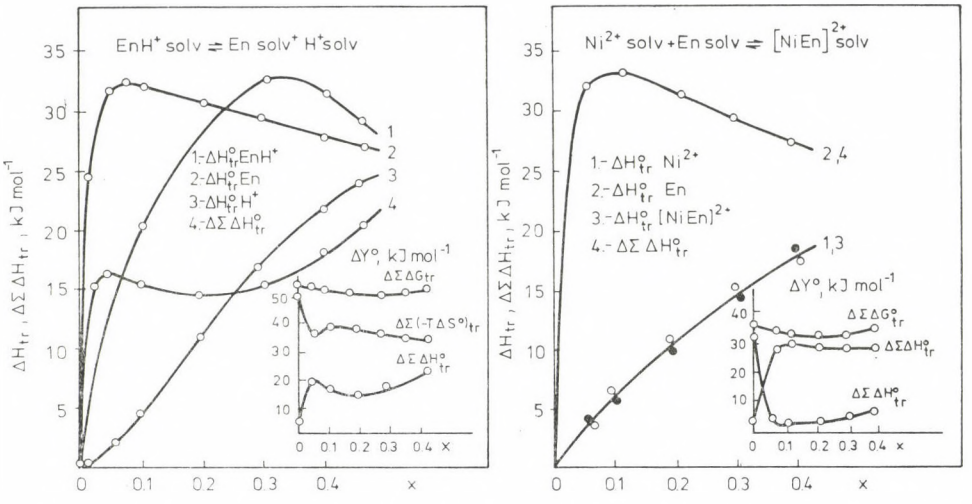

Fig. 12. Composition dependences of the thermodynamic characteristics of transfer of the reactions of dissociation of EnH^+_{solv} and of complex formation of $(NiEn)^{2+}_{solv}$ in mixed solvents at 298.15 K

$$\Delta G^{\circ}_{solv} = \Delta G^{m}_{solv} - \frac{1000}{M_1 \cdot m_2} RT \ln a_1 - RT \ln (m_2 \gamma_2) \tag{1}$$

$$\Delta H^{\circ}_{soln} = \Delta H^{m}_{soln} + \frac{1000}{M_1 \cdot m_2} RT^2 \frac{\partial \ln a_1}{\partial T} + RT^2 \frac{\partial \ln \gamma_2}{\partial T} \tag{2}$$

$$\Delta H^{\circ}_{soln} = \Delta H^{m}_{soln} + \frac{1000}{M_{a \cdot v} \cdot m} \Delta H_{mix} + \frac{1000}{M_{a \cdot v} \cdot m} \sum_{i=1}^{n} X_i \frac{\partial \ln a_1}{\partial T} + RT^2 \frac{\partial \ln \gamma_2}{\partial T} \tag{3}$$

For their determination it is necessary to have data on the thermal effects of solution (solvation) at ultimate concentrations of an electrolyte ΔH^{m}_{soln} temperature dependences of solvent activity (a_1), and activity coefficients of a solute (γ_2). This method is free of the assumptions for extrapolation methods and is applicable, both for electrolyte and non-electrolyte solutions. The accuracy of the results obtained is determined by the accuracy of the derivatives $\partial \ln a_1/\partial T$ and $\partial \ln \gamma_2/\partial T$. In those cases when the extrapolation laws are not known (e.g. weak electrolyte and non-electrolyte solutions) the use of the given equations is the only possibility. Table I shows examples illustrating the applicability of this method for electrolyte and non-electrolyte solutions.

Attention should be paid to the incorrect use in the literature of the practical osmotic coefficient, which is referred to the scale of molal concentra-

Table I

System	H_2O—NaI			H_2O—C_2H_5OH	
m	0.1	1.0	2.0	14.5	86.96
$\Delta H^{\circ calc}_{soln}$, kJ · mol^{-1}	4.07	4.04	4.08	11.79	11.38
ΔH^{exp}_{soln}, kJ · mol^{-1}		3.89		10.17	

tions; at the same time, the rational osmotic coefficient is used in the mole fraction concentration scale. A different interpretation of osmotic coefficients is given in the IUPAC recommendations. Together with this, the analysis [21] shows that the osmotic coefficients in both cases are introduced with the use of the mole fraction concentration scale. Actually,

$$\ln a_1 = \Phi \ln X_i, \text{ but } \ln a_1 = -\Phi \frac{m \cdot M_1}{1000}, \text{ if } \frac{m \cdot M_1}{1000} \ll 1 \qquad (4)$$

In the general case the second expression is approximate. Instead of various designations of the osmotic coefficients g and φ, it is advisable to use only Φ. If for aqueous solutions, the difference between them is not great up to large electrolyte concentrations, this difference may be essential for non-aqueous solution with a considerably greater mass as compared with water. For the system NaI—H_2O ($m = 1.0$) and are 1.99 and 1.98, respectively, and for the system NaI—C_3H_7OH ($m = 1.0$) they are 2.76 and 2.66.

The problem of the determination of the thermodynamic characteristics of individual ions in solutions is a matter of principle in the thermodynamics of solutions. It is a very complicated problem, and, as a rule, it can not be solved without the introduction of some non-thermodynamic assumptions.

The necessity of finding the properties of individual ions is universally recognized at present. Nevertheless, up to now there is no unanimous opinion, not only concerning the numerical magnitudes of the values, but also with respect to the methods of their determination.

Obtaining the thermodynamic properties of individual ions in connection with the presence of the data for stoichiometric mixtures of ions in solutions amounts to finding the properties of at least one of the ions by one method or another.

For these purposes, various experimental and theoretical methods are tried, and also methods of dividing the thermodynamic characteristics of stoichiometric mixtures into ionic components.

Among experimental methods we can mention the volt-potential method, mass spectrometry, measurement of electron removal work at its emission from the solution, of free energy of transfer of ions from one solvent to another, electrochemical and other methods.

However, the effective use of experimental methods for the determination of the thermodynamic properties of individual ions is hindered by numerous difficulties and certain broad assumptions. In this connection we can not be sure of the absolute reliability of the qualitative description of ion properties, and the limit of error in their measurement is great. Thus, to obtain the thermodynamic characteristics of individual ions in solutions there is wide use of theoretical methods of calculation, the correlation of their different properties, the division of summary values into ionic components with the use of non-thermodynamic assumptions and, finally, the replacement of "absolute" values of thermodynamic characteristics by "relative" ones.

The theoretical methods of determination of the thermodynamic characteristics of solvation of individual ions are based on the Bohrn theory and modifications, the use of structural representations, thermodynamic cycles, etc . . . In the past decade theoretical methods of determination of the thermodynamic characteristics of ion solvation have been developed on the basis of statistical thermodynamic methods, and quantum-chemical calculations of all kinds of interactions in solutions.

A review of experimental and theoretical methods is given, for example, in the work [3].

At the present stage of development of solution theory and the accumulation of experimental material, a great role, and, sometimes, the most important, is played by the determination of the thermodynamic characteristics of ion solvation, by the division of the experimentally determined values into ionic components, followed by processing them on the basis of approximate correlations. It is possible to single out at least four groups of division methods.

An essential drawback of the method, which based on the assumption of the equality of the thermodynamic characteristics of solvation of cations and anions considered as standard, is the absence of correspondence of various thermodynamic characteristics of ion solvation in solution obtained in this way. In principle, the question of the possibility of separating the sum values $\Sigma \Delta Y_{\text{solv}}$ into ionic components in connection with the presence of charges of solvated particles remains open.

Another type of division of thermodynamic characteristics of solvation of stoichiometric ion mixtures lies at the basis of the second group of methods. This type of division is carried out on the basis of extrapolation of $\Delta\Sigma(\Delta Y_{\text{solv}})_i$ for ion pairs with a common cation or a common anion from ion properties. The application of the extrapolation method is considerably limited by the absence of reliable experimental data on the thermodynamic characteristics

of solvation of stoichiometric ion mixtures. This applies first of all non-aqueous and mixed solvents. In connection with the use of different systems of ionic radii in calculation, the thermodynamic parameters of ionic solvation obtained by the method described differ greatly.

The third method is based on the division of changes in thermodynamic characteristics of transfer of the stoichiometric mixture from one solvent to another into their components. These given values can be calculated with sufficient accuracy, not being complicated by errors connected with the calculation of the thermodynamic parameters of the crystal lattice. The majority of the methods of determining the thermodynamic characteristics of ion transfer are based on the assumption of the equality of the changes of these values for the determination of ion pairs, taken as standard.

An analysis of the third group shows that, despite the possibility of their application to a wide range of individual and mixed solvents, they have their shortcomings. It is hardly to be expected that all the components of ion-solvent interaction of a standard ion pair should be equal. Moreover, there are no criteria for the equality of the radii of ions included in standard pairs. That is why, the data obtained by these methods are of a quantitative nature and have importance for a limited number of solvents.

The fourth group of methods comprises a number of other methods of division. They include the method of the division of the medium summary effect into its components, the division of the isotopic effects of hydration on the basis of their equality to zero for Na^+, of a consideration of the energy of H-bonds between solvent molecules and anions, the use of the constancy of the ratio $(\Delta Y_{solv})_c/\Delta(Y_{solv})_a$ in any solvents, and a consideration of the electrostatic interaction of ions with the charge centres of the solvent dipoles in the short-range surrounding, and the distribution of these charges, and the constancy of coordination numbers, and many other methods.

The majority of the methods mentioned does not allow for the varying nature of ion-molecular interactions for cations and anions, which serves as a vivid example of their limited character.

Figure 1 shows the dependences ΔH°_{solv} for some single-charged ions on donor-acceptor ability of the solvent [22].

It follows from Figure 13 that the state of solvated ions varies with the donor-acceptor characteristics of individual solvents, which are calculated as the difference of ΔH°_{solv} of an electrolyte in a non-aqueous solvent (R) and the one taken as standard (H_2O). This circumstance testifies to the different nature of cation and anion solvation. The ion-solvent interaction is realized by the donor-acceptor mechanism for cations, and for anions, it is H-bonds that play a great role. These data make it possible to conclude that cations are solvated preferably in amides, and anions are better solvated in water or alcohols.

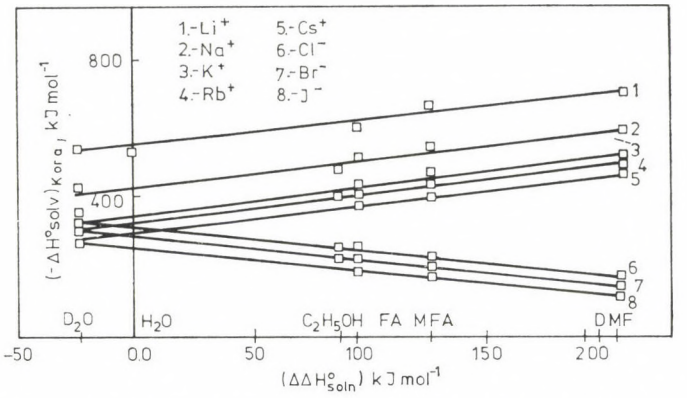

Fig. 13. Dependences ΔH°_{solv} of cations or anions for a series of single-charged ions versus donor-acceptor characteristics of individual solvents

The specific nature of cation and anion solvation follows also from the data on the entropy characteristics of ions versus mixed solvent composition [23] (Fig. 14).

It can be supposed that the phenomenon of heteroselective ion solvation occurs in water-methanol mixtures, in which case cations are preferably hydrated and anions are solvated by methanol molecules. Here, too, cation-solvent interaction is of a donor-acceptor nature, and anion-solvent interaction is performed through H-bonds.

On the basis of the above consideration, the basic drawbacks of the majority of the division methods considered are as follows:

1. They give the approximate magnitudes of the values obtained, which is associated with a more or less arbitrary assumption adopted during the division;

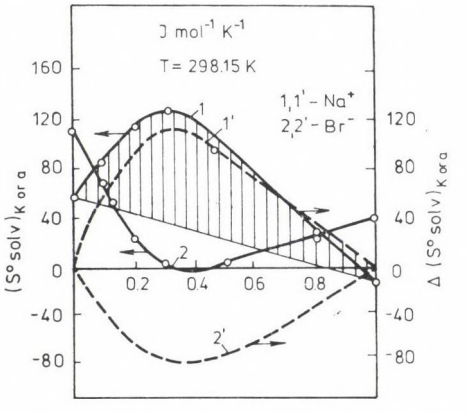

Fig. 14. Composition dependences of the entropy of ions in aqueous methanol at 298.15 K

2. There are no corresponding levels of calculating various thermodynamic characteristics of the solvation of individual ions;

3. No regard is paid to the different natures of ion-molecular interactions of cations and anions;

4. There is an arbitrary choice in the calculation of the thermodynamic characteristics of electrons in solutions and in the gaseous phase, as a result of which the thermodynamic characteristics of cation solvation are higher, and those of anion solvation are lower by the value of $|Z|(\Delta Y^{\circ}_{\mathrm{solv}})\bar{e}$.

Thus, the problem of the determination of the thermodynamic characteristics of ion solvation remains urgent.

REFERENCES

[1] Krestov, G. A.: J. Struc. Khim., **25,** 90 (1984)
[2] Krestov, G. A.: J. All-Un. Khim. Soc., **28,** 70 (1983)
[3] Krestov, G. A.: Thermodynamics of Ionic Processes in Solutions Chemistry, ed. 1 (1973), p. 303, ed. 2 (1984), p. 272
[4] Krestov, G. A., Kolker, A. M., Korolev, V. P.: J. Sol. Chem., **11,** 593 (1982)
[5] Krestov, G. A., Kolker, A. M., Vatagin, V. S., Kinchin, A. N.: DAN SSSR, **268,** 1150 (1983)
[6] Kolker, A. M., Alper, G. A., Krestov, G. A.: DAN SSSR (in press)
[7] Durov, O. A., Usacheva, T. M.: Zh. Fiz. Khim., **56,** 648 (1982)
[8] Krestov, G. A., Egorova, I. V., Korolev, V. V., Safonova, L. P., In: Thermodynamic Properties of Solutions, Ivanovo 28 (1984)
[9] Kukharenko, V. A., Korolev, V. P., Krestov, G. A.: Zh. Obshch. Khim. **55,** 971 (1985)
[10] Kukharenko, V. A., Korolev, V. P., Krestov, G. A.: Zh. Fiz. Khim. (in press)
[11] Krestov, G. A., Vinogradov, V. I., Kononenkova, T. V., Sergeyev, E. N., Gorelov, V. N.: DAN SSSR, **272,** 680 (1983)
[12] Krestov, G. A., Vinogradov, V. I.: DAN SSSR **276,** 616 (1984)
[13] Krestov, G. A., Vinogradov, V. I., Sergeyev, E. N.: Izv. AN SSSR, Chemical Series **10,** 2373 (1984)
[14] Kononenkova, T. V., Vinogradov, V. I., Krestov, G. A.: Zh. Fiz. Khim., **57,** 2074 (1983)
[15] Krestov, G. A., Vinogradov, V. I., Parfenuke, V. I.: Zh. Inorg. Khim., **25,** 584 (1984)
[16] Shormanov, V. A., Trupikov, E. A., Gusev, V. D., Krestov, G. A.: Izv. Vuzov, Khim. and Khim. Technol., **19,** 523 (1976)
[17] Shormanov, V. A., Sharnin, V. A., Krestov, G. A.: Zh. Fiz. Khim., **53,** 121 (1979)
[18] Gusev, V. D., Shormanov, V. A., Krestov, G. A.: Koord. Khim., **5,** 706 (1979)
[19] Kolker, A. M., Vatagin, V. S., Krestov, G. A.: Izv. Vuzov, Khim. and Khim. Technol. **28,** 116 (1985)
[20] Krestov, G. A., Kolker, A. M., Safonova, L. P.: DAN SSSR **280,** 404 (1985)
[21] Kolker, A. M., Safonova, L. P., Krestov, G. A.: Zh. Fiz. Khim. (in press)
[22] Krestov, G. A., Zakharov, A. G., Romanov, V. K.: Izv. Vuzov, Khim. and Khim. Technol., **19,** 1276 (1976)
[23] Sokolov, V. P., Kobenin, V. A., Krestov, G. A., In: Thermodynamics and Solution Structure, Ivanovo, v. **10,** 33 (1982)

Acta Chimica Hungarica 121 (1—2), pp. 107—117 (1986)

DIELECTRIC GRADIENT AROUND THE IONS IN SOLUTIONS+

János Liszi

(University of Veszprém, Department of Analytical Chemistry, H-8201 Veszprém, P.O.B. 158.)

Received January 18, 1985

The dielectric saturation caused by the strong electric field of the ions in the solvent is considered. The dielectric gradient around the ions is approximated by step-like and continuous profiles. The various representations of the dielectric profile are tested via comparisons of calculated and observed electrostatic free energies of solvation. A simple one-step dielectric profile seems to be preferred because of its relative simplicity, and predictive power.

Introduction

There are two main groups of theoretical models that have been used for the calculation of thermodynamic parameters of ionic solvation [1, 2]. In the 1st group the environment of the ion is considered to consists of individual particles, the real or "simplified" structure of the solvent is taken into account [3, 4, 5]. In the 2nd group the ionic environment is viewed as a structureless dielectric continuum [1, 6]. Whichever type of models is used one has to take into account the dielectric saturation caused by the strong electric field of the ions in the solvent. By other words the non-linear dielectric behaviour of the solvent has to be considered. In this paper the continuum approach is used because of its relative simplicity. In this approach the ion-solvent interaction can be treated either by the reaction field technique [7, 8, 9, 10] or by charging up model [6, 10]. Both give the same final results, but the second is simpiler, therefore this has been used. The fundamental question is the selection of a suitable dielectric profile for the description of the dielectric gradient around the ions. However, it is of limited use just to compare one theoretical profile with another, because there is then no rigorous criterion that can be used to select the "best" profile. It is more useful to calculate e.g. the electrostatic free energy of solvation from the various representations of the dielectric profile and then to compare these calculated values with experiment.

+ This paper was presented at the Symposium on Structure of Liquids and Solutions at Veszprém, August 27—30, 1984.

The electrostatic free energy density

The solvation free energy can be divided into a non-electrostatic and an electrosatatic part [11, 12, 13]*:

$$\Delta G_s = \Delta G_n + \Delta G_e. \tag{1}$$

Then ΔG_n is taken as a solvation free energy of an inert non-electrolyte of the same radius as the ion in question, so that ΔG_e may then be deduced. Therefore we consider only the electrostatic free energy of solvation which comes from the integration of the electrostatic free energy density:

$$\Delta G_e = \iiint\limits_{r>a} g \, \mathrm{d}V - \iiint\limits_{r>a} g_v \, \mathrm{d}V. \tag{2}$$

Here the free energy density in solution is g, in vacuum is g_v, and the integration range refers to the entire space existing outside the ion, the latter being a charged sphere of radius a.

In this treatment the ion is taken to be a charged conducting sphere, whilst the sphere is charged up to the ionic charge, it dielectrically saturates the solvent in its neighbourhood. The free energy density of the electrostatic field in a dielectric is given by eq. (3):

$$g = \frac{1}{4\pi} \int_0^D E \, \mathrm{d}D, \tag{3}$$

where E is the electric field strength and D is the displacement vector, $D = \varepsilon E$ with ε as the static relative permittivity. In a strong field, such as that occurring in the vicinity of the solvated, ion, ε depends on E. This field dependence according to Booth [15]:

$$D = n^2 E + 4\pi N \mu \left(\mathrm{cth} \frac{3\mu E}{2kT} - \frac{2kT}{3\mu E} \right), \tag{4}$$

where n is the internal refractivity of the solvent, N is the number of the molecules in unit volume, k is the Boltzmann constant, T is the temperature and μ is the actual dipole moment valid in the liquid. This last quantity can be calculated from the gas-phase dipole moment via $\mu = \mu_g(n^2 + 2)/3$.

Introducing the $\varepsilon_d = \mathrm{d}D/\mathrm{d}E$ differential relative permittivity eq. (3) gives

$$g = \frac{1}{4\pi} \int_0^E \varepsilon_d \, E \, \mathrm{d}E. \tag{5}$$

* One advantage of this division is that provide ΔG_s and ΔG_n refer to the same standard states, the numerical value of ΔG_e is independent of any standard state.

From eqs (4) and (5) the free energy density is given by

$$g = \frac{\varepsilon E^2}{8\pi} + \frac{3}{2} NkT\left[\frac{x}{2}\left(\text{cth } x - \frac{1}{x}\right) + \ln\left(\frac{x}{\text{sh } x}\right)\right], \tag{6}$$

where $x = 3\mu E/2kT$ (It has to be mentioned that a similar result has been obtained by Lengyel and Kempelen [16]). In order to make the interpretation of eq. (6) easier, in Fig. 1 a sketch of the D vs. E function is given. For weak fields, where E is small, the plot is an approximately straight line of slope ($\varepsilon = \varepsilon_d = \varepsilon_0$). For strong fields, where E is large, there is again a straight line but of slope ($\varepsilon_d = n^2$). Between the two linear sections, at intermediate field strengths, the curvature of the plot indicates the saturation of the dielectric medium. In Fig. 1 the quantity $4\pi g$ is also given for a dielectric medium polarized up to the point P [see eq. (3)]. The exact value of g can be calculated from eq. (6). Let us consider now only the final state corresponding to point P and use a relative permittivity $\varepsilon = D/E$ appropriate to the point P. In this case we neglect the process due to the charging up of the conducting sphere. Then the "4π times density" is represented by the triangle OQP, equivalent to $ED/2$. This result corresponds to the approximation of calculating the free energy density using only the first term in eq. (6) with $\varepsilon = D/E$ at point P. In other words, the first term in eq. (6) gives the free energy density of the electrostatic field, of strength E, in a non-saturated dielectric medium of

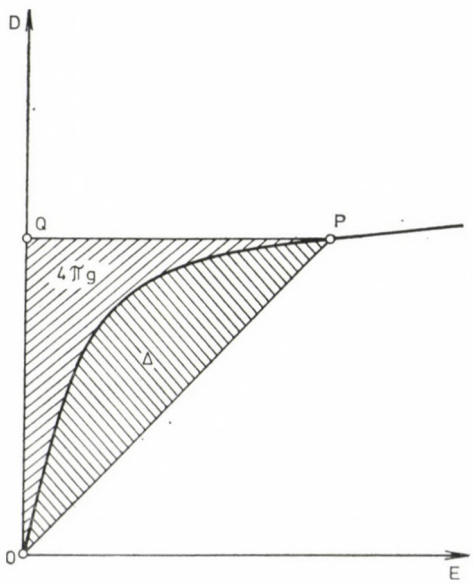

Fig. 1. Plot of the displacement vector D against the field strength E. Δ originates in the second term of eq. (6)

relative permittivity ε. If the permittivity decreases owing to dielectric saturation, then the free energy density is smaller than $\varepsilon E^2/8\pi$ (valid for the linear case) by a value Δ that is given by the second term in eq. (6). In Fig. 1 the area that corresponds to Δ is shown, too. It is the difference in the calculated value of the free energy density between the approximate result (neglect of dielectric saturation) and the exact result (with dielectrid saturation taken into account). If Δ is small, then the saturated dielectric medium at point P can be replaced by a non-saturated medium of relative permittivity $\varepsilon = D/E$ without introducing a significant error in the calculation of the electrostatic free energy density.

The dielectric gradient around the ions

Eq. (4) refers to a homogeneous electrid field. If one neglects the difference between the effects of the homogeneous and non-homogeneous fields, a combination of eq. (4) and the Coulomb's law gives the relative permittivity in the field of a point charge as a function of the distance. Such functions are given in Fig. 2 as examples for methanol and acetonitrile around univalent ions. The more simple case is that of acetonitrile which is less organized liquid than the methanol. Its relative permittivity decreases from the bulk value (ε_0) to about two at the narrow neighbourhood of the point charge. The originally organized liquid methanol shows a curve with "two steps". This indicates that the lowering of the relative permittivity of organized solvents in the vicinity of ions originates from two superimposed effects of the destruction of the original structure of the solvent and its dielectric saturation in the narrower sense [17]. In the following only the simple case is considered when the lowering of the relative permittivity comes from dielectric saturation.

The ε vs r function has no meaning for distances smaller than the ionic radius a. Therefore it is evident that the larger ions bring about weaker dielectric saturation in their close neighbourhood than do the smaller ions. In Fig. 2 some ionic radii are marked to illustrate this effect.

Between the surface of the ion and the nearest permanent dipoles of the solvent molecules will be a region, without permanent dipoles, in which the relative permittivity is $\varepsilon = n^2$. Consequently, in the close neighbourhood of the ion, there will exist a region of low relative permittivity even in the absence of the dielectric saturation effect of the ion. This is an "apparent dielectric saturation" which modifies the dielectric gradient around the ion as shown in Fig. 3. (For example in acetonitrile ions of radious >0.6 nm do not cause dielectric saturation (see Fig. 3), but the phenomenon of "apparent dielectric saturation" must be present for these large ions, too). The thickness of this region of low relative permittivity depends on the dimensions of the

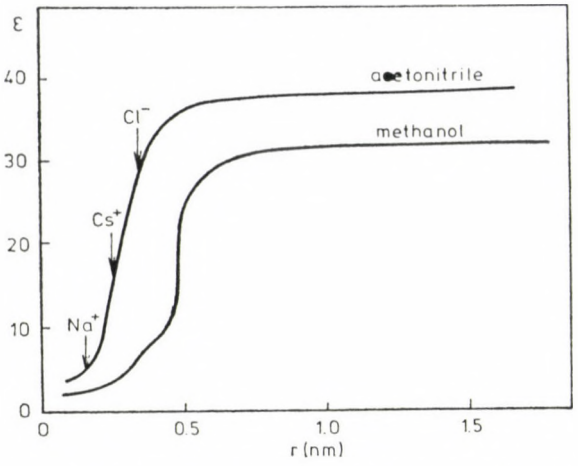

Fig. 2. The relative permittivity of methanol and acetonitrile in the field of a univalent ion

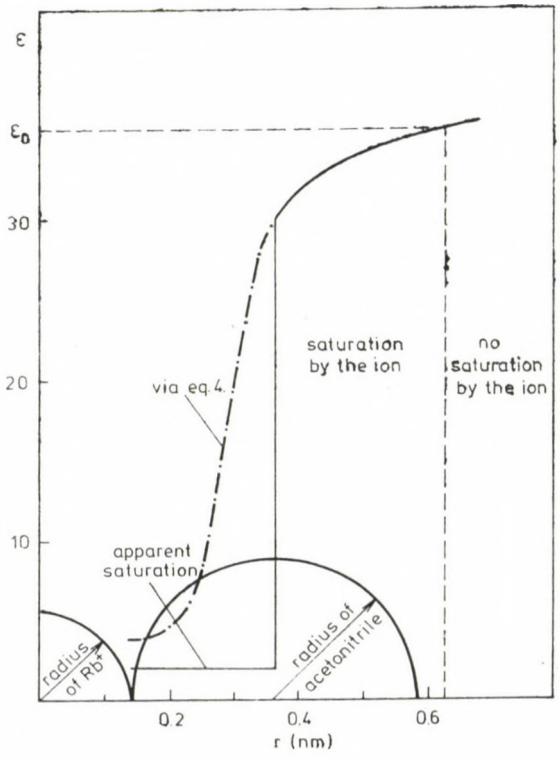

Fig. 3. A plot of ε of acetonitrile in the field of a Rb^+ ion including the effect of apparent dielectric saturation

solvent molecule and on the position of its permanent dipole. If the dipole is not symmetrically situated in the molecule, the thickness of this region may be different for anions and cations in the same solvent. Nevertheless, for the sake of simplicity spherical solvent molecules will be considered with dipoles, situated at the center of the molecules, so that the thickness of this layer will be the same for anions and cations.

There is another consequence of the apparent dielectric saturation and the finite dimension of the ion, too. As the distance r becomes larger, the field strength becomes less, Δ becomes more negligible, and the calculation of g by the first term in eq. (6) becomes a better approximation. In the case of univalent ions in acetonitrile only when $r < 0.3$ nm does the second term make a very significant contribution to the overall value of the free energy density. Bearing in mind that the Stearn—Eyring radius of the acetonitrile molecule is $R = 0.224$ nm, for ions with radius more than 0.1 nm (i.e. for ions with $(a + R) > 0.324$ nm) the electrostatic free energy density can be calculated by the first term in eq. (6) without significant error. Similar calculations for many solvents including 1,1-di-chlorethane, ammonia, acetone, *N*,*N*-dimethyl-formamide, DMSO, *N*-methylformamide, formamide, 1-propanol, ethanol, methanol and water yield the same result. One can conclude that for the usual solvents the electrostatic free energy density can be calculated from the first term only in eq. (6) without significant error, provided that the univalent ion has a radius larger than about 0.1 nm.

Dielectric profiles and the electrostatic free energy of solvation

Although there is no disagreement over the form of the dielectric profile [see eq. (6) together with Coulomb's law], there are difficulties over the representation of the profile in a way that can lead to a reasonable simple calculation of the electrostatic free energy of solvation of an ion. Eq. (4) and accordingly eq. (6) does not give a simple way for calculation of ΔG_e, even if we consider only the first member of eq. (6). Therefore efforts are made to find a suitable dielectric profile. The profiles have been applied are either step-like or continuous ones.

In terms of eq. (2) the electrostatic free energy of solvation is the difference between the electrostatic free energy of the solvent and that of the vacuum in the field of the ion. The second term via the Coulomb's law is

$$\Delta G_{ev} = z^2/2a, \tag{7}$$

where z is the ionic charge and a is the ionic radious. The first term of eq. (2) quite generally can be given by a multilayer model. One supposes that a

sphere of radius a and relative permittivity unity is surrounded by concentric dielectric continua of radii $b_1, b_2, \ldots, b_k$ and of respective relative permittivities $\varepsilon_1, \varepsilon_2, \ldots, \varepsilon_k$. Beyond these concentric shells, or layers, from b_k to infinity there lies the homogeneous bulk of the solvent with relative permittivity ε_0. The free energy can then be obtained as the sum of integrals corresponding to the layers. From eq. (2) and Coulomb's law, $|E| = z/\varepsilon r^2$, comes

$$G_e = \frac{z^2}{2} \sum_{j=1}^{k} \int_{b_{j-1}}^{b_j} \frac{\mathrm{d}r}{\varepsilon_j r^2} + \frac{z^2}{2} \int_{b_k}^{\infty} \frac{\mathrm{d}r}{\varepsilon_0 r^2} = \frac{z^2}{2} \sum_{j=1}^{k} \frac{1}{\varepsilon_j} \left(\frac{1}{b_{j-1}} - \frac{1}{b_j} \right) + \frac{z^2}{2} \left(\frac{1}{\varepsilon_0 b_k} \right). \tag{8}$$

(In this equation the radius corresponding to b_{j-1}, where $j = 1$ is actually a, the ionic radius.) The first k members of the series give the free energy of the layers and the last term gives the free energy of the dielectric existing beyond b_k. In the integration ε_j was considered to be independent of r and hence in eq. (8) the average relative permittivity of each layer must be used. In the following the electrostatic free energy of solvation, $\Delta G_e = G_e - G_{ev}$ is given for some particular models:

The Born model (zero layer):

$$\Delta G_{e0} = \frac{z^2}{2} \left(\frac{1}{\varepsilon_0 a} - \frac{1}{a} \right), \tag{9}$$

The one-layer model (first layer $r = b$ and $\varepsilon = \varepsilon_l$):

$$\Delta G_{e1} = \frac{z^2}{2} \left[\frac{1}{\varepsilon_l} \left(\frac{1}{a} - \frac{1}{b} \right) + \frac{1}{\varepsilon_0 b} - \frac{1}{a} \right], \tag{10}$$

The two-layer model (first layer $r = b$ and $\varepsilon = \varepsilon_l$, second layer $r = c$ and $\varepsilon = \varepsilon_m$):

$$\Delta G_{e2} = \frac{z^2}{2} \left[\frac{1}{\varepsilon_m} \left(\frac{1}{b} - \frac{1}{c} \right) + \frac{1}{\varepsilon_l} \left(\frac{1}{a} - \frac{1}{b} \right) + \frac{1}{\varepsilon_0 c} - \frac{1}{a} \right]. \tag{11}$$

In order to test the electrostatic models, two univalent ions, Rb^+ and Br^- are considered. In acetonitrile the following ΔG_e (gas, 1 atm → solvent, unit mole fraction) values were found [11]: for Rb^+ —329 kJ mol^{-1} and for Br^- —254 kJ mol^{-1}. These electrostatic free energies of solvation of gaseous ions may be directly compared to values calculated on the basis of a continuum theory, using various representations of the dielectric profile. In Table I solvation free energies, calculated via various stepwise dielectric profiles, are given. In the calculations $\varepsilon_l = 2$ or $\varepsilon_l = 1.9$ is used; these values are close to the square of the internal refractivity of the solvent. The thickness of the first layer, $(b - a)$ would be close to the Stearn—Eyring radius of the solvent molecule (0.222 nm for acetonitrile, [11]), and for simplicity $(c - b) = (b - a)$

Table I

ΔG_e for Rb^+ *sand* Br^- *in acetonitrile via various step-like dielectric profiles;* $a = 0.143$ nm *for* Rb^+ *and* $a = 0.195$ nm *for* Br^-

Dielectric profile	ΔG_e (calc) in kJ mol^{-1}	
	Rb^+	Br^-
Born equation, eq. (9)	−472	−346
One-layer, eq. (10), $\varepsilon_l = 2.0$; $(b - a) = 0.222$*	−333	−257
One-layer, eq. (10), $\varepsilon_l = 1.9$; $(b - a) = 0.205$	−330	−255
One-layer, $\varepsilon_l = 2.0$; $(b - a) = 0.222$; ε = Booth-Onsager value for $r > 0.365$	−332	−256
Two-layer, eq. (11) $\varepsilon_l = 2.0$; $\varepsilon_m = 33.1$; $(b - a) = (c - b) = 0.222$	−333	−256
Two-layer, eq. (11) $\varepsilon_l = 1.9$; $\varepsilon_m = 33.1$; $(b - a) = (c - b) = 0.205$	−329	−255
Observed value	−329	−254

* Distances in nm.

would be taken. The relative permittivity of the second layer is selected on the basis of the Booth—Onsager profile using the distances given above. The results show that there is actually very little difference between ΔG_e values calculated via a one-step or a two-step profile. Since more constants are needed for the two-step calculations, it seems that there is no need to use any further approximation than a one-step dielectric profile. This result is not special to the cases of Rb^+ and Br^- in acetonitrile, but it is quite general.

The idea of the continuous profile was introduced by Stiles [18] and the general form of such a profile was given by us [19]. The distance dependence of the relative permittivity in terms of a continuous profile is given by eqs (12), (13):

$$\varepsilon = \varepsilon_a(\varepsilon_b/\varepsilon_a)^{f(r)}, \qquad a < r \leq b, \tag{12}$$

$$f(r) = 1 - [(b - r)/(b - a)]^n. \tag{13}$$

The electrostatic free energy of solvation via these equation is

$$\Delta G_e = \frac{z^2}{2}\left[\frac{1}{b\,\varepsilon_0} - \frac{1}{a} + \frac{1}{\varepsilon_a}\int_b^a \left(\frac{\varepsilon_a}{\varepsilon_0}\right)^{f(r)} r^{-2}\,\mathrm{d}r\right]. \tag{14}$$

A disadvantage of this treatment is that the equations contain five undetermined constants (a, b, ε_a, ε_b and n). Some of them can be fixed on the basis of the step-like models given above, namely, a can be taken as ionic radius, ε_a as the square of the internal refractivity, or approximately $\varepsilon_a = 2$ and $\varepsilon_b = \varepsilon_0$, the bulk permittivity. Then one may use the remaining two parameters (b and n) as adjustable constants. Although the method looses its predictive power in this way, one can get reasonable results for the solvation

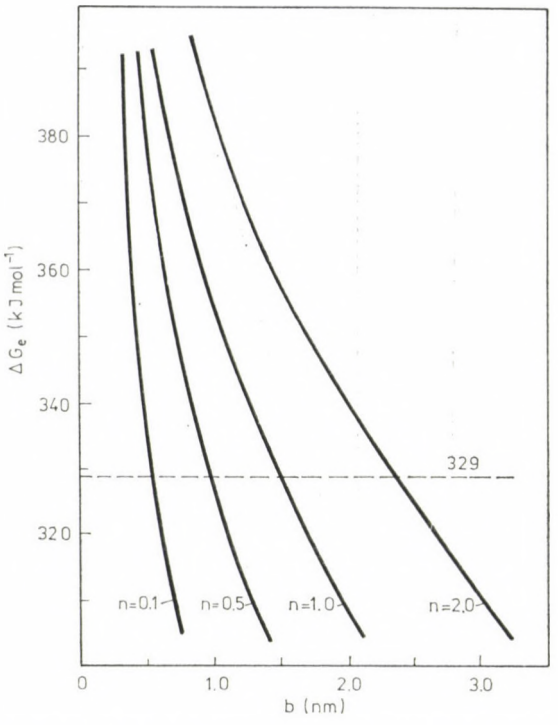

Fig. 4. Plots of ΔG_e for Rb^+ in acetonitrile as calculated from eqs. (12)—(14) for various n values

free energy. The calculated values of ΔG_e for Rb^+ in acetonitrile are plotted against b for various n in Fig. 4, where the observed ΔG_e value of —329 kJ mol^{-1} is also shown. There is a very strong dependence of the calculated ΔG_e on b, especially for the cases where n is small. From the calculated values one can obtain the b value that leads to the correct ΔG_e as follows: $n = 2$, $b = 2.4$ nm; $n = 1$, $b = 1.6$ nm; $n = 0.5$, $b = 1.0$ nm; $n = 0.1$, $b = 0.5$ nm. Therefore in this system $n = 0.1$ seems to be preferred. Interestingly, the continuous dielectric profile given by this value is very close indeed to the one-step profile (see Fig. 5). Fig. 5 also shows that the continuous profile with $n > 0.1$ as well as the Born model overestimates the relative permittivity at smaller distances and hence both lead to too negative calculated ΔG_e values, unless the value of b in the continuous profile is taken to be very large.

From the discussion given above shows that it is possible to choose a mathematical function relating local solvent relative permittivity to the distance from an ion on the basis of criteria such as:

1. the calculation of thermodynamic parameters for solvation that are in agreement with experiment,

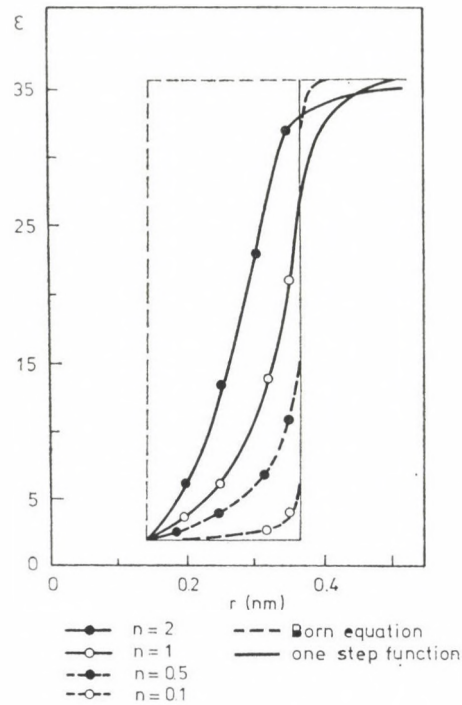

Fig. 5. A comparison of continuous and step-like profiles

2. the possibility of predicting such parameters for systems that have not been experimentally studied,

3. the convenience of use of the function, without regard to the physical significance of such a function, especially in terms of the solvent region close to the ion.

The simple one-step dielectric profile, yielding eq. (10) as an expression for ΔG_e, is actually quite a reasonable approximation. Beside its *simplicity*, fixing ε_l as 2 and $(b - a)$ as the Strearn—Eyring radius of the solvent molecule, it has a valuable *predictive power*. It can be used for the calculation of solvation free energies of ions in widely different solvent [11], the calculation of solvation entropies of ions in numerous aprotic solvents [11], and the calculation of partition coefficients of ions between water and immiscible non-aqueous solvents [18].

*

This work was done in cooperation with M. H. Abraham (Dept. Chem. University of Surrey, Guildford, U. K.), Mrs. E. Kristóf (Dept. Anal. Chem., University of Veszprém), L. Mészáros (Hungarian Academy of Sciences, Laboratories of Inorganic Chemistry, Budapest) and I. Ruff (Lab. Theor. Chem., Eötvös University, Budapest). The author is grateful to them for the kind cooperation.

REFERENCES

[1] Saluja, P. P. S.: International Review of Science, Physical Chemistry Series Two (Butterworths, London, 1976), Vol. **6**, pp. 1—51.
[2] O'M Bockris, J., Saluja, P. P. S.: J. Phys. Chem., **76**, 2298 (1972)
[3] Frank, H. S., Wen, W. Y.: Disc. Faraday Soc., **24**, 133 (1957)
[4] Ruff, I.: J. Chem. Soc. Faraday Trans., 2, **73**, 1858 (1977)
[5] Arányi, L., Liszi, J.: Acta Chim. Hung., **106**, 325 (1981)
[6] Born, M.: Z. Phys., **1**, 45 (1920)
[7] Linder, B.: Adv. Chem. Phys., **12**, 225 (1967)
[8] Böttcher, C. J. F.: The Theory of Electric Polarisation (Elsevier, Amsterdam, 1973) 2nd Ed., Vol. **1**.
[9] Beveridge, D. L., Schnuelle, G. W.: J. Phys. Chem., **79**, 2562 (1975)
[10] Abraham, M. H., Liszi, J., Mészáros, L.: J. Chem. Phys., **70**, 2491 (1979)
[11] Abraham, M. H., Liszi, J.: J. Chem. Soc., Faraday Trans. 1, **74**, 1604, 2858 (1978); **76**, 1219 (1980)
[12] Bjerrum, N., Józefowicz, E. Z.: Phys. Chem., Abt. A, **159**, 194 (1932)
[13] Alfenaar, M., de Ligny, C. L.: Rec. Trav. Chim. Pays-Bas, **86**, 929 (1967)
[14] Noyes, R. M.: J. Am. Chem. Soc., **84**, 513 (1962)
[15] Booth, F.: J. Chem. Phys., **19**, 391, 1327, 1615 (1951)
[16] Lengyel, S., Kempelen, M.: MTA Alk. Mat. Int. Közl., **2**, 489 (1952)
[17] Liszi, J., Mészáros, L., Ruff, I.: J. Chem. Phys., **74**, 6896 (1981)
[18] Stiles, P. J.: Aust. J. Chem., **33**, 1389 (1980)
[19] Abraham, M. H., Liszi, J., Kristóf, E.: Aust. J. Chem., **35**, 1273 (1982)
[20] Abraham, M. H., Liszi, J.: J. Inorg. Nucl. Chem., **43**, 143 (1981)

Acta Chimica Hungarica 121 (1—2), pp. 119—145 (1986)

ROLE OF HYDROGEN BONDING IN THE STRUCTURE OF LIQUIDS+

Werner A. P. Luck

(Physikalische Chemie der Universität Marburg, D-3550 Marburg, Germany)

Received January 18, 1985

A simple model for nonpolar liquids is discussed in the first section along with formulae for the specific heats of intermolecular degrees of freedom and for heats of evaporation. The dominant role of abnormally high H-bond energies for H-bonded liquids is stressed. The second important factor is the angle dependence of the H-bonds which induces a structure with coordination numbers of about 4 instead of 12 in the H-bonded regions of liquid water. The variation in the density of liquids as a result of this effect is discussed.

Spectroscopic methods to determine the content of H-bonded OH or NH groups and the H-bond energies are reviewed. As a consequence of the above discussion the important role of van der Waals forces on H-bonded liquids including water is stressed. An attempt is made to clear up the difference in the properties of water and alcohols.

The role of the repulsion term in cases where two protons or two lone pairs of electrons are neighbours for the H-bonded liquids is demonstrated.

The possibility to describe the caloric data of H-bonded liquids quantitatively by the simplified equilibrium of H-bonded and non-H-bonded OH groups is now established by the calculation of the specific heat, the liquid enthalpy and the inner heat of evaporization of ethanol and methanol till the critical point. The reasons for the efficiency of this simplified equilibrium are discussed. The usefulness of the dependence of intermolecular degrees of freedom for the specific heat is established by the above result. The importance of the abnormal H-bonded influence on liquid properties for the living organism is reported.

The dominant role of H-bonds on liquid mixtures and solutions is demonstrated. The similarity between the interaction of anions with OH and H-bonds is stressed. Electrolyte solutions are found to behave similarly to mixtures of H-bonded systems.

The structure of normal liquids

We should understand the structure of non-polar liquids before we look at the anomalies of hydrogen-bonded liquids. The development of suitable models for liquids got interrupted in the beginning of this century by the increasing interest of physical chemists in quantum phenomena. In the last decade the interest in liquid revived, however, the knowledge of the complicated partition functions reduced the courage to develop simple models of liquids like we use for the vapour state. To develop such a model [1] let us consider a few interesting features.

We start with the experience that upon melting the density decreases by about 10% (Lorentz rule [2], Fig. 1), whereas the distances between the

+ This paper was presented at the Symposium on Structure of Liquids and Solutions at Veszprém, August 27—30, 1984.

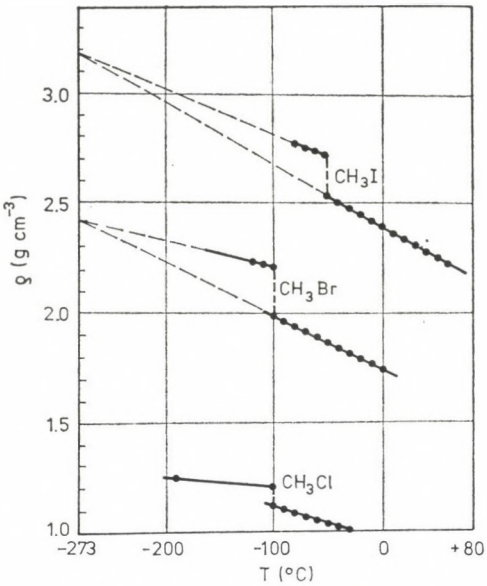

Fig. 1. Density change at the melting point T_m is mainly about 10%, an indication that the molecular distances in liquids near T_m are similar to those in crystals (data of [3])

molecules increase only by about 2.2%. This means that the mean positions of molecules in melts cannot be much different from the crystals. In agreement with this conclusion the enthalpies of fusion are mostly small compared to the enthalpies of vaporization. The intermolecular potentials of melts are therefore very similar to crystals, which are arranged in a densed package (Fig. 2 left). The understanding of the melting process has been described efficiently by Bresler [4, 1], who demonstrated that if the energy U to introduce a defect depends linearly on the degree of order η, than

$$U = U_0 + U_1\eta. \tag{1}$$

(U_0, U_1: constants)

Calculations based on statistical thermodynamics show a jump of the degree of order η at a certain temperature T, which we could assume to be the melting temperature T_m [1, 4].

The cooperativity assumed in Eq. (1) could be described as the interaction energy in a crystal and in a liquid and is given by the term $ZE_{11}/2$, where Z is the coordination number of next neighbours and E_{11} is the pair potential of intermolecular forces [1]. Z_0 is the coordination number at $T = 0$ K. Around a hole defect the interaction energy is reduced to $(Z_0 - 1)\, E_{11}/2$; the energy is reduced to introduce a second defect in this disturbed area. The liquid at

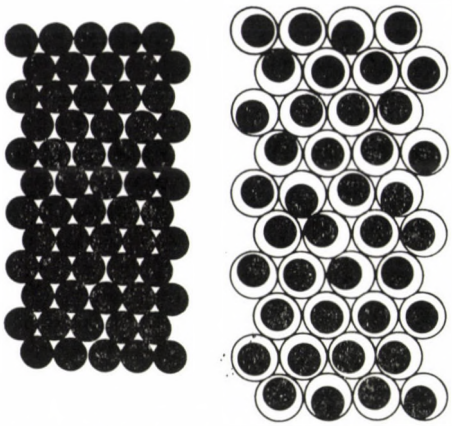

Fig. 2. Left: two dimensional model of a crystal as a dense package. Right: two dimensional model of a liquid near T_m; crystal-like package of the vibration volume included is the molecular volume

T_m differs according to Bresler from a solid only by a small increased number of defects, which could induce a decoupling of the thermal molecular movements (Fig. 2, right). This decoupling decreases the viscosity of the liquid but cannot change the averaged structure significantly. Thus we can start the description of a nonpolar liquid with a crystal-like packing for the averaged molecular positions (Fig. 2). This is established by X-ray scattering experiments, which demonstrate peaks of the radial distribution curves of liquids near the peak positions of a crystal. The broadening of these peaks indicates the difference between a liquid and a crystal, viz. more or less disordered thermal movements.

These thermal movements decrease the density of most liquids with increasing T linearly in a T-region [1]:

$$T < T_B \ (T_B\text{: boiling } T)\text{:}$$
$$\varrho = \varrho_0 - bT \tag{2}$$

This linear decrease in ϱ corresponding to an increase in molecular distances induces a linear decrease |1| in the heat of evaporations ΔU_{vap} for:

$$\Delta U_{\text{vap}} = \Delta U_0 - aT \quad \text{for} \quad T < T_B$$
$$\Delta U_0 = ZfE_{11}/2 \tag{3}$$

The factor f, not far from unity, includes the influence of second and higher next neighbours [1].

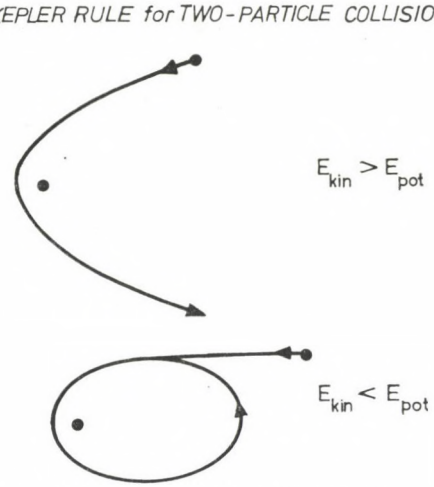

Fig. 3. A two body encounter gives a hyperbola or ellipse if kinetic energy is bigger or smaller than potential energy; model for condensation below critical temperature if kinetic energy 3 $RT/2$ is smaller than potential one 3 $RT_c/2$

With the empirical rule* [1]: $E_{11} = 3RT_c/2$ (T_c: critical temperature) we get:

$$\Delta U_{\text{vap}} = \frac{Zf}{2} R \left(\frac{3}{2} T_c - T\right) \quad \text{for} \quad T < T_B \tag{4}$$

The factor $-ZfRT/2$ may be described as heat content of the intermolecular degrees of freedom, which reduced the intermolecular potential energy [5, 6].

Recently we have established with spectroscopic exactness [5, 6] the efficiency of Eq. (4) and the use of our simplified liquid model by the demonstration that the frequency shift $\Delta\nu$ of OH vibrational bands by van der Waals forces is strictly linear too for $T < T_B$ ($\Delta\nu \sim \Delta U_{\text{vap}}$ is a measure of the total interaction energy). The spectroscopic results also show that the slope $\mathrm{d}(\Delta\nu)/\mathrm{d}T$ is very similar for many nonpolar liquids, with Eq. (4) being ($\mathrm{d}(\Delta\nu)/\mathrm{d}T \sim$ $\sim ZfR/2$). Therefore, we can conclude that the packing of such liquids is very similar.

The Eötvös rule

Honouring the famous Hungarian scientist Eötvös, we give his rule:

$$\frac{d\sigma_M}{\mathrm{d}T} = \text{constant} = 2.1\ N_A^{1/3}\ (\text{erg/mol K}) = 17.73\ (\text{J/mol K}) \tag{5}$$

* This relation is related to Keplers law of planet movements: two bodies move on a hyperbola if $E_{\text{kin}} > E_{\text{pot}}$ and on a circle or on an ellipse if $E_{\text{kin}} < E_{\text{pot}}$; at T_c is $E_{\text{kin}} = RT_c$ 3/2, liquefaction is possible if RT 3/2 $< RT_c$ 3/2 $= E_{\text{pot}}$ (Fig. 3).

(N_A: Avogadro's number, σ: surface tension (erg/cm^2);

$$\sigma_M = \sigma \cdot V^{2/3} \cdot N_A^{1/3}\text{: molar surface tension)}$$

This expression gives very similar results. In our simplified model [1, 7] we have concluded:

$$\frac{d\sigma_M}{dT} = (Z - X)\, fR \cdot \frac{3}{4} \tag{6}$$

(X: coordination number at the surface)
and found experimentally as average [7]: $(Z - X) = 2.85$; in consequence: $d\sigma_M/dT = 17.76$ J/mol K.

Some authors have criticized that the Eötvös coefficient seems to be T-dependent and changes from one compound to the other. They have suggested erroneous: $d\sigma_M/dT = V^{2/3}N_A^{1/3}d\sigma/dT$ instead of the correct relation $d\sigma_M/dT = N_A^{1/3}\, d(V^{2/3}\sigma)/dT$. But Eötvös is more correct at his reviewer claim.

Small real deviations from the Eötvös rule are given by Eqs. (5) and (6) in terms of different values of $(Z - X)$ and f.

We may add that at high $T(>T_B)$, deviations from the linear T-relations are observed, and we may correlate such observation with the Lennard—Jones potential curve at higher distances or simplified heuristically by the so-called hole model [1, 8, 9].

H-bond energies

The normal van der Waals energies in homologous series are proportional to the electron numbers or to the molecular weight [1]. In Fig. 4 are plotted the heats of vaporization at the boiling point T_B:

$$\Delta U_{vap} = \Delta H_{vap} - RT_B \tag{7}$$

as a function of the number of closed 8-electron shells of noble gases or as a function of the number of carbon atoms of n-paraffins. If we compare similar data on n-alcohols or amines counting one OH or NH group similar to one C-atom we recognize the greater influence of the H-bonds on the intermolecular interactions at T_B.

Water is especially abnormal, in which the H-bonds of two OH groups dominate. It has the same electron number as CH_4. therefore, expecting similar van der Waals forces in water and CH_4, water would have an excess energy of $\Delta U_{vap}(H_2O) - \Delta U_{vap}(CH_4) = 7.3$ kcal/mol or 30.5 kJ/mol; the excess energy per OH band is 3.65 kcal/mol or 15.25 kJ|mol. In Fig. 5 are

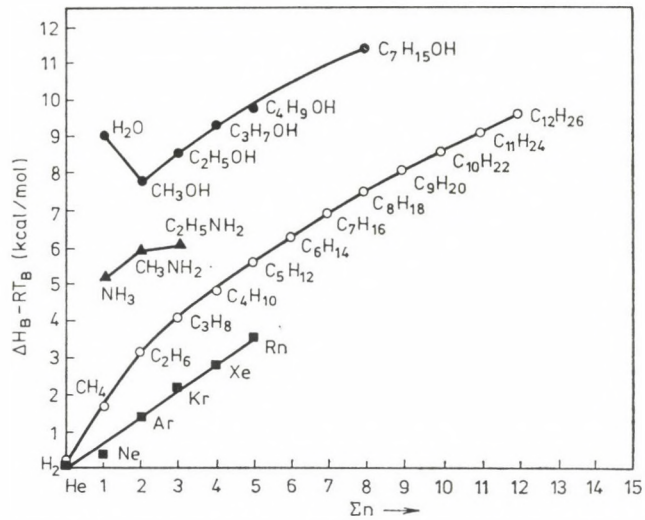

Fig. 4. Internal energy of vapourization: $\Delta U_B = \Delta H_B - RT_B$ at the boiling point T_B as a function of the number n of closed electron shells (rare gases) or the number of atoms (protons not counted). Higher values of OH or NH compounds are induced by H-bonds

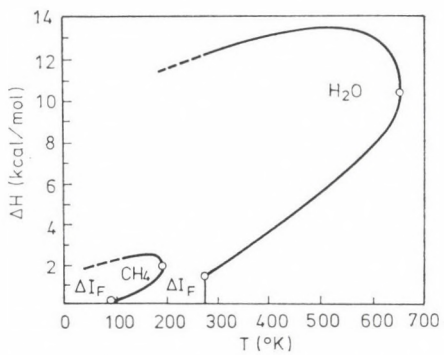

Fig. 5. Comparison of enthalpies CH_4/H_2O. Above: vapour state; down: liquid state; both in equilibrium. The difference is mainly given by the high H-bond energy of H_2O

given the enthalpy of CH_4 and H_2O (lower curves for liquid state and upper curves for vapours) at liquid/vapour equilibrium. The enthalpy of the solid at T_m is assumed as the zero point. The comparison of both enthalpy curves in Fig. 5 demonstrates the large energy influence of H-bonds on the energetic properties of H-bonded liquids.

If we extrapolate the boiling temperature and the melting temperature T_m of hybrides in the series: H_2Te, H_2Se, H_2S to H_2O, we would expect for water: $T_m = -100$ °C, $T_B = -80$ °C. Only the higher interaction energies induced by the H-bonds enable life on our planet. The higher enthalpies of vaporizations by H-bonds become intensified by the small size of water molecules if we calculate the enthalpy of vaporization per gram (Table I).

Table I

Enthalpies ΔH of vaporization of liquids

	ΔH (kJ/mol)	ΔH (kJ/g)	t (°C)
H_2O	43.9	2.45	20
CH_3OH	39.3	1.20	20
C_2H_5OH	42.3	1.00	20
$C_2H_5—O—C_2H_5$	28.9	0.39	34
$CHCl_3$	31.4	0.263	20
C_3H_8	19.7	0.867	—44
C_2H_6	16.3	0.54	—88

The mobile thermostat of the human body can be efficiently regulated by the cooling process of evaporating liquid water by its high ΔH_{vap}-values per gram.

Table II

Volume change: $\Delta V = [V(T/T_c) - V(T/T_c = 0.6)]/V(T/T_c = 0.6)$ in percent

T/T_c	water	ethanol	CCl_4	Benzene	*n*-Hexane	Cyclohexane	Methyl acetate
0.6	0	0	0	0	0	0	0
0.65	3.0	3.1	3.8	3.7	4	3.8	3.9
0.7	6.7	6.7	8.2	8.1	8.4	8.1	8.2
0.8	17.2	17	19.4	19.8	19.8	19.4	19.9
0.9	36.8	34.8	38.5	38.1	39	38	39

Properties of non-polar molecules, determined by the intermolecular potentials, are similar if we compare them at reduced temperatures T/T_c [1]. For instance the relative volume-change of vapours or liquids with increasing T are similar (see Table II)*. The corresponding values of the H-bonded liquids, water and C_2H_5OH are higher but are similar. We can conclude that the stronger bonded OH group determines the increase in volume with T. The values in Table II demonstrate that the volume expansion is smaller in the case of H-bonded liquids due to the greater interaction energy and due to the more porous structure by the angle dependence of the H-bonded energies. To estimate the caloric properties of molecules we should know the coordination numbers and the pair potential.

Coordination numbers

In addition to higher H-bond interaction energies the orientation dependent H-bond energy is the second abnormal factor of H-bonded liquids. The dispersion energy of a group in the molecule has a spherical symmetry having

* The scattering of values in Table II are partially induced by the necessary linear interpolation between density-data given in 10 or 20 degrees distances.

repulsion at low distances and attraction at higher distances. The depth of the potential minimum is equal in any direction in the case of dispersion interaction but it is angle dependent in the case of H-bonds. The H-bond energy ΔH_H is maximum if the angle between the proton axis and the axis of the lone pair electron is zero [10, 11]. Quantum chemical calculations [12] have shown that ΔH_H goes down by 40% if the OH groups are antiparallel. In Fig. 6 curve *C* gives the total energy of a "cyclic" water dimer; the energy per OH bond of this angle-unfavoured-H-bond is about 50% of this value.

The angles of H-bonds in crystals — determined by scattering methods — deviate seldom more than about 14% of the linear H-bond (see Fig. 7) if the O . . . O distance is smaller than 2.84 Å; a distance at which the H-bond energy becomes small. Scattering measurements of H-bonded liquids demonstrate a similar preference of the optimal H-bond angle [15a].

In water, which is an extremely H-bonded liquid, this angle effect of H-bonds has the consequence of a coordination number of 4 in ice contrary to nonpolar liquids or crystals of spherical molecules condensing in a dense

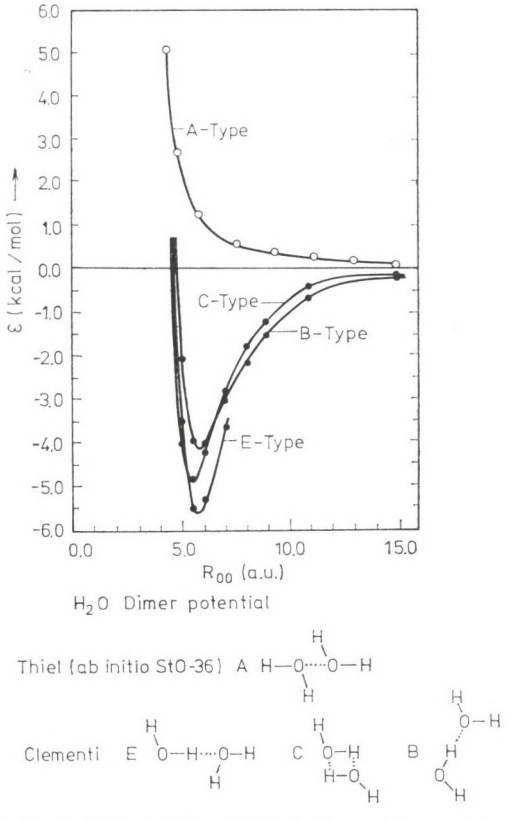

Fig. 6. Quantum chemical calculations [12, 13] of the interact on potential of a water dimer in different positions

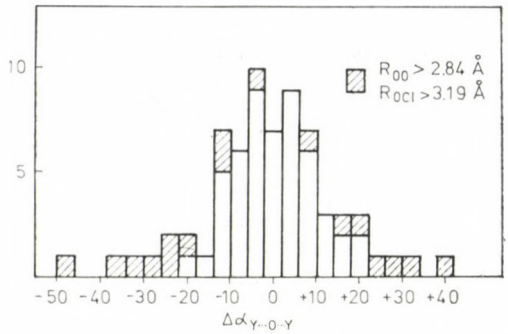

Fig. 7. Number of observed deviations of the H-bond angle zero in solid hydrates; data taken from the neutron scattering review of Falk and Knop [14]

packing which have a coordination number of $Z = 12$. The linear H-bonds of water together with the tetrahedral angle between protons and lone pair electrons induces hexagonal rings of 4-coordinate water molecules in the tridymite ice structure (Fig. 8). This preferred hexagonal structure of the H-bond acceptor groups is also observed in H-bonds of organic molecules like the dimers of lactams [11] or carboxylic acids or the trimers of oximes [16]. This intermolecular hexagonal symmetry of water induces directly the hexagonal symmetry of snowflakes which are grown near saturation conditions.

Coordination numbers of nearly 4 are observed in liquid water in the vicinity of the melting point (see Table III). Contrary to nonpolar liquids like

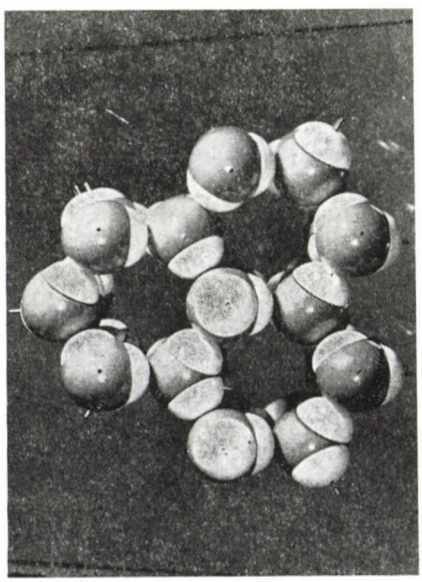

Fig. 8. The model of the normal ice structure with a coordination number of 4 and the fundamental unit of a six-membered H_2O-ring

Table III

Average number N of nearest neighbours

Solid	Ice 4	Solid argon 12
T/T_c	Liquid water	Liquid argon
0.428	4.37	
0.499	4.39	
0.538	4.42	
0.56		10.5
0.61		7
0.654	4.5	
0.731	4.5	6
0.99		

argon with Z-values near 12 at the melting point and decreasing Z-values by thermal vibrations at increasing T in the case of water, it is observed that the coordination number of $Z = 4$ at T_m increases with increasing T (Table III). This increase in Z-values of water is attributed to the vanishing trend of the angle dependence of the interaction energies of molecules which H-bond because of the sufficiently high thermal energy. At this point the coordination number is similar to that of nonpolar liquids, because the interaction energy of such OH groups is of the van der Waals type. The coordination number of such an OH group may be assumed to be 6, which is one half of that for a spherical nonpolar molecule, which has $Z = 12$. This effect is overlapped by the normal thermal expansion. The overlapping of these effects induces the known abnormal density maximum at 4 °C of H_2O which is of vital importance for fish in areas of temperatures below the freezing point. The coordination number 4 in liquid water is given too with computer simulations by Pálinkás et al. [43].

Density of liquid water

The volume of liquids or crystals as a function of T can be described often by a linear T-function; which, for example, for ice is given as:

$$V_i(\mathrm{cm^3/g}) = 1.035\,(\mathrm{cm^3/g})(1 + 1.741 \times 10^{-4}\,(\mathrm{g\,cm^{-3}\,°C^{-1}})\,T\,(°\mathrm{C}))$$

In the region of the critical temperature T_c a factor of higher T-exponents has to be added.

The volume of liquid water could be taken as the sum of a certain percentage $(1 - O_F)$ of ice-like H-bonded OH groups with ice-like partial molar volume and the partial molar volume V_F of the O_F-percent non H-bonded OH groups [17, 18]:

$$V = 1/\varrho = (1 - O_F)\,V_i + O_F V_F \qquad (8)$$

V_F can be adjusted to:

$$V_F = 0.64006\,(\mathrm{cm^3\,g^{-1}})(1 + 5.7249\times10^{-3}\,(\mathrm{g\,cm^{-3}\,°C^{-1}})T(°\mathrm{C}))$$

O_F is a temperature function which we can determine spectroscopically. O_F increases and $(1 - O_F)$ decreases with T, the first term $(1 - O_F)V_i$ decreases and $O_F V_B$ increases with T. The sum of both gives the density maximum at 4 °C and the density decrease above 4 °C [17].

Determination of the content of H-bonded OH groups

The influence of H-bonding on the structure of liquids depends on the content of H-bonds. Infrared spectroscopy is a sensitive tool to determine the content of non-H-bonded OH groups [1, 19—21]. They give in the vibration spectrum a sharp band near the absorption in vapour (Fig. 9). H-bonded OH groups shift the stretching vibration frequency and increase the band-intensity [22]. This increase disturbes the determination of the unshifted band of the non-H-boned OH. Fortunately, this intensity change does not appear in the overtone spectra (Fig. 9). In this region the band-area does not change much but the band half widths increase by a factor of about 15 and as a consequence the band maximum decreases. This means that overtone spectroscopy gives good information on the content of the non-H-bonded OH groups [18—21]. We call these groups "free OH". It may, however, be noted that free means only free of H-bonds but not free of van der Waals interactions.

In Fig. 10 the result of this efficient method: the content O_F of liquid water, liquid CH_3OH and liquid C_2H_5OH in equilibrium with its own vapour pressure are given. In the first papers on water we gave $O_F(T_c) = 100\%$. In the region of critical temperature T_c the spectroscopic measurements are disturbed by the large density gradient in the gavitational field [23]. By more detailed discussion of the spectra in this region we have later changed to this picture 10*. The low content of O_F near the melting point means that the molecules give a network of H-bonds with some free OH. In this system the equilibrium between the potential minimum of the H-bonds and the thermal vibrations cannot be described well by the statistics of monomers and small or medium sized aggregates. In a simplified fashion we assume the equilibrium [18]:

$$OH_F + \Theta_F \rightleftharpoons OH_B \qquad (9)$$

(OH_F: OH groups free of H-bonds; Θ_F: lone pair electrons free of H-bonds OH_B: bonded OH groups).

* A similar content of O_F for water could be established by Horváth et al. by the method of pion-decay [Chem. Phys. Letters, **87,** 304 (1982)], and by Jorgensen by computer methods [Chem. Phys. Letters, **70,** 326 (1980).

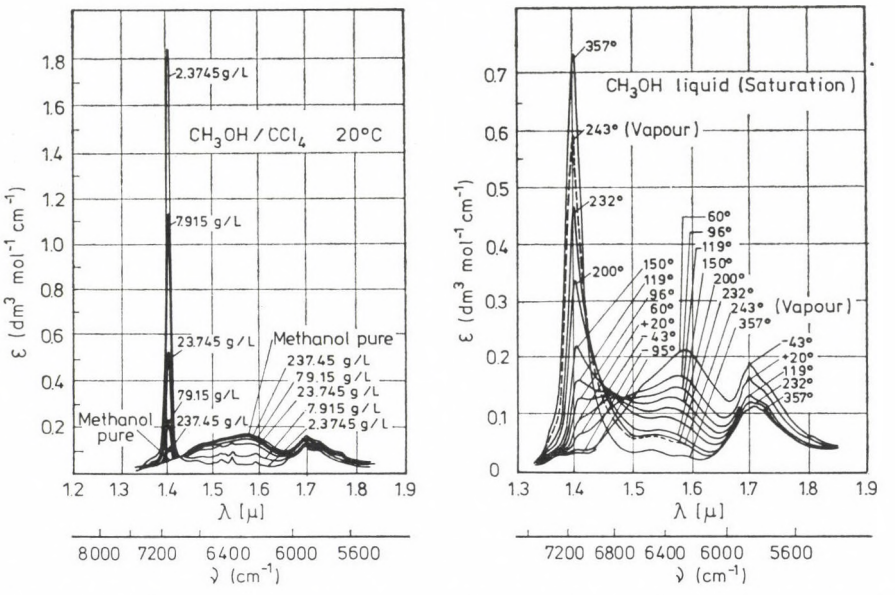

Fig. 9. Left: OH stretching overtone spectra of dilute methanol solutions showing the sharp peak of non-H-bonded OH groups. Right: same spectra of liquid methanol demonstrating the increase of the non-bonded OH groups with increasing T, peak heights are directly proportional to the content of "free" OH

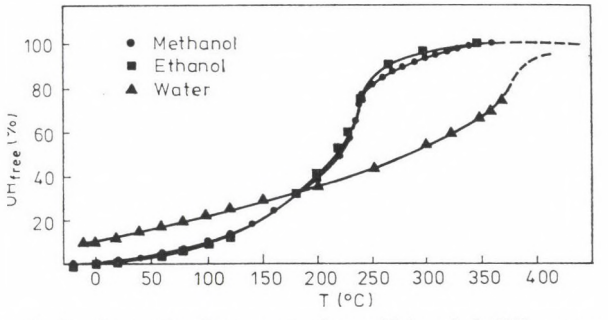

Fig. 10. Spectroscopically determined percent of non-H-bonded OH groups under saturation conditions [18]

The temperature dependence of OH_F allows us to estimate the H-bond energy [24]:

$$\Delta H'(\text{water}) = -3.7 \text{ (kcal/mol OH groups)} = -15.48 \text{ (kJ/mol OH groups)}$$

The total H-bond energy of water is: $\Delta H_H = 2 \cdot \Delta H' = 30.96$ kJ/mol; ΔH_H (methanol, ethanol) = —(4 kcal/mol) = —16.74 kJ/mol).

The ΔH_H-values of alcohols can be established by the IR spectroscopy of diluted solutions [25].

Table IV

Comparison between the total interaction energy ΔU_S, the H-*bond energy ΔH_H and van der Waals energies ΔW of liquids in kJ/mol*

	$\Delta U_S = \Delta H_S - RT$	ΔH_H	ΔW	$\Delta H_H/\Delta U_S$
water	48.53	30.96	17.57	64%
CH_3OH	39.6	16.74	22.9	42%
C_2H_5OH	47.5	16.74	31.03	35%
CH_4	8.4	—	8.4	0%

If we assume ΔH_H (solid) = ΔH_H (liquid), we can calculate the van der Waals energy ΔW of these three H-bonded liquids by ΔH_H and the heat of sublimation ΔH_s as the sum of all intermolecular interactions.

In Table IV the intermolecular interactions of H-bonded liquids are given in kJ/mol. Table IV demonstrates that the H-bonds play a dominant role for liquid water, but the van der Waals interactions should not be neglected [18] with their contribution of about one third of the total interaction energy.* This remark is not widely known. For instance the famous Stillinger potential of water for computer simulation has not taken this into account. For alcohols the H-bonds form only a smaller part of the total energy (see Table IV). The van der Waals energy of one OH group corresponds nearly to its value of about two CH_2-groups [26]. Therefore, the H-bonds in organic molecules play the role of an excess energy which may be dominant for instance in enthalpies of mixing [26].

Similar values of ΔH_H for water and alcohols seem to be contrary to the observed difference of O_F (see Fig. 10). Water has less H-bonds at T_m contrary to its content of two OH groups and similar ΔH_H-values. This can be explained on the basis of Eq. (8): the difference between water and alcohols lies in equal concentration of OH and lone pair electrons in water but an excess of 50% lone pairs in alcohols. If we increase the concentration of lone pairs relative to OH — the way nature does in alcohols — we shift the equilibrium Eq. (8) to the bonded state.

Importance of the repulsion term of H-bond

If the H-bonds with its angle dependence induce the coordination number 4 instead if 12, which we observe with dispersion forces of similar molecules, we could conclude an energy excess of $(\Delta H_H^2 + \Delta W')$ 4/2 compared with

* Jancsó, Bopp and Heinzinger calculated with a central force potential at the minimum of the Coulomb energy a ratio of non-coulombic to Coulombic energy: $\approx 1 : 5$ [Chem. Phys., **85,** 383 (1984)].

$\Delta W' \cdot 12/2$ ($\Delta W' = \Delta W/2$:van der Waals interaction of one OH in a water dimer).

But the result gives: ((—15.48 + (—8.78)) 2 (kJ/mol) = —48.52 kJ/mol compared with: $\Delta W' = (-8.78 \cdot 6)$ (kJ/mol) = —52.68 (kJ/mol). Based on this idea the H-bond structure with $Z = 4$ does not seem to be probable.

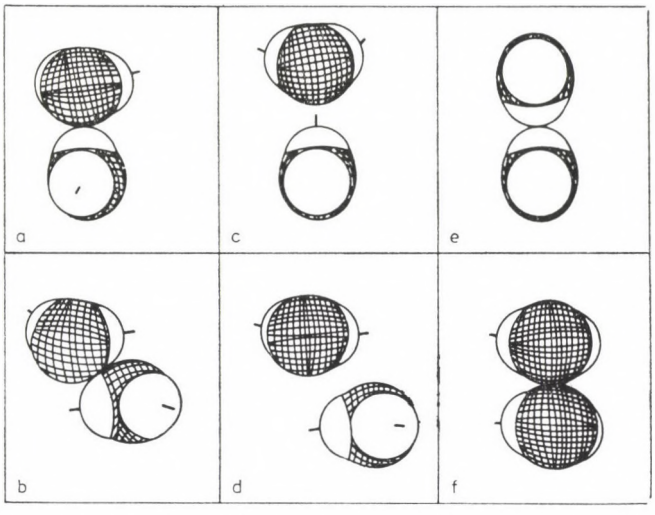

Fig. 11. H_2O dimer model of angle dependent interaction; a: Optimum H-bond, b: Angle-unfavoured antiparallel H-bond, c: Position (a) with longer distance, H-bond energy nearly vanishing, d: Position (b) with longer distance, H-bond energy nearly vanishing, e and f: H-bond repulsion

This shows that we should not neglect the repulsion effect of H-bonds of two protons or two lone pair electrons of neighbouring water molecules (in positions e or f of Fig. 11).

Contrary to the dispersion forces which given an attraction minimum in any direction, the H-bonds induce repulsion too at a distance of the normal H-bond minimum (in ice 2.47 Å). Figure 6 demonstrates this high repulsion with two opposite protons [13]. At small distances this repulsion is large compared with RT, the thermal energy. Consequently, such configurations could exist only very seldom and have to be excluded from the comparison between the H-bond structure with $Z = 4$ in water and the dispersion interaction with $Z = 12$. In statistics with any configuration with equal probability, half of the $Z = 12$ configurations should be canceled by the repulsions and would induce a total energy $\Delta W'$ smaller than (52.68 kJ/mol). The repulsion term enforces the coordination number of 4!

H-bonds could be called "Nebenvalenz". They are similar to valence forces for instance for H_2. The encounter of two H-atoms induces binding

in H_2 with a minimum in its potential curve if the spins are antiparallel and repel at any distance if their spins are parallel [27]. Similarly, two OH groups attract with a minimum of the intermolecular potential curve if one proton meets one lone pair and two OH groups induce a repulsion term at any distances if one proton meets another proton or one lone pair meets another lone pair.

The possibility to describe the H-bond interactions by the simple chemical equilibrium of Eq. (9) seems to be allowed because, like in a chemical bond, the energy is high compared with RT. The nearly isosbestic points in the IR spectra, the observation of one or a maximum of two relaxation times of liquid water establish this assumption. The necessity to describe liquids with a partition function, in the way present day research in liquids often claims, does not seem to be more preferred than in the description of the thermal movement by a partition function. We can approximate this by the average value of its temperature. The reason for partition functions for liquids is the same, namely: the Maxwell partition of the thermal energy. Why should we not apply the same method to use average values — averaged on the thermal partition — if we wish to describe the properties of liquids?

Caloric properties of liquids

We have applied the technique of calculated average values to the description of the abnormal properties of liquid water with good success [17, 18]. At the time of the calculations on water, we did not have enough data on alcohols till T_c. In the meantime we have such data on ethanol [29—34]. In the following section we will apply the same formulas for *ethanol* used in the calculations on water and demonstrate that the description of the caloric properties of ethanol is sufficiently good too.

a) *The specific heat*

We do not come across sufficiently simple theories on intermolecular influence on the specific heats, which are very important for liquids, for instance for liquid water $C_p = 18$ cal/mol compared with 8 cal/mol for ideal water vapour.

There is a very useful relationship to give the intermolecular part of specific heats both for nonpolar and H-bonded liquids: we assume [1, 18] that every molecular pair induces one degree of intermolecular vibration freedom leading to the intermolecular part of the specific heat as given below:

$$fZR/2$$

With this important and simple equation we describe the specific heat of nonpolar liquids as:

$$C_p = \frac{(12-3)}{2} R + C_p^\circ \tag{10}$$

(C_p°: specific heat of the ideal vapour as a measure of the intramolecular degrees of freedom).

$Z = 12$ would be valid for dense packing of sphere-like-molecules, the other packings and the higher order neighbours could be taken into acount by the factor f. The constant C_p° has to be corrected in condensed media by the disappearance of the translation by a factor of (3/2) R. At the saturation line we have to add a term for the energy which is needed to change the intermolecular energy. In the case of dominating H-bonds this gives a term $(dO_F/dT)\Delta H_H$, if O_F is the content of non H-bonded OH groups. The specific heat C_σ of ethanol at the saturation line of liquid ethanol is given by:

$$C_\sigma = \frac{(12-3)}{2} R + C_p^\circ + \frac{dO_F}{dT} \Delta H_H \tag{11}$$

In a first attempt to describe the specific heats of liquid ethanol [17] in a small T-region, we have chosen $Z = 8$, but during the detailed analysis based on newer and better experimental data we came to the conclusion that we should take $Z = 12$ for liquid ethanol. That would mean that the big contribution of dispersion forces induces the description with the normal packing of $Z = 12$.

Equation (11) does not need any further adjusted constants. We take our spectroscopically determined, T-dependent O_F-values [21] (Table V). For C_P°-values of the ideal vapour state we took known tabulated values [35, 36]: $C_p^\circ/R = 8.85$ (300 K); 10.55 (400 K); 12.1 (500 K) and 13.4 (600 K). The value at melting T has been extrapolated to 6.1; C_p°/R-values between the tabulated temperatures have been interpolated linearly.

Figure 12 shows a reasonably good agreement between the experimental values of the specific heat of liquid ethanol [31, 34] and our simple Eq. (11), which has been applied together with our spectroscopic O_F-values.

Table V

Spectroscopically determined content O_F of non H-*bonded* OH *in liquid ethanol*

T (°C)	−25	0	25	50	75	100	150	200	225	240	243
O_F (%)	0.3	0.5	2.4	3.3	5.8	9.2	20.8	41.5	56	75	77.5

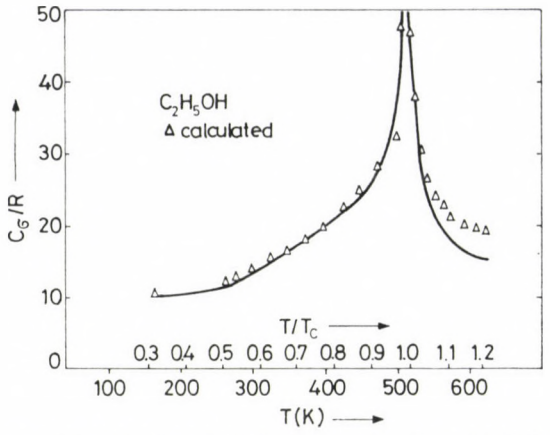

Fig. 12. Specific heats of liquid ethanol at the saturation line. (1) Full line: literature data [31, 34], (2): calculated equation (11)

Our spectroscopic data of O_F with its turning point at T_c are able to describe the big C_δ maximum at T_c. Similar good results are got for water too [18]. In this case we have measured the pressure dependence of O_F near T_c till 400 °C. With pressure higher as the critical one the H-bond equilibrium shifts to H-bonded OH groups and the turning point of O_F shifts at $T > T_c$ and becomes more flat. As consequence the C_σ-maximum shifts to higher T and becomes more flat.

The correctness of the assumption that $Z = 12$ is established by the agreement of the calculated and literature values and in addition by the value C_p (Liquid) $= 12.43\ R$ at T_m for ethanol given by Kelley [34]; at T_m: $(dO_F/dT) = 0$ and $(12.43 - 4.5)\ R = 5.9\ R$ corresponds to the literature value of $C_p^\circ(T_m)$.

Small deviations between our values of Eq. (11) and the literature values near T_c are expected. In this T-region we should add a non-linear T-term of the intermolecular term of the specific heat, which we have demonstrated with unpolar liquids [1].

Table VI demonstrates the high values of the specific heat per gram of liquid water. This uses the nature of the human body as mobile thermostat with a high heat capacity but low weight.

b) *Enthalpy of H-bonded liquids*

In a similar way we could calculate the enthalpy H_L of liquid water at equilibrium with its vapour [18]. The lower curve in Fig. 13 shows experimental values of H_L of liquid ethanol given till 390 K in [30] with $H_L\ (T_m) = 0$, at $T > 390$ K, values of Yukalovich [31] have been taken, standardized for

Table VI

Specific heats C_p of different liquids

	J/mol K	J/g K	T (°C)
H_2O	75.3	4.18	20
CH_3OH	77	2.38	20
C_2H_5OH	107	2.34	20
$CH_3-CO-CH_3$	124	2.13	20
$C_2H_5-O-C_2H_5$	172	2.32	20
$CHCl_3$	112	0.92	20
C_2H_6	71.5	2.38	−100
C_3H_8	96.7	2.18	−53

390 K. Based on our assumptions we would expect:

$$H_L = \frac{(12-3)}{2} R(T - T_m) + \bar{C}_p^{\circ}(T - T_m) + O_F \, \Delta H_H \qquad (12)$$

The nearly linear T-dependence of C_p° was taken into account by an average value: $\bar{C}_p^{\circ} = [C_p^{\circ}(T) - C_p^{\circ}(T_m)]/2$.

Like we have found with water [18], Eq. (12) agrees with the literatures values of H_L of ethanol fairly well (Fig. 13).

Contrary to water, the last term $O_F \, \Delta H_H$ in eq. (12) is smaller for ethanol. The reasons are: (1) the H-bond energy of ethanol is 4 kcal/mol and for water 2×3.7 kcal/mol = 7.4 kcal/mol; (2) and O_F of ethanol is smaller than that for water for $T < 200$ °C (Fig. 10). As a consequence, the role of H-bonds in the properties of ethanol is smaller than for water. In addition the coordination number of water is smaller with $(4 + O_F)$ (see [18]) but 12 for ethanol.

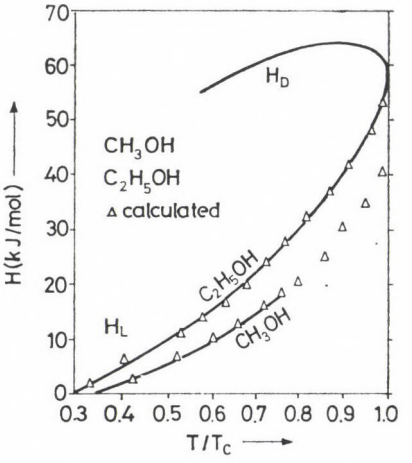

Fig. 13. Enthalpy of ethanol and methanol vapour (*D*) and liquid (*L*) in equilibrium; (1) Full line: literature data [30, 31], (2): calculated equation (12)

For ethanol we get the following values for $O_F \times \Delta H_H/H_L$: 2% (25 °C); 6.3% (100 °C); 11% (150 °C); 16.5% (200 °C) and 24% (240 °C). Corresponding values for water are about 50% and do not vary significantly with T [18].

The agreement with the H_L-values of the two different liquids with completely different behaviour increases the confidence in these simple equations (11) and (12) and in the spectroscopic interpretations. The eq. (12) can describe the enthalpy values of methanol too based on our O_F-measurements (Fig. 13). Unfortunately we have not found experimental values for methanol at higher T.

c) *The internal energy of evaporation*

Figure 14 gives the literature values [33] of the internal heat of evaporation ΔU_{vap} of CH_3OH and C_2H_5OH. These values of Mellon [32] agree with older data given at low T. The ΔH_{vap} values published by Yukalovich [31] seem unequivocally a little to high.

Our modell would give the following equation for ΔU_{vap}:

$$\Delta U_{vap} = \Delta H_{vap} - p\Delta V = \Delta U_s - O_F \Delta H_H - \frac{(12-3)}{2} RT + (1 - 2x_F) \times \frac{3}{2} RT - W_{real} \tag{13}$$

$\Delta U_s = 47.5$ kJ/mol: total intermolecular energy of ethanol, measured by the heat of sublimation (obtained by the extrapolation of ΔU_{vap} to 0 K to $\Delta U_{vap,0} = 42.5$ kJ/mol $+ \Delta U_m = 5$ kJ/mol (heat of fusion: ΔU_m)).

The RT 3/2 term in Eq. (13) gives the excitation of translation in the vapour state, its correction $2x_F$ considers the deviation from the linear T-

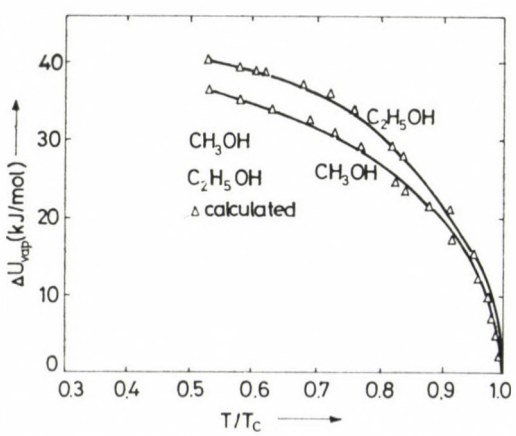

Fig. 14. Internal energy of ethanol and methanol vapourization [33]. (1) Full line: literature data, (2): calculated equation (13)

-dependence of the intermolecular thermal energy [1]. $\Delta U_{vap}+W_{real}$ calculates the vapourization to the ideal vapour state. W_{real} gives the intermolecular energy of the real gas. It has been calculated by:

$$W_{real} = C_p^\circ(T - 273) - [H_D(T) - H_D(273))] \tag{14}$$

H_D: enthalpy of the vapour phase [31].
Figure 14 demonstrates that Eq. (13) interprets the internal energy of vapourization of CH_3OH and C_2H_5OH sufficiently well, like a similar term could do for water too [17, 18].

d) *Surface energy*

Another abnormal property of H-bonded liquids is the surface energy U_σ. It is T-independent* for $T < 0.9\ T_c$ in the case of nonpolar liquids [1, 7], but has a T-maximum for H-bonded liquids like water, alcohols and carboxylic acids (Fig. 15). The reason is that at low T the weakest bonded areas in the liquid are transported to the enlarged surface. These are the van der Waals bonds between the hydrophobic groups of the alcohols. At higher T, "free" OH groups with higher van der Waals forces W_{OH} compared with the CH_2--contributions W_c are transported to the surface too. The surface energy U_σ of alcohols becomes [18]:

$$U_\sigma = W_c + O_F W_{OH} \tag{15}$$

This equation was able to predict that U_σ of alcohols should become T-independent at low T, because there O_F is nearly zero. Our own measurements of U_σ of different alcohols (Fig. 15) could establish this prediction and increase the confidence in our simplified models [18]. Equation (15) gives too the increase of U_σ with T. The surface energy of alcohols has at low T — if O_F can be neglected — similar behaviour as nonpolar liquids: a T-independence of U_σ. Normally more at high T the abnomal H-bond properties are canceled and all liquids become similar. But in the case of surface properties, the

Table VII

$U_\sigma = f(Z - X)^3_4 RT_c$

Stoffpaar	U_σ (Alkohol) / $\frac{3}{4} RT_c$ (paraffin)
C_2H_5OH/C_2H_6	2.85
n-C_3H-OH/C_3H_8	2.85
n-C_4H-OH/C_4H_{10}	2.85

* As consequence we have to assume that the specific heat are equal at the surface and in bulk.

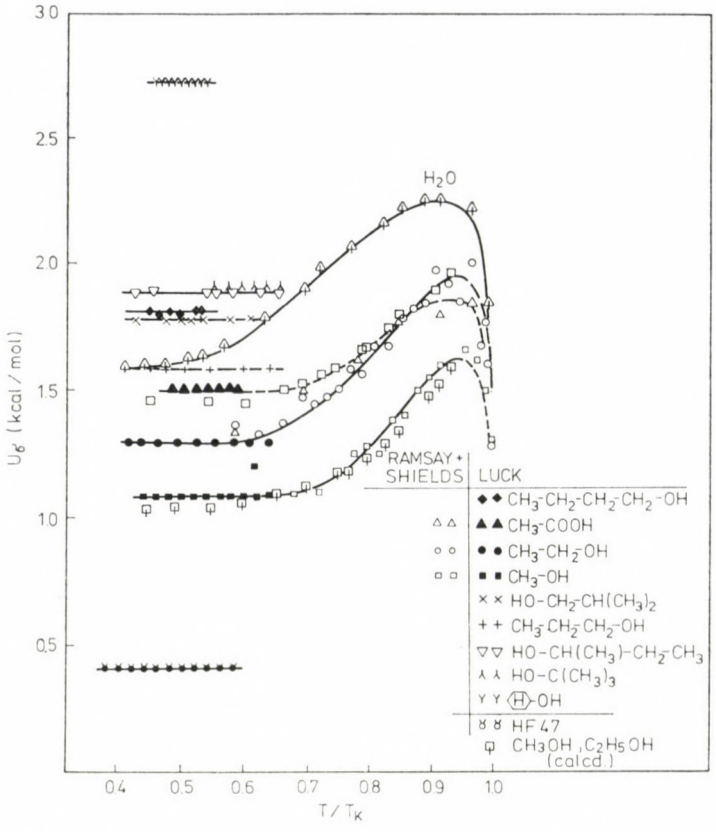

Fig. 15. Surface energy U_0 as a function of T over critical T_c, experimental and calculated values (Eq. 15)

weakest group dominates the behaviour. As consequence the surface energy of alcohols at low T is similar to the surface energy of the corresponding paraffin, or U_σ of alcohols at low T is given by T_c of its corresponding paraffin (see Table VII).

Therefore, the Stefan rule, the ratio Φ of the inner heat of vapourization to the surface energy U_σ gives a much higher value for H-bonded liquids compared with nonpolar ones [7] (at $T/T_c = 0.6$: $CH_3OH : \Phi = 7.4$; $C_2H_5OH : : \Phi = 7.1$; $H_2O : \Phi = 5.05$; $CCl_4 : \Phi = 2.85$). In this case of Φ H-bonds play an especially important role.

The energy partition function

The calculations based on the very simple Eqs. (11)—(15) have been unexpected successfully. H-bonded liquids depend on the partition function of distances and orientation angles. The IR spectra too demonstrate a certain

partition of H-bond energies with different frequency shifts $\Delta\nu$ and in addition to the solution spectra higher intensities in the region of low $\Delta\nu$ or low H-bond interactions are observed [18, 20, 36].

Why do we not need to take into account this partition of H-bond energies in Eqs (11)—(15)? We think that at unfavoured H-bond angles both O-atoms of one H-bridge could come closer together and induce higher van der Waals energies. Estimations of this effect show that the lost of H-bond energy by unfavoured H-bond angles could be nearly compensated by a gain in van der Waals energy [18]. The spectra are able to differentiate between both types of energies ΔH_H and W. If we plot [26] the internal energies of evaporation of ethanol from dilute solutions of different solvents as a function of the $\Delta\nu$-values (Fig. 16) we recognize that nonpolar solvents induce a much smaller $\Delta\nu$ compared with H-bond acceptor solvents. By this incident IR spectra are a useful tool to distinguish between H-bonds and van der Waals interactions. The content of non-H-bonded groups can be determined with the highest accuracy. The simplified adjustment of the energy partition function by a model of two different OH groups — bonded and "free" — seems to world because both OH groups seem to show two different energies: "free" OH have only van der Waals interactions and different bonded groups seem to have nearly similar total energies: $\Delta H''_H + W \approx \Delta H_H$. Bonds with lower $\Delta H''_H$ have greater W and vice versa.

Our results seem to be supported by the computer simulations. For instance Geiger has produced a movie of the time dependence of the water orientations calculated by computer simulation. He has shown that the OH groups oscillate around the H-bond potential minimum and very seldom

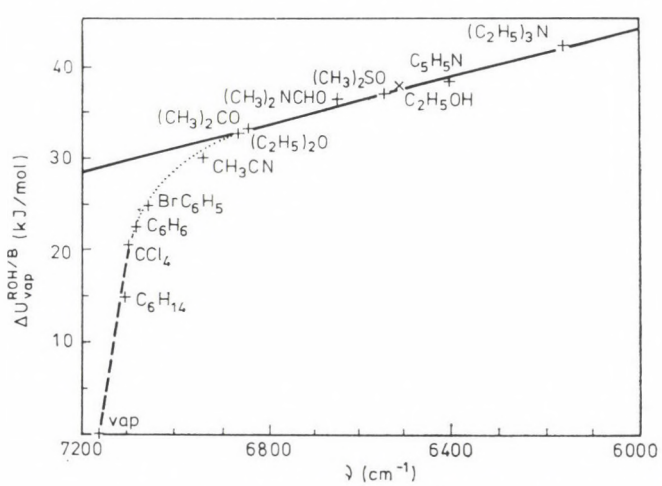

Fig. 16. Ethanol: Internal energy of vapourization $\Delta U_{vap}^{ROH/B}$ from dilute solution in different solvents as a function of the OH combination band frequency [2, 6]. Van der Waals shift much less than by H-bonds

escape this minimum. Correspondingly we observe a broad H-bonded band in our spectra which we could characterized by its band maxima which is related to the mean H-bond energy.

Mixture experiments

H-bonds play a dominant role in the abilities of mixing different liquids. In the case of nonpolar organic liquids the van der Waals forces between the groups of molecules are similar. That means that the pair potentials U_{12} between two unlike molecules 1—2 are similar to the potential of pure liquids: U_{11} or U_{12}. For dispersion forces we can assume: $U_{12} = (U_{11}U_{22})^{1/2}$. The heat of mixing is proportional to:

$$U_{\text{mix}} = (U_{11}U_{22})^{1/2} - (U_{11} + U_{22})/2 \tag{16}$$

The last term gives the energy which we need to solve the bonds in both pure liquids.

If we remember that:

$$|(U_{11}U_{22})^{1/2}| < |(U_{11} + U_{22})/2| \tag{17}$$

and the difference in Eq. (16) becomes greater with higher differences between U_{11} and U_{22}, we expect that U_{mix} of nonpolar liquids always gives endothermic values, if the distances between molecules ar similar in the mixture or in pure liquids. Experimental observations establish that there are a lot of endothermic mixtures and U_{mix} are of a similar order of magnitude. Exothermic mixtures should shorten the intermolecular distances by better packing. Another consequence of Eq. (16) is the demixing of nonpolar liquids in certain T- and p-regions as observed for instance in mixtures of rare gases too.

The mixture rule for U_{mix} could be completely different in mixtures of H-bonded liquids. The most favoured case is the mixing of a H-bonded liquid with aprotic solvent having high H-bond acceptor groups. In such a case mixing takes place without problems. On the other hand a mixture of two H-bonded substances like H_2O/phenol of H_2O/nicotine could give problems if $|\Delta H_{H11}| + |\Delta H_{H22}| > |\Delta H_{H12}|$2. Similar difficulties of mixing may arise if we mix an H-bonded liquid with a nonpolar liquid like in CCl_4/H_2O. The necessary opening of H-bond in such mixture would need too much energy compared with the van der Waals energy between CCl_4 and H_2O molecules. This effect may be reduced if aggregates of the H-bonded liquid are dissolved in the nonpolar solvents. This is favoured in the case of alcohols which have similar van der Waals interactions compared with the nonpolar solvents. As proof of this we

found that [25] U_{mix} of hexane/hexanol is directly proportional to the H-bond energy consumed.

Water also has van der Waals forces and they enable water to dissolve nonpolar molecules to a certain amount in such a way that no H-bonds have to be broken [37, 38]. But the van der Waals energy between H_2O/nonpolar solvent is not large enough to dissolve each other in great amounts; the formation of small water aggregates via the two OH groups cannot give nonpolar aggregates compared with alcohols.

Anions as H-bond acceptors

In the complicated description of mixtures of H-bonded liquids we can include aqueous electrolyte solutions. The ion interactions with acid protons or lone pair electrons seem to be similar to the H-bonds. The order of magnitude of anion . . . OH interaction energy seems to be similar to OH . . . OH interaction [38, 39 40], therefore, electrolyte solutions correspond to the mixture rules of two H-bonded liquids with similar H-bond energies.

This conclusion is in accordance with the spectroscopic results. The frequency shifts $\Delta\nu$ of water in crystalline hydrates are smaller or rather not too higher than in ice. From the so-called Badger—Bauer rule:

$$\Delta\nu \sim \Delta H_H$$

we can conclude on similar interaction energies of anions to OH (the disturbances of the lone pair electrons by cations influence the OH valence vibrations much less than the anion-proton effects). The similarity between the OH . . . base and OH . . . anion interactions is demonstrated by Figs. 17 and 18. Figure 17 shows the position and shift of the two water OH stretching bands ν_1 and ν_3 in socalled 1 : 1 complexes of one OH group of water with one base. Figure 18 shows the same plot for 1 : 1 interactions of one OH group of water with one anion measured in systems: water(CH_2Cl_2) salt/cryptate [40].

A difference between H-bond acceptors and anions is that in base acceptors the lone pair electrons of organic acceptors have the coordination number of one for H-bonds, whereas anions have higher coordination numbers for OH groups.

The apparant discrepancy between the statement of similar interaction energies OH . . . anions and OH . . . OH and the high hydration energies of salts in water can be explained if we suppose that the hydration energies are only given by a group of water molecules [37] and by spectroscopy we determine the interaction of an anion with one OH group and the cation . . . water interaction is found to be higher. Strong acids and bases induce much higher

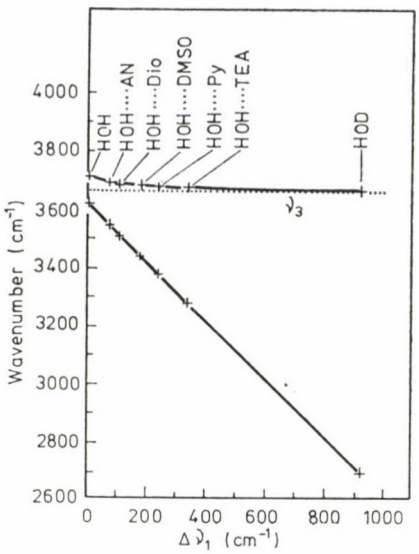

Fig. 17. Frequency of the symmetric ν_3 and asymmetric ν_1 stretching band of water in 1 : 1 complexes 1 H_2O : 1 solvent as a function of the frequency shift $\Delta\nu$ [41]. AN: acetonitrile, Dio: dioxane, DMSO: dimethyl sulfoxide, Py: Pyridine, TEA: triethylamine

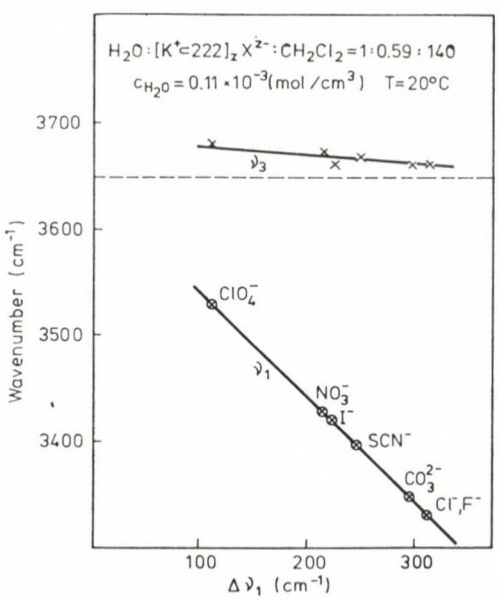

Fig. 18. ν_1 and ν_3 of water as a function of $\Delta\nu$ by different anions in diluted solutions: H_2O/salt/cryptate/CH_2Cl_2 [40]. Anions act similarly to H-bonds on OH spectra

interactions with water than salts. In addition the lifetime of an H-bond is reduced in such systems. Nature has a wide variety of factors to induce the scale of behaviour of mixtures and solutions: strengths of H-bonds, number of H-bonding groups, lifetime of H-bonds and the ratio of H-bonded groups to hydrophobic groups should all be considered. The role of H-bonds, however, seems to be a very important factor.

The H-bonds of NH groups could be described similarly to the OH groups but the spectroscopic experiments for NH are more difficult. In this paper we have discussed mainly liquids under saturation condition. In liquids at higher pressures than the saturation pressures p_s the equilibrium (8) is shifted to the bonded OH or NH groups. This can be established by IR spectroscopy too [42]. These measurements have shown that the turning point of the $O_F - T$ function at T_c is shifted to higher T under higher $p > p_s$. This clarifies the p-dependence of the maximum of the specific heat near T_c.

*

I thank my coworkers who helped me to bring some light in the complicated field of H-bonded systems especially W. Ditter, O. Schrems, H. Kleeberg, D. Schiöberg, W. Thiel and guests from foreign countries, namely, Buanam-Om, Thailand; O. Koçak, Turkey; Surjit Singh, India and H. Y. Zheng, China, gave interesting contributions to this paper.

REFERENCES

[1] Luck, W .A. P.: Angew. Chem., **91,** 408 (1979); Angew. Chem. Int. Ed. Engl., **18,** 350 (1979)
[2] Luck, W. A. P.: Ullmanns Enzyklopädie der techn. Chem., 4. Aufl., Verlag Chemie, Weinheim, Bd. **I** 1/1, S. 55—82 (1972)
[3] Morgan, P.: J. Phys. Chem., **34,** 2417 (1930)
[4] Bresler, E.: Acta Physicochim., **10,** 491 (1939)
[5] Luck, W. A. P., Zheng, H. Y.: J. Chem. Soc., Faraday Trans. 2, **80,** 1253 (1984)
[6] Luck, W. A. P., Zheng, H. Y.: Z. Naturforsch., **39a,** 888 (1984)
[7] Ditter, W., Luck, W. A. P.: Tetrahedron, **27,** 201 (1971)
[8] Eyring, H.: Z. Phys. Chem., **4,** 283 (1936)
[9] Cremer, E.: Z. Phys. Chem., **A 193,** 287 (1944)
[10] Luck, W. A. P.: "The Angle Dependence of Hydrogen-Bond-Interactions", in The Hydrogen Bond, Hrsg.: Schuster-Zundel-Sandorfy, Verlag North Holland Publ. Vol. **II.** Kap. 11 (1976) S. 527—562
[11] Luck, W. A. P.: Naturwissenschaften, **52,** 25, 49 (1965); ibid., **54,** 601 (1967)
[12] Clementi, E.: Lecture Notes in Chemistry, Vol. **2,** Springer Verlag 1976
[13] Thiel, W.: Theor. Chem. Acta, **48,** 357 (1978)
[14] Falk, M., Knop, O.: in "Water: Comprehensive Treatise" ed. F. Franks, Vol. **II,** p. 55. Plenum Press, New York 1973
[15] a) Narten, A. H., Danford, M. D., Levy, H. A.: Discuss. Faraday Soc., **43,** 97 (1967); b) Eisenstein, A., Gingrich, N. S.: Phys. Rev., **62,** 261 (1942)
[16] Luck, W. A. P.: Z. Elektrochem., **65,** 355 (1961)
[17] Luck, W. A. P.: Discuss. Faraday Soc., **43,** 115 (1967)
[18] Luck, W. A. P.: Angew. Chem., **92,** 29 (1980); Int. Ed. Engl., **19,** 28 (1980)
[19] Luck, W. A. P.: "Infrared Studies of Hydrogen Bonding in Pure Liquids and Solutions", in "The Hydrogen Bond in Water: A Comprehensive Treatise", ed. Felix Franks, Vol. **II,** p. 235, Chapter 4, Plenum, New York 1973
[20] Luck, W. A. P., Ditter, W.: Z. Naturforsch., **24b,** 482 (1969)
[21] Luck, W. A. P., Ditter, W.: Ber. Bunsenges. Phys. Chem., **72,** 365 (1968)
[22] Singh, S., Schiöberg, D., Luck, W. A. P.: Spectr. Lett., **14,** 141 (1981)
[23] Luck, W. A. P., Ditter, W.: Ber Bunsenges. Phys. Chem., **70,** 1113 (1966)

[24] Luck, W. A. P.: "Infrared Overtone Region", in "Structure of Water and Aqueous Solutions", Kap. **III**, 3., Verlag Chemie, Physik Verlag Weinheim 1974
[25] Schiöberg, D., Buanam-Om, C., Luck, W. A. P.: Spectr. Lett., **12**, 83 (1979)
[26] Kleeberg, H., Kocak, O., Luck, W. A. P.: J. Solution Chem., **11**, 611 (1982)
[27] Luck, W. A. P.: Z. Elektrochem., **61**, 1057 (1957)
[28] Volyak, L. D.: Teploenergetika, **7** (1958)
[29] Vargaftik, N. B.: "Tables on the Thermophysical Properties of Liquids and Gases" English Ed. J. Wiley and Sons, New York
[30] Engineering Sciences Data No. 79028, London 1979
[31] Yukalovich, M. P.: Teploenergetika, **2,** 70 (1960); **10,** 63 (1960)
[32] Mellan: Industrial Solvents Handbook, 2. Ed. Noyes Data Corp. Park Ridge (1977)
[33] Kelley, K. K.: J. Am. Chem. Soc., **51,** 182 (1929)
[34] Landold-Börnstein "Zahlenwerte und Funktionen" Vol. II, 4, (1961), Springer Verlag Heidelberg
[35] Zeise, H.: "Thermodynamik/Tabellen" Vol. **III**/1, Hirzel-Verlag Stuttgart 1954
[36] Luck, W. A. P.: Ber. Bunsenges. Phys. Chem., **85,** 959 (1981)
[37] Luck, W. A. P.: Schriftenreihe des Deutschen Wollforschungsinstitutes Aachen, **84,** 215 (1981) und in Flüssige Arzneiformen- und Arzneimittelsicherheit, hrsg. von D. Essig, P. Schmidt und H. Stumpf, Wissenschaftliche Verlagsges. mbH, Stuttgart 1981, S. 17—47
[38] Luck, W. A. P.: "Structure of Water and Aqueous Systems" in Synthetic Membrane Processes. Fundamentals and Water Applications, Ed. G. Belfort, pp. 21—72, Academic Press, New York 1984
[39] Buanam-Om, C., Luck, W. A. P., Schiöberg, D.: Z. Phys. Chem. Neue Folge, **117,** 19 (1979)
[40] Kleeberg, H., Luck, W. A. P.: J. Solution Chem., **12,** 369 (1983)
[41] Luck, W. A. P., Schiöberg, D.: Advan, Mol. Relax. Proc., **14,** 277 (1979)
[42] Luck, W. A. P.: Discuss. Faraday Soc., **43,** 135 (1967)
[43] Pálinkás, G., Bopp, P., Jancsó, G., Heinzinger, K.: Z. Naturforsch., **39a,** 179 (1984)

Acta Chimica Hungarica 121 (1—2), pp. 147—171 (1986)

MÖSSBAUER SPECTROSCOPY APPLIED TO SOLUTION CHEMISTRY+

STEEN MØRUP* and Jørgen E. KNUDSEN**

(Laboratory of Applied Physics II, Technical University of Denmark, DK-2800 Lyngby, Denmark)

Received January 18, 1985

The application of Mössbauer spectroscopy to studies of solution chemistry is discussed. Since Mössbauer spectra can only be obtained after freezing of the solutions the first part of the paper deals with the freezing process and the relation between the structure of the liquid and that of the frozen solution. In the second part of the paper we discuss complex formation in solutions of Fe^{3+}, emphasizing the information which can be obtained from paramagnetic hyperfine split Mössbauer spectra of solutions dilute in Fe^{3+} ions. Specifically, complexes of the type $[Fe(H_2O)_{6-n}Cl_n]^{3-n}$ and $[Fe(H_2O)_{6-n}F_n]^{3-n}$ are discussed. Moreover, some examples of studies of tetrahedral complexes and dimeric complexes are given. Finally it is illustrated how Mössbauer spectroscopy can be used to obtain information about the dynamic properties of highly viscous supercooled liquids.

Introduction

Mössbauer spectroscopy is a technique which allows measurements of the electric and magnetic interactions between an atomic nucleus and its surroundings. Specifically, it gives information about the electron density at the nucleus (via the isomer shift), the electric field gradient at the nucleus (via the nuclear quadrupole splitting), and the magnetic field at the nucleus (via the nuclear Zeeman splitting). Therefore, the technique gives information on important parameters such as the valence state of the atoms, the coordination numbers, the distribution of charge around the nucleus, and the magnetic properties of the material which is investigated.

Since Mössbauer spectroscopy is based on recoil-free emission and absorption of gamma radiation it can in general only be used for studies of solids and not gases or liquids. Consequently, Mössbauer spectroscopy cannot be directly used for studies of solutions. Solutions can easily be studied after they are frozen, but the structure of the frozen solutions may, however, not be identical to that of the liquid. For example, in many systems some crystallization takes place even if the solutions are cooled very rapidly, and the structure

* To whom correspondence should be addresse.
** Present address: Dansk Olie og Naturgas, DK-2950 Hørsholm, Denmark
+ This paper was presented at the Symposium on Structure of Liquids and Solutions at Veszprém, August 27—30, 1984.

will then of course be very different from that of the liquid. Crystallization may be avoided by adding an appropriate glass-forming agent to the solution combined with a sufficiently high cooling rate. The liquid then solidifies as an amorphous phase with a structure which is presumably very similar to that of the liquid. In the first part of the paper we discuss how Mössbauer spectroscopy can be used for studies of the formation of crystalline and amorphous phases during the freezing process.

Mössbauer spectroscopy has been extensively used for studies of frozen solutions. Since the discovery of the Mössbauer effect about 400 papers have been published on the subject. The pioneering work was made by the Hungarian scientists I. Dézsi, L. Keszthelyi, A. Vértes, and their co-workers [1—4]

A comprehensive review of Mössbauer spectroscopy studies of frozen solutions has recently been published by Vértes et al. [5].

Most of the Mössbauer work has been done using the isotope ^{57}Fe and in the present paper we only discuss studies of iron complexes in solution. A section is devoted to studies of complex formation in solution, emphasizing investigations of solutions with very low concentrations of Fe^{3+}, which allow observation of paramagnetic hyperfine split Mössbauer spectra. Such spectra give very detailed information about the Fe^{3+} complexes present in the solution.

Finally, in the last section we briefly discuss how Mössbauer spectroscopy can be used for studies of the dynamic properties of supercooled liquids.

Studies of crystallization and glass formation

In frozen solutions of Fe^{3+} complexes, the sensitivity of Mössbauer spectroscopy to paramagnetic relaxation effects may, as discussed below, be used for studies of crystallization and glass formation.

The magnetic interaction between a ^{57}Fe nucleus and the atomic electrons can often be described in terms of an effective magnetic field acting at the nucleus. In paramagnetic materials this magnetic hyperfine field varies both in size and direction because of paramagnetic relaxation processes. If the relaxation time, τ, of these fluctuations is of the order of 10^{-7}—10^{-10} s the Mössbauer spectra are very sensitive to the relaxation process. If $\tau < 10^{-10}$ s the magnetic interaction cannot be observed by Mössbauer spectroscopy and then only the electric interaction can be detected. When $\tau > 10^{-7}$ s the spectra reflect a static magnetic interaction. For intermediate values of τ, the lines of the spectra are broadened.

Two types of relaxation processes may contribute to the relaxation, namely spin-spin relaxation and spin-lattice relaxation. The spin-spin relaxation is due to magnetic interactions among the paramagnetic ions. Therefore the spin-spin relaxation frequency increases with increasing concentration of

paramagnetic ions. Spin-lattice relaxation is induced by the interactions of lattice vibrations (phonons) with the magnetic moments of the paramagnetic ions. The spin-lattice relaxation frequency increases with increasing temperature. Often spin-lattice relaxation of Fe^{3+} ions is so slow that it is negligible below 80 K. Reviews of Mössbauer studies of relaxation effects have recently been published [6, 7].

It is interesting that the sensitivity of Mössbauer spectroscopy to spin-spin relaxation can be used for studies of crystallization and glass formation during freezing of solutions. The reason is that the local concentration of paramagnetic ions determines the spin-spin relaxation time [8].

It order to illustrate the sensitivity of Mössbauer spectra to the Fe^{3+} concentration we show in Fig. 1 spectra obtained at 80 K of frozen aqueous solutions of $Fe(NO_3)_3$ in different concentrations. The amount of nitric acid was adjusted to $[Fe(NO_3)_3] + [HNO_3] \approx 7$ *M* in order to ensure formation

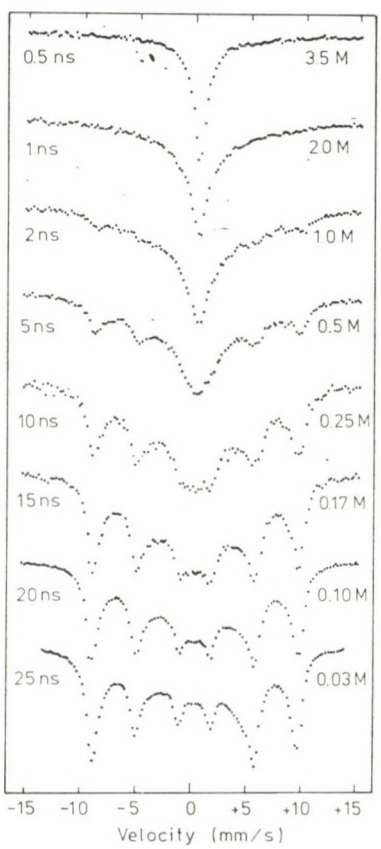

Fig. 1. Mössbauer spectra of some aqueous $Fe(NO_3)_3 + HNO_3$ glasses. The iron concentration is indicated. An estimate of the relaxation time is given

of homogeneous glasses (see below). The numbers on the left side of the figure are the approximate relaxation times estimated from the spectra. These measurements clearly illustrate that the spectra are very sensitive to the concentration of Fe^{3+} ions. For spectra with a relaxation time shorter than about 5 ns the line width of the spectra may serve as a parameter which reflects the relaxation time and therefore also the concentration.

In order to study crystallization and glass formation during freezing of solutions, Mørup et al. [8] studied a number of aqueous solutions of $FeCl_3$ with different concentrations x, given in mol $FeCl_3$ per 100 mol H_2O. The absorbers were frozen by immersion into liquid nitrogen and the freezing time, i.e., the time needed for cooling from room temperature to liquid nitrogen temperature was about 10 s. Mössbauer spectra were obtained at 80 K in applied fields of 1.24 T and in the remanent field of the electromagnet which was about 0.005 T.

In Fig. 2 is shown the line width at the two different applied magnetic fields as a function of the concentration of $FeCl_3$. The increase in the line width with increasing field is due to an increase in the spin-spin relaxation time. This effect is related to the amorphous nature of the iron-containing phases and has been discussed elsewhere [6—9]. A study of the temperature dependence of the spectra has shown that spin-lattice relaxation can be neglected at 80 K. In Fig. 2 the line width is shown for rapidly frozen absorbers and also after a subsequent heating of the absorbers to 200 K for one hour. Before the heating at 200 K the Mössbauer line width (and thus the spin-spin relaxation time) of the absorbers exhibits a pronounced maximum for $x \simeq 3.5$.

By visual inspection it was found that the absorbers with $x > 3.5$ were transparent with some cracks, indicating that a glassy state was formed by rapid cooling of these absorbers. However, the less concentrated absorbers were opaque and seemed to contain a large number of small crystals. Heating of the absorbers with $x < 5.5$ to 200 K for one hour resulted in a change in their visual appearance indicating some crystallization, whereas the more concentrated absorbers were unaffected by this treatment.

In the fast frozen absorbers with $x \geq 3.5$ the line width decreases with increasing iron concentration in accordance with the expected influence of spin-spin relaxation in a system with a uniform distribution of paramagnetic ions. These absorbers therefore seem to be glasses with a uniform distribution of ferric ions. None of the spectra of these absorbers showed any trace of the spectrum of crystalline $FeCl_3 \cdot 6\ H_2O$.

Before heating to 200 K, all the absorbers with $x \leq 3.0$ showed identical Mössbauer line widths, namely about 1.6 mm/s at $B = 0.005\ T$ and 3.3 mm/s at $B = 1.24\ T$. These values are identical with those of a homogeneous glass with $x \simeq 5.5$ (see Fig. 2). The results therefore indicate that before heating to 200 K the iron is found in amorphous regions with a composition corre-

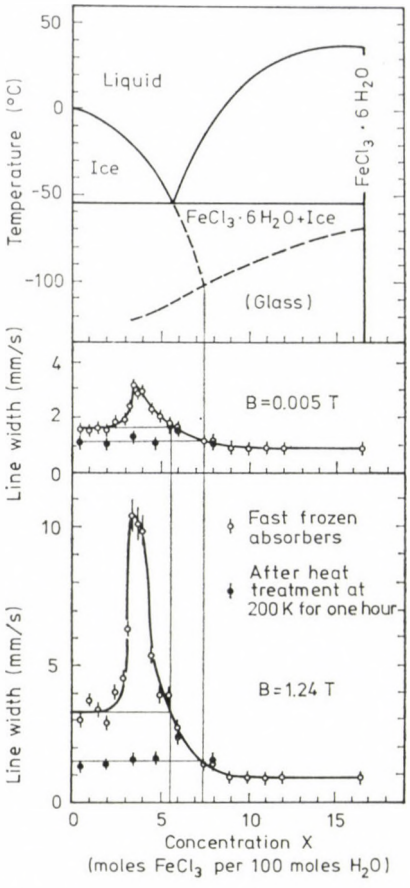

Fig. 2. The upper part of the figure shows the phase diagram of the $FeCl_3-H_2O$ system. The dotted lines indicate the metastable phase diagram including the extrapolated hypoeutectic liquids curve and the glass curve. In the lower part of the figure is shown the Mössbauer line width (FWHM) of frozen aqueous solutions of $FeCl_3$ at 80 K at applied fields of 0.005 T and 1.24 T as a function of the concentration (adapted from [8])

sponding to $x \simeq 5.5$, independent of the initial composition of the solutions. Similar results have been found in studies of frozen aqueous solutions of $Fe(ClO_4)_3$ [10].

After heating to 200 K for one hour and recooling to 80 K the Mössbauer spectra of the samples with $x < 5.0$ had changed irreversibly, whereas the spectra of the more concentrated samples were unaffected by this treatment. For all the spectra with $x < 5.0$ the line width decreased to about 1.2 mm/s at 0.005 T and 1.5 mm/s at 1.24 T. These values are identical to those of a homogeneous glass with $x \simeq 7.3$ and this suggests that the Fe^{3+} ions are present in a glass with a local concentration corresponding to $x \simeq 7.3$ in all these samples.

On the basis of these observations a simple model can be evaluated for the kinetics of the freezing process in the $FeCl_3$—H_2O system [8]. When a sample of an initial concentration of $x < 3.0$ is cooled, nucleation and growth of ice crystals start at a certain supercooling. As the temperature is decreased the crystal growth continues, while the iron concentration in the liquid increases following a curve below the hypoeutectic liquidus curve of the equilibrium phase diagram. The detailed relation between temperature and composition of the liquid presumably depends on the freezing rate. At a certain temperature T_0 and a certain composition of the liquid, x_0, the crystal growth rate becomes slow compared to the cooling rate and eventually the remaining liquid solidifies into a glass with the iron concentration $x \simeq x_0$. According to this model, samples with different initial concentration $x < 3.0$ will only differ with respect to the amount of ice, when cooled to the temperature T_0, but not with respect to the composition of the glass. This explains why samples, in which ice crystallized during cooling, all have the same iron concentration in their glassy phase, when cooled at the same cooling rate. The local iron concentration in the glass phase of the absorbers frozen in about 10 s is $x_0 \simeq 5.5$.

After heat treatment for one hour at 200 K (which is above the glass temperature, T_g) and recooling to 80 K, the spectra indicate that the Fe^{3+} ions are present in amorphous regions with a local concentration corresponding to $x = 7.3$. Furthermore, it was observed that the absorbers with $3.5 < x < 5.0$, which initially were glassy, became opaque during the heat treatment. Therefore, it can be concluded that both nucleation and growth of ice crystals do take place in these samples at 200 K, when sufficient time is available.

Since $FeCl_3 \cdot 6\ H_2O$ did not crystallize in any of the samples discussed here, the state of the dilute absorbers at 200 K may be found from the extrapolated liquids curve shown in Fig. 2. When the samples are recooled slowly (cooling time for cooling to 80 K was about 30 min), growth of ice crystals may take place, while the concentration of the liquid follows the extrapolated liquidus curve. During slow cooling the crystal growth terminates at a certain temperature, which is supposed to be close to the glass temperature of the liquid. In fact, it is seen in Fig. 2 that the local concentration, $x \simeq 7.3$, of the heated absorbers is close to the concentration at the intersection of the extrapolated liquids curve and the glass curve. Thus, the results can be explained on the basis of the metastable phase diagram shown by the dotted lines in Fig. 2.

The role of the freezing rate has also been studied by freezing a number of absorbers of identical composition (0.5 M $Fe(NO_3)_3$, 2.0 M HNO_3 and 3.0 M $NaNO_3$) at various freezing rates by changing the thermal contact to the liquid nitrogen bath [8]. During cooling, the temperature was measured with a thermocouple inside the absorber (expect for the fastest rate $r \simeq 5000$ K/min, which was obtained by dipping into liquid nitrogen pieces of filter paper

wetted by the solution. The freezing rate, r, was defined as the average rate in the temperature range 273 — 125 K. For these samples it was found that there exists a critical rate, $r = r_0$, 220 K/min $< r_0 <$ 570 K/min. The quickly frozen absorbers ($r > r_0$) had a glassy appearance and showed identical Mössbauer spectra, indicating that they consists of homogeneous glasses, whereas the slowly frozen absorbers ($r < r_0$) were opaque and showed identical spectra with less resolved magnetic hyperfine splitting indicating that some crystallization of ice had taken place during the freezing.

Studies of a number of samples with different glass formers have shown that glycerol seems to give a quite homogeneous glass, and glycerol is therefore commonly used as a glass former in Mössbauer studies of frozen solutions. It has also been found that glass formers such as nitrates, perchlorates and glycerol do not affect the complexes of Fe^{3+} in the solutions [8].

The measurements discussed in this section illustrate how the sensitivity of Mössbauer spectroscopy to spin-spin relaxation can be used to obtain information on crystallization and glass formation during cooling of solutions of ferric ions. The results indicate that both the composition of the solutions (the amount of glass forming agents) and the cooling rate are parameters which have a strong influence on the structure of the frozen solutions.

When the solutions contain a suitable amount of glass forming agents and the cooling rate is sufficiently high, a homogeneous glass is formed during freezing.

The structure of this glass is presumably closely related to the structure of the liquid.

Complex formation in solution

A major part of the publications on Mössbauer studies of frozen solutions deal with the nature of the complexes formed by Fe^{2+} and Fe^{3+} ions. In this section we shall mainly discuss the information that can be obtained from magnetically split spectra of dilute solutions of Fe^{3+}. Such spectra give very detailed information about the spin Hamiltonian of the Fe^{3+} ions and, therefore the coupling of the ligands to the Fe^{3+} ions can be elucidated.

The spin Hamiltonian, $\hat{H}$, of a Fe^{3+} ion in the high spin state ($S = 5/2$) is composed of terms due to the crystal field interaction, $\hat{H}_{cf}$, the electronic Zeeman interaction, $\hat{H}_Z$, the magnetic dipole interaction between the Mössbauer ion (i) and the neighbouring ions or ligands (j), $\hat{H}_{dd}$, the exchange interaction with neighbouring ions, $\hat{H}_{ex}$, the magnetic hyperfine interaction, $\hat{H}_{hf}$, and the nuclear quadrupole interaction, $\hat{H}_Q$ [11, 12]:

$$\hat{H} = \hat{H}_{cf} + \hat{H}_Z + \hat{H}_{dd} + \hat{H}_{ex} + \hat{H}_{hf} + \hat{H}_Q \qquad (1)$$

where

$$\hat{H}_{\mathrm{cf}} = D\left[\hat{S}_z^2 - \frac{1}{3}S(S+1) + \lambda(\hat{S}_x^2 - \hat{S}_y^2) + \right.$$
$$\left. + \frac{1}{6}a\left(\hat{S}_\xi^2 + \hat{S}_\eta^2 + \hat{S}_\zeta^2 - \frac{707}{16}\right)\right] \tag{2}$$

$$\hat{H}_{\mathrm{Z}} = g\mu_B \vec{B}\cdot\hat{\vec{S}} \tag{3}$$

$$\hat{H}_{\mathrm{dd}} = \sum_{j\neq i}\hat{H}_{ij} = \frac{\mu_0}{4\pi}\sum_{j\neq i} g_i g_j \mu_B^2 r_{ij}^{-5}[\hat{\vec{S}}_j r_{ij}^2 - 3r_{ij}(\hat{\vec{S}}_j\cdot\vec{r}_{ij})]\cdot\hat{\vec{S}}_i \tag{4}$$

$$\hat{H}_{\mathrm{ex}} = -\hat{\vec{S}}_i\cdot\sum_{j\neq i} 2J_{ij}\vec{S}_j \tag{5}$$

$$\hat{H}_{\mathrm{hf}} = A\hat{\vec{S}}\cdot\hat{\vec{I}} \tag{6}$$

$$\hat{H}_{\mathrm{Q}} = P\left[\hat{I}_z^2 - \frac{1}{3}I(I+1) + \frac{1}{3}\eta(\hat{I}_x^2 - \hat{I}_y^2)\right] \tag{7}$$

Often the magnetic hyperfine coupling constant A is expressed in terms of the saturation hyperfine field B_0 (for the $S_z = 5/2$ state. It is convenient to define the parameters Δ_{cf} and Δ_{Z} as the total energy splittings due to $\hat{H}_{\mathrm{cf}}$ and $\hat{H}_{\mathrm{Z}}$, respectively.

$\hat{H}_{\mathrm{cf}}$ gives rise to a splitting of the ionic ground state into three Kramers doublets. The eigenstates of the electronic system depend critically on small perturbations that lift the degeneracy. For $\hat{H}_{\mathrm{Z}} = \hat{H}_{\mathrm{dd}} = \hat{H}_{\mathrm{ex}} = 0$, the hyperfine interaction alone lifts the degeneracy. The spectrum is then very sensitive to the values of the parameters λ and $\mu = a|D$. The magnetic hyperfine interaction gives rise to a splitting of the order of 10^{-8} eV. Therefore, applied magnetic fields of the order of only 0.001 T result in a Zeeman splitting of the ionic states of the same size. Such fields therefore have a significant influence on the eigenstates and are in fact difficult to avoid. For instance, the dipolar fields from the ligand nuclei can easily be of this order of magnitude and the dipolar fields due to the neighbouring paramagnetic ions may be considerably larger. If a field of about 0.01 T is applied, the Zeeman interaction is large compared to the hyperfine interaction. Then the electronic eigenstates are essentially determined by $\hat{H}_{\mathrm{cf}}$ and $\hat{H}_{\mathrm{Z}}$ and the Mössbauer spectrum consists of three Zeeman components each described by an effective magnetic field. When the electronic Zeeman splitting is comparable to the crystal field splitting, the electronic eigenstates, and therefore also the size and direction of the hyperfine fields, depend on the relative size of Δ_{cf} and Δ_{Z}. Finally, for $\Delta_{\mathrm{Z}} \gg \Delta_{\mathrm{cf}}$, the electronic eigenstates are essentially determined by $\hat{H}_{\mathrm{Z}}$. In this simple case the Mössbauer spectrum can essentially be described in terms of

six Zeeman split spectra with magnetic hyperfine fields in the ratio 5 : 3 : 1 arising from the electronic states $S_z = \pm 5/2, \pm 3/2, \pm 1/2$, respectively.

An investigation of the spectrum as a function of the applied field allows a determination of the parameters of the spin Hamiltonian [13, 14].

A detailed study of the ferric hexaaqua complex $[Fe(H_2O)_6]^{3+}$, in frozen aqueous solutions has been performed by Knudsen [13—15]. He prepared several absorbers with low concentrations of Fe^{3+} and studied the magnetic field dependence of the spectra at 78 K and at 4.5 K. The samples were prepared with different glass formers (e.g. gylcerol and different nitrates) in order to ensure formation of homogeneous glasses.

Typical spectra of an absorber containing 0.03 *M* $Fe(NO_3)_3$, 0.5 *M* HNO_3 and 5.4 *M* $LiNO_3$ as a glass forming agent are shown in Fig. 3. The

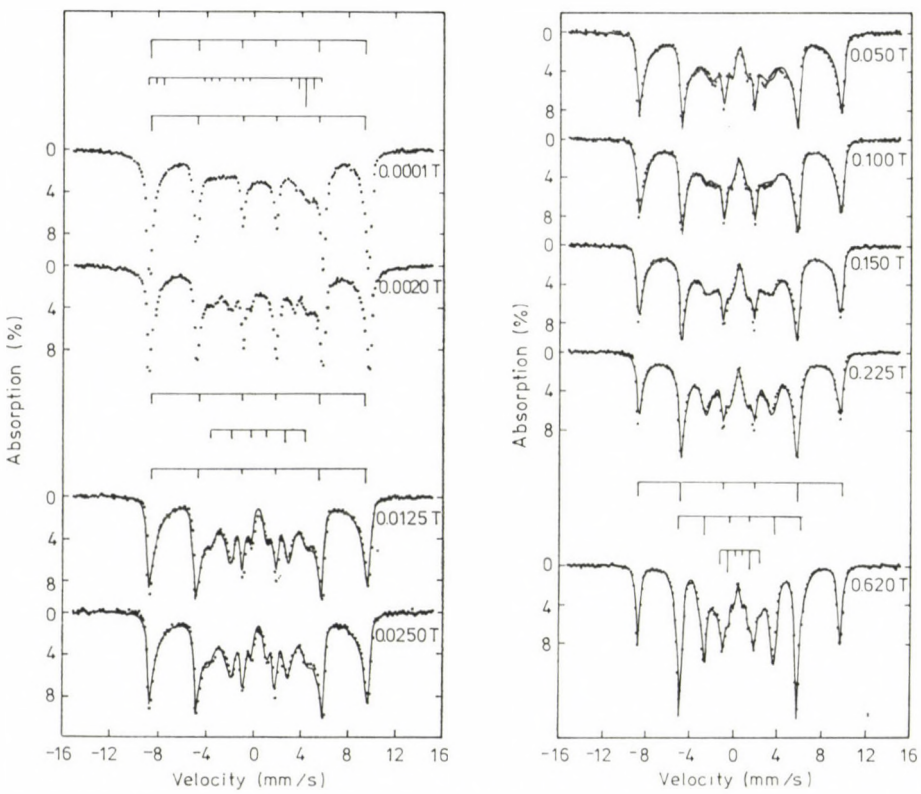

Fig. 3. Mössbauer spectra of an absorber of a frozen aqueous solution with 0.03 *M* $Fe(NO_3)_3$, 0.5 *M* HNO_3, 5.4 *M* $LiNO_3$ obtained at 4.5 K with various applied transverse magnetic fields. The full curves show theoretical fits. The bar diagram above the 0.0001 *T* and the 0.0125 *T* spectra show a simplified interpretation in terms of spectra related to the three Kramers doublets. The bar diagram above the 0.620 *T* spectrum shows an interpretation in terms of three magnetically split spectra with hyperfine fields in the ratio 5 : 3 : 1. The line intensities are indicated by the lengths of the bars (Reprinted with permission From J. Phys. Chem. Solids, **38,** 883 (1977), Pergamon Press [14])

spectra were obtained at 4.5 K. At $B = 0.0001$ T the spectrum essentially consists of an asymmetric component superimposed on a six-line component.

The spectra are drastically changed when the applied magnetic field is increased. For $B \gtrsim 0.01$ T the spectra are symmetric. It was found that the spectra obtained at 0.0125 T and 0.0250 T are essentially identical, but at larger applied fields the spectra again change with the applied field.

Qualitatively, the results are in accordance with a crystal field Hamiltonian with the parameters $D \simeq 0.10$ cm^{-1}, $\lambda \simeq 0.26$ and $a \simeq 0.017$ cm^{-1}. The spectrum obtained with $B = 0.0001$ T can be explained by two magnetically anisotropic Kramers doublets and an isotropic doublet [13, 14]. The bar diagrams above the spectrum indicate theoretical line positions. A detailed study of the low-field spectra has shown that the line positions of the isotropic doublet are affected by random dipolar fields of the order of 0.0006 T from neighbouring atoms [15].

For $A \ll g\mu_B B \ll \Delta_{cf}$ the spectrum is stabilized and is not expected to depend on the external field. This situation is achieved for applied magnetic fields of the order of 0.01—0.03 T. At applied magnetic fields in this range the spectrum consists of the three six-line components indicated by the bar diagram shown above the 0.0125 T spectrum.

For $B > 0.05$ T the electronic Zeeman interaction becomes comparable to Δ_{cf} and therefore the spectrum again changes with the applied magnetic field. The spectrum obtained with $B = 0.62$ T indicates that Δ_Z can be considered much larger than Δ_{cf} and this spectrum essentially consists of three six-line components with hyperfine fields in the ratio 5 : 3 : 1 (indicated by the bar diagrams).

A detailed analysis of the spectra showed, however, that completely satisfactory fits could not be made with such a model. This is illustrated in Fig. 4 which shows the experimental spectrum obtained at 0.0250 T together with a theoretical spectrum calculated by use of the spin Hamiltonian parameters given above. Clearly, the line shape of the outer lines as well as the intensity ratios indicate that the theoretical model is unable to explain the experimental results.

It was therefore attempted to fit the spectra with a model in which a distribution of crystal field parameters was assumed. Such a distribution may in fact be expected in an amorphous sample because of the variation in the surroundings of the ferric ions in an amorphous phase. The best fits of the spectra (shown by the solid lines in Fig. 3) were obtained with the parameters:

Saturation hyperfine field $B_0 = 58.5$ T; quadrupole coupling constant, $P = 0$ mm/s; isomer shift, $\delta_{Fe} = 0.50$ mm/s; line width $\Gamma = 0.34$ mm/s. Crystal field parameters: $\langle D \rangle = 0.10$ cm^{-1}; $\sigma_D = 0.02$ cm^{-1}, $|\langle \lambda \rangle| = 0.20$, $\sigma_\lambda = 0.10$, $a = 0.017$ cm^{-1}; $\sigma_a = 0$.

In the fits the values of D and λ were assumed to have Gaussian distributions with the indicated standard deviations.

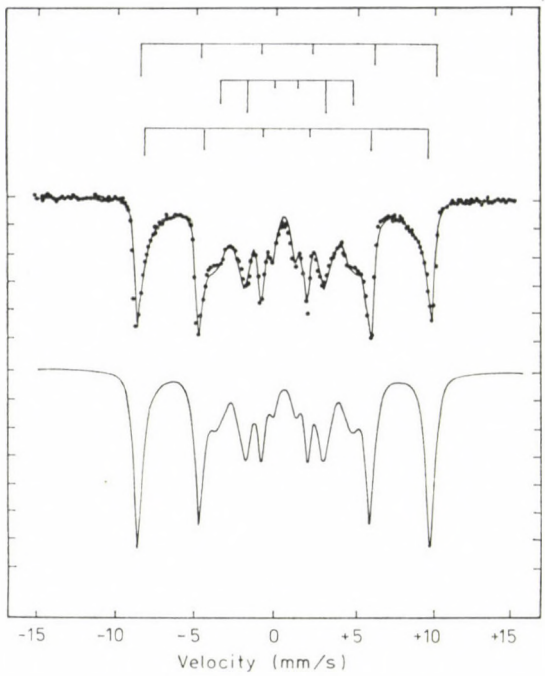

Fig. 4. Mössbauer spectrum of the ferric hexaaqua complex in frozen aqueous solution, obtained at 4.5 K with an applied field of 0.025 *T*. The curve below the experimental spectrum shows the best fit obtained with sharply defined crystal field parameters. The curve shown together with the experimental spectrum is the best fit obtained by admitting a spread in the crystal field parameters

The fits show that the spectra can be explained in detail with this model. The low-field spectra can also be fitted with the same crystal field parameters [15].

These studies of the $[Fe(H_2O)_6]^{3+}$ complex illustrate that quite detailed information on Fe^{3+} complexes with slow paramagnetic relaxation can be obtained. It is of particular interest that the variation in the local environments of the Fe^{3+} ions can be studied by this method.

The method has been applied in an investigation of Fe^{3+} complexes extracted by diethyl ether from aqueous solutions with 0.03 *M*—0.1 *M* $Fe(NO_3)_3$ and 6 *M* HCl, 6 *M* HBr, or 0.5 *M* NH_4SCN. In these three absorbers the ether serves a double purpose as a complex extractant and as a glass former when freezing the absorber. Spectra obtained at 5 K of the frozen absorbers are shown in Figs. 5—7 together with fits calculated from the spin Hamiltonian formalism of Eqs (1)—(7).

The well resolved paramagnetic hyperfine splittings show that the Fe^{3+} complexes are extracted as monomers.

The key parameters of the fits are given in Table I. The values of the isomer shifts δ_{Fe} and the saturation hyperfine fields B_0 show definitively that

Cl^- and Br^- are extracted as tetrahedral complexes, whereas SCN^- is extracted octahedrally.

For the tetrahedral complexes, $FeCl_4^-$ and $FeBr_4^-$, the hyperfine field decreases significantly with increasing covalency of the chemical bond, whereas

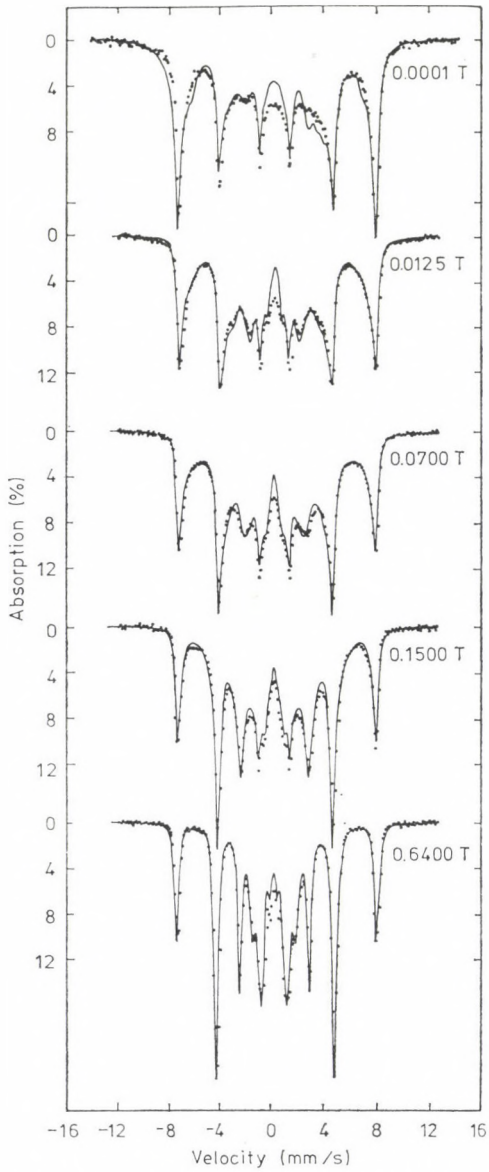

Fig. 5. Mössbauer spectra of an absorber frozen from an ether extracted solution of Fe^{3+} and Cl^-. The spectra were obtained at 5 K with various applied magnetic fields. The curves show the best fits obtained within the spin Hamiltonian formalism, admitting some spread in the spin Hamiltonian parameters

Table I

Mössbauer and crystal field parameters of diethyl ether extracted Fe^{3+} *complexes*
Isomer shifts are given relative to metallic iron at room temperature

Complexing ligand	Saturation hyperfine field $B_0(T)$ (T)	Isomer shift δ_{Fe} (mm/s)	Quadrupole coupling constant P (mm/s)	Crystal field parameters		
				D (cm^{-1})	λ	a (cm^{-1})
Cl^-	48.2	0.35	0.0	0.041	0.20	0.0041
Br^-	43.7	0.37	0.0	0.16	0.19	0.0026
SCN^-	56.8	0.55	−0.60	−0.27	0.12	0.0

the crystal field splitting, as given by D, shows the opposite dependence. The crystal field symmetry (λ) is identical for the two complexes. For both complexes, the quadrupole interaction is zero.

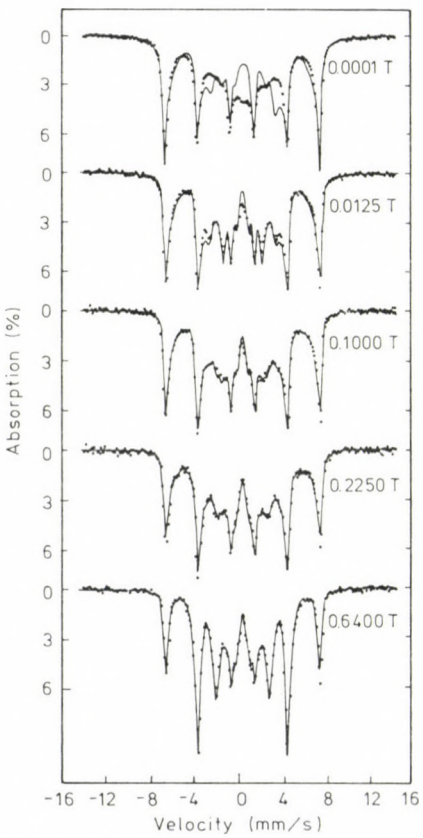

Fig. 6. Mössbauer spectra of an absorber frozen from an ether extracted solution of Fe^{3+} and Br^-. The spectra were obtained at 5 K with various applied magnetic fields. The curves show the best fits obtained within the spin Hamiltonian formalism, admitting some spread in the spin Hamiltonian parameters

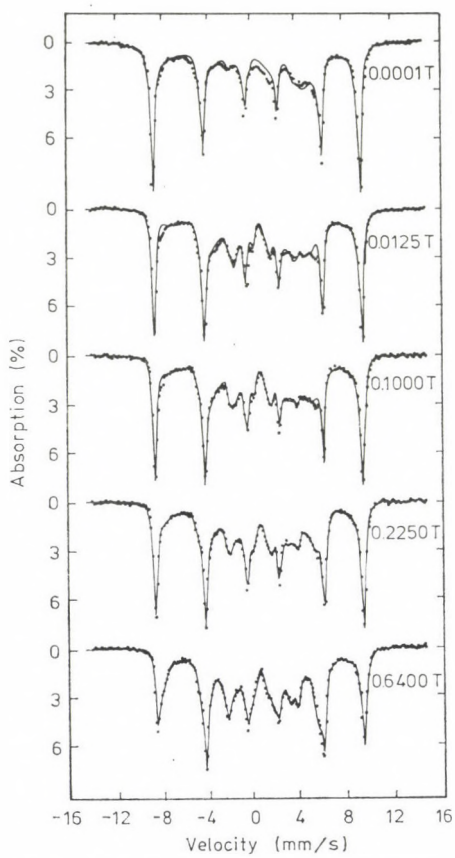

Fig. 7. Mössbauer spectra of an absorber frozen from an ether extracted solution of Fe^{3+} and SCN^-. The spectra were obtained at 5 K with various applied magnetic fields. The curves show the best fits obtained within the spin Hamiltonian formalism, admitting some spread in the spin Hamiltonian parameters

The octahedral complex, Fe^{3+} with SCN^-, has a higher crystal field splitting and a large quadrupole coupling of *axial* symmetry.

In another investigation the complex formation of Fe^{3+} in the aqueous system $HCl/HNO_3/H_2O$ was studied. The complexing tendency of the Cl^--ion to Fe^{3+} is well established, whereas the NO_3^- ion does not form complexes. The presence of HNO_3 in suitable concentration ($[HCl + HNO_3] \simeq 7\ M$) ensures the formation of an amorphous state upon freezing.

By the preparation of absorbers of various concentrations of Cl^-, referred to by the ratio $R = [Cl_{total}]/[Fe_{total}]$, it is possible successively to study the complexes $[Fe(H_2O)_{6-n}Cl_n]^{3-n}$, $n = 0, 1, \ldots$ The absorbers were prepared with $[Fe] = 0.03\ M$ or $0.02\ M$ and $R = 0$, 1.0, 5.5, 12, 33, 90, 300, and 530. Figures 8—11 show spectra obtained at 5 K for a few characteristic values of R.

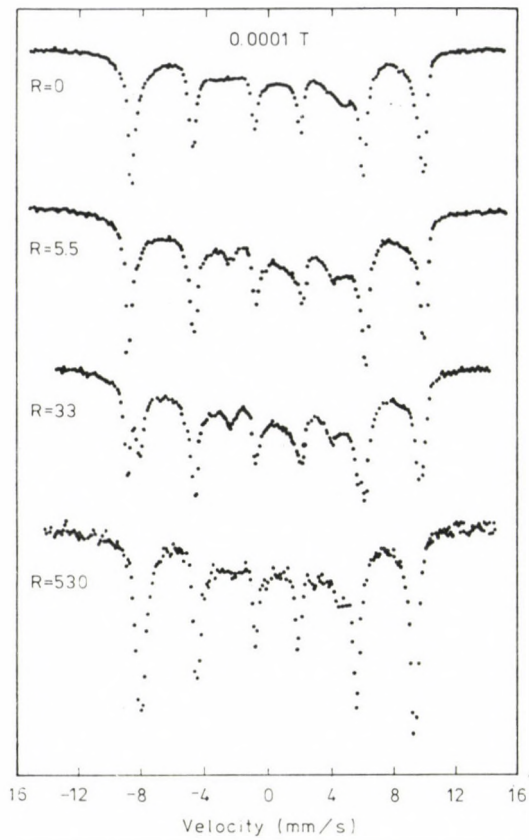

Fig. 8. Mössbauer spectra of frozen aqueous solutions of Fe^{3+} and Cl^- ions obtained at 5 K in an applied magnetic field of 0.0001 *T*. The values of R indicate the relative molar concentration of Cl^-, $R = [Cl^-]/[Fe^{3+}]$

From the well resolved magnetic hyperfine splitting it can be concluded that the complexes are present as monomers.

It appears clearly that besides the spectrum of $[Fe(H_2O)_6]^{3+}$, spectra of three different complexes can be distinguished, interpreted as $n = 1$, 2, and 3. However, the simultaneous presence of several complexes (n) in each absorber (R) presents a major difficulty for the interpretation. In order to obtain a consistent description, the following method was applied. First, complex formation constants (K_n) were assumed, and the distribution of individual complexes (n) in every absorber calculated. Next, for each complex (n) and for each applied magnetic field B a theoretical spectrum was derived from the experimental ones by means of a least squares method. Finally, all the theoretical spectra of the individual complexes were fitted within the spin Hamiltonian formalism, assuming a statistical distribution between *cis* and *trans* coordinated complexes. This procedure, starting with adjustments of

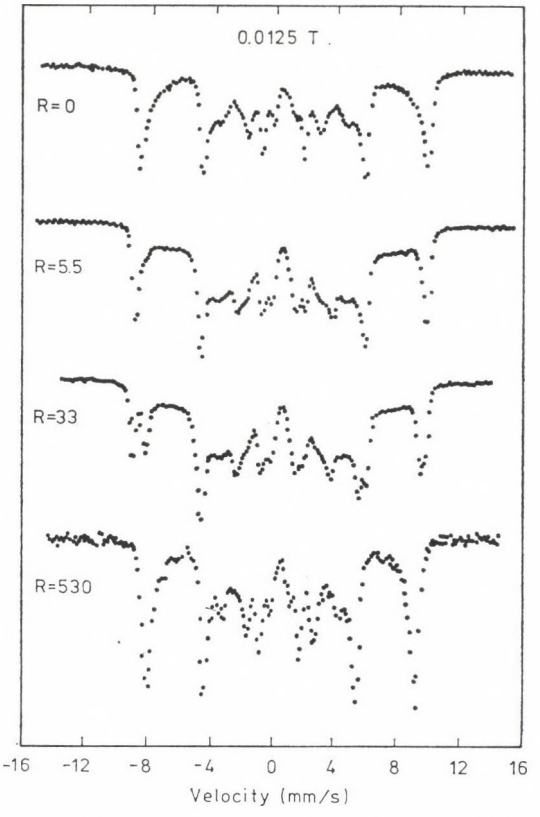

Fig. 9. Mössbauer spectra of frozen aqueous solutions of Fe^{3+} and Cl^- ions obtained at 5 K in an applied magnetic field of 0.0125 *T*. The values of *R* indicate the relative molar concentration of Cl^-, $R = [Cl^-]/[Fe^{3+}]$

the equilibrium constants K_n, was repeated until a reasonable consistent description was obtained.

The equilibrium constants of the best description are $K_1 = 13.2$, $K_2 = 0.86$, and $K_3 = 0.11$. The key parameters of the fits are given in Table II. The isomer shifts indicate octahedrally coordinated complexes. The decrease in saturation hyperfine field B_0 with increasing number of Cl^- ligands reflects the higher covalency of the Fe^{3+} —Cl^- bond in comparison to the Fe^{3+}—H_2O bond, which is also supported by the presence of large crystal field splittings in the mono- and dichloro complexes.

The variation in magnitude and symmetry of the crystal field of the chloro complexes may to some extent be explained within the so-called spin Hamiltonian superposition model [16—18]. According to this concept each ligand contributes a term

$$\hat{H}_p = d[3\hat{S}_z^2 - S(S+1)] \tag{8}$$

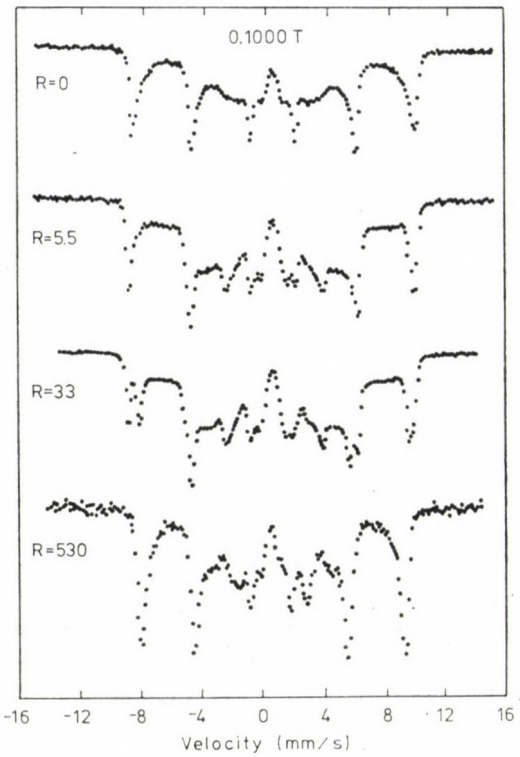

Fig. 10. Mössbauer spectra of frozen aqueous solutions of Fe^{3+} and Cl^- ions obtained at 5 K in an applied magnetic field of 0.1000 *T*. The values of *R* indicate the relative molar concentration of Cl^-, $R = [Cl^-]/[Fe^{3+}]$

where the quantization axis ζ has been chosen in the direction of the Fe^{3+}-ligand bond. The crystal field constant d depends on the type of ligand and the bond length. The total crystal field spin Hamiltonian is obtained by adding the terms for all the ligands.

Assuming octahedral complexes and constant bond length, the relative magnitude and symmetry of the crystal field interaction of the different iron-chloro complexes can easily be found. The results of the calculation are given in Table III, together with similar relations of the quadrupole interactions, derived from a simple electrostatic picture. It appears from a comparison of the results given in Tables II and III that the crystal field interactions of the mono- and chloro complexes follow the superposition model rather well. It is also seen that the quadrupole interaction of these complexes is in reasonable agreement with the electrostatic model.

However, the trichloro complexes do not fit well into this picture. For the *cis-trans* complex the value determined for *D* is much smaller than expected from the model, but the higher value of λ is expected. For the *cis-cis* complex

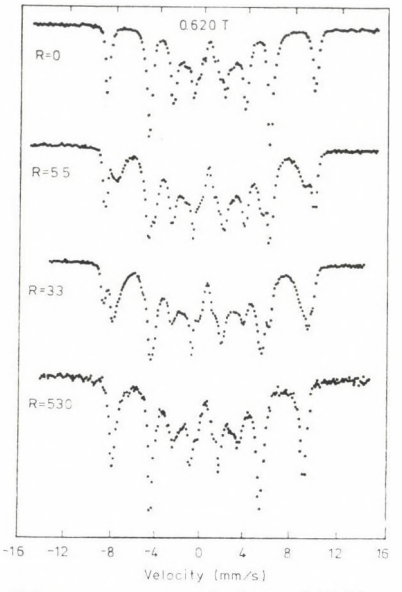

Fig. 11. Mössbauer spectra of frozen aqueous solutions of Fe^{3+} and Cl^- ions obtained at 5 K in an applied magnetic field of 0.6200 *T*. The values of *R* indicate the relative molar concentration of Cl^-, $R = [Cl^-]/[Fe^{3+}]$

(as for $[Fe(H_2O_6)]^{3+}$) this simple model predicts that $D = 0$, but non-zero values are actually found. These disagreements could be due to the presence of deviations from the strict octahedral symmetry anticipated or to a change in bond lengths. Moreover, the distribution of *cis-trans* and *cis-cis* complexes may be different from the assumed statistical ratio, and this would also influence the fitting procedure.

In a similar work, the fluoro complexes, $[Fe(H_2O)_{6-n}F_n]^{3-n}$, were investigated in frozen aqueous solution, using 40% glycerol as a glass former [19].

Table II

Mössbauer and crystal field parameters of $[Fe(H_2O)_{6-n}Cl_n]^{3-n}$ *complexes.*
Isomer shifts are given relative to metallic iron at room temperature

Complex	Saturation hyperfine field B_0 (*T*)	Isomer shift δ_{Fe} (mm/s)	Quadrupole interaction		Crystal field parameters		
			P (mm/s)	η	*D* (cm^{-1})	λ	*a* (cm^{-1})
$[Fe(H_2O)_6]^{3+}$	58.5	0.50	0.0	0	0.10	0.20	0.017
$[Fe(H_2O)_5Cl]^{2+}$	58.1	0.52	−0.20	0	0.50	0	0
$[Fe(H_2O)_4Cl_2]^+$							
cis	55.0	0.53	+0.18	0	−0.60	0.07	0
trans	55.0	0.53	−0.28	0	+0.90	0	0
$Fe(H_2O)_3Cl_3$							
cis-trans	53.7	0.55	−0.20	1	0.20	0.45	0.01
cis-cis	53.7	0.55	+0.10	0	0.10	0	0.02

Table III

Crystal field parameters derived from the superposition theory.
d_a and d_b are crystal field interaction constants for the ligands A = H_2O and B = Cl^-. The quadrupole coupling constants are evaluated from individual electrostatic contributions a and b of the two ligands

Complex	Crystal field parameters		Quadrupole interaction constants	
	D	λ	P	η
FeA_5B	$3(d_a - d_b)$	0	$a - b$	0
FeA_4B_2				
— *cis*	$-3(d_a - d_b)$	0	$-(a - b)$	0
— *trans*	$6(d_a - d_b)$	0	$2(a - b)$	0
FeA_3B_3				
— *trans-cis*	$\frac{9}{2}(d_a - d_b)$	$\frac{1}{3}$	$\frac{3}{2}(a - b)$	1
— *cis-cis*	0		0	

Spectra of absorbers with $n = 0, 1, 2, 3$, and 4, were observed, according to generally accepted values of the equilibrium constants. However, as the spectra were obtained at 78 K the hyperfine resolution is lower than that in the studies discussed above, because of the finite spin-lattice relaxation time. A detailed interpretation within the spin Hamiltonian formalism was therefore not attempted. Instead, the maximum observed magnetic hyperfine splitting, the isomer shift and the quadrupole shift were read directly from the spectra and an evaluation of the crystal field splitting Δ_R was carried out by comparison of the field dependence of the observed spectra with that of the $[Fe(H_2O)_6]^{3+}$ spectrum. The results are shown in Fig. 12 from which it appears that the magnetic hyperfine splitting increases with increasing number of F^--ligands, whereas the crystal field splitting first increases and then decreases with increasing n. These results are in accordance with the fact that the character of the Fe^{3+}—F^- bond is less covalent than that of the Fe^{3+}—H_2O bond. The isomer shifts indicate octahedral coordination.

The examples outlined here demonstrate the suitability of Mössbauer Spectroscopy of frozen solutions in the achievement of a detailed understanding of complex formation by Fe^{3+} in solution. The method can be used for other ligands as well. However, the necessity of the formation of a homogeneous amorphous state upon freezing should be stressed. So, in a study of complex chemistry in frozen solutions it is of utmost importance to find a suitable glass former that does not disturb the system under investigation. Here HNO_3 and $LiNO_3$ at concentrations near 7 M and glycerol have turned out to be promising for studies of aqueous solutions.

In the examples discussed above, the spectra show magnetic hyperfine splittings because the ferric ions are well separated and therefore exhibit a long spin-spin relaxation time. As shown in Fig. 1, the magnetic splitting

collapses due to fast relaxation when the concentration of Fe^{3+} ions is increased.

An extreme case of strong magnetic interaction is found in dimetric complexes. In such complexes the exchange interaction (Eq. 5) between the ions is often predominant in the spin Hamiltonian. For a dimeric complex Eq. (5) reduces to:

$$\hat{H}_{ex} = -2J\hat{\vec{S}}_1 \cdot \hat{\vec{S}}_2 \tag{9}$$

where $\hat{\vec{S}}_1$ and $\hat{\vec{S}}_2$ are the spin operators for the two ions. The eigenvalues of this spin Hamiltonian are

$$E = -J[S'(S'+1) - 2S(S+1)] \tag{10}$$

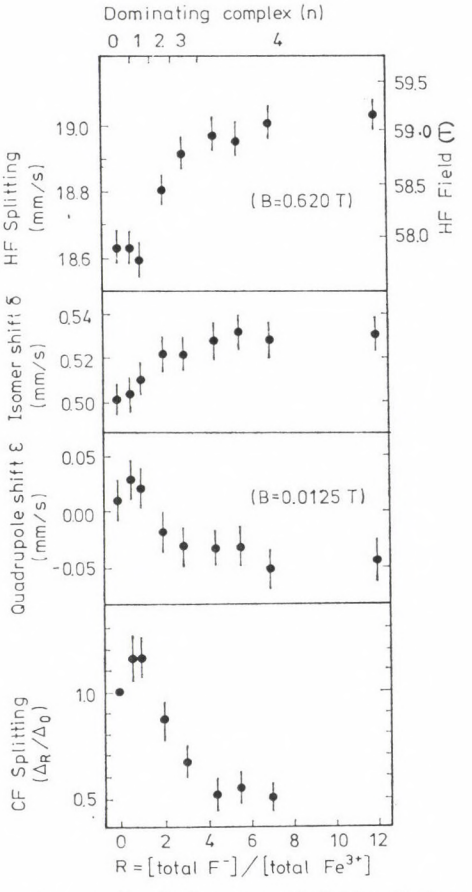

Fig. 12. Hyperfine parameters and relative crystal field splittings in absorbers of frozen aqueous solutions of $[Fe(H_2O)_nF_{6-n}]^{3-n}$ complexes (adapted from [19])

where S' is the total spin quantum number for the complex. For negative values of J, the lowest state corresponds to $S' = 0$. Therefore, such complexes are diamagnetic at very low temperatures and, consequently, the Mössbauer spectrum does not exhibit magnetic splitting as the magnetic hyperfine field at each ^{57}Fe nucleus is zero. Even at low temperatures the application of an external magnetic field only results in a magnetic field at the nucleus equal to the applied field. Such dimeric complexes can therefore easily be identified by Mössbauer spectroscopy.

Dézsi et al. [20] observed such a dimeric complex in a study of frozen aqueous solution of $Fe(ClO_4)_3$ at different pH. At a pH value of 1.45 a quadrupole doublet was found in the Mössbauer spectrum, and it was attributed to a dimetric complex.

This complex was later investigated in detail by Knudsen et al. [21]. Some of their spectra for 0.67 M aqueous solutions of $Fe(ClO_4)_3$ with different pH values are shown in Fig. 13. In this study the pH was changed by adding

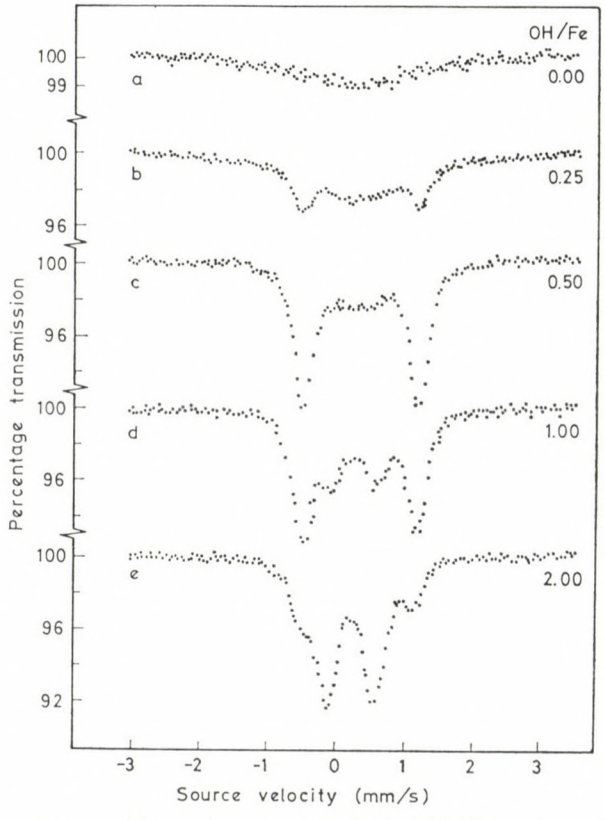

Fig. 13. Mössbauer spectra of frozen aqueous solutions of $Fe(ClO_4)_3$ at various values of the ratio [OH]/[Fe]. [OH] is determined from the amount of base added. The spectra were recorded at $T = 77$ K. (Adapted from [21])

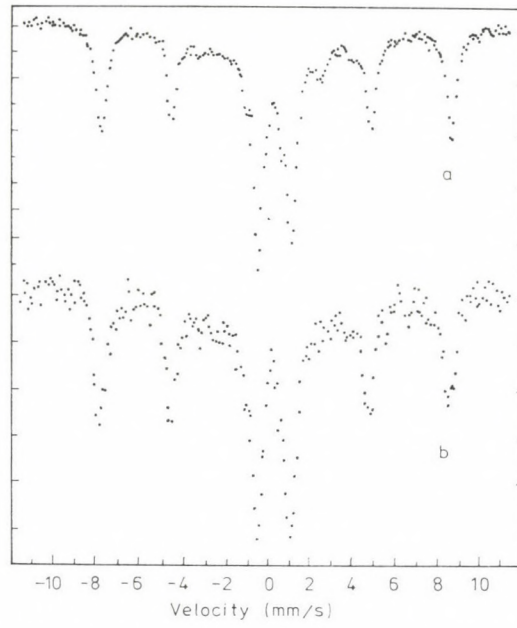

Fig. 14. Mössbauer spectra of a solution of $FeCl_3$ in pyridine at 4.2 K. (a) $B = 0$; (b) $B = 0.88\ T$ (adapted from [22])

various amounts of $NaHCO_3$ to the solutions. The ratio of OH^- and Fe^{3+} are indicated in the figure. At the lowest pH, (spectrum a, $\sim$pH $\simeq$ 0.5) only the monomeric $[Fe(H_2O)_6]^{3+}$ complex is present. The spectrum does not exhibit magnetic hyperfine splitting, but consists of a single broad line. This is due to fast spin-spin relaxation in this relatively concentrated frozen solution.

When the pH is increased a quadrupole doublet appears in the spectra, similar to that observed by Dézsi et al. [20]. The quadrupole splitting of this doublet is about 1.67 mm/s. A detailed analysis led to the conclusion that it is due to a mono-oxo bridged dimer, $[(H_2O)_5Fe—O—Fe(H_2O)_5]^{4+}$ with a strong exchange coupling ($J \approx -100\ cm^{-1}$).

At higher pH values (spectra d and e) a new quadrupole doublet with a splitting of about 0.66 mm/s appears. This components is due to the formation of polymeric iron hydroxo complexes [21].

Dimeric complexes may also be present in non-aqueous solutions. For example, Vértes et al. [22] found evidence for the formation of dimeric complexes in frozen solutions of $FeCl_3$ in pyridine. Spectra obtained at 4.2 K in zero applied field and at $B = 0.88\ T$ are shown in Fig. 14. Both spectra consist of a magnetically split (six-line) component due to monomeric complexes and a quadrupole doublet. The latter component is essentially unaffected by the applied magnetic field, indicating that it is due to a diamagnetic complex.

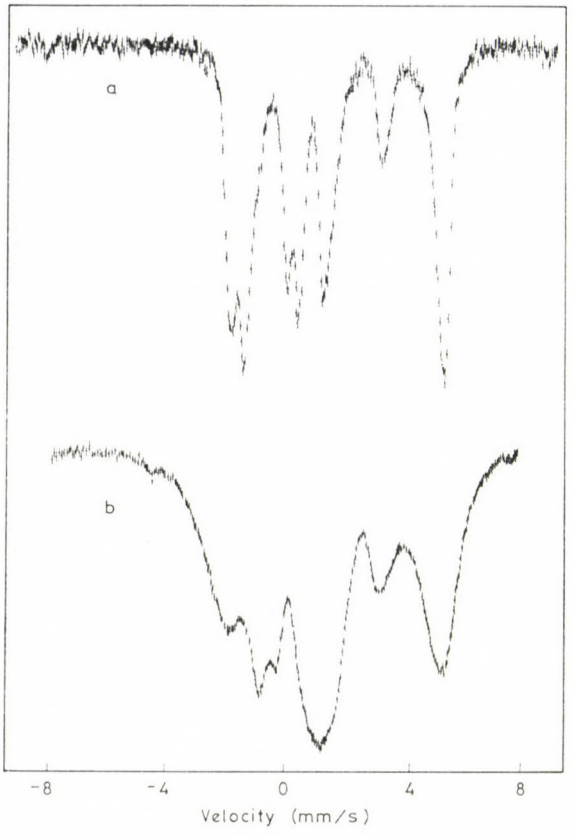

Fig. 15. (a) Mössbauer spectrum of a polycrystalline sample of $Fe(ClO_4)_2 \cdot 6H_2O$ (adapted from [24]). (b) Mössbauer spectrum of an amorphous frozen aqueous solution of $Fe(ClO_4)_2$ (adapted from [23]). Both spectra were obtained at 4.2 K in an applied magnetic field of 5.0 *T*

In contrast to monomeric Fe^{3+} complexes, complexes of Fe^{2+} do normally not exhibit a magnetic hyperfine splitting, even at liquid helium temperature. The magnetic properties of such complexes may, however, be elucidated by Mössbauer spectra obtained in an applied magnetic field, which induces a substantial magnetic splitting at low temperatures.

Studies of frozen aqueous solutions of Fe^{2+} at 4.2 K and in large applied magnetic fields have shown the presence of a distribution in magnetic hyperfine fields [23]. As in the spectra of $[Fe(H_2O)_6]^{3+}$ discussed above, this presumably reflects the amorphous nature of the samples. The difference between the spectra of a crystalline and an amorphous sample is illustrated in Fig. 15, which shows spectra of a frozen solution of $Fe(ClO_4)_2$ and a polycrystalline sample of $Fe(ClO_4)_2 \cdot 6\ H_2O$ [24]. Both spectra were obtained at 4.2K in an applied magnetic field of 5 *T*.

Dynamic properties of viscous liquids

As mentioned in the introduction, Mössbauer spectroscopy can in general not be used for studies of liquids and the solutions therefore have to be solidified by cooling. It is, however, possible to obtain Mössbauer spectra of very viscous liquids and the technique then gives information not only about the chemical state of the atoms but also on the dynamics of the liquid.

The parameters related to the dynamic properties, that can be determined are the mean square amplitude, $\langle x^2 \rangle$, of the vibrational motion of the Mössbauer atom and the diffusion coefficient, D.

Information on $\langle x^2 \rangle$ can be obtained since the total area of the Mössbauer spectrum is proportional to the so-called f-factor (the probability for recoil-free absorption of the gamma rays) which is given by:

$$f = \exp\left\{-\left(\frac{2\pi}{\lambda}\right)^2 \langle x^2 \rangle\right\} \tag{11}$$

where λ is the wavelength of the gamma radiation.

Using the Debye model for the vibrations one finds in the high temperature approximation:

$$f = \exp\left\{-\frac{3E_\gamma^2 T}{Mc^2 k\Theta_D^2}\right\} \tag{12}$$

Here E_γ is the gamma ray energy, M is the mass of the atom and Θ_D is the Debye temperature. This approximation is applicable for $T > 1/2\Theta_D$. According to Eq. (12), the logarithm of the area of the spectrum depends linearly on the temperature. This behaviour has in fact been found in a number of studies of solids.

Studies of frozen solutions have also shown a similar behaviour below the glass transition temperature, T_g. However, several studies have shown that above T_g, $\langle x^2 \rangle$ increases much more rapidly with increasing temperature than it does in the solid state. Thus new types of vibrations are present in the supercooled liquid, and it has been suggested that these vibrations are related to the diffusional motion of the atoms.

The diffusional motion of the atom gives rise to an extra line broadening given by [25]:

$$\Delta\Gamma = 2\hbar\left(\frac{2\pi}{\lambda}\right)^2 D \tag{13}$$

Thus the diffusion constant, D, can easily be estimated from the Mössbauer spectrum (unless the spectrum is also broadened because of other effects such as paramagnetic relaxation).

Mössbauer studies of the temperature dependence of D in viscous liquids have shown that the diffusion constant follows an Arrhenius law. Simulta-

neous studies of the temperature dependence of the spectral area and the diffusional line broadening have suggested that the vibrational mean square amplitude above T_g and the diffusional motion are closely related [26, 27].

Conclusions

In the present work we have demonstrated that Mössbauer spectroscopy gives several types of information about solutions. Specifically, we have illustrated how the method can be used to study crystallization and glass formation during freezing of the liquids. Moreover, we have shown that detailed information about the iron complexes in solutions can be obtained. Finally we have discussed how the dynamic properties of viscous liquids can be studied by use of Mössbauer spectroscopy.

*

The authors wish to thank the Danish Natural Science Research Council for financial support.

REFERENCES

[1] Dézsi, I., Keszthelyi, L., Pocs, L., Korecz, L.: Phys. Lett., **14,** 14 (1965)
[2] Dézsi, I., Keszthelyi, L., Molnár, B., Pocs, L.: Phys. Lett., **18,** 28 (1965)
[3] Dézsi, I., Gorobchenko, V. D., Lukashevich, I. I., Vértes, A.: Chem. Phys. Lett., **2,** 665 (1968)
[4] Dézsi, I., Keszthelyi, L., Molnár, B., Pocs, L.: in "Hyperfine Structure and Nuclear Radiations", ed. F. Matthias and D. Shirley, p. 566, North Holland, Amsterdam 1968
[5] Vértes, A., Korecz, L., Burger, K.: Mössbauer Spectroscopy. Elsevier Scientific Publishing Company, Amsterdam 1979
[6] Mørup, S.: Paramagnetic and Superparamagnetic Relaxation Phenomena Studied by Mössbauer Spectroscopy. Polyteknisk Forlag, Lyngby 198'
[7] Mørup, S.: Proc. Indian National Science Academy, Physical Sciences, International Conference on the Applications of the Mössbauer Effect Jaipur, India, 1981, p. 91
[8] Mørup, S., Knudsen, J. E., Nielsen, M. K., Trumpy, G.: J. Chem. Phys., **65,** 536 (1976)
[9] Mørup, S., Thrane, N.: Chem. Phys. Lett., **21,** 363 (1973)
[10] Ohya, T., Ono, K.: J. Phys. Soc. Japan, **34,** 376 (1973)
[11] Pake, G. E.: Paramagnetic Resonance. W. A. Benjamin, New York 1962
[12] Abragam, A., Bleaney, B.: Electron Paramagnetic Resonance of Transition Ions. Clarendon Press, Oxford 1970
[13] Knudsen, J. E.: J. Physique Colloq., **37,** C6-735 (1976)
[14] Knudsen, J. E.: J. Phys. Chem. Solids, **38,** 883 (1977)
[15] Knudsen, J. E.: J. Phys. Chem. Solids, **41,** 545 (1980)
[16] Novak, P., Veltrusky, I.: Phys. Stat. Sol., (b), **73,** 575 (1976)
[17] Newman, D. J., Siegel, E.: J. Phys. C, **9,** 4285 (1976)
[18] Eremin, M. V., Kornienko, A. A.: Phys. Stat. Sol. (b), **79,** 775 (1977)
[19] Knudsen, J. E., Mørup, S.: J. Physique Colloq., **37,** C6-535 (1976)
[20] Dézsi, I., Gorobchencko, V., Komor, M., Vértes, A., Tsirskishviei, K.: Acta Chim. Acad. Sci. Hung., **70,** 329 (1971)
[21] Knudsen, J. M., Larsen, E., Moreira, J. E., Nielsen, O. F.: Acta Chem. Scand., **A29,** 833 (1975)
[22] Vértes, A., Nagy-Czakó, I., Burger, K.: J. Phys. Chem., **82,** 1469 (1978)
[23] Nagy, D. L., Horváth, D., Ritter, G., Spiering, H., Szücs, I. S., Volland, U.: Nucl. Instr. Meth., **199,** 223 (1982)
[24] Spiering, H., Nagy, D. L., Zimmermann, R.: J. Physique Colloq., **35,** C6-231 (1974)
[25] Singwi, K. S., Sjölander, A.: Phys. Rev., **120,** 1093 (1960)
[26] Jensen, J. H.: Phys. Kondens. Material., **13,** 273 (1971)
[27] Keller, H., Debrunner, P. G.: Phys. Rev. Lett., **45,** 68 (1980)

Acta Chimica Hungarica 121 (1—2), pp. 173—185 (1986)

DIFFRACTION STUDIES OF LIQUIDS+*

A. H. NARTEN

(Chemistry Division, Oak Ridge National Laboratory, Oak Ridge, Tennessee 37830, U.S.A.)

Received January 18, 1985

The aim of modern diffraction studies should be to extract unique information about liquid structure as described by the atom pair distribution functions. The past decade has seen the application of neutron diffraction with isotopically substituted samples toward this aim. A number of ionic liquids have thus been completely characterized, and detailed comparison between theory and experiment has become possible. Unique information on ion-water interactions in ionic solutions has been obtained by this methods. The next decade will see a new impetus in x-ray diffraction as the new synchrotron sources come into operation.

I. Introduction

It is important to realize at the outset that the term "structure", as used in studies of the liquid state, usually means something quite different from the same word used to describe crystalline solids.

The structure of a crystalline solid is specified by the symmetry of the space group and by the mean atomic positions in the unit cell, together with estimates of the amplitudes of thermal vibration of each of the nuclei. The periodicity of the lattice allows one to construct a model of the unit cell which is representative of the entire crystal.

In a liquid there is no such periodicity. The short-range ordering or structure, found in liquid materials is completely described by probability functions of position and orientation. If we choose the symbol X_i to denote the set of all coordinates needed to specify the position and orientation of a particle, and we let dX_2 be the volume of a differential volume element in the coordinate space of particle 2, then we may define a pair distribution function $g(X_1, X_2)$ so that $\varrho g(X_1, X_2)dX_2$ is the average number of particles at X_2 is the volume element dX_2 when another particle is at X_1. Hence, the function $g(X_1 \quad X_2)$ is a measure of the local particle density in the vicinity

+ This paper was presented at the Symposium on Structure of Liquids and Solutions at Veszprém, August 27—30, 1984.

* Research sponsored by the Division of Material Sciences, U. S. Department of Energy under contract DE-AC05-840R21400 with the Martin Marietta Energy Systems, Inc.

of any origin particle of bulk density ϱ. In principle, knowledge of the pair distribution function $g(X_1, X_2)$ and the pair potential $V(X_1, X_2)$ is sufficient for the prediction of all equilibrium properties of fluids through standard methods of statistical mechanics [1]. While this sounds very simple, it can be done in practice with useful results only for the simplest types of fluids.

For monatomic fluids (Ar, Na) the pair distribution function depends only on the scalar distance, r, between the atoms, and we usually write the function as $g(r)$. The atom pair distribution function of a monatomic fluid can be obtained from a single diffraction experiment using thermal neutrons, x-rays, or electrons. If the interatomic potential $V(r)$ is known, the function $g(r)$ can also be obtained from computer experiments involving the Monte Carlo or the molecular dynamics method, and from statistical mechanical integral equations. For simple fluids such as argon the agreement between experiment, computer simulation, and the general theory is quite satisfactory.

For molecular fluids the situation is not so clear, even for the simple case of linear molecules the function $g(X_1, X_2)$ now depends on four relative coordinates of the two molecules and a single diffraction experiment does not provide enough information to determine a function of four or more variables. For fluids with nearly spherical molecules a multipole expansion of molecular properties leads to a converging series, the coefficients of which can be determined from one or two diffraction experiments [1]. This approach is promising for the analysis of x-ray diffraction data because many non-spherical molecules have a very nearly spherical distribution of electron density. An example is liquid water, for which the pair distribution function for molecular centers has been derived from a single x-ray diffraction experiment [2].

The expansion method appears less promising for the analysis of neutron diffraction data, because the molecular neutron scattering density is highly non-spherical and the resulting series does not converge. An alterntaive approach, which has been the traditional one, is to describe the structure of molecular fluids in terms of atom pair distribution functions, $g_{\alpha\gamma}(r)$. In this picture, the function $g_{\alpha\gamma}(r)$ are related to the probability of finding an atom of type γ at a scalar distance r from an atom of type α of some different molecule. Knowledge of all atom pair distribution functions is not sufficient for a complete description of the structure of a molecular fluid. This may be visualized by considering a fluid with homonuclear diatomic molecules such as N_2 which is described by a single atom pair distribution function, $g_{NN}(r)$. Clearly, the function $g_{NN}(r)$ does not tell us whether the N_2 molecules are aligned mostly parallel or perpendicular to each other.

Despite these limitations, the description of liquid structure in terms of atom pair distribution functions will be adopted in this discussion because the experimental determination of these quantities is feasible for many liquids of practical interest. This will be discussed in the next section.

II. Diffraction experiments

In a diffraction experiment with a source of monochromatic radiation a detector is used to count the scattered radiation at a preset angle Θ. The measured intensity may quite generally be written as

$$I(\Theta) = \alpha(\Theta)[\mathrm{d}\sigma/\mathrm{d}\Omega + \delta(\Theta)] \tag{1}$$

The parameters $\alpha(\Theta)$ and $\delta(\Theta)$ depend on the nature of the scattered radiation and on the experimental geometry [1, 3]. A properly designed experiment will permit the precise determination of these calibration parameters. The quantity then available for further analysis is the static coherent differential scattering cross-section

$$N^{-1}\,\mathrm{d}\sigma/\mathrm{d}\Omega = \sum_{\alpha} c_\alpha f_\alpha f_\alpha^* + F(k) \tag{2}$$

with $k = 4\pi \sin\Theta/\lambda$ the momentum transfer coordinate, and the scattering function

$$F(k) = \sum_{\alpha}\sum_{\gamma} c_\alpha c_\gamma f_\alpha f_\gamma^* \hat{h}_{\alpha\gamma}(k) \tag{3}$$

In these defining equations N is the total number of scattering sites in the sample, and c_α the atom fraction of species α. The type of radiation used enters Eqs. (2) and (3) through the scattering factors f_α which are, in general, complex and assumed to be known. The partial structure functions $\hat{h}_{\alpha\gamma}(k)$ are related to the atom pair correlation functions $h_{\alpha\gamma}(r) = g_{\alpha\gamma}(r) - 1$ by the Fourier integral

$$\hat{h}_{\alpha\gamma}(k) = 4\pi\varrho \int_0^\infty r^2 h_{\alpha\gamma}(r)\, j_0(kr)\, \mathrm{d}r \tag{4}$$

with $j_0(x) = x^{-1}\sin x$. Only for monatomic and homonuclear diatomic liquids can the structure function $\hat{h}(k)$ be obtained from a single diffraction experiment. The structure of a liquid with m different kinds of atoms is described by $m(m+1)/2$ different atom pair distribution functions, and an equal number of diffraction experiments with different values of the scattering factors f must be performed for their complete determination. For fluids with more than one kind of atom only the total scattering function $F(k)$ can be obtained from a single experiment. This function is not a particularly useful quantity because its interpretation is always difficult, often ambiguous, and never unique. The contemporary aim of diffraction studies is to decompose $F(k)$ into the partial functions $\hat{h}_{\alpha\gamma}(k)$. This can be done by changing the scattering factors f in (3) by an appropriate systematic procedure.

The two principal types of radiation used in diffraction experiments are x-rays and neutrons. For neutrons, the coherent, scattering length is iso-

tropic, isotope-dependent, and bears no simple relation to the atomic weight. These properties makes neutrons particularly useful for the study of light elements. But the most significant property of the coherent neutron scattering length is its isotopic dependence, for this allows the factors f in (2) and (3) to be changed systematically without significantly changing the chemical and physical properties of the system.

X-ray scattering arises from electron-proton interactions. Therefore the atomic x-ray scattering factors are proportional to the atomic number Z and depend strongly on the variable k. The fall-off, and therefore the low scattered intensity at large values of k, is more than offset by the much larger intensity of the available x-ray sources. Neutron sources are weak when compared to standard x-ray tubes, and the flux from the best available neutron sources is only $\sim 10^{-7}$ of that in a 1 eV energy band of synchrotron x-rays. We have mentioned that scattering factors are in general complex, and dispersion occurs in the vicinity of an absorption edge. Unlike neutrons, x-rays have strong resonances with every atom at energies of the electron binding energies. Synchrotron sources emit intense photon fluxes from the visual into the hard x-ray region. This provides for the selectrion of a particular energy (wavelength) to enhance or decrease the x-ray scattering factor of any element.

III. Recent results

The determination of the total scattering function $F(k)$ from a single diffraction experiment [Eq. (3)] is useful in order to determine nearest-neighbour distances and, sometimes, coordination numbers. It may also be used to test models of the liquid structure. However, the partial structure and atom-pair distribution functions [Eq. (4)] contain so much more detailed information that their determination should be the aim of moden diffraction experiments. The following discussion is therefore restricted to studies in which this has been attempted. Only some typical examples, or results that have not been discussed in recent reviews, will be presented.

A. Monatomic and homonuclear molecular liquids

Studies of atomic liquids have concentrated almost entirely on liquid metals which will be discussed in Section *C*. For liquids with molecules in which the electron density can be represented by a rapidly converging multipole expansion [4] the scattering of x-rays can be described by a single scattering factor. If the expansion is made about a suitably chosen center atom, the distribution function for these center atom pairs can be obtained, to good approximation, from a single x-ray diffraction experiment. Examples are

[4, 2, 5, 6] H_2O, HF, NH_3, and CH_4 for which the distribution functions for the heavy atom pairs can be thus determined. The function $g_{CC}(r)$ for liquid methane is shown in Fig. 1 together with that for liquid argon [7] in reduced units. The scaled distribution functions for methane and argon are remarkably similar beyond the first maximum, indicating that the structure of liquid-methane differs very little from a monatomic fluid.

In a similar manner, the scattering of x-rays from the $(CH)_n$ groups in hydrocarbon liquids can be described by a single scattering factor. In this way the C . . . C distribution functions for liquid benzene [8], ethylene [9], and ethane [10] have been derived from a single x-ray diffraction experiment. Ethylene and ethane may be regarded as "pseudodiatomics" in that the hydrogen atoms in these molecules are mere bulges in the electron density distribution around the carbon atoms. The C . . . C distribution functions for ethylene and ethane are compared with the atom pair distribution functions for liquid nitrogen [11] and bromine [12] in Fig. 2. The main first peak in each of the curves is followed by a shoulder which develops into a second peak with increasing elongation (L/σ = bond length/atomic diameter) of the molecule. This structure is explained as follows: When two molecules touch, there is at least one highly probable intermolecular distance at $r = \sigma$, and two others between σ and $L + \sigma$. Beyond $L + \sigma$ there is therefore a sudden drop in probability. Another interesting feature is that the structure beyond $L + \sigma$ is gradually washed out as the elongation increases. All these features are in good qualitative agreement with results from computer simulations [13]. The simulations show, in addition, that the transformation of the shoulder

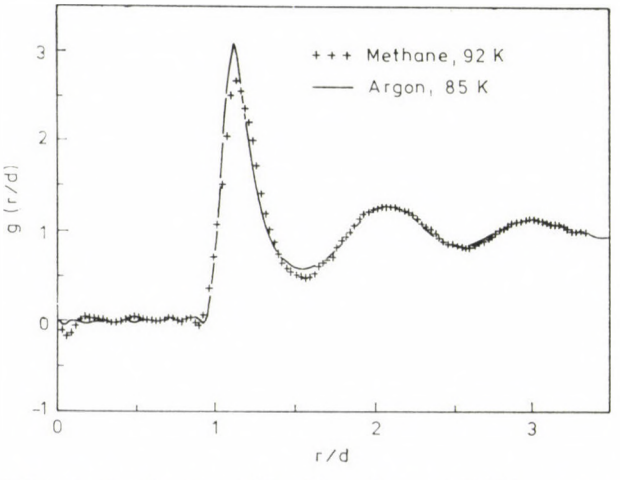

Fig. 1. The C. . . C distribution function of liquid methane at 92 K is compared with the atom pair distribution function of liquid argon at 85 K in reduced units. The scaling parameters d have the values 3.59 Å for methane and 3.37 Å for argon

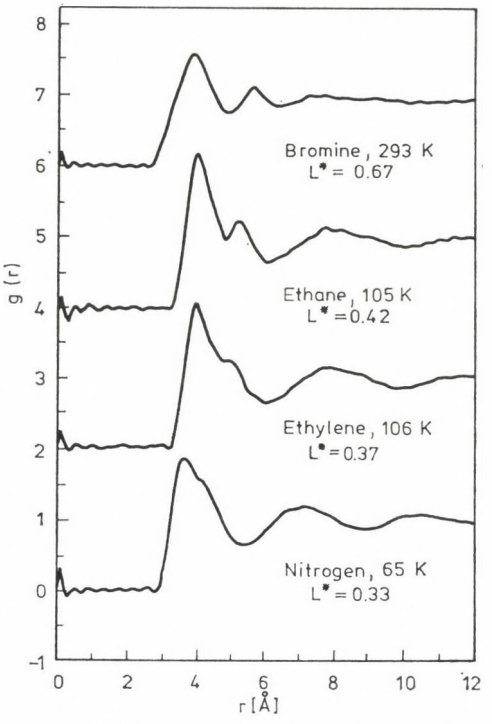

Fig. 2. Intermolecular atom pair distribution functions derived from x-ray diffraction. The elongation L^* is the ratio of bond length over atomic diameter

at $L + \sigma$ into a peak is due to an increase of T-shaped configurations, since in this orientation there are two atom pair distances approximately equal to $L + \sigma$.

B. Heteratomic molecular liquids

For a liquid with molecules containing two kinds of atoms a minimum of three experiments is required to determine the three atom pair distribution functions. A case in point is water, characterized by the functions $g_{OO}(r)$, $g_{OH}(r)$ and $g_{HH}(r)$.

The first attempt to produce this information was to use a combination of x-ray, electron, and neutron diffraction data (XEN-data) [14]. In 1982 two independent attempts to solve the problem using neutrons and isotopic substitution of H/D in water were reported: At the High Flux Isotope Reactor (HFIR) in Oak Ridge four data sets were analyzed to yield the three atom pair distributions (HFIR-data); [15] at the Weapons Neutron Research Facility (WNR) in Los Alamos three data sets were measured to yield only the hydrogen air distribution function (WNR-data) [16]. The neutron experi-

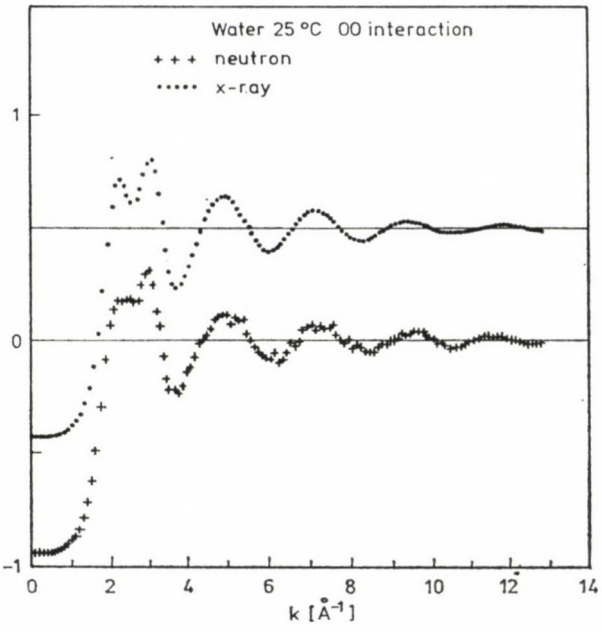

Fig. 3. Partial structure functions $\hat{h}_{00}(k)$ for oxygen atom pairs in water at 25 °C derived from neutron [15] and from x-ray [2] diffraction. The upper curve has been displaced along the ordinate for clarity

ment were done with different sources (reactor and pulsed) and the methods of analysis were different. Yet, the partial structure functions $h_{HH}(k)$ are not very different: the oscillations are in phase. The main difference between the HFIR and the WNR-data is the amplitude of the oscillations beyond $k \sim 6$ A^{-1}, which are strongly damped in the WNR-data. This implies much sharper near-neighbor peaks in the H . . . H pair distribution function derived from the HFIR-data. The nearest neighbor distances at 2.3 Å and 3.9 Å are in excellent agreement; they differ significantly from the H . . ..H distances derived from the XEN-data. It should be pointed out that the structure function $\hat{h}_{00}(k)$ derived from the HFIR-data is in excellent agreement with that obtained much earlier from x-ray diffraction [2], as shown in Fig. 3. A third attempt to obtain the atom pair distribution functions for water by isotopic H/D substitution has been made using the High Flux Reactor at Grenoble (ILL-data) [17]. Comparison of these results with the HFIR and WNR results is almost impossible because analysis of the ILL data appears to have been carried out in *r*-space, a highly unusual practice.

The conclusion is that diffraction results for water must be compared in *k*-space, because serious truncation problems obscure the comparison of *r*-space data. The same conslusion applies to comparison with results from computer simulations. One should also bear in mind that computer simulations

are tests of mathematically defined models for the interaction between a relatively small number of particles which obey classical statistical mechanics [18]. The model for water has been systematically tuned to reproduce the basic tetrahedrality of the structure of water as determined by the experimental structure function for O . . . O interactions. There is no assurance that such a model should describe the orientational correlations between water molecules, i.e., the O . . . H and H . . . H interactions correctly. Clearly, the experimenters must agree among themselves, and then the theoreticians must tune their models to match the experimental results.

The only liquid with molecules containing three different kinds of atoms for which the complete set of six atom pair distributions has been determined is chloroform [19]. This painstaking work was carried out with x-rays and with five neutron experiments on $CDCl_3$, $CD^{35}Cl_3$, $CD^{37}Cl_3$, $CHCl_3$, and a null mixture of $CDCl_3/CHCl_3$. From the distribution functions the most probable configurations between pairs of molecules in the liquid were investigated, and found to be one in which the molecular dipole axes are inclined with respect to each other, and the hydrogen atom is tilted toward the hollow between two chlorine atoms of the next molecule.

C. Ionic liquids

Metals. Interest in the structure of metals and alloys has clearly shifted from the liquid to the amorphous solid state. A number of partial structure functions for these materials have been obtained from combined x-ray and neutron studies, neutron diffraction with isotopic substitution, and near-resonant x-ray diffraction using synchrotron radiation [20].

Salts. Molten salts were among the first liquids to which the method of multi-pattern analysis with isotopic substitution was applied [21, 22] and a large number of systems have been studied. Extensive recent reviews on the subject are available [23, 24]; only some recent examples will be discussed.

Among liquid inorganic halides, $ZnCl_2$ is unusual for its high viscosity at the melting point (318 °C), and for its consequent low electrical conductivity and its ability to supercool into a glass, metastable at room temperature. It has been studied by EXAFS [25], x-ray [26], and neutron diffraction [27], the latter using the isotopic substitution method. The complete set of ion pair distribution functions derived from the neutron work is shown in Fig. 4. The distance ratio of the $g_{ClCl}(r)$ peak at 3.7 Å and the $g_{ZnCl}(r)$ peak at 2.3 Å is close to the value $(8/3)^{1/2}$, which is the expected value for tetrahedral coordination of the Cl^- ions around the Zn^{2+} ions. The area under the Zn—Cl peak at 2.3 Å is 4.3, in agreement with this view. These results rule out the existence of $ZnCl_4^{2-}$ complexes in the melt. They strongly suggest a close packing of Cl^- ions with the Zn^{2+} ions located in the tetrahedral holes typical

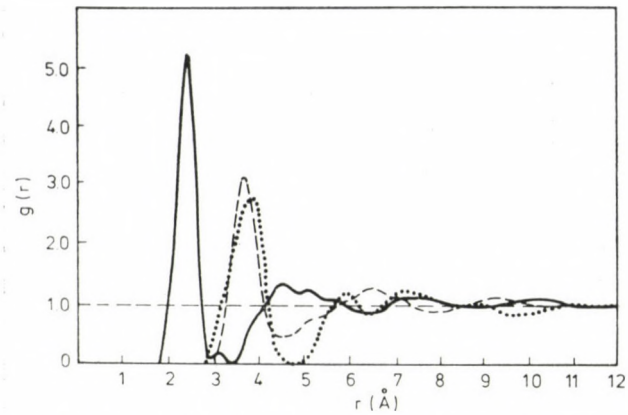

Fig. 4. Ion-ion pair distribution functions for liquid $ZnCl_2$ at 600 K from neutron diffraction [27]; solid line, g_{+-}; broken line, $g_{--}(r)$; dotted curve, $g_{++}(r)$

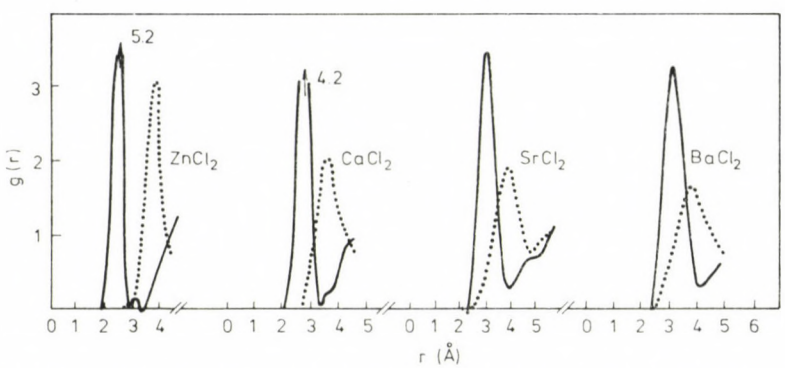

Fig. 5. First-neighbor distributions in molten salts from neutron diffraction [24]; with increasing cation size there is increasing penetration of anion-anion interactions (broken curves) into the nearest-neighbor anion-cation (solid lines) distance distributions

of such a structure. These results are in good agreement with the interpretation of x-ray data; they disagree with the EXAFS results.

The well-defined coordination of Zn^{2+}, a manifestation of the ability of this small ion to occupy tetrahedral sites in the Cl^- substructure, becomes progressively less defined as the cation size increases [24]. Fig. 5 clearly shows the marked tendency for penetration of like ions into the first coordination shell for the larger cations.

D. Aqueous solutions

Aqueous solutions are, of course, in general ionic liquids. In view of their enormous importance to whole branches of science they deserve special consideration: "the developments in solution diffraction techniques alone are revolutionary" [28].

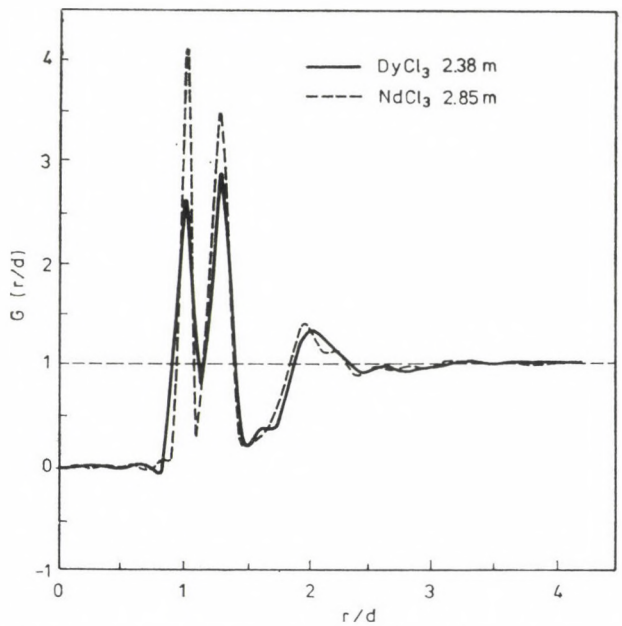

Fig. 6. Comparison of the radial distribution functions for Nd^{3+} and Dy^{3+}-water interactions. The radial distances have been scaled by d, the cation-oxygen distance (2.48 Å for $NdCl_3$ and 2.37 Å for $DyCl_3$)

An aqueous solution of monatomic ions is characterized by ten different pair distribution functions, and an equal number of experiments with different scattering factor combinations is necessary for their determination. While this sounds hopeless, it will be feasible with the next generation of neutron and synchrotron x-radiation sources. In the meantime, it has been the pioneering work of Enderby and his Leicester—Bristol group [29] to show that useful information on ion-water interactions can often be uniquely obtained from only two neutron diffraction experiments, and that each properly designed additional experiment gives information on the ion pair interactions [30, 31]. The method consists of measuring the neutron diffraction pattern of two solutions, identical in every respect except the isotopic state of one of the ions. The arithmetic difference between the two data sets then yields directly the weighted sum of the ion-water and ion-ion interactions. A number of mono and divalent metal chlorides have been studied by this method [31]. In Fig. 6 radial distribution functions for two lanthanide chlorides [32, 33] are compared in reduced distance units $r^* = r/d$, with d the value of the first maximum in the radial distribution functions for the two solutions, namely 2.48 Å for $NdCl_3$ and 2.37 Å for $DyCl_3$. The first peak at $r^* = 1$ is due to $M^{3+} \ldots O$ interactions, and the second to $M^{3+} \ldots D$ interaction (the experiments were done with solutions in heavy water to minimize incoherent scattering). The

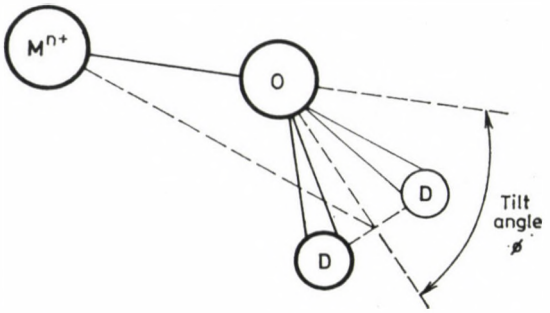

Fig. 7. Typical orientation of a water molecule in the first hydration sphere of a cation determined by neutron diffraction

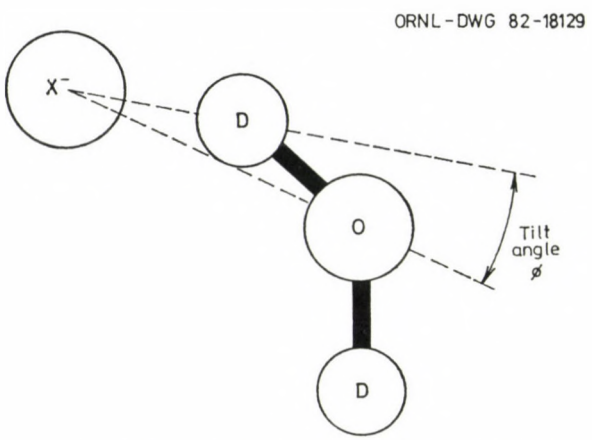

Fig. 8. Typical orientation of a water molecule in the first hydration sphere of a chloride ion determined by neutron diffraction

ratios of the areas under these peaks are close to 1 : 2 as expected for water molecules, and their magnitude yields directly the coordination numbers 8.5 for Nd^{3+} and 7.4 for Dy^{3+}. This decrease in coordination number along the lanthanide series is barely outside the error limits of these absolute measurements. The sharp second peak for the $M^{3+} \ldots D$ interactions suggests a coplanar arrangement of deuterium atoms, as indicated in Fig. 7 for one ion-water pair. The tilt angle Φ, determined by the $M^{3+} \ldots O$ and $M^{3+} \ldots D$ distances, is of considerable interest; values of $24° \pm 4°$* and $17° \pm 3°$ have been found for Nd^{3+} and Dy^{3+}, considerably smaller than the values of $\Phi \sim 30°$—$40°$ reported for concentrated mono and divalent metal chloride solutions [31]. The hydration of anions in D_2O has been studied with matched solutions that differ only in the isotopic state of the anion. For the chloride ion it was found [31, 34] that the $Cl^- \ldots D$ distance (Fig. 8) is independent

* Not 55° as erroneously reported in [32].

of the cation size, charge, and electronic structure. The average number of water molecules around a Cl^- ion seems to be six, decreasing with concentration, and the tilt angles have values close to 0°.

Results for ion-ion pair interactions in water, obtained from analyses of multi-pattern neutron diffraction data, have been reported for one solution, namely 4.35 m NiCl in D_2O [35]. These measurements are extremely difficult and the accuracy of the results derived from them is, at present difficult to judge.

IV. Summary and outlook

The aim of statistical mechanical theory is to predict the properties of liquids from models for the interaction of the particles (atoms, ions, molecules). The theory can be tested in computer simulations which yield accurate results for a particular model. An example is the test of RISM theory for hard sphere and Lennard—Jones (12/6) interaction models of molecular fluids. The computer simulations showed that RISM provided a good description of these systems. The theory was then used to improve the interaction model by comparing computed atom pair distribution functions with those obtained from diffraction studies [6, 8, 9]. More experimental data are needed for molecular fluids: in addition to isotopic H/D substitution which is problematical because of the large inelasticity corrections, isotopic substitution experiments with $^{15}N/^{14}N$, $^{34}S/^{32}S$, and even $^{13}C/^{12}C$ are feasible with present day techniques.

Diffraction data on molten salts and metals have also been used to test interaction models [29] for ionic systems.

The situation is not so clear for metallic glasses and amorphous solid semiconductors. These materials seem poorly understood at the atomic level and diffraction studies of both liquids and amorphous solids of this class seem very promising.

Single difference experiments with neutrons on isotopically substituted ions have become almost routine and provide an invaluable tool for the study of ionic hydration, complexation, and other solution phemona. The determination of ion pair interactions by multipattern analysis will become possible in the next few years, to concentrations below $\sim$1 *m*. This will make possible the testing of statistical mechanical theories for ion-ion interactions in water.

The exciting rseults of the last decade came overwhelmingly from neutron scattering results. The next decade will se new impetus in x-ray scattering from work carried out at the second generation of synchrotron radiation facilities. This will require a change in attitude for the scientists who want to remain in the forefront of x-ray research. As has happened with neutron scattering, the exciting results will come from the new national or regional facilities.

It is a pleasure to acknowledge many stimulating discussions with Brian Annis, Sue Biggin, Tony Habenschuss, Dick Hahn, and Elijah Johnson during the preparation of this manuscript.

REFERENCES

[1] Blum, L., Narten, A. H.: Adv. Chem. Phys., **34,** 203 (1976)
[2] Narten, A. H., Levy, H. A.: J. Chem. Phys., **55,** 2263 (1971)
[3] Enderby, J. E., Neilson, G. W.: Adv. Phys., **29,** 323 (1980)
[4] Blum, L.: J. Comp. Phys., **7,** 592 (1971)
[5] Narten, A. H.: J. Chem. Phys., **66,** 3117 (1977)
[6] Habenschuss, A., Johnson, E., Narten, A. H.: J. Chem. Phys., **74,** 5234 (1981)
[7] Yarnell, J. L., Katz, M. J., Wenzel, R. G., Koenig, S. H.: Phys. Rev., **A7,** 2130 (1973)
[8] Narten, A. H.: J. Chem. Phys., **67,** 2102 (1977)
[9] Narten, A. H., Habenschuss, A.: J. Chem. Phys., **75,** 3073 (1981)
[10] Sandler, S. I., Lombardo, M. G., Wong, S. S.-H., Habenschuss, A., Narten, A. H.: J. Chem. Phys., **77,** 2144 (1982)
[11] Narten, A. H., Johnson, E., Habenschuss, A.: J. Chem. Phys., **73,** 1248 (1980)
[12] Narten, A. H., Agrawal, R., Sandler, S. I.: Mol. Phys., **35,** 1077 (1978)
[13] Streett, W. B., Tildesley, D. J.: Proc. Roy. Soc. London **A355,** 239 (1977)
[14] Pálinkás, G., Kalman, E., Kovács, P.: Mol. Phys., **34,** 525 (1977)
[15] Thiessen, W. E., Narten, A. H.: J. Chem. Phys., **77,** 2656 (1982); Narten A. H., Thiessen, W. E., Blum, L.: Science, **217,** 1033 (1982)
[16] Soper, A. K., Silver, R. N.: Phys. Rev. Let., **49,** 471 (1982)
[17] Dore, J. C.: private communication
[18] Wood, D. W.: in Water a Comprehensive Treatise, Vol. **6,** p. 279 (Ed. F. Franks), Plenum Press, New York 1979
[19] Bertagnolli, H., Chieux, P.: Mol. Phys., **51,** 617 (1984)
[20] For a recent review see: Steeb, S., Lamparter, P.: in Liquid and Amorphous Metals V, Vol. **I,** p. 237 (Eds. C. N. J. Wagner and W. L. Johnson), North-Holland Physics Publishing, Amsterdam 1984
[21] Page, D. I. and Mika, K.: J. Phys. C, **4,** 3034 (1971)
[22] Edwards, F. G., Enderby, J. E., Howe, J. E., Page, D. I.: J. Phys. C, **8,** 3483 (1975)
[23] Enderby, J. E., Neilson, G. W.: Adv. Phys., **29,** 323 (1980)
[24] Enderby, J. E., Biggin, S.: Adv. Molten Salt Chem., **5,** 1 (1983)
[25] Wong, J., Lytle, F. M.: J. Non-Cryst. Solids, **37,** 273 (1980)
[26] Triolo, R., Narten, A. H.: J. Chem. Phys., **74,** 703 (1981)
[27] Biggin, S., Enderby, J. E.: J. Phys. C, **14,** 3129 (1981)
[28] Friedman, H. L.: Ann. Rev. Phys. Chem., **32,** 179 (1981)
[29] Enderby, J. E., Howells, W. S., Rowe, R. A.: Chem. Phys. Letters, **21,** 109 (1973)
[30] Enderby, J. E., Neilson, G. W.: in Water a Comprehensive Treatise, Vol. **6,** p. 1 (Ed. F. Franks), Plenum Press, New York 1979
[31] Enderby, J. E.: Ann. Rev. Phys. Chem., **34,** 155 (1983)
[32] Narten, A. H., Hahn, R. L.: J. Phys. Chem., **87,** 3193 (1983)
[33] Annis, B. K., Hahn, R. L., Narten, A. H.: J. Chem. Phys., **82,** 2086 (1985)
[34] Biggin, S., Enderby, J. E., Narten, A. H.: J. Phys. Chem. **88,** 3634 (1984)
[35] Neilson, G. W., Enderby, J. E.: Proc. Roy. Soc. Lond., **A390,** 353 (1983)

Acta Chimica Hungarica 121 (1—2), pp. 187—202 (1986)

DIFFRACTION STUDIES ON SOLVENT AND SOLUTIONS+

Gábor PÁLINKÁS and Erika KÁLMÁN*

(Central Research Institute for Chemistry of the Hungarian Academy of Sciences, H-1525 Budapest, P.O. Box 17)

Received May 10, 1985

The present paper is concerned primarily with the current state of development of methods by diffraction measurements for obtaining the distribution functions which describe structural consequences due to ionic solvation.

1. Introduction

A survey of the literature of diffraction investigations on liquids leads to the striking observation that the majority of these studies deal with aqueous electrolyte solutions. On reason for this marked interest may be due to the phenomenon of hydration which has been a central problem of physical chemistry from the very beginning. Another explanation is perhaps, that for a long time the theory of liquids could be successfully applied only in the interpretation of properties of the simple van der Waals liquids and dilute electrolyte solutions.

The history of X-ray diffraction experiments of aqueous solutions dates back to nearly 55 years. Neutron and electron diffraction studies have started only with the last decade and so far, only few solutions have been investigated. Although diffraction studies cover mainly X-ray investigations, the use of the other two, relatively new liquid diffraction methods offers new possibilities in the structure investigation of solvents and solutions. In spite of the progress made in experiment techniques, the X-ray method had shown very slow development for a long time. A characteristic feature of these efforts was repeated reinvestigation of the solutions at different stages of development of the X-ray method. At the very beginning, the analysis of experimental data was restricted to the observation of intensity and the shape of the first main peak of the diffraction pattern as a function of increasing ion concentration. Later on, by introducing the Fourier transformation in data treatment,

+ This paper was presented at the Symposium, on Structure of Liquids and Solutions at Veszprém, August 27—30, 1984.

* To whom correspondence should be addressed.

analysis in most cases was henceforward limited to the interpretation of the first peak in the radial distribution function. Interpretation of the whole intensity distribution curve is, however, the result of only ten years.

2. H-bonded solvents

Although, molecular liquids were among the first to which the method of X-ray diffraction was applied, for the time being the structure of only few hydrogen bonded solvents has been investigated by diffraction methods. These are liquid water, some alcohols and simple liquid amides.

Liquid water

The averaged molecular structure of liquid water has been a subject of interest for many years, but despite the number of diffraction experiments and models, proposed to explain the experimental data, no definite solution has been obtained, yet. During the past fifteen years, interest has been focused on intensive neutron diffraction investigations and on the introduction of electron diffraction experiments. The main objective of diffraction experiments was the accurate measurement of experimental data in a broad temperature and scattering variable range. The structure of water molecules in the liquid state was investigated with neutron and electron diffraction experiments, and by combination of the data of different diffraction methods, the first attempts to determine experimentally the three pair-correlation functions of liquid water has been made.

In an extensive study, Narten and Levy [1] have determined the high quality X-ray structure and correlation functions $H^{X}(k)$, $G^{X}(r)$ for water between 4 and 200 °C. The results have shown that the structure functions $H^{X}(k)$ for liquid water below 100 °C rise monotonously through a pronounced double maximum centered around 2.5 $Å^{-1}$ and oscillate with decreasing amplitude around the asymptotic value $H^{X}(\infty) = 0$. The double maximum merges gradually into a simple peak with increasing temperature. The first peak in the experimental functions derived, indicates a nearest neighbour separation of 2.84 Å at 4 °C, increasing to 2.94 Å at 200 °C. The coordination number for first neighbors is about four which is invariant with respect to the temperature. The maxima at 4.5 and 7 Å in the correlation function disappear with increasing temperature.

Reinvestigation of the X-ray scattering of liquid water at 4°, 25° and 50 °C Hajdu et al. [2] has led results close to those of Narten and Levy.

The neutron diffraction structure function $H^{N}(k)$ of heavy water was first measured by Page and Powles [3]. The results have been interpreted

by the authors using models for the correlation between the orientation of molecular pairs ranging from completely uncorrelated orientation to the orientation of adjacent molecules in ice I. The conclusion was drawn that neither these nor any of the popular models for liquid water — e.g. the watery model or the clathrate model, nor a non-hydrogen-bonded model — fit the neutron-diffraction data obtained over a whole range of k. The same conclusion was drawn by Ohtomo and Arakawa [4] analysing the neutron structure function of heavy water derived by means of the time-of-flight method using a pulsed neutron beam produced by a linear accelator. Neutron diffraction studies of Narten [5] and Powles, Dore and Page [6] have suggested similar structures for light and heavy water.

The systematic change of neutron diffraction structure functions of D_2O were investigated by Walford, Clarke and Dore [7] and Gibson and Dore [8] at temperatures in the range 11—75 °C. The analysis of the temperature variation of data showed that the intermolecular OD separation which corresponds to an effective hydrogen bonded distance increases as the temperature rises. Variations at larger distances were attributed to a change in the relative orientation of neighbouring molecules.

Electron diffraction measurements for heavy and light water at 5 °C were presented and analysed by Kálmán, Pálinkás and Kovács [9]. In agreement with earlier neutron and X-ray data, ED studies also predicted nearly identical structures for heavy and light water. The structure of water molecules in the liquid was found to be same as that of free molecules, the rms variations of intramolecular distance were, however, larger in liquid. This conclusion is in agreement with Narten's neutron results [5] and slightly differs from the findings of Walford et al. [7] which were also based on neutron data. The nearest intermolecular O—O and O—H separations were found to be 2.85 Å and 1.95 Å indicating deviations from linear hydrogen bonding. The distance spectra derived from ND, ED and XD measurements are shown in Fig. 1. Many efforts have been made recently for the experimental isolation of $g_{OO}(r)$, $g_{OH}(r)$ and $g_{HH}(r)$ partial pair correlation functions of liquid water. The first separation of partials was obtained by Pálinkás, Kálmán and Kovács [10] using a combination of XD, ED and ND data on liquid D_2O. Neutron diffraction measurements for the derivation of OO, OD and DD correlation functions applying isotope substitution techniques were reported by Thiessen, Blum and Narten [11—12], and by Reed and Dore [13—14]. Neutron diffraction measurement of $g_{HH}(r)$ was presented by Soper and Silver [15]. A comparison between experimental results for first and second peak positions of partial correlation functions is given in Table I.

Different experimental data for oxygen-oxygen distance distribution are in close agreement. However, significant discrepancies can be found between available sets of data of O—H and H—H distributions. The data

Table I

First (r_1) and second (r_2) peak positions in Å *of partial* O—O, O—H *and* H—H *pair correlation functions obtained by different experimental techniques.*
IS stands for isotopic substitution method

	O—O		O—H		H—H	
	r_1	r_2	r_1	r_2	r_1	r_2
1) ED, XD, ND [10]	2 85	4.40	1.95	2.95	2.45	3.80
2) ND-IS [13—14]	2.85	4.40	1.95	3.02	2.45	3.80
3) ND-IS [11]	2.85	4.50	1.86	3.20	2.29	3.90
4) ND-IS [15]	—	—	—	—	2.34	3.82

set (3) in Table I is consistent with linear hydrogen bond formation while data set (1—2) predict deviations from linearity. At large r-values (>3 Å) the various data exhibit more varied discrepancies.

Liquid alcohols

X-ray data on methanol [16—17], ethanol [16] and tertiary butyl alcohol [16] show clear evidence for hydrogen bonding in these liquids (Fig. 2). The most striking feature of distance spectra in Fig. 2 is the presence of a strong peak near 2.8 Å. This peak must be ascribed to hydrogen bonded hydroxil groups. In alcohols each hydroxil group has nearly two hydroxil neighbours on the average. The experimental results could be interpreted in terms of chain formation. The large local instantaneous deviations from the average chain configuration lead to a decrease in correlations for distances greater than few molecular diameters from any molecule. Structural parameters of hydrogen bonded OH . . . OH interactions are given in Table II.

Results of the neutron diffraction studies on CD_3OH, CD_3OD and mixtures of these compounds [18] are in close agreement with X-ray results an interpretation of liquid structure.

Table II

Mean O—O *distances r_{00}, with r.m.s. deviations and number of hydrogen bonds as derived by* X*-ray diffraction* [16]

	r_{00} (Å)	l_{00} (Å)	n_{00}
Methanol	2.798	0.142	1.77
Ethanol	2.808	0.113	1.81
CMeOH	2.740	0.08	~2

Liquid amides

The first X-ray study on liquid formamide has been made by De Sando and Brown [19]. The authors assigned to the O . . . N interaction a length of 3.05 Å and suggested that formamide in the liquid state has a short range

order which resembles that in the crystalline state. The crystal structure of formamide consists of puckered sheets of molecules. Within the sheets, pairs of formamide molecules associate around the symmetry centers to form almost coplanar dimers. Within each sheet two types of hydrogen bond are found.

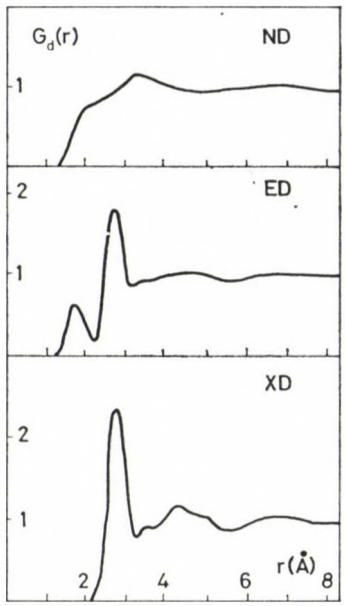

Fig. 1. Intermolecular distance spectra of liquid water: ND [7], ED [9], XD [2]

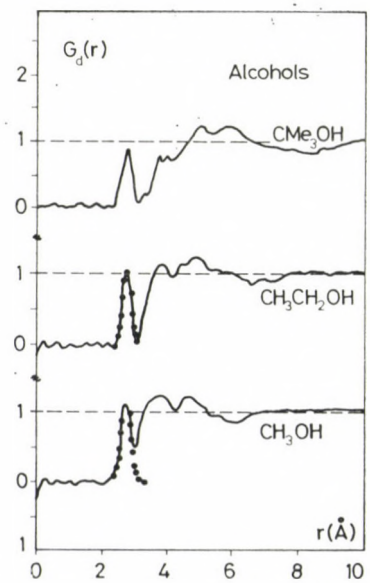

Fig. 2. Intermolecular distance spectra of alcohols derived by X-ray diffraction [16]

One of these is 2.93 Å and links molecules to form bimolecular units, the other which is 0.05 Å shorter, links the bimolecular units together to form sheets. Both cyclic dimers and linear chains are formed in the crystal phase.

Recent combined ND, ED, XD measurements have yielded the accurate molecular structure $H_m(k)$ and the average geometry of the hydrogen bond $H_d(k)$ in liquid state at a temperature of 25 °C [20]. The molecular parameters resulting from liquid electron and X-ray diffraction experiments were found in good agreement with those from gas electron diffraction. The structure of the formamide molecule was found to be the same as that of a free molecule. Analysis of the three distinct structure functions (Fig. 3) has lead to the nearest

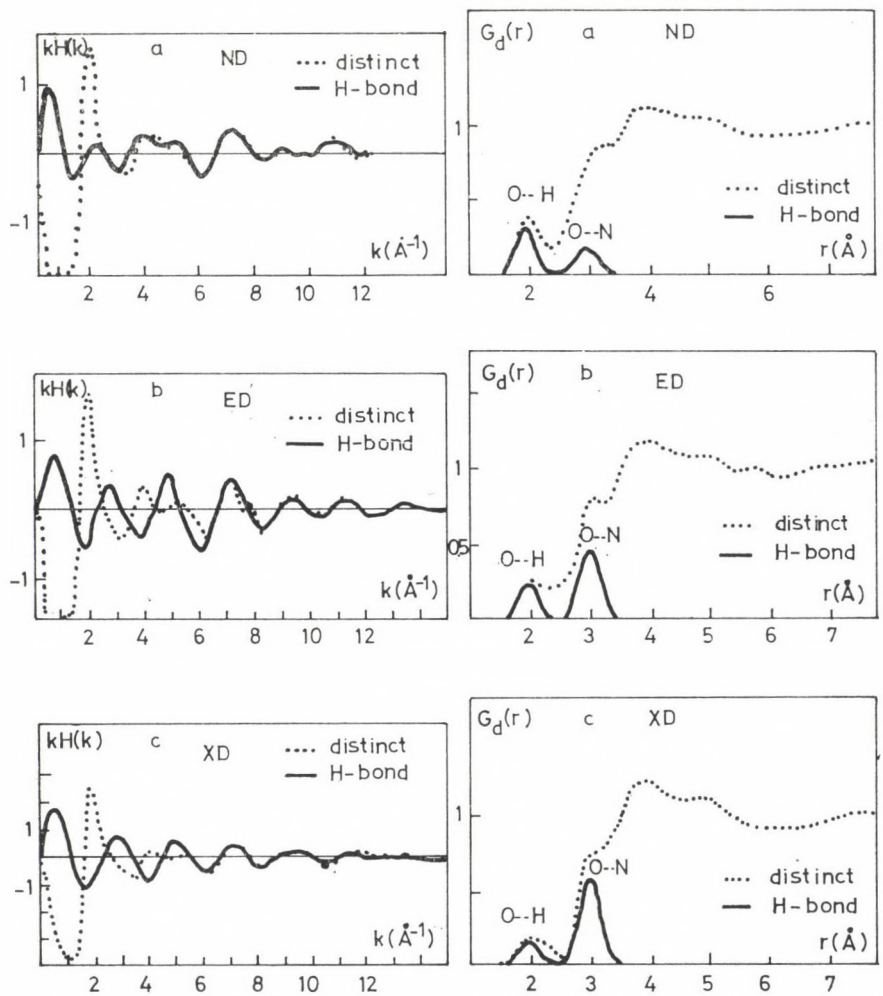

Fig. 3. The distinct structure functions $kH_d(k)$, and distance spectra $G_d(r)$ got by ND, ED, XD measurements for liquid formamide at 250 °C. The full lines represent the contributions of the O . . . N and O . . .H-bond interactions

Table III

Mean O . . . N and O . . . H intermolecular distances (r) and associated r.m.s. variations (l) and average number of H-bonds per molecule (n)

		r (Å)	l (Å)	n
ED	O . . . N	2.90 (1)	0.161	4.08
	O . . . H	1.90 (1)	0.147	4.00
ND	O . . . N	2.90 (4)	0.169	4*
	O . . . H	1.90 (2)	0.152	3.9
XD	O . . . N	2.92 (4)	0.175	3.54
	O . . . H	1.93 (6)	0.070	4*

* Values were maintained.

neighbour O . . . N and O . . . H distance, r.m.s. deviations and average number of H-bonds in liquid formamide given in Table III. These values of mean distances allowed estimation of an average N—H . . . O angle of about 10 degrees.

A further analysis of the X-ray structure function [21] has lead to the conclusion that liquid formamide mainly consists of a chain-like hydrogen bonded structure of formamide molecules, however, the existence of ring dimers in liquid cannot be excluded by the X-ray diffraction method.

The structure function of N,N-dimethyl formamide (DMF) was determined at 25 °C by means of X-ray diffraction [22]. The least-squares analysis of the total structure function resulted in a polar skeletal structure of the molecules in liquid phase not appreciable different from those found in the gas phase. The featureless distance spectrum of DMF showed that the intermolecular arrangement of DMF molecules is practically fully disordered and no evidence has been found for cluster formation of DMF molecules in liquid phase.

3. Structure of solutions

In the past ten years many diffraction studies have been made to describe the structure of the solvation shell of ions and to characterize the influence of ions on solvent structure or to gain information on the orientation of solvent molecules near to ions. It is characteristic of the investigations that most measurements were carried out by means of X-ray diffraction and the methods were very seldom applied for salts in organic solvents. The reason for latter is due to difficulties arising in the analysis of total structure functions with increasing number of site-site interactions for organic solvent. There are also differences in the methods of analysis applied to different types of data sets. The analyses of diffraction data have mainly been carried out on structure

functions in XD and ED methods while the ND experimental data have been interpreted in the r-space on the basis of $G_M(r)$ and $G_A(r)$ ion-water difference functions. — No measurement has been carried out on organic solutions with the ND method yet. — In the following section the solvation of ions presented by different methods will be discussed to illustrate the description of ionic solvation by diffraction techniques.

The description of the hydration shell has usually been confined to the second coordination shell of ions in terms of structural parameters. Octahedral hydration around cations was found to be the most common. Of course one cannot expect rigid structure in solution, and the symmetry of a hydration shell has to be thought in sense of an averaged picture from which great deviations are also allowed. Tetrahedral configurations have been reported for Zn [23] and Hg [24] in solutions with halide ions. The existence of inner shell complex formation $M(H_2O)_{6-x}A_x$ ($x \sim 0.1$—0.9) has been predicted for several double and triple charged cations [25—35]. Concerning the data available the structural parameters obtained by X-ray diffraction method are hardly dependent on the counterion and concentration of solutions except in a few cases. Typical experimental structure functions together with the best model structure functions are shown in Fig. 4 for aqueous $FeCl_3$ [36] and for some transient metal halide solutions [25]. Some relevant results inferred on ionic hydration are given in Table IV.

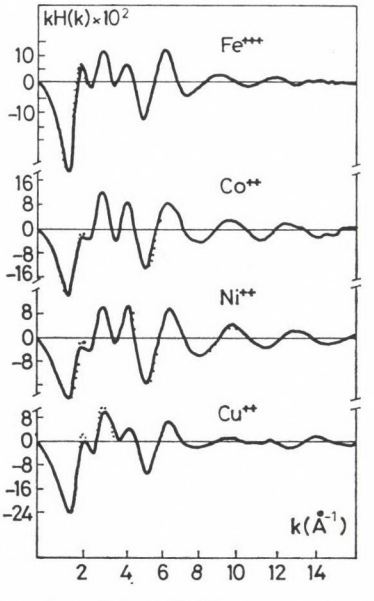

Fig. 4. Experimental (dots) and model (full) X-ray structure functions $kH(k)$ of 2 molar aqueous $FeCl_3$ [36] and transient metal halide solutions [25]

Table IV

Nearest neighbour ion-oxygen distances r_{Iw}(Å), rms variations ($l^2_{Iw} = (r_{Iw} - r)^2$), distances r_{w1w2} and rms variations l_{w1w2} for water molecules in the first and second hydration shell. The concentration of solutions (M = molal, m = molar) and references [ ] are given in the last two columns. R_{Ion} denotes Pauling radii of ions

	R_{Ion}	r_{Iw}	l_{Iw}		r_{w1w2}	l_{w1w2}	conc.	[1]
Li	0.60	2.10	0.12	6	2.72	0.10	2.2 M LiI	33
Na	0.95	2.42	0.27	6	—	—	2 M NaCl	37
K	1.33	2.80	0.19	6	—	—	2 M KCl	37
Cs	1.69	3.15	0.22	8	—	—	2 M CsCl	37
Tl	1.4	3.22	0.17	0.8	—	—	Tl formate	38
Mg	0.65	2.12	0.04	6	2.79	< 0.02	1.1 M $MgCl_2$	34
Ca	0.99	2.44	0.15	6	—	—	2 m $CaBr_2$	35
Mn	0.80	2.20	0.10	6	2.78	0.04	2 m $MnSO_4$	26
Co	0.77	2.10	0.10	6	2.75	0.05	3 m $CoCl_2$	25
Ni	0.69	2.07	0.09	6	2.74	0.05	3 m $NiCl_2$	25
Zn	0.74	2.10	0.16	6	2.70	0.11	3 M $ZnSO_4$	29
Cd	0.97	2.32	0.10	6	2.81	0.15	3 M $CdSO_4$	32
Al	0.50	1.89	0.10	6	2.68	0.09	2 m $AlCl_3$	31
Cr	0.53	1.94	0.10	6	2.71	0.07	1.44 m $Cr_2(SO_4)_3$	27
Fe	0.53	2.08	0.14	6	2.77	0.04	2.3 m $FeCl_3$	36
In	—	2.16	0.11	6	2.67	0.06	1.71 m $In_2(SO_4)_3$	28
Ce	1.01	2.25	0.12	8	2.90	0.14	2 m $Ce(NO_3)_3$	30
Cl	1.81	3.10	0.20	6	—	—	3 m $CoCl_2$	25
I	2.16	3.63	0.26	6.9	—	—	2.2 M LiI	33
Br	1.95	3.34	0.26	6	—	—	2 m $CaBr_2$	35
NO_3	—	3.40	0.28	7	—	—	2 m $Ce(NO_3)_3$	30
SO_4	—	3.83	0.27	8.2	—	—	3 m $ZnSO_4$	29

Some general conclusions deducible from the data in Table IV are as follows:

(i) Cation-water distances are nearly equal to the sum of the radii of cations and of the water molecule.

(ii) The first hydration shell of divalent and trivalent cations is much better localized around ions — as revealed by l_{Iw} parameters — than that for single charged cations and anions.

(iii) A secondary hydration shell is observable for double and triple charged cations with strongly shortened H-bond interaction between water molecules in primary and secondary hydration shells (r_{w1w2}, l_{w1w2}).

Habenschuss and Spedding showed measurability of small changes in hydration of ions by the X-ray diffraction method investigating a series of concentrated aqueous rare earth chloride solutions [39]. Careful examination of the X-ray diffraction results for ten solutions (Fig. 5) has proved that the coordination number for primary hydration shells of the rare earth ions decreases from nine to eight due to the decreasing ionic radii.

The structural parameters for $[RE(H_2O)_x]^{3+}$ complexes shown in Fig. 6 were obtained by least-squares analysis applied to distance spectra given in Fig. 6. Crystal hydrates supports the existence of the hydration change.

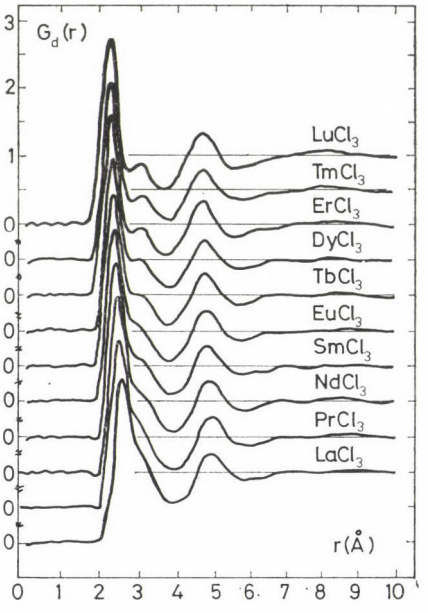

Fig. 5. Distance spectra $G_d(r)$ for ten concentrated aqueous rare earth chloride solutions [39] (reproduced by premission of J. Chem. Phys.)

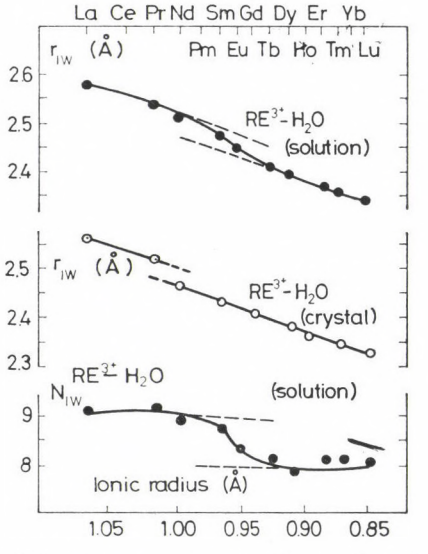

Fig. 6. The average $Re^{3+}-H_2O$ distances, coordination numbers in the crystals and solutions [39] (reproduced by permission of J. Chem. Phys.)

4. Complex formation as studied by X-ray and electron diffraction

The complexes are held together by chemical bonds resulting in long-lived structure with well-defined symmetry properties in contrast to short lived structures of ion-solvent aggregates produced by intermolecular force. The existence of strong chemical interactions between atoms in the complex results in a decrease in the r.m.s. variation of mean distances between pairs of atoms and in a corresponding increase in the structure functions at high scattering variable ranges which increases the accuracy of the determination of structural parameters as well.

Although diffraction method is at present the best means for obtaining direct structural information on complex formation in solutions, no unambiguous structure determination of the complexes can be made merely on the basis of diffraction data. This requires the combination of equilibrium data and information on the symmetry properties derived from spectroscopic and crystal structure data. If complex formation is weak — as it is in the case of $M(H_2O)_{6-x}A_x$ aqueous transition metal complexes, with $x < 1$ — diffraction data give only slight indications for existence of a given complex. By diffraction data analysis, however, only the presence or absence of a given type of complex can be determined.

An earlier X-ray study [40] of nine concentrated aqueous $ZnBr_2$ solutions indicated, based on the analysis of the areas under the peaks in the radial distribution functions, that the Zn^{++} ion is coordinated by two bromide and two water molecules. It also showed that the zinc ion becomes totally four coordinated by bromide if the bromide/zinc ratio increases by the addition of hydrobromic acid. The concentration in Zn^{++} of the solutions investigated ranged from 3.5 up to 17.7 molal for $Br^-/Zn^{++} = 2$ and from 4.2 up to 23 molal at higher Br^-/Zn^{++} ratios. Interatomic distances for Zn^{++}—Br^- Br^-—Br^- and Br—O contacts were found to be at 2.4 A, 3.9 A and 3.2 A, respectively. A tetrahedral symmetry of the complexes was suggested.

Contrary to zinc solutions recent X-ray diffraction studies of aqueous nickel bromide solutions with $Br^-/Ni^{++} = 2$ [41—42] and nickel chloride solutions with $Cl^-/Ni^{++} = 2.4$ [43], showed the presence of octahedral $Ni(H_2O)_6^{++}$ and $Ni[Br(H_2O)_5]^+$ as well as octahedral $Ni(H_2O)_6^{++}$, $Ni(H_2O)_5Cl^+$ and $Ni(H_2O)_4Cl_2$ complexes. The Cl^- in the 1 : 2 complexes were found in transpositions as in crystalline $NiCl_2 \cdot 6\ H_2O$.

The above results show some differences between the complex formation of similar sized zinc and nickel ions. In order to reinvestigate the structure of bromide complexes of Zn^{++} we measured the X-ray and electron scattering of an aqueous solution (1.64 molar in Zn^{++}), as well as the electron scattering of an dimethylformamide solution (1.77 molar in Zn^{++}) with a Br^-/Zn^{++} ratio of 3 [44—45]. The excess of bromide ions was achieved by the addition of LiBr salt.

Table V

Mean distances $r_{\alpha\beta}$ [Å], r.m.s. variations $l_{\alpha\beta}$ and coordination numbers $N_{\alpha\beta}$ for nearest neighbour interactions obtained from the electron (E) and the X-ray (X) structure functions for the aqueous solution

	$r_{\alpha\beta}$	$l_{\alpha\beta}$	$N_{\alpha\beta}$	$R_{\alpha\beta}$	$L_{\alpha\beta}$
E					
Zn^{++}—O	2.23	0.083	2.40	2.63	0.05
Zn^{++}—Br^-	2.40	0.126	2.22	3.48	0.01
O—O	2.93	0.102	1.12	2.88	0.29
Br^-—O	3.49	0.195	4.36	3.26	0.19
Br^-—Br^-	3.91	0.116	1.36	5.27	0.15
Zn^{++}—O	2.21	0.093	2.42	3.06	0.09
Zn^{++}—Br^-	2.42	0.116	2.26	3.69	0.02
O—O	2.90	0.082	1.09	2.83	0.21
Br^-—O	3.45	0.25	4.20	3.36	0.13
Br^-—Br^-	3.95	0.132	1.28	.483	0.17

The structural parameters (Table V) obtained from the two independent diffraction experiments on aqueous solution are in good agreement which supports their reliability. The bond distance of Zn^{2+}—Br^- indicates that the bromo complex belongs to the inner type of coordination. Its value of 2.41 Å is significantly smaller than the expected value from ionic radii, 2.65 Å. A similar phenomenon was observed for Ni^{2+}—Br^- interactions in the aqueous $NiBr_2$ solutions [41]. The bond distance of 2.22 Å for Zn^{2+}—H_2O contact is greater than that for the hexaaquo complex in $Zn(NO_3)_2$ [42] and $ZnSO_4$ [29] solutions. The r.m.s. variations of the mean distances, $l_{\alpha\beta}$, are generally, low, except for Br^-—O interactions. The low values of $l_{\alpha\beta}$ indicate strong interactions between the particles which are characteristic for complex formation [25, 43, 44].

The value of 2.2 for the average number of zinc bromide contacts results in a concentration of about 1.4 mol/L for free hydrated bromide ions. Mean coordination numbers given in Table V are not far from those characteristic for $ZnBr_2(H_2O)_2$ complexes ($N_{Zn-O} = 2$, $N_{Zn-Br} = 2$, $N_{O-O} = 1$, $N_{Br-Br} = 1$). However, the significance of deviations between these parameters is supported by the fact that similar values resulted from both types of diffraction experiments.

The independent refinement of the Zn^{2+}—Br^- and the Br^-—Br^- interactions leads to a tetrahedral Br—Zn—Br angle. This result (together with the low values found for Zn^{2+}—O and O—O contacts) strongly indicates formation of a tetrahedral inner sphere complex.

Complex formation of the Zn^{++} ion in dimethylformamide has been studied by electron diffraction. The Raman spectra of the solution has shown that the only species present in the system is the $ZnBr_3^-$ complex.

Table VI

Structural parameters obtained from ED *structure function for* DMF *solution*

	$r_{\alpha\beta}$	$l_{\alpha\beta}$	$N_{\alpha\beta}$
$Zn^{++}—O$	2.22	0.101	0.28
$Zn^{++}—Br^-$	2.52	0.1040	0.63
O—O	3.45	0.130	1.04
$Br^-—Br^-$	4.06	0.201	0.42

The most remarkable result of the fit is connected with the coordination numbers for Zn—Br and Br—Br interactions (Table VI). Combined with the numbers of corresponding distances within a $ZnBr_3^-$ unit, they indicate that only a fraction $\alpha = 0.21$ of the total number of Zn^{++} ions is bound in such complexes.

The Zn—Br and Br—Br distances are slighly larger than those obtained in the aqueous solution. The values of r_{ZnBr} and r_{BrBr}, parameters indicate a piramidal geometry of the $ZnBr_3$ complex. The Br—Zn—Br angle is calculated to be 107.4° quite close to the tetrahedral value. Although the Li^+—O interaction itself is not detectable in the diffraction pattern because of its low weight, we could derive some information about the Li^+ solvation from the combined N_{ZnO} values. The value of 1.04 obtained for N_{OO} corresponds to an average number of $\approx$3 DMF molecules around each Li^+ ion.

The results reveal stricking differences regarding zinc bromide complex formation in concentrated aqueous and DMF solutions. The fraction of Zn^{2+} ions involved in such complexes is considerably lower in DMF. The reasons for this different complexation behaviour might be the poor solvating ability of DMF molecules for anions and their size.

A direct information can be obtained about the orientation of water molecules using the isotopic substitution method in neutron diffraction. Based on $\Delta H(k)$ and $\Delta G(r)$ difference functions, with assumptions on the geometry of water molecules, the most probable values of angles shown in Fig. 7 are deducible for concentrated aqueous solutions. Data accumulated on the orientation of water molecules near to ions in different concentrations are summarized in a recent review of Enderby and Neilson [46]. Typical difference functions are shown in Fig. 8 for Ni^{++} and Ca^{++} ions.

The mean cation-oxygen r_{C-O} and cation-hydrogen r_{C-D} nearest neighbour distance derived from the peak positions of $\Delta G_C(r)$ difference functions shown in Fig. 8 are given in Table VII. Both the distances and coordination numbers N_{C-O}, calculated from the peak areas of $\Delta G_c(r)$, are in good agreement with those derived from X-ray diffraction data in the accuracy limit of the methods. The angular data in Table VII. strongly favour the nearly lone pair orientation of water molecules in hydration shell of Ni^{++} and Ca^{++} ions in concentrated

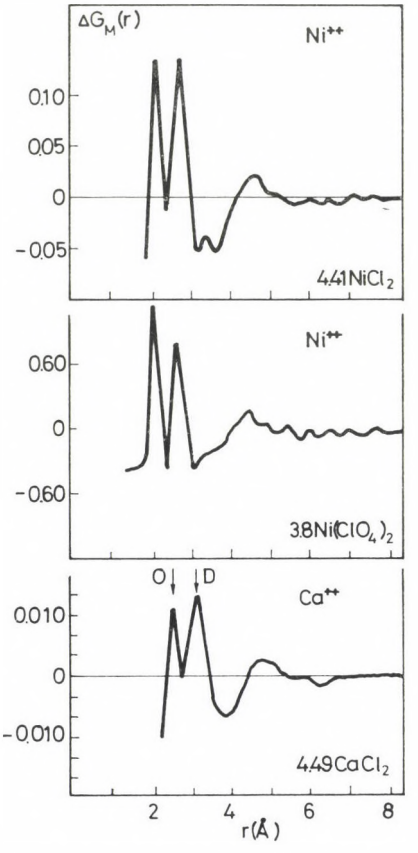

Fig. 7. Angles characterizing orientation of water molecular near to cations (C) and anions (A)

solutions. The same conclusion can be drawn for Li^+ and Cu^{++} ions based on difference functions derived for concentrated LiCl [47] and $CuCl_2$ [46] solutions

ND studies with $^{35}Cl : {}^{37}Cl$ isotopic substitution have shown that the hydration of the chloride ion is essentially independent of the counter cation (Li, Na, Rb, Ca, Ni, Ba) and concentration (1—9 molal) [49—51].

Table VII

Structural parameters derived by ND *method with isotropic substitution for* Ni^{++} *and* Ca^{++} *ions*

Solution	Isotopes	Molarity	r_{C-O} (Å)	r_{C-D} (Å)	N_{C-O}	[ ]
$NiCl_2$ (D_2O)	Ni: ^{62}Ni	4.41	2.07	2.67	42 ± 5.8	48
$Ni(ClO_4)_2$ (D_2O)	Ni: ^{62}Ni	3.8	2.07	2.67	42 ± 5.8	49
$CaCl_2$ (D_2O)	Ca: ^{44}Ca	4.41	2.40	2.93	51 ± 5.5	50

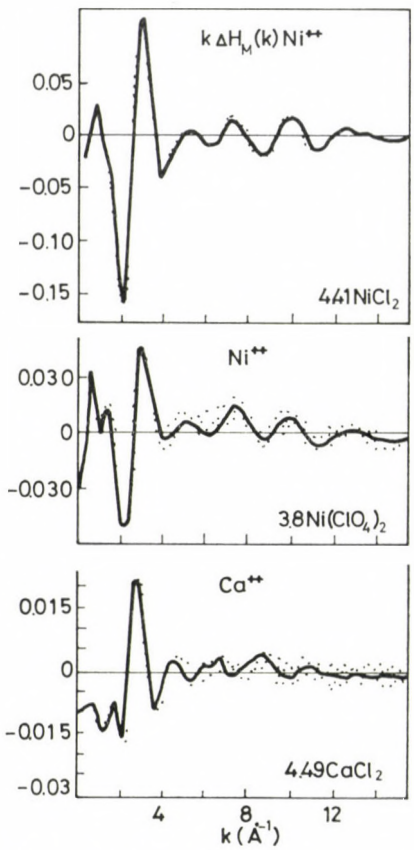

Fig. 8. Cation difference functions $k\Delta H_c(k)$ and $\Delta G_c(k)$ for different aqueous solutions [48—50]

REFERENCES

[1] Narten, A. H., Levy, H. A.: J. Chem. Phys., **55,** 1136 (1971)
[2] Hajdú, F., Lengyel, S., Pálinkás, G.: J. Appl. Cryst., **9,** 184 (1976)
[3] Page, D. I., Powles, J. G.: Mol. Phys., **21,** 901 (1971)
[4] Ohtomo, N., Arakawa, K.: Bull. Chem. Soc. Japan, **51,** 1649 (1976)
[5] Narten, A. H.: J. Chem. Phys., **56,** 5681 (1972)
[6] Powles, J. C., Dore, J. C., Page, D. F.: Mol. Phys., **24,** 1025 (1972)
[7] Walford, C., Clark, J. H., Dore, J. C.: Mol. Phys., **34,** 21 (1977)
[8] Gibson, I. P., Dore, J. C.: Mol. Phys., **48,** 1019 (1983)
[9] Kálmán, E., Pálinkás, G., Kovács, P.: Mol. Phys., **34,** 505 (1977)
[10] Pálinkás, G., Kálmán, E., Kovács, P.: Mol. Phys., **34,** 525 (1977)
[11] Thiessen, W. D., Blum, L., Narten, A. H.: Science, **217,** 1033 (1982)
[12] Thiessen, W. D., Narten, A. H.: J. Chem. Phys., **77,** 2625 (1982)
[13] Reed, J.: Thesis, University of Kenti, 1981
[14] Dore, J. C., ILL Workshop on Water, Grenoble, 1984: Private communication
[15] Soper, A. K., Silver, R. N.: Phys. Rev. Lett., **49,** 471 (1982)
[16] Narten, A. H., Habenschuss, A.: J. Chem. Phys., **80,** 3387 (1984)
[17] Magini, M., Paschina, G., Piccaluga, G.: J. Chem. Phys., **77,** 2051 (1982)
[18] Montague, D. C., Dore, J. C., Cummings, S.: Mol. Phys., **53,** 1049 (1984)
[19] de Sando, R. J., Brown, G. H.: J. Phys. Chem., **72,** 1083 (1968)

[20]Kálmán, E., Serke, I., Pálinkás, G., Zeidler, M. D., Siesman, F. J., Bertagnoli, H., Chichieux, P.: Z. Naturforsch., **38a,** 281 (1982)
[21] Ohtaki, H., Funkai, A., Rhode, B. M., Rebnegger, G.: Bull. Chem. Soc. Japan, **56,** 2116 (1983)
[22] Ohtaki, H., Itoh, S., Yamaguchi, T., Ishihuro, S., Rods, E. M.: Bull. Chem. Soc., Japan, **56,** 3406 (1983)
[23] Wertz, D. L., Bell, J. R.: J. Inorg. Nucl. Chem., **35,** 861 (1973)
[24] Sandstrom, M., Johansson, G.: Acta Chem. Scand., **81a,** 132, 141 (1977)
[25] Magini, M.: J. Chem. Phys., **74,** 2523 (1981)
[26] Caminit, R., Maronqui, G., Paschina, G.: Z. Naturforsch., **37a,** 581 (1982)
[27] Caminit, R.: Chem. Phys. Lett., **36,** 214 (1982)
[28] Caminit, R., Paschina, G.: Chem. Phys. Lett., **82,** 487 (1981)
[29] Radnai, T., Pálinkás, G., Caminiti, R.: Z. Naturforsch., **37a,** 1247 (1982)
[30] Caminit, R., Cucca, P., Dandrea, A.: Z. Naturforsch., **38a,** 533 (1983)
[31] Caminit, R., Licheri, G., Piccaluga, G., Pinna, G.: J. Chem. Phys., **71,** 2473 (1979)
[32] Caminit, R.: Z. Naturforsch., **36a,** 1062 (1981)
[33] Radnai, T., Pálinkás, G., Szász, G., Heinzinber, K.: Z. Naturforsch., **36a,** 1076 (1981)
[34] Pálinkás, G., Radnai, T., Dietz, W., Szász, G., Heinzinber, K.: Z. Naturforsch., **37a,** 1049 (1982)
[35] Licheri, G., Piccaluga, G., Pinna, G.: J. Chem. Phys., **63,** 4412 (1975)
[36] Magini, M., Radnai, T.: J. Chem. Phys., **71,** 4255 (1979)
[37] Pálinkás, G., Radnai, T., Hajdú, F.: Z. Naturforsch., **35a,** 107 (1979)
[38] Ozutsumi, K., Ohtaki, H., Kusumeg, A.: Bull. Chem. Soc. Japan, **57,** 2612 (1984)
[39] Habenschuss, H., Spedding, F. H.: J. Chem. Phys., **70,** 2797, 3758 (1979); **73,** 442 (1980)
[40] Wertz, D. L., Lawrance, R. M., Kruh, R. F.: J. Chem. Phys., **43,** 2163 (1965)
[41] Wakita, H., Ichihashi, M., Mibuchi, T., Masuda, I.: Bull. Chem. Soc. Japan, **55,** 817 (1982)
[42] Raminiti, R., Cucca, P.: Chem. Phys. Lett., **89,** 110 (1982)
[43] Magini, M., Paschina, G., Piccaluga, G.: J. Chem. Phys., **76,** 1116 (1982)
[44] Kálmán, E., Serke, I., Pálinkás, G., Johansson, G., Kabisch, G., Maeda, M., Ohtaki, H.: Z. Naturforsch., **38a,** 225 (1983)
[45] Kabisch, G., Kálmán, E., Pálinkás, G., Radnai, T.: Chem. Phys. Lett., **107,** 463 (1984)
[46] Enderby, J. E., Neilson, G. W.: Rep. Prog. Phys., **44,** 593 (1981)
[47] Newsome, J. R., Neilson, G. W., Enderby, J. E.: J. Phys. C. Solid St. Phys., **13,** 1923 (1980)
[48] Newsome, J. P., Neilson, G. W., Enderby, J. E., Sandstrom, M.: Chem. Phys. Lett., **82,** 399 (1981)
[49] Cummings, S., Enderby, J. E., Howe, R. A.: J. Phys. C. Solid St. Phys., **13,** 1 (1980)
[50] Soper, A. K., Neilson, G. W., Enderby, J. E., Howe, R. A.: J. Phys. C. Solid St. Phys., **10,** 1973 (1977)
[51] Cummings, S., Enderby, J. E., Neilson, G. W., Newsome, J. P.: Nature, **287,** 714 (1980)

Acta Chimica Hungarica 121 (1—2), pp. 203—213 (1986)

RECENT DEVELOPMENTS IN THE THEORY OF THE NON-LINEAR DIELECTRIC BEHAVIOUR OF LIQUIDS+

Imre RUFF

(Laboratory of Theoretical Chemistry, L. Eötvös University, H-1088 Budapest, Múzeum krt. 6—8.)

Received January 18, 1985

The non-linear dielectric behaviour of both polar and apolar liquids gives information on correlations between molecular dipoles and polarizability due to electrodynamic forces as well as due to forces of other effects such as hydrogen bonding, dispersion interactions, etc. While there seems to be a stagnation in the experimental research in this field, the theoretical interpretation of non-linear dielectric effects shows a considerable advance owing to sophisticated statistical mechanical methods introduced recently in the theory of liquids. This paper gives a review of theoretical results published in the last decade.

Introduction

Studies on the non-linear dielectric behaviour of liquids have been published since the 1920's. Most of the experimental results stem from two famous schools, a Polish one founded and led by A. Piekara and a British one established by M. Davies. Although some members of these schools are excellent theoreticians, too, the theoretical foundations of non-linear dielectric effects as well as their development are contributed by authors not belonging to these groups.

An outstanding review of the entire field was published by S. Kielich in 1972 covering both the experimental and theoretical results achieved that far [1]. Since then, quite a number of experimental reports have appeared (see e.g. Refs. [2—8]) extending our knowledge about non-linear effects both in pure liquids and liquid mixtures, yet it seems that nothing strikingly new has been discovered during the last decade. The only exceptions are a few papers of Kielich and his coworkers [9—12] which report on the first measurements of the time evolution of non-linear dielectric effect and on the theoretical basis of the interpretation of these results.

In contrast to experimental studies, the recent development in the theory of non-linear dielectric effects in liquids produced some important results owing mainly to more sophisticated solutions of integral equations

+ This paper was presented at the Symposium on Structure of Liquids and Solutions at Veszprém, August 27—30, 1984.

outlined in the 1970's [13—18]. In addition, some other theoretical results, based on macroscopic electrodynamics [19, 20] and on unconventional treatments [21—25] contributed to the field.

In this paper we confine ourselves to a selection of theoretical results which—by our subjective judgement—appear to the most important ones. First, we emphasize a fundamental relationship clarifying the nature of the quantity measured in high-field experiments. In the next section, a comparison of theoretical results is given with respect to the cavity field treatment and some others avoiding its use. Finally we discuss the effect of high field on the Kirkwood *g*-factor.

What is measured in high-field experiments?

In *linear* dielectrics, the fundamental equation defining the relationship between the dielectric displacement vector, **D** and the electric field vector, **E**, is:

$$\mathbf{D} = \varepsilon\mathbf{E} \tag{1}$$

where the relative permittivity, ε, is a constant. Thus:

$$\mathrm{d}\mathbf{D} = \varepsilon \cdot \mathrm{d}\mathbf{E}. \tag{2}$$

Equation (1) represents a relationship of *vectorial* nature.

In *non-linear* dielectrics, however, the **D**(**E**) function is *tensorial:*

$$\mathbf{D} = \varepsilon(\mathbf{E}) \cdot \mathbf{E} \tag{3}$$

where ε is a function of **E** in a tensorial form:

$$\varepsilon = \begin{pmatrix} \varepsilon_{xx} & \varepsilon_{xy} & \varepsilon_{xz} \\ \varepsilon_{yx} & \varepsilon_{yy} & \varepsilon_{yz} \\ \varepsilon_{zx} & \varepsilon_{zy} & \varepsilon_{zz} \end{pmatrix} \tag{4}$$

For this case, instead of eq. (2), we have:

$$\mathrm{d}\mathbf{D} = \mathbf{E} \cdot \mathrm{d}\varepsilon + \varepsilon \cdot \mathrm{d}\mathbf{E} \tag{5}$$

which, if **D** is parallel with **E**, can serve as a definition of the *differential relative permittivity*, ε_d:

$$\varepsilon_d \equiv \frac{\mathrm{d}D}{\mathrm{d}E} = \varepsilon + \frac{\mathrm{d}\varepsilon}{\mathrm{d}E}E. \tag{6}$$

In the usual experiments, the field dependence of the relative permittivity is measured by a low-amplitude but high-frequency analysing field, E_a, superimposed on high-amplitude but low-frequency rectangular pulses of a polarizing field, E_p. Under such conditions, the analysing field is a small perturbation to the polarizing one. Thus, eq. (3) can be written in the form:

$$D(E_p, E_a) = \varepsilon(E_p, E_a) \cdot E_a$$
$$= \left[\varepsilon(E_p) + \left(\frac{\mathrm{d}\varepsilon}{\mathrm{d}E_a}\right)_{E_p} E_a\right] E_a = \varepsilon_d(E_p) \cdot E_a \tag{7}$$

Consequently, the analysing field tests the *slope* of the **D(E)** function as shown in Figure 1.

On the basis of eq. (6), one would think that the logarithmic differential of the relative permittivity with respect to field intensity, which is the difference between ε_d, and ε, is negligibly small for the field strengths applied in experiments (usually less than 60 to 100 kV/cm). However, this conclusion proves to be false, if ε and ε_d is compared by their definition. Let us consider the power series of the **D(E)** function:

$$\mathbf{D(E)} = \varepsilon_0 \mathbf{E} + \xi E^2 \mathbf{E} + \ldots \tag{8}$$

where ξ is the first non-linearity coefficient. If higher order terms are neglected —which can be done in all experiments carried out so far—, the quantity $\Delta\varepsilon/E^2$ usually given by experimentalists is thought to be:

$$\frac{\Delta\varepsilon}{E^2} \equiv \frac{\varepsilon - \varepsilon_0}{E^2} = \xi \tag{9}$$

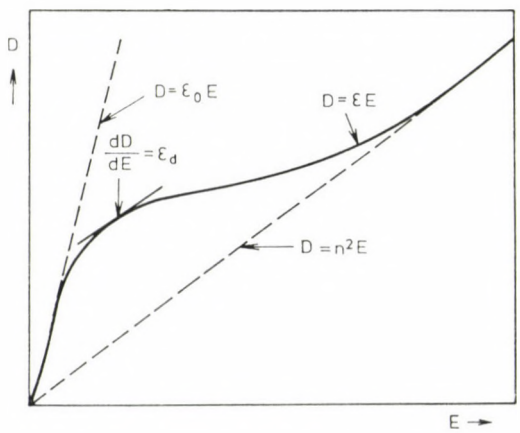

Fig. 1. Schematic representation of the field dependence of dielectric displacement

whereas they really measure the quantity:

$$\frac{\Delta\varepsilon_d}{E^2} \equiv \frac{\varepsilon_d - \varepsilon_0}{E^2} = 3\xi \tag{10}$$

Thus the difference between the two is not minor at all.

In light of this, it must be emphasized that *most of the evaluation and interpretation of experimental results published so far are to be revised.* Comparison with theoretical results usually indicates a difference even higher than the factor of 3 in eq. (10) which was explained by assuming dipole-dipole correlations due to forces other than electrostatic ones (e.g. hydrogen bonds). Although such forces play a considerable role in many cases, their effect seems to be less when the measured quantity is taken—correctly—according to eq. (10) [21].

Theoretical treatment by cavity and non-cavity models and the effect of electrostriction

In the continuum theory of dielectrics, the effective field acting on molecular dipoles has been conventionally calculated by the cavity model. One or a few orientationally correlated molecules are represented by a spherical cavity surrounded by a spherical layer of a continuum dielectric bearing the macroscopic properties of the liquid (see Figure 2). In some models the cavity is assumed to be filled with a polarizable continuum whose polarizability is characterized by the square of the refraction index or in general with a medium of relative permittivity ε_∞. In some others, the cavity is considered empty. In the middle of the cavity, there is a point dipole whose moment is taken equal either to the dipole moment of a single molecule or to the resultant moment of the correlated molecules modelled by the cavity. If the cavity is

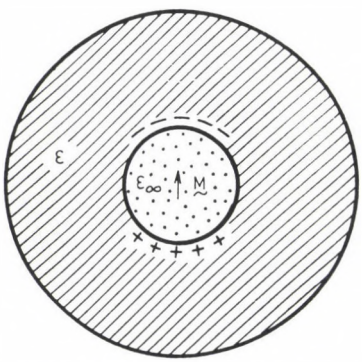

Fig. 2. A schematic representation of a cavity with a spherical layer of the surrounding continuum (see text)

filled with a continuum of relative permittivity ε_∞, the "vacuum" dipole moment, μ is corrected as follows:

$$M = \frac{\varepsilon_\infty + 2}{3} \mu . \tag{11}$$

This dipole moment, M, polarizes the surrounding continuum which, in turn, modifies the external field. This can be calculated by solving the Laplace equation for the spherically symmetrical system. The final result for a macroscopic liquid can be obtained by taking the limiting case when the outer boundary of the surrounding continuum tends to infinity.

The cavity treatment of the above scheme can be applied to calculate the first non-linear coefficient, ξ, in approximation. Fröhlich [26] assumed that the continuum surrounding the cavity is polarized *linearly*. In this case the first non-linear coefficient is:

$$\xi = \frac{3\langle M^4 \rangle_0 - 5\langle M^2 \rangle_0^2}{(k_B T)^3 V_m} \cdot f(\varepsilon) \tag{12}$$

where the first term represents the average dipole moment of the molecules in the cavity, k_B is the Boltzmann constant, T the temperature, and V_m the molar volume. The subscript O indicates that the resultant average dipole moment within the cavity is calculated with the assumption that the dipole—dipole correlation is *not* altered by the high field, i.e. these averages are taken in the low-field limit.

The continuum environment of the cavity results in a correction represented by $f(\varepsilon)$ which, according to Fröhlich, is:

$$f(\varepsilon) = \frac{3\varepsilon^4}{10(2\varepsilon^2 + \varepsilon_\infty^2)(2\varepsilon + \varepsilon_\infty)^2} \tag{13}$$

Bordewijk [19] carried out the cavity treatment with the assumption that the continuum surrounding the cavity is also non-linearly polarized, but preserved the supposition that dipole correlations can be treated in the low-field limit. His result, thus, differs only in $f(\varepsilon)$:

$$f(\varepsilon) = \frac{3\varepsilon^4}{\frac{2}{3}(148\varepsilon^4 + 5\varepsilon^3\varepsilon_\infty + 258\varepsilon^2\varepsilon_\infty^2 - 43\varepsilon\varepsilon_\infty^3 + 37\varepsilon_\infty^4)} \tag{14}$$

Taking water as an example with $\varepsilon = 80$ and $\varepsilon_\infty = 2$, Bordewijk's eq. [14] would predict a value higher of about 23% than Fröhlich's eq. (13).

Instead of a cavity treatment Fulton [23, 24] deduced an expression for the first non-linearity coefficient by a four-point correlation function

taking into account both the polarizability of the electron shell of the molecules and the orientational polarization of permanent dipoles as well as their cross effects. Below we shall return to his complete results. Here we cite only his formula for $f(\varepsilon)$:

$$f(\varepsilon) = \frac{3\varepsilon^4}{\frac{5}{2}(2\varepsilon + \varepsilon_\infty)^4 + 4(\varepsilon - \varepsilon_\infty)^4} \tag{15}$$

For water, eq. (15) would yield a value of about 32% lower than Fröhlich's eq. (13).

Since Fulton avoided the use of the cavity model and handled *all* polarization effects non-linearly up to the fourth order in the dipole moments, his calculation seems to be the most reliable. This means that theoretical results based so far on Fröhlich's equation are *too high*. It can also be concluded that the error originating from the approximate nature of eq. (13) is mainly due to the cavity model rather than to the neglect of the non-linear polarization of the surrounding continuum, since Bordewijk's result, which accounts for the latter effects but within the framework of a cavity treatment, increases the difference even more.

Fulton's calculations clarify another uncertain point of the theory of non-linear dielectric effects, too, viz. the influence of electrostriction. Previously, Kielich [1] called the attention to the problem that the change of the density due to high electric field is to be taken into account. However, he suggested an additional correction in which he seems to double-count the effect of electrostriction. Fulton—in agreement with Carnie and Stell [16]—treats this effect along with other polarizations, and obtains the following result:

$$\xi = f(\varepsilon)\frac{\pi\varrho}{2k_BT}(\varepsilon_\infty + 2)^4 \cdot$$

$$\cdot\left[\left(\bar{\alpha} + \frac{\mu^2}{3k_BT}\right)^2 \varrho k_BT\varkappa_T + \frac{2}{15}\left(\mathbf{Tr}\Delta\alpha^2 + \frac{2}{k_BT}\boldsymbol{\mu}\cdot\Delta\alpha\cdot\boldsymbol{\mu}\right) - \frac{2}{45}\left(\frac{\mu^2}{k_BT}\right)^2\right] \tag{16}$$

where ϱ is the number density of molecules, $\bar{\alpha}$ the average of the polarizability matrix, $\boldsymbol{\mu}$ the permanent dipole moment of the molecules, $\Delta\alpha$ the difference polarizability matrix with respect to the average polarizability, and $\varkappa_T$ the isothermal compressibility. The first term in the square brackets represents the non-linear contribution due to electrostriction, the second to the polarization of electron shells, the third to the cross effects of electronic polarization and permanent dipole orientation, and the fourth to the pure dipole orientation.

The restristions to the application of eq. (16) are the following. It is valid only for "normal" liquids in which there are no special forces influenc-

Table I

Comparison of experimental and theoretical non-linearity coefficents for carbon tetrachloride

	$3\xi_{exp.}$	$3\xi_{calc.}$
	$\times 10^{16}$ cm²/V²	
from direct measurement	[27] 18.4	13.2 [23]
from light scattering	[28] 9.9	13.2 [23]

ing dipole correlations, i.e. the Kirkwood g-factor is unity. Thus, it does not account for cases when the external field alters dipole correlations due to non-electrostatic forces, either. Hence examples for which eq. (16) can be tested are rather limited.

For apolar liquids these restrictions are unimportant, since all terms involving μ in eq. (16) cancel. In such cases, ξ can be determined experimentally either by the direct measurement of the non-linearity coefficient under the effect of high field or, indirectly by measuring the light scattering. The relationship giving this latter quantity is:

$$\xi = \frac{3\lambda^4 R^2}{4\pi^3 k_B T V} \frac{I_{\text{incid.}}}{I_{\text{scatt.}}} \tag{17}$$

where λ is the wavelength of the light *in vacuo*, R the distance from the scattering volume V, and I the light intensity.

Fulton—being also unaware of the fact that the direct measurement yields 3ξ instead of ξ as pointed out in the previous section—reports of a disagreement between the non-linearity coefficient measured directly and that calculated as well as between the directly measured one and that obtained from light scattering. The correct comparison, however, reveals an acceptable agreement as shown in Table I, particularly if the rather large experimental error of the direct measurements is taken into consideration.

Thus, it can be concluded that—for apolar liquids—Fulton's eq. (16) is a good approximation of the first non-linearity coefficient.

It is rather difficult to find a real liquid which behaves "normally" in the sense that there are no special forces influencing the correlation of permanent dipoles. Thus, the test of eq. (16) for polar liquids remains yet untested.

Field dependence of dipole correlations

The exact treatment of the effect of high field on the dipole correlations due to non-electrostatic forces—such as hydrogen bonds or strong, angle--dependent, dispersion forces—is a very complicated problem. Fulton [23, 24]

has deduced an equation including such special correlations, too, however its concrete application would require rather cumbersome calculations.

This problem has been approached recently in a more phenomenological way by Liszi, Mészáros and Ruff [21] and by Liszi, Papp, and Ruff [22]. Their treatment is based on the original cavity treatment modified by the introduction of a field dependent Kirkwood g-factor.

The field dependent relative permittivity is given by the following equation:

$$\varepsilon(E) = \varepsilon_\infty + \frac{2\pi\varrho M}{k_B T E}\sqrt{g(E)} \cdot L\left[\frac{3ME}{2k_B T}\sqrt{g(E)}\right] \tag{18}$$

where L is the Langevin function and eq. (11) is valid, while

$$g(E) = g_0 + g_1 E^2 + \ldots \tag{19}$$

since the Kirkwood g-factor is scalar.

Equation (18) involves the following approximate assumptions:

— the compressibility term is neglected,

— the cavity field is approximated by its limiting case when $\varepsilon \to \infty$,

— the non-linearity of the electronic polarization is neglected.

These equations are, first of all, suitable for a qualitative discussion of the effect of high field on the non-linear behaviour of polar liquids. Figure 3 shows schematically the four possible cases of the field effect on the Kirkwood factor. Two of them correspond to the *structure breaking effect* of the field, while the other two represent cases when the field has a *structure making*

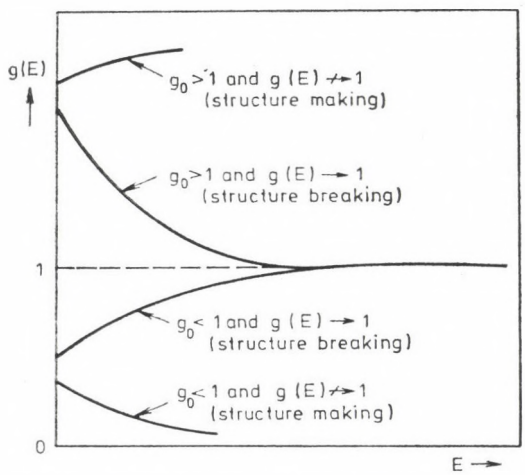

Fig. 3. A schematic representation of the possible variation of the Kirkwood g-factor with field intensity

effect. If the term "structure" is used for the specific dipole correlations caused by interactions other than electrostatic, structure breaking means the effect of the external field diminishing the correlations due to these special forces and making electrostatic interactions predominant. Whereas structure making means the strengthening of the effect of special forces by a cooperating action of the external field and these non-electrostatic interactions.

The case when $g_0 < 1$ and $\lim_{E\to\infty} g(E) = 1$ can be illustrated by the most simple example. If the Kirkwood factor is less than unity, the orientations of the dipoles are biassed toward somewhat more antiparallel positions than "normal". A typical liquid in this group is nitrobenzene in which the parallel disc-shaped molecules are favourably placed with antiparallel dipole moments ($g_0 = 0.92$).

This is probably due to the rather strong dispersion forces in the position when the benzene rings are plane-parallel and, thus, the large dipole moments are acting at a short distance.

The effect of the external field on such associates increases the Kirkwood factor by breaking up this "structure". With increasing field intensity the liquid would approach its "normal" state when the dipole correlations are only due to electrostatic interactions.

When eq. (18) is simplified by expanding the Langevin function upto third order terms, the first non-linearity coefficient can be obtained as follows:

$$\xi = -\frac{2\pi\varrho M^2}{k_B T}\left[\frac{9M^2}{(2k_B T)^2} g_0^2 - g_1\right] \tag{20}$$

If $g(E)$ tends monotonously to unity "from below", g_1 must be positive, thus ξ may be positive provided that g_1 overcompensates the first term in the square brackets. This would mean that the liquid behaves anomalously in the sense that its relative permittivity would increase with increasing field intensity as far as higher terms can be neglected in the non-linear effect. This is exactly what has been measured e.g. for nitrobenzene.

Specific dipole correlations, however, may not only decrease but increase the effective dipole moment. If $g_0 > 1$ and $\lim_{E\to\infty} g(E) = 1$, i.e. the Kirkwood factor approaches unity "from above", the molecular dipole moments are more or less lined-up parallel with each other and the primary effect of the external field would break up these associates making dipole correlations more random. Examples for this case are water and normal alcohols in which hydrogen bonded chains with zig-zag dipole moments represent the original structure. These chains are broken up under the effect of the external field.

In these cases g_1 is negative and, according to eq. (20), the observed non-linearity coefficient would be a larger negative value than for the corresponding "normal" liquid.

Table II

Kirkwood factors and their first coefficients of field dependence for some liquids

Liquid	μ/D	g_0	$g_1/10^{-14}$ cm^{2}V^{-2}
Water	1.85	2.8	— 6.2
Methanol	1.71	2.8	—14.3
Ethanol	1.70	3.1	—12.8
n-propanol	1.69	3.1	—11.7
n-butanol	1.67	3.1	—10.1
n-pentanol	1.65	3.1	—10.4
n-hexanol	1.63	3.1	—11.1
Nitrobenzene	4.22	0.92	+6.2

In principle, there are two cases when the external field may have structure making effect.

If $g_0 > 1$ and g_1 is positive, the original structure of the liquid with mainly parallel dipole correlation is further strengthened by the field. Although this makes sense physically, since higher fields would favour higher effective dipole moment, no such cases have been observed to occur so far.

If $g_0 < 1$ and g_1 is negative the external field would have also a structure making effect by lowering further the originally low Kirkwood factor. This case, however, is likely never to occur, since a higher field would disfavour a less polarizable medium.

The quantitative analysis of experimental data by eq. (20) yields g_1 values given in Table II. It is seen that practically all hydrogen-bonded liquids can be characterized with the same g_1.

These calculations can be extended to liquid mixtures too [22] whereby the concentration dependence of g_0 and g_1 is responsible for the non-linear behaviour of each polar component.

Conclusions

With this review we intended to emphasize three main points which could influence the further development of the study of non-linear dielectric effects in liquids:

1) Experimental results should be analysed with regard to the fact that high-field measurements give information on the *change in the differential relative permittivity* of liquids.

2) Theoretical results indicate that *electrostriction*—though a minor effect—must be properly accounted for.

3) There are many interesting features to be explained yet considering the effect of external high field on the changes of the specific dipole correlations.

REFERENCES

[1] Kielich, S.: General Molecular Theory and Electric Field Effects in Isotropic Dielectrics, in: M. Davies (ed.): Dielectric and Related Molecular Processes, The Chemical Society, London, 1972, pp. 198—387
[2] Parry Jones, G., Krupkowski, T.: JCS Faraday Trans. II, **70,** 862 (1974)
[3] Krupkowski, T., Parry Jones, G., Davies, M.: JCS Faraday Trans. II, **70,** 1348 (1974)
[4] Kołodziej, H. A., Parry Jones, G., Davies, M.: JCS Faraday Trans. II, **71,** 269 (1975)
[5] Bradley, P. A., Parry Jones, G., Kołodziej, H. A., Davies, M.: JCS Faraday Trans. II, **71,** 1200 (1975)
[6] Brown, B. L., Parry Jones, G.: JCS Faraday Trans. II, **71,** 1657 (1975)
[7] Balanicka, S., Małecki, J.: Bull. Acad. Pol., Ser. Chim., **29,** 77 (1982)
[8] Mészáros, L., Liszi, J.: Acta Chim. Acad. Sci. Hung., **104,** 397 (1980); **112,** 153 (1983)
[9] Buchert, J.: Nonlinear Behaviour of Molecules, Atoms, and Ions in Electric, Magnetic, and Electromagnetic Fields, Elsevier, Amsterdam, 1979, pp. 423—437
[10] Buchert, J., Kaprowicz-Kielich, B., Kielich, S.: Adv. Mol. Relax. and Interact. Processes, Elsevier, Amsterdam, 1977, pp. 115—128
[11] Alexiewicz, W., Buchert, J., Kielich, S.: Faraday Symposium, No. 11/1, 1977
[12] Alexiewicz, W., Buchert, J., Kielich, S.: Acta Phys. Pol., **A52,** 445 (1977)
[13] Ramshaw, J. D.: J. Chem. Phys., **73,** 5294 (1980)
[14] Rasaiah, J. C.: J. Chem. Phys., **77,** 5710 (1982)
[15] Høye, J. S., Stell, G.: J. Chem. Phys., **77,** 5173 (1982)
[16] Carnie, S. L., Stell, G.: J. Chem. Phys., **77,** 1017 (1982)
[17] Kusalik, P. G., Patey, G. N.: J. Chem. Phys., **79,** 4468 (1983)
[18] Troll, M., Zimm, B. H.: J. Phys. Chem., **87,** 3197 (1983)
[19] Bordewikl, P.: J. Chem. Phys., **58,** 1220 (1973)
[20] Logan, D. E.: Mol. Phys., **44,** 1271 (1981)
[21] Liszi, J., Mészáros, L., Ruff, I.: J. Chem. Phys., **74,** 6896 (1981)
[22] Liszi, J. Papp, E., Ruff, I.: JCS Faraday Trans. II, **78,** 915 (1982)
[23] Fulton, R. L.: J. Chem. Phys., **78,** 6865 (1983)
[24] Fulton, R. L.: J. Chem. Phys., **78,** 6877 (1983)
[25] Małecki, J.: JCS Faraday Trans. II, **72,** 104 (1976)
[26] Fröhlich, H.: Theory of Dielectrics, Clarendon, Oxford 1949

Acta Chimica Hungarica 121 (1—2), pp. 215—231 (1986)

MÖSSBAUER STUDIES ON THE STRUCTURE OF SOLUTIONS+

Attila VÉRTES* and Ilona CZAKÓ-NAGY

(Laboratory of Nuclear Chemistry, Eötvös University, H-1088 Budapest, Puskin u. 11—13.)

Received January 18, 1985

The Mössbauer spectra recorded in quenched liquids at low temperature gives information about the following properties of the studied solutions.

Hydration and solvation of the salts containing Mössbauer active isotopes.

Complexes formation and hydrolysis in the solutions of compounds possessing iron, tin, europium, or antimony.

Electron-exchange reactions between tin(II) and tin(IV) and iron(II) and iron(III).

The equilibrium and stability constants of the species of the solutes can be obtained on the basis of the line intensities of the Mössbauer spectra.

The Mössbauer study of the paramagnetic spin relaxation and superparamagnetic behaviour of the iron(III)- salt solutions can inform us about the polymerization and particle size distribution of the iron(III)-compounds respectively.

This paper will demonstrate the above applications of the Mössbauer technique.

The Mössbauer effect, i.e. the recoilless nuclear resonance absorption of γ-rays, takes place with measurable probability only in materials of solid state. Nevertheless, liquids or solutions containing Mössbauer active atoms can be studied by Mössbauer spectroscopy in quenched state. The Mössbauer spectra of glasses produced by quenching closely reflect the structure and chemical properties of "liquid" solutions prior to quick freezing. During quick freezing the oxidation levels and covalent bonds of the Mössbauer atoms are always stable, but the chemical coordination and its geometry may slightly change [1]. In order to hinder any change in the structure of the solutions in the course of quenching it is advisable to promote glass formation applying simultaneously more than one of the following possibilities:

(a) An increase in the concentration of the solute up to the eutectic composition.

(b) A decrease in the difference between the temperature of the solution prior to quick freezing and its solidification temperature.

(c) Increase in the viscosity of the solution.

(d) An increase in the rate of freezing (optimal rate $\sim$8—10 Ks^{-1}).

* To whom correspondence should be addressed.

+ This paper was presented at the Symposium on Structure of Liquids and Solutions at Veszprém, August 27—30, 1984.

(e) Addition of glass-forming materials (e.g., methanol, ethanol) to the solution.

In this paper we intend to demonstrate by examples the applicability of Mössbauer spectroscopy in different fields of solution chemistry.

Hydration of iron(II) salts

The Mössbauer parameters of aqueous iron(II) salt solutions containing various anions (Cl^-, SO_4^{2-}, ClO_4^-) are similar, from which it can be concluded that the Fe^{2+} ions in these solutions are probably present in the form of hexaaqua complexes [2]. The Mössbauer spectra of aqueous iron(II) chloride solutions of different composition are shown in Fig. 1. Not even a considerable increase in the concentration of the iron(II) salt leads to the breakdown of the species $[Fe(H_2O)_6]^{2+}$. However, if the activity of water (a_0) is decreased by some additive, e.g. LiCl, then in case of $a_0 < 0.2$ the quadrupole splitting (ΔE) of Fe(II) species decreases significantly (see Fig. 1/c) indicating that the Cl^- ions enter the inner coordination sphere of the iron(II) ion. The formation of the following complexes are supposed in case $a_0 < 0.2$:

$$[Fe(H_2O)_5Cl]^+$$

$$[Fe(H_2O)_6]^{2+} \xrightarrow{LiCl} \quad \xrightarrow{LiCl} [Fe(H_2O)_4Cl_2]$$

Mössbauer spectra of frozen aqueous solution of $FeCl_2$ showed a line broadening in applied magnetic fields of 5 T and 4.2 K comparing to the Mössbauer spectra of frozen aqueous solution of $Fe(ClO_4)_2$ at the same circumstances [3]. This experimental result suggests that the chloride coordinates to the central iron(II) ion in the outer sphere.

Solvation studies

When metal salts are dissolved in non-aqueous solvents the two fundamental effects that determine the electronic structure and hence the Mössbauer spectra of the metal are (1) the coordination of the solvent molecule to the cation and (2) the extent of association between the cation and the anion.

A solvation process can be described by the following equation:

$$MA + (n + k + 1)D \rightleftharpoons [MD_{n+1}]^+ + [AD_k]^+$$

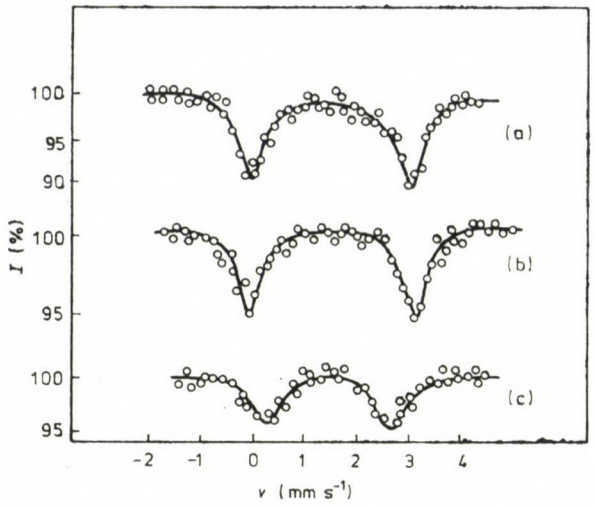

Fig. 1. Mössbauer spectra of the three-component systems $FeCl_2$—LiCl—H_2O at liquid nitrogen temperature. (a) 24.64 wt.% $FeCl_2$, 0.00 wt.% LiCl, 75.36 wt.% H_2O; (b) 6.91 wt.% $FeCl_2$, 34.20 wt.% LiCl, 58.89 wt.% H_2O; (c) 6.31 wt.% $FeCl_2$, 39.70 wt.% LiCl, 53.99 wt.% H_2O. Radiation source: ^{57}Co in stainless steel

where MA is the dissolved salt molecule and D is a solvent molecule of donor character. The donor ability of a solvent molecule can be characterized by the donor number (DN) defined by Gutmann as the solvation entalphy (in kcal mol^{-1}) of $SbCl_5$ by the solvent in question. When M is a Mössbauer active atom the Mössbauer spectra of the quenched solutions yield information regarding the structure and stability of the solvated species even in solvent mixtures.

The Mössbauer spectra of solutions of Fe(II) chloride in hexamethylphosphoramide (HMPA) — water mixtures (Fig. 2) revealed the superposition of two components [4, 5]. The Mössbauer parameters of these solvates agreed with the parameters of Mössbauer spectra recorded in pure water or in pure HMPA, that is in HMPA-water mixtures the bulk of the Fe(II) is present in the form of $[Fe(HMPA)_xCl_y]^{(2-y)+}$ and $[Fe(H_2O)_xCl_y]^{(2-y)+}$ solvates.

In contrary, the separation of Mössbauer spectra of $FeCl_2$ in dimethylformamide (DMF)-methanol (M) mixtures into components was not possible and this suggests the formation of solvates of mixed ligand sphere in this system $[(Fe(DMF)_xM_yCl_{(6-x-y)}]^{(x+y-4)+}$, see Fig. 3).

In stepwise solvation reactions the electronic structure of the solvate complexes existing side by side in solution may be so different (primarily because of the different symmetries of the coordination spheres) that the individual species may each appear as separate lines in the Mössbauer spectrum of the quenched solution. Assuming that the Debye—Waller factors of the stepwise formed species in a given solution are the same, the areas under the

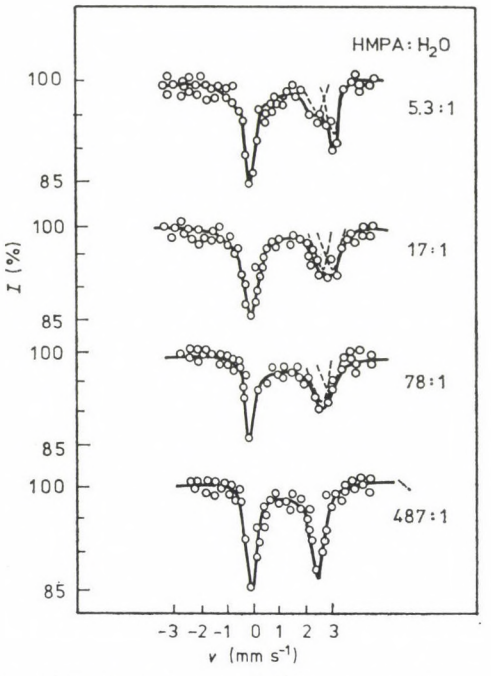

Fig. 2. Mössbauer spectra of $FeCl_2$ in hexamethylphosphoramide-water mixtures of various compositions, at liquid nitrogen temperature. Radiation source: ^{57}Co in stainless steel

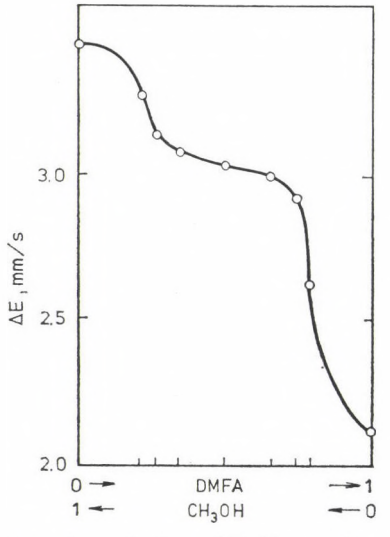

Fig. 3. Dependence of quadrupole splitting of $FeCl_2$ on the composition of the solvent, expressed as a volumetric ratio, in dimethylformamide-methanol mixtures

line can be regarded as being directly proportional to the concentrations of the species relating to them. Determining the concentrations of the different solvates from the Mössbauer spectra of series of quenched solutions with various concentrations, one can simply calculate the equilibrium constants of the stepwise solvation reactions.

This procedure is rather time-consuming contrary to the other, well-known methods applied for complex equilibrium studies, therefore the Mössbauer procedure described above is justified only when other methods are not available for the measurement of the concentration of the species in the solution.

The tin(IV) halides are solvated by donor solvents in one step, according to the following equation.

$$SnX_4 + 2D \rightleftharpoons D_2SnX_4 \quad K = \frac{[D_2SnX_4]}{[SnX_4]\,[D]^2}$$

In inert media (low relative permittivity, e.g. CCl_4 or benzene) only two species are present in the solution, viz., the tetrahedral unsolvated tin(IV) halide (the right-hand line in Fig. 4) and its solvated form with distorted octahedral symmetry (the left-hand line). The two species can be well distinguished and thus the spectrum is suitable for the determination of the equilibrium constant of the above equilibrium.

In Table I the equilibrium constants are summarized for the solvation process of $SnBr_4$ in different donor solvents [6].

The Mössbauer study of paramagnetic spin-relaxation can give information on the structure of non-aqueous Fe(III) salt solutions.

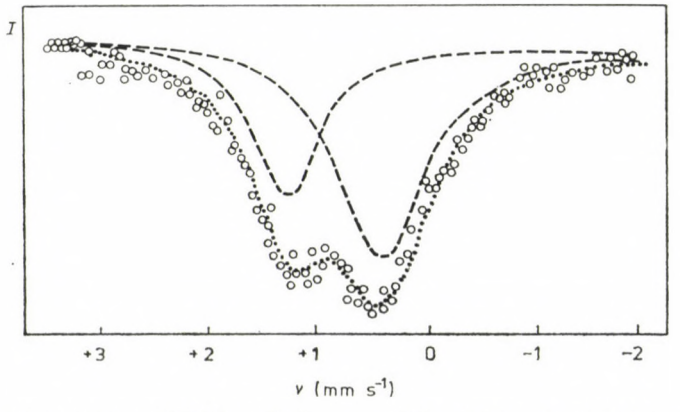

Fig. 4. Mössbauer spectrum of $SnBr_4$ solution containing 0.18 mole of $SnBr_4$ + 1.0 mole of acetic anhydride per kilogram of benzene, at liquid nitrogen temperature. Radiation source: $Ba^{119}SnO_3$

Table I

Mössbauer parameters and equilibrium constants of solvates $SnBr_4D_2$ *in various donor solvents*

Solvent	Donicity (DN)	Relative permittivity (ε)	Isomer shift δ, SnB_4 (mm s^{-1})	Isomer shift δ, SnB_4D_2 (mm s^{-1})	K (mole $kg^{-1})^{-2}$	log K
Acetic anhydride	10.5	20.7	1.22 ± 0.08	0.41 ± 0.09	3.2	0.5 ± 0.05
Acetonitrile	14.1	38.0	1.23 ± 0.05	0.35 ± 0.02	25.2	1.40 ± 0.05
Acetone	17.0	20.7	1.18 ± 0.08	0.24 ± 0.04	38.9	1.60 ± 0.1
Tetrahydrofuran	20.0	7.6	1.28 ± 0.04	0.22 ± 0.01	93.2	1.97 ± 0.1

According to the theory of paramagnetic spin-relaxation when paramagnetic Fe(III) ions in a solution are far apart and the temperature is low enough a spectrum with magnetic hyperfine structure (MHS) will be observed, such as in the case of mononuclear solvates and of the low concentration (slow spin-spin relaxation: $\tau_R \geq \omega_L{}^{-1}$) while on the other hand, when the ions are close together, such as in dimers or polymers, the MHS is collapsed because of the resulting decrease of spin-spin relaxation time.

It has been established that the iron(III)-chloride is in dimeric or polymeric form in benzene, nitrobenzene and partially in acetone, acetonitrile, pyridine and dimethylformamide, while it is monomeric in ethanol [7]. The ability of the monomer formation depends on the donicity and relative permittivity of the solvent. The order of this ability is: ethanol > dimethylformamide > pyridine > acetone > acetonitrile > nitrobenzene > benzene. Some of the spectra are shown in Fig. 5.

The transversely applied magnetic field of 8.8 T resulted in the splitting of the central line only in the solution of Fe(III)-chloride in acetone, which proves that in the dimeric solvates, except the acetone dimer, the iron(III) atoms are antiferromagnetically coupled (see Fig. 6).

Complex formation in solution

In the course of complex formation a coordinate bond is established between the central atom and the ligand, the electron configuration of both is altered, and this change may be clearly reflected in the Mössbauer spectrum. Thus, the Mössbauer spectroscopy is suitable for the study of complexes formed in solutions. The greater the change in electronic structure as a result of a complex formation reaction, or the greater the difference between the electronic structures of the complex species formed in a given solution, the more suitable Mössbauer spectroscopy is for the study of such systems.

For example, in reactions that lead to the formation of a low-spin complex, the Mössbauer spectrum of the quick-frozen solution reveals the

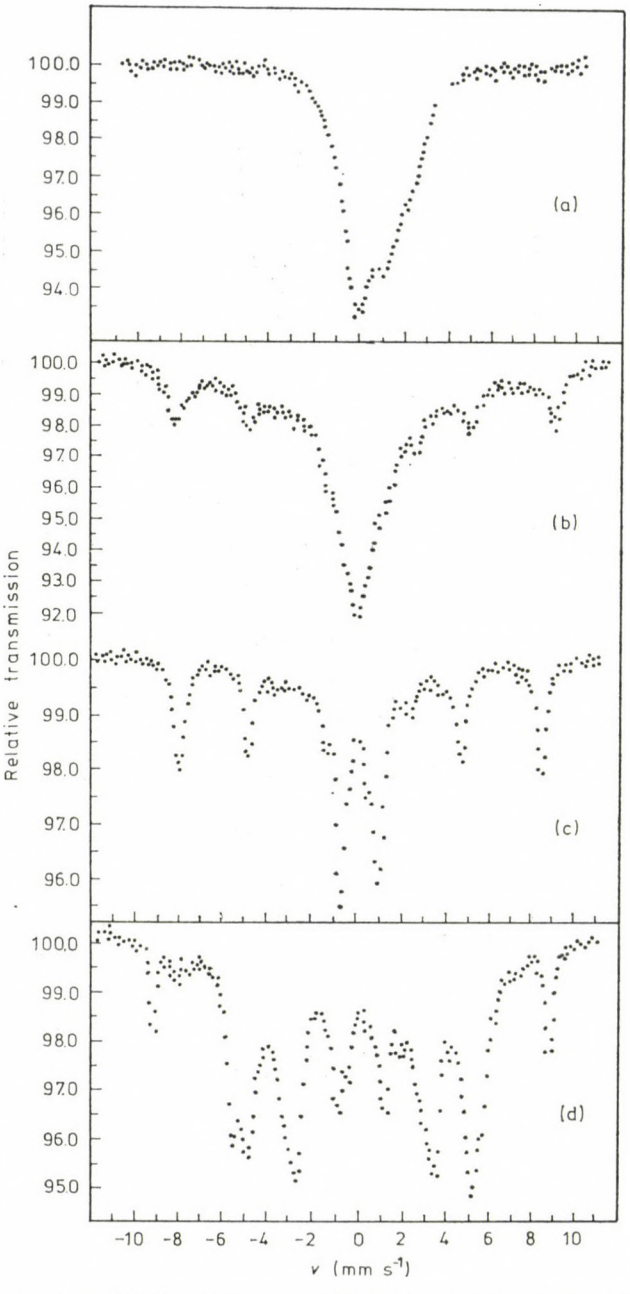

Fig. 5. Mössbauer spectra of $FeCl_3$ solution at 4.2 K. (a) 1.4×10^{-2} mole dm^{-3} $FeCl_3$ in benzene; (b) 1.0×10^{-2} mole dm^{-3} $FeCl_3$ in acetone; (c) 1.4×10^{-2} mole dm^{-3} $FeCl_3$ in pyridine; (d) 1.4×10^{-2} mole dm^{-3} $FeCl_3$ in ethanol. Radiation source: ^{57}Co (Rh)

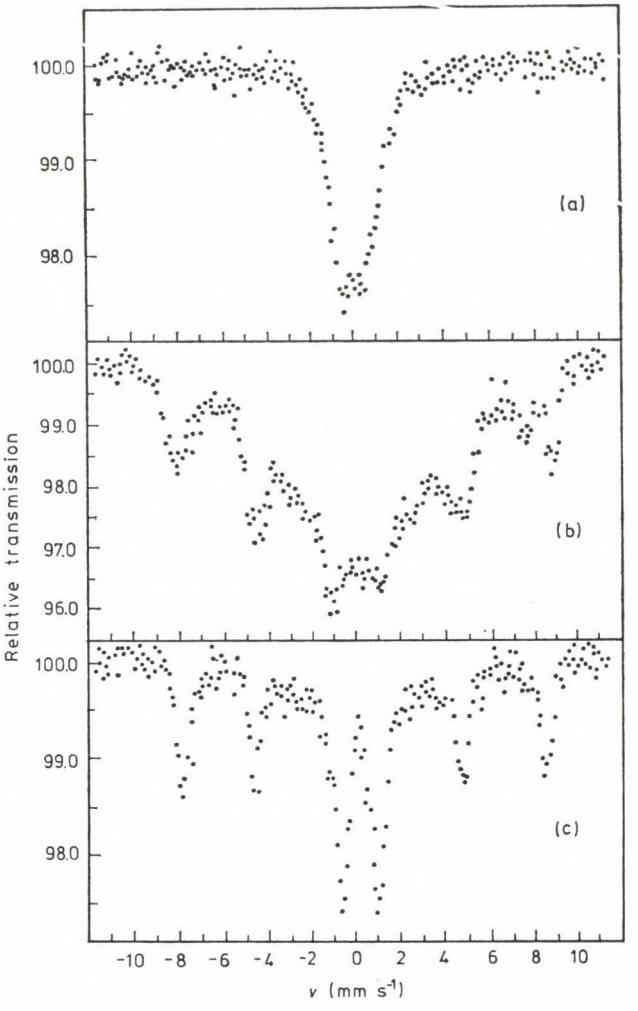

Fig. 6. Mössbauer spectra of $FeCl_3$ solution at 4.2 *K* and at 8.8 *T* external magnetic field. (a) 1.4×10^{-2} mole dm^{-3} $FeCl_3$ in benzene; (b) 1.0×10^{-2} mole dm^{-3} $FeCl_3$ in acetone; (c) 1.4×10^{-2} mole dm^{-3} $FeCl_3$ in pyridine. Radiation source: ^{57}Co (Rh)

clear separation of the Mössbauer lines of the high-spin metal ion and the low-spin metal complex. This effect was shown on the formation of the iron(II)-bipyridyl complex in aqueous solution [8].

Figures 7 (a), (b), (c), illustrate the spectra of solutions in which the amount of α,α'-bipyridyl was insufficient to bind the iron quantitatively in the form of bipyridyl complex. The superpositioned spectra can be resolved into two components, one of which can in each case be identified with the spectrum obtained in an aqueous solution of iron(II) chloride ($\delta = 1.40$ mm s^{-1}, $\Delta E =$ $= 3.28$ mm s^{-1}), while the other component is the Mössbauer spectrum of

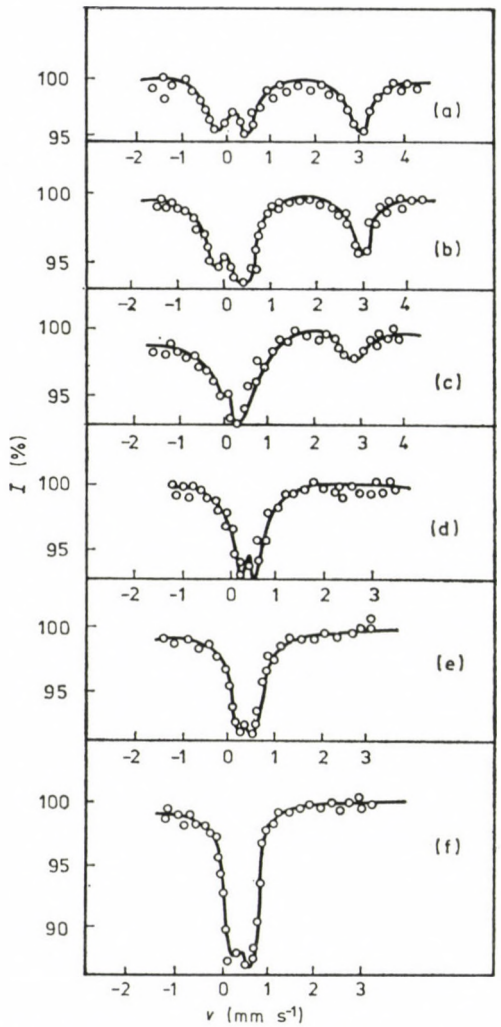

Fig. 7. Mössbauer spectra of frozen aqueous solutions of $FeCl_2$ and α,α'-bipyridyl at liquid air temperature. The molar ratio of α,α'-bipyridyl and $FeCl_2$ in the solution, normalized to the moles of $FeCl_2$, is: (a) 0.75, (b) 1.51, (c) 2.40, (d) 3.01, (e) 3.60

$[Fe(bip)_3]^{2+}$ ($\delta = 0.46$ mm s^{-1}, $\Delta E = 0.33$ mm s^{-1}. Fig. 7 (e) shows the Mössbauer spectrum of the solution in which the amount of α,α'-bipyridyl was enough to transform the $[Fe(H_2O)_6]^{2+}$ complex ions into the $[Fe(bip)_3]^{2+}$ complex. These results demonstrate that in the solution examined the inner coordination sphere of the iron(II) consists either completely of water molecules or bipyridyl molecules, and mixed ligand complexes are not present in detectable amount.

Electron exchange in solution between tin(II) and tin(IV)

The Mössbauer spectroscopy can be easily applied for following the progress of electron exchange processes continuously, without the need to separate the exchange components (as it is necessary using the isotopic tracer method). The electron exchange between tin(II) and tin(IV) in aqueous solution has been studied by using $SnCl_4$ labelled with ^{119}Sn Mössbauer active isotope and $SnCl_2$ prepared from natural tin [9]. Aqueous solution in which the concentration of both $^{119}Sn(IV)$ and Sn(II) was approximately 0.06 mole dm^{-3}, has been prepared. Under such concentration conditions only the $^{119}Sn(IV)$ may yield Mössbauer spectra with suitable high line intensities, however, the line intensity of Sn(II) in the Mössbauer spectra is virtually zero.

The equation describing the electron exchange of ^{119}Sn is:

$$^{119}Sn(IV) + Sn(II) \underset{k_2}{\overset{k_1}{\rightleftharpoons}} Sn(IV) + {}^{119}Sn(II)$$

where k_1 and k_2 are rate constants.

Fig. 8(a) shows the Mössbauer spectrum of a solution prepared by mixing of the two components just before the quenching. The Sn(IV) line ($\delta = 0.20$ mm s^{-1}) appears with high intensity whereas the corresponding line ($\delta = 3.4$ mm s^{-1}, $\Delta E = 0.95$ mm s^{-1}) for Sn(II), prepared from natural tin, is not

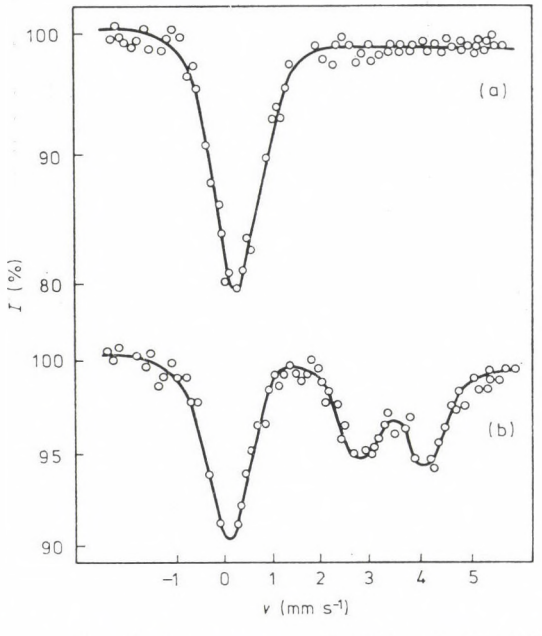

Fig. 8. Mössbauer spectra at liquid air temperature of 0.063 mole dm^{-3} $^{119}SnCl_4$ + 0.057 mole dm^{-3} $SnCl_2$ solution. (a) $t = 2$ s; (b) $t = 3.9 \times 10^3$ s. Radiation source: $Ba^{119}SnO_3$

visible. The spectrum in Fig. 8(b) is that of a sample in which the mixture of $^{119}SnCl_4$ and $SnCl_2$ was allowed to stand for 65 minutes at 20 °C before quenching. As a result of the electron exchange, part of the ^{119}Sn was converted from Sn(IV) to Sn(II) and thus the intensity of the line pair corresponding to the latter increased considerably.

The Mössbauer measurements enabled us to determine the rate constant of the electron exchange ($k = k_1 = k_2$ as the isotope effect of the electron exchange can be neglected) at different temperatures. Using these data an activation energy of the electron-exchange process: 20.2 ± 2 kcal mol^{-1} has been obtained. The relatively high activation energy of the electron exchange between tin(II) and tin(IV) indicates that the process proceeds via a transition complex, probably in the following steps:

$$[^{119}SnCl_6]^{2+} + [SnCl_4]^{2-} \rightarrow [^{119}SnSnCl_{10}]^{4-} \rightarrow$$
$$\rightarrow [^{119}SnCl_4]^{2-} + [SnCl_6]^{2-}.$$

Hydrolysis studies of Fe(III) salts

Others than Mössbauer technique (e.g., potentiometric titration, spectrophotometry magnetic measurements) have revealed that various complex ions are formed in solution of iron(III) salts when the pH is changed. For instance Mulay and Selwood [10] described $[Fe(H_2O)_6]^{3+}$; $[Fe(OH)(H_2O)_5]^{2+}$; $[Fe(OH)_2(H_2O)_4]^{+}$ species in aqueous iron(III) perchlorate solution in case of pH < 2, and at pH > 2 $[Fe_2(OH)_2(H_2O)_8]^{4+}$ dimer ions. The changes that occur in the structure of the iron(III) salt solutions as the pH is changed are reflected closely in the Mössbauer spectra. Fig. 9 shows the liquid helium temperature (4.5 K) Mössbauer spectra of 0.05 molar $^{57}Fe(NO_3)_3$ aqueous solutions at different pH's [11]. At pH < 2 the spectra show well resolved magnetic hyperfine structure indicating the presence of mononuclear species in the solution. The high value of $H_{5/2}$ can be attributed to hexaqua complex ions. The quadrupole line pair in Fig. 9(e) can be related to the formation of dimeric iron(III) species at pH $= 2$.

The above mentioned monomeric or dimeric aqua-complex iron(III) ions are in equilibrium and generally formed very quickly (within a few minutes) after adjustment of pH, however, it should be pointed out that a fairly slow polymerization process may occur even at room temperature in these systems. The polymerization during aging or at elevated temperature is indicated by opalescence or suspension formation. The polymer species are usually magnetically ordered and show superparamagnetic behaviour. As it is known the magnetically ordered materials have a long relaxation time (τ_R) because of the long-range cooperative interaction, and therefore they

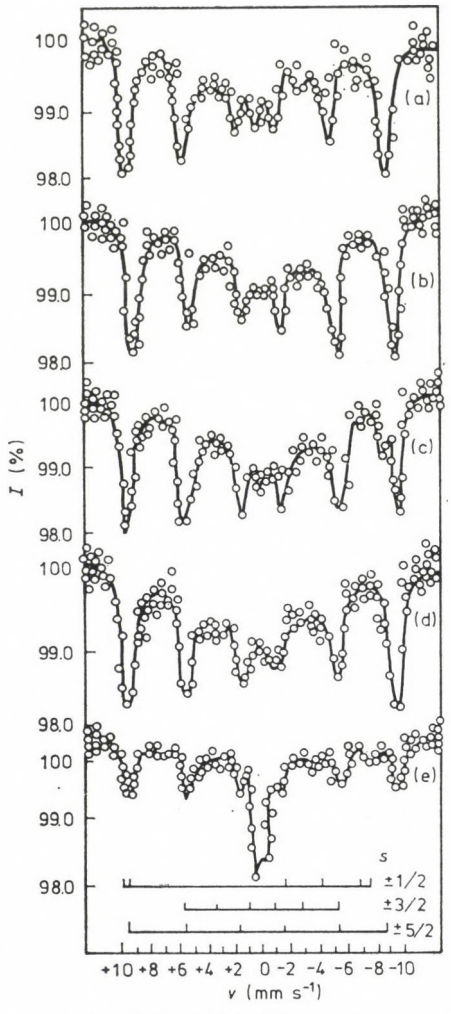

Fig. 9. Mössbauer spectra of 0.05 mole kg^{-1} $^{57}Fe(NO_3)_3$ solutions at 4.5 *K*. Radiation source: $^{57}Co(Pt)$. (a) 65 wt.% HNO_3; (b) 30 wt.% HNO_3; (c) 11.2 wt.% HNO_3; (d) pH: 1.0; (e) pH: 2.0. The positions of the lines relating to the various Kramers' doublets are also visible in the spectra

usually show magnetic hyperfine splitting below the magnetic ordering temperature ($\tau_R > \omega_L^{-1}$). In case of small particles ($\sim$10—10^3 ions) the relaxation time depends on the particle size in the following way

$$\tau_R = \frac{1}{f_0} \exp \frac{2KV}{kT}$$

where f_0 and K are the frequency and anisotropy constants, V is the volume of the particle, k is the Boltzmann constant and T is the absolute temperature. Thus, with extremely small particles, magnetic hyperfine structure may be

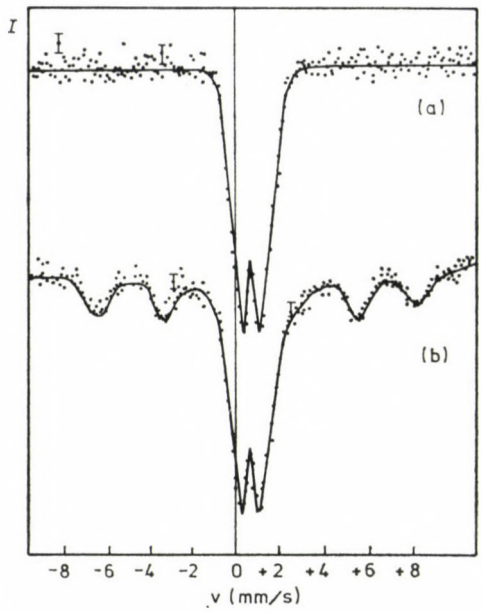

Fig. 10. Mössbauer spectra of 0.06 mole kg^{-1} $^{57}Fe(ClO_4)_3$ solution of pH: 2.3, at liquid nitrogen temperature. Radiation source: ^{57}Co in stainless steel. (a) Immediately after preparation; (b) after standing for 1 month at room temperature

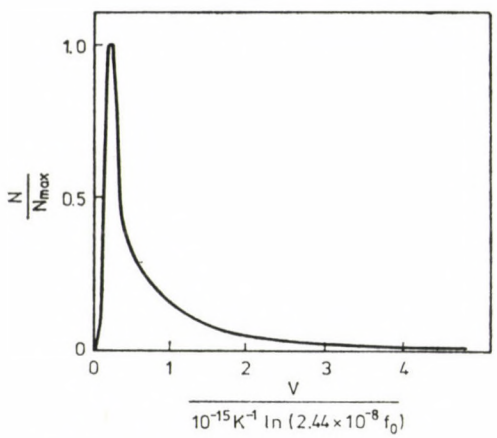

Fig. 11. Particle size distribution of the superparamagnetic polymers formed in 0.04 mole kg^{-1} $^{57}Fe(ClO_4)_3$ solution of: pH 2.3 during aging for 4 weeks. The maximum of the particle size distribution corresponds to a polymer containing 300 iron atoms

absent below the magnetic ordering temperature ($\tau_R < \omega_L{}^{-1}$) that is the magnetically ordered material behaves as a typical paramagnetic one. This phenomenon is called superparamagnetism. At low enough temperatures when $\tau_R \geq \omega_L^{-1}$, the magnetic hyperfine splitting may appear even with fine particles.

The Mössbauer spectrum of the frozen solution containing superparamagnetic iron(III) polymer compounds consists of paramagnetic singlet or doublet and magnetic sextet due to the smaller and bigger particle size, respectively (see Fig. 10.). The border between the "smaller" and "bigger" particle size is defined by τ_R and it depends on the volume of the particles (V) and on the temperature (T). Consequently the temperature dependence of the area ratio of the paramagnetic and magnetic spectral components gives information about the size distribution of iron(III)-polymer-species in the solution [12] (see Fig. 11.).

Mössbauer spectroscopy of liquids trapped in the pores of thirsty glass

The preceeding section showed that Mössbauer spectroscopy can be used for the study of the chemical properties of solutions and liquids if the studied system was quenched to a frozen state before recording of the Mössbauer spectrum. Nevertheless, Mössbauer spectra of liquids can be recorded at room temperature if the molecules of liquids are trapped in the cavities of a special porous silicate glass of a mean pore diameter of 4 nm [13—15].

Liquids containing Mössbauer active elements can be divided into three groups on the basis of their Mössbauer parameters recorded in the thirsty glass carrier at room temperature (see Table II).

(1) The Mössbauer parameters for the quenched (frozen) solutions or liquids are similar as those measured for the solutions or liquids trapped in the porous glass. The differences between the Mössbauer parameters achieved at the temperature of liquid nitrogen and at room temperature in the glass carrier are due mostly to the second order Doppler shift that is to the normal temperature dependence. Such kinds of systems are the aqueous solutions of Mössbauer active salts.

(2) Mössbauer parameters measured in the frozen state and in the carrier at room temperature are considerably different, e.g. SnI_4 dissolved in carbon tetrachloride or iron pentacarbonyl a liquid itself (see Table II).

(3) Mössbauer spectra recorded in the porous glass consists of two components. One of these is identical or very similar to that measured in a quenched (frozen) solution or liquid, the other one differs from it. Such a kind of system is $SnCl_4$ (see Fig. 12).

On the basis of the experimental data in systems characteristic for group (1)only the solvent molecules (e.g. water) can be supposed to be in chemical interaction with the wall of the capillaries in the glass and the Mössbauer active species [e.g. Fe(II)] have the same near surroundings (first coordination sphere) they have in normal liquid state [see Fig. 13(a)].

In systems characteristic of the second group all Mössbauer active atoms trapped in the carrier are in direct chemical interaction with the wall

Table II

Mössbauer parameters (mm|s) *of the systems studied*

	Trapped in thirsty glass 293 K			80 K			Frozen solution 80 K			Solid crystal 293 K	
	IS[a]	QS[b]	c	IS[a]	QS[b]	I[c]	IS[a]	QS[b]	c	IS[a]	QS[b]
$SnCl_4$	0.72	0	0.029	0.82	0	0.15	0.80	0	0.297		
	−0.20	0	0.023	−0.02	0	0.11					
0.01 *M* SnI_4 in CCl_4	−0.04	0	0.011	0.13	0	0.138	1.60	0	0.087		
0.01 *M* SnI_4 in DMF + CCl_4	−0.10	0	0.015	0.00	0	0.149	0.76	0	0.063		
0.01 *M* SnI_4 in 1 *M* $C_2H_5OH+CCl_4$	−0.11	0	0.036	0.02	0	0.251					
50−50 w% $Fe(CO)_5$ + CH_3OH	0.35	0.79	0.003	0.47	0.84	0.01	0.08	2.52			
0.01 *M* $Fe(dip)_3Cl_2$ in H_2O	0.30	0.30	0.020	0.35	0.33	0.021	0.35	0.34	0.022	0.28	0.31
0.5 *M* $Fe(H_2O)_6SO_4$ in H_2O	1.25	3.17					1.35	3.28			
$FeSO_5 \cdot 7\ H_2O$ crystals										1.25	3.20
$FeSO.\ H_2O$ crystals										1.23	2.70
FeSO										1.31	2.94

[a] IS = isomer shift referred to SnO_2 and α-iron, respectively, reproducibility ±0.01 mm/s

[b] QS = quadrupole splitting

[c] I = integral intensity

[d] $FeSO_4 \cdot 7\ H_2O$, in this compound the Fe^{2+} has the same hexaaqua ligand sphere as in solution. The component with 0.01 *M* concentrations were prepared from enriched ^{119}Sn and ^{57}Fe, respectively.

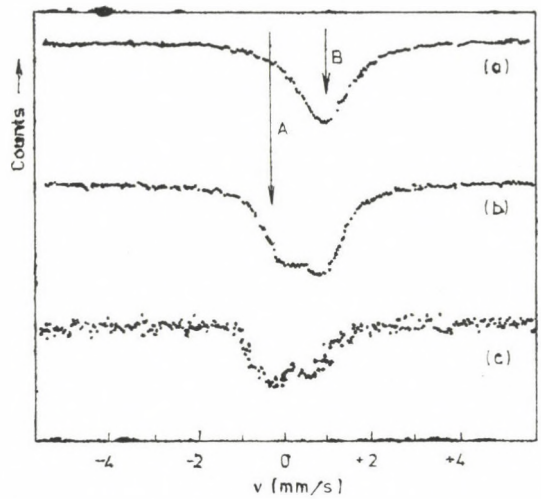

Fig. 12. The Mössbauer spectra of $SnCl_4$ samples: (a) frozen and measured at 80 K; (b) trapped in the pores of thirsty glass, measured at 80 K; (c) trapped in the pores of thirsty glass, measured at room temperature

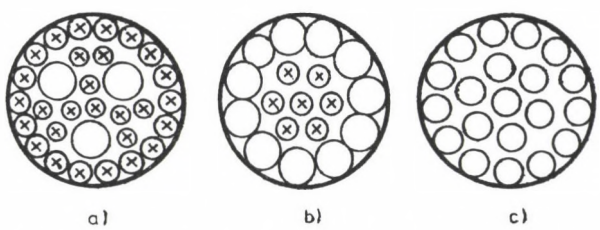

Fig. 13. Typical positions of the Mössbauer active molecules in the cavities: O represents the Mössbauer active ions or molecule (e.g., $^{57}Fe^{II}(bipy)_3$, $^{119}SnI_4$, $^{119}SnCl_4$ a.s.o.) and X represents the solvent molecules (H_2O, CCl_4 a.s.o.)

of its cavities (e.g. SnI_4). This situation is favoured when the size of the molecule containing the Mössbauer active element is relatively large [Fig. 13(b)].

In systems characteristic of group (3) only one part of the Mössbauer active molecules is in direct chemical interaction with the wall of the pores in the carrier, the remaining part show Mössbauer parameters characteristic of the free species. This situation is realized e.g. when the liquid, trapped in the pores, consists of only the Mössbauer active molecules [e.g. $SnCl_4$, see Fig. 13(c)].

The recoilless gamma-resonance absorption can take place in the Mössbauer active molecule adsorbed directly on the wall of the cavities in the glass carrier due to the interaction between the silicate oxygen of the wall and the adsorbed species.

On the other hand, in the molecules located in the second or third layers to the capillary wall the Debye—Waller factor will depend on the direction

of the recoil. (It should be mentioned that there is space only for the formation of a few layers of molecules between the walls of the cavities of the porous glasses.)

It is interesting to mention that the relative intensity of the line A in Fig. 12 is higher at room temperature due to the effect of the direct interaction between the inner surface of the thirsty glass and the $SnCl_4$ molecules. And on the other hand the Debye—Waller factor of the bulk $SnCl_4$ molecules decreases considerably when the temperature increases from nitrogen to room temperature.

The results presented above rises some hope that the application of thirsty glasses will extend the usefulness of the Mössbauer spectroscopy in the field of solution chemistry.

REFERENCES

[1] Vértes, A., Korecz, L., Burger, K.: Mössbauer Spectroscopy, Elsevier, Amsterdam 1979
[2] Vértes, A.: Acta Chim. Acad. Sci. Hung., **63,** 9 (1970)
[3] Domes, H., Leupold, O., Molnár, B., Nagy, D. L., Ritter, G., Szűcs, I. S.: Symposium on the Structure of Liquids and Solutions 27—30 August, 1984, Veszprém, Hungary
[4] Vértes, A., Burger, K., Molnár, B., Pálfalvy, M.: J. Inorg. Nucl. Chem., **35,** 691 (1973)
[5] Vértes, A., Burger, K., Suba, M.: Acta Chim. Acad. Sci. Hung., **63,** 123 (1970)
[6] Vértes, A., Nagy-Czakó, I., Burger, K.: J. Phys. Chem., **80,** 1314 (1976)
[7] Vértes, A., Czakó-Nagy, I., Burger, K.: J. Phys. Chem. **82,** 1469 (1978)
[8] Vértes, A., Dézsi, I., Suba, M.: Acta Chim. Acad. Sci. Hung., **64,** 347 (1970)
[9] Vértes, A.: Radiochem. Radioanal. Lett., **4,** 337 (1970)
[10] Mulay, L. N., Selwood, P. W.: J. Am. Chem. Soc., **77,** 2693 (1955)
[11] Vértes, A., Parak, F.: J. Chem. Soc. Dalton Trans., **1972,** 2062
[12] Vértes, A., Komor, M., Gelencsér, P.: Acta Chim. Acad. Sci. Hung., **77,** 55 (1973)
[13] Burger, K., Vértes, A., Zay, I.: Inorg. Chim. Acta, **76,** L247 (1983)
[14] Burger, K., Vértes, A.: Nature, **306,** 353 (1983)
[15] Vértes, A., Burger, K., Takács, L., Horváth, I.: J. Radioanal. Nucl. Chem. Lett. **86** 195 (1984)

PRINTED IN HUNGARY
Akadémiai Kiadó és Nyomda, Budapest

Text

The text of the paper should be concise. The description of new compounds (in the Experimental) must include the complete analytical data. Special attention must be paid to structural formulas given within the text. Complicated (non-linear) formulas should be drawn on separate sheets of paper and their position in the text should be clearly marked. The numbering of formulas and equations (in parentheses on the right-hand side) is only needed if they are referred to in the text. Units should conform to the International System of Units (SI). In nomenclature the rules of the I.U.P.A.C. are accepted as standard. Symbols for physical quantities are printed in italic type and should, therefore, be underlined in the manuscript.

References

References should be numbered in order of appearance in the text (where the reference number appears in brackets) and listed at the end of the paper. The reference list, too, should by typed double-spaced. Journal titles are to be abbreviated as defined by the Chemical Abstracts Service Source Index.

Examples:

[1] Brossi, A., Lindlar, H., Walter, M., Schneider, O.: Helv. Chim. Acta, **41**, 119 (1958)
[2] Parr, R. G.: Quantum Theory of Molecular Electronic Structure, Benjamin, New York 1964
[3] Warshel, A.: in Modern Theoretical Chemistry, Vol. **7**, Part A (Ed. G. A. Segal), Plenum Press, New York 1977

Tables

Each table should be given a Roman number and a brief informative title. Structural formulas should not be used in column headings or in the body of tables.

Figures

Figures should be numbered consecutively with Arabic numerals. Their approximate place should be indicated in the text on the margin. Allfigures must be identified on the back by the author's name and the figure number in pencil. Standard symbols (such as circles, triangles, squares) are to be used on line-drawings to denote the points determined experimentally. Line-drawings must not contain structural formulas and comments. Spectra or relevant segments thereof, chromatograms, and X-ray diffraction patterns will be reproduced only if concise numerical summaries are inadequate to replace them. Drawings and graphs should be prepared in black ink on good-quality white or tracing paper. Photographs should be submitted on glossy paper as high-contrast copies. Xerox or similar copies are not suitable for reproduction, but may be used for duplicate copies.

Redrawn illustrations will be sent to the authors for checking. No corrections of figures will, therefore, be accepted in the proofs.

Submission of manuscript

After having completed the corrections suggested by the referees and editors, the final manuscript should be submitted in duplicate, in a form ready for publication. If the corrected manuscript is not returned to the editots *within six weeks*, the intended publication of the paper will be regarded as withdrawn by the authors.

Page charge will not be assessed for the publication, however, authors from overseas countries must contribute to the postage of correspondence by sending, together with the manuscript, international postal coupons to the value of U.S. $ 10.—

Proofs and reprints

A set of proofs will be sent to the submitting author. The proofs must be returned within 48 hours of receipt. Late return may cause a delay in the publication of the paper. 100 reprints will be supplied to the authors free of charge.

Periodicals of the Hungarian Academy of Sciences are obtainable at the following addresses:

AUSTRALIA
C.B.D. LIBRARY AND SUBSCRIPTION SERVICE
Box 4886, G.P.O., *Sydney N.S.W. 2001*
COSMOS BOOKSHOP, 145 Ackland Street
St. Kilda (Melbourne), Victoria 3182

AUSTRIA
GLOBUS, Höchstädtplatz 3, *1206 Wien XX*

BELGIUM
OFFICE INTERNATIONAL DE LIBRAIRIE
30 Avenue Marnix, *1050 Bruxelles*
LIBRAIRIE DU MONDE ENTIER
162 rue du Midi, *1000 Bruxelles*

BULGARIA
HEMUS, Bulvar Ruszki 6, *Sofia*

CANADA
PANNONIA BOOKS, P.O. Box 1017
Postal Station "B", *Toronto, Ontario M5T 2T8*

CHINA
CNPICOR, Periodical Department, P.O. Box 50
Peking

CZECHOSLOVAKIA
MAD'ARSKÁ KULTURA, Národní třida 22
115 66 Praha
PNS DOVOZ TISKU, Vinohradská 46, *Praha 2*
PNS DOVOZ TLAČE, *Bratislava 2*

DENMARK
EJNAR MUNKSGAARD, Norregade 6
1165 Copenhagen K

FEDERAL REPUBLIC OF GERMANY
KUNST UND WISSEN ERICH BIEBER
Postfach 46, *7000 Stuttgart 1*

FINLAND
AKATEEMINEN KIRJAKAUPPA, P.O. Box 128
SF-00101 Helsinki 10

FRANCE
DAWSON-FRANCE S. A., B. P. 40, *91121 Palaiseau*
EUROPÉRIODIQUES S. A., 31 Avenue de Versailles, *78170 La Celle St. Cloud*
OFFICE INTERNATIONAL DE DOCUMENTATION ET LIBRAIRIE, 48 rue Gay-Lussac
75240 Paris Cedex 05

GERMAN DEMOCRATIC REPUBLIC
HAUS DER UNGARISCHEN KULTUR
Karl Liebknecht-Straße 9, *DDR-102 Berlin*
DEUTSCHE POST ZEITUNGSVERTRIEBSAMT
Sraße der Pariser Kommüne 3–4, *DDR-104 Berlin*

GREAT BRITAIN
BLACKWELL'S PERIODICALS DIVISION
Hythe Bridge Street, *Oxford OX1 2ET*
BUMPUS, HALDANE AND MAXWELL LTD.
Cowper Works, *Olney, Bucks MK46 4BN*
COLLET'S HOLDINGS LTD., Denington Estate
Wellingborough, Northants NN8 2QT
WM. DAWSON AND SONS LTD., Cannon House
Folkstone, Kent CT19 5EE
H. K. LEWIS AND CO., 136 Gower Street
London WC1E 6BS

GREECE
KOSTARAKIS BROTHERS INTERNATIONAL BOOKSELLERS, 2 Hippokratous Street, *Athens-143*

HOLLAND
MEULENHOFF-BRUNA B.V., Beulingstraat 2,
Amsterdam
MARTINUS NIJHOFF B.V.
Lange Voorhout 9–11, *Den Haag*
SWETS SUBSCRIPTION SERVICE
347b Heereweg, *Lisse*

INDIA
ALLIED PUBLISHING PRIVATE LTD., 13/14
Asaf Ali Road, *New Delhi 110001*
150 B-6 Mount Road, *Madras 600002*
INTERNATIONAL BOOK HOUSE PVT. LTD.
Madame Cama Road, *Bombay 400039*
THE STATE TRADING CORPORATION OF INDIA LTD., Books Import Division, Chandralok
36 Janpath, *New Delhi 110001*

ITALY
INTERSCIENTIA, Via Mazzé 28, *10149 Torino*
LIBRERIA COMMISSIONARIA SANSONI, Via Lamarmora 45, *50121 Firenze*
SANTO VANASIA, Via M. Macchi 58
20124 Milano
D. E. A., Via Lima 28, *00198 Roma*

JAPAN
KINOKUNIYA BOOK-STORE CO. LTD.
17-7 Shinjuku 3 chome, Shinjuku-ku, *Tokyo 160-91*
MARUZEN COMPANY LTD., Book Department,
P.O. Box 5050 Tokyo International, *Tokyo 100-31*
NAUKA LTD. IMPORT DEPARTMENT
2-30-19 Minami Ikebukuro, Toshima-ku, *Tokyo 171*

KOREA
CHULPANMUL, *Phenjan*

NORWAY
TANUM-TIDSKRIFT-SENTRALEN A.S., Karl Johansgatan 41–43, *1000 Oslo*

POLAND
WĘGIERSKI INSTYTUT KULTURY, Marszałkowska 80, *00-517 Warszawa*
CKP I W, ul. Towarowa 28, *00-958 Warszawa*

ROUMANIA
D. E. P., *Bucureşti*
ILEXIM, Calea Grivitei 64–66, *Bucureşti*

SOVIET UNION
SOJUZPECHAT — IMPORT, *Moscow*
and the post offices in each town
MEZHDUNARODNAYA KNIGA, *Moscow G-200*

SPAIN
DIAZ DE SANTOS, Lagasca 95, *Madrid 6*

SWEDEN
ALMQVIST AND WIKSELL, Gamla Brogatan 26
101 20 Stockholm
GUMPERTS UNIVERSITETSBOKHANDEL AB
Box 346, *401 25 Göteborg 1*

SWITZERLAND
KARGER LIBRI AG, Petersgraben 31, *4011 Basel*

USA
EBSCO SUBSCRIPTION SERVICES
P.O. Box 1943, *Birmingham, Alabama 35201*
F. W. FAXON COMPANY, INC.
15 Southwest Park, *Westwood Mass. 02090*
THE MOORE-COTTRELL SUBSCRIPTION AGENCIES, *North Cohocton, N. Y. 14868*
READ-MORE PUBLICATIONS, INC.
140 Cedar Street, *New York, N. Y. 10006*
STECHERT-MACMILLAN, INC.
7250 Westfield Avenue, *Pennsauken N. J. 08110*

YUGOSLAVIA
JUGOSLOVENSKA KNJIGA, Terazije 27, *Beograd*
FORUM, Vojvode Mišića 1, *21000 Novi Sad*

Index: 26.007

Acta Chimica Hungarica

VOLUME 121, NUMBER 3, MARCH 1986

Akadémiai Kiadó, Budapest
ACTA CHIM. HUNG. ACHUDC 121 (3) 233–331 (1986) HU ISSN 0231–3146

ACTA CHIMICA HUNGARICA

A JOURNAL OF THE HUNGARIAN ACADEMY OF SCIENCES

Acta Chimica publishes original reports on all aspects of chemistry in English.

Acta Chimica is published in three bolumes per year, each volume consisting of four issues, by

AKADÉMIAI KIADÓ

Publiching House of the Hungarian Academy of Sciences
H-1054 Budapest, Alkotmány u. 21.

Manuscripts and editorial correspondence should be addressed to

Acta Chimica
H-1450 Budapest P.O. Box 67

Subscription information

Orders should be addressed to

KULTURA Foreign Trading Company
H-1389 Budapest P.O. Box 149

or to its representatives abroad

Acta Chimica is indexed in Current Contents.

NOTICE TO AUTHORS

Acta Chimica publishes original papers on all aspects of chemistry in English. Before preparing a manuscript for submission to this journal authors are advised to consult recent issues.

Form of manuscript

Manuscripts, tables and illustrations should be submitted in triplicate. Manuscripts should be typewritten double spaced (25 lines, 50 characters per line including spaces). The *title page* should include (1) the title of the paper, (2) the full names of the author(s) in the sequence to be published; apply an asterisk to designate the name of the author to whom correspondence should be addressed, (3) name and address of the institution where the work was done. If the paper is part of a series, reference to the previous communication must be given as a footnote.

Abstract

A summary is printed at the head of each paper. This should not exceed 200 words and should state briefly the principal results and major conclusions of the work. It should be suitable for use by abstracting services.

CONTENTS

PHYSICAL AND INORGANIC CHEMISTRY

ORGANIC CHEMISTRY

Acta Chimica Hungarica 121 (3), pp. 233—236 (1986)

BROMINATION OF 5α-CHOLESTANE-3,6-DIONE

Rubina HABIB, Mubarak HUSAIN, Mashkoor HUSAIN and Naseem Hasan KHAN*

(Department of Chemistry, Aligarh Muslim University, Aligarh-202 001, India)

Received July 25, 1984
Accepted for publication October 23, 1984**

Bromination of 5α-cholestane-3,6-dione (**I**) was effected using different molar concentrations of bromine in acetic acid. One mole equivalent of bromine gave cholest-4-ene-3,6-dione (**II**). With two mole equivalents and excess of bromine, products **III** and **IV** were, respectively, obtained. These products were characterized on the basis of their elemental analyses, spectral properties and by comparison with authentic samples where available.

Compound **I** on reaction with one mole equivalent of bromine in acetic acid gave a product, m.p. 122 °C, which was identified as cholest-4-ene-3,6-dione (**II**) on the basis of its identity (m.p., m.m.p., co-TLC and IR) with an authentic sample of II [1]. This compound is probably a dehydrobromination product of 5α-bromocholestane-3,6-dione (**V**).

A similar treatment of the title compound with 2 mole equivalents of bromine afforded another product with melting point 159 °C, which had a positive Beilstein test for halogen and correct analysis for $C_{27}H_{41}O_2Br$ (M^+ 476, 478; 1 : 1). The UV spectrum of this compound having an absorption maximum at 255 nm (ε 10658) suggested the presence of an enedione chromophore. The presence of α-substituted enedione was further supported [2] by two absorption bands at 1670 and 1700 cm^{-1}. The latter band [2] suggested the attachment of bromine adjacent to one of the C=O groups. The position of bromine was ascertained from its NMR spectrum wherein a broad singlet at δ 4.40 integrating for one proton is undoubtedly [3] due to the C7-proton, oriented *equatorially* (the Dreiding stereomodel showed the dihedral angle between C7 and C8 protons to be almost 90°). Had the bromine been at C2, the signal for the C2-proton in the NMR spectrum should have been observed as a doublet of doublet [4, 5]. A sharp singlet for 1H seen at δ 6.5 is ascribable to C4 vinylic proton. On the basis of this spectral evidence, the compound of m.p. 159 °C has been considered as 7α-bromocholest-4-ene-3,6-dione (**III**).

* To whom correspondence should be addressed.
** In final form May 24, 1985.

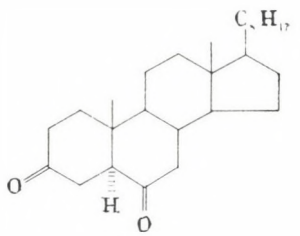

I

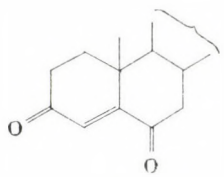

II

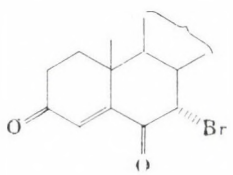

III

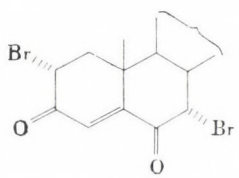

IV

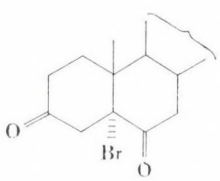

V

With an excess of bromine compound **I** furnished a third product which melted at 168 °C. This also showed positive Beilstein test indicating the presence of halogen and had analysis correct for $C_{27}H_{40}O_2Br_2$ (M^+ 554, 558; 1 : 1). The UV absorptiom maximum at 242 nm (ε 11620) suggested the presence of an enone. This was further substantiated by a strong band at 1700 cm^{-1}, which is characteristic of α-substituted ketones [2]. The NMR spectrum lends further support to structure **IV** by exhibiting a broad signal at δ 4.41 for one proton (C7-proton), which is *equatorially* oriented. A doublet of doublet (J_1 = 12 Hz; J_2 = 6 Hz) at δ 4.85 can be assigned to the proton present at C2. The splitting constants [4] $J_{a,a}$ = 12 Hz and $J_{a,e}$ = 6 Hz confirm the presence of bromine at C2 having α-orientation; consequently, the proton at this position is axial. Moreover, the α-oriented *(equatorial)* bromine at C2 would be preferred, since the alternative structure, with β-oriented bromine, is less favourable due to 1,3-*diaxial* interaction between the C10 methyl and C2 β-bromine. Thus, the compound melting at 168 °C has been represented by the structure **IV**.

Furthermore, the bromination under similar conditions of cholest-4-ene-3,6-dione (**II**) yielding products **III** and **IV** can be explained via the dehydrobromination of the likely primary product **V** formed from the title compound (**I**), resulting in unsaturation at C4.

Experimental

M.p.'s are uncorrected. UV spectra were recorded on a PYE-UNICAM PU 8800 spectrophotometer. IR spectra were obtained on a PYE-UNICAM SP-300 infrared spectrophotometer. NMR were taken on a Varian A60 instrument using TMS as internal standard. TLC plates were coated with silica gel G and sprayed with a 25% aqueous solution of perchloric acid.

Reaction of 5α-cholestane-3,6-dione(I) with 1 mole equivalent of bromine

5α-Cholestane-3,6-dione **I**; (1 g) was dissolved in ether (30 mL). To this a solution of bromine in glacial acetic acid (0.2 mL taken up in 8 mL acetic acid) was added over a period of 45 min and the mixture was kept at room temperature for 2 h when the reaction was complete. The reaction mixture was extracted with ether and the ethereal layer washed with water, dried over anhydrous sodium sulfate and filtered. Removal of the solvent gave an oily residue which was crystallized from petroleum ether to obtain **II**, m.p. 122 °C (reported [1] m.p. 122—123 °C); yield 0.6 g (identified as cholest-4-ene-3,6-dione on the basis of its identity in m.p., m.m.p., co-TLC and IR with an authentic sample of **II**).

Reaction of (I) with 2 mole equivalents of bromine

To a solution of **I** (1 g) in ether (30 mL) was added a solution of bromine (0.4 mL dissolved in 10 mL of glacial acetic acid), dropwise, over a period of 45 min at 0—5 °C. The reaction mixture was kept at a temperature of 0—5 °C for 5 days when the reaction was over; the mixture was then extracted with ether. The ethereal layer was washed with water and dried over anhydrous Na_2SO_4. Removal of the solvent gave an oily residue which was chromatographed over silica gel to yield 0.4 g of a compound, m.p. 159 °C (other compounds present in minute quantities were not isolated) characterized as 7α-bromocholest-4-ene-3,6-dione (**III**).

UV: λ_{max} 255 nm (ε 10658) (C=C—C=O).

IR: ν_{max} 1700 (—CO—CH—Br), 1670 (C=C—C=O), 1620 (C=C), 640 cm^{-1} (C—Br).

^{1}H-NMR: δ 4.40 (br, s, 1H, C7-βH) (Dreiding stereomodel of this compound showed the dihedral angle between C7 and C8 protons to be ~90°), 6.5 (s, 1H, C4-vinylic proton), 1.14 (s, 3H, C10-CH_3), 0.87 ppm (s, 3H, C13-CH_3).

MS (*m/e*): (M^+; 476, 478; 1 : 1).

$C_{27}H_{41}O_2Br$. Calcd. C 67.92; H 8.59. Found C 67.86; H 8.54%.

Reaction of (I) with an excess of bromine

A solution of compound **I** (1 g) in ether (30 mL) was subjected to reaction with a bromine solution (2 mL of Br_2 dissolved in 12 mL of acetic acid) in a similar way as described above. The reaction mixture was kept in a freezer for 7 days, when the reaction was complete. The mixture was then worked-up in the usual manner. Removal of the solvent furnished an oily residue which was purified on a silica gel column and crystallized from petroleum ether to give the product (0.7 g), m.p. 168 °C, characterized as 2α,7α-dibromocholest-4-ene-3,6-dione (**IV**).

UV: λ_{max} 242 nm (ε 11620).

IR: ν_{max} 1700 (strong band, Br—CH—CO—C=C—CO—CH—Br), 1625 (C=C), 680, 640 cm^{-1} (C—Br).

^{1}H-NMR: δ 4.41 (br, s, 1H, C7-βH; the Dreiding model showed the angle between C7 and C8 protons as 90°), 4.85 (dd, $J_1 = 12$ Hz; $J_2 = 6$ Hz, 1H, C2-H; *axial);* 6.35 (s, 1H, C4-vinylic H); 1.13 (s, 3H, C10-CH_3); 0.68 ppm (s, 3H, C13-CH_3).

MS (*m/e*): (M^+; 554, 558; 1 : 1).

$C_{27}H_{40}O_2Br_2$. Calcd. C 58.27; H 7.19. Found C 58.23; H 7.25%.

*

The authors are grateful to Prof. M. S. Ahmad, Chairman, Chemistry Department, for research facilities and to CSIR (New Delhi) for financial support (MH, MH).

REFERENCES

[1] Fieser, L. F.: J. Am. Chem. Soc., **75,** 4386 (1953)
[2] Ahmad, M. S., Khan, I. A., Pillai, N. K.: Tetrahedron, **36** (16), 2341 (1980)
[3] Shafiullah, Husain S., Ali, H.: Indian J. Chem., **22B,** 71 (1983)
[4] Abraham, R. J., Holker, J. S. E.: J. Chem. Soc., **1963,** 806
[5] Komeno, T., Tori, K., Takeda, K.: Tetrahedron, **21,** 1635 (1965)

Acta Chimica Hungarica 121 (3), pp. 237–242 (1986)

SYNTHESIS AND CYCLIZATION OF BIS-AMIDES INTO ISOQUINOLINONES

(SHORT COMMUNICATION)

László Hazai and Gyula Deák*

(Institute of Experimental Medicine, Hungarian Academy of Sciences, H-1450 Budapest, P.O.B. 67,)

Received January 15, 1985
Accepted for publication April 15, 1985

1-Phenyl-1,4-dihydro-3(2*H*)-isoquinolinone was first prepared by Deák et al. [1] by the cyclization of benzaldehyde and benzyl cyanide in acid medium (polyphosphoric acid). During the kinetic investigation of the reaction it was established [2] that phenylacetamide, formed by hydration from the nitrile in polyphosphoric acid (further on: PPA), yields in the reaction with benzaldehyde benzylidene-bis(phenylacetamide). From this intermediate isoquinolinone is formed by cyclizing amidoalkylation, with the cleavage of one molecule of phenylacetamide (see Scheme 1: **1a**, **2a**). By this method several 1-aryl-1,4-dihydro-3(2*H*)-isoquinolinones, substituted in different positions, have been synthesized [3].

In the course of further investigations the presumed intermediate bis--amide, which could be isolated so far only in a single case (R^1 = 4-pyridyl group, $n = 1$ [4]), was prepared by two methods: starting from nitrile (Q: —C≡N) in acetic acid, catalyzed by *conc.* sulfuric acid, at room temperature, or by Gilbert's method [5], that is, by boiling the amide (Q: —$CONH_2$) with toluene**, similarly using *conc.* sulfuric acid as catalyst. The bis-amides obtained in this way were converted in PPA into the expected 1,4-dihydro--3(2*H*)-isoquinolinones [6].

In continuation of this work, we wished to extend our investigations to the synthesis of 1-unsubstituted or 1-benzyl-substituted isoquinolinones, further to the preparation of isoindolones. Therefore, we studied the preparation of bis-amides containing H or an aralkyl group instead of the R^1 = aryl group with $n = 1$, and their cyclization into isoquinolinones. Results of the experiments pertaining to the bis-amides are summarized in Table I.

In view of the fact that methylene-bis(phenylacetamide) (**1b**) could be prepared by both methods, the question arose whether the reaction of phenyl-

* To whom correspondence should be adressed.

** In general, the toluene method was used only if the acetic acid process failed for some reason.

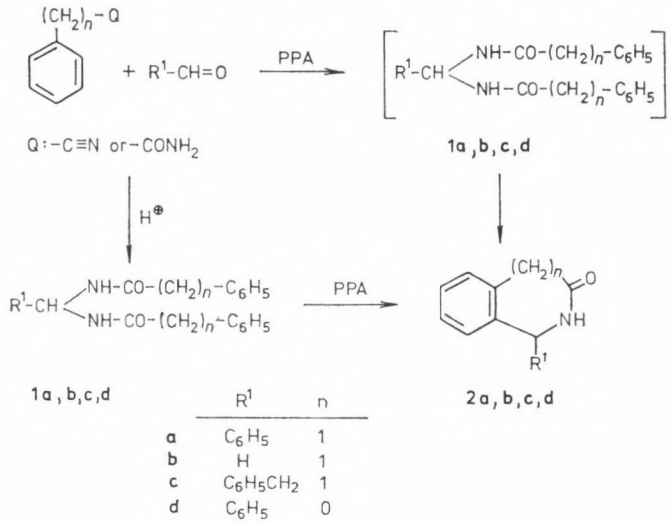

	R^1	n
a	C_6H_5	1
b	H	1
c	$C_6H_5CH_2$	1
d	C_6H_5	0

Scheme 1

acetamide or benzyl cyanide with formaldehyde could not lead through **1b** directly to 1,4-dihydro-3(2*H*)-isoquinolinone (**2b**), unsubstituted in position 1, under the conditions of the synthesis method generally used by us (see above).

Several methods are described in the literature for the preparation of **2b**, e.g. the Schmidt reaction of 2-indanone [9], synthesis from sulfur-containing homophthalimide derivatives by desulfuration [10, 11], the cyclization of *N*-hydroxymethylphenylacetamide [12], and some recently published Japanese patents (e.g. Ref. [13]), according to which the compound is prepared by the cyclization of phenylacetamide and formaldehyde in acid medium, the acid being phosphoric acid, methanesulfonic acid, PPA, using occasionally toluene or xylene as diluting agent.

Table I

Bis-amides			Yield (%)	
	R^1	*n*	Toluene method	Acetic acid method
1a	C_6H_5	1	75.6	75 [7]
1b	H	1	33*	88 [8]**
1c	$C_6H_5CH_2$	1	—	—
1d	C_6H_5	0		55

* Yield of the crude product of good m.p.: 96.4%, nearly quantitative; the large loss of crystallization is due to the poor solubility.

** In the literature process [8] no acetic acid was used; the reaction was carried out by boiling in *conc.* sulfuric acid in the presence of aqueous formaldehyde.

The effecting of the reactions in polyphosphoric acid medium was attempted also by us; however, in 1 : 1 PPA* (in which our synthesis can be suitably performed) neither the reaction of phenylacetamide with formaldehyde, nor the heating of methylene-bis(phenylacetamide) (**1b**) gave the expected isoquinolinone **2b**; unidentifiable decomposition products were formed, from which the required product could not be isolated.

As a further cyclizing medium a 10 : 1 mixture of methanesulfonic acid and phosphorus pentoxide was investigated, which, according to Eaton et al. [14] may replace in several cases the otherwise impracticable polyphosphoric acid in various reactions. With this reagent, both benzyl cyanide (Q: —C≡N) and phenylacetamide (Q: —$CONH_2$), as model compounds (Scheme 1), could be cyclized with benzaldehyde to the respective 1-phenyl--1,4-dihydro-3(2*H*)-isoquinolinone (**2a**) in good yields. However, when formaldehyde was applied instead of benzaldehyde, the use of this reagent also failed in giving the expected isoquinolinone **2b** as an isolable product.

Ben-Ishai et al. [15] obtained the derivative of **2b** containing dimethyl substituent in position 4 under conditions actually similar to those of the bis-amide preparation, by the reaction of α,α-dimethylphenylacetamide with formaldehyde in acetic acid—sulfuric acid mixture, with 16-hour refluxing, in a yield of 82%. Tikk et al. [16], applying the reaction to phenylacetamide, isolated **2b** in a very poor yield. A detailed investigation of this reaction was undertaken with the aim to elucidate the cause of the low yield, and possibly to optimize the reaction conditions.

Following, by thin-layer chromatography, the reaction of phenylacetamide with formaldehyde in acetic acid—sulfuric acid mixture at reflux temperature, the examination of the samples taken each 10 minute showed that even after reaction times of 50 or 60 minutes 1,4-dihydro-3(2*H*)-isoquinolinone (**2b**) could be isolated from many unidentifiable by products only in a poor yield, similarly to the experience of Tikk et al. [16]. Moreover, it was found that the primary product of the reaction was the bis-amide **1b**; from a reaction carried out at 95 °C this bis-amide could be isolated after a reaction time of 10 minutes in crude yet already pure state in nearly 50% yield. During the further reaction of the bis-amide presumably decomposition processes predominate, and these may be responsible for the low yield of **2b**. The isolation of **1b** is a new example that this intermediate can be separated during isoquinolinone synthesis, which, as mentioned above, was achieved previously only in a single case.

In our further work the cyclization of benzylidene-bis(benzamide) (**1d**) was studied. However, in PPA medium **1d** was not converted into the expected 3-phenyl-2,3-dihydroisoindolone (**3**) (Scheme 2) under the usual reaction con-

* 85% phosphoric acid (mL); phosphorous pentoxide (g).

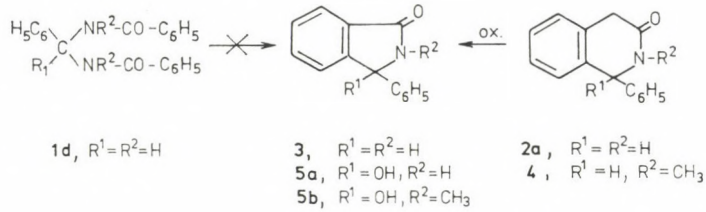

1d, $R^1=R^2=H$ **3**, $R^1=R^2=H$; **5a**, $R^1=OH, R^2=H$; **5b**, $R^1=OH, R^2=CH_3$ **2a**, $R^1=R^2=H$; **4**, $R^1=H, R^2=CH_3$

Scheme 2

ditions, and only decomposition products were detected. Thus the isoquinolinone synthesis developed by us could not be extended to the 5-membered ring analogues.

It should be mentioned here that the 3-hydroxy derivative of isoindolone **3*** (**5a**) [17] and its *N*-methyl analogue (**5b**) [18] was isolated from the oxidation with potassium permanganate of the 1-phenyl-1,4-dihydro-3(2*H*)-isoquinolinones **2a** and **4**. The structures of the compounds were proved by IR, UV, NMR and mass spectroscopy.

Experimental

M.p.'s were measured with a Büchi—Tottoli melting point determinating apparatus and are uncorrected. The IR spectra were recorded with a Perkin Elmer 457 spectrophotometer, the NMR spectra with a JEOL FX-100 instrument and the UV spectra with an OPTON-DMR 21 spectrophotometer. The mass spectra were obtained with an AEI MS-902 type instrument (70 eV, direct insertion, 110 °C).

Benzylidene-bis(phenylacetamide) (1a)

Phenylacetamide (27.0 g; 0.2 mol) and 10.6 g (0.1 mol) benzaldehyde were refluxed in 450 mL dry toluene in the presence of a few drops of *conc.* sulfuric acid for 4 h, using a water separator headpiece. The product which separated was filtered off and recrystallized from ethyl alcohol to give 27.1 g (75.6%) of **1a**; m.p. 228—230 °C, *lit.* [20] m.p. 231 °C.

N,N'-Methylene-bis(phenylacetamide) (1b)

Phenylacetamide (27.0 g; 0.2 mol) and 3.3 g (0.1 mol) formaldehyde were boiled in 400 mL anhydrous toluene in the presence of a few drops of *conc.* sulfuric acid, using a water separator headpiece, until water formation had ceased (12—13 h). The precipitate was filtered off and dried. Recrystallization from ethyl alcohol gave 9.3 g (33%) of **1b**, m.p. 214 °C, *lit.* [8] m.p. 210 °C.

Benzylidene-bis(benzamide) (1d)

Glacial acetic acid (10 mL) was mixed with 5.23 g (0.05 mol) benzaldehyde, then, under cooling the mixture in ice-water, 1 mL *conc.* sulfuric acid was added. After 10 min 10.3 g (0.1 mol) benzonitrile was added dropwise, and the reaction mixture was allowed to stand

* The oxidation of 1-phenylisoquinoline with $KMnO_4$ presumably leads also through the 3,4-dioxo-1-hydroxy compound to **5a** [19].

for 4 days. The precipitate, which separated on dilution of the reaction mixture with water, was filtered off, washed with water, then with *conc.* ammonia diluted to 1 : 1, and with ether, and dried. Recrystallization from dimethylformamide gave 9.1 g (55.2%) of **1d**, m.p. 231—233 °C.

$C_{21}H_{18}N_2O_2$. Calcd. C 76.34; H 5.49; N 8.48. Found C 76.33; H 5.73; N 8.45%.

IR (KBr): 1665 cm^{-1} (amide I), 1550 cm^{-1} (amide II).

Isolation of *N,N'*-methylene-bis(phenylacetamide) (1b) during the preparation of 1,4-dihydro-3(2*H*)-isoquinolinone (2b)

Phenylacetamide (2.7 g; 0.02 mol), paraformaldehyde (0.7 g; 0.0232 mol) and *conc.* sulfuric acid (1.6 mL) were weighed into 32 mL of glacial acetic acid. After stirring for 30 min the mixture became homogeneous. It was heated to 95 °C and stirred at this temperature for 10 min. The reaction mixture was then neutralized with 800 mL saturated $NaHCO_3$ solution. The solid which separated was filtered off and dried to obtain 1.4 g (49.6%) of the product, m.p. 215—216 °C (ethanol), identical with the compound prepared earlier.

Preparation of 1-phenyl-1,4-dihydro-3(2*H*)-isoquinolinone (2a) in 10 : 1 methanesulfonic acid-phosphorus pentoxide reagent

(a) From nitrile (Q: —C≡N)

P_2O_5 (5 g) was added to 50 g of methanesulfonic acid, and the mixture was stirred until dissolution was complete (2 h). Benzyl cyanide (1.17 g; 0.01 mol) was then added and the mixture agitated at 80 °C for 30 min. Benzaldehyde (1.06 g; 0.01 mol) was added to the reaction mixture and after stirring for 2 h at 80 °C, it was poured into 500 mL saturated $NaHCO_3$ solution. The solid was filtered off and dried to obtain 1.1 g (49.3%) of the product m.p. 166—168 °C (ethanol); *lit.* [1] m.p. 168 °C.

(b) From amide (Q: —$CONH_2$)

Phenylacetamide (1.35 g; 0.01 mol) and 1.06 g (0.01 mol) benzaldehyde were weighed into the reagent prepared according to method *(a)*; carrying out the reaction as described above gave 1.15 g (51.5%) of **2a** m.p. 167 °C (ethanol); *lit.* [1] m.p. 168 °C.

3-Phenyl-3-hydroxy-2,3-dihydroisoindolone (5a)

Compound **2a** (2.23 g; 0.01 mol) was stirred in 50 mL water, and, at 70 °C, 4.1 g (0.025 mol) potassium permanganate was added over 1 h. The reaction mixture maintained for 30 min at 100 °C. The hot mixture was then filtered, the filter was washed with water, and the filtrate was acidified. A solid separated, which was filtered off and dried to give 0.5 g (22.2%) of the product, m.p. 158—160 °C (water); *lit.* [17] m.p. 162—163 °C.

3-Phenyl-3-hydroxy-2-methyl-2,3-dihydroisoindolone (5b)

Compound **4** (2.37 g; 0.01) [21] was mixed with 50 mL water, and 4.1 g (0.025 mol) potassium permanganate was added in small portions, while the temperature of the mixture was raised to 100 °C. After stirring for 30 min the hot solution was filtered, and the solid which separated on cooling was filtered off and washed with water. The product was triturated with chloroform, the chloroform solution was evaporated to dryness, and the residual oil was rubbed with ether to obtain 0.55 g (23%) of **5b**, m.p. 186—188 °C (1 : 1 acetone-water); *lit.* [18] m.p. 187—188 °C.

The agreement of the spectroscopic data [18] adequately supported the structures of both compounds (**5a**, **5b**).

*

The authors' thanks are due to Dr. J. Haskó-Breuer for recording the IR spectra, to Dr. G. Tóth for recording the NMR spectra and to Dr. J. Tamás for the mass spectra. The authors are grateful to the analytical team, headed by Miss M. Fodor, for microanalyses, and to Miss K. Juhász for excellent technical assistance.

REFERENCES

[1] Csűrös, Z., Deák, Gy., Hoffmann, I.: Acta Chim. Acad. Sci. Hung., **55,** 125 (1968)
[2] Deák, Gy., Gáll-Istók, K., Kálmán, Zs., Haskó-Breuer, J.: Acta Chim. Acad. Sci. Hung., **76,** 299 (1973)
[3] Deák, Gy.: Magy. Kém. Lapja, **39,** 285 (1984) and references cited therein
[4] Hazai, L., Deák, Gy., Szabó, G., Koltai, E.: Acta Chim. Acad. Sci. Hung., **102,** 305 (1979)
[5] Gilbert, E. E.: Synthesis, **1972,** 30
[6] Deák, Gy., Gáll-Istók, K., Hazai, L., Sterk, L.: Synthesis, **1975,** 393
[7] Deák, Gy., Gáll-Istók, K., Hazai L.: Acta Chim. Acad. Sci. Hung., **84,** 477 (1975)
[8] Haworth, R. D., MacGillivray, R., Peacock, D. H.: J. Chem. Soc., **1950,** 1496
[9] Jean, T., Dienel, B., Dowalo, F., van Hoeven, H., Bender, P., Loev, B.: J. Med. Chem., **16,** 633 (1973)
[10] Kim, Y. C.: Canad. J. Chem. **47,** 3259 (1969)
[11] Tamura, Y., Uenishi, J., Maeda, H., Choi, H., Ishibashi, H.: Synthesis, **1981,** 534
[12] Watanabe, Y., Kamochi, Y., Miyazaki, T.: Heterocycles, **16,** 609 (1981)
[13] Jpn. Kokai Tokkyo Koho, JP 82 88, 163 (1982); Chem. Abstr., **97,** 162597e (1982)
[14] Eaton, P. E., Carlson, G. R., Lee, J. T.: J. Org. Chem., **38,** 4071 (1973)
[15] Ben-Ishai, D., Inbal, Z., Warshawsky, A.: J. Heterocycl. Chem., **7,** 615 (1970)
[16] Tikk, I., Tóth, G., Deák, Gy.: Acta Chim. Hung., **114,** 355 (1983)
[17] Rabjon, N., Drumm, M. F., Elliott, R. L.: J. Am. Chem. Soc., **78,** 1631 (1956)
[18] Armarego, W. L., Sharma, S. C.: J. Chem. Soc. (C), **1970,** 1600
[19] Davies, W., Ramsay, T. H., Stove, E. R.: J. Chem. Soc., **1949,** 2633
[20] Csűrös, Z., Deák, Gy., Haraszty-Papp, M., Hoffmann, I.: Acta Chim. Acad. Sci. Hung., **59,** 119 (1969)
[21] Hazai L., Deák, Gy., Szőllősy, Á., Tóth, G., Bitter, I.: Acta Chim. Hung., **121,** 263 (1986)

Acta Chimica Hungarica 121 (3), pp. 243—253 (1986)

ION EXCHANGE PROPERTIES OF A HUNGARIAN SEDIMENTARY MORDENITE

Elisabeth CZÁRÁN*, Elisabeth DOMOKOS, Ágnes MÉSZÁROS-KISS and János PAPP

(Central Research Institute for Chemistry, Hungarian Academy of Sciences, H-1525 Budapest, P.O. Box 17)

Received February 22, 1985
Accepted for publication April 15, 1985

Mordenite-containing tuff from the Tokaj Hills (Hungary) has been studied. The mordenite content of the rock has been determined from its ion exchange capacity and has been found to be about 78%. Based on ion exchange experiments, chemical and X-ray microanalytical results, the composition of the mordenite phase has been established as $Na_{2.07}K_{1.13}Ca_{2.4}[(Al_8\ Si_{40})O_{96}] \cdot 22.7H_2O$. The selectivity sequence of the original rock to the cations studied is: $K > NH_4 > Na > Ca$. Upon ion exchange with $NaNO_3$, KNO_3, NH_4NO_3 and $CaCl_2$ the different "monocationic" forms have been prepared and, by a second ion exchange, the following integral, selectivity sequences have been found for them:

$Na-M$: $NH_4 > K > Ca$
$K-M$: $NH_4 > Na > Ca$
$Ca-M$: $Na > NH_4 > K$

Introduction

In the last few decades sedimentary zeolites have been continuously gaining in importance in several fields of application. Zeolites of mineral origin can be successfully used in fields where the heterogeneity, i.e. the non-zeolite accompanying materials in the samples do not interfere with the properties to be utilized, e.g. in industrial, agricultural and environmental use, mainly as sorbents, ion exchangers, carriers, etc. For all these purposes the investigation of the physico-chemical properties to be exploited is of primary importance.

There is substantial literature on ion exchange in zeolites, but the majority of these works deal with the synthetic variants, and especially with those of the faujasite type, e.g. [1—5]. The ion exchange properties of mordenite have been studied in detail by Barrer and co-workers [6—8], but they mainly focused attention on the so-called large port, synthetic mordenite. The ion exchange of aqua and ammine complexes of silver into a synthetic Na-mordenite has been described by Fletcher and Townsend [8].

As to natural zeolites, Barrer and Townsend investigated the introduction of ammine complexes of transition metals into mordenite, clinoptilolite

* To whom correspondence should be addressed.

and phillipsite by ion exchange [7], whereas Rees and Rao [9] and Rao and Rees [10] studied the kinetics of ion exchange into natural mordenite.

In a review on ion exchange in zeolites [11] Barrer mentions the following parameters as influencing factors:

— topology of the anion lattice,
— shape and size of the participating cations,
— charge density in the lattice (Si/Al ratio),
— valency of the cations,
— concentration of the electrolyte in the ion exchange solution.

In addition to these, the hydration ability of the cations also plays a very important role. If the affinity of the cation to water is too high, an additional factor is operating, which diminishes the extent of ion exchange, namely the hydrate shell of the cation shields its positive charge, decreasing thereby the electrostatic attraction. As a result, the strongly hydrated cation cannot reach the less accessible positions. This speculation is supported by the experimental work of Coughlan [12], who has measured the degree of ion exchange attainable for divalent cations in mordenite as a function of the hydrated ionic radius and found a linear correlation. Extrapolation to 100% ion exchange corresponds to a hydrated ionic radius of 0.375 nm. The hydrated ionic radii of alkali metal ions are below this value with the exception of Li, and, in fact, most alkali metal ions can be exchanged into mordenite to nearly 100%. However, the hydrated ionic radii of alkaline earth metal ions, and even more so those of the transition metal ions impose a restriction on the degree of ion exchange.

Experimental

Characterization of the mordenite-containing tuff

As starting material, mordenite-containing rock from Tokaj Hills was used (location Bodrogkeresztúr). Qualitative identification of the zeolite contained in the rock was performed by X-ray powder diffraction and transmission electron microscopy. For its quantitative determination the adsorption capacity for CO_2 has been measured [3], but satisfactory results have been obtained also by simpler methods, e.g. by measuring the temperature rise upon wetting, or the ignition loss in a certain temperature range, mainly for zeolite-rich tuffs. Upon comparing the results obtained for a sample with those measured for a reference sample, the zeolite content could be determined. The results provided by the different methods agree within 5 – 8%. A better agreement cannot be expected owing to the heterogeneity of such mineralic samples.

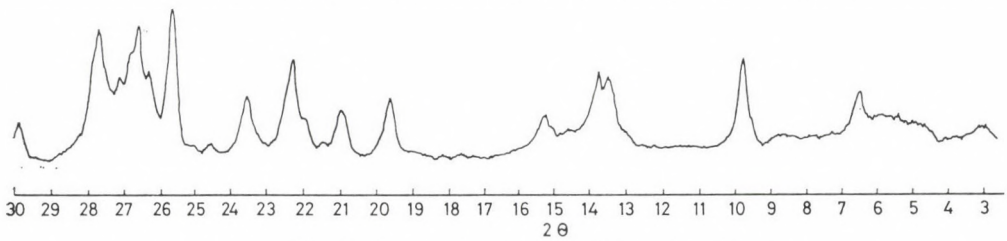

Fig. 1. X-ray diffractogram of the original rock

The selection of the suitable mordenite-containing rock for ion exchange experiments was made by taking into account that clay minerals, which very often accompany zeolites in sedimentary deposits, are interfering in ion exchanges. (This is due to their lamellar structure, where they also can bind cations and, in addition, a significant amount of water, which results in a swelling in the course of ion exchange from aqueous solutions.) The starting material chosen is a tuff containing about 80% of mordenite, the other components being mainly volcanic glass and quartz (see Fig. 1).

The X-ray diffractogram of the original tuff is shown in Fig. 1. Figures 2 and 3 represent the replicas prepared from the fractured surface of the tuff, taken in a Zeiss EF transmission

Fig. 2. Transmission electron micrograph of the replica prepared from a fracture surface of the rock. Needle-like individual crystals of mordenite. Magnification: × 10,000

Fig. 3. Transmission electron micrograph of the block formation of mordenite in the volcanic tuff. Magnification: × 10,000

electron microscope. From our earlier experience we know that in cases where the amount of mordenite is high in the sample, besides the characteristic individual needle crystals of mordenite (Fig. 2), also larger blocks of the mineral are formed during the crystallization process, as is shown in Fig. 3.

Ion exchange experiments

For ion exchange measurements the rock was ground below a particle size of 100 μm. Experiments were carried out with air dry samples. For ion exchange, the following solutions were used: 2 *M* and 0.2 *M* NH_4NO_3, 2 *M* and 0.2 *M* $NaNO_3$, 2 *M* and 0.2 *M* KNO_3, 2 *M* and 0.2 *M* $CaCl_2$ and 0.15 *M* $AgNO_3$. For the preparation of the "monocationic" forms, 20 g of the original rock was refluxed 3 times for 4 h each, renewing every time the 200 cm^3 portions of the 2 *M* ion exchange solution. An exception was the ion exchange with $AgNO_3$; in this case 0.15 *M* solutions were used in the dark at ambient temperature in order to prevent the reduction of silver ions.

In the study of the ion exchange properties of the "monocationic" samples, ion exchange was carried out by refluxing 1 g "monocationic" samples with 50 cm^3 of the appropriate solution portions, 2 times for 3 h each.

After ion exchange, the derivatives were washed with distilled water about 8—10 times, and dried in air at ambient temperature.

Both solid and liquid phases were analyzed. For the determination of the elemental composition of the different solid samples, they had to be digested. This was carried out with HF and H_2SO_4 in a platinum crucible, with each process repeated two times by evaporating the digestions to dryness. The residue was taken up with distilled water, heated on a water bath for 20—30 minutes, filled up to a known volume and analyzed.

The amounts of Na and K in both the digestions and ion exchange solutions were determined by atomic absorption spectrophotometry (AAS). For Ca, in addition to AAS, complexometric titration was also used, whereas Ag was only titrated. For the AAS measurements a Zeiss AAS-1N type instrument was applied, Na and K were determined in the emission mode (in an air-acetylene flame). whereas Ca in the absorption mode in N_2O-acetylene flame at wavelengths of 589.0 nm for Na, 766.5 nm for K and 422.6 nm for Ca. For calibration, the actual concentrations were adjusted in the calibrating solutions in order to compensate for matrix effects, i.e. for the eventual interfering effect of the high amounts of exchanging cations.

As the wet chemical analysis of the rock provides an overall chemical composition but not that of the zeolite phase, the Si/Al ratio of the mordenite phase had to be determined by some other method, e.g. X-ray microanalysis performed in the electron microscope [13]. In this method, a mordenite crystal identified in the electron microscope by its crystal shape, is excited by the electron beam, producing thereby a characteristic X-ray spectrum of the elements present in the analyzed volume of the samples. This spectrum can be evaluated for the Si/Al ratio in the crystal. As to the determination of the other components (cations) in the samples, this method is not sensitive enough for Na. (This element has the lowest atomic number among the elements analyzable by energy dispersive X-ray method.)

Results and Discussion

Determination of the cation composition of the mordenite phase

First the overall chemical composition of the rock has been determined from the wet chemical analysis of the tuff. The cations in this starting material are distributed between the zeolitic and non-zeolitic phase, but only those in the zeolite phase can be exchanged by other cations. Due to this fact, on ion exchanging the mordenite-containing rock with different solutions, in these solutions the mobile, zeolitic cations exchanged by this special cation can be determined. Thus, upon treating the starting material with the different solutions mentioned in the experimental part, two aims can be achieved at the same time:

— the preparation of the "monocationic" samples,

— by mobilizing the exchangable cations, a possibility arises for the separate determination of the zeolitic cations.

It is known from the literature [14] on mordenite that NH_4 and alkali metal ions can be exchanged practically quantitatively into this zeolite. Therefore, we assumed that on exchanging with NH_4, Na and K ions, the maximum amount of cations leaving the mordenite and appearing in the solution, can be assigned to the zeolitic phase. Thus, amounts of cations representing the difference between the cation content in the rock as found by the wet chemical analysis and the maximum amount of the respective cations found in the ion exchange solutions can be regarded as belonging to the non-zeolitic phase.

In Table I the results of wet chemical analysis are given (column 2) together with the maximum amounts of exchangeable cations assigned to the mordenite phase (column 8) and, as a difference between these two, the amounts of cations contained in the non-zeolitic part of the rock (column 9) are shown. The columns 3—7 contain the results of analysis of the ion exchange solutions after exchanging according to the procedure given in the experimental part.

The Si/Al ratio in the mordenite phase was determined by X-ray microanalysis. Mordenite crystals were chosen in positions where no other interfering particles were present in the analyzed volume. Point analyses were made at about 10—15 points and averaged. This average agreed satisfactorily with the Si/Al ratio of synthetic mordenite, i.e. 5, with an accuracy of about 5—7%. Therefore, we considered this ratio to be 5. By knowing this, we can determine the distribution of the three cations present in the unit cell of mordenite, if we take the data from Table I. As the analyses did not show the presence of Mg, and from the ignition loss of the samples the real water con-

Table I

Cation content of the starting material, of its zeolite and non-zeolitic phases (meq/g)

Cation	Starting material	Cation content of ion exchange solutions					Zeolitic cations	Non-zeolitic cations
		2 *M* NH_4NO	2 *M* $NaNO_3$	2 *M* KNO_3	2 *M* $CaCl_2$	0.15 *M* $AgNO_3$		
1	2	3	4	5	6	7	8	9
Na	0.52	0.47	—	0.47	0.33_5	0.47	0.47	0.05
K	0.49	0.26	0.22	—	0.11	0.18	0.26	0.23
Ca	1.22_5	1.05	1.05	1.08_5	—	0.65	1.08_5	0.14
Exchanged cations in the solutions		1.78	1.27	1.55_5	0.44_5	1.30		
Sum of mobile cations		1.78	1.74	1.81_5	1.53	1.30	1.81_5	—
Degree of ion exchange		98%	96%	100%	84%	72%		

tent of the rock is also known, the stoichiometric formula of this special mordenite can be given. This corresponds to the following unit cell composition:

$$(Ca_{2.4}Na_{2.07}K_{1.13}) \cdot Al_8Si_{40}O_{96} \cdot 22.7\ H_2O$$

As is seen from Table I, the total ion exchange capacity of our mordenite is 1.810 mg/g. Upon comparing this value with those calculated for a 100% pure mordenite with the same distribution of cations (2.31 mg/g), the zeolite content of our sample can be calculated as being 78%. This value agrees well with those determined earlier by other methods mentioned in the Introduction.

On inspecting columns 8 and 9 it is apparent that whereas the major part of Na and Ca ions belongs to the zeolite phase (91% of the Na ions and 89% of Ca ions), only about one half of the K ions can be assigned to the mordenite (52.5%).

It is also seen from Table I that on exchanging with NH_4 and Ag ions not present in the original rock, 98% ion exchange can be achieved by NH_4 ions, whereas Ag ions can replace (however, under the different conditions of exchange) only 73% of the cations. In this case the total amount of Na, but only a fraction of K and Ca (70% and 62%, respectively) can be exchanged for Ag.

Upon studying ion exchange with counterions present originally in the zeolite (Na, K, Ca), it can be seen that the sample shows the highest selectivity for K ions, i.e. the exchange of Na and Ca ions for K is practically complete — as is seen from the wet chemical analysis of the K-form — under the conditions applied. This behaviour corresponds to the rule observed earlier by Barrer and Klinovski [14], viz. that larger, less hydrated cations prefer the zeolite to the solution.

On exchanging with $NaNO_3$, almost all Ca ions, but only 87% of the K ions can be replaced by Na.

Mordenite is the least accessible to the strongly hydrated Ca ions; under identical conditions of ion exchange only 85% of all cationic positions are occupied by Ca ions, i.e. the originally present 40% of (Na + K) ions can only be exchanged in 62% by Ca.

Study of the "monocationic" forms

After determining the maximum amount of exchangeable cations in the different ion exchange solutions, the composition of the "monocationic" mordenites was also examined in the solid phase. For this purpose, samples obtained in the previous experiments were digested and the cations in the digestions were determined by AAS. The "monocationic" forms with respective degrees of ion exchange of 96, 100, 85 and 98% will be designated in

Table II

Amounts of mobile and immobile cations in "monocationized" mordenite-containing rock
(results of wet chemical analysis)

Sample (total ion exchange capacity) [meq/g]		Na, K and Ca content in meq/g, after ion exchange		
		in the rock	in the "monocationized" mordenite	in the non-zeolite phase*
1		2	3	4
Na-M (1.789)	Na	1.74	1.70	0.05
	K	0.26	0.03	0.23
	Ca	0.18	0.04	0.14
	Total	2.18	1.77	0.42
K-M (1.726)	Na	0.05	—	0.05
	K	1.90	1.67	0.23
	Ca	0.19	0.05	0.14
	Total	2.14	1.73	0.42
Ca-M (1.802)	Na	0.18	0.13	0.05
	K	0.37	0.14	0.23
	Ca	1.67_5	1.53_5	0.14
	Total	2.22_5	1.80_5	0.42

* Data from Table I.

the following as Na—M, K—M, Ca—M and NH_4—M. Results are summarized in Table II.

In column 2 of Table II the results of wet chemical analyses of ion exchanged rocks are shown. Assuming again that the immobile ions belong to the non-zeolitic phase, and taking their values from Table I, upon subtracting these values from the amounts determined in the ion exchanged tuff, the corresponding amounts of the different cations in the mordenite phase are obtained. These data are shown in column 3, whereas the cations of the non-zeolitic part are seen in column 4. As is seen, the agreement between the calculated ion exchange capacity and the total amount of cations determined in the mordenite phase is satisfactory. The deviation does not exceed 5% in either cationic form as related to the value corresponding to a 100% ion exchange with the appropriate cation.

Ion exchange properties of "monocationic" mordenite

In order to characterize the ion exchange properties of the "monocationic" forms, a second ion exchange was performed with Na—M, K—M and Ca—M mordenites. Solutions used were 2M $NaNO_3$, KNO_3, $CaCl_2$ and NH_4NO_3, and for comparison, tenfold diluted (0.2 *M*) solutions, as described in the experimental part. Another aim of these experiments was to check whether a redistribution of ions occurs during the first exchange, as a result

of which cations located earlier in inaccessible positions could be exchanged by the second treatment. Therefore, in these experiments in the ion exchange solutions after exchange not only the main ions, but the ones remaining from the first treatment and removed by the second one were also determined. The results of these measurements are summarized in Table III. In column 2 the theoretical ion exchange capacity for the respective ion exchanged forms calculated for 78% zeolite content are shown, numbers in column 3 refer to the steps of the three ion exchange treatments, in columns 4, 5, 6 and 7 the amounts of the "main" ions removed by the different solutions, then the amount of cations remaining in the sample after the preparation of the „monocationic" form, but removed by a further exchange treatment, and finally the sum of these two as "total" are shown.

From the data in Table III the following conclusions can be drawn:

— With NH_4NO_3 as ion exchange solution the sum of cations removed is higher than expected, though the error remains mostly within the limit of the accuracy of AAS measurements of about 5%. However, these values allow the conclusion that on exchanging with NH_4NO_3 (2 *M* solution) for the second

Table III

Exchangeable cations in the different "monocationic" mordenites

Sample	Total ion exchange capacity for Na, K and Ca forms (meq/g)	Amounts of ion-exchanged cations (in meq/g) by exchange with				
		Step	2 *M* $NaNO_3$	2 *M* KNO_3	2 *M* NH_4NO_3	2 *M* $CaCl_2$
1	2	3	4	5	6	7
Na-M	1.789	1		1.68	1.79	1.05
		2		0.01	0.01	0.22
		3		0.01	0.01	0.09
		Total Na		1.70	1.81	1.36
		Other exchanged ions		0.09	0.04	—
		Sum		1.79	1.85	1.36
K-M	1.726	1	1.52		1.61	0.97
		2	0.13		0.07	0.15
		3	0.02		0.02	0.05
		Total K	1.67		1.70	1.17
		Other exchanged ions	0.05		0.11	0.07
		Sum	1.72		1.81	1.24
Ca-M	1.802	1	1.37	1.31	1.33	
		2	0.12	0.04	0.08	
		3	0.06	0.02	0.05	
		Total Ca	1.55	1.37	1.46	
		Other exchanged ions	0.20	0.22	0.35	
		Sum	1.75	1.59	1.81	

time, all the cations contained in the Na—M, K—M and Ca—M samples can be removed, which is equivalent to complete ion exchange for the NH_4-form.

— It is also seen from Table III that Ca behaves differently, both as cation in the mordenite and as exchanging ion. This is not surprising, as it is well known that among the cations studied the Ca ion has the highest hydration ability. In the aqueous ion exchange solution it always has a coordinated hydrate shell in which the cation-water interaction is very strong. The radius of hydrated Ca ion is — according to Coughlan et al. [12] — about 0.42—0.45 nm, thus it is strongly hindered in entering or leaving the mordenite channels. In fact, it had to be stripped of at least a part of this water shell, which requires energy. The level of attainable ion exchange given in the literature lies at about 72—85%, depending on the conditions of ion exchange. According to the assignment of cations to the positions made by Meier [15] and Mortimer et al. [16], these two values correspond to the removal or introduction of Ca from or into positions I and VI and I, IV and VI, respectively.

In the case of the natural Hungarian mordenite, we should take into account that in the original mordenite more than 50% (see Table I) of the cation positions are occupied by "built in" Ca ions, thus the achievement of 85% ion exchange is understandable.

— On considering the respective ion contents of Na—M, K—M and Ca—M in the three successive ion exchange treatments, it can be established that upon exchanging Na—M with NH_4NO_3 and KNO_3, practically the total amount removable is contained in the first ion exchange solution (99 and 91%, respectively). Ion exchange with $CaCl_2$ is not so effective, the amount of parent Na and K ions removed from Na—M and K—M by the first treatment are about 73 and 56%.

In the case of K—M, NH_4NO_3 seems to be acting the most quickly (hardly any K in fractions 2 and 3), but $NaNO_3$ is also capable of removing 97% of the total K content in the three steps of exchange. On the contrary, $CaCl_2$ removes 68% only of the total K.

For Ca—M, the total Ca removed is almost the same with the three different ion exchange solutions (76% with KNO_3, 86% with $NaNO_3$ and 82% with NH_4NO_3).

For comparison, some preliminary experiments were performed with 0.2 *M* $NaNO_3$, KNO_3, $CaCl_2$ and NH_4NO_3 ion exchange solutions. From Na—M, 0.2 *M* solutions of KNO_3 and NH_4NO_3 remove almost the same amounts of Na as the 2 *M* solutions, whereas 0.2 *M* $CaCl_2$ does not.

For K—M, 0.2 *M* NH_4NO_3 and $CaCl_2$ solutions are nearly as effective as the more concentrated solutions, while $NaNO_3$ does not work well at this lower concentration.

In the case of Ca—M, 0.2 *M* KNO_3 effects the removal of Ca-ions almost to the same extent as do the more concentrated solutions.

In general it is seen that 0.2 *M* $NaNO_3$ is not effective in ion exchanging either "monocationic" form, 0.2 *M* KNO_3 is effective for both Na—M and Ca—M, whereas 0.2 *M* NH_4NO_3 is efficient in the ion exchange of K and Na from their "monocationic" variants, but does not work well for Ca, whereas 0.2 *M* $CaCl_2$ is suitable for exchanging K, but not for Na.

Conclusions

Upon ion exchanging a natural, sedimentary, mordenite-containing rock, a comparison of the zeolite content of the original rock measured earlier by other physico-chemical methods and the results of ion exchange showed a satisfactory agreement. The amount of mordenite determined is about 78%. The cation composition of the mordenite phase has been determined based on the ion exchange ability of the sample, by wet chemical analysis the composition of the original rock has been found. Cations studied were Na, K and Ca. Their distributions in the zeolite and non-zeolitic phases are different, almost all of Na and Ca is contained in the zeolite phase, whereas a significant amount of K has to be assigned to the non-zeolitic part.

Ion exchange experiments were carried out with 2 *M* $NaNO_3$, KNO_3, $CaCl_2$ and NH_4NO_3 solutions. The selectivity of the original (heterocationic) mordenite shows the following sequence:

$$K > NH_4 > Na > Ca$$

On transforming the original sample into the so-called "monocationic" Na—M, K—M and Ca—M forms, and then ion exchanging them further with the above 2 M solutions, the selectivity sequences for the individual "monocationic" forms can be determined as follows:

$$\text{for Na—M: } NH_4 > K > Ca$$

$$\text{for K —M: } NH_4 > Na > Ca$$

$$\text{for Ca—M: } Na > NH_4 > K$$

The behaviour of Ca ions differs from that of the other ions studied due to its strong hydration ability under the conditions of ion exchange, which hinders both the entering and removal of hydrated Ca-ions into or from the channels of mordenite.

A study of the exchange properties with more dilute solutions (and eventually also) at room temperature is also planned, as these conditions are

more promising from the point of view of practical applications of these materials.

*

The authors thank Dr. D. Kalló for careful reading of, and his useful comments on, the manuscript.

REFERENCES

[1] Sherry, H. S.: J. Phys. Chem., **70,** 1158 (1966)
[2] Sherry, H. S.: J. Phys. Chem., **72,** 4086 (1986)
[3] Fletcher, P., Townsend, R. P.: JCS Faraday Trans. I, **78,** 1741 (1982)
[4] Coughlan, B., Carrol, W. M.: JCS Faraday Trans. I, **72,** 2016 (1976)
[5] Maes, A., Cremers, A.: JCS Faraday Trans. I, **71,** 265 (1975)
[6] Barrer, R. M., Townsend, R. P.: JCS Faraday Trans. I, **72,** 661 (1976)
[7] Barrer, R. M., Townsend, R. P.: JCS Faraday Trans. I, **72,** 2650 (1976)
[8] Fletcher, P., Townsend, R. P.: JCS Faraday Trans. I, **77,** 497 (1981)
[9] Rees, V. L. C., Rao, A.: Trans. Faraday Soc., **68,** 2103 (1966)
[10] Rao, A., Rees, V. L. C.: Trans. Faraday Soc., **62,** 2505 (1966)
[11] R. M. Barrer in: Natural Zeolites. Occurrences, Properties, Use, Eds.: E. B. Sand, F. A. Mumpton, p. 385. Pergamon Press 1976
[12] Cughlan, B., Carroll, W. M., McCann, W. A.: JCS Faraday Trans, I, **73,** 1612 (1977)
[13] Papp, J., Czárán, E., Jánossy, A.: Anal. Chem., **50,** 1265 (1978)
[14] Barrer, R. M., Klinowski, J.: JCS Faraday Trans. I, **70,** 2362 (1974)
[15] Meier, W. M.: Z. Kristallogr., **115,** 439 (1961)
[16] Mortimer, W. J. J., Pluth, J. J., Smith, J. V.: Materials Res. Bull., **10,** 1037, 1319 (1975)

Acta Chimica Hungarica 121 (3), pp. 255—262 (1986)

HYDROXYIMINOISOQUINOLIN-3(2*H*)-ONES, V*

SYNTHESIS OF 4-AMINO-1,2,3,4-TETRAHYDROISOQUINOLINES

István TIKK[1], Gyula DEÁK[1]**, Gábor TÓTH[2], Áron SZŐLLŐSY[2] and József TAMÁS[3]

([1]Institute of Experimental Medicine, Hungarian Academy of Sciences, H-1450 Budapest, P.O.B. 67., [2]N.M.R. Laboratory of the Institute for General and Analytical Chemistry, Technical University, H-1521 Budapest, Gellért tér 4. [3]Central Research Institute of Chemistry, Hungarian Academy of Sciences, H-1525 Budapest, P.O.B. 17,)

Received March 25, 1985
Accepted for publication April 17, 1985

Reductive acylation of 4-hydroxyimino-1,4-dihydroisoquinolin-3(2*H*)-ones gave 4-acetylamino-1,4-dihydroisoquinolin-3(2*H*)-ones which were reduced further, then deacetylated to yield 4-amino-1,2,3,4-tetrahydroisoquinolines. In several cases the *cis* and *trans* isomers were separated and their steric structures elucidated.

8-Amino-4-phenyl-2-methyl-1,2,3,4-tetrahydroisoquinoline is a known antidepressive agent [2] of a novel type; our aim was to synthesize a new skeletal isomer of this compound, 4-amino-1-phenyl-2-methyl-1,2,3,4-tetrahydroisoquinoline, starting from 1,4-dihydroisoquinolin-3(2*H*)-one.

In the first series of experiments the preparation of 4-nitro-1,4-dihydroisoquinolin-3(2*H*)-one was attempted by nitration, but only the aromatic rings became nitrated or the decomposition of the isoquinolinone skeleton occurred. As it is known [3] that in many cases the isonitrosation of a methylene group adjacent to a carbonyl group yields oximes, this method was used; *n*-butyl nitrite in the presence of potassium *t*-butoxid gave the 4-(hydroxyimino) derivatives in satisfactory yields at 0 °C [4].

Since purification of the 4-amino-1,4-dihydroisoquinolin-3(2*H*)-ones (Scheme 1) obtained by chemical reduction of the oximes (**8**—**12**) [5] and the reduction of the 3-oxo group presented difficulties, and catalytic reduction yielded 5,6,7,8-tetrahydroisoquinoline derivatives (**13**), reductive acylation (Scheme 2) was employed to prepare the 4-acetylamino derivatives (**15**—**19**) and the steric structures of these compounds were determined. According to the ^{1}H n.m.r. spectra in the mixture of the *cis* and *trans* isomers the latter were predominating. The *cis-trans* mixture obtained by reductive acylation of 6,7-dimethoxy-1-phenyl-4-(hydroxyimino)-2-methyl-1,4-dihydroisoquinolin-3(2*H*)-one **12** could be separated into the homogeneous components, and their structures were determined.

* Part IV: See Ref. [1].
** To whom correspondence should be addressed.

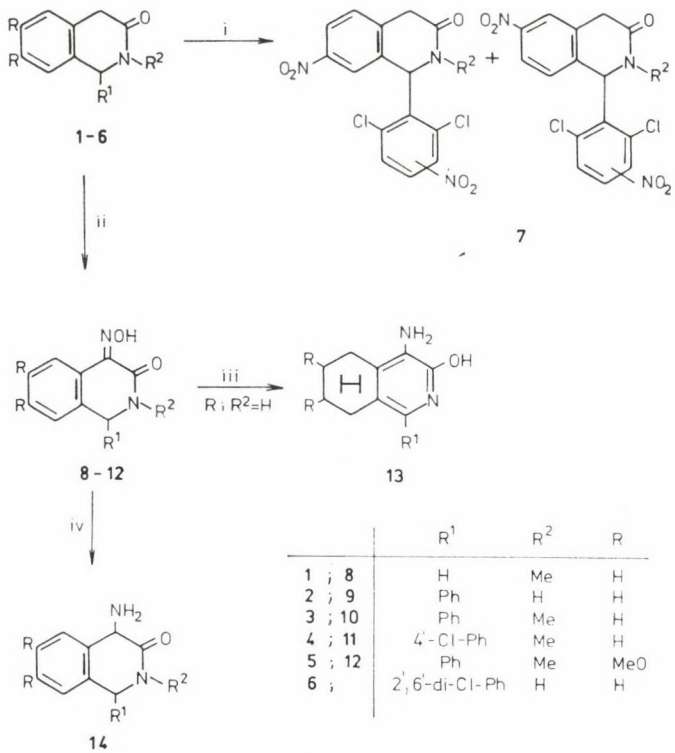

	R^1	R^2	R
1 ; 8	H	Me	H
2 ; 9	Ph	H	H
3 ; 10	Ph	Me	H
4 ; 11	4'-Cl-Ph	Me	H
5 ; 12	Ph	Me	MeO
6 ;	2',6'-di-Cl-Ph	H	H

Scheme 1

In the course of our earlier examinations [6, 7] it was shown that in the case of the analogous 4-benzyl derivatives the chemical shift of the H-1 proton had a significant deviation if the position of the 1-phenyl group was *quasiaxial* (5.64 p.p.m.) or *quasiequatorial* (4.48 p.p.m.). In the ^{1}H n.m.r. (Table II) spectra of **19-*cis*** and **19-*trans***, the chemical shifts of the H-1 proton (5.36 and 5.42 p.p.m.) indicate that in both compounds the 1-phenyl substituent occupies *quasiaxial* position, similarly to the case of 4-hydroxy-1,4-dihydroisoquinolin-3(2*H*)-ones [1]. It follows that **19-*cis*** and **19-*trans*** are 4-epimers.

Further the selective reduction of the lactam carbonyl group (in **15**—**19**) was investigated. Although the tetrahydroisoquinoline derviatives can be obtained by means of sodium ethoxide, satisfactory yields of **20**—**24** are attained only by the use of lithium aluminium hydride.

The steric structures of the new compounds **20**—**24** were investigated by ^{1}H n.m.r. spectroscopy (Scheme 3). The steric position of the C-4 substituent

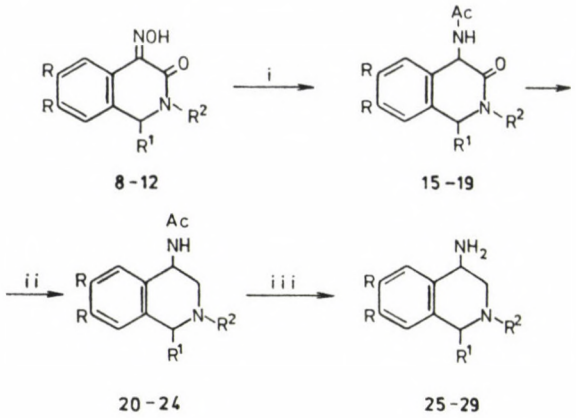

	R^1	R^2	R
15 ; 20 ; 25	H	Me	H
16 ; 21 ; 26	Ph	H	H
17 ; 22 ; 27	Ph	Me	H
18 ; 23 ; 28	4' Cl Ph	Me	H
19 ; 24 ; 29	Ph	Me	MeO

Reagents: i, Zn, AcOH, Ac_2O; ii, $LiAlH_4$, THF; iii, HCl-HOH (1:1)

Scheme 2

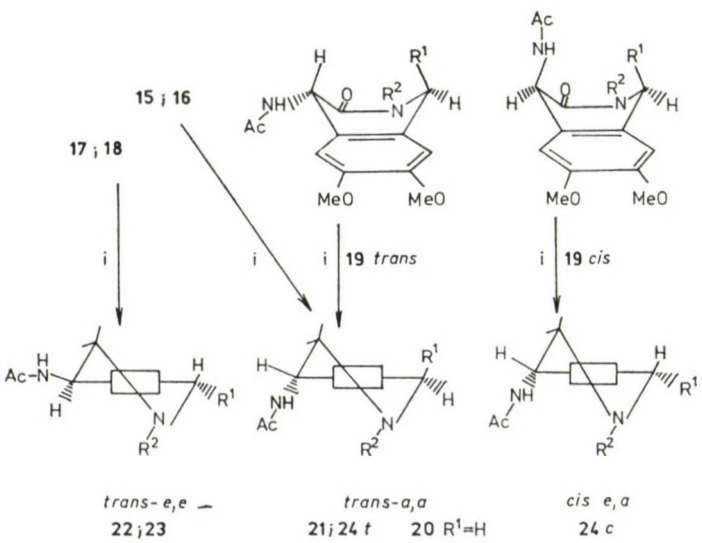

Reagent: i, $LiAlH_4$

Scheme 3

Table I

Analytical and i.r. data of the 4-*acetylamino- and* 4-*amino*-1,2,3,4-*tetrahydroisoquinolines* (**15**—**29**)

Compound (formula)	M. w.	Yield (%)	M.p. (°C) (solvent)	Found (%) / (Required, %) C	H	N	Cl	ν_{max} (KBr), cm^{-1}
15 ($C_{12}H_{14}N_2O_2$)	218.2	71	176—177 (CH_2Cl_2)	66.0 66.2	6.5 6.4	12.8 12.8		1670, 1638 (amide I)
16 ($C_{17}H_{16}N_2O_2$)	276.3	80	195—196 (MeHO)	72.8 72.9	5.7 5.8	10.0 9.8		1692, 1675, 1650 (amide I)
17 ($C_{18}H_{18}N_2O_2$)	294.3	81	189—190 (CH_2Cl_2)	73.4 73.4	6.2 6.3	9.5 9.7		1675, 1640 (amide I)
18 ($C_{18}H_{17}N_2O_2Cl$)	328.8	76	165—167 (Et_2O)	65.7 65.5	5.2 5.4	8.5 8.2	10.8 10.5	1635 (amide I)
19 *trans* ($C_{20}H_{22}N_2O_4$)	354.4	72	217—220 (Me_2CO)	67.8 67.8	6.3 6.3	7.9 8.0		1665, 1630 (amide I)
19 *cis*		9	227—229 (Me_2CO)	67.8 67.9	6.3 6.2	7.9 8.2		1655, 1635 (amide I)
20 ($C_{12}H_{16}N_2O$)	204.3	70	137—139 (EtOAc)	70.6 70.4	7.9 8.2	13.7 13.7		1632 (amide I)
21 ($C_{17}H_{18}N_2O$)	266.3	58	158—160 (Et_2O)	76.6 76.5	6.8 6.7	10.5 10.6		1625 (amide I)
22 $C_{18}H_{20}N_2O$)	280.4	78	223—226 (*i*-PrOH—Et_2O)	77.1 77.3	7.2 7.4	10.0 10.3		1640 (amide I)
23 ($C_{18}H_{19}N_2OCl$)	314.8	81	237—239 (CH_2Cl_2)	68.7 68.7	6.1 6.1	8.9 9.0	11.3 11.4	1628 (amide I)
24 *trans* ($C_{20}H_{24}N_2O_3$)	340.4	50	190—192 (EtOAc)	70.6 70.8	7.1 7.2	8.2 8.3		1634
24 *cis*		26	165—167 (EtOAc)	70.6 70.9	7.1 7.4	8.2 8.5		
25 ($C_{10}H_{14}N_2 \cdot 2HCl$)	162.2	46	223—225 (EtOH)	51.1 51.1	6.9 6.9	11.9 11.9	30.1 29.9	
26 ($C_{15}H_{16}N_2$)	224.3	49	130—133 (EtOAc—MeOH)	80.3 80.1	7.2 7.3	12.5 12.6		3340, 3255 (NH_2)
27 ($C_{16}H_{18}N_2 \cdot$ dimaleate)	238.3	64	156—158 (EtOH)	61.3 61.3	5.6 5.9	5.9 5.8		
28 ($C_{16}H_{18}N_2Cl$)	273.7	89	110—111 (EtOH)	70.5 70.9	6.3 6.4	10.3 10.3	13.0 12.9	3370, 3300 (NH_2)
29 *trans* ($C_{18}H_{22}N_2O_2 \cdot 2HCl + EtOH$)	298.4	40	218—220 (EtOH)	57.5 57.3	7.2 7.3	6.7 6.9	17.0 17.0	

Table II

^{1}H *n.m.r. data of the* 4-*acetylamino*-1,4-*dihydroisoquinolin*-3(2*H*)-*ones* (**15**—**19**) *in* $CDCl_3$ (*δ*-s are given in p.p.m., *J* in Hz)

Compound	MeCO	N—Me	MeO	C_1—H	C_4—H	$J_{CH,NH}$	$H_{arom.}$	NH
15	22.2	3.08	—	4.13 4.64	5.36	7.0	7.0—7.3	—
16	2.12	—	—	5.62	5.42	8.0	6.8—7.6	7.80; 8.66 (N_2—H)
17	2.21	3.19	—	5.49	5.46		7.0—7.3	
18	2.17	3.08	—	5.41	5.44	9.0	7.0—7.3	6.92
19 *trans*	2.23	3.13	3.83 3.86	5.36	5.47	7.5	7.1—7.3 6.68; 6.73	6.77
19 *cis*	2.17	2.85	3.62 3.83	5.42	5.60	7.5	7.2—7.4 6.18; 6.81	6.42

can be established on the basis of the vicinal coupling constants of the H-4 protons. Accordingly, in compound **20** the predominating conformer contains the acetylamino group in *quasiaxial* position. The position of the C-1 substituent can be decided only in the case of *cis-trans* pairs of isomers. Therefore, the reduction of **19**-*cis* and **19**-*trans* was also effected and the spectral data of **24**-*cis* and **24**-*trans* were compared (Table III). In the **24**-*cis* compound, the *axial* position of the 4-acetylamino group is confirmed by the vicinal coupling constants, while the chemical shift for H-1 (4.11 p.p.m.) is lower by about 0.4 p.p.m. than in **24**-*trans* 4.48 p.p.m. Using the empirical rule δH-*e* > > δH-*a* generally holds for cyclohexane derivatives, this difference can serve as a proof that H-1 is *quasiaxial* in **24**-*cis* while it is *quasiequatorial* in **24**-*trans* in the predominant conformations. Consequently, the predominating conformations are *cis e, a* and *trans a, a* in the *cis* and *trans* compounds, respectively. The *axial* position of the 4-aminoacetyl group in tetrahydroisoquinolines is in agreement with the data observed by Borossi et al. [8], for 4-hydroxy-1-methyl-1,2,3,4-tetrahydroisoquinolines where the OH group occupies the *quasiaxial* position in both the *cis* and the *trans* isomers.

Finally, the acetylamino derivatives **20**—**24** were deacetylated to obtain the 4-amino-1,2,3,4-tetrahydroisoquinolines **25**—**29**, among them the required skeletal isomer **27**. Investigations of the steric structures of these compounds showed that the predominating conformer was the *trans e, e* in each of the 1,4-disubstituted 1,2,3,4-tetrahydro derivatives [9], however, in the 4-monosubstituted compound **25** the coupling constants indicate the conformer containing the 4-amino group in *quasiaxial* position to be predominating.

Table III

^{1}H *n.m.r. data of the* 4-*acetylamino- and* 4-*amino*-1,2,3,4-*tetrahydroisoquinolines* (**20**—**29**) δ *in* $CDCl_3$ *p.p.m.*, (*J in* Hz)

	NH_2	MeCO	MeO	Me	C_3—H	^3J ^2J	C_1—H	C_4—H	$J_{CH,NH}$	C_5H	NH	$H_{ar.}$
20	—	1.96	—	2.38	2.50 2.85	3.0; 12.0 2.5	3.20 3.58	5.12	9.0	6.52		
21	—	1.98	—	—	2.79 3.29	5.0; 12.5 3.5	5.00	5.18	9.0	6.29	6.42	6.95—7.40
22	—	2.07	—	2.22	2.46 3.30	8.0; 12.0 5.0	4.50	5.49	9.0		6.08	6.7 —7.5
23	—	2.04	—	2.18	2.40 3.25	8.0; 11.5 5.0	4.40	5.45		6.62	5.85	6.90—7.40
24$_t$	—	2.01	3.58 3.82	2.19	2.40 3.18	5.0; 12.5 4.0	4.48	5.32	9.0		6.09	6.9 —7.3; 6.12; 6.80
24$_c$	—	2.08	3.59 3.90	2.23	2.83 3.08	3.0; 12.0 3.0	4.11	5.20	9.0	7.02		7.3 —7.50; 6.10
25					2.63	4.0 4.0	3.36 3.62	3.90				
26	1.82	—	—	—	2.77 3.31	7.0; 13.0 5.0	5.08	4.02		6.72		6.85—7.50
27	—	—	—	2.18	2.34 3.19	9.5; 11.0 4.5	4.25	4.26		7.50		6.85—7.30
28	1.62	—	—	2.20	2.39 3.23	9.0; 11.5 5.0	4.30	4.30		6.62		6.95—7.30; 7.18; 7.32
29			3.56 3.87	2.19	2.35 3.18	9.5; 11.0 4.5	4.23	4.22				7.0—7.3

Experimental

M.p.'s were determined with a Büchi—Tottoli apparatus and are uncorrected. The i.r. spectra were recorded in KBr pellets (Perkin Elmer Model 457). The ^{1}H n.m.r. spectra were recorded on a JEOL FX-100 spectrometer and chemical shifts are given in p.p.m. relative to tetramethylsilane used as internal standard.

Nitration of 1-(2',6'-dichlorophenyl)-1,4-dihydroisoquinolin-3(2*H*)-one

1-(2',6'-Dichlorophenyl)-1,4-dihydroisoquinolin-3(2*H*)- one (1.15 g 4 mmol) was dissolved in concentrated sulfuric acid (6.0 mL) and mixed acid (12 mL) was added while maintaining the temperature below 5 °C. The solution was poured into water, the product (1.15 g 76%) was filtered off and purified by recrystallization from acetonitrile, m.p. 251—253 °C.

$C_{15}H_9N_3Cl_2O_5$ (382.2); requires C, 47.1; H, 2.3; N, 11.0; Cl, 18.5% Found: C, 47.0; H, 2.8; N, 11.1; Cl, 18.6%.

I.R. (KBr) 3180, 3060, 2930, 1670, 1530, 1352 cm^{-1}.

^{1}H n.m.r. (DMSO-d_6): 3.85 (2H, s, C_4-H); 6.28 (1H, m, C_1-H); 7.05 (1H, d, C_8-H); 7.0—8.2 (5H, m, H_{ar}); 8.50 (1H, m, NH) p.p.m.

4-Amino-3-hydroxy-1-phenyl-5,6,7,8-tetrahydroisoquinoline (13)

Platinium(IV) oxide (2.3 g) was wetted with 99% acetic acid (60 mL) in a glass hydrogenation vessel, and a solution of 4-(hydroxyimino)-1-phenyl-1,4-dihydroisoquinolin-3(2*H*)-one **9**, (10 g 40 mmol) in acetic acid (200 mL) was added to the catalyst. The reduction with hydrogen was effected at room temperature and continued until the absorption of the gas had stopped. The catalyst was filtered off, the solution evaporated to dryness and the residual oil rubbed with water to obtain the crude product (2.1 g 22%), which was recrystallized from ethanol (200 mL) to yield **13** (1.5 g 15.7%) m.p. 258—260 °C.

$C_{15}H_{16}N_2O$ (M: 240.3); requires C, 74.98; H 6.71; N, 11.65%. Found: C 74.81; H, 6.82; N, 11.47.

I.R. (KBr): 3450, 3340, 2920, 2842, 1630, 1585, 1450, 1432, 762, 695 cm^{-1}.

^{1}H n.m.r. (DMSO-d_6): 1.40—1.95 (4H, m, CH_2); 2.35—2.70 (4H, m, C_5-H_2, C_8-H_2); 4.70 (2H, m, NH_2); 7.39 (5H, s, H_{ar}); 11.05 (1H, s, OH) p.p.m.

4-Amino-2-methyl-1-(4'-chlorophenyl)-1,4-dihydroisoquinolin-3(2*H*)-one (14)

4-(Hydroxyimino)-2-methyl-1-(4'-chlorophenyl)-1,4-dihydroisoquinolin-3(2*H*)-one **11** (2.0 g) was dissolved in acetic acid (50 mL), zinc powder (4.8 g) was added and the mixture was stirred at 55—60 °C for 30 minutes. After filtration the solution was evaporated to dryness under reduced pressure. The oily residue was rubbed with ether to obtain the crude product as a solid which was washed with water to give pure **14** (1.1 g 57.8%) m.p. 110—114 °C.

$C_{16}H_{15}N_2OCl$ (M: 286.5); requires C, 67.02; H, 5.27; N, 9,77; Cl, 12.36%. Found: C, 66.68; H, 5.33; N, 9.72; Cl, 12.80.

I.R. (KBr): 3380, 3305, 3050, 2920, 2810, 1660, 1555, 1488, 1450, 1400, 1310, 1188, 1010, 885, 800, 755 cm^{-1}.

^{1}H n.m.r. ($CDCl_3$): 2.10 (2H, s, NH_2); 3.17 (3H, s, NMe); 4.35 (1H, s, C_4-H); 5.46 (1H, s, C_1-H); 7.0—7.5 (7H, m, H_{ar}); 7.70 (1H, m, C_5-H) p.p.m.

General procedures

Reductive acetylation

4-(Hydroxyimino)-1,4-dihydroisoquinolin-3(2*H*)-one **8**—**12** (15 mmol) was dissolved in a mixture of 96% acetic acid (140 mL) and acetic anhydride (28 mL) and zinc powder (10 g) was added to the solution at room temperature. It was heated to 70 °C, with stirring, filtered, and the filtrate was evaporated to dryness. The product separated on treatment of the residue with ether.

Reduction of the lactam carbonyl group

4-Acetylamino-1,4-dihydroisoquinolin-3(2*H*)-one (10 mmol) **15**—**19** was dissolved in anhydrous tetrahydrofuran (120 mL) and the solution was added to a suspension of lithium aluminium hydride (2.4 g) in anhydrous tetrahydrofuran (60 mL), with cooling and vigorous stirring, while keeping the temperature of the mixture below 10 °C. It was stirred until complete reaction had occured, then the complex was decomposed by the dropwise addition of ethyl acetate and water, also decomposing the excess of reagent. The precipitate was removed by filtration, the mother liquor evaporated to dryness and the resulting oil treated with ether to give the crystalline product **20**—**24**.

Deacetylation

4-Acetylamino-1,2,3,4-tetrahydroisoquinoline (**20**—**24**) (7.1 mmol) was dissolved in dilute (1 : 1) hydrochloric acid (40 mL), refluxed for 4 h and poured onto ice. The mixture was made alkaline (pH 10) with 6n sodium hydroxide solution. After extraction with chloroform, the organic phase was evaporated to dryness. Compounds **26** and **28** are crystalline also in the base form, the others are oily products. The latter were crystallized in the form of maleates or hydrochlorides **25**—**29**.

*

The authors gratefully acknowledge the support of this work by the EGIS Pharmaceuticals, Budapest.

REFERENCES

[1] Tikk, I., Tóth, G., Tamás, J., Deák, Gy.: J. Chem. Soc., Perkin Trans 1, **1984,** 619
[2] Hoffmann, K., Erhardt, G., Schmitt, K.: Arzneim.-Forsch., **21,** 1045 (1971)
[3] Litvan, F., Robinson, R.: J. Chem. Soc., **1938,** 1997; Cova, M. P., Glamkovski, E. J., Weintraub, P. M.: J. Org. Chem., **31,** 2755 (1966)
[4] Tikk, I., Deák, Gy., Tóth, G.: Acta Chim. Hung., **114,** 69 (1983)
[5] Tahara, S., Shigetsuna, M., Otomasu, H.: Chem. Pharm. Bull., **30,** 3133 (1982)
[6] Deák, Gy., Hazai, L., Tóth, G.: J. Heterocycl. Chem., **14,** 583 (1977)
[7] Tóth, G., Hazai, L., Deák, Gy., Duddeck, H.: Justus Liebigs Ann. Chem. **1978,** 1103
[8] Grethe, G., Uskokovic, M., Williams, T., Brossi, A.: Helv. Chim. Acta, **50,** 2397 (1969)
[9] Kametani, T., Sugi, H., Yagi, H., Fukomoto, K., Shiuya, S.: J. Chem. Soc. (C), **1970,** 2213

Acta Chimica Hungarica 121 (3), pp. 263—269 (1986)

LITHIATION OF 1-ARYL-1,4-DIHYDRO-3(2*H*)--ISOQUINOLINONES AND THEIR *N*-METHYL DERIVATIVES

László Hazai[1], Gyula Deák[1]*, Áron Szőllősy[2], Gábor Tóth[2] and István Bitter[3]

([1]Institute of Experimental Medicine, Hungarian Academy of Sciences, H-1450 Budapest, P.O.B. 67, [2]General and Analytical Chemical Department, N.M.R. Laboratory, Technical University, H-1521 Budapest, Gellért tér 4, and [3]Department for Organic Chemical Technology, Technical University, H-1521 Budapest, Műegyetem rkp. 3.)

Received January 4, 1985
Accepted for publication April 18, 1985

N-Methyl analogues of several 1,4-dihydro-3(2*H*)-isoquinolinone derivatives have been prepared via methylation with dimethyl sulfate; in some experiments the *O*-methyl lactim ethers have also been isolated. The incorporation of lithium into the *N*-methyl compounds was examined by labelling with deuterium and it was found that, preferably when using *n*-butyllithium, the lithium was incorporated in the C-4 methylene group of the compounds. The incorporation of lithium could be utilized only in the reaction with 4-nitrobenzaldehyde; 1-phenyl-2-methyl-4-(4'-nitrobenzylidene)-1,4-dihydro-3(2*H*)-isoquinolinone (**8**) was succesfully prepared. In the other cases the reagents employed did not yield isolable products.

Organolithium compounds, particularly lithium alkyls are well-known and widely employed reagents in preparative organic chemistry; they are useful for introducing substituents into given sites of a molecule in such a way which otherwise would be impracticable or very complicated (see corresponding entries in Refs. [1—2]). This was the reason why we selected these compounds to attempt the introduction of carboxyl, formyl, hydroxyalkyl, etc., substituents into the C-4 methylene group of 1-phenyl-1,4-dihydro--3(2*H*)-isoquinolinone (**1a**), a compound prepared by us earlier [3]. In the attempted reaction of **1a** with butyllithium, however, after pouring the reaction mixture onto dry ice, the expected 4-carboxy derivative could not be isolated from among the several unidentifiable decomposition products. Although it has been described in the literature [4] that an active methylene group adjacent to an acid amide can be alkylated on treatment with butyllithium, we attributed the failure of the above reaction to the non-protected lactam nitrogen atom. Therefore, the possibilities of the incorporation of lithium were examined in *N*-substituted derivatives. In view of the fact that, according to our earlier experience [5], the acylated lactam is very sensitive to hydrolysis and other effects, the experiments were made with *N*-methyl

* To whom correspondence should be addressed.

compounds (Scheme 1). Compounds **1b**—**4b** have already been described in the literature (e.g. [6, 17]), but it seemed to be practical to synthesize the corresponding *N*-methylisoquinolinones by direct methylation of the readily available lactams in one step, instead of using the rather cumbersome cyclization

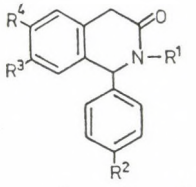

	R^1	R^2	R^3	R^4
1a	H	H	H	H
1b	CH_3	H	H	H
2a	H	H	OCH_3	OCH_3
2b	CH_3	H	OCH_3	OCH_3
3a	H	NO_2	H	H
3b	CH_3	NO_2	H	H
4a	H	NO_2	OCH_3	OCH_3
4b	CH_3	NO_2	OCH_3	OCH_3

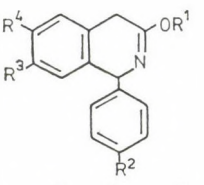

	R^1	R^2	R^3	R^4
3c	CH_3	NO_2	H	H
4c	CH_3	NO_2	OCH_3	OCH_3

Scheme 1

methods. Thus, the following conversions were successfully realized using dimethyl sulfate in the presence of a phase-transfer catalyst:

1a [3] $\xrightarrow{Q}$ **1b** [6]

2a [3] $\xrightarrow{Q}$ **2b** [6]

3a [7] $\xrightarrow{Q}$ **3b** [17] + **3c**

4a [8] $\xrightarrow{Q}$ **4b** [17] + **4c**

where Q = dimethyl sulfate.

The reactions were effected in benzene-water medium in the presence of sodium hydroxide at room temperature, with vigorous stirring. It is noteworthy that in the case of nitro derivatives, lactim ethers (**3c**, **4c**) could also be isolated, even if in only low yields. This indicates that in the mesomeric anion formed by the action of alkali, the centre of the negative charge is not localized exclusively at the nitrogen atom, owing to the strong electron-withdrawing effect of the nitrophenyl group.

The corresponding unsaturated 3(2*H*)-isoquinolinones, in which tautomerism was studied in detail previously [9], could be transformed into lactim ethers only by treatment with triethyloxonium tetrafluoroborate [10]; the use of conventional alkylating agents yielded in the main mixed *N*- and

O-alkyl products (see, e.g. Ref. [11]). Using methyl iodide*, the possibility of alkylation of the unsaturated derivative, 4-benzyl-1-phenyl-3(2*H*)-isoquinolinone **5** has also been examined by us, and the *o*-quinoidal structure of the *N*-methyl derivative **6**, isolated in 44.6% yield, was confirmed via the

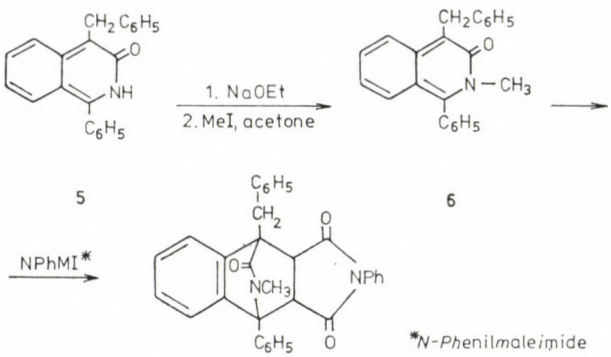

7

Scheme 2

formation of a Diels-Alder adduct (**7**) (Scheme 2). The presence of lactim ether could not be detected in the end-product.

After having synthesized the required *N*-methyl derivatives, the most suitable of the reagents capable of introducing lithium was to be decided, and also the problem had to be solved which of the carbon atoms in the isoquinolinone will bind the lithium when employing the different reagents. The latter problem was investigated by deuterium labelling [12]; after the treatment with alkyllithium, deuterium oxide was added to the reaction mixture and the site and extent of the incorporation of deuterium was detected by NMR spectroscopy.

First the reaction of metallic lithium was examined; this gave highly contaminated **1b**, yet containing deuterium at site 4. A similar result was obtained with phenyllithium: the incorporation of deuterium was about 25%, but the product was very contaminated. Effective introduction of lithium could be achieved by the use of butyllithium; here 4-^{2}H-**1b** was obtained as a pure compound, incorporation was higher than 70%; thus this reagent seemed to be the most suitable for mediating the introduction of various substituents. The 6,7-dimethoxy compound (**2b**), too, was examined. Also in this case *one*

* Compound **1a** reacted with methyl iodide only in the presence of sodium hydride, and the end-product was not homogeneous, owing to reactions taking place also on the C-4 methylene group.

hydrogen atom was exchanged for deuterium in the C-4 methylene group. The incorporation of deuterium was also confirmed by NMR spectroscopy.

Various reagents were then added to compounds of type **b** which had been made to react with butyllithium; such reagents were dry ice (in different solvents), dimethylformamide and paraformaldehyde, under various reaction conditions. However, no homogeneous compound could be isolated from among the decomposition products, although the incorporation of lithium had been confirmed previously. It was only the reaction of **1b** with 4-nitrobenzaldehyde which gave 4-(4'-nitrobenzylidene) isoquinolinone (**8**). In this case,

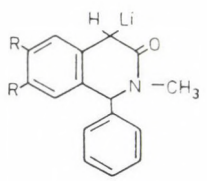

R = H, OMe

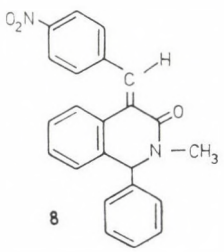

8

literature references describe the formation of carbinol [13], yielding the alkylidene derivative on treatment with dehydrating agents. In the conversion **1b** → **8**, the presence of the carbinol derivative could not be detected; the formation of compound **8** is interesting, since carbonyl condensation reactions could be effected up to now only with isoquinolinones carrying no nitrogen-substituent [10]. Compound **8** proved to be the homogeneous *E*-isomer, similar to the derivatives prepared in the presence of sodium hydride [10].

Experimental

M.p.'s were measured with a Büchi—Tottoli melting point determining apparatus and are uncorrected. The IR spectra were recorded with a Perkin Elmer 457 spectrophotometer; the NMR spectra were obtained on a JEOL-FX-100 instrument.

1-Phenyl-2-methyl-1,4-dihydro-3(2*H*)-isoquinolinone (1b)

To a vigorously stirred suspension of 1-phenyl-1,4-dihydro-3(2*H*)-isoquinolinone (**1a**) (6.7 g; 0.03 mol) in benzene (50 mL) were added 50% NaOH solution (8 g), 4 drops of Aliquat-336 (tricaprylmethylammonium chloride) and dimethyl sulfate (4.5 mL). The temperature rose to 30 °C; this was reduced to room temperature by cooling in ice-water, then the reaction mixture was stirred at this temperature for 3 h. The solid was removed by filtration, the two phases were separated, the benzene fraction was dried over Na_2SO_4 and evaporated to dryness. The residual yellow solid was washed with petroleum ether and subjected to chromatographic purification on a column packed with Al_2O_3. The homogeneous fractions were combined, the solvent ($CHCl_3$) was evaporated and the residue rubbed with petroleum ether to obtain the product (3.8 g; 53.5%), m.p. 93 °C, *lit.* [6] m.p. 93—94 °C.

IR (KBr): νC=O 1635 cm^{-1}.

^{1}H-NMR ($CDCl_3$): NMe 3.02 s (3), H_2-4 3.72 broad s (2), H-1 5.42 s (1), ArH 7.0—7.3 m (9).

6,7-Dimethoxy-1-phenyl-2-methyl-1,4-dihydro-3(2*H*)-isoquinolinone (2b)

6,7-Dimethoxy-1-phenyl-1,4-dihydro-3(2*H*)-isoquinolinone (**2a**) (8.5 g; 0.03 mol) was suspended in benzene (80 mL) and 50% NaOH solution (8 g), 4 drops of Aliquat-336 and dimethyl sulfate (4.5 mL) were added, with stirring, and the mixture was stirred for 6.5 h. After the addition of another portion of dimethyl sulfate (2 mL) and stirring for 8.5 h, the solid was filtered off, the benzene fraction was dried over Na_2SO_4 and evaporated to dryness. The residue was rubbed with ether to obtain the product (3.2 g; 36%), m.p. 139 °C (ethanol-petroleum ether), *lit.* [6] m.p. 140 °C.

IR (KBr): νC=O 1640 cm^{-1}.

^{1}H-NMR ($CDCl_3$): NMe 3.00 s (3), OMe 3.78 s (3), 3.84 s (3), H-1 5.31 (1), 3.60 d (1), 3.77 d (1); J_{gem} = 20 Hz, ArH 7.1—7.4 m (7), H-5,8 6.51 s (1) and 6.53 s (1).

2-Methyl-1-(4'-nitrophenyl)-1,4-dihydro-3(2*H*)-isoquinolinone (3b) and 3-methoxy-1-(4'-nitrophenyl)-1,4-dihydroisoquinoline (3c)

1-(4'-Nitrophenyl)-1,4-dihydro-3(2*H*)-isoquinolinone (**3a**) (8.04 g; 0.03 mol) was suspended in benzene (50 mL), and 50% NaOH solution (8 g), Aliquat-336 (2 drops) and dimethyl sulfate (4.5 mL) were added. The temperature of the reaction mixture rose to 36 °C; it was cooled in ice-water to room temperature, then the mixture was stirred at room temperature for 2 h. The red suspension was filtered, the benzene phase was dried over Na_2SO_4 and evaporated to dryness. The residue was triturated first with ethanol then with petroleum ether and the resulting solid was subjected to chromatographic separation on a column packed with Al_2O_3. The fractions eluted with chloroform were examined by TLC, combined on the basis of the R_f values, evaporated to dryness and the residue was rubbed with ether; the solid was filtered off and dried under an infrared lamp.

3b (3.1 g; 36.9%), m.p. 176—178 °C (ethanol-petroleum ether), *lit.* [17] m.p. 176—177 °C.
$C_{16}H_{14}N_2O_3$. Calcd. C 68.08; H 5.00; N 9.92. Found C 68.18; H 5.23; N 10.17%.
IR (KBr): νC=O 1645 cm^{-1}, NO_2 1530, 1350 cm^{-1}.

3c (0.2 g; 2.5%), m.p. 153—156 °C.
$C_{16}H_{14}N_2O_3$. Calcd. C 68.08; H 5.00; N 9.92. Found C 68.26; H 4.93; N 10.11%
IR (KBr): νC=N 1625, νNO_2 1520, 1350 cm^{-1}.

6,7-Dimethoxy-2-methyl-1-(4'-nitrophenyl)-1,4-dihydro-3(2*H*)-isoquinolinone (4b) and 1-(4'-nitrophenyl)-3,6,7-trimethoxy-1,4-dihydroisoquinoline (4c)

6,7-Dimethoxy-1-(4'-nitrophenyl)-1,4-dihydro-3(2*H*)-isoquinolinone (**4a**) (9.85 g; 0.03 mol) was suspended in benzene (50 mL) and 50% NaOH solution (8 g), Aliquat-336 (4 drops) and dimethyl sulfate (4.5 mL) were added to the suspension. After stirring at room temperature for 5.5 h, another portion of dimethyl sulfate (2.0 mL) was added, and the reaction mixture was stirred for 6 h more. The mixture was then filtered, the benzene phase separated, dried over Na_2SO_4 and evaporated to dryness. The residue was subjected to chromatographic separation on a column packed with Al_2O_3. The appropriate fractions were combined and evaporated to dryness; the residue was rubbed with ether, filtered off and dried under an infrared lamp.

4b (4.8 g; 46.7%), m.p. 195—197 °C (ethanol-petroleum ether), *lit.* [17] m. p. 203 °C.
$C_{18}H_{18}N_2O_5$. Calcd. C 63.15; H 5.30; N 8.18. Found C 63.09; H 5.50; N 8.11%.
IR (KBr): νC=O 1645, NO_2 1520, 1350 cm^{-1}.

4c (0.2 g; 1.95%), m.p. 218—220 °C.
$C_{18}H_{18}N_2O_5$. Calcd. C 63.15; H 5.30; N 8.18. Found C 63.37; H 5.48; N 8.00%.
IR (KBr): νC=N 1625, NO_2 1510, 1340 cm^{-1}.

4-Benzyl-2-methyl-1-phenyl-3(2*H*)-isoquinolinone (6)

4-Benzyl-1-phenyl-3(2*H*)-isoquinolinone (**5**) (3.11 g; 0.01 mol) [14] was suspended in anhydrous benzene (100 mL) and a solution of sodium ethoxide, prepared from metallic sodium (0.23 g; 0.01 g-atom) and anhydrous ethanol (10 mL), was added to it dropwise. In a few minutes the orange suspension turned into a greenish-yellow solution; then it was evaporated to dryness. The residual solid was dissolved in anhydrous acetone (50 mL), methyl iodide (0.69 mL; 1.56 g; 0.011 mol) was added, and the mixture was stirred at 40 °C for 5 h. The

resulting solid was filtered off to obtain the product (1.45 g; 44.6%), m.p. 203—205 °C (acetonitrile).

$C_{23}H_{19}NO$. Calcd. C 84.89; H 5.88; N 4.30. Found C 85.15; H 6.28; N 4.50%.

IR (KBr): νC=O 1635 cm^{-1}.

1-Benzyl-4,7-diphenyl-10-methyl-4,10,diazabenzo-[8,9]-tricyclo[2,2,0,3]-8--undecene-3,5,11-trione (7)

Compound **6** (0.5 g; 1.54 mmol) was dissolved in dry xylene (25 mL), *N*-phenylmaleimide (0.29 g, 1.7 mmol) was added, and the mixture was refluxed for 1 h, when reaction of the starting materials was complete. The mixture was evaporated to dryness and the residual oil rubbed with ether to obtain the product (0.15 g; 19.7%), m.p. 260—262 °C.

$C_{33}H_{26}N_2O_3$. Calcd. C 79.50; H 5.26; N 5.62. Found C 79.76; H 5.22; N 5.63%.

IR (KBr): νC=O 1780, 1715, 1670 cm^{-1}.

Investigations of the incorporation of lithium in compound 1b

Reaction with metallic lithium

A solution of **1b** (0.5 g; 2.11 mmol) in THF (5 mL) was added dropwise to a suspension of metallic lithium (0.15 g, 21.1 mg-atom) in tetrahydrofuran (5 mL). The mixture was stirred at room temperature for 8 h, then cooled to below 10 °C, and deuterium oxide (1.8 mL) dissolved in THF (5 mL) was added, and stirring was continued for 1.5 h. The reaction mixture was acidified with 2 *N* hydrochloric acid and extracted with chloroform. The organic phase was dried over Na_2SO_4 and evaporated to dryness to obtain an oil (0.5 g), which could not be crystallized. The integrated intensity of the ^{1}H-NMR ($CDCl_3$) spectra indicated that incorporation of deuterium at site 4, had occurred, however, the extent of incorporation could not be established exactly because of the high concentration of contaminants.

Reaction with phenyllithium

A solution of phenyllithium [15] prepared from bromobenzene (0.53 mL; 0.785 g; 5 mmol) and metallic lithium (0.086 g; 12.3 mg-atom) in ether (8 mL) was added dropwise to a solution of **1b** (0.5 g; 2.11 mmol) in THF (7 mL) at room temperature. The mixture was stirred for 3 h and allowed then to react with deuterium oxide in the manner described above. After processing, the oil obtained (0.5 g) was examined by ^{1}H-NMR spectroscopy, which showed that one of the hydrogen atoms in the C-4 methylene group of the very strongly contaminated material had been exchanged for deuterium to an extent of about 20—25%.

Reaction with butyllithium

A solution of butyllithium [16] prepared from butyl bromide (0.54 mL, 0.685 g; 5 mmol) and metallic lithium (0.086 g; 12.3 mg-atom) in ether (7 mL) was added dropwise to a solution of **1b** (0.5 g; 2.11 mmol) in THF (7 mL) at room temperature. The mixture was then stirred for 8 h. Deuterium oxide (3 mL) diluted with THF (3 mL) was added dropwise at 10 °C, the mixture was acidified and extracted with $CHCl_3$. The organic phase was dried over Na_2SO_4 and evaporated to dryness. The NMR spectra, based on the H-1 signal, indicated that the intensity of H-4 was equal to 1.3 H, implying that the incorporation of deuterium was at least about 70%.

Investigation of the incorporation of lithium into compound 2b

The lithium derivative was prepared from butyllithium (the amount given above) and from **2b** (0.6 g; 2.11 mmol) in THF (5 mL). It was then allowed to react with deuterium oxide as described above. The product was examined by the ^{1}H-NMR and ^{2}H-NMR techniques; in the deuterium resonance spectrum there was a single signal at 3.7 ppm, indicating that incorporation had occurred at site 4 in this case, too. According to the integrated intensities of the ^{1}H-NMR spectrum, one deuterium atom was incorporated.

1-Phenyl-2-methyl-4-(4'-nitrobenzylidene)-1,4-dihydro-3(2*H*)-isoquinolinone (8)

The required lithium compound was synthesized from butyllithium prepared from butyl bromide (1.1 mL; 1.37 g; 0.01 mol) and metallic lithium (0.17 g; 0.0246 g-atom) in ether (14 mL); this was allowed to react with **1b** (1.0 g; 4.22 mmol) dissolved in THF (14 mL). The reaction was effected at room temperature for 8 h. After cooling to −50 °C, a solution of 4-nitrobenzaldehyde (0.95 g; 6.33 mmol) in THF (7 mL) was added dropwise to the solution of the lithium compound. The reaction mixture was stirred at −50 °C for 30 min, at −8 °C for 30 min and at room temperature for 4 h. It was then poured into water (60 mL). The oil which separated was extracted with $CHCl_3$, the organic phase was dried and evaporated to dryness. The residual oil gave several spots in TLC. It was subjected to chromatographic purification on a column packed with Al_2O_3. The identified fractions were combined, the solvent was evaporated and the residue rubbed in ether to give the product (0.3 g; 19.2%), m.p. 207–208 °C (ethanol).

$C_{23}H_{18}N_2O_3$. Calcd. C 74.38; H 4.90; N 7.56. Found C 74.71; H 4.92; N 7.45%.

IR (KBr): νC=C 1615, νC=O 1655, NO_2 1510 and 1345 cm^{-1}.

^{1}H-NMR ($CDCl_3$): NMe 3.13 s (3), H-1 5.41 s (1), =CH 7.82 s (1), ArH 6.95–7.4 (9), *p*-NO_2–C_6H_4– 7.46 d (2), 8.09 d (2) type AA'BB').

*

The authors' thanks are due to Mrs. G. Kalász for recording the IR spectra and for the microanalyses, and to Miss É. Draskóczy for excellent technical assistance.

REFERENCES

[1] Houben–Weyl–Müller: Methoden der Organischen Chemie, **XIII/*1***, p. 97. George Thieme Verlag, Stuttgart 1970
[2] Fieser, L. F., Fieser, M.: Reagents for Organic Synthesis, John Wiley and Sons, New York–London–Sydney, 1967, Vol. **1** and subsequent volumes
[3] Csűrös, Z., Deák, Gy., Hoffmann, I., Török-Kalmár, A.: Acta Chim. Acad. Sci. Hung., **60,** 177 (1969)
[4] Gay, R. L., Boatman, S., Hauser, C. R.: Chem. Ind., **1965,** 1789
[5] Zára-Kaczián, E., Deák, Gy., Hazai L., Gáll-Istók, K., Haskó-Breuer, J.: Acta Chim. Acad. Sci. Hung., **100,** 37 (1979)
[6] Finkelstein, J., Brossi, A.: J. Heterocycl. Chem., **4,** 315 (1967)
[7] Deák, Gy., Gáll-Istók, K., Hazai, L., Sterk, L.: Synthesis, **1975,** 393
[8] Deák, Gy., Gáll-Istók, K., Sterk, L.: Acta Chim. Acad. Sci. Hung., **88,** 87 (1976)
[9] Hazai, L., Deák, Gy., Schnitta, A., Haskó-Breuer, J., Horváth, E.: Acta Chim. Hung., **116,** 303 (1984)
[10] Deák, Gy., Hazai L., Tóth, G.: J. Heterocycl. Chem., **14,** 583 (1977)
[11] Kreighbaum, W. E., Kavanaugh, W. F., Comer, W. T.: J. Med. Chem., **15,** 1131 (1972)
[12] Poindexter, G. S.: J. Org. Chem., **47,** 3787 (1982)
[13] Mayrhofer, R., Otto, H.-H.: Synthesis, **1980,** 247
[14] Deák, Gy., Hazai L.: Acta Chim. Acad. Sci. Hung., **79,** 113 (1973)
[15] Organic Reactions, Vol. **VI,** pp. 353. Wiley, New York–London 1951
[16] Shirley, D. A.: Preparation of Organic Intermediates, Wiley, New York, 1951. p. 65.
[17] Mollov, N. M., Venkov, A. P.: Acta Chim. Acad. Sci. Hung., **98,** 315 (1978)

Acta Chimica Hungarica 121 (3), pp. 271—279 (1986)

INFRARED AND RAMAN SPECTRA OF TRISUBSTITUTED ACETOPHENONES

T. V. K. SARMA*

(Molecular Spectroscopy Laboratories, Department of Physics, Andhra University, Visakhapatnam 530.003, India)

Received January 4, 1985
In revised form April 16, 1985
Accepted for publication May 8, 1985

The infrared and Raman spectra of 2,4,6-trimethylacetophenone, 2,4,6-trihydroxyacetophenone, 3,4,5-trimethoxyacetophenone and 2,3,4-trimethoxyacetophenone were recorded. The far infrared spectra of the two solids — 2,4,6-trihydroxyacetophenone and 3,4,5-trimethoxyacetophenone — were also recorded. Assuming C_s symmetry for all the molecules the vibrational analysis is reported.

The vibrational spectra of acetophenone and a number of mono- and disubstituted acetophenones have been studied earlier [1—13]. However, only for a few tri- and other polysubstituted acetophenones these spectral studies have been extended so far [4, 13—16]. The present communication deals with the recording and analysis of the infrared and Raman spectra of a few trisubstituted acetophenones — 2,4,6-trimethylacetophenone (**A**), 2,4,6-trihydroxyacetophenone (**B**), 3,4,5-trimethoxyacetophenone (**C**) and 2,3,4-trimethoxyacetophenone (**D**). The experimental details are the same as described earlier [17]. The spectra are shown in Figs 1—10.

The observed frequencies (in cm^{-1}), their visual intensities and probable assignments are shown in Table I. All the four molecules are assumed to belong to C_s point group. Under this symmetry the 72 vibrations of molecule **A** divide among themselves as $49a' + 23a''$ whereas molecule **B** gives rise to 54 vibrations which can be classified as $37a' + 17a''$. Molecules **C** and **D** have 81 normal modes as $55a' + 26a''$. Both the species are allowed in the infrared and Raman spectra. The vibrational analysis is carried out following the classification of molecules [4, 18] for the identification of the vibrational frequencies of benzene derivatives and a comparison with the spectra of similar and related molecules [4, 19—38]. Molecules **A**, **B** and **C** belong to the 1,2,3,5-tetralight substituted class of benzenes whereas molecule **D** comes under 1,2,3,4-tetralight type based on the above classification. As the molecules **A**, **B** and **C** belong to the 1,2,3,5-tetralight substituted benzenes, a closer comparison of the spectra of molecules **A**, **B** and **C** with those of 44 such molecules, reported by Varsányi et al. [15] is taken into consideration in identifying the 30 benzene-like modes. A comparison of the spectra of mole-

* Present address: Department of Physics, Mrs. A.V.N. College, Visakhapatnam — 530.001, India

Table I

Infrared and Raman frequencies observed for 2,4,6-trimethylacetophenone; 2,4,6-trihydroxyacetophenone; 3,4,5-trimethoxyacetophenone and 2,3,4-trimethoxyacetophenone and their probable assignments

2,4,6-trimethylacetophenone (A)		2,4,6-trihydroxyacetophenone (B)		3,4,5-trimethoxyacetophenone (C)		2,3,4-trimethoxyacetophenone (D)		Probable assignments		
Infrared (cm^{-1}) (1)	Raman (cm^{-1}) (2)	Infrared (cm^{-1}) (3)	Raman (cm^{-1}) (4)	Infrared (cm^{-1}) (5)	(Raman) (cm^{-1} (6)	Infrared (cm^{-1}) (7)	Raman (cm^{-1}) (8)	Species (9)	Mode No. § (10)	Description (11)
—	—	3545 sb	—	—	—	—	—	a'	—	νO—H
—	—	3474 s	—	—	—	—	—	a'	—	νO—H
3388 w	—	—	—	—	—	—	—	A'	—	2×1170+1041
—	—	3133 sb	—	—	—	—	—	a'	—	νO—H
—	—	—	—	3107 vw	—	—	—	A'	—	1594+1510
3037 sh	3020 mw	3100 sh	—	3031 w	—	—	3096 msp	a'	20*a*,7*b*	νC—H
3005 vvw	—	—	—	3012 mw	3012 mw	3008 sh	—	a'	20*b*	νC—H
2979 sh	—	—	—	2975 ms	—	2979 w	2985 vw	a'	—	ν_{as} CH_3
2960 w	—	—	—	2950 ms	—	2950 s	2935 sp	a'		$\nu_s CH_3$
2926 vs	2923 vvsp	2933 w	—	2925 vw	—	2916 sh	—	a'	—	$\nu_s CH_3$
2866 w	2865 sh	—	—	2867 vvw	—	2887 vvw	—	A'	—	2×1433; 1459+1416; 1467+1416
—	—	—	—	2841 ms	—	2849 ms	2848 sp	a'	—	$\nu_s CH_3(OCH_3)$
2741 mw	2745 mwp	—	—	—	—	—	—	A'	—	1385+1358
—	—	2625 vw	—	—	—	—	—	A'	—	1372+1258
2408 w	—	—	—	—	—	—	—	A'	—	1358+1066
2304 w	—	—	—	—	—	—	—	A''	—	1258+1041
2033 vw	—	—	—	—	—	—	—	A'	—	1066+970
—	—	—	—	—	—	2000 vvwb	—	A'	—	1024+975
1966 mw	—	—	—	—	—	1937 vw	—	A'	—	1358+596; 1296+640
1925 wb	—	—	—	—	—	—	—	A'	—	970+952
—	—	—	—	—	—	1892 vw	—	A''	—	1217+675
—	—	—	—	—	—	1800 vw	—	A'	—	1100+709
—	—	—	—	—	—	1774 vvw	—	A''	—	1100+675
1716 vvs	—	—	—	—	—	—	—	a'	—	νC=O; 2×863
1699 vvs										
—	1703 sp	1637 vvs	—	1685 vvs	1677 ms	1683 vs	1678 vvsp	a'	—	νC=O
—	—	—	—	—	—	1641 vw	—	A'	—	932+709
1618 vvs	1617 sp	1575 ms	—	1594 vvs	1582 ms	1598 vvs	1591 vvsp	a'	8*a*	νC—C

1582 w	1585 w	1541 ms	—	—	—	—	—	a'	8*b*	νC—C
—	1487 w	1479 ms	—	1510 vs	—	1501 vs	1500 mwp	a'	19*a*	νC—C
1468 sh	—	1462 sh	—	1467 sh	—	1467 vs	1468 sp	a'	—	δ_{as} CH_3
1458 vvsb	1455 wb	—	—	1459 vvs	—	—	—	a'	—	δ_{as} CH_3
—	—	—	—	1441 mw	1432 ms	1440 sh	—	a'	—	δ_{as} CH_3
1433 vvsb	—	1420 ms	—	1416 vvs	—	1416 vs	—	a'	19*b*	νC—C
1385 ms	1388 vsp	1372 s	—	1365 vvs	—	1366 vs	1364 mw	a'	—	$\delta_s CH_3$
1358 vvs	—	—	—	1340 vvs	1325 s	—	1332 vw	a'	—	$\delta_s CH_3$
1304 ms	1300 vvsp	1292 vs	1293 ms	1229 vvs	1215 w	1296 vvsb	1291 vvsp	a'	2	νC—$COCH_3$ (**A, B, D**) νC—OCH_3(**C**)
1258 vvs	1258 msp	1320 s	—	1252 s	—	1217 vs	1215 msp	a'	14	νC—C
—	—	1258 s	—	—	—	—	—	a'	—	δO—H
—	—	1214 ms	—	—	—	—	—	a'	—	δO—H
—	—	—	—	1237 sh	—	—	—	A'	—	2×610
1184 sh	—	—	—	—	—	1241 mw	1240 vvw	a'	18*b*, 18*a*	βC—H
—	—	—	—	1183 vs	—	1179 ms	1193 msp	a'	—	νO—CH_3
1170 vvs	1170 mwp	1175 vs	—	1139 vvsb	—	1100 vvs	1098 msp	a'	13	νC—CH_3(**A**); νC—OH(**B**); νC—OCH_3(**C, D**)
—	—	1096 mw	—	—	—	—	—	A''	—	575+525
—	—	1071 vs	1075 mw	1100w	1092 ms	1133 vs	1133 msp	a'	18*a*, 9*a*	βC—H
1066 vvs	1065 vsp	—	—	1041 mw	1034 w	—	—	a''	—	$\delta_{as}CH_3$
1041 s	—	1029 ms	1023 ms	1033 w	—	1024 vs	1020 msp	a''	—	$\delta_{as}CH_3$
1000 vvw	—	—	—	1002 vs	1000 w	—	—	a''	—	$\delta_{as}CH_3$
970 s	—	968 s	973 w	987 ms	986 w	975 s	973 vsp	a'	—	νC—C($COCH_3$)
952 ms	953 sp	—	—	894 s	894 vw	932 ms	928 msp	a'	7*b*, 7*a*	νC—CH_3(**A**); νC—OCH_3(**C, D**)
933 sh	—	820 sh	—	782 s	—	883 ms	880 msp	a'	7*a*, 20*a*	νC—CH_3(**A**); νC—OH(**B**); νC—$COCH_3$(**C**); νC—OCH_3(**D**)
891 w	—	—	—	868 sh	—	—	—	a''	17*a*	ΦC—H
872 sh	—	—	—	864 vs	—	866 sh	—	a'	—	δC=O
863 vvs	—	835 s	—	833 s	—	815 vs	812 vw	a''	11, 17*b*	ΦC—H
*845.8		*814.3		*840.3		*773.6				
—	—	771 mwb	—	—	—	—	—	a''	—	γO—H
745 s	—	750 w	—	756 ms	756 vw	709 ms	708 sp	a'	12	βC—C—C
672 s	678 vsp	717 w	713 w	673 w	—	675 mwb	680 msp	a''	4	ΦC—C
620 w	630 w	658 mwb	—	655 s	—	618 mw	620 msp	a''	—	γC=O
596 vvs	580 vvsp	612 mw	613 mw	610 vs	615 vw	640 mw	645 sp	a'	1	νC—C
		**615 ms		**610 s						

Table I (contd.)

2,4,6-trimethylacetophenone (A)		2,4,6-trihydroxyacetophenone (B)		3,4,5-trimethoxyacetophenone (C)		2,3,4-trimethoxyacetophenone (D)		Probable assignments		
Infrared (cm^{-1}) (1)	Raman (cm^{-1}) (2)	Infrared (cm^{-1}) (3)	Raman (cm^{-1}) (4)	Infrared (cm^{-1}) (5)	Raman (cm^{-1}) (6)	Infrared (cm^{-1}) (7)	Raman (cm^{-1}) (8)	Species (9)	Mode No. § (10)	Description (11)
529 vs	520 sdp	575 s	—	537 w	—	551 ms	—	a''	16*b*	ΦC—C
		**578 ms		**545 ms						
512 vvw	505 sh	525 ms	—	512 mw	—	538 s	540 msp	a'	6*b*	βC—C—C
		**525 ms		**510 ms						
466 vvw	465 vvw	450 mw	—	**460 w	—	500 vw	508 mwp	a''	16*a*	ΦC—C
		**440 ms								
—	443 wp	**395 w	—	**445 w	—	433 vw	430 vw	a'	6*a*	βC—C—C
—	345 sp	**362 mw	—	**352 s	—	—	328 msp	a'	3	βC—CH_3; βC—OH; βC—OCH_3; βC—OCH_3
—	—	—	—	**390 vw	382 ms	408 mw	413 mwp	a'	—	δO—CH_3
—	—	—	—	—	—	—	385 wp	a'	—	δO—CH_3
—	—	**316 w	—	**335 ms	—	—	—	a''	10*b*	ΦC—OH; ΦC—OCH_3
—	283 mwp	—	—	**295 mw	—	—	283 mw	a'	9*b*, 18*b*	βC—CH_3(**A**); βC—OCH_3(**C, D**)
—	—	**258 mw	—	—	—	—	—	a'	9*a*	βC—OH
—	231 sp	**230 ms	—	**235 s	236 vw	—	—	a''	10*a*	ΦC—CH_3(**A**); ΦC—OH(**B**); ΦC—OCH_3(**C**)
—	183 wdp?	**185 s	—	—	—	—	193 mwp	a''	5, 11	ΦC—CH_3(**A**); ΦC—OH(**B**); ΦC—OCH_3(**D**)
—	—	**172 w	—	—	—	—	—	—	—	νCO...H
—	—	**140 ms	—	—	—	—	—	a''	17*b*	ΦC—$COCH_3$

§ First number refers to molecules **A, B, C**; second refers to molecule **D**; a single number refers to **A—D**.

* Calculated frequencies.

** Bands observed in the far infrared spectra.

ν — Stretching; β — in-plane ring bending; Φ — out-of-plane ring bending.

δ_{as} — asymmetric deformation of the substituent group; δ_s — symmetric deformation of the substituent group; δ_{as}^{-} — rocking of the substituent group; δ — in-plane bending of the substituent group; γ — out-of-plane bending of the substituent group.

s — strong; v — very; m — medium; w — weak; sh — shoulder; b — broad; p — polarised; dp — depolarised.

cule **D** with its isomer, molecule **C** is also attempted to arrive at some significant factors which may be attributable to the spectra of isomeric molecules.

In addition to the identification of most of the fundamental frequencies in all the four molecules, the following are a few significant results worthy to mention. The calculated values of the C—H out-of-plane bending mode 11 in

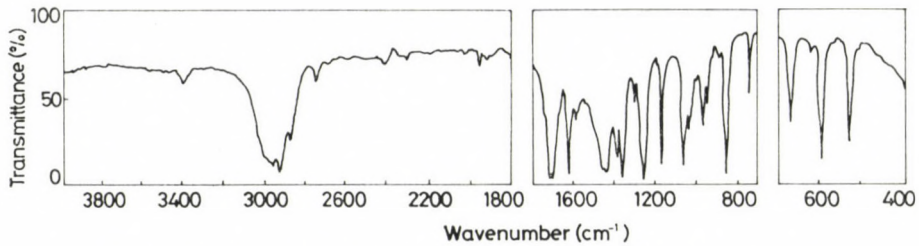

Fig. 1. Infrared absorption spectrum of 2,4,6-trimethylacetophenone

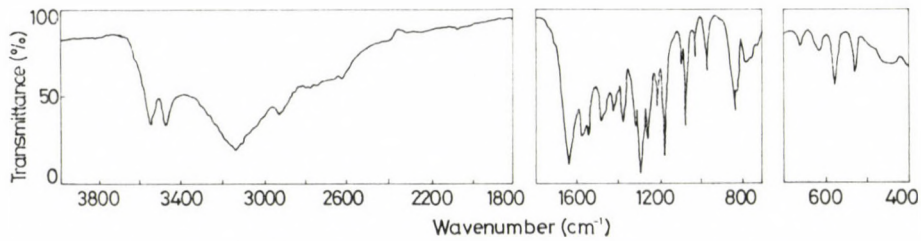

Fig. 2. Infrared absorption spectrum of 2,4,6-trihydroxyacetophenone

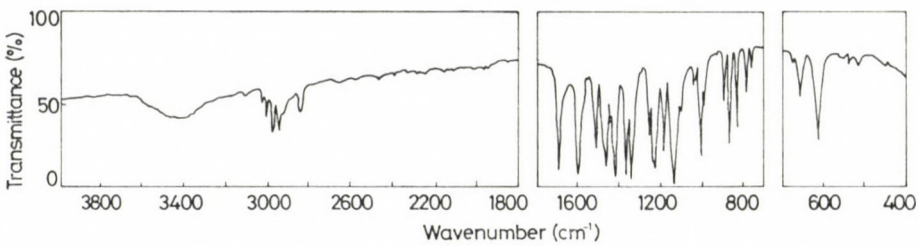

Fig. 3. Infrared absorption spectrum of 3,4,5-trimethoxyacetophenone

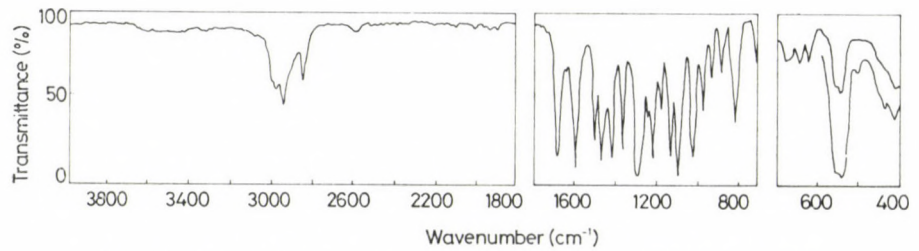

Fig. 4. Infrared absorption spectrum of 2,3,4-trimethoxyacetophenone

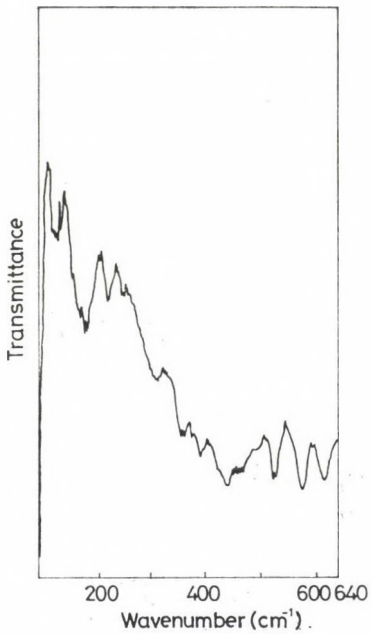

Fig. 5. Far infrared absorption spectrum of 2,4,6-trihydroxyacetophenone

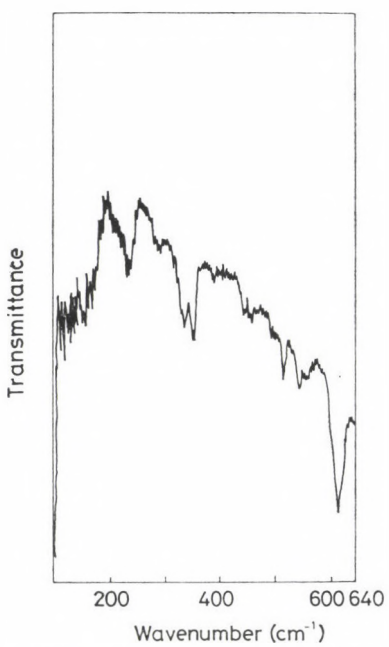

Fig. 6. Far infrared absorption spectrum of 3,4,5-trimethoxyacetophenone

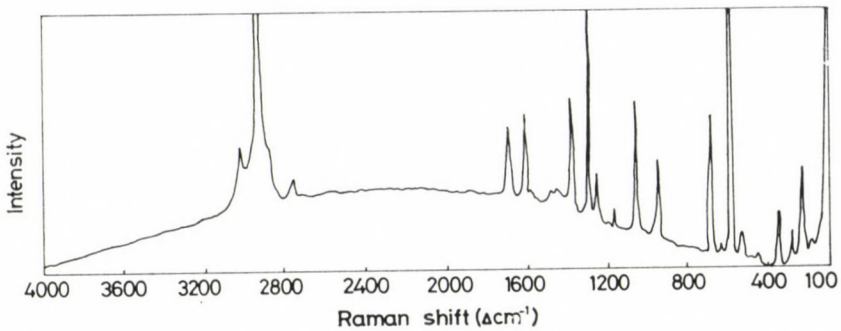

Fig. 7. Laser Raman spectrum of 2,4,6-trimethylacetophenone

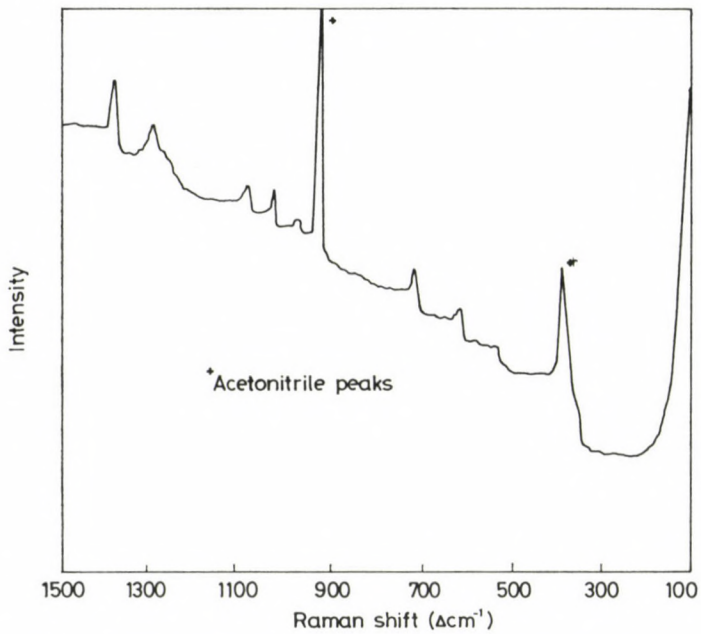

Fig. 8. Laser Raman spectrum of 2,4,6-trihydroxyacetophenone

2,4,6-trimethylacetophenone, 2,4,6-trihydroxyacetophenone and 3,4,5-trimethoxyacetophenone and mode 17*b* in 2,3,4-trimethoxyacetophenone, using spectroscopic moments [14, 32] are well comparable with the assignments made in the present work. Fermi resonance between the C=O stretching mode and the first overtone of C—H out-of-plane bending mode 11, is believed to be present in 2,4,6-trimethylacetophenone. Inter- and intramolecular hydrogen bondings could be established from the position and nature of OH stretching and out-of-plane bending modes in 2,4,6-trihydroxyacetophenone.

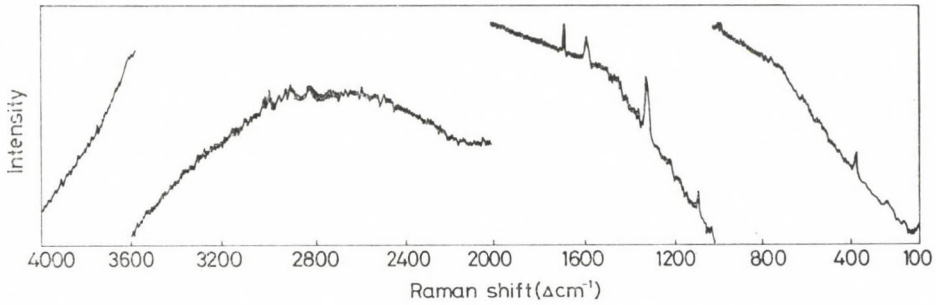

Fig. 9. Laser Raman spectrum of 3,4,5-trimethoxyacetophenone

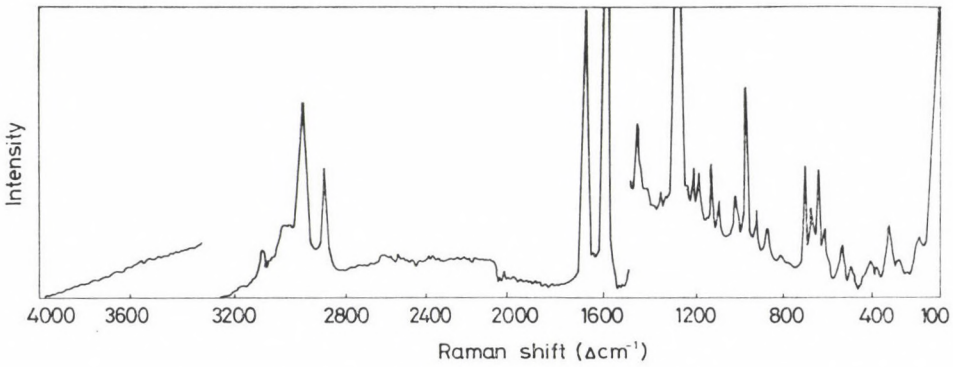

Fig. 10. Laser Raman spectrum of 2,3,4-trimethoxyacetophenone

The decrease in the carbonyl stretching frequency in this molecule is due to the intramolecular hydrogen bonding between the carbonyl oxygen atom and the hydrogen atom of the adjacent hydroxyl group.

*

The author wishes to acknowledge with gratitude Prof. J. Ramakrishna, Dr. A. Selvarajan and Mr. A. Ganesan of the I. I. Sc., Bangalore for their help in recording the infrared spectra. The author is thankful to Prof. B. N. Bhattacharya, Prof. G. Thyagarajan and Dr. T. K. Gundu Rao of the R. S. I. C., I. I. T., Bombay for providing the facilities to record the Laser Raman spectra. The author is grateful to the Head, R.S.I.C., I.I.T., Madras and in particular to Mr. M. Mylarajan for running the Laser Raman and far infrared spectra. Financial assistance from the U.G.C., New Delhi is gratefully acknowledged. The author is deeply indebted to Prof. (Mrs.) C. Santhamma, for her valuable guidance during the course of the present investigation.

REFERENCES

[1] Cherrier, M. C.: C. R. Acad. Sci. Paris, **228,** 307 (1947)
[2] Weckherlin, S., Luttke, W.: Z. Elektrochem., **64,** 1228 (1960)
[3] Mross, W. D., Zundel, G.: Spectrochim. Acta, **26A,** 1097 (1970)
[4] Varsányi, G.: Assignments for Vibrational Spectra of Seven Hundred Benzene Derivatives, Vols. **I** and **II,** Adam Hilger, London 1974
[5] Green, J. H. S., Harrison, D. J.: Spectrochim. Acta. **33A,** 583 (1977)

[6] Pajeau, R.: Bull. Soc. Chim. Fr., **13,** 544 (1946)
[7] Ansari, A. K., Verma, P. K.: Proc. 6th Int. Conf. Raman Spectroscopy, **2,** 16 (1978)
[8] Tripathi, G. N. R., Sitaram, Pandey, V. M.: Indian J. Pure Appl. Phys., **11,** 842 (1973)
[9] Maltese, M., Ercolani, C.: J. Chem. Soc., (B), **1970,** 1147
[10] Gambi, A., Giorgianni, S., Passerini, A., Visinoni, R., Ghersetti, S.: Spectrochim, Acta, **38A,** 871 (1982)
[11] Garrigou-Lagrange, C., Lebas, J. M., Josien, M. L.: Spectrochim. Acta, **12,** 305 (1958)
[12] Lebas, J. M., Garrigou-Lagrange, C., Josien, M. L.: Spectrochim. Acta, **15,** 225 (1959).
[13] Gupta, V. P., Devinder Gupta, Jain, S. M.: Indian J. Pure Appl. Phys., **14,** 846 (1976)
[14] Varsányi, G., Sohár, P.: Acta Chim. Acad. Sci. Hung., **76,** 243 (1973)
[15] Varsányi, G., Horváth, G., Imre, L., Schawartz, L., Sohár, P., Soti, F.: Acta. Chim. Acad. Sci. Hung., **93,** 315 (1977)
[16] Singh, K., Singh, I. S.: Curr. Sci., **41,** 513 (1972)
[17] Sarma, T. V. K.: Acta Chim. Hung., **115,** 89 (1984)
[18] Varsányi, G.: Vibrational Spectra of Benzene Derivatives, Academic Press, New York 1969
[19] Singh, R. B.: Ph. D. thesis, Bhagalpur University, 1980
[20] Verma, V. N.: Spectrosc. Lett., **8,** 349 (1975)
[21] Goel, R. K., Sharma, S. D., Sharma, S. N.: Indian J. Pure Appl. Phys., **17,** 55 (1979)
[22] Sharma, S. N.: Acta Phys, Polonica, **A62,** 449 (1982)
[23] Green, J. H. S., Harrison, D. J., Kynaston, W.: Spectrochim. Acta, **27A,** 2199 (1971)
[24] Chattopadhyay, S.: Indian J. Phys., **45,** 564 (1971)
[25] Green, J. H. S.: Spectrochim. Acta, **18,** 39 (1962)
[26] Pathak, A. N., Sinha, B. K.: Indian J. Pure Appl. Phys., **18,** 619 (1980)
[27] Pathak, A. N., Sinha, B. K.: Indian J. Pure Appl. Phys., **19,** 678 (1981)
[28] Sarma, T. V. K.: Indian J. Phys., **59B,** 477 (1985)
[29] Venkoji, P.: Acta Chim. Hung., **117,** 163 (1984)
[30] Colthup, N. B., Daly, L. H., Stephen, E. W.: Introduction to Infrared and Raman Spectroscopy, Academic Press, New York 1964
[31] Freeman, F., Bentley,H. R., Smithson, L. D., Rozek, A. L.: Infrared Spectra and Characteristic Frequencies $\sim 700-300$ cm^{-1}, Interscience Publishers, New York 1968
[32] Varsányi, G., Sohár, P.: Acta Chim. Acad. Sci. Hung., **74,** 315 (1972)
[33] Nyquist, R. A.: Spectrochim. Acta, **19,** 1655 (1963)
[34] Verma, V. N.: The J. Sci. Res. Banaras Hindu Univ., **21,** 239 (1970—71)
[35] Gambi, A., Ghersetti, S.: Spectrosc. Lett., **9,** 211 (1976)
[36] Mercer, G. D.: J. Chem. Eng. Data, **14,** 262 (1969)
[37] Schubert, W. M., Sweeney, W. A.: J. Am. Chem. Soc., **77,** 4172 (1955)
[38] Bellamy, L. J.: The Infrared Spectra of Complex Molecules, Chapman and Hall, London 1975

Acta Chimica Hungarica 121 (3), pp. 281—289 (1986)

STUDIES OF SOME METAL CHELATES OF KETOANILS, I

Raj Kumar UPADHYAY[1]*, Kamlesh RATHORE[1], Arun Kumar BAJPAI[1] and Deo Swarup MAHESHWARI[2]

([1]Chemical Laboratories, N.R.E.C. College, Khurja-203131, India, [2]Physics Department, D.S. College, Aligarh, India)

Received December 16, 1983
In revised form March 27, 1985
Accepted for publication May 14, 1985

p-Dimethylamino- and *p*-diethylamino-anils of 2-thiopheneglyoxal form stable dark coloured chelates with Cr(III), Mn(II), Fe(III), Co(II), Ni(II), Cu(II), Zn(II), Cd(II), Hg(II) and Au(III), which have been characterized by analysis, molar conductance, magnetic susceptibility, IR and electronic spectroscopy.

Introduction

Ketoanils, prepared from aromatic glyoxals and parasubstituted primary amines, and coordinating through azomethine and carbonyl groups of quinonoid structures, have novel ligand properties [1—3], forming complexes of generally unusual stereochemistries and isomeric compositions. Coordination chemistry of ketoanils obtained from 2-thiopheneglyoxal and parasubstituted primary aromatic amines has not been described as yet, though, a few references [4, 5] dealing with bonding and structure of metal chelates of Schiff's bases obtained by condensing 2-thiophenealdehyde with alkylamines are available. We now report the synthesis, properties and structures of Cr(III), Mn(II), Fe(III), Co(II), Ni(II), Cu(II), Zn(II), Cd(II), Hg(II) and Au(III) complexes containing *p*-dimethylamino- and *p*-diethylamino-anils of 2-thiopheneglyoxal (abbreviated as DMATG and DEATG, respectively) ligands with three donor sites.

Experimental

Preparation of ketoanils and their complexes

DMATG and DEATG [6] were precipitated on mixing solutions of 2-thiopheneglyoxal (1 mol) and the corresponding amine (1 mol) in ether. The brown precipitates washed with ether were recrystallized from benzene or acetone.

For the preparation of complexes, ligand and metal chloride solutions in acetone ($AuCl_3$ in 95% ethanol) mixed in stoichiometric proportions (ligand in slight excess) were refluxed, concentrated and crystallized. Crystalline products washed with ether and recrys-

* To whom correspondence should be addressed.

tallized from methyl cyanide, chloroform, dioxane or ethanol-HCl (9 : 1, *v/v*) and finally washed with ether, were dried under reduced pressure.

In the preparative work laboratory reagents obtained from BDH and Johnson Matthey (London) were used as supplied.

Analysis and physical measurements

For carbon, hydrogen and nitrogen contents samples were analysed microanalytically, whereas chlorine was estimated as AgCl gravimetrically. Conductance was measured on a Toshniwal conductivity bridge using a dip-type cell with a cell constant of 0.61. Infrared spectra were recorded in Nujol on a Perkin Elmer-577 spectrophotometer. Absorbance of complex solutions was measured on a Beckmann DU-2 spectrophotometer. Magnetic susceptibility measurements on powdered solids were done with a Gouy balance at room temperature using $CoHg(SCN)_4$ calibrant.

Results and Discussion

The colour, m.p. and analytical results, which agree with the proposed stoichiometries of the complexes are listed in Table I. Silver nitrate test and molar conductance data (Table II) reveal that except Fe(III) and Au(III) complexes all are non-electrolytes. Low ΛM values obtained generally may be attributed to large cations.

IR spectra of DMATG, DEATG and their complexes reveal considerable lowering in the stretching frequencies and/or intensities and changes of band shapes corresponding to C=O, C—S, 1 : 4 disubstitution and C=C (aromatic) groups of ligands on complexation. This indicates that both ligands are coordinated with metal ions in quinonoid structures through their carbonyl oxygen and heterocyclic sulphur atoms; new low frequency peaks corresponding to M—O and M—S stretching in the spectra of complexes support the participation of C=O and C—S (heterocyclic) groups in coordination. Undisturbed position of the azomethine band evidently shows that, probably due to its remote position from the coordinating groups, it is prevented from coordination.

Six coordination species of the type ML_2X_2 (where L and X are bidentate ligand and monodentate halide, respectively) are capable of exhibiting *cis*- and *trans*-isomerism [7] in octahedral geometry. In the *cis*- isomer of C_{2v} symmetry with halides in *axial* positions, one would expect two IR-active terminal M—X stretching modes, whereas in the *trans*-isomer of D_{4h} symmetry only one normal mode is expected. These considerations lead us to suggest that only the *cis*-configuration is obtained with the complexes of Mn(II), Fe(III), Ni(II) and Cd(II). In some cases the doublet structure of M—X peaks could be attributed to incomplete degeneracy of the two normal modes.

In several complexes one or two strong, broad IR bands in the 3320—3440 cm^{-1} range, and the analytical data indicate water molecules which, however, do not seem to be coordinated to metal ions as additional M—O bands are absent from the IR spectra.

Table I

Colour, m.p., molar conductance and analytical data for the complexes

Complex	Colour	Melting point (°C)	Molar conductivity, ΛM (Ω^{-1} cm^2 mol^{-1})	Found (Calcd.) %			
				C	H	N	Cl
$Cr(DMATG)Cl_3 \cdot 4H_2O$	Gray brown	195	14.8 ($CHCl_3$)	34.45 (34.38)	4.33 (4.50)	5.79 (5.73)	21.65 (21.80)
$Cr(DEATG)Cl_3 \cdot 4H_2O$	Black	210	18.3 ($CHCl_3$)	37.08 (37.20)	5.10 (5.03)	5.38 (5.42)	21.00 (20.64)
$Mn(DMATG)_2Cl_2 \cdot 2H_2O$	Gray brown	250	21.9 (MeCN)	49.38 (49.55)	4.60 (4.71)	8.38 (8.25)	10.12 (10.47)
$Mn(DEATG)_2Cl_2 \cdot 2H_2O$	Black	—	22.4 (Me_2CO)	52.40 (52.31)	5.60 (5.44)	7.45 (7.62)	10.00 (9.67)
$Fe(DMATG)_2Cl_3$	Dark brown	250	107.6 (Me_2CO)	49.78 (49.53)	4.24 (4.12)	8.49 (8.24)	16.02 (15.70)
$Fe(DEATG)_2Cl_3$	Brown black	178	89.5 (Me_2CO)	52.45 (52.29)	5.06 (4.90)	7.62 (7.62)	14.75 (14.50)
$Co(DMATG)Cl_2 \cdot 2H_2O$	bray Brown	198	26.6 (MeCN)	40.15 (39.62)	4.11 (4.24)	6.72 (6.60)	16.54 (16.75)
$Co(DEATG)Cl_2$	Black	190	25.4 (Me_2CO)	46.06 (46.16)	4.70 (4.34)	6.58 (6.73)	16.78 (17.07)
$Ni(DMATG)_2Cl_2$	Dark brown	192	16.9 (MeCN)	52.14 (52.04)	4.29 (4.32)	8.75 (8.67)	10.82 (11.00)
$Ni(DEATG)_2Cl_2$	Black	195	22.9 ($CHCl_3$)	54.88 (54.73)	5.06 (5.13)	7.86 (7.98)	9.88 (10.12)
$Cu_2(DMATG)Cl_4 \cdot 8H_2O$	Brown	280	5.0 (Dioxane)	24.86 (25.02)	4.51 (4.47)	4.12 (4.17)	20.00 (21.15)
$Cu(DEATG)(OH)Cl$	Brown black	285	2.2 (Dioxane)	48.74 (49.80)	4.73 (4.67)	6.96 (7.27)	8.83 (9.21)
$Zn(DMATG)Cl_2$	Black	170	19.2 (Me_2CO)	42.98 (42.60)	3.85 (3.54)	7.15 (7.09)	17.88 (18.00)
$Zn(DEATG)Cl_2 \cdot 2H_2O$	Dark brown	168	14.0 (Me_2CO)	42.78 (41.89)	4.79 (4.79)	5.30 (5.27)	15.32 (15.49)
$Cd(DMATG)_2Cl_2 \cdot 2H_2O$	Gray brown	195	—	46.60 (46.83)	4.32 (4.46)	7.77 (7.81)	9.62 (9.90)
$Cd(DEATG)_2Cl_2$	Dark brown	215	18.4 (Me_2CO)	50.98 (50.83)	5.08 (4.77)	7.72 (7.41)	9.28 (9.40)
$Au(DMATG)Cl_3 \cdot H_2O$	Gray brown	232	79.5 (EtOH—HCl, 6 : 1, *v/v*)	27.52 (27.26)	2.82 (2.76)	4.85 (4.83)	18.60 (18.38)
$Au(DEATG)Cl_3 \cdot 3H_2O$	Black	230	72.3 (EtOH—HCl, 6 : 1, *v/v*)	30.83 (31.10)	3.40 (3.29)	4.68 (4.60)	17.42 (17.52)
$Hg(DMATG)Cl_2 \cdot 3H_2O$	Brown	—	—	29.00 (28.81)	3.35 (3.42)	4.90 (4.80)	12.00 (12.17)
$Hg(DEATG)Cl_2 \cdot H_2O$	Black	—	21.1 (Me_2CO)	33.27 (33.35)	3.53 (3.47)	4.92 (4.86)	12.18 (12.33)

On the basis of analytical and molar conductance data, and of the abcence of water molecule(s) in the coordination sphere Cr(III) complexes can be proposed to be chloride-bridged dimers, although, the Cr—Cl—Cr stretching bands in their IR spectra could not be identified, probably due to its mixing with ligand bands or rotational oscillations of lattice water occurring in the same frequency region. Similarly, in the halide-bridged cquare planar $Cu_2(DMTAG)Cl_4 \cdot 8H_2O$, dimer i.e. Cu—Cl—Cu stretching bands

Table II

Principal infrared bands (cm^{-1}) *for the ligands and their complexes*

Compound	ν(C=O)	ν(C=N)	ν(C=C) aromatic	1 : 4 Disubstitution	ν(C—S)	ν(M—O)	ν(M—S)	ν(M—Cl)
DMATG	1650 s, sh	1610 s	1565 s, 1540 m, 1515 s	830 s, d	860 s, 645 m	—	—	—
DEATG	1660 s, sh	1610 s	1520 s, d, 1470 s, 1450 s	820 s, d	850 s, 665 m	—	—	—
$Cr(DMATG)\ Cl_3 \cdot 4H_2O$	1640 s	1610 s	1515 s	825 s	850 m, sh, 665m	535 m	210 m	335 m
$Cr(DEATG)Cl_3 \cdot 4H_2O$	1650 s, sh	1610 s	1515 s, 1470 s	835 s	—	560 s	205 m	370 m
$Mn(DMATG)_2Cl_2 \cdot 2H_2O$	1640 s, sh	1610 s	1518 s	830 s	650 m	540 m	215 m	285 s, d
$Mn(DEATG)_2Cl_2 \cdot 2H_2O$	1645 s, sh	1610 s	1520 s, 1465 s	825 m	855 m, sh	575 m	—	295 w, 235 m
$Fe(DMATG)_2Cl_3$	1630 s, sh	1610 s	1510 s	830 s	675 s	—	215 s	285 s, d
$Fe(DEATG)_2Cl_3$	1650 s, sh	1610 s	1510 s, 1470 s	840 s	—	560 m	—	380 m, 295 m
$Co(DMATG)Cl_2 \cdot 2H_2O$	1640 s	1610 s	1515 s	825 s	850 s, sh	535 m	210 m	310 w
$Co(DEATG)Cl_2$	1650 s	1610 s	1515 s, 1470 s	825 m	—	560 m	210 m	315 m
$Ni(DMATG)_2Cl_2$	1635 s	1610 s	1512 s	820 s	850 s, sh, 660 m	530 m	—	370 m, 240 m
$Ni(DEATG)_2Cl_2$	1640 s, sh	1610 m	1510 s	820 m	845 m, sh	550 m	205 w	260 w, 240 w
$Cu_2(DMATG)Cl_4 \cdot 8H_2O$	1625 s, b	1610 s	1535 m, 1515 m	840 m, b	855 m, 660 m	510 w	205 w	320 m
Cu(DEATG)(OH)Cl	1650 s	1610 s	1510 s	835 s	—	535 s	210 s	380 m
$Zn(DMATG)Cl_2$	1640 s	1610 s	1510 s	820 s	850 m, sh, 650 m	530 m	—	280 s, 250 s
$Zn(DEATG)Cl_2 \cdot 2H_2O$	1645 m, sh	1610 s	1520 s, 1460 m	840 m	—	560 m	210 m	300 m, 230 m
$Cd(DMATG)_2Cl_2 \cdot 2H_2O$	1620 s, b	1620 s, b	1590 s, 1495 s	810 s	840 m, sh	550 m	—	275 s, sh, 250 s
$Cd(DEATG)_2Cl_2$	1625 s, sh	1610 s	1495 s	810 s	—	520 s	250 s	275 s, 250 s
$Au(DMATG)Cl_3 \cdot H_2O$	1625 s	1610 s	1590 s, 1485 s	810 s	—	550 s	225 s	275 s, 250 s
$Au(DEATG)Cl_3 \cdot 3H_2O$	1620 s, sh	1610 s	1590 s	820 s	—	545 s	—	290 s, 250 s
$Hg(DMATG)Cl_2 \cdot 3H_2O$	1625 m, b	1610 m, b	—	815 m	840 m	557 m, b	—	280 s, 270 s
$Hg(DEATG)Cl_2 \cdot H_2O$	1590 s	1610 s, sh	—	820 s	—	545 s	225 s	280 s, 250 s

s — strong; m — medium; w — weak; sh — shoulder; b — broad.

could not be identified. In both Co(II) compounds a band at ca. 313 cm^{-1} attributable to Co—Cl stretching, reveals monomeric structures for the four-coordinate species.

The magnetic moments of Cr(III) complexes indeed correspond to three unpaired electrons, but they are considerably lower than the spin-free value (3.87 B.M.). For ligands that are normal molecules with no large numbers of low lying electronic states, one would expect small contributions of spin-orbit coupling and $(1—4\lambda/10Dq)$ to the lowering of magnetic moments of complexes. As in many instances [8] polymerization could considerably reduce the magnetic moments, in the present compounds major contributions to the observed lowering could be attributed to dimerization. Band splitting pattern in the absorption spectra is consistent with the octahedral geometry of the complexes. Ligand field parameters have been calculated by standard methods [9]. The observed $10Dq$ values are lower as compared with that for $[Cr(NH_3)_6]^{3+}$, 2200 cm^{-1}. Therefore, it is reasonable to assume that ligands are lower than ammonia in the spectrochemical series. The B values are 60—62% of the free ion value in the complexes, suggesting a highly covalent nature of metal-ligand bonds.

Complexes of Mn(II) and Fe(III) are simple paramagnetics. The observed magnetic moments falling in the range of values reported for compounds involving high spin d^5 configuration indicate the presence of this configuration in these complexes. Electronic spectra are also characteristic of high spin d^5 octahedral stereochemistry. In these complexes a band corresponding to $^4A_{1g}(G) \leftarrow {}^6A_{1g}$ transition could not be identified on account of its mixing with the closely spaced band of $^4E_g(G) \leftarrow {}^6A_{1g}$. The energy of $^4E_g(G)$ and $^4A_{1g}(G)$ degenerate states, which are independent of Dq, do not change much relative to the ground term $^6A_{1g}$ as Dq changes and, therefore, their bands in the spectra are not appreciably broadened either by vibronic coupling or by spin-orbit coupling [10]. Consequently, both of these bands generally remain unresolved. The β values reveal the covalent nature of coordinate bonds in the complexes. However, Fe(III) complexes involving sufficient metal-ligand orbital overlap, as indicated by a strong reduction of B relative to the free ion value are more covalent than Mn(II) complexes.

The magnetic moment of $Co(DMATG)Cl_2 \cdot 2H_2O$ seems to fall in the range of Co(II) complexes displaying anomalous behaviour. In spin-paired square planar complexes of divalent cobalt, the total magnetic moment including orbital contribution is expected to be 1.9 B.M. and any high value will lead to the presence of spin-free octahedral complexes along with a square planar compound, whereas low values will lead to low-spin square planar $\rightleftarrows$ octahedral configurational equilibrium. The observed moment of 2.24 B.M. could be accounted for by considering spin-paired square planar $\rightleftarrows$ spin-free octahedral configurational equilibrium. Such complexes are not uncommon

Table III

Magnetic and electronic spectral data for the complexes

Complex	Magnetic moment (μ_{eff}) (B.M.)	Wave number (cm^{-1})	Band assignment	$10Dq$ (cm^{-1})	Racah's parameters (cm^{-1})	Nephelauxetic ratio (β)	LFSE (cm^{-1})
$Cr(DMATG)Cl_3 \cdot 4H_2O$	3.61	16,289 16,667 19,417 21,978 25,316	$^2E_g \leftarrow {}^4A_{2g}(F)$ $^2T_{1g} \leftarrow$ $^4T_{2g}(F) \leftarrow$ $^2T_{2g} \leftarrow$ $^4T_{1g}(F) \leftarrow$	19,417	$B = 551.8$ $C = 2041.6$	0.60	23,300
$Cr(DEATG)Cl_3 \cdot 4H_2O$	3.55	14,286 16,000 18,692 24,691 27,027	$^2E_g \leftarrow {}^4A_{2g}(F)$ $^4T_{2g}(F) \leftarrow$ $^4T_{1g}(F) \leftarrow$	18,692	$B = 666.9$ $C = 2097.5$	0.62	22,430
$Mn(DMATG)_2Cl_2 \cdot 2H_2O$	5.64	17,397 19,048 20,619 32,258 45,455	$^4T_{1g}(G) \leftarrow {}^6A_{1g}$ $^4T_{2g}(G) \leftarrow$ $^4E_g(G) \leftarrow$ $^4T_{1g}(P) \leftarrow$ M Charge transfer $\leftarrow$ L	9,971	$B = 724.6$ $C = 2536.0$	0.76	—
$Mn(DEATG)_2Cl_2 \cdot 2H_2O$	5.73	16,129 18,519 19,608 20,833 22,727d 24,390 27,390 29,850	$^4T_{1g}(G) \leftarrow {}^6A_{1g}$ $^4T_{2g}(G) \leftarrow$ $^4E_g(G) \leftarrow$ $^4T_{2g}(D) \leftarrow$ $^4E_g(D) \leftarrow$ $^4T_{1g}(P) \leftarrow$ $^4A_{2g}(F) \leftarrow$ $^4T_{1g}(F) \leftarrow$	7,393	$B = 672.0$ $C = 2352.0$	0.70	—
$Fe(DMATG)_2Cl_3$	5.78	18,692 19,418 20,619 27,778 29,851	$^4T_{1g}(G) \leftarrow {}^6A_{1g}$ $^4T_{2g}(G) \leftarrow$ $^4E_g(G) \leftarrow$ $^4T_{1g}(P) \leftarrow$ $^4A_{2g}(F) \leftarrow$	8,567	$B = 778.8$	0.60	
$Fe(DEATG)_2Cl_3$	5.65	17,391 18,349 19,048 23,529 24,691 28,169 30,030	$^4T_{1g}(G) \leftarrow {}^6A_{1g}$ $^4T_{2g}(G) \leftarrow$ $^4E_g(G) \leftarrow$ $^4T_{2g}(D) \leftarrow$ $^4E_g(D) \leftarrow$ $^4T_{1g}(P) \leftarrow$ $^4A_{2g}(F) \leftarrow$	7,971	$B = 724.6$	0.56	—
$Co(DMATG)Cl_2 \cdot 2H_2O$	2.24	12,195 16,667 19,048 24,096sh 26,667 37,037	$^2E_g(F) \leftarrow {}^4T_{1g}(F)$ $^4A_{2g}(F) \leftarrow$ $^4T_{1g}(P) \leftarrow$ M $\leftarrow$ L Charge transfer	9,093	$B = 866.0$ $C = 3377.4$	0.89	5,456
$Co(DEATG)Cl_2$	4.40	12,821 16,109 19,048 24,691 27,027 37,037	$^2E_g(F) \leftarrow {}^4T_{1g}(F)$ $^4A_{2g}(F) \leftarrow$ $^4T_{1g}(P) \leftarrow$ M $\leftarrow$ L Charge transfer	8,593	$B = 840.6$ $C = 3278.3$	0.87	5,156

Table III (contd.)

Complex	Magnetic moment ($\mu_{eff.}$) (B.M.)	Wave number (cm^{-1})	Band assignment	10 Dq (cm^{-1})	Racah's parameters (cm^{-1})	Nephelauxetic ratio (β)	LFSE (cm^{-1})
$Ni(DMATG)_2Cl_2$	2.15	11,765	$^3T_{2g}(F) \leftarrow {}^3A_{2g}$	11,765	$B = 571.0$	0.55	14,118
		17,544	$^3T_{1g}(F) \leftarrow$		$C = 2569.5$		
		24,096	$^1E_g(D) \leftarrow$				
		26,316	$^3T_{1g}(P) \leftarrow$				
		36,364	M Charge transfer $\leftarrow$ L				
$Ni(DEATG)_2Cl_2$	2.67	10,989	$^3T_{2g}(F) \leftarrow {}^3A_{2g}$	10,989	$B = 632.0$	0.61	13,187
		16,807	$^3T_{1g}(F) \leftarrow$		$C = 2844.0$		
		22,478	$^1E_g(D) \leftarrow$				
		25,641	$^3T_{1g}(P) \leftarrow$				
		36,364	M Charge transfer $\leftarrow$ L				
$Cu_2(DMATG)Cl_4 \cdot 8H_2O$	1.84	16,667	$^2A_{1g} \leftarrow {}^2B_{1g}$	—	—	—	—
		17,857	$^2E_g \leftarrow$				
		18,692sh					
		32,787	M Charge transfer $\leftarrow$ L				
$Cu(DEATG)(OH)Cl$	1.92	15,625	$^2A_{1g} \leftarrow {}^2B_{1g}$	—	—	—	—
		17,241	$^2E_g \leftarrow$				
		18,868					
		20,408					
		32,787	M Charge transfer $\leftarrow$ L				
$Au(DMATG)Cl_3 \cdot H_2O$	Diamag.	17,544	$^3A_{2g} \leftarrow {}^1A_{1g}$	—	—	—	—
		19,231	$^1A_{2g} \leftarrow$				
		23,809	$^1B_{1g} \leftarrow$				
		25,974					
		31,428	$^1A_{2u} \leftarrow$				
		42,735	$^1E_u \leftarrow$				
$Au(DEATG)Cl_3 \cdot 3H_2O$	Diamag.	16,260	$^3A_{2g} \leftarrow {}^1A_{1g}$	—	—	—	—
		20,408b	$^1A_{2g} \leftarrow$				
		25,000	$^1B_{1g} \leftarrow$				
		26,667					
		32,258	$^1A_{2u} \leftarrow$				
		44,444	$^1E_u \leftarrow$				

d — doublet; sh — shloulder; b — broad.

[11—14]. Magnetic moment of $Co(DEATG)Cl_2$ is typical of Co(II) compounds with tetrahedral symmetry. The assumed tetrahedral geometry of the complex is, of course, a simplification, however, it seems justified to assume tetrahedral $\rightleftharpoons$ octahedral configurational equilibrium on account of the $\mu_{eff.}$ value higher than the spin-only value of 3.87 B.M. Although $\mu_{eff.}$ values, which are consistent with IR and analytical results, indicate anomalous behaviour of the solid complexes, the electronic spectra of their solutions are characteristic [11—15] of an octahedral Co(II) ion. Assignment of bands and ligand field parameters as calculated by Konig's equations [9], are noted in Table III.

For high-spin tetrahedral or tetragonally distorted octahedral nickel(II) complexes, the magnetic moments, in general, are higher (> 3.4 B.M.) than those for high-spin octahedral compounds (< 3.4 B.M.); square planar complexes are diamagnetic. In complexes exhibiting moments between zero and 2.8 B.M., most probably, spin-free $\rightleftharpoons$ spin-paired equilibrium occurs involving either square planar-octahedral or square planar-tetrahedral geometries. The low magnetic moment values, viz. 2.15 B.M. and 2.67 B.M. are consistent with low-spin square planar $\rightleftharpoons$ high-spin octahedral equilibrium in both $Ni(DMATG)_2Cl_2$ and $Ni(DEATG)_2Cl_2$. Although, magnetic results indicate both solids to be equilibrium mixtures of octahedral and square planar forms, electronic spectra display patterns characteristic [11, 16, 17] of octahedral nickel(II). Electronic spectral results are corroborated by molar conductance data. Racah's interelectronic repulsion parameters and nephelauxetic ratios calculated by standard methods [9] reveal a highly covalent character of nickel-ligand bonds in the octahedral complexes.

For perfectly tetrahedral copper(II) compounds having a degenerate ground state, crystal field theory predicts large orbital contributions to the spin-only value and the magnetic moment should be about 2.20 B.M., whereas distorted tetrahedral complexes should have lower values of $\mu_{eff.}$ (2.00 B.M.). However, in planar complexes which do not have a degenerate ground state, the $\mu_{eff.}$ values are close to the spin-only value. The magnetic moments of the present complexes indicate [16] their square planar geometry. In electronic spectra of the complexes, the first two bands, corresponding to characteristic crystal field transitions [18—20] of a square planar geometry, indicate this configuration in them.

The diamagnetism exhibited by Au(III) complexes is indicative of their low-spin square planar configuration as usual. Splitting patterns of the first four bands in the electronic spectra confirms square planar stereochemistry of both the complexes. Based on the fact that in square planar complexes of d^8 configuration involving ligands having no π orbitals, two ligand $\rightarrow$ metal charge transfer bands are spaced at energy difference of 10,000 cm^{-1}, the last two bands of high intensity can be assigned [21] to spin-allowed charge transfer transitions $^1A_{2u} \leftarrow {}^1A_{1g}$ and $^1E_u \leftarrow {}^1A_{1g}$, respectively.

*

We are grateful to Dr. G. S. Vashishtha, Principal, N.R.E.C. College, Khurja, for providing facilities needed in this work. One of us (K.R.) extends thanks to C.S.I.R., New Delhi, for the award of J.R.F.

REFERENCES

[1] Upadhyay, R. K.. Rathore, K., Bajpai, A. K.: Tran. Met. Chem., **10,** 24 (1985)
[2] Bajpai, A. K.: Ph. D. Thesis, Meerut University, Meerut, India (1983)
[3] Upadhyay, R. K., Kumari, V., Singh, V. P.: J. Liq. Chromatogr., **5,** 1141 (1982)
[4] Coakley, M. P. et al.: J. Inorg. Nucl. Chem., **31,** 1449 (1969); **34,** 1937 (1972)
[5] Kuma, H., Motobe, K., Yamada, S.: Bull. Chem. Soc. Japan, **51,** 2489 (1978); **51,** 1101 (1978)
[6] Upadhyay, R. K.: Chromatographia, **11,** 197 (1978)
[7] Nakamoto, K.: Infrared Spectra of Inorganic and Coordination Compounds, Wiley, New York 1963
[8] Figgis, . N.: Introduction to Ligand Fields, Interscience, New York 1966
[9] Konig, E.: Structure and Bonding, Vol. **9,** p. 175, Springer-Verlag, Berlin 1971
[10] Dunn, T. M., McClure, Pearson, R. G.: Some Aspects of Crystal Field Theory p. 47 1965.
[11] Sinha, B. K., Singh, R., Srivastava, J. P., Misra, L. K.: J. Inorg. Nucl. Chem., **39,** 1797 (1977)
[12] Williams, D. L., Smith, D. W., Stoufer, R. C.: Inorg. Chem., **6,** 590 (1967)
[13] Figgis, B. N., Nyholm, R. S.: J. Chem. Soc., **1954,** 12
[14] Zaidi, S. A. A., Neyazi, M. A.: Tran. Met. Chem., **4,** 164 (1979)
[15] Tanabe, Y., Sugano, S.: J. Phys. Soc. Japan, **4,** 293 (1949)
[16] Ali, M. A., Tarafdar, M. T. H.: J. Inorg. Nucl. Chem., **39,** 1785 (1977)
[17] Lever, A. B. P.: Inorganic Electronic Spectroscopy, Elsevier, Amsterdam 1968
[18] Ali, M. A., Livingstone, S. E., Phillips, D. J.: Inorg. Chim. Acta, **5,** 119 (1971)
[19] Meeks, M. J., Flackler, J. P.: Inorg. Chem., **7,** 2548 (1968)
[20] Sacconi, L., Bertini, I.: Inorg. Chem., **5,** 1521 (1966)
[21] Gray, H. B., Ballhausen, C. J.: J. Amer. Chem. Soc., **85,** 260 (1968)

Acta Chimica Hungarica 121 (3), pp. 291—303 (1986)

INVESTIGATIONS ON THE THERMAL PROPERTIES OF TWO NEW PLANT-PROTECTING AGENTS OF DIFFERENT TYPES

Teréz FLÓRA

(Research Institute for Heavy Chemical Industries, H-8201 Veszprém, Wartha V. u. 1—3.)

Received October 3, 1984
Accepted for publication May 22, 1985

Derivatographic investigations were carried out on plant-protecting agents of different types developed in NEVIKI, such as phosmethylane (*O,O*-dimethyl-*S*-(*N*-2-chlorophenylpropane-1-carboxylamidomethyl)dithiophosphate) with insecticide activity, having the commercial name Nevifosz, and *N*-phenylphthalaminic acid with hormone activity (commercial name: Nevirol). By analyzing the decomposition products (IR spectra, elemental analysis, determination of the melting point) the thermal processes taking place were elucidated. The kinetic parameters of thermal dissociation (E, n, $\tau_{1/2}$) were calculated and determined for both compounds from the data of curves recorded with continuous heating and under isothermal conditions. The curves recorded for phosmethylane under isothermal conditions show that the heat liberated during the polymerization process overlapping thermal dissociation, affects the temperatures produced by the heating and thus the activation energy calculated from the temperature data.

Introduction

Successful application of thermal analysis in the chemistry of plant-protecting agents has been reported in several papers. Thermal analysis has been employed with good results in research aiming at the synthesis of plant-protecting agents, for qualitative and quantitative analysis of the products, for studying the reactions taking place between the individual components under heating and for the determination of solubility [1—11].

It is important to know the mechanism of the thermal decomposition of plant-protecting agents. On one hand, new, effective plant-protecting agents can be obtained on thermal treatment; on the other hand, the protection of environment also demands the knowledge of the stability of plant-protecting agents, their important decomposition reactions, the persistency [12], the time required for their decomposition and the nature of the decomposition products.

In the present paper, the thermal decomposition and the kinetics of decomposition of two new plant-protecting agents developed in our institute will be discussed; these are *N*-phenylphthalaminic acid (commercial name: Nevirol) with hormone activity, and a phosphoric ester insecticide *O,O*-dimethyl-*S*-(*N*-2-chlorophenylpropane-1-carboxylamidomethyl)-dithiophosphate (proposed common name of the active ingredient is phosmethylane, the product containing this substance has the commercial name Nevifosz).

Literature review

Thermal isomerization of alkyl thiophosphates of the phosphoric ester type has been known for a long time. In 1911, Emmett and Jones [13] described the isomerization of *O,O,O*-trimethyl thiophosphate and the corresponding triethyl esters:

Schrader [14] reported a similar reaction in the case of parathion (*O,O*-diethyl-*O*-(4-nitrophenyl)-thio-phosphate), which occurred on heating of the insecticide to 130—140 °C. The same reaction was the basis of the patent claimed by Morril [15], dealing with the preparation of the *S*-ethyl isomer of parathion, having a high insecticide activity, the procedure included heating of parathion at 160—170 °C for 10 h. Metcalf and March [16] heated a parathion methyl homologue at 150 °C for 3.5 h to obtain a yellow viscous liquid with a mercaptan-like odour. When heating was effected for 24 h, two phases were obtained: a very volatile mobile liquid and a solid fraction. Similar phases appeared on heating of the isopropyl homologue of parathion at 150 °C for 3 h. During the thermal treatment of purified parathion at 150 °C for 24 h, the presence of eight compounds could be detected chromatographically: five of them could be identified:

(1) *O*-ethyl-*O,O*-bis(*p*-nitrophenyl thiophospate)
(2) *O,O*-diethyl-*O*-(4-nitrophenyl) thiophosphate (parathion)
(3) *O,S*-diethyl-*O*-(4-nitrophenyl) thiophosphate
(4) diethyl-4-nitrophenyl phosphate
(5) *p*-nitrophenol

McPhusin et al. [17] stated that the decomposition of the methyl homologue of parathion takes place in two steps, the first of them results in the formation of a mixture of dimethyl sulfide, sulfur dioxide and mixed polyaryl metaphosphates.

In our Institute, thermal decomposition of several effective substances of the phosphoric ester type has been studied. Thermal properties of fosmet (*S*-(*N*-phthalimidomethyl)*O,O*-dimethyldithiophosphate) have been investigated on a derivatography [8]. It was stated that the decomposition process starts with isomerization. This is followed by the split-off of the methyl groups and simultaneous polymerization at 210 °C, while a polymeric compound containing S—S and P—O—P bonds is formed. Further decomposition, after the cleavage, of the S—S, P—S and C—N bonds (at about 310 °C) yields phthalimide and polyphosphoric acid. The other compound examined [18] was

ditalimphos (*O,O*-diethylthiophosphoric phthalimide) being more stable than fosmet: in the first process characterized by the peak temperature 260 °C, the split-off of the ethyl groups takes place simultaneously with the cleavage of the P—N bond. The decomposition of this compound results in the formation of polyphosphoric acids and phthalimide. Phthalimide and the polyphosphoric acids react with each other, yielding new compounds at a temperature nearly identical with that of the decomposition.

Beyond the compounds of phosphoric ester type listed above, the thermal decomposition and its kinetics have been investigated in the case of trichlorophon (*O,O*-dimethyl-1-hydroxy-2,2,2-trichloroethyl phosphonate), too. The compound melts at about 80 °C, after melting, decomposition starts and consists of two steps. According to literature data [21], in the first step the decomposition yields dichlorophos (*O,O*-dimethyl-2,2-dichlorovinyl phosphate) via the release of hydrochloric acid. In connection with the thermal properties of compounds of the phosphoric acid type, let us mention the results obtained in studies on the thermal decomposition of the effective agent glyphosate (*N*-phosphonomethylglycine, registered names: Nitosorg or Glialka) [10, 11]: during heating of the substance, polycondensation yielding polyphosphate and internal salt formation take place.

The thermal properties of *N-meta*-tolylphthalic acid (Akperol, in other countries, it is the active ingredient in Duraset or Solanaset preparations) having a structure similar to *N*-phenylphthalaminic acid (active ingredient in the preparation Nevirol) have also been investigated in this Institute [22]. In the first thermal step (DTG peak at 133—164 °C, depending on the experimental conditions) the decomposition product was examined by the IR technique and it was shown that *N-meta*-tolylphthalaminic acid released one molecule of water to yield *N-meta*-tolylphthalimide. The weight loss (8.8—12.8%) during the decomposition is somewhat higher than the theoretical value (7.05%) calculated for the loss of one molecule of water, since the compound melts simultaneously with the decomposition (under microscope with a heated objective plate the m.p. was found to be 159 °C), and slow evaporation starts. The processes, viz. melting, evaporation and decomposition overlap each other. The decomposition product (*N-meta*-tolylphthalimide) is again a solid, melting at 169 °C when measured under microscope having a heated objective plate. This melting process produces a definite, separate peak on the DTA curve.

Experimental

The derivatograms were recorded with a derivatograph of MOM type [23] under various experimental conditions, employing different heating rates, in a stream of nitrogen gas or of air, in a crucible equipped with a platinum top (when employing a stream of nitrogen). Phosmethylan was studied in a thermoceram crucible, too. The sample mass was 100 mg in all cases, after appropriate pulverizing. The derivatograms were transformed into linear temperature scale by the Paulik—Paulik method [24].

The kinetics of decomposition was determined from the curves obtained under continuous heating by the Freeman—Carrol method [25] modified by us, the half-time of the decomposition was calculated at different temperatures by the correlation holding for primary reactions [26]. The kinetics of decomposition was determined under isothermal conditions, too.

The isothermal curves were recorded with a Paulik—Paulik—Erdey derivatograph of MOM type equipped with a temperature regulator [23], using a Cr—Al thermocouple and adjusting the temperature control switch to the temperature desired. The oven was heated first without the sample by a heating program which ensured reaching of the desired constant temperature in a short time. When reaching the stable temperature desired, the oven was lifted and the platinum crucible containing the sample was placed onto the thermocouple holding the sample. Now the oven was rapidly placed back. Quartz beakers were not used. The sample reached the temperature given in about 20—25 minutes. The apparatus simultaneously recorded the weight losses occurring at the given temperature for different periods (TG curve) and the temperature difference observed in the "DTA" circuit (Fig. 3). The calculations on the data of the isothermal curves have already been described in detail earlier [27].

The IR spectra were recorded with a Carl Zeiss UR-10 spectrophotometer.

Sulfur was determined by combustion in a Grote—Krekeler apparatus, precipitation in the form of $BaSO_4$ and gravimetric measurement.

Results and Discussion

a. Studies on thermal properties of phosmethylane

Phosmethylane

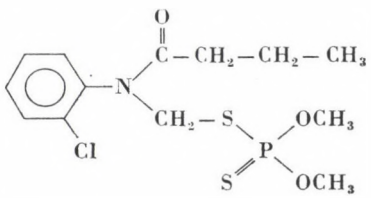

produced derivatograms both in the presence of air and in a stream of nitrogen similar in shape, thus in Fig. 1 only the derivatograms recorded in the presence of air (using different heating rates) are presented. According to the derivatographic DTA curves, the melting of the compound took place at about 50 °C, followed by a step involving evolution of heat (exothermic DTA peak) and loss of weight (DTG peak temperatures appeared at about 160—180 °C, depending on the rate of heating). Starting temperature of weight loss was 80—140 °C. In order to elucidate the thermal processes taking place in the first step, at the end of the step (about 15% loss in weight) the heating was stopped and the IR spectrum of the heating residue was recorded (Fig. 2). It could be established that during heating the CH_2—CH_2—CH_3 fragment remained unaltered (aliphatic chain, 732 cm^{-1} and 2935 cm^{-1}, $\delta_s CH_3$ at 1302 cm^{-1}). In the spectrum of the residue of heating, the band characteristic of secondary amides

appeared at 1520 cm^{-1}, while the bands characteristic of the

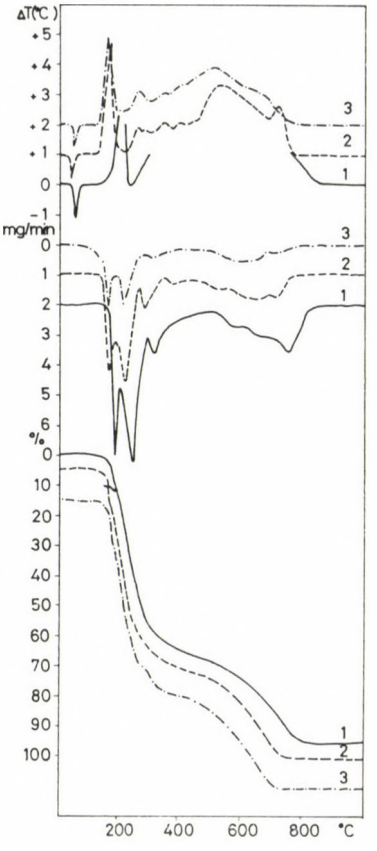

Fig. 1. Derivatograms recorded for phosmethylane in the presence of air, at different heating rates. Curve 1: heating rate: 10 °C/min; Curve 2: heating rate: 5 °C/min; Curve 3: heating rate: 2.6 °C/min

tertiary amide (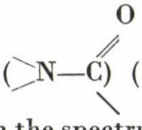) (1650 cm^{-1}) and the N—CH_2— bond (1410 cm^{-1}) disappeared from the spectrum. On the basis of these observations, the splitting took place probably at the —N—CH_2 bond (see the molecular formula). The bands indicating the presence of ortho-substituted aromatic ring could be identified (1060, 1110, 1267 cm^{-1}). According to this, on decomposition of the molecule, a compound with the formula

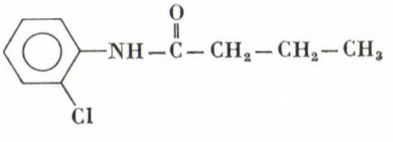

was formed. This compound was available and its IR spectrum was also known. The characteristic IR bands could be recognized in the spectrum of the heating residue and this also confirmed our hypothesis.

The other part of the molecule contained phosphorus: here isomerization took place between the $—OCH_3$ groups containing oxygen and the sulfur atom: the band characteristic of the P=S bond (650 cm^{-1}) disappeared from

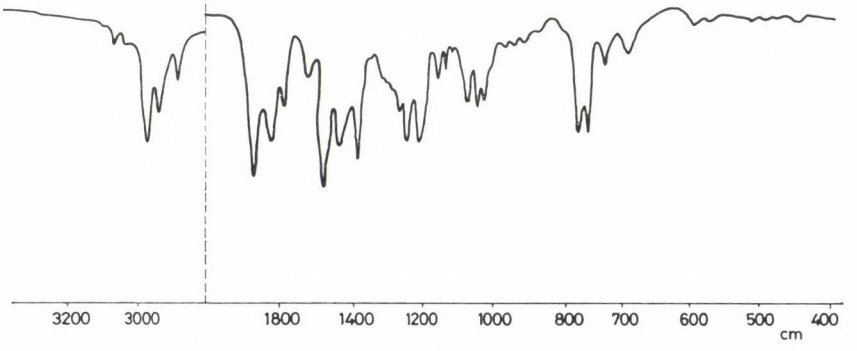

Fig. 2. Infrared spectrum of the heating residue of phosmethylane

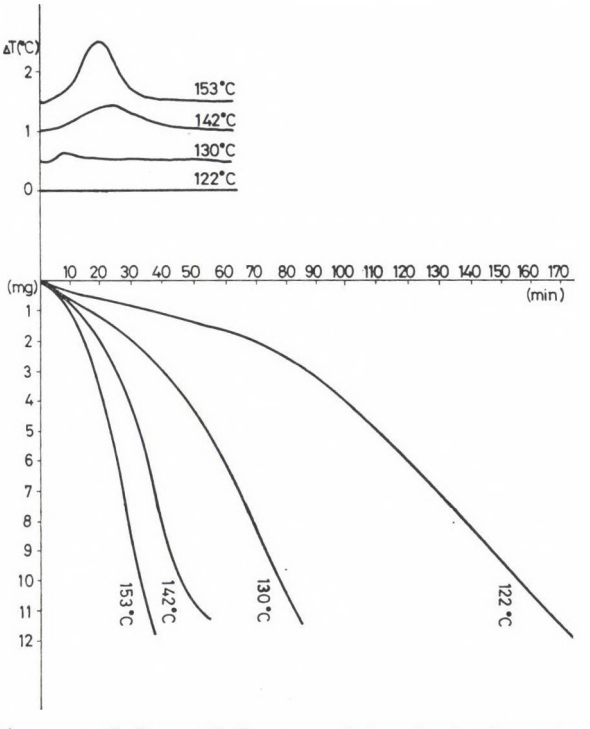

Fig. 3. TG and DTA curves of phosmethylane recorded under isothermal conditions. Sample: 100 mg

the spectrum of the residue of heating and a band characteristic of the P=O bond appeared at 1150 cm^{-1}.

The sulfur content of the heating residue was determined, it was 13.69% in the residue obtained at 14.45% loss of weight. According to this, two sulfur atoms are released from three molecules of the compound. The exothermic peak accompanying the loss of weight also indicates polymerization. On the basis of the sulfur content, polymerization can be assumed as follows:

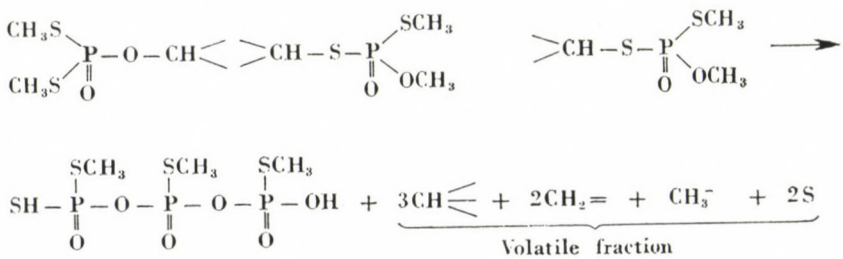

According to this, a polyphosphate would be formed, which, on the basis of our earlier studies on phosphoric esters [18], seemed to be very probable. Formation of mercapto groups is also supported by the odour of the residue characteristic of mercaptanes.

The loss of wieght calculated on the basis of the equation given is 13.2%, which, owing to the slight evaporation of the melt is somewhat lower than the weight loss obtained (15%).

The kinetic parameters obtained for the first step of the decomposition obtained from the curves recorded under continuous heating are shown in Table I.

Table I

Kinetic parameters obtained for phosmethylane from the curves recorded under continuous heating

Heating rate (°C/min)	Activation energy (*E*)		Reaction order (*n*)
	(kcal/mol)	(kJ/mol)	
10	−32.4	−135.5 (thermoceram crucible)	1.0
	−32.7	−136.6	1.0
	−26.4	−110.4	0.7
5	−41.7	−174.6	0.2
Mean value	−33.3	−139.3	
2.6	−14.6	−61.1	−0.6

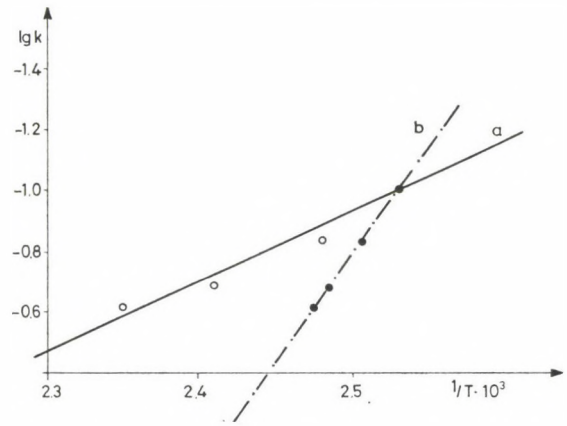

Fig. 4. Kinetic curve obtained from the data from isothermal measurements (phosmethylane a) using the temperature values measured, b) using the temperature values calculated

In the discussion of the mechanism of thermal decomposition it was established that in the first step thermal dissociation, the process of polymerization and, of course, diffusion, overlap each other. Kinetically, the processes can be separated best at the highest heating rate (10 °C/min), where thermal dissociation is predominating: this is indicated by the primary reaction order obtained by the methods suggested by Freeman—Carroll [28]. Varying values were obtained for the activation energy by varying the heating rate, as was observed in earlier research [26], too. It was also stated that the activation energy most characteristic of thermal dissociation (also considering the phenomenon of diffusion) can be obtained at relatively high rates of heating. Therefore, in the following calculations aimed at determination of half-lives, we used the activation energy obtained in a platinum crucible, and at a 10 °C/min heating rate. $E = -32.65$ kcal/mol, and the results were in good agreement with those obtained in thermoceram crucibles, too. Owing to the experimental errors, there are deviating results, too (Table I), but when averaging the results of the first four measurements, a value near the activation energy chosen (—33.28 kcal/mol) is obtained.

The thermal curves obtained in the isothermal measurements "DTA"* and TG are shown in Fig. 3. As shown by the "DTA"* curves, of the overlapping processes, thermal dissociation predominates most strongly in experiments at the lowest temperature (122 °C), since in the measurements at this temperature the exothermic peak disappeared completely on the "DTA"* curve. With increasing temperature, gradually increasing "DTA"* peaks are obtained, owing to incipient polymerization. The kinetic curve obtained from the data

* The temperature difference observed in the "DTA" circuit.

of isothermal measurements is shown in Fig. 4 (curve "a"), the activation energy obtained from its slope (10.09 kcal/mol and 42.24 kJ/mol) is significantly lower than that obtained from any of the heating curves with continuous heating (Table I). This is due to the fact that in the measurements effected at different temperatures the exothermic reaction is effective to different extents (Fig. 3): the temperature observed in the isothermal measurement is usually higher, owing to the occurrence of the polymerization process, than that produced in the presence of thermal dissociation only, and this falsifies the $1/T$ values characteristic of thermal dissociation used in constructing the isothermal kinetic curve (4 "a" curve) and thus the slope of the curve, too. The temperatures originating from heating (taking into account the increase in temperature caused by the exothermic reaction) can be calculated in the knowledge of the activation energy (E) accepted as realistic (136.61 kJ/mol) obtained from the continuous heating curves.

1. When using the correct activation energy (E), the isothermal kinetic curve expected for the thermal dissociation, in accordance with the kinetic equations, will have the slope

$$\mathrm{tg}\alpha = \frac{E}{19.134} = \frac{-136.61}{19.134} = -7.1387$$

Here the value 19.134 is a constant obtained from the universal gas constant ($R = 1.986 \cdot 10^{-3}$), the conversion factor into natural logarithm (2.303) and from kcal into kJ (4.184).

2. Using the slope obtained (Fig. 4, curve b) a straight line was drawn in Fig. 4 across the point established at the lowest temperature measured (122 °C, which corresponds to 2.53 $(1/T)\cdot 10^3$), at which temperature the exothermic effect is the weakest as shown by the "DTA" curve in Fig. 3.

3. In Fig. 4b, the isothermal temperature belonging to various lg k values calculated earlier due to the heating of the sample only (the lg k value was not affected by this condition, since in the calculation of the rate constants, the temperature had no role). The correlated lg k $(1/T)\cdot 10^3$, T (K) (and t (°C)) values are summarized in Table II, taking into account the rise in temperature due to the exothermal reaction (measured values) and without taking into account this reaction (calculated values).

Finally, the half-lives obtained for thermal dissociation at different temperatures from the activation energy (131.61 kJ/mol) which was obtained from the continuous heating curves and accepted as correct (the calculation method is given in Ref. [26]), were compared with the half-lives read from the isothermal curves (Fig. 3) at certain temperatures and presented in Table III.

According to the Table, the half-lives calculated from the curve obtained by continuous heating show satisfactory agreement with the values read from the isothermal curves.

Table II

Temperature values in the isothermal experiments (calculated and measured) (phosmethylane)

log k	$1/T \cdot 10^3$ found	$1/T \cdot 10^3$ calcd.	T (K) found	T (K) calcd.	t (°C) found	t (°C) calcd.
−1.0544	2.53	2.53	395.26	395.26	122.00	122.00
−0.8323	2.48	2.51	403.23	399.04	130.00	126.04
	(2.45)*		(407.00)		(134.00)	
−0.6770	2.41	2.48	414.93	402.90	142.00	129.90
	(2.39)		(418.24)		(145.24)	
−0.6055	2.36	2.47	425.53	404.53	153.00	131.53
	(2.36)		(424.09)		(151.09)	

* The values in parentheses are the theoretical values falling on the curve constructed from the average of the experimental points.

Table: III

Half-life ($\tau_{1/2}$) *of the decomposition of phosmethylan at different temperatures*

Temperature (°C)	$\tau_{1/2}$, calculated from the continuous heating curve	$\tau_{1/2}$ obtained from the isothermal curve
20	$6.48 \cdot 10^2$ years	
50	3.50 years	
75	33.80 days	
100	46.60 h	
122	2.95 h	2.23 h
130	1.22 h	1.12 h
140	22.76 min	39.00 min
153	8.21 min	28.00 min

b. Studies on thermal properties of the Nevirol active ingredient

The active ingredient in Nevirol is N-phenylphthalaminic acid

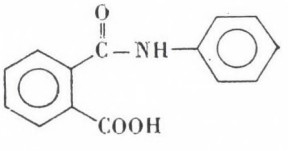

is a long-known compound. However, only the biological experiments supported by NEVIKI revealed its excellent hormone activity [29] and, under Hungarian conditions, it can be produced much more cheaply than the active agent in Akperol, *N-meta*-tolyl-phthalaminic acid, having similar plant-protecting effects.

For the sake of simplicity, of the derivatograms recorded in *N*-phenylphthalaminic acid under various experimental conditions, only the corrected derivatogram recorded at a heating rate of 9.9 °C/min in a stream of nitrogen is presented here (Fig. 5), which is quite identical with the derivatogram of the active agent in Akperol, thus the details of the decomposition process will not be discussed here. From studies on the decomposition of the active substance in Akperol [22], it can be stated that, according to the date of the curve discussed, the decomposition of the active ingredient in Nevirol starts at about 100 °C and takes place at maximum rate at 145 °C, accompanied by the melting of the sample. During the decomposition process, one molecule of water is released to produce *N*-phenylphthalimide, while the molten substance slowly undergoes evaporation. The overlapping processes of evaporation and decomposition are also shown by splitting of the peak in the DTG curve (140—150 °C). According to the DTA curve, *N*-phenylphthalimide is formed during the decomposition and being a solid it melts at 205 °C. This is followed by the sublimation and decomposition of *N*-phenylphthalimide, but further elucida-

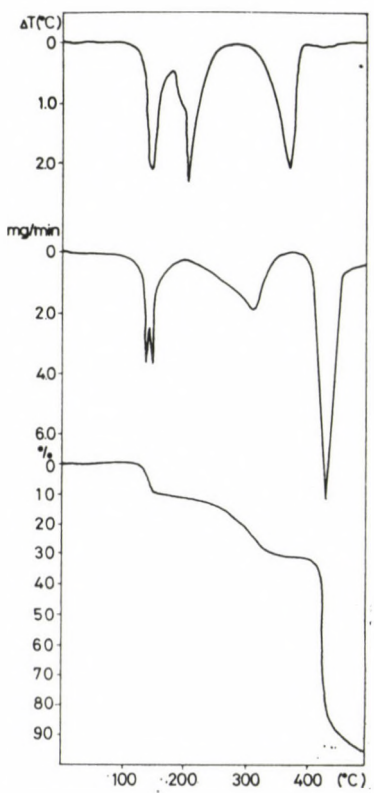

Fig. 5. Derivatogram of *N*-phenylphthalaminic acid (in a stream of nitrogen, heating rate 9.9 °C/min)

Table IV

Kinetic data obtained for N-phenylphthalaminic acid from the continuous heating curve

Heating rate (°C min)	E (kcal/mol)	E (kJ/mol)	n
9.9	−33.7	−140.9	1
6.6	−30.4	−127.2	1
5.3	−32.1	−134.4	1
Mean value	−33.9	−134.2	

Table V

Half-life ($\tau_{1/2}$) of the decomposition of the active ingridient in Nevirol, at different temperature

Temperature (°C)	Half-life
20	47.3 years
50	10.6 weeks
75	1.7 days
100	1.5 h
120	8.6 min
130	3 min

tion of this process was beyond the scope of the present work. The further course of the derivatogram shows, however, that the DTA and DTG curves are not concerted: there are complex processes involving changes in weight, accompanied partly by endothermic, partly by exothermic effects. When combining them it can be stated that, for example, only a very slight endothermic effect belongs to the decomposition process taking place at maximum rate 430 °C (Fig. 5, DTA curve), while at 370 °C the DTA curve indicates a physical change not accompanied by a change in weight.

The kinetic data regarding the decomposition of the active agent in Nevirol obtained from the continuous heating curves (activation energy and reaction order) are shown in Table IV.

In order to check the values of activation energy obtained under continuous heating, the activation energy was also determined from the isothermal curves. The isothermal measurements required in the determination of the rate constants were carried out at two temperatures, 120 and 130 °C only, in the presence of air, for orientation purposes. The isothermal curve yielded 30.71 kcal/mol for the activation energy of the decomposition which — in view of the low number of points recorded — can be considered as to be in satisfactory agreement with the results obtained from the continuous heating curves. In

the next step, the half-life in the decomposition of the compound was calculated using the activation energies (mean) obtained from the continuous heating curves. The half-lives for the different temperatures are shown in Table V.

REFERENCES

[1] Flóra, T.: Z. Anal. Chem., **207,** 345 (1965)
[2] Flóra, T., Almásy, A.: Acta Chim. Acad. Sci. Hung., **54,** 189 (1967)
[3] Flóra, T.: Nehézvegyip. Kut. Int. Közl., **3,** 99 (1966)
[4] Flóra, T.: Hung. Sci. Instrum., **19,** 3 (1970)
[5] Pfeifer, Gy., Flóra, T.: Acta Chim. Acad. Sci. Hung., **52,** 223 (1967)
[6] Flóra, T., Pfeifer, Gy.: 3rd Analytical Conference, August 1970, pp. 24—29. Akadémiai Kiadó, Budapest
[7] Flóra, T.: 3rd Analytical Conference, August 1970. p. 357. Akadémiai Kiadó, Budapest
[8] Pfeifer, Gy., Flóra, T.: Nehézvegyip. Kut. Int. Közl., **4,** 175 (1972)
[9] Pfeifer, Gy., Flóra, T., Kovács, M.: Nehézvegyip. Kut. Int. Közl. **4,** 143 (1972)
[10] Flóra, T., Simon, Z.: Magy. Kém. Folyóirat, **87,** 419 (1981)
[11] Flóra, T., Simon, Z.: Thermochim. Acta, **59,** 125 (1982)
[12] Pfeifer, Gy.: Magy. Kém. Lapja, **32,** 186 (1977)
[13] Emmett, W. C., Jone, H. O.: J. Chem. Soc., **99,** 713 (1911)
[14] Coates, H., Toply, B.: PB **95,** 312 (B. 10S 1808) "Synthetic Insecticides" interrogation of Gerhard Schrader, 1947. Technical Information and Document Unit, Mo. Cadogan Square, London, S. W. 1.
[15] Morrill, M. L.: U. S. Patent 2,601,219 (June 17, 1952)
[16] Metcalf, R. L., March, R. B.: J. Econ. Entomol., **46,** 288 (1953)
[17] McPhuson, J. B., Johnson, G. A.: Agric. Food Chem., **4,** 42 (1956)
[18] Flóra, T., Simon, Z., Bokor-Lanszky, E.: Nehézvegyip. Kut. Int. Közl., **11,** 105 (1981)
[19] Flóra, T., Choinka, A.: Nehézvegyip. Kut. Int. Közl., **4,** 179 (1972)
[20] Flóra, T.: Magy Kém. Lapja, **28,** 278 (1973)
[21] Mattson, A. M.: J. Agric. Food Chem., **3,** 319 (1953)
[22] Flóra, T., Pfeifer, Gy.: IX. Dunántúli Analitikai Konferencia, Szombathely, 1973 (lecture)
[23] Paulik, F., Paulik, J., Erdey, L.: Z. Anal. Chem., **160,** 241 (1958)
[24] Paulik, J., Paulik, F.: Per. Polytechn. Chem. Eng., **14,** 141 (1970)
[25] Flóra, T.: Acta Chim. Acad. Sci. Hung., **48,** 225 (1966)
[26] Flóra, T.: Magy. Kém. Lapja, **36,** 623 (1981)
[27] Gór Nagy S., Bésán, J., Flóra, T., Szántó, A.: Magy. Kém. Lapja, **32,** 169 (1977)
[28] Freeman, E. S., Carroll, B.: J. Phys. Chem., **62,** 394 (1958)
[29] Pfeifer, Gy., Kovács, M., Prágai, I., Nádasy, M.: Nehézvegyip. Kut. Int. Közl., **6,** 21 (1976)

Acta Chimica Hungarica 121 (3), pp. 305—312 (1986)

PHOTOEVOLUTION OF HYDROGEN FROM WATER ON MODIFIED TiO_2, II

METALLIC IRON, COBALT AND NICKEL ON TiO_2

Stanisław ZIELIŃSKI* and Andrzej SOBCZYŃSKI

(Laboratory of General Chemistry and Catalyst Synthesis, Faculty of Chemistry, A. Mickiewicz University, 60-780 Poznan, Poland)

Received December 17, 1984
In revised from April 9, 1985
Accepted for publication May 22, 1985

TiO_2-samples with admixtures of metallic iron, cobalt and nickel were prepared by the reduction of Fe_2O_3, Co_3O_4 and NiO-doped samples in hydrogen at higher temperatures. Some of the catalysts were studied by means of X-ray diffraction and specific surface areas were measured. Composition studies show incomplete reduction of iron, cobalt and nickel to metals. The activity of the samples in hydrogen photogeneration from 0.01 *M* EDTA increases in the order $Co/TiO_2 < Fe/TiO_2 < Ni/TiO_2$.

A possible explanation of the difference in activity is given. The influence of pH of reaction medium and of various electrolyte solutions on H_2 photogeneration was also studied.

Introduction

A great number of papers has been devoted to properties of metallic platinum supported on various semiconductors in the reaction of photoassisted hydrogen evolution from water. Refs. [1—10] represent some examples. Other noble metals have also been studied as catalysts for the above process [11—15]. Only a few papers, however, deal with the application of other transition metals, which could replace the very expensive noble metals as the catalysts for hydrogen evolution. Sakata and Kawai [16] observed hydrogen photoevolution from a mixture of ethanol and water on Ni/TiO_2. The activity of this catalyst was about six times lower than that of Pt/TiO_2. A systematic study of photoassisted hydrogen evolution from aliphatic alcohols on Ni/TiO_2 was carried out by Prahov et al. [17]. The authors established the influence of nickel content and degree of metal reduction on the rate of hydrogen production. Lehn et al. [11] observed slow hydrogen and oxygen evolution from irradiated slurry of $Co/SrTiO_2$ in water. Moreover, metallic iron on titania has been used as a catalyst for ammonia photoproduction from water and nitrogen [18—21].

The present paper deals with the influence of metallic iron, cobalt and nickel admixtures on the rate of hydrogen evolution on TiO_2 from an illuminated of 0.01 *M* EDTA solution in water.

* To whom correspondence should be addressed.

Experimental

Metal-covered TiO_2 was prepared by reduction of Fe_2O_3, Co_3O_4, and NiO-doped samples (preparation of which was described in Part I of this article [22]) in a stream of hydrogen at elevated temperatures for 6 hours. The temperatures were: 673 K for Ni/TiO_2 and 773 K for Fe/TiO_2 and Co/TiO_2.

Methods of characterization of the samples: specific surface area measurements, X-ray diffraction analysis, a composition study and hydrogen evolution experiments were described previously [22].

The incident light flux, measured by oxalate-uranyl actinometry [23] was assumed to be 7.2×10^{-2} μmol of quanta per second for the 366 nm wavelength and 11.5×10^{-2} μmol of quanta per second for the whole spectrum of a medium pressure mercury lamp.

Results and Discussion

Catalysts characterization

As it was mentioned in the Experimental, three series of metal-covered TiO_2 were used for this study: Fe/TiO_2, Co/TiO_2 and Ni/TiO_2. The amounts of dopants are listed in Table I. These values are related to the amount of oxides of iron, cobalt and nickel before reduction of the samples. Precise amount of iron, cobalt and nickel are not known owing to the only partial reduction of the appropriate oxide (see below). The use of various temperatures for sample reduction (viz. 673 K for Ni/TiO_2, 773 K for Fe/TiO_2 and Co/TiO_2) was due to the impossibility of the reduction of Co_3O_4/TiO_2 and Fe_2O_3/TiO_2 at 673 K. Specific surface areas of metal-covered titania (see Table I) are a little lower than that of pure TiO_2 and decrease with increasing reduction temperature. X-ray diffraction spectra of the samples with the highest metal loading show only lines characteristic of anatase, similarly as it is in the case of samples doped with the appropriate oxide [22]. A composition study (dissolution in a boiling, concentrated HCl followed by atomic spectroscopy measurements)

Table I

Data on the samples investigated and their photoactivity in hydrogen evolution from water

Catalyst	Amount of dopant (wt.%) xx	Solubility of dopant (%)	Sp. surface area ($m^2\,g^{-1}$)	Rate of hydrogen evolution ($\mu mol\,s^{-1}\times10^4$)	Rate of hydrogen evolution ($cm^3\,h^{-1}\times10^3$)	Quantum efficiency (%)
TiO_2	—	—	128	1.8	14.7	0.50
Fe/TiO_2 (1)	0.5	x	90	3.1	25.0	0.86
Fe/TiO_2 (2)	1.0	58	85	3.8	30.5	1.06
Fe/TiO_2 (3)	2.0	x	88	4.4	35.5	1.23
Co/TiO_2 (2)	1.0	72	82	1.3	10.9	0.38
Co/TiO_2 (3)	2.0	x	82	2.4	19.3	0.69
Ni/TiO_2 (1)	0.5	x	106	16.2	130.6	4.50
Ni/TiO_2 (2)	1.0	54	112	25.1	101.4	7.00
Ni/TiO_2 (3)	2.0	x	107	22.0	177.4	6.10

x — the solubility of dopant was not measured.
xx — this value is referred to the amount of metal oxide before reduction of the samples.

performed for the samples of Fe/TiO_2 (2), Co/TiO_2 (2) and Ni/TiO_2 (2) revealed that only a fraction of Fe_2O_3, Co_3O_4 and NiO has been transformed to the corresponding metal during heating in hydrogen. The colour of the residue after dissolution in hydrochloric acid was similar to that of Fe_2O_3, Co_3O_4 and NiO-doped titania, which additionally confirms that only a part of introduced foreign oxide underwent reduction. However, the solubility of dopants is somewhat higher than in the case of oxide-doped TiO_2 [22]. This indicates that during annealing in hydrogen not only the "islands" of foreign oxides but a part of Fe_2O_3, Co_3O_4 and NiO, which reacted with TiO_2 (probably on the surface or near the surface of the last), were also reduced to metals. The above results allow us to state that, although there is no direct evidence, our samples consist of TiO_2 grains with a thin layer of a solution of Fe_2O_3, Co_3O_4 and NiO on or near the surface of titania and of a layer of metallic iron, cobalt and nickel, respectively, on the surface.

Hydrogen evolution from a solution of EDTA in water

Activity of the metal-covered samples was studied in a photo-accompanied reaction of hydrogen production from 0.01 *M* EDTA solution in water. The measurements were performed at 298 K in flowing argon (oxygen free) and under illumination with light of 366 nm wavelength. Rates of hydrogen production and quantum efficiencies on metal-covered TiO_2 and, for comparison, on pure TiO_2 are listed in Table I. These values correspond to the steady state of the photoreaction, i.e. proceeding after the initial step (see Figs 1 and 3).

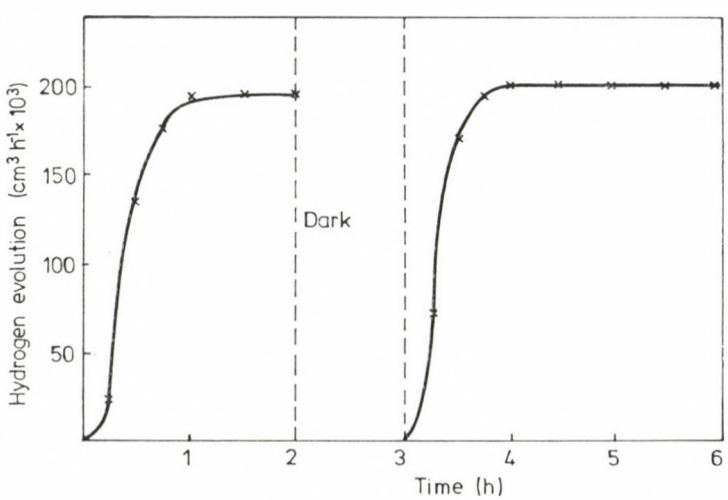

Fig. 1. Light induced water decomposition. Volume of H_2 produced on Ni/TiO_2(2) in 0.01 *M* EDTA as a function of irradiation time

The data given in Table I show that the presence of metallic nickel distinctly improves the photoactivity of titania. Metallic iron increases the activity of TiO_2 to a much smaller extent; the influence of cobalt is negligible. We should add here that the activity of Pt/TiO_2, which is the most widely used as a photocatalyst for water splitting, is about four times higher than that of the most active Ni/TiO_2 (2) sample under the same conditions (0.01 *M*

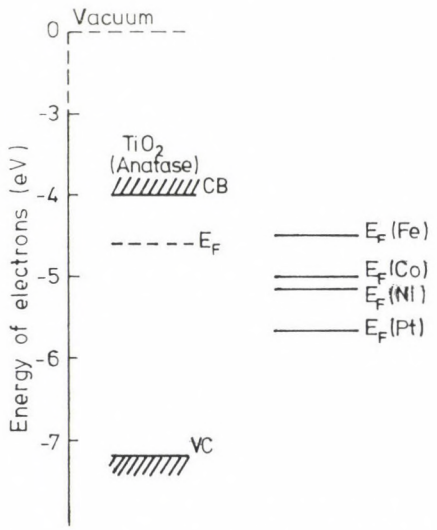

Fig. 2. Work functions of metallic iron, cobalt, nickel and platinum, band edges and Fermi level of TiO_2-anatase under illumination

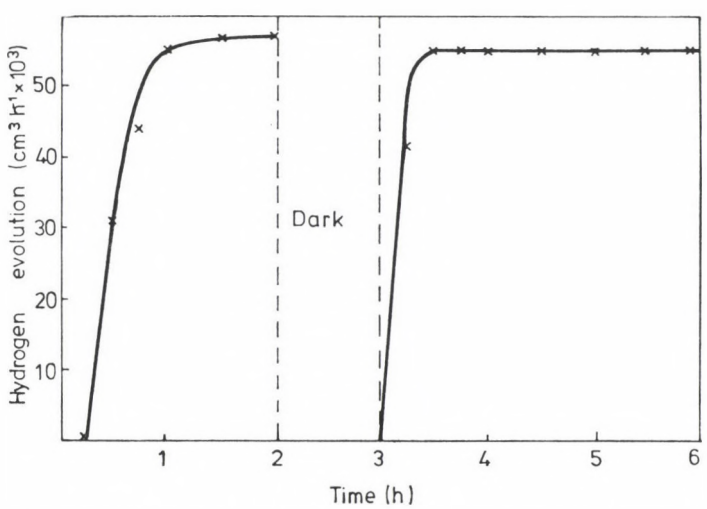

Fig. 3 Light induced water decomposition. Volume of H_2 produced on Ni/TiO_2(2) in 1.0 *M* NaOH as a function of irradiation time

EDTA, 366 nm wavelength) [24]. The question is why various metals have very different effects on hydrogen generation. Let us consider the influence of some factors on the photoactivity of Me/TiO_2. Anatase-TiO_2 is an n-semiconductor with a band gap of 3.2 eV. The electron affinity of titania is about 4.0 eV and its Fermi level under illumination amounts to about 4.6 eV in vacuum [25]. Work functions of powdered metals: Pt, Fe, Co and Ni are 5.65, 4.5, 5.0 and 5.15 eV, respectively [26]. Figure 2 shows the work functions and electron affinity for the discussed metal—semiconductor junctions (authors omitted a band bending of titania in contact with electrolyte). It is clear that when Pt, Co or Ni are in contact with TiO_2, electrons flow from the n-semiconductor to the metal (the Fermi level in TiO_2 before the contact is higher than that in the metal) [27]. Such systems (metal/TiO_2) can be considered as short-circuited photoelectrochemical cells in which small islets of metal play the role of a cathode [28]. When such n-semiconductors are illuminated in the presence of water with a light of energy equal to or higher than the band gap of TiO_2, hydrogen is evolved on the metal. We can see from Fig. 2 that Pt, Co and Ni can play role of the cathode if they are connected with TiO_2. In the case of iron, however, the position of the Fermi level is similar to that of TiO_2 and it is not clear in what direction the electrons flow.

To support our considerations we can add that, according to literature data the three metals regarded here (Co, Ni, Pt) are in SMSJ state if they are deposited onto TiO_2 particles in a way similar to that described in the Experimental [2, 29, 30]. Such strong metal-support interaction leads to a negative charge on the metal [2, 30, 31] and changes the adsorptive and catalytic properties of the supported metals [32—35]. Very distinct SMSJ effect was found for Ni/TiO_2 [30, 33—35] and Pt/TiO_2 [2, 30, 31]. In the case of iron on TiO_2 the existence of SMSJ is limited to samples reduced in hydrogen at high temperature (above 770 K). Moreover, the SMSJ between iron and TiO_2 can be partially destroyed by exposing the sample to air at room temperature [36, 37].

Let us recall here that for our catalysts the photoactivity increases in the order Co < Fe < Ni ($\ll$ Pt), at the same time the work functions of the metals change in the order Fe < Co < Ni ($\ll$ Pt.).

The second factor which can influence the activity of metals in this reaction is the overvoltage of hydrogen evolution. Although this factor seems to be the most important in the process of hydrogen evolution, the overvoltages for Fe, Co and Ni are very close [38] (the hydrogen overvoltage of Pt, which is the best catalyst for hydrogen evolution, is very small indeed) and should not have much influence on the activity of our supported metal catalyst.

The third factor results from the nature of our catalysts. As was mentioned above, only part of the dopant oxide (i.e. Fe_2O_3, Co_3O_4 and NiO) was reduced to the metal. The rest forms solid solutions or some compounds with the TiO_2 support. It seems to be likely that the solid solution of iron, cobalt or

nickel oxides in TiO_2 (or any new phase) retards the activity, similarly as was observed for Fe_2O_3/TiO_2, Co_3O_4/TiO_2 and NiO/TiO_2 [22].

The influence of Ni^{2+} ions on the properties of TiO_2 has been studied [39, 40, 41]. It was found that nickel additives caused the drop of electrical conductivity [39] and lowered the quantum efficiency of photocurrent and water photodecomposition [40, 41]. The authors ascribed the above changes to the defects induced by doping which acted as recombination centers in TiO_2.

We can see from Figs 1 and 3 that after removing the light source, hydrogen stopped to evolve. When the slurry was irradiated again, the rate of hydrogen evolution achieved the same values as before. Careful observations of the curve shapes show that after a dark period of the reaction, the rate of H_2 production attains a maximum much earlier than for fresh catalysts. In our opinion the difference results from the migration of photogenerated hydrogen atoms from the metal to the support (spillover effect) followed by subsequent reduction of some surface Ti^{4+} according to the reaction

where $$Me_s—H + O_s^{2-} + Ti^{4+} \rightarrow Me_s + OH_s^- + Ti^{3+}$$

s-denotes the surface.

The hydrogen uptake on platinized TiO_2 under illumination has been described. Disdier et al. [25], based on their photoactivity studies, ascribed this phenomenon to a migration of adsorbed hydrogen atoms from Pt to TiO_2 (hydrogen spillover), where they form OH^- ions. Aspnes and Heller [42] observed hydrogen uptake in the initial stage of water photodecomposition on Pt/TiO_2. According to the authors, the catalyzed hydrogen evolution cannot take place unless part of the catalyst is hydrogen-saturated because of the barrier which prevents electron flow from the semiconductor to the metal. We can add here that the hydrogen adsorption on TiO_2 in the initial step of the photoreaction of water splitting was observed previously by us for pure TiO_2 and for Fe_2O_3, Co_3O_4 and NiO doped titania [22]. Hence metal deposition is not necessary for hydrogen photouptake on TiO_2 (i.e. for TiO_2 photoreduction).

Hydrogen photogeneration from aqueous NaOH *solution*

This experiment was performed in a quartz reaction cell using the whole spectrum of a medium pressure mercury lamp (180 V) for irradiation of the reaction mixture. The hydrogen production rate was about 55 $\mu L\, h^{-1}$ when the catalyst Ni/TiO_2 (2) was immersed in 1.0 *M* aqueous NaOH solution (see Fig. 2). Irradiation of the catalyst in neutral or less basic media did not give any amount of hydrogen. The similar effect of pH has been discussed in the literature [1, 6, 12, 14].

Table II

Rates of hydrogen production during irradiation of Ni/TiO_2 (2) *in* 0.01 *M* EDTA *aqueous solution in the presence of various electrolytes*

Electrolyte	Conc. of electrolyte (mol dm^{-3})	Rate of hydrogen evolution ($\mu mol\ s^{-1} \times 10^4$)	($cm^3\ h^{-1} \times 10^3$)	Quantum efficiency (%)
KCl	0.1	22.8	183.9	6.35
KCl	1.0	24.1	193.9	6.70
$BaCl_2$	1.0	18.3	147.6	5.10
NaOH	0.0001	18.6	149.9	5.18
NaOH	0.001	23.0	185.5	6.41
NaOH	0.1	1.3	10.5	0.36
NaOH	1.0	1.6	12.6	0.46

Influence of some salts and pH *of the medium on hydrogen evolution from* 0.01 *M* EDTA *solution*

It is well known that semiconductor particles immersed in an electrolyte solution adsorb some ions on the solid-liquid interface. Some works on the adsorption of various ions on pure TiO_2 [43] and on Pt/TiO_2 [44] have been done. Table II shows the influence of mono- (K^+) and divalent (Ba^{2+}) ions on the H_2 production. A distinct effect, namely the decrease of hydrogen production rate was observed only for 1.0 *M* $BaCl_2$ solution. KCl solutions (0.1 and 1.0 *M*) did not change the rate of H_2 photogeneration. We must add here that according to the above mentioned authors [43], Ba^{2+} ions show specific adsorption on TiO_2, which causes a change in the electronic state of the surface. Contrary to Ba^{2+}, the adsorption of monovalent ions (Na^+) does not influence the surface properties of TiO_2.

The effect of pH on H_2 production from 0.01 *M* EDTA solution in water is opposite to that observed for a slurry of Ni/TiO_2 in pure water (see above) — here the rise in pH causes a decrease in hydrogen evolution. The strong retardation of hydrogen photoproduction in 0.1 *M* and 1.0 *M* NaOH solutions is surprising. Unfortunately, the explanation of this phenomenon is not possible on the grounds of our experimental data.

Conclusions

Among the three metals which were subjected to the examination, nickel seems to be promising as a catalyst for hydrogen evolution. The advantage of nickel over noble metals is its much lower price; the disadvantages are lower activity and impossibility of use in an acidic medium. The present work should be considered as a contribution to the study of mainly Ni/TiO_2. It shows the possibility of water splitting on this catalyst and the influence of various factors, like pH or some electrolyte solutions on H_2 photoproduction. It indi-

cates the necessity of complete NiO reduction in accordance with recentyl published paper of Prahov et al. [17]. We think that further study on nickel on titania (or other semiconductors) can give, in the future, efficient photocatalysts for water splitting.

REFERENCES

[1] Sato, S., White, J. M.: J. Catal., **69,** 128 (1981)
[2] Chen, B. H., White, J. M.: J. Phys. Chem., **86,** 3534 (1982)
[3] Kirch, M., Lehn, J. M., Sauvage, J. P.: Helv. Chim. Acta, **62,** 1345 (1979)
[4] Wagner, F. T., Somorjai, G. A.: J. Amer. Chem. Soc., **102,** 5494 (1980)
[5] Vidyarth, S. K., Bharucka, N. R.: J. Electrochem. Soc., **128,** 2046 (1981)
[6] Kiwi, J., Greatzel, M.: J. Phys. Chem., **88**$_1$ 1302 (1984)
[7] Degani, Y., Willner, J.: J. Amer. Chem. Soc., **105,** 6228 (1983)
[8] Matsumura, M., Saho, Y., Tsubomura, H.: J. Phys. Chem., **87,** 3807 (1983)
[9] Kalyanasundaran, K., Borgarello, S., Greatzel, M.: Helv. Chim. Acta, **64,** 362 (1981)
[10] Miller, D. S., Bard, A. J., McLendon, G., Ferguson, J.: J. Amer. Chem. Soc., **103,** 5336 (1981)
[11] Lehn, J. M., Sauvage, J. P., Ziessel, R.: Nouv. J. Chim., **4,** 623 (1980)
[12] Lehn, J. M., Sauvage, J. P., Ziessel, R., Hilaire, L.: Isr. J. Chem., **22,** 168 (1982)
[13] Magliozzo, R. S., Krasna, A. I.: Photochem. Photobiol., **38,** 15 (1983)
[14] Yesodharan, E., Greatzel, M.: Helv. Chim. Acta, **66,** 2145 (1983)
[15] Kawai, T., Sakata, T.: J. Chem. Soc., Chem. Comm., **1980,** 649
[16] Sakata, T., Kawai, T.: Chem. Phys. Lett., **80,** 341 (1981)
[17] Prahov, L., Disdier, J., Herrmann, J. M., Pichat, P.: Int. J. Hydrogen Energy, **9,** 397 (1984)
[18] Auguliaro, V., Lauricella, A., Rizzuti, L., Schiavello, M., Sclafani, A.: Int. J. Hydrogen Energy, **7,** 845 (1982)
[19] Auguliaro, V., Lauricella, A., Rizzuti, L., Schiavello, M., Sclafani, A.: ibid., **7,** 851 (1982)
[20] Yue, P. L., Khan, F., Rizzuti, L.: Chem. Eng. Sci., **38,** 1893 (1983)
[21] Radford, P. P., Francis, C. G.: J. Chem. Soc. Chem. Comm., **1983,** 1520
[22] Zieliński, S., Sobczyński, A.: Acta Chim. Hung. (submitted for publication)
[23] Murov, S. L.: Handbook of Photochemistry. Marcel Dekker, Inc. New York 1973
[24] Zieliński, S., Sobczyński, A.: to be published
[25] Disdier, J., Herrmann, J. M., Pichat, P.: J. Chem. Soc., Faraday Trans 1, **79,** 651 (1980)
[26] Handbook of Chemistry and Physics, 60th Ed., 1979—1980, CRS Press, Inc. Boca Raton, Florida 33431
[27] Bube, R. H.: Photocunductivity of Solids, p. 110—115. Wiley, New York 1960
[28] Bard, A. J.: J. Photochem., **10,** 50 (1979)
[29] Tauster, S. J., Fung, S. C., Garten, R. L.: J. Amer. Chem. Soc., **100,** 170 (1978)
[30] Herrmann, J. M.: J. Catal., **89,** 404 (1984)
[31] Koudelka, M., Augustynski, J.: J. Chem. Soc., Chem. Comm., **1983,** 856
[32] Solymosi, F.: Catal. Rev., **1,** 233 (1967)
[33] Vannice, M. A., Garten, R. L.: J. Catal., **56,** 236 (1979)
[34] Ozdogan, S. Z., Gochis, P. D., Falconer, J. L.: J. Catal., **83,** 257 (1983)
[35] Vance, C. K., Bartholomew, C. H.: Appl. Catal., **7,** 169 (1983)
[36] Tatarchuk, B. J., Dumesic, J. A.: J. Catal., **70,** 308 (1981); **70,** 323 (1981); **70,** 335 (1981)
[37] Santos, J., Philips, J., Dumesic, J. A.: J. Catal., **81,** 141 (1983)
[38] Krishtalik, L. I.: in "Advances in Electrochemistry and Electrochemical Engineering" (Ed. P. Delahay), Vol. **7,** p. 283. Wiley Intersciences, New York 1970
[39] Choi, J. S., Kim, K. H.: J. Phys. Chem., **80,** 666 (1976)
[40] Matsumoto, Y., Kurimoto, J., Shimizu, T., Sato, E.: J. Electrochem. Soc., **128,** 1040 (1981)
[41] Monnier, A., Augustynski, J.: J. Electrochem. Soc., **127,** 1576 (1980)
[42] Aspnes, D. E., Heller, A.: J. Phys. Chem., **87,** 4919 (1983)
[43] Tasev, D. K., Kolmakova, G. A., Sidorova, M. P., Fridrikhsberg, D. A.: Kolloidn. Zh., **44,** 373 (1982)
[44] Tsai, W., Schwarz, J. A., Driscoll, C. T.: J. Phys. Chem., **87,** 1619 (1983)

Acta Chimica Hungarica 121 (3), pp. 313—322 (1986)

SYNTHETIC, STRUCTURAL AND ANTIBACTERIAL STUDIES OF Co(II), Ni(II), Cu(II) AND Zn(II) COMPLEXES OF PYRIDINE-2--CARBOXYALDEHYDE THIOISONICOTINOYL HYDRAZONE

Nand Kishor SINGH*, Namita AGRAWAL and Ram Chandra AGGARWAL

(Department of Chemistry, Banaras Hindu University, Varanasi-221,005, India)

Received January 11, 1985
Accepted for publication May 22, 1985

Pyridine-2-carboxaldehyde thioisonicotinoyl hydrazone (2-PTINH) gave adducts with Co(II), Ni(II), Cu(II) and Zn(II) chloride, bromide, iodide and thiocyanate and an orange diamagnetic complex Cu(2-PTIN) (NCS) which shows a d-d transition band at 20,000 cm^{-1} characteristic of dimeric Cu(II) species. Magnetic, electronic and ESR spectral studies suggested high-spin octahedral geometry for all Ni(II) and Co(II) chloride and bromide adducts, tetrahedral geometry for Co(II) iodide and thiocyanate complexes and distorted octahedral geometry for Cu(II) halide and thiocyanate complexes. Infrared spectral studies showed neutral bidentate behaviour of the ligand in all the adducts except Cu(2-PTIN) (NCS), where it acted as an uninegative bidentate ligand, the bonding sites being the thione/thiol sulfur and azomethine nitrogen. ESR spectral studies suggested monomeric nature for $Cu(2\text{-}PTINH)_2Cl_2$ and dimeric nature for Cu(2-PTIN)(NCS) and the presence of unpaired electron in $d_{x^2-y^2}$ orbital of Cu(II). Antibacterial activities of 2-PTINH and their (Co(II), Ni(II), Cu(II) and Zn(II) complexes tested against *Klebsiella pneumoniae*, *E. coli* and *V. cholerae* showed that the metal complexes are good antibacterial agents.

Introduction

There are a few papers on the transition metal complexes of Schiff bases derived from the condensation of dithiocarbazate and thiosemicarbazide with pyridine-2-carboxaldehyde [1]. Domagk reported [2] the antitubercular activity of thiosemicarbazone. Recently, some first row transition metal complexes of α-*N*-heterocyclic carboxaldehyde thiosemicarbazones have been shown to possess very significant antibacterial [3] and antineoplastic [4] activities. Iron(II) and copper(II) complexes of 5-substituted-2-formylpyridine thiosemicarbazone have both in vitro and in vivo activities against tumour cells [4—6], which is thought to be due to their ability to chelate trace metals.

* To whom correspondence should be addressed.

Since thiosemicarbazones are structurally very similar to thiohydrazones in having sulfur and nitrogen as donor atoms, the 3d-metal complexes of pyridine carboxaldehyde thiohydrazones are also expected to show similar interesting biological and ligational behaviour because of the presence of as many as five potential donor sites and a possibility of thione-thiol tautomerism which may lead to varied bonding and stereochemical behaviour in the complexes. The present paper describes the synthesis, structural characterization and antibacterial screening of pyridine-2-carboxaldehyde thioisonicotinoyl hydrazone (2-PTINH, **a**) and its 3d-metal complexes.

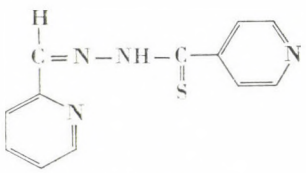

a (2-PTINH)

Experimental

Preparation of ligand

INH was obtained from Sigma Chem. Co., U.S.A. All. other chemicals used were of analytical or equivalent quality.

Pyridine-2-carboxaldehyde thioisonicotinoyl hydrazone was prepared following the procedure described by Engelbert et al. [7] for the pyridine-4-carboxaldehyde thioisonicotinoyl hydrazone. Thus, a mixture of INH, 2-picoline and sulfur powder was heated in 1 : 1 : 2 molar ratio at 130—140 °C for ~10 h or till the evolution of H_2S almost ceased, then about one equivalent of acetonitrile was added to the warm mixture, cooled, filtered and the product was recrystallized from DMF, m.p. 190 °C.

Analysis ($C_{12}H_{10}N_4S$). Found C 59.10, H 3.58, N 22.28 and S 14.20; Calcd. C 59.51, H 4.13, N 23.14 and S 13.22%.

Preparation of complexes

Metal(II) halide and thiocyanate complexes [M(2-PTINH)X_2] [M(II) = Ni for X = Cl, Br and Co for NCS] and [M(2-PTINH)$_2X_2$] [M(II) = Co, Cu, Zn for X = Cl, Br, I and Ni for X = I and NCS] were prepared by mixing together an ethanolic solution of the appropriate metal(II) salt and the ligand in a 1 : 1 molar ratio. [Cu(2-PTINH)$_2$(NCS)$_2$] was obtained by adding a hot DMSO solution of the ligand to $Cu(NCS)_2$ in the same solvent in a 1 : 2 molar ratio, whereas the sequence of addition was reversed in the case of Cu(2-PTIN)(NCS).

All the complexes which precipitated on stirring and digesting the above reaction mixture on a water bath for ~30 minutes, were suction filtered, washed with hot ethanol and dried in vacuum.

The complexes thus obtained were analyzed for their metal, halogen/thiocyanate and sulfur contents employing standard literature procedures [8]. The metal contents were estimated after destroying the organic matter first with aqua regia and then with *conc.* H_2SO_4.

Physical measurements

The methods and apparatus employed for studying molar conductance, magnetic susceptibility, electronic and infrared spectra and the procedures for calculating the ligand-field parameters were the same as described elsewhere [9]. The pertinent experimental data are given in Tables I and II.

ESR spectra of $[Cu(2\text{-}PTINH)_2Cl_2]$ doped in the diamagnetic host lattice of $[Zn(2\text{-}PTINH)_2Cl_2]$ and Cu(2-PTIN) (NCS) as polycrystalline sample were recorded at LNT on a Varian E-112 spectrometer using TCNE ($g = 2.00277$) as a standard.

Far-infrared spectra of Ni(II) chloride and bromide adducts were recorded on a Polytec FIR-30 Fourier Far-infrared spectrometer.

The antibacterial activity of the compounds under investigation was studied in vitro against three bacteria species viz. *V. cholerae*, *E. coli* and *Klebsiella pneumoniae* in DMF at the concentrations of 10, 5 and 1 mg/mL by paper disc method using peptone water for making inoculum and the results are given in Table III.

Table I

Analytical data, colour, molar conductance and magnetic moment of 2-PTINH complexes

Complex		Found (Calcd.) %				$\Lambda M(ohm^{-1} cm^2 mol^{-1})$	$\mu_{eff.}$ (B.M.)
		Metal	X/SCN	S	N		
1	2	3	4	5	6	7	8
$Co(2\text{-}PTINH)_2Cl_2$	Light violet	9.45 (9.61)	12.00 (11.54)	10.50 (10.43)	17.85 (18.24)	53.44	5.20
$Ni(2\text{-}PTINH)Cl_2$	Green	15.40 (15.80)	18.85 (19.08)	8.65 (8.61)	14.95 (15.08)	—	3.07
$Cu(2\text{-}PTINH)_2Cl_2$	Green	10.45 (10.28)	11.50 (11.47)	10.42 (10.35)	18.50 (18.10)	—	1.85
$Zn(2\text{-}PTINH)_2Cl_2$	White	10.45 (10.54)	11.25 (11.43)	10.35 (10.32)	18.35 (18.05)	9.53	Diamagnetic
$Co(2\text{-}PTINH)_2Br_2$	Light pink	8.25 (8.39)	22.65 (22.75)	9.15 (9.11)	15.55 (15.94)	55.22	5.31
$Ni(2\text{-}PTINH)Br_2$	Light green	12.68 (12.75)	34.50 (34.59)	7.01 (6.95)	12.15 (12.16)	—	2.99
$Cu(2\text{-}PTINH)_2Br_2$	Green	8.85 (8.99)	22.55 (22.59)	9.10 (9.05)	15.27 (15.83)	—	1.84
$Zn(2\text{-}PTINH)_2Br_2$	White	9.20 (9.22)	21.59 (22.53)	9.10 (9.02)	15.50 (15.79)	16.03	Diamagnetic
$Co(2\text{-}PTINH)_2I_2$	Yellow	7.25 (7.39)	31.85 (31.88)	8.15 (8.03)	13.95 (14.06)	136.30	4.61
$Ni(2\text{-}PTINH)_2I_2$	Red	7.36 (7.41)	31.86 (31.88)	8.10 (8.04)	13.95 (14.06)	—	3.27
$Zn(2\text{-}PTINH)_2I_2$	White	8.10 (8.14)	31.50 (31.62)	7.98 (7.96)	13.85 (13.94)	59.00	Diamagnetic
$Co(2\text{-}PTINH)(NCS)_2$	Yellow	14.10 (14.14)	27.75 (27.83)	22.95 (23.03)	20.12 (20.15)	54.30	4.53
$Ni(2\text{-}PTINH)_2(NCS)_2$	Green	8.80 (8.91)	17.25 (17.61)	19.25 (19.44)	21.35 (21.24)	54.22	3.06
$Cu(2\text{-}PTINH)_2(NCS)_2$	Yellowish green	9.55 (9.57)	17.50 (17.49)	19.35 (19.30)	20.84 (21.10)	41.14	1.97
Cu(2-PTINH)(NCS)	Orange	17.26 (17.47)	15.68 (15.95)	17.25 (17.61)	19.16 (19.26)	—	Diamagnetic

Table II

Electronic spectral data and ligand-field parameters of the complexes

Complex	Band maxima (cm^{-1})	Assignments	D_q (cm^{-1})	B (cm^{-1})	β	β° (%)	LFSE (kJ/mol)
1	2	3	4	5	6	7	8
$Co(2\text{-}PTINH)_2Cl_2$	9090, 19,050, 20,180	$^4T_{1g}(F) \rightarrow {}^4T_{2g}(F)(\nu_1)$; $^4A_{2g}(F)\,(\nu_2)$; $^4T_{1g}(P)(\nu_3)$	1077	718	0.74	26	103.00
$Co(2\text{-}PTINH)_2Br_2$	8700, 18,870	$^4T_{1g}(F) \rightarrow {}^4T_{2g}(F)(\nu_1)$; $^4T_{1g}(P)(\nu_3)$	979	753	0.77	23	93.70
$Co(2\text{-}PTINH)_2I_2$	9090, 14,810, 22,220	$^4A_2(F) \rightarrow {}^4T_1(F)(\nu_2)$; $^4T_1(P)(\nu_3)$	561	467	0.48	52	53.69
$Co(2\text{-}PTINH)(NCS)_2$	10,000, 15,665	$^4A_2(F) \rightarrow {}^4T_1(F)(\nu_2)$; $^4T_1(P)(\nu_3)$	652	408	0.42	58	62.38
$Ni(2\text{-}PTINH)Cl_2$	10,200, 15,750, 25,000	$^3A_{2g}(F) \rightarrow {}^3T_{2g}(F)(\nu_1)$; $^3T_{1g}(F)(\nu_2)$; $^3T_{1g}(P)(\nu_3)$	1020	714	0.67	33	146.40
$Ni(2\text{-}PTINH)Br_2$	9615, 16,000, 25,640	$^3A_{2g}(F) \rightarrow {}^3T_{2g}(F)(\nu_1)$; $^3T_{1g}(F)(\nu_2)$; $^3T_{1g}(P)(\nu_3)$	1013	750	0.71	29	145.40
$Ni(2\text{-}PTINH)_2I_2$	8620, 17,860, 22,220	$^3A_{2g}(F) \rightarrow {}^3T_{2g}(F)(\nu_1)$; $^3T_{1g}(F)(\nu_2)$; $^3T_{1g}(P)(\nu_3)$	862	.	.	.	124.00
$Ni(2\text{-}PTINH)_2(NCS)_2$	10,000, 16,130, 26,670	$^3A_{2g}(F) \rightarrow {}^3T_{2g}(F)(\nu_1)$; $^3T_{1g}(F)(\nu_2)$	990	861	0.82	18	142.10
$Cu(2\text{-}PTINH)_2Cl_2$	14,290	$^2B_{1g} \rightarrow {}^2E_g$; $^2B_{2g}$ and $^2A_{1g}$	1429	.	.	.	102.60
$Cu(2\text{-}PTINH)_2Br_2$	14,280, 22,220	$^2B_{1g} \rightarrow {}^2E_g$; $^2B_{2g}$ and $^2A_{1g}$	1428	.	.	.	102.50
$Cu(2\text{-}PTINH)_2(NCS)_2$	15,380, 22,220	$^2B_{1g} \rightarrow {}^2E_g$; $^2B_{2g}$ and $^2A_{1g}$	1538	.	.	.	110.40
Cu(2-PTIN)(NCS)	18,180, 20,000	Envelope of $^2B_{1g} \rightarrow {}^2A_{1g}$; $^2B_{2g}$ and ^2E_g	1818	.	.	.	.

Table III

Antimicrobial activity of pyridine-2-carboxaldehyde thioisonicotinoyl hydrazone and their metal(II) complexes
Incubation temp. = 37 °C
Incubation time = 24 h

Compound	Inhibitory concentration (mg/mL)	Microbial species		
		Klebsiella pneumoniae	*E. coli*	*V. cholerae*
2-PTINH	10	+	+	+
	5	+	+	+
	1	+	+	+
$Co(2\text{-}PTINH)_2Cl_2$	10	+	+	+
	5	+	+	+
	1	+	+	+
$Cu(2\text{-}PTINH)_2(NCS)_2$	10	+	+	+
	5	+	+	+
	1	+	+	+
$Ni(2\text{-}PTINH)Cl_2$	10	—	—	—
	5	—	—	—
	1	—	—	—
$Zn(2\text{-}PTINH)_2Cl_2$	10	—	—	—
	5	—	—	—
	1	—	—	—

— = Inhibition.
+ = Growth.

Results and Discussion

2-PTINH has been found to form 1 : 1 or 1 : 2 adducts with Co(II), Ni(II), Cu(II) and Zn(II) halides and thiocyanate and also gives a deprotonated complex Cu(2-PTIN)(NCS) with copper(II) thiocyanate. All the complexes have high melting or decomposition temperatures (about 300 °C) except $[Cu(2\text{-}PTINH)_2Cl_2]$ which melts at $\sim$ 294 °C, and are generally insoluble in water, ethanol and methanol but some of them are slightly soluble in coordinating solvents like DMF and DMSO.

The molar conductance values of the soluble complexes in DMF at 10^{-3} M show that they are non-electrolytes except $Co(2\text{-}PTINH)_2I_2$, which is a 2 : 1 electrolyte [10]. The slightly high values for the non-electrolytic nature of some complexes may be due to solvolysis as shown below:

$$[M(2\text{-}PTINH)_xX_2] + DMF \rightleftharpoons [M(2\text{-}PTINH)_xX \cdot DMF]^+ + X^-$$

Magnetic moments

The magnetic moment data given in Table I suggest octahedral geometry for all the Ni(II) complexes. The $\mu_{eff.}$ values of the Co(II) chloride and bromide adducts suggest them to be octahedral while those of the Co(II) iodide and

thiocyanate complexes are indicative of a tetrahedral geometry around Co(II). The magnetic moments of Cu(II) complexes are normal (except [Cu(2-PTIN)(NCS)] which is diamagnetic) and correspond to the presence of one unpaired electron.

Electronic spectra

The electronic spectra of $[Co(2\text{-}PTINH)_2Cl_2]$ and $[Co(2\text{-}PTINH)_2Br_2]$ show two bands in the 8700—9090 and 18870—19050 cm^{-1} regions assigned to $^4T_{1g}(F) \rightarrow {}^4T_{2g}(F)(\nu_1)$; $\rightarrow {}^4T_{1g}(P)(\nu_3)$ transitions, respectively, in an octahedral environment of cobalt(II) [11]. The bands occurring in the 9090—10000 and 14810—15665 cm^{-1} regions in the spectra of $Co(2\text{-}PTINH)_2I_2$ and $Co(2\text{-}PTINH)(NCS)_2$ may be assigned to $^4A_2(F) \rightarrow {}^4T_1(F)(\nu_2)$ and $\rightarrow {}^4T_1(P)(\nu_3)$ transitions, respectively, in tetrahedral geometry of the complexes [11].

All the Ni(II) complexes exhibit three bands in 8620—10,200, 15,750—17,860 and 22,220—26,670 cm^{-1} regions attributed to $^3A_{2g}(F) \rightarrow {}^3T_{2g}(F)(\nu_1)$; $\rightarrow {}^3T_{1g}(F)(\nu_2)$ and $\rightarrow {}^3T_{1g}(P)(\nu_3)$ transitions, respectively, in octahedral geometry around Ni(II) [12].

Tbe spectra of Cu(II) complexes show a broad band in 14,280—15,380 cm^{-1} region assigned to the envelope of $^2B_{1g} \rightarrow {}^2E_g$; $^2B_{2g}$ and $^2A_{1g}$ transitions in distorted octahedral geometry of Cu(II) [13]. The spectrum of the orange, diamagnetic complex, Cu(2-PTIN)(NCS), however, shows two bands, at 18,180 and 20,000 cm^{-1}. The first one may be attributed to d-d transition in square-planar geometry and the second one to the dimeric Cu(II) species [14, 15]. The diamagnetism of this complex indicates strong spin-spin interaction between two cupric ions [15].

ESR spectra

The ESR spectrum of the doped sample of $[Cu(2\text{-}PTINH)_2Cl_2]$ at LNT shows a high field transition at $\sim$ 3200 G ($\Delta ms = 1$) with the parallel, perpendicular and average g values of 2.25, 2.03 and 2.11 respectively. The trend $g_{||} > g_{\perp} > g_e$ (free-ion value, 2.0023) shows that the unpaired electron is in the $d_{x^2-y^2}$ orbital of Cu(II) [16]. The $g_{||}$ and $g_{\perp}$ values in the complex deviate considerably from the free-spin value and are close to those reported for a number of distorted octahedral Cu(II) complexes [17]. The ESR powder spectrum of Cu(2-PTIN)(NCS) at LNT shows four peaks on the low field side of the parallel region and the analysis of the spectrum gives $g_{||} = 2.10$, $g_{\perp} = 2.04$ and $g_{av.} = 2.06$. The presence of a weak half-field signal at about 1600 G indicates its dimeric nature [16].

Infrared spectra

The infrared spectrum of 2-PTINH in nujol/KBr shows a band at 3180 cm^{-1} assigned to ν(N—H) which remains practically unchanged in adducts but disappears in Cu(2-PTIN) (NCS) presumably via thioenolization. The bands occurring at 1620 and 985 cm^{-1} in the ligand due to ν(C=N) and ν(N—N) modes, respectively, show a negative and positive shifts of 10—20 and 20—30 cm^{-1}, respectively, in the complex indicating that azomethine nitrogen is involved in bonding [18]. Thioamide band I (βNH + νCN) and thioamide band II (νCN + βNH) occurring at 1410 and 1310 cm^{-1}, respectively, in the ligand undergo positive shifts of 25—40 cm^{-1} in the complexes indicating

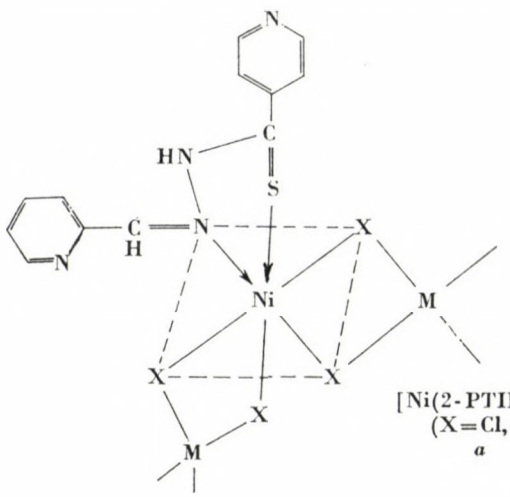

[Ni(2-PTINH)X_2]
(X=Cl, Br)
a

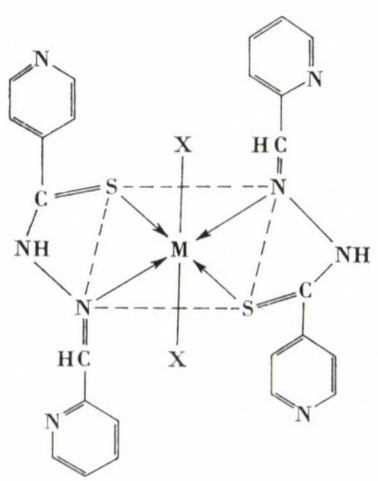

[M(2-PTINH)$_2X_2$]
M = Co(II), X = Cl, Br;
Ni(II), X = I, NCS;
Cu(II), X = Cl, Br, NCS;
Zn(II), X = Cl, Br, I
b

that the sulfur of the thioamide group is involved in bonding [19]. The thioamide band I, mainly due to ν(C=S), observed at 845 cm^{-1} in the ligand is shifted to 790—825 cm^{-1} in the adducts suggesting bonding through sulphur of >C=S group. This band, however disappears in Cu(2PTIN) (NCS) and a new band at 720 cm^{-1} due to ν(C—S) is observed, indicating that the enolized

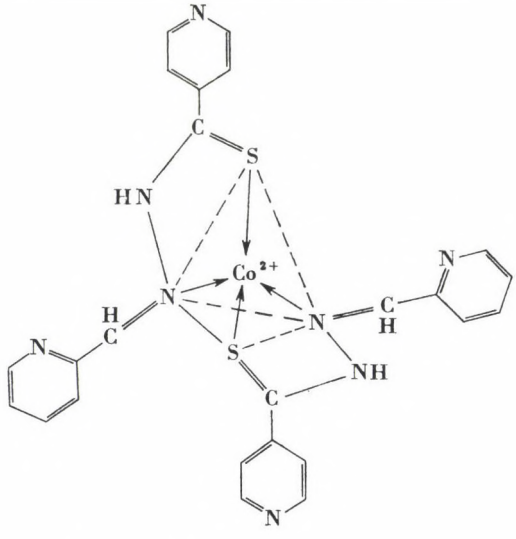

c [Co(2-PTINH)$_2$] I_2

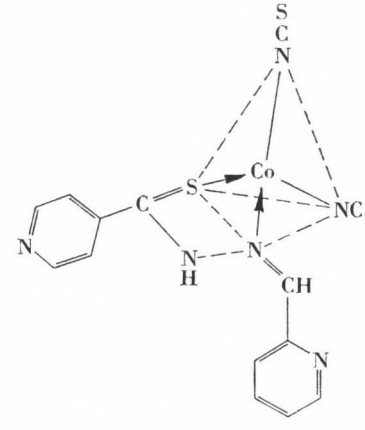

d [Co(2-PTINH)(NCS)$_2$]

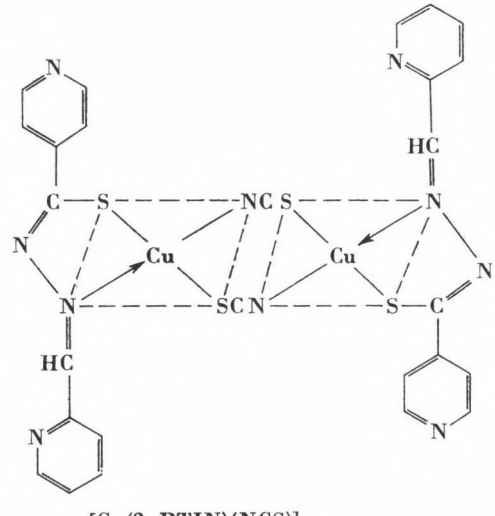

e [Cu(2-PTIN)(NCS)]

form of νC=S is involved in bonding [20]. The pyridine ring vibrations remain practically unchanged in all the Co(II), Ni(II), Cu(II) and Zn(II) adducts, indicating non-involvement of pyridine nitrogen in bonding.

In the thiocyanate complexes of Co(II), Ni(II) and Cu(II), the bands appearing at $\sim$ 2080 cm^{-1} (ν_1), 470—480 cm^{-1} (ν_2) and 760—780 cm^{-1} (ν_3) due to ν(C≡N), δ(NCS) and ν(C=S) modes, respectively, clearly indicate the presence of monodentate and N-bonded thiocyanate group in these complexes. The ν(C≡N) band is, however, observed at a higher frequency at 2115 cm^{-1} in Cu(2-PTIN) (NCS) suggesting the presence of bridging thiocyanate group [21].

The far-infrared spectra of Ni(II) chloride and bromide complexes show non-ligand bands at 170 and 184 and 128 and 140 cm^{-1}, respectively, which may be assigned to ν_b(Ni—Cl) and ν_b(Ni—Br) modes, respectively, clearly indicating the halide bridging in these complexes [22]. The non-ligand bands due to ν(M—S) and ν(M—N) observed in all the complexes at 360 $\pm$ 10 and 310 $\pm$ 10 cm^{-1} regions further support coordination through thione/thiolato sulfur and azomethine nitrogen [20].

Antibacterial activity

The results of antibacterial activity given in Table III show that 2-PTINH and its Co(II) and Cu(II) complexes show no inhibition at any of the concentrations studied against the three bacteria species viz., *V. cholerae*, *E. coli* and *Klebsiella pneumoniae*. However, an impressive increase in antibacterial activity is observed in the case of Ni(II) and Zn(II) complexes for which almost complete inhibition of bacterial growth at all the three concentrations of the compounds against all bacteria have been observed. Thus the above result shows that these metal complexes are effective antibacterial agents [23].

Based on the analytical data and physico-chemical studies described above, the structures of the complexes are shown in Figs *a* — *e*.

*

Authors' thanks are due to Professor P.C. Sen, Head of Microbiology Section, Institute of Medical Sciences, B.H.U.; the Incharges of Regional Sophisticated Instrumentation Centre, I.I.T., Madras and Bombay, for their kind help in studying the antibacterial activity, far-infrared and ESR spectra, respectively. One of the authors (N.A.) is also thankful to CSIR, New Delhi for the award of a Junior Research Fellowship.

REFERENCES

[1] Ali, M. A., Livingstone, S. E.: Coord. Chem. Rev., **13,** 101 (1974)
[2] Domagk, G., Behnisch, R., Mietzsch, F., Schmidt, H.: Naturwissenschaften, **33,** 315 (1946)
[3] Dave, L. D., Thampy, S. K., Shelat, Y. A.: J. Inst. Chem., **53,** 237 (1981)
[4] Antholine, W. E., Knight, J. M., Petering, D. H.: J. Med. Chem., **19,** 339 (1976)
[5] Agrawal, K. C., Booth, B. A., Moore, E. C., Sartorelli, A. C.: Proc. Am. Ass. Cancer Res., **15,** 289 (1974)

[6] Antholine, W. E., Knight, J., Whelan, H., Petering, D. H.: Molec. Pharmacol., **13,** 89 (1977)
[7] Kuhle, E. et al.: Chem. Abst., **51,** 6705 (1957)
[8] Vogel, A. I.: "Text-book of Quantitative Inorganic Analysis" E L B S and Longmans, London 1971
[9] Singh, N. K., Agrawal, S., Aggarwal, R. C.: Indian J. Chem., **21A,** 973 (1982)
[10] Geary, W. J.: Coord. Chem. Rev., **7,** 81 (1971)
[11] Lever, A. B. P.: "Inorganic Electronic Spectroscopy", p. 320. Elsevier, Amsterdam
[12] Ali, M. A., Tarafdar, M. T. H.: J. Inorg. Nucl. Chem., **39,** 1785 (1977)
[13] Patel, K. C., Goldberg, D. E.: J. Inorg. Nucl. Chem., **34,** 637 (1972)
[14] Khullar, I. P., Agarwala, U.: Canad. J. Chem., **53,** 1165 (1975)
[15] Harris, C. M., Hoskins, B. F., Martin, R. L.: J. Chem. Soc., **1959,** 3728
[16] Felthouse, T. R., Hendrickson, D. N.: Inorg. Chem., **17,** 444 (1978)
[17] Van Landschoot, R. C., Van Hest, J. A. M., Reedijk, J.: J. Inorg. Nucl. Chem., **38,** 185 (1976)
[18] Rastogi, D. K., Sahni, S. K., Rana, V. B., Dua, S. K.: J. Coord, Chem., **8,** 97 (1978)
[19] Campbell, M. J., Grzeskowiak R.: J. Chem. Soc., *A*, **1967,** 396
[20] Geetharani, K., Sathyanarayana, D. N.: Aust. J. Chem., **30,** 1617 (1977)
[21] Nakamoto, K.: "Infrared and Raman Spectra of Inorganic and Coordination Compounds", p. 270. Wiley-Interscience, New York 1978
[22] Postmus, C., Ferraro, J. R., Quattrochi, A., Shobatake, K., Nakamoto, K.: Inorg. Chem., **9,** 1851 (1969)
[23] Anjaneyulu, Y., Rao, R. P., Swamy, R. Y., Eknath, A., Rao, K. N.: J. Indian Chem. Soc., **LIX,** 1024 (1982)

Acta Chimica Hungarica 121 (3), pp. 323—328 (1986)

STRUCTURE-ACTIVITY STUDIES ON NEW INHIBITORY ANALOGS OF LH-RH

Anikó HORVÁTH[1]*, David H. COY[2], Mary V. NEKOLA[2], Esther J. COY[2], Simon J. HOCART[2], György KÉRI[1] and István TEPLÁN[1]

([1]1st Institute of Biochemistry, Semmelweis University Medical School, H-1444 Budapest P.O.B. 260, and [2]Department of Medicine, Tulane University School of Medicine, New Orleans, LA 70112 U.S.A.)

Received October 10, 1984
Accepted for publication May 24, 1985

The effect of different substitutions in positions 2, 3, 8 and 10 on inhibitory analogs of LH-RH has been investigated in the series of D-Arg[6]-antagonist analogs. Sixteen analogs have been synthesized and tested for antiovulatory activity. The potency of the analogs was compared with Ac-D-*p*-Cl-Phe[1,2], D-Trp[3], D-Arg[6], D-Ala[10]-LH-RH which shows 78% inhibition of ovulation in a dose of 3 μg/rat. Insertion of D-homoPhe or D-Arg in position 2 and 3 resulted in lower biological activity. The analogs exhibiting high antiovulatory activity with D-Ala substitution in position 10 had reduced activity when D-Ala was changed for Gly. The D-*p*-Br-Phe or D-*p*-F-Phe substitutions both in positions 1 and 2 had the same effect as the corresponding counterparts had in position 1. Ac-D-*p*-Br-Phe[1,2], D-Trp-, D-Arg-, D-Ala[10]-LH-RH exhibited full blockade of ovulation at a dose of 3 μg per animal. The different substitutions in position 8 expressed the importance of a basic amino acid in this position.

Introduction

During the past few years considerable progress has been made in the development of highly potent inhibitory analogs of the LH-RH decapeptide (*p*Glu-His-Trp-Ser-Tyr-Gly-Leu-Arg-Pro-GlyNH_2). The purpose of these studies was to achieve a therapeutically useful level by s.c. route and even oral activity, too. While the first LH-RH antagonists completely inhibited ovulation in rats at a single s.c. injection of about 1 mg/per rat, recently the most potent antagonists cause full blockade of ovulation at the μg range per animal. For instance, (Ac-D-*p*-Cl-Phe[1,2], D-Trp[3], D-Phe[6], D-Ala[10])-LH-RH [1] (Ac-dehydroPro[1], D-*p*-Cl-Phe[2], D-Trp[3,6], *N*-Me-Leu[7])-LH-RH [2] and (Ac-Gly[1], D-*p*-Cl-Phe[2], D-Trp[3,6])-LH-RH [3] are fully active in doses of 10—20 μg.

Further studies on the relationship between structure and activity of LH-RH antagonists have led to the preparation of a new type of these peptides. Incorporation of a basic D-amino acid in the six-position resulted in a large increase in antiovulatory activity in a certain combination of substitutions. (Ac-D-*p*-Cl-Phe[1,2], D-Trp[3], D-Arg[6], D-Ala[10])-LH-RH [4] not only has 78%

*To whom correspondence should be addressed.

Table I

Amino acid analyses and R_f values of peptides

Compound	Ser	Pro	Gly	Ala	Leu	Tyr	Lys	His
I	0.83	0.91	1.00		1.00	0.90		
II	0.84	0.84	0.99		1.00	0.93		
III	0.87	0.96	1.00		1.02	1.00		
IV	0.72	0.94	1.02		1.04	1.00		1.20
V	0.85	0.90		1.00	1.01	1.00		
VI	0.88	1.05		0.98	1.00	1.00		
VII	0.84	1.00		1.05	0.94	0.90		
VIII	0.90	1.07		1.00	1.00	1.00		
IX	0.86	1.00		1.05	1.04	1.03		
X	1.02	0.99		1.00	1.01	0.99		
XI	0.80	0.95		0.97	1.01	1.00	1.02	
XII	0.98	0.96		0.97	1.02	1.00	1.02	
XIII***	—	—		—	—	—	—	
XIV	1.00	0.78		1.08	1.14	1.07		0.84
XV	0.90	1.00		1.00	1.03	1.06		
XVI	0.80	0.92		1.00	1.07	1.06		

* Amino acids were not calculated except Glu.
A *n*-BuOH : AcOH : H_2O — 4 : 1 : 1.
B EtOAc : Pyridine : AcOH : H_2O — 10 : 5 : 1 : 3.
C *n*-BuOH : AcOH : H_2O : EtOAc — 1 : 1 : 1 : 1.

inhibitory potency at s.c. injection of 3 μg per rat, but also oral administration of 2 mg completely blocked ovulation [5]. Our purpose was to clarify structural requirements at different positions in combination with D-Arg^6. As a part of this study we have found that bulky aromatic substituents in position 1 improve antiovulatory activity. (Ac-D-β-Nal^1 or Ac-D-*p*-Br-Phe^1, D-*p*-Cl-Phe^2, D-Trp^3, D-Arg^6, D-Ala^{10})-LH-RH have 100% activity at 3 μg dose levels [6]. In this paper we report further details about the different substitutions in the series of D-Arg^6 antagonist analogs.

Materials and Methods

Synthesis

The desired protected peptides were synthesized by a standard solid phase method [7] on a Beckman 990 Automatic Peptide Synthesizer, using benzhydrylamine resin. HCl (0.49 meq/g) (Beckman). The individual amino acids were coupled to the resin as their *N*-α-*tert*-butyloxycarbonyl (Boc) derivatives using three-fold excess of each. Reactive side chains of the amino acids were protected as follows: Arg, N^G-tosyl; Ser, *O*-benzyl; Tyr was incorporated without OH protection [8]; His, N^{im}-dinitrophenyl; *p*-NH_2-Phe, N^p-benzyloxycarbonyl. All amino acids were coupled using *N*,*N*'-diisopropylcarbodiimide (Aldrich). The completeness of the coupling reaction was measured by ninhydrin test [9]. If the test was positive, the coupling was repeated. The duration of the coupling changed between 1 and 16 hours, depending on the amino acid. The acetylations were carried out on the protected peptide-resin using 5% acetic anhydride in CH_2Cl_2 for 60 min.

The peptides were cleaved from the resin with simultaneous deprotection by anhydrous hydrogen fluoride [10]. The protected peptide-resin (0.5 mmol) was treated with 30 mL of redistilled HF in the presence of 10% anisole and 100 mg dithiothreitol for 60 min at 0 °C.

Trp	Arg	Cpa	X+	R_f				
				A	B	C	D	E
—*	1.97	1.06	β-Nal**	0.27	0.59	0.62	0.78	0.55
—	2.05	1.05		0.35	0.30	0.55	0.72	0.56
0.92	2.11	1.06	$Phe(CH_3)_5$	0.36	0.27	0.69	0.81	0.57
—	2.07	1.18		0.24	0.07	0.62	0.71	0.36
—	2.03		p-F-Phe	0.30	0.44	0.61	0.87	0.59
0.80	2.00		p-Br-Phe	0.38	0.41	0.64	0.82	0.60
0.98	1.74	0.97	homo-Phe	0.36	0.32	0.58	0.73	0.59
0.98	2.91	1.06		0.28	0.14	0.57	0.71	0.43
	2.84	2.00		0.18	0.19	0.64	0.57	0.41
	1.96	2.19	homo-Phe	0.40	0.32	0.66	0.78	0.62
—	0.97	2.19		0.34	0.34	0.56	0.76	0.56
0.90	0.99	1.09	β-Nal	0.33	0.47	0.58	0.79	0.55
—	—	—	—	—	—	—	—	—
0.84	0.96	1.75		0.38	0.42	0.67	0.86	0.59
—	1.03	1.80	p-NH_2-Phe	0.47	0.55	0.71	0.93	0.72
0.90	1.05	2.30	Glu (1.00)	0.46	0.70	0.70	0.87	0.69

D EtOAc : Pyridine : AcOH : H_2O — 5 : 5 : 1 : 3.
E 2-PrOH : 1 *N* AcOH — 2 : 1.
** β-Naphthylalanine.
*** Ref. [11].

The hydrogen fluoride was eliminated in dry nitrogen gas stream. The resin was then suspended in absolute ether and filtered off. The solid residue was washed with 50% acetic acid, then the solution was evaporated in vacuum at 37 °C. In the case of His-containing peptides, to remove the dinitrophenyl protecting group, the peptide-resin was stirred in DMF containing a few drops of propylamine for 60 min. Then the peptide-resin was filtered off and treated with hydrogen fluoride in the usual manner.

Purifications

Crude peptides obtained after HF cleavage were purified first on a column of Sephadex G-25 (2.5×100 cm) in 50% acetic acid. The separation was monitored by UV absorption at 280 nm and by TLC. Fractions, separated from shorter fragments, were collected and lyophilized; yields: 65—85%. Yields are based on the amine content (substitution) per gram of starting resin.

Gel filtration was followed by reversed-phase C_{18}-bonded silica gel LRP-1 (13—24 μm) (Whatman) preparative HPLC column (2.5×45 cm) eluted with a *n*-PrOH — 20% AcOH linear gradient solvent system (10—60% *n*-PrOH) at a pressure of 3 atm and a flow rate 2 mL/min. The contents of the fractions were measured by UV absorption at 280 nm and by TLC. Fractions were pooled to favor purity rather than quantity; yields: 15—29%. The purity of the peptides was tested by TLC in five solvent systems and by amino acid analysis (Table I). Peptide contents (based on amino acid analysis): 90—98%.

Biological assay

Antiovulatory tests [12] were carried out to determine the biological activity of the peptides. The analogs were dissolved in 40% propylene glycol—saline, and s.c. injections were given at noon on the proestrous day to adult Charles River CD rats showing regular 4-day cycles. On the morning of estrus the number of ova was counted from isolated oviducts. Tables II—IV express the results of these assays as the percentage blockade of ovulation. It was calculated from the ratio of rats which did not ovulate to the total number of rats treated with a given dose of analog. An average of eight animals were tested per group.

Table II

Antiovulatory activities of LR-RH *analogs with* Gly *or* D-Ala *in position* 10

	Peptide	Gly		D-Ala	
		Dose μg/rat	% Blockade of ovulation	Dose μg/rat	% Blockade of ovulation
I	Ac-D-β-Nal[1], D-*p*-Cl-Phe[2], D-Trp[3],	7.5	100	3	100
	D-Arg[6]-LH-RH	1	0	1	77
II	Ac-D-Trp[1,3], D-*p*-Cl-Phe[2], D-Arg[6]-LH-RH	5	33	3	91
III	Ac-D-Phe-$(CH_3)^1_5$, D-*p*-Cl-Phe[2], D-Trp[3], D-Arg[6]-LH-RH	15	10	—	—
IV	Ac-D-His[1], D-*p*-Cl-Phe[2], D-Trp[3], D-Arg[6]-LH-RH	15	0	5	20

Table III

Antiovulatory activities of LR-RH *antagonists modified in positions* 2 and 3

		Dose μg/rat	% Blockade of ovulation
*R[1]	Ac-D-*p*-Cl-Phe[1,2], D-Trp[3], D-Arg[6], D-Ala[10]-LH-RH	3	78
		1.5	10
V	Ac-D-*p*-F-Phe[1,2], D-Trp[3], D-Arg[6], D-Ala[10]-LH-RH	5	40
VI	Ac-D-*p*-Br-Phe[1,2], D-Trp[3], D-Arg[6], D-Ala[10]-LH-RH	3	100
		1	10
VII	Ac-D-*p*-Cl-Phe[1], D-homoPhe[2], D-Trp[3], D-Arg[6], D-Ala[10]-LH-RH	15	0
VIII	Ac-D-*p*-Cl-Phe[1], D-Arg[2,6], D-Trp[3], D-Ala[10]-LH-RH	15	12.5
IX	Ac-D-*p*-Cl-Phe[1,2], D-Arg[3,6], D-Ala[10]-LH-RH	15	12
X	Ac-**D**-*p*-Cl-Phe[1,2], D-homoPhe[3], D-Arg[6], D-Ala[10]-LH-RH	7.5	0

*R: Reference compounds.

Table IV

Antiovulatory activities of LR-RH *antagonists modified in position* 8

	Peptide	Dose μg/rat	% Blockade of ovulation
*R[1]	Ac-D-*p*-Cl-Phe[1,2], D-Trp[3], D-Arg[6], D-Ala[10]-LH-RH	3	78
XI	Ac-D-*p*-Cl-Phe[1,2], D-Trp[3], D-Arg[6], Lys[8], D-Ala[10]-LH-RH	3	50
*R[2]	Ac-D-*p*-Cl-Phe[1,2], D-Trp[3], D-Lys[6], D-Ala[10]-LH-RH	3	50
*R[3]	Ac-D-β-Nal[1], D-*p*-Cl-Phe[2], D-Arg[6], D-Trp[3] D-Ala[10]-LH-RH	3	100
		1	77
XII	Ac-D-β-Nal[1], D-*p*-Cl-Phe[2], D-Trp[3], D-Arg[6], Lys[8], D-Ala[10]-LH-RH	3	100
		1	50
XIII	Ac-D-*p*-Cl-Phe[1,2], D-Trp[3], D-Arg[6], Dab[8], D-Ala[10]-LH-RH	3	18
XIV	Ac-D-*p*-Cl-Phe[1,2], D-Trp[3], D-Arg[6], His[8], D-Ala[10]-LH-RH	7.5	15
XV	Ac-D-*p*-Cl-Phe[1,2], D-Trp[3], D-Arg[6], *p*-NH_2-Phe[8], D-Ala[10]-LH-RH	7.5	20
XVI	Ac-D-*p*-Cl-Phe[1,2], D-Trp[3], D-Arg[6], Gln[8], D-Ala[10]-LH-RH	15	0

*R: Reference compounds.

Results and Discussion

Previous results have shown the strict steric restraints in position 10 [1] and the favorable modifications in position 1 by large aromatic substituents [6]. Therefore we synthesized some new analogs by combining the above requirements inserting Gly in position 10 and different aromatic amino acids in position 1, such as D-β-naphthylalanine, D-tryptophan, D-pentamethylphenylalanine and D-histidine. Table II shows the antiovulatory activities of these peptides compared with the corresponding D-Ala^{10} analogs [6]. The size and the hydrophobicity of the side-chain of the first amino acid preserved its effect on the activity. The largest substituent (D-β-naphthylalanine, peptide **I**) exhibits the highest activity, while the more polar and smallest D-His-containing peptide (**IV**) represents the least potent antagonist in this series. However, all of the new peptides (**I**—**IV** with Gly in position 10) have reduced activity compared to the parent peptides suggesting that the side-chain and/or the optical activity of D-Ala have an important role in position 10.

Systematically changing the substituents in the LH-RH antagonist molecule, we incorporated new amino acids in positions 2 and 3 as well (Table III). The phenyl ring substituents (F, Cl, Br) on D-Phe [6] showed the sensitivity of the position 1 side-chain to the size of the halogen atom. A similar strategy also in position 2 revealed a similar trend.

(Ac-D-*p*-F-Phe^1, D-*p*-Cl-Phe^2, D-Trp^3, D-Arg^6, D-Ala^{10})-LH-RH was less active (33%, 3 μg) than the D-*p*-Cl-Phe^{1,2}-peptide (R^1, 78%, 3 μg), while the D-*p*-Br-Phe^1 substitution resulted in an improved activity (100%, 3 μg). The same correlation exists in position 2. The D-*p*-F-Phe^{1,2} analog (peptide **V**) was partially active even at a 5-μg dose, while the D-*p*-Br-Phe^{1,2} analog preserved its highly potent activity.

In the case of the D-homoPhe^2 analog (**VII**) the absence of a halo-substituent and the extension of the amino acid side-chain by one CH_2 group resulted in severely reduced activity. The peptide was not active at 15 μg dose. Surprisingly, the exchange of the halogen-substituted aromatic side-chain for an aliphatic basic one (peptide **VIII**) did show some activity at 15 μg dose level.

Analogs obtained by the incorporation of these two amino acids in position 3 (peptides **IX** and **X**) were about as active as the two above peptides (**VII** and **VIII**) and both of them had decreased activity as compared with the D-Trp^3 parent peptide.

The substitution of aromatic amino acids in position 6 by D-Arg yielded an improvement in the hydrophilic character of the whole molecule. It was reasonable to test whether the role of the original Arg in position 8 was still so important. Furthermore, the fact that the native chicken LH-RH structurally differs from the mammalian peptide by the substitution of Gln for Arg in position 8 [13] supported our aim to check the variability of position 8. We

synthesized new analogs with different basic amino acids and Gln in position 8 (Table IV). The most remarkable substitution was the incorporation of Lys. Comparison of peptide **XII** to its corresponding Arg^8 counterparts (R^3) shows a little dose-dependent difference, but both of them have 100% activity at 3 μg. In the case of the R^1 analog the insertion of Lys into position 8 (**XI**) resulted in some decrease in the percentage of the blockade of ovulation, but it has the same activity as the D-Lys^6 (R^2) analog. A highly active inhibitor of LH-RH [(Ac-D-$Trp^{1,3}$, D-*p*-Cl-Phe^2, D-Lys^6, D-Ala^{10})-LH-RH] was published recently [14]. The peptide was found to completely inhibit ovulation at an extremely low daily dose (5 μg/rat) in the case of long-term application. In this peptide the Arg was changed for Lys in position 6. Considering the above results, it is important to point out that Lys can be a suitable substitution, or certain sequences more favourable than Arg in position 8, too. All of the other basic amino acids severely reduced the activity of the peptides (**XII**, **XIII**, **XIV**, **XV**) which suggests that the structure and the basicity of the amino acid side-chain have an important role in the biological activity. The case of Gln (**XVI**) also seems to support this view. The peptide lost its activity even at a dose of 15 μg. It is in keeping with the fact that natural chicken LH-RH has approximately 1% of the potency of mammalian LH-RH stimulating LH release from cultured ovine anterior pituitary cells [15].

REFERENCES

[1] Érchegyi, J., Coy, D. H., Nekola, M. V., Coy, E. J., Schally, A. V., Mező, I., Teplán, I.: Biochem. Biophys. Res. Commun., **100,** 915 (1981)
[2] Rivier, C., Rivier, J., Vale, W.: Endocrinology, **108,** 1425 (1981)
[3] Spatola, A. F., Nirankar, S. A.: Biochem. Biophys. Res. Commun., **97,** 1571 (1980)
[4] Coy, D. H., Horvath, A., Nekola, M. V., Coy, E. J., Érchegyi, J., Schally, A. V.: Endocrinology, **110,** 1445 (1982)
[5] Nekola, M. V., Horváth, A., Ge, L. J., Coy, D. H., Schally, A. V.: Science, **218,** 160 (1982)
[6] Horváth, A., Coy, D. H., Nekola, M. V., Coy, E. J., Schally, A. V., Teplán, I.: Peptides, **3,** 969 (1982)
[7] Merrifield, R. B.: J. Am. Chem. Soc., **85,** 2149 (1963)
[8] Coy, D. H., Baranyas, N.: Int. J. Peptide Protein Res., **14,** 339 (1979)
[9] Kaiser, E., Colescott, R. L., Bossinger, C. D., Cook, P. I.: Anal. Biochem., **34,** 595 (1970)
[10] Sakakibara, S., Shimonishi, Y., Kishida, Y., Okada, M., Sugikara, H.: Bull. Chem. Soc. Jpn, **40,** 2164 (1967)
[11] Hocart, S. J., Coy, D. H., Coy, E. J., Horvath, A., Nekola, M. V.: Peptides. Proc. 8th American Peptide Symp., Pierce, Rockford, IL., 1983
[12] de la Cruz, A., Coy, D. H., Vilchez-Martinez, Arimura, A., Schally, A. V.: Science, **191,** 195 (1976)
[13] King, J. A., Millar, R. P.: J. Biol., Chem., **257,** 10729 (1982)
[14] Kovács, M., Mező, I., Flerkó, B., Teplán, I., Nikolics, K.: Biochem. Biophys., Res. Commun., **118,** 351 (1984)
[15] Millar, R. P., King, J. A.: Endocrinology, **113,** 1364 (1983)

Acta Chimica Hungarica 121 (3), pp. 329—331 (1986)

BOOK REVIEWS

Stucture and Bonding, Vol. 57

Springer-Verlag, Berlin, Heidelberg, New York, Tokyo, 1984

R. D. Ernst: Structure and Bonding in Metal-Pentadienyl and Related Compounds (pp. 1—53);

B. J. Hathaway: A New Look at the Stereochemistry and Electronic Properties of Complexes of the Copper(II) Ion (pp. 55—118);

K. D. Warren: Calculations of the Jahn-Teller Coupling Constants for d^x Systems in Octahedral Symmetry via the Angular Overlap Model (pp. 119—145);

J. Emsley: The Composition, Structure and Hydrogen Bonding of the β-diketones (pp. 147—191).

(1) Metal complexes of the allyl (C_3H_5) and cyclopentadienyl (C_5H_5) ligands have played a major role in the development of inorganic and organometallic chemistry. Metal allyl complexes are well known for the many organic transformations which they may mediate, while metal cyclopentadienyl complexes possess very high stabilities but only very limited catalytic chemistry. Although the first transition metal-pentadienyl compound, $Fe(C_5H_7)(CO)_3^+ClO_4^-$, was reported in 1962, this ligand has been greatly neglected in comparison to the cyclopentadienyl and allyl ligands. Only recently has it become clear that pentadienyl ligands offer substantial promise for the future of inorganic and organomentallic chemistry. The chemistry of the pentadienyl ligand has similarities to the chemistry of both the allyl and cyclopentadienyl ligands, and it has now been demonstrated that metal pentadienyl complexes posses not only thermal stability but also chemical and catalytic reactivities.

It is the purpose of this article to present a perspectivic view of some of the more important physical, structural, and chemical aspects of pentadienyl and metal-pentadienyl chemistry. Particular emphasis is given to the bis(pentadienyl)metal complexes, which have been referred to as the "open metallocenes" (271 references).

(2) Like all transition metal ions the copper(II) ion is characterized by an ability to form coordination complexes with a wide range of ligands, exhibiting a variety of stereochemistries. It is less typical in that these stereochemistries are dominated by the formation of nonregular structures, involving significant bond length and bond angle distortions from the regular octahedral, tetrahedral and square coplanar geometries as a consequence of the non-spherical symmetry of the copper(II) ion, d^9 configuration, and of the influence of the Jahn—Teller, and pseudo Jahn—Teller effect on six-coordinate geometries. However, there are secondary consequences of the Jahn—Teller effect that must also be considered: (1) The Plasticity Effect; (2) Cooperative Jahn—Teller Effect; (3) Second Order Jahn—Teller Effects; (4) Fluxional Copper(II) Stereochemistries.

An earlier attempt to establish a correlation of the structural data with the electronic properties (such as electronic and ESR spectra) was limited to the more regular stereochemistries of copper(II) ions, but this picture is now sufficiently out of date to justify a new look at the relationship in question. This review is an attempt to do this. In order to keep the article to a reasonable length, and as the literature on the copper(II) ion is now very extensive, this reappraisal is carried out with particular emphasis on the authors' own fields of interest (98 references).

(3) Recently Bacci demonstrated that the Jahn—Teller coupling constants, hitherto only accessible theoretically with considerable difficulty, could be derived in a remarkably simple manner using the framework of the angular Overlap Model. He gave the results for

d^1 (and equivalent) systems both for ML_6O_4 species and for a number of lower symmetries and more recently has listed his findings for various other d^x ground states in O_h symmetry. These latter calculations were carried out only in the strong field basis and neglected the effects of spin-orbit coupling. Although the strong field formalism lends itself most readily to the evaluation of the Jahn—Teller coupling constants, there may still arise situations in which a weak field approximation might be more appropriate. The article in question therefore presents results for all the d^x ground states of ML_6O_4 systems in both the weak and strong field bases and considers specifically the consequences of spin-orbit coupling in either formalism (20 references).

(4) β-Dicarbonyl compounds have been of considerable interest to organic, inorganic and physical chemists over the years. The review in question concentrates principally on β-diketones and β-ketoaldehydes, their tautomeric composition, structure and bonding. As is well known, proton transfer and hydrogen bonding are two aspects of the chemistry of hydrogen that, respectively, govern the behaviour and structure of many molecules, both simple and complex. The β-dicarbonyls exhibit both of these features, and in ways which have singled them out for detailed study for many years. They provide the best known examples of keto/enol proton transfer and high concentration of the enol tautomers in most cases. Research involving structural, spectroscopic and computational techniques has deepened our understanding of these compounds and changed our picture of them. The hydrogen bonding is surprisingly strong, surprising since it is neither centered, nor linear, nor involved in the ring's delocalized bonding, although it is certainly coupled to it. The review deals with controversies that have surrounded the β-dicarbonyls (156 references).

Veszprém University of Chemical Engineering,
Department of General and Inorganic Chemistry,
Veszprém

Sándor PAPP

I. Ugi, J. Dugundji, R. Kopp, D. Marquarding: *Perspectives in Theoretical Stereochemistry*
Springer-Verlag, Berlin—Heidelberg—New York—Tokyo 1984, pp. 247 + XVII

The knowledge in stereochemistry is expanding enormously, owing to the rapid development in the NMR, IR, ORD, CD, MS techniques and the chromatographic separation techniques, which information cannot be processed and classified consistently by the "classical" stereochemictry based on geometric and energetical concepts. The utilization of computers has become unavoidable and desirable in this discipline, too. The pioneers of this direction are the authors of the present work, they summarized here the results of a decade-long research mainly published in various journals, while considering the points of view of non-experts, too, completing it with basic principles in stereochemistry and the theory of sets.

After the Introduction (pages VI—XIII) reasoning for the development of a new stereochemical theory detached from the geometric aspect, the authors describe their theory based on permutational approximation in Parts I, II and III divided into further subchapters.

Part I is devoted to the introduction of the main concepts and principles, thus in Chapter I they described the striking deficiencies of the classical theory in the case of flexible models, the definitions of chemical identity, stereoisomerism, chirality are given in new or somewhat reconstructed forms, corresponding to the purposes of permutational formalism. According to the definition, two molecules are identical, when they belong to the same compound, that is, they cannot be separated from each other by chemical methods. Although the definition is based purely on empirical fundamentals and consists no geometrical or energetical conditions, just owing to its empirical character, it is a function of the actual technical knowledge, is open in its meaning and can change in time. Since in the formalism introduced the almost only fundamental new concept is the identity group (Chapter II) reflecting the chemical identity, the not sharply outlined definition indicates non-final state of the theory. In Chapter III they discuss the geometrical interpretation of the "asymmetric carbon atom" stating that the permutational formalism does not demand the symmetry of the skeleton (valence bonds) that can be described by a T_d point group. This abstraction is, however, not implicated by the geometrical concept, either, thus this cahpter can be regarded as a "fingerwork" attached to the new theory.

Part II contains a detailed formulation of the mathematical theory of the chemical identity group. The understanding of Chapters IV—VI requires a more profound knowledge in the theory of groups than that usual for stereochemists in the practice, therefore it is advisable

to study the concepts in the theory of groups, the notations and terminology summarized in the Appendix before reading Part II; due to the repetitorium character of this summary, great persistence is required for doing it by beginners. The families of the permutational isomers (Chapter IV), analysis of the isomerization schemes (Chapter V), the discussion on the structure of the identity group (Chapter VI) are the following topics, however, in these chapters several mathematically defined definitions, axiomas, theoremas, propositions crystallize in the form of corollariums, which, being isolated from reality to be reflected seem rather to be the application of the theory of sets than to a new stereochemical theory.

Chapter VII in Part III, presents the application of permutational formalism to actual stereochemical problems by the determination of the stereoisomers of pentacoordinated arsenic compounds, allene derivatives, cyclobutane derivatives and trihydroxyglutaric acid. The widespread analytical efficiency of the method is presented by the interpretation of the pseudorotation of pentacoordinated molecules, of the sigmatropic 1,5-hydrogen migration examined in the case of an octadiene derivative, as well as of the Cope rearrangement of bullvalene and the S_N2 processes. Stereochemists interested not in the mathematical relationships can judge and study the perspectives and limits of the theory in this chapter, while omitting Part II. Chapter VIII contains the description of a uniform nomenclature and documentation system serving computerized data processing. The CANON procedure developed by the authors and the method of permutational groups was coupled to provide an alternative possibility for this.

The title of the book is a bit too promising as compared to its content, since it is limited to the description of permutational formalism, omitting other developing perspectives of theoretical stereochemistry. Its style is sometimes talkative, sometimes laconic, rather elegant than easy to understand. The way of presentation seems to be unsettled didactically, which can be attributed to the pioneer nature of the work. It can be recommended to experts deeply involved in stereochemistry or to those working on the application of computers.

Central Research Institute for Chemistry,
Hungarian Academy of Sciences,
Budapest

István TÖMÖSKÖZI

PRINTED IN HUNGARY

Akadémiai Kiadó és Nyomda, Budapest

RECENT DEVELOPMENTS IN THE CHEMISTRY OF NATURAL CARBON COMPOUNDS

Vol. 10.

Edited by

R. BOGNÁR and CS. SZÁNTAY

In English. 1984. 303 pages. 198 figures. 24 tables. 15×23 cm
Hardcover $ 18.00/DM 44,—/£ 9.90
ISBN 963 05 3255 7

Two interesting groups of biologically active natural products are discussed in the present volume.

I. Ninomiya and *T. Naito* give a survey of recent results in the research of benzo/c/phenanthridine alkaloids. Synthetic methods, grouped in a well arranged system, constitute the main part, followed by descriptions of the syntheses of prominent representatives of the group, such as nitidine, a compound with antitumour activity.

The authenticity of the report on vancomycin antibiotics by *F. Sztaricskai* and *R. Bognár* is guaranteed by the authors' own achievements in the pertaining research. The isolation, activity, details of structural studies and syntheses of these glycopeptide antibiotics are surveyed and their uses (medical, agricultural or diagnostic) are also mentioned.

The volume is of primary interest to researchers, organic and pharmaceutical chemists, biochemists and pharmacologists.

AKADÉMIAI KIADÓ
Publishing House of the Hungarian
Academy of Sciences
Budapest

PROCEEDINGS OF THE FIFTH TIHANY SYMPOSIUM ON RADIATION CHEMISTRY

Edited by: J. Dobó, P. Hedvig, R. Schiller

In two volumes. 1983. 1188 pages. Numerous figures. 17 × 25 cm. Hardcover. $ 75.00/DM 165,—
ISBN 963 05 3429 0

These volumes contain the papers and discussions of the Fifth Tihany Symposium on Radiation Chemistry held traditionally at Lake Balaton, Hungary. Similarly to its predecessors, the first of which was in 1962, all important aspects of the radiolysis of aqueous solutions, organic and inorganic materials, and polymers were discussed. Papers dealing with biological aspects were also included. It is rewarding to see how new fields, such as the physics of exotic atoms, i.e. muonium and positronium chemistry, is being incorporated into the traditional area of radiation research. Besides studies of basic processes, various problems of applications were presented and discussed by some 170 participants.

The volumes provide an up-to-date overview of the present state of this rapidly developing field.

AKADÉMIAI KIADÓ
BUDAPEST

Text

The text of the paper should be concise. The description of new compounds (in the Experimental) must include the complete analytical data. Special attention must be paid to structural formulas given within the text. Complicated (non-linear) formulas should be drawn on separate sheets of paper and their position in the text should be clearly marked. The numbering of formulas and equations (in parentheses on the right-hand side) is only needed if they are referred to in the text. Units should conform to the International System of Units (SI). In nomenclature the rules of the I.U.P.A.C. are accepted as standard. Symbols for physical quantities are printed in italic type and should, therefore, be underlined in the manuscript.

References

References should be numbered in order of appearance in the text (where the reference number appears in brackets) and listed at the end of the paper. The reference list, too, should by typed double-spaced. Journal titles are to be abbreviated as defined by the Chemical Abstracts Service Source Index.

Examples:

[1] Brossi, A., Lindlar, H., Walter, M., Schneider, O.: Helv. Chim. Acta, **41**, 119 (1958)
[2] Parr, R. G.: Quantum Theory of Molecular Electronic Structure, Benjamin, New York 1964
[3] Warshel, A.: in Modern Theoretical Chemistry, Vol. 7, Part A (Ed. G. A. Segal), Plenum Press, New York 1977

Tables

Each table should be given a Roman number and a brief informative title. Structural formulas should not be used in column headings or in the body of tables.

Figures

Figures should be numbered consecutively with Arabic numerals. Their approximate place should be indicated in the text on the margin. Allfigures must be identified on the back by the author's name and the figure number in pencil. Standard symbols (such as circles, triangles, squares) are to be used on line-drawings to denote the points determined experimentally. Line-drawings must not contain structural formulas and comments. Spectra or relevant segments thereof, chromatograms, and X-ray diffraction patterns will be reproduced only if concise numerical summaries are inadequate to replace them. Drawings and graphs should be prepared in black ink on good-quality white or tracing paper. Photographs should be submitted on glossy paper as high-contrast copies. Xerox or similar copies are not suitable for reproduction, but may be used for duplicate copies.

Redrawn illustrations will be sent to the authors for checking. No corrections of figures will, therefore, be accepted in the proofs.

Submission of manuscript

After having completed the corrections suggested by the referees and editors, the final manuscript should be submitted in duplicate, in a form ready for publication. If the corrected manuscript is not returned to the editots *within six weeks*, the intended publication of the paper will be regarded as withdrawn by the authors.

Page charge will not be assessed for the publication, however, authors from overseas countries must contribute to the postage of correspondence by sending, together with the manuscript, international postal coupons to the value of U.S. $ 10.—

Proofs and reprints

A set of proofs will be sent to the submitting author. The proofs must be returned within 48 hours of receipt. Late return may cause a delay in the publication of the paper. 100 reprints will be supplied to the authors free of charge.

Periodicals of the Hungarian Academy of Sciences are obtainable at the following addresses:

AUSTRALIA
C.B.D. LIBRARY AND SUBSCRIPTION SERVICE
Box 4886, G.P.O., *Sydney N.S.W. 2001*
COSMOS BOOKSHOP, 145 Ackland Street
St. Kilda (Melbourne), Victoria 3182

AUSTRIA
GLOBUS, Höchstädtplatz 3, *1206 Wien XX*

BELGIUM
OFFICE INTERNATIONAL DE LIBRAIRIE
30 Avenue Marnix, *1050 Bruxelles*
LIBRAIRIE DU MONDE ENTIER
162 rue du Midi, *1000 Bruxelles*

BULGARIA
HEMUS, Bulvar Ruszki 6, *Sofia*

CANADA
PANNONIA BOOKS, P.O. Box 1017
Postal Station "B", *Toronto, Ontario M5T 2T8*

CHINA
CNPICOR, Periodical Department, P.O. Box 50
Peking

CZECHOSLOVAKIA
MAD'ARSKÁ KULTURA, Národní třida 22
115 66 Praha
PNS DOVOZ TISKU, Vinohradská 46, *Praha 2*
PNS DOVOZ TLAČE, *Bratislava 2*

DENMARK
EJNAR MUNKSGAARD, Norregade 6
1165 Copenhagen K

FEDERAL REPUBLIC OF GERMANY
KUNST UND WISSEN ERICH BIEBER
Postfach 46, *7000 Stuttgart 1*

FINLAND
AKATEEMINEN KIRJAKAUPPA, P.O. Box 128
SF-00101 Helsinki 10

FRANCE
DAWSON-FRANCE S. A., B. P. 40, *91121 Palaiseau*
EUROPÉRIODIQUES S. A., 31 Avenue de Versailles, *78170 La Celle St. Cloud*
OFFICE INTERNATIONAL DE DOCUMENTATION ET LIBRAIRIE, 48 rue Gay-Lussac
75240 Paris Cedex 05

GERMAN DEMOCRATIC REPUBLIC
HAUS DER UNGARISCHEN KULTUR
Karl Liebknecht-Straße 9, *DDR-102 Berlin*
DEUTSCHE POST ZEITUNGSVERTRIEBSAMT
Sraße der Pariser Kommüne 3–4, *DDR-104 Berlin*

GREAT BRITAIN
BLACKWELL'S PERIODICALS DIVISION
Hythe Bridge Street, *Oxford OX1 2ET*
BUMPUS, HALDANE AND MAXWELL LTD.
Cowper Works, *Olney, Bucks MK46 4BN*
COLLET'S HOLDINGS LTD., Denington Estate
Wellingborough, Northants NN8 2QT
WM. DAWSON AND SONS LTD., Cannon House
Folkstone, Kent CT19 5EE
H. K. LEWIS AND CO., 136 Gower Street
London WC1E 6BS

GREECE
KOSTARAKIS BROTHERS INTERNATIONAL BOOKSELLERS, 2 Hippokratous Street, *Athens-143*

HOLLAND
MEULENHOFF-BRUNA B.V., Beulingstraat 2,
Amsterdam
MARTINUS NIJHOFF B.V.
Lange Voorhout 9–11, *Den Haag*

SWETS SUBSCRIPTION SERVICE
347b Heereweg, *Lisse*

INDIA
ALLIED PUBLISHING PRIVATE LTD., 13/14
Asaf Ali Road, *New Delhi 110001*
150 B-6 Mount Road, *Madras 600002*
INTERNATIONAL BOOK HOUSE PVT. LTD.
Madame Cama Road, *Bombay 400039*
THE STATE TRADING CORPORATION OF INDIA LTD., Books Import Division, Chandralok
36 Janpath, *New Delhi 110001*

ITALY
INTERSCIENTIA, Via Mazzé 28, *10149 Torino*
LIBRERIA COMMISSIONARIA SANSONI, Via Lamarmora 45, *50121 Firenze*
SANTO VANASIA, Via M. Macchi 58
20124 Milano
D. E. A., Via Lima 28, *00198 Roma*

JAPAN
KINOKUNIYA BOOK-STORE CO. LTD.
17-7 Shinjuku 3 chome, Shinjuku-ku, *Tokyo 160-91*
MARUZEN COMPANY LTD., Book Department,
P.O. Box 5050 Tokyo International, *Tokyo 100-31*
NAUKA LTD. IMPORT DEPARTMENT
2-30-19 Minami Ikebukuro, Toshima-ku, *Tokyo 171*

KOREA
CHULPANMUL, *Phenjan*

NORWAY
TANUM-TIDSKRIFT-SENTRALEN A.S., Karl Johansgatan 41–43, *1000 Oslo*

POLAND
WĘGIERSKI INSTYTUT KULTURY, Marszałkowska 80, *00-517 Warszawa*
CKP I W, ul. Towarowa 28, *00-958 Warszawa*

ROUMANIA
D. E. P., *Bucureşti*
ILEXIM, Calea Grivitei 64–66, *Bucureşti*

SOVIET UNION
SOJUZPECHAT — IMPORT, *Moscow*
and the post offices in each town
MEZHDUNARODNAYA KNIGA, *Moscow G-200*

SPAIN
DIAZ DE SANTOS, Lagasca 95, *Madrid 6*

SWEDEN
ALMQVIST AND WIKSELL, Gamla Brogatan 26
101 20 Stockholm
GUMPERTS UNIVERSITETSBOKHANDEL AB
Box 346, *401 25 Göteborg 1*

SWITZERLAND
KARGER LIBRI AG, Petersgraben 31, *4011 Basel*

USA
EBSCO SUBSCRIPTION SERVICES
P.O. Box 1943, *Birmingham, Alabama 35201*
F. W. FAXON COMPANY, INC.
15 Southwest Park, *Westwood Mass. 02090*
THE MOORE-COTTRELL SUBSCRIPTION AGENCIES, *North Cohocton, N. Y. 14868*
READ-MORE PUBLICATIONS, INC.
140 Cedar Street, *New York, N. Y. 10006*
STECHERT-MACMILLAN, INC.
7250 Westfield Avenue, *Pennsauken N. J. 08110*

YUGOSLAVIA
JUGOSLOVENSKA KNJIGA, Terazije 27, *Beograd*
FORUM, Vojvode Mišića 1, *21000 Novi Sad*

Index: 26.007

Acta Chimica Hungarica

VOLUME 121, NUMBER 4, APRIL 1986

Akadémiai Kiadó, Budapest
ACTA CHIM. HUNG. ACHUDC 121 (4) 333–411 (1986) HU ISSN 0231–3146

ACTA CHIMICA HUNGARICA

A JOURNAL OF THE HUNGARIAN ACADEMY OF SCIENCES

Acta Chimica publishes original reports on all aspects of chemistry in English.

Acta Chimica is published in three bolumes per year, each volume consisting of four issues, by

AKADÉMIAI KIADÓ

Publiching House of the Hungarian Academy of Sciences
H-1054 Budapest, Alkotmány u. 21.

Manuscripts and editorial correspondence should be addressed to

Acta Chimica
H-1450 Budapest P.O. Box 67

Subscription information

Orders should be addressed to

KULTURA Foreign Trading Company
H-1389 Budapest P.O. Box 149

or to its representatives abroad

Acta Chimica is indexed in Current Contents.

NOTICE TO AUTHORS

Acta Chimica publishes original papers on all aspects of chemistry in English. Before preparing a manuscript for submission to this journal authors are advised to consult recent issues.

Form of manuscript

Manuscripts, tables and illustrations should be submitted in triplicate. Manuscripts should be typewritten double spaced (25 lines, 50 characters per line including spaces). The *title page* should include (1) the title of the paper, (2) the full names of the author(s) in the sequence to be published; apply an asterisk to designate the name of the author to whom correspondence should be addressed, (3) name and address of the institution where the work was done. If the paper is part of a series, reference to the previous communication must be given as a footnote.

Abstract

A summary is printed at the head of each paper. This should not exceed 200 words and should state briefly the principal results and major conclusions of the work. It should be suitable for use by abstracting services.

CONTENTS

Acta Chimica Hungarica 121 (4), pp. 333—338 (1986)

SYNTHESES WITH AROMATIC NITRAMINES, VI*

SUBSTITUENT EFFECT IN THE PHOTOLYTIC REARRANGEMENT OF NITRAMINOPYRIDINES

Jadwiga SEPIOŁ and Piotr TOMASIK**

(Department of Chemistry and Physics, The Hugon Kołłataj Academy of Agriculture, 30059 Cracow, Poland)

Received December 17, 1984
Accepted for publication May 24, 1985

All isomeric ring-substituted methyl-2-nitraminopyridines, both 3-nitro- and 5-nitro-2-nitraminopyridines, 5-chloro- and 3-carboxy-2-nitraminopyridines, as well as 3,5-dibromo-2-nitraminopyridine were photolyzed in methanol by irradiation with a low-pressure mercury lamp (253.7 nm). Preference was generally noted for the migration of the side-chain nitro group to the vicinal β-position. 3,5-Dibromo-2-nitraminopyridine gave both 2-amino-3,5-dibromopyridine and 3,5-dibromo[1*H*]pyridine-2-one. The ratio of the preparative and quantum yields of the two products were 2.5 and 3.0, respectively.

Introduction

2-Nitraminopyridine yields in acid-catalyzed rearrangement a mixture of 2-amino-3-nitro- and 2-amino-5-nitropyridines with an isomer ratio of about 1 : 4, and this is almost independent of the reaction conditions [1]. This ratio of the isomers is reversed in the free radical (photolytic) rearrangement [2]. The substituent effect observed in the acid-catalyzed rearrangement is due to the electronic effect of the given group, but also the size and the position of such a group in the ring play an essential role.

It has been reported that in the acid-catalyzed process 3-substituted 2-nitraminopyridines rearrange more readily into the 5-position than 5-substituted isomers do it into the 3-position (see [3] and references cited therein). Our recent studies [4] have shown that it is not so; on the other hand the results published by Deady et al. [5] may cast doubts on our point of view. In the present paper the substituent effect in the photolytic rearrangement is presented based on the determination of the quantum yields of decay of nitraminopyridines, as well as the preparative and quantum yields of the formation of the rearrangement products are given. The photolysis reactions of all isomeric ring substituted methyl-2-nitraminopyridines, 5-chloro- and 3-carboxy-2-nitraminopyridines and 3,5-dibromo-2-nitraminopyridine were studied.

* Preceding paper of this series: J. Sepioł, P. Tomasik, This Journal, **113**, 159 (1983)
** To whom correspondence should be addressed

Results and Discussion

Table I shows the results of the irradiation of particular 2-nitraminopyridine derivatives, together with the preparative yields of the products.

Table II presents the decay of the nitramines as a function of the irradiation time and the concentration increase of the products. The quantum yields of these processes supplemented by some experimental details are listed in Table III.

Table I

Results of the irradiation of 2-nitraminopyridines

Substrate	Initial concentration $x10^{-3}$ mol · dm^{-3}	Irradiation time, s	Chomatographic developing solvent
3-Methyl-2-nitraminopyridine [6]	5.524	1800	chloroform : acetone, 1 : 1
4-Methyl-2-nitraminopyridine [6]	1.949	1500	chloroform : acetone, 1 : 1
5-Methyl-2-nitraminopyridine [6]	3.918	2400	chloroform : acetone, 1 : 1
6-Methyl-2-nitraminopyridine [6]	6.597	4800	chloroform : acetone, 1 : 1
3-Nitro-2-nitraminopyridine [7]	4.432	21600	chloroform : acetone, 1 : 1
5-Nitro-2-nitraminopyridine [8]	4.237	2700	chloroform : acetone, 1 : 1
5-Chloro-2-nitraminopyridine [9]	6.388	2400	chloroform
3,5-Dibromo-2-nitraminopyridine [10]	9.388	7200	chloroform
2-Nitraminonicotinic acid [11]	0.915	1200	ethanol

[a] M.p.s. agree with those reported in the literature (see Refs.).
[b] The product was crystallized from aqueous ethanol.
[c] The isomers were separated by steam distillation [12], followed by crystallization from aqueous ethanol.
[d] The products were separated by sublimation, followed by crystallization from aqueous ethanol.
[e] The crude product was dissolved in dilute sodium hydroxide solution and precipitated with hydrochloric acid added to pH 5 [11].

Products	M. p.,[a] °C	Elemental analysis		Yield, %
		%N Calcd.	%N Found	
3-Methyl-5-nitro-2-aminopyridine[b]	255	27.44	27.24	19.4
4-Methyl-3-nitro-2-aminopyridine[c]	135	27.44	27.53	4.2
4-Methyl-5-nitro-2-aminopyridine[c]	220	27.44	27.33	26.6
5-Methyl-3-nitro-2-aminopyridine[b]	190	27.44	27.29	28.2
6-Methyl-3-nitro-2-aminopyridine[b]	141	27.44	27.55	7.2
3,5-Dinitro-2-aminopyridine[b]	191	30.43	30.31	17.6
3,5-Dinitro-2-aminopyridine[b]	191	30.43	30.35	12.8
5-Chloro-3-nitro-2-aminopyridine[b]	195	24.21	24.38	8.5
3,5-Dibromo-2-aminopyridine[d]	105	11.12	11.09	22.3
1*H*-3,5-Dibromopyridine-2-one[d]	208	5.54	5.38	8.9
2-Amino-5-nitronicotinic acid[e]	318	22.95	23.10	14.1

It can be seen from Tables I and III that the preparative yields roughly parallel the quantum yields of the product formation. Significant differences and the increase of the concentrations of the irradiated substrates and the products formed, respectively, are due to the formation of tarry by-products. In the case of all 3-, 4- and 5-methyl-2-nitraminopyridines approximately one of each two molecules yields aminonitropyridines, whereas in the case of the majority of the other nitramino derivatives only one of each five molecules is converted into the aminonitro product. These results are better than those for unsubstituted 2-nitraminopyridine [2] where only 3 of each 25 molecules gave aminonitropyridines. Following the observation of Deady et al. [5], reaction mixture obtained on the irradiation of 3-nitro- and 5-nitro-2-nitraminopyridines were examined for the content of the corresponding β-nitro-2-pyridones. They were absent among the products. The low yield is not necessarily due to decomposition of the amino-nitro products. As we have shown previously, 2-amino-β-nitropyridines are stable under the conditions of the irradiation applied.

It can be seen that the decay of nitramines does not too clearly depend on the electrical effects of the substituents. Perhaps the substituent effect observed is due to an influence also on the tautomeric equilibrium. 2-Nitraminopyridine and its methyl derivatives take the form of 1*H*-2-nitriminopyridine [13, 14] whereas 3-nitro- and 5-nitro-2-nitraminopyridines take the nitramino form [15]. Simultaneously, the effect of substituents on the pK_a of nitraminopyridines should also be taken into account. From a comparison of the quantum yields of the decay of the isomeric methyl-2-nitraminopyridines and isomeric nitro-2-nitraminopyridines one may conclude that a preference exists for the migration of the side-chain nitro group to the vicinal 3-position rather than to the 5-position. It is the opposite tendency to that observed in the acid-catalyzed process [3], and it simultaneously confirms our recent observation [2] in the photolytic rearrangement of unsubstituted 2-nitraminopyridine. The rearrangement of 4-methyl-2-nitraminopyridine does not follow this rule, perhaps for steric reasons. The varying proneness of the isomeric β-monosubstituted nitraminopyridines to rearrangement may be due to differences in the electrical effect of a given substituent exerted on the nitramino group from the 3- or 5-position. It has been shown that the electron donating effect from the 2-methyl group to the reaction site in the 3-position is stronger than the effect transmitted across the ring to the 5-position [16]. Hence 6-methyl-2-nitraminopyridine rearranges solely into 6-methyl-3-nitro-2-aminopyridine because the energy of localization of the unpaired electron is lower in the 3-position. The substituent constants for the $NHNO_2$ and NNO_2^- groups clearly suggest [17] that the localization of the unpaired electron should be preferred in the 3-position rather than in the 5-position. Our studies on the conformation and tautomeric equilibria in 2-nitraminopyridine and its

Table II

Decay of nitraminopyridines and the formation of products (all in mol · dm^{-3}) *as the function of the*

Irradiation time s	3-Methyl-2-nitraminopyridine →	3-Methyl-5-nitro-2-aminopyridine	4-Methyl-2-nitraminopyridine →	4-Methyl-3-nitro-2-aminopyridine +	4-Methyl-5-nitro-2-aminopyridine	5-Methyl-2-nitraminopyridine →	5-Methyl-3-nitro-2-aminopyridine	6-Methyl-2-nitraminopyridine →	6-Methyl-3-nitro-2-aminopyridine
	x10^{-3}	x10^{-4}	x10^{-3}	x10^{-4}	x10^{-4}	x10^{-3}	x10^{-4}	x10^{-3}	x10^{-4}
0	5.524		1.949			3.918		6.597	
180									
300								5.654	2.940
360			1.280	0.348	2.879				
600			1.010	0.554	3.852	2.974	5.467	5.238	3.060
900	4.248	6.654	0.845	0.729	4.649				
1200	3.956	7.754				2.624	7.852		
1500	3.766	8.643	0.680	0.827	5.189				
1800	3.646	10.695				2.180	9.912		
2400						2.040	11.053	3.800	4.030
2700									
3600								3.445	4.340
4800								3.360	4.740
5400									
7200									
10800									
14400									
21600									

derivatives [13—15] suggest that within pairs of isomers the influence of a β-substituent is less essential on both these properties.

In 3,5-disubstituted 2-nitraminopyridines rearranged in acidic media, the nitramino group is replaced by a hydroxyl group [18]. Now the partial conversion of the nitramino group to amino group has been shown. This seems to be a novel feature of the reactivity of this substituent.

Experimental

Methanolic solutions of the analytically pure nitraminopyridines were irradiated under nitrogen between two low-pressure Phillips TUV 30 W (253.7 nm) mercury lamps. The course of the reaction was monitored on TLC silica gel 60 F_{254} covered (0.25 mm) sheets. The identity of the resulting products with authentic samples (see Refs in Table I) was confirmed by comparison of their IR (KBr) spectra, elemental analyses, as well as by mixed m.p. determinations. References to the preparation methods of the nitramines and experimental details are given in Table I and footnotes to it.

The quantum yields were calculated based on determinations of the decay of nitraminopyridines and formation of the products as a function of the irradiation time (Table II). These determinations as well as the procedure of the determination of the quantum yields were followed as described in our preceding paper [2]. The experimental details necessary for this purpose are shown in Table III.

irradiation time

3-Nitro-2-nitramino-pyridine →	3,5-Dinitro-2-amino-pyridine	5-Nitro-2-nitramino-pyridine →	3,5-Dinitro-2-amino-pyridine	5-Chloro-2-nitramino-pyridine →	5-Chloro-3-nitro-2-amino-pyridine	3,5-Dibromo-2-nitramino-pyridine →	3,5-Dibromo-2-amino-pyridine +	3,5-Dibromopyridine-2-one	2-Nitraminonicotinic acid →	2-Amino-5-nitronicotinic acid
x10^{-3}	x10^{-4}	x10^{-3}	x10^{-4}	x10^{-3}	x10^{-4}	x10^{-3}	x10^{-3}	x10^{-4}	x10^{-4}	x10^{-4}
4.432		4.237		6.388		9.388			9.147	
									3.455	0.668
				4.900	2.098	8.415				
									1.590	0.880
		3.330	1.940						0.936	1.112
		3.135	2.130	3.440	3.535					
									0.549	1.292
				2.930	4.513					
		2.436	4.542			7.230	1.584	4.342		
3.093	3.733			2.120	5.451	6.665	1.699	5.258		
		2.019	5.409							
						5.685	1.962	7.634		
2.574	4.215					4.530	2.227	9.196		
						3.790	2.466	9.805		
1.662	4.908									
1.362	5.326									
1.023	7.790									

REFERENCES

[1] Pasternak, E. E., Tomasik, P.: Bull. Acad. Pol. Sci., Ser. Sci. Chim., **26,** 417 (1978)
[2] Sepioł, J., Tomasik, P.: Acta Chim. Hung., **113,** 159 (1983)
[3] Tomcufcik, A. S., Starker, L. N.: "Pyridine and Its Derivatives" (E. Klingsberg, Ed.), Chapter 9.4, p. 50, Part **3,** Interscience, New York 1962
[4] Kokocińska, H., Thomas, A., Tomasik, P., Zalewski, R.: Bull. Acad. Pol. Sci., Ser. Sci. Chim., **24,** 535 (1976)
[5] Deady, L. W., Grimmett, M. R., Potts, C. H.: Tetrahedron, **35,** 2895 (1979)
[6] Pino, L. N., Zehrung, W. S.: J. Am. Chem. Soc., **77,** 3154 (1955)
[7] Chichibabin, A. E., Konovalova, R. A.: Ber., **58,** 1717 (1925)
[8] Chichibabin, A. E., Rasorenov, B. A.: Zh. Russ. Fiz. Khim. Obshch., **47,** 1286 (1915)
[9] Chichibabin, A. E., Jegorov, A.: Zh. Russ. Fiz. Khim. Obshch., **60,** 687 (1982); Chem. Zentr., **1928 II,** 1670
[10] Chichibabin, A. E., Kirssanov, A. V.: Ber., **61,** 1241 (1928)
[11] Bojarska-Dahlig, H.: Roczniki Chem., **30,** 493 (1953)
[12] Seide, O.: Ber., **57,** 794 (1924)
[13] Kraus, W., Pietrzycki, W., Tomasik, P.: Chem. Scripta, **23,** 97 (1984)
[14] Kraus, W., Pietrzycki, W., Tomasik, P.: Chem. Scripta, **19,** 158 (1982)
[15] Kraus, W., Pietrzycki, W., Tomasik, P., Zawadzki, W.: Chem. Scripta (in the press)
[16] Achremowicz, L., Tomasik, P.: Bull. Acad. Pol. Sci., Ser. Sci. Chim., **24,** 853 (1976)
[17] Thomas, A., Tomasik, P.: Bull. Acad. Pol. Sci., Ser. Sci. Chim., **23,** 65 (1975)
[18] Chichibabin, A. E., Kirssanov, A. V.: Ber., **61,** 1236 (1928)

Table III

Quantum yields of photochemical rearrangement of nitraminopyridines

Compounds	Irradiation intensity, 10^{-6}E · dm^{-3} · s^{-1}	Quantum yield, mol · E^{-1}		Extinction coefficient, dm^2 · mol	Chromatographic column and temperature[b], °C
		substrate decay	product formation[a]		
3-Methyl-2-nitraminopyridine	5.90	0.634		$\varepsilon_{275} = 722.7$	
3-Methyl-5-nitro-2-aminopyridine			0.329 (0.52)	$\varepsilon_{275} = 27.5$	3% SE-30, 260°
4-Methyl-2-nitraminopyridine	12.52	0.768		$\varepsilon_{270} = 1781.1$	
4-Methyl-3-nitro-2-aminopyridine			0.047 (0.48)	$\varepsilon_{270} = 214.4$	3% OV-17, 130—250°
4-Methyl-5-nitro-2-aminopyridine			0.320	$\varepsilon_{270} = 93.0$	3% OV-17, 130—250°
5-Methyl-2-nitraminopyridine	5.90	0.741		$\varepsilon_{275} = 773.3$	
5-Methyl-3-nitro-2-aminopyridine			0.434 (0.59)	$\varepsilon_{275} = 165.6$	3% SE-30, 210°
6-Methyl-2-nitraminopyridine	5.90	0.886		$\varepsilon_{275} = 610.2$	
6-Methyl-3-nitro-2-aminopyridine			0.172 (0.19)	$\varepsilon_{275} = 258.3$	3% SE-30, 110—230°
3-Nitro-2-nitraminopyridine	5.90	0.251		$\varepsilon_{265} = 622.7$	
3,5-Dinitro-2-aminopyridine			0.056 (0.22)	$\varepsilon_{265} = 181.5$	3% OV-17, 210°
5-Nitro-2-nitraminopyridine	5.90	0.382		$\varepsilon_{310} = 1396.2$	
3,5-Dinitro-2-aminopyridine			0.083 (0.22)	$\varepsilon_{310} = 169.0$	3% OV-17, 210°
5-Chloro-2-nitraminopyridine	12.52	0.887		$\varepsilon_{292} = 1169.0$	
5-Chloro-3-nitro-2-aminopyridine			0.115 (0.13)	$\varepsilon_{292} = 79.6$	3% OV-17, 130—250°
3,5-Dibromo-2-nitraminopyridine	5.90	0.309		$\varepsilon_{285} = 628.5$	
3,5-Dibromo-2-aminopyridine			0.175 (0.76)	$\varepsilon_{285} = 95.3$	3% OV-17, 110—230°
1*H*-3,5-Dibromopyridine-2-one			0.059	$\varepsilon_{285} = 168.6$	3% OV-17, 110—230°
2-Nitraminonicotinic acid	12.52	0.728		$\varepsilon_{285} = 1847.0$	
2-Amino-5-nitronicotinic acid			0.095 (0.13)	$\varepsilon_{285} = 64.8$	3% SE-30, 330°

[a] The ratio of the quantum yields of the substrate decay and product formation is given in parentheses.
[b] If the range of temperature is given, the temperature increase was programmed.

Acta Chimica Hungarica 121 (4), pp. 339—344 (1986)

GAS CHROMATOGRAPHIC DETERMINATION OF C_1—C_4 NORMAL PRIMARY AMINES AS THE SCHIFF BASES OF FURFURAL AND THE CORRESPONDING SECONDARY AND TERTIARY AMINES AS FREE AMINES

László Maros

(Institute of Inorganic and Analytical Chemistry, Eötvös Loránd University, H-1088, Múzeum krt. 4/B, Budapest)

Received January 30, 1985
Accepted for publication May 24, 1985

A gas chromatographic method was developed for the quantitative determination of C_1—C_4 normal aliphatic primary and the corresponding secondary and tertiary amines. Primary amines were separated as the Schiff bases of furfural, secondary and tertiary amines were separated simultaneously in the free form on a potassium hydroxide-treated PEG-20M packed column.

Introduction

For the separation of mixtures of amines by gas chromatography PEG-20M + KOH [1, 2], tetrahydroxyethylenediamine and tetraethylenepentamine [3], triethanolamine [4], Amine 220 + KOH [5], Pennwalt + KOH [6], Chromosorb 103 + KOH [7], TENAX-GC [8] and GHP-l + KOH [9] packed columns have been used.

Primary amines can be derivatized with carbonyl compounds to form Schiff bases [10]. Hoshika [11] used benzaldehyde to form Schiff bases with lower primary aliphatic amines. The mixture of the Schiff bases and the free secondary and tertiary amines were separated by a TENAX-GC packed column by temperature programmed gas chromatography. Tavakkol and Drucker [12] found that for the gas chromatographic separation of bacterial primary amines the benzaldehyde Schiff bases were the most suitable, using columns of OV-17 on Chromosorb W. However, secondary and tertiary amines cannot be separated on this column.

In this study, to achieve separations of free primary, secondary, tertiary amines and the furfural Schiff base derivates of the primary amines, they were chromatographed using a column of PEG-20M with potassium hydroxide on Chromosorb G. It will be shown that the furfural Schiff bases of methylamine and ethylamine can be separated from the reagent furfural, while the benzaldehyde Schiff bases of these amines and the reagent benzaldehyde overlap.

Experimental

Reagents and materials

The amines used were obtained from Fluka (Buchs, Switzerland). A 200-mL aqueous amine hydrochloride stock solution was prepared from accurately weighed methylamine hydrochloride (1.000 g), dimethylamine hydrochloride (0.993 g), trimethylamine (1.00 mL 21,3% aqueous solution), ethylamine hydrochloride (1.001 g), diethylamine (1.00 mL), triethylamine (1.00 mL), *n*-propylamine (1.00 mL), di-*n*-propylamine (2.00 mL) tri-*n*-propylamine (0.50 mL), *n*-butylamine (1.00 mL), di-*n*-butylamine (1.00 mL) and tri-*n*-butylamine (0.50 mL) by acidifying with concentrated hydrochloric acid in the presence of 10 drops of 0.2% aqueous Thymol Blue indicator solution until the red colour appeared, and by diluting with distilled water. *Sec*-butyl alcohol was used as a solvent, which contains 1.00% (v/v) mesitylene as internal standard. Redistilled furfural was used for derivatization. The solvent and all other reagents used were guaranteed or reagent grade chemicals from Reanal (Budapest, Hungary).

Apparatus

A Chromatron Model GCHF-4 (Berlin, GDR) gas chromatograph with flame ionization detector, and a Chinoin Model Digint 34 μ (Budapest, Hungary) electronic integrator was used for sample analysis. The column used was a 6 m 4 mm i.d. stainless steel column packed with 5% PEG-20M and 2% potassium hydroxide on Chromosorb G WAW (80–100 mesh). Nitrogen was used as carrier gas at a flow rate of 45 mL/min. Injector and detector temperatures were set at 250 °C. The column was preconditioned at 210 °C for 12 hours in a stream of nitrogen.

Temperature programmed gas chromatographic determinations were performed for the analysis: 10 min at 80 °C, programmed to 180 °C by a 48 °C/min rate, and 20 min at 180 °C.

Procedure

To an aliquot portion (0.100 or 1.00 mL) of the aqueous amine hydrochloride solution 1 drop of Thymol Blue indicator solution and 1 drop of *conc.* hydrochloric acid was given. The solution was evaporated to dryness in vacuum at 60—70 °C. The residue was dissolved in 1.00 mL of *sec*-butyl alcohol (containing the internal standard mesitylene). The solution was transferred to a small glass-stoppered test tube and made alkaline with 1—3 drops of aqueous 20% sodium hydroxide solution till the appearance of the blue colour. (Solutions must be shaken well to observe the point of change of colour).

A 1- μL aliquot was injected to the column. After the GC analysis of the free amines, 10—40 μL furfural was added to the solution (10 μL to the 0.100 mL, and 40 μL to the 1.00 mL originally used stock solution). After 30 min reaction time a 1- μL aliquot was injected to the column for analysis of the free secondary, tertiary amines, and the Schiff bases formed from the primary amines.

Results and Discussion

In gas chromatographic amine separations potassium hydroxide-treated PEG-20M columns are commonly used. On these columns the methyl- and dimethylamine, *n*-butylamine and di-*n*-propylamine peaks overlap, but in the form of Schiff bases primary amines can be well separated from the secondary and tertiary amines.

The gas chromatograms of the free amine mixtures and of the furfural Schiff bases of primary amines with the free secondary and tertiary amines are shown in Figs 1a and 1b. Comparison of the gas chromatograms of the benzaldehyde Schiff bases of primary amines (Fig. 1c) with these of the furfural derivatives shows that the methylamine and ethylamine Schiff bases of furfural

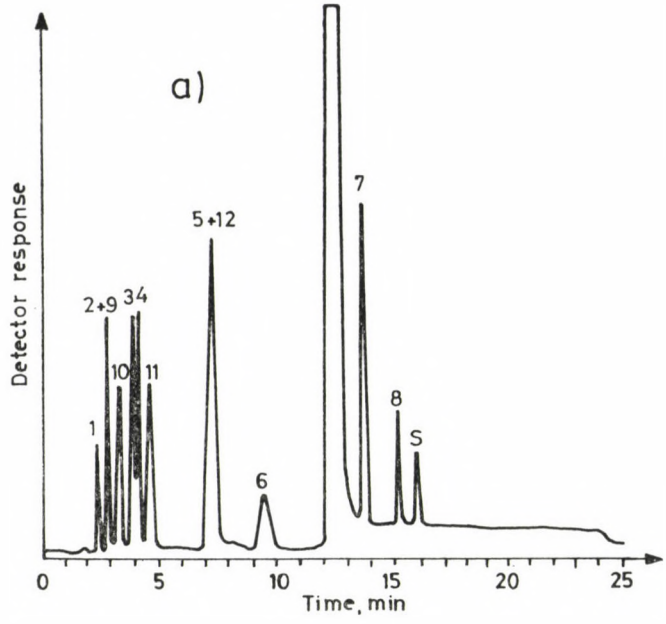
a)
Detector response
1
2+9
3
4
10
11
5+12
6
7
8
S
0
5
10
15
20
25
Time, min

Fig. 1/a.

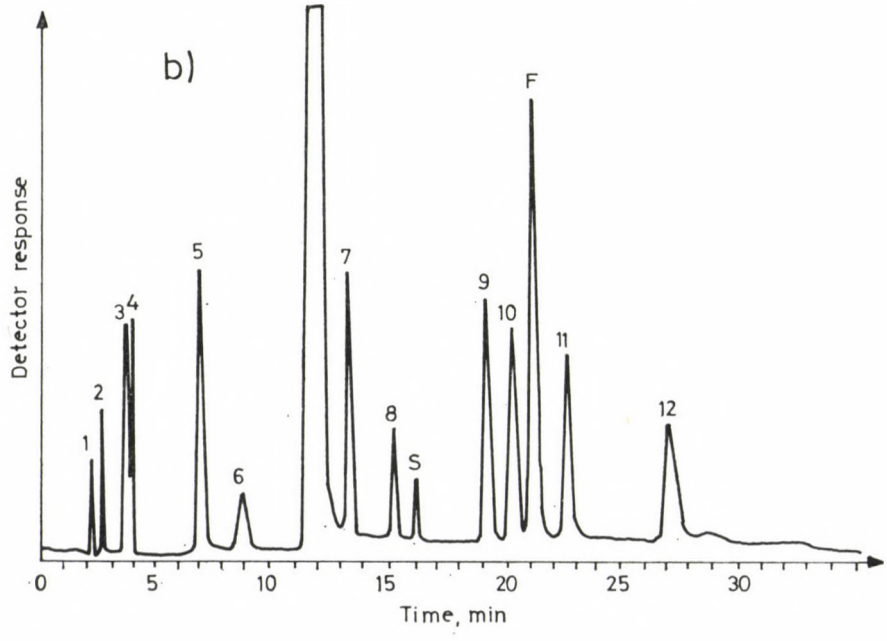
b)
Detector response
1
2
3
4
5
6
7
8
S
9
10
F
11
12
0
5
10
15
20
25
30
Time, min

Fig. 1/b.

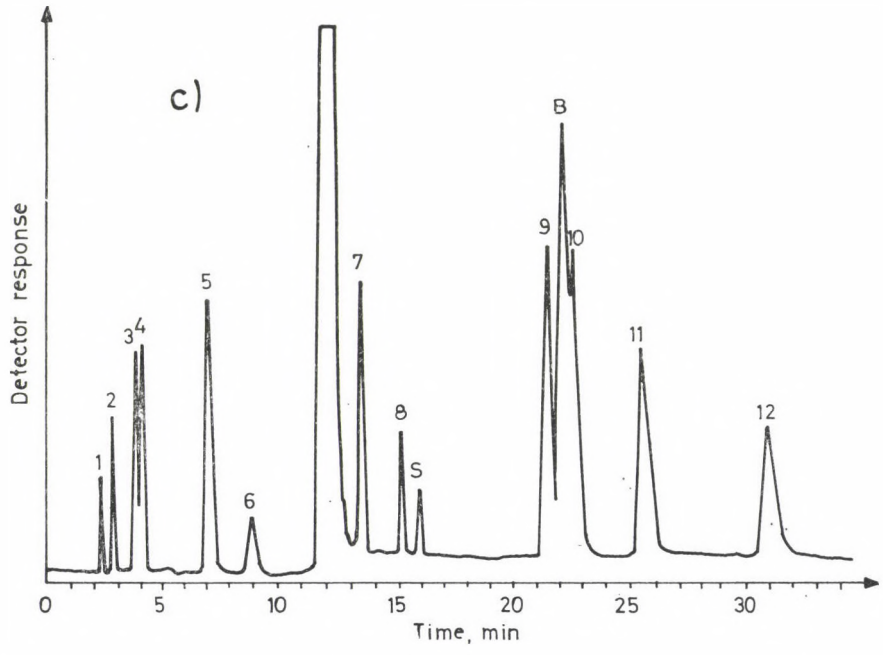

Fig. 1/c.

Fig. 1. Gas chromatogram for C_1—C_4 normal aliphatic primary amines and the corresponding secondary and tertiary amines; *a* — Free amines; *b* — Free secondary and tertiary amines and the furfural Schiff bases of primary amines; *c* — Free secondary and tertiary amines and the bezaldehyde Schiff bases of primary amines.
1 — trimethylamine, 2 — dimethylamine, 3 — diethylamine, 4 — triethylamine, 5 — dipropylamine, 6 — tripropylamine, 7 — dibutylamine, 8 - tributylamine, 9 — methylamine, 10 — ethylamine, 11 — propylamine, 12 — butylamine, S — mesitylene, F — furfural, B — benzaldehyde

are better separated on the potassium hydroxide-treated PEG-20M column, than the Schiff bases of benzaldehyde.

In alcoholic solutions Schiff base formation with furfural is as rapid as with benzaldehyde. A 50—100% molar excess of furfural is sufficient to achieve quantitative reactions. Slow and incomplete reactions were found in dioxan and in aqueous solutions. Some of the C_1—C_4 alcohols and some of these amines overlap in the gas chromatographic separation, with the exception of *sec*-butyl alcohol, which was found to be a good solvent for both the amines and Schiff bases. Furfural for Schiff base formation was introduced directly in the samples after making the solutions alkaline. This was done to avoid acid-catalyzed acetal formation of the aldehyde with alcohols, especially in the presence of ammonium chloride, which is an effective catalyst of this reaction. Furfural reacts with ammonia similarly to benzaldehyde [13], and on the gas chromatogram a peak appears closely following the furfural peak. This volatile reaction product, probably furfurimide, $OC_4H_3 \cdot CH{:}NH$, however, does not seem to be stable. The amount of this reaction product decreases in

the solution after a longer reaction time forming the high-boiling furfuramide, $OC_4H_3 \cdot CH(N{:}CH \cdot C_4H_3O)_2$, which does not give the corresponding peak in the chromatogram.

The Canizzaro reaction of furfural gives furfuryl alcohol, which is eluted after the Schiff base of *n*-butylamine, and does not interfere in the gas chromatographic amine analysis. Brown colouring of the alkaline amine solution occurs on adding furfural to the mixture. This does not interfere in the analysis when gas chromatographic measurements are performed within a time interval of 0.5—10 hours. A 5—10% decrease of the amount of dimethyl- and diethylamine was found only after 36 hours.

Table I

Analytical data of determinations of free amines

Amine	mg/mL	R^a	RSD[b]%	R^c_M
Trimethylamine	1.07	0.796	3.3	0.318
	0.107	0.080	5.6	
Methylamine	2.30	0.830		0.081
	0.230	0.082		
Dimethylamine	2.75	1.66	2.1	0.196
	0.275	0.158	8.8	
Ethylamine	2.77	1.72		0.202
	0.277	0.161		
Diethylamine	3.56	2.91	1.5	0.430
	0.356	0.281	4.2	
Triethylamine	3.65	3.62	2.3	0.724
	0.365	0.335	3.2	
n-Propylamine	3.59	2.45		0.290
	0.359	0.225		
n-Butylamine	3.70	2.88		0.410
	0.370	0.287		
Di-*n*-propylamine	7.39	6.88	1.2	0.678
	0.739	0.672	5.8	
Tri-*n*-propylamine	1.89	2.05	1.6	1.118
	0.189	0.208	10.7	
Di-*n*-butylamine	3.84	3.28	2.5	0.795
	0.384	0.241	8.3	
Tri-*n*-butylamine	1.95	1.88	1.4	1.29
	0.195	0.184	4.4	

[a] Ratio of peak area of the amine and that of the internal standard mesitylene (0.865 mg/mL).

[b] Relative standard deviation of R (calculated from 5 measurements)

[c] Molar response ratio: (response/mol) amine/(response/mol) mesitylene

Incomplete resolution of isopropylamine and ethylamine was found in both the free and the Schiff base form. Isobutylamine and *sec*-butylamine were well separated from the other amines in the free form, but the *sec*-butylamine peak partially overlapped the Schiff base peak of isopropylamine. Analytical results of the gas chromatographic analysis of the free amines examined are summarized in Table I, and those of the Schiff bases in Table II.

Table II

Analytical data of determinations of primary amines as the Schiff bases of furfural

Amine	mg/mL	R^a	RSD[b]%	R_M[c]
Methylamine	2.30	5.54	1.2	0.539
	0.230	0.550	2.7	
Ethylamine	2.77	5.39	1.2	0.632
	0.277	0.536	2.6	
n-Propylamine	3.59	6.16	1.5	0.730
	0.359	0.561	4.5	
n-Butylamine	3.70	5.42	1.5	0.772
	0.370	0.508	4.6	

[a] Ratio of the peak area of the Schiff base and that of the internal standard mesitylene (0.865 mg/mL).
[b] Relative standard deviation of R (calculated from 5 measurements).
[c] Molar response ratio: (response/mol) Sch. base /(response/mol) mesitylene

REFERENCES

[1] Smith, E. D., Radford, R. D.: Anal. Chem., **33,** 1160 (1961)
[2] Di Corcia, A., Samperi, R.: Anal. Chem., **46,** 977 (1974)
[3] Sze, Y. L., Borke, M. L., Ottenstein, D. M.: Anal. Chem., **35,** 240 (1963)
[4] Burks, Jr. R. E., Baker, E. B., Clark P., Esslinger, J., Lacey, Jr. J. C.: J. Agric. Food Chem., **7,** 778 (1959)
[5] Dunn, S. R., Simenhoff, M. L., Wessen, Jr. L. G.: Anal. Chem., **48,** 41 (1976)
[6] Moiser, A. R., Andre, C. E., Viets, Jr. F. G.: Environ. Sci. Technol., **7,** 642 (1973)
[7] Andre, C. E., Moiser, A. R.: Anal. Chem., **45,** 1971, (1973)
[8] Daemen, J. M. H., Dankelman, W., Hendriks, M. E.: J. Chromatogr., Sci., **13,** 73 (1975)
[9] Kuwata, K., Akiyama, E., Yamazaki, Y., Yamazaki, M., Kuge, Y., Kiso, Y.: Anal. Chem., **55,** 2199 (1983)
[10] Blau, K., King, G. S.: "Handbook of Derivatives for Chromatography", p. 237. Heyden, London 1978
[11] Hoshika, Y.: Anal. Chem., **48,** 1716 (1976)
[12] Tavakkol, A., Drucker, D. B.: Chromatographia, **17,** 318 (1983)
[13] Sprung, M. M.: Chem. Rev., **26,** 297 (1939)

Acta Chimica Hungarica 121 (4), pp. 345–361 (1986)

INTERFACIAL RHEOLOGICAL PROPERTIES OF CRUDE OIL–WATER SYSTEMS, I

EFFECT OF CONTACT TIME, SHEAR RATE AND COMPOSITION OF THE AQUEOUS PHASE ON INTERFACIAL VISCOSITY

Julianna LAKATOS-SZABÓ and István LAKATOS*

(Chemical Research Laboratory of Mining, Hungarian Academy of Sciences, H-3515 Miskolc-Egyetemváros, P. O. B. 2)

Received February 28, 1985
Accepted for publication May 24, 1985

Investigations were carried out with Hungarian crude oils of different character, using distilled water, sodium chloride solution and formation water as aqueous phase. Interfacial viscosity was determined with Contraves Low Shear 30 viscometer in rotational mode of operation at 303 K in the shear rate range between 10^{-3} and 10^{2} s^{-1}.

On the basis of experimental results it was established that there is a difference of several orders of magnitude between the interfacial viscosities of the different oil–water systems. Films formed at the water–oil interface have generally non-Newtonian flow behaviour, and both interfacial viscosity and deviation from Newtonian flow behaviour increase with contact time. Inorganic electrolytes diminish interfacial viscosity. Experience proves that, on the one hand, interfacial rheological properties can be used for the characterization and identification of natural water–oil systems, and, on the other hand, that interfacial viscosity may play a decisive role in oil displaacement processes, and consequently in the efficiency of petroleum production.

Introduction

Interfacial phenomena play a fundamental role in the displacement processes and phase-exchange mechanism in the hydrocarbon reservoirs. Of the secondary, tertiary production processes chemical floodings are based on the changing of just these interfacial properties in a favourable direction, but it is beyond doubt that the interfacial tension of the oil–water system and the wetting conditions of the rock become key issues also in the conventional reservoir engineering operation of the system .It is curious, however, that of the interfacial properties of the system, rather complicated from the physico-chemical aspect, only the two characteristics mentioned are taken into account, while a fundamental fact is neglected that in the formation of the interface not only composition and energy differences are produced between the interface and the bulk phases, but the bulk phase and its boundary are different also from the rheological point of view.

Reisberg and Doscher [1], and Bourgoyne et al. [2] have shown that irreversible rigid films are formed at the crude oil–water interface, which may strongly influence spontaneous adsorption or displacement processes in porous rocks. Though this phenomenon is well known, no adequate explanation

* To whom correspondence should be addressed

could be given for the anomalies of flow processes neglecting the rheological properties of the interface. In recent years studies were published in which the authors emphatically called attention to the role of interfacial viscosity played in the displacement mechanism [3, 4].

A decisive part of petroleum produced in the world reaches the surface in the form of W/O emulsions. Strange and Talash [5], Whiteley and Ware [6], and Widmyer et al. [7] explain the generally characteristic low displacement efficiency by spontaneous emulsification and the high stability of the emulsions formed, and attribute to these the fact that the excellent laboratory results of surfactant flooding could not be reproduced under field conditions. Wasan et al. [8, 9], and Neustadter et al. [10] proved that spontaneous demulsification of the emulsion, the coalescence of particles and the formation of a so-called oil bank, which is the precondition of efficient oil displacement, are to be expected only if a low interfacial tension is accompanied by a similarly low interfacial viscosity.

Starting from these data in the literature, it seemed necessary to investigate in connection with conventional hydrocarbon production and with oil displacement by intensive chemical methods, the interfacial rheological properties of Hungarian oil–water systems. As the first step of this work the fundamental interfacial rheological properties of crude oils having different composition and origin will be given as a function of the composition of the aqueous phase, and of the contact time and shear rate.

Experimental

Arising from the stepwise character of the displacement process taking place in a porous system, the oil–water interface is characterized by alternating rest and dynamic states. From time to time the duration of rest state is sufficient for the establishing of sorption equilibrium between bulk phases and interface. Thus, the measuring technique to be applied must make possible the determination of interfacial viscosity both under steady state and dynamic conditions. In steady state measurements the viscosity of the interface, formed between the superlayered phase in rest, was determined at different time as a function of shear rate. In this case, interfacial viscosity is characteristic of the interface moving toward adsorption equilibrium between the two immiscible phase. Shear rate changed in the 10^{-3} to 10^{2} s^{-1} range according to a linear program of 2 min.

As opposed to this, interfacial viscosity was measured under dynamic conditions continuously at constant shear rate. In such measuring technique constantly acting shear forces retarded the establishment of adsorption equilibrium in the interfacial layer, so that information obtained concerned primarily the emulsifying tendency of the two phases, and the rheological properties of the W/O type emulsion, formed at the interfacial layer.

Measurements were carried out with a Contraves Low Shear 30 viscometer, the edge of the biconical measuring head of which was located in the boundary layer. Measurement required approximately 1 cm^3 each hydrocarbon and aqueous phase.

For the investigation of fundamental rheological phenomena, crude oils not solidifying at the measurement temperature were used. Crude oils characterized in Table 1 belong to light Hungarian oils and can be considered as characteristic with respect to their chemical composition, physical properties and storability. As aqueous phase, natural formation water, 5—10 g dm^{-3} NaCl solution and distilled water were used. Interfacial properties were measured in the 303—343 K temperature range. The interfacial tension of oil-water systems was determined by the pendent drop method.

Table I

Properties of the crude oils investigated

Denomination, symbol	Character	Density* of crude oil g cm^{-3}	Viscosity** mPa s	Depth m	Age or reservoir	Nature
Algyő-426 (Alg-426)	paraffinic-intermediate	0.783	4.6	1823.5—1828.0	upper Pannonian	sandstone
Battonya-Kelet-55 (Ba-K-55)	paraffinic	0.800	3.8	950.0—995.0	lower Pliocene	limestone
Battonya-Kelet-65 (Ba-K-65)	paraffinic	0.807	4.4	950.0—995.0	lower Pliocene	limestone
Forráskút-5 (Fkút-5)	intermediate	0.843	11.0	2931.5—2938.5	lower Pannonian	lime marl
Kelebia-24 (Ke-24)	naphthenic	0.951	634.2	817.0—825.0	Paleogen	quartzporphyry
Kismarja-3 (Kism-2)	intermediate	0.826	6.0	766.0—769.0	upper Pannonian	sandstone
Ruzsa-2 (Ru-2)	paraffinic	0.940	794.3	2799.0—2809.0	Miocene	conglomerate

* $T = 298$ K
** $T = 303$ K; $\dot{\gamma} = 118.24$ s^{-1}

Results and Discussion

At the boundary of two immiscible liquids, the free energy of the system, consisting of bulk phases and an interface between them, considerably diminishes on formation of monomoleculat films, rigid membranes, if a distinguished component is enriched in the boundary layer. Moreover, it is characteristic of rigid film that the number of molecules leaving the interfacial layer by diffusion is negligible as compared with those in the boundary layer [11]. It was shown for oil-water systems already in the beginning of the 1950's that natural surfactants becomə highly enriched in the interfacial layer, and their presence fundamentally diminishes interfacial tension [12]. Owing to the composition of crude oils, the interfacial layer formed is generally of composite character, multicomponent and heterogeneous. In many cases a penetrated film, containing also asphaltene particles is formed.

Many publications deal with the theoretical problems of surface and interfacial rheology, which are summarized in the excellent monograph of Joly [11, 13]. However, regrettably, it does not offer a practical possibility for the correct theoretical treatment of our experimental results, because crude oil-water systems cannot be considered 2-component systems. Thus, we mostly must be content with the empirical description of phenomena, investigating those factors which influence interfacial properties in the flow of crude oil in porous media. Of these we investigate as a first step the effect of time elapsed from the contact of the two phases, on interfacial viscosity.

At the water–oil interface of crude oils, active compounds, generally containing heteroatoms, have a high molecular mass and large molecular size. Together with the relatively high viscosity of the hydrocarbon bulk phase, this makes diffusion besides adsorption the decisive factor in the formation of the interface. Thus, depending on the concentration and nature of amphipathic compounds present in the crude oil and on the viscosity of the bulk phase, different times are necessary for the development of the interfacial layer and for the attaining of equilibrium state, as shown in Fig. 1. The figure gives for various crude oil–distilled water systems the change with time of the interfacial viscosity, measured at constant shear rate and 303 K.

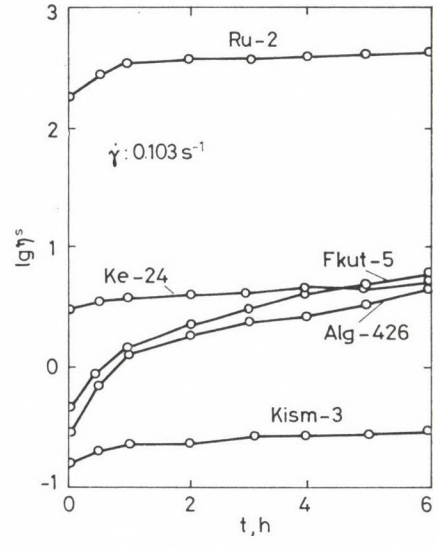

Fig. 1. Change in interfacial viscosity of different crude oil–water systems as a function of time

Two essential facts can be concluded on the basis of Fig. 1. It will be noted that there are differences of orders of magnitude between the interfacial viscosities of the individual crude oils. The interfacial viscosity of the system Ru-2–distilled water is nearly 1000 times higher than that obtained for the system Kism-3–distilled water. There are rather few properties (composition, viscosity, density, interfacial tension, etc.) of crude oil–water systems showing such large differences depending on the origin of the crude oil. We think it likely that interfacial viscosity is a property of crude oil–water systems that can be used, similarly to other methods, for the identification of crude oils. This is illustrated by Fig. 2, showing the change in interfacial viscosity against water of crude oils from two different wells of the field Battonya-Kelet, as a function of time. Differences in composition between the two oils (Table II),

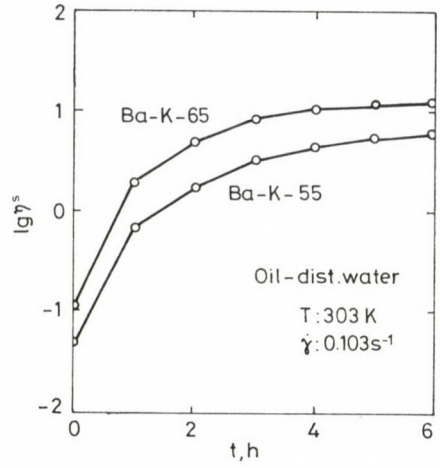

Fig. 2. Change in interfacial viscosity of crude oils from two wells of the field Battonya-Kelet as a function of time in distilled water system

Table II

Composition of the crude oils Ba-K-55 *and* Ba-K-65

Symbol of the oil	Atmospheric distillate %	Vacuum* up to 473 K %	Asphaltene content %	Resin content %	Residue %
Ba-K-55	33.00	57.26	1.09	0.22	8.43
Ba-K-65	23.50	62.58	0.79	0.37	12.76

* 0.1 Torr

a few tenth of a per cent of deviation in asphaltene and resin content, are well reflected in the shaping of interfacial viscosity.

The other important finding on the basis of the curves in the two figures may be that for some crude oils the equilibrium interfacial viscosity is established in a very short time (e.g. Kism-3), while in other cases (e.g. Alg-426, Ba-K-55, -65) the formation of the stable interfacial layer is a slow process, needing as much as 4—10 hrs. Against this, in the given crude oil–water systems, considerably less time is needed for the attainment of the equilibrium value of interfacial tension, as can be seen on Fig. 3. The view became generally accepted on the basis of interfacial tension measurements that in the interfacial layers of natural crude oil–water systems at most 1—2 hours are needed for the establishment of equilibrium. Our experience proves that the formation of the interfacial layer is not always terminated during this period. The contradiction or the discrepancy of conclusions drawn from the results of the two methods, is attributed to the fact that the development of a monomolecular layer is sufficient for the attainment of equilibrium interfacial tension, while

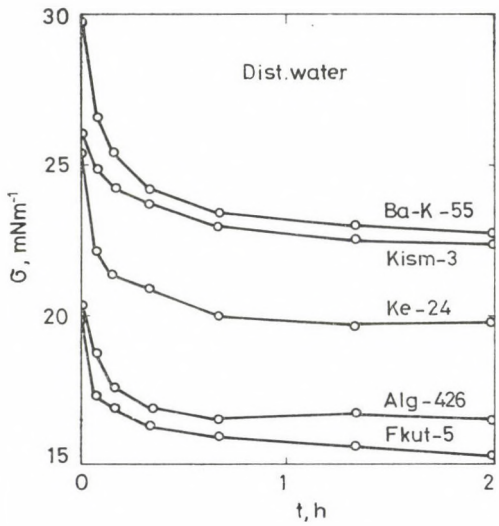

Fig. 3. Change in interfacial tension of different crude oil–distilled water systems as a function of time

a thicker, multilayer film belongs to the equilibrium interfacial viscosity, the development of which requires more time.

Films developing at the interface of crude oil–water systems are usually viscoelastic from the rheological aspect, and can seldom be considered as completely viscous [10]. Results of our oscillorheometric investigations for the determination of elastic properties will be summarized in a later study; here we deal only with the dependence of interfacial viscosity upon the shear rate. The contribution of the elastic component of the viscoelastic system is considered in the present case as equivalent viscous effect.

In Fig. 4 the interfacial viscosities of five different crude oils against distilled water are plotted as a function of shear rate at 303 K. The courses of the curves belonging to one hour contact time are rather varied. With one exception (Ke-24), the interfacial layer is, for all the crude oils, bearing more or less non-Newtonian flow behaviour. However, there are great differences among the crude oils with respect to non-Newtonian properties. While in the case of oil Kism-3 Newtonian flow is characteristic of the interfacial layer both at low and high shear rates, and the region of structural viscosity is restricted to a small section, for oil Alg-426 and Ru-2 the interfacial viscosity decreases steeply with shear rate. The latter curve differs from those of the other crude oils investigated, besides its steepness, also with respect to the absolute magnitude of the interfacial viscosity already mentioned. The curve representing oil Fkút-5 forms a separate case: the horizontal section is preceded and followed by a steep non-Newtonian section in the range of low and high

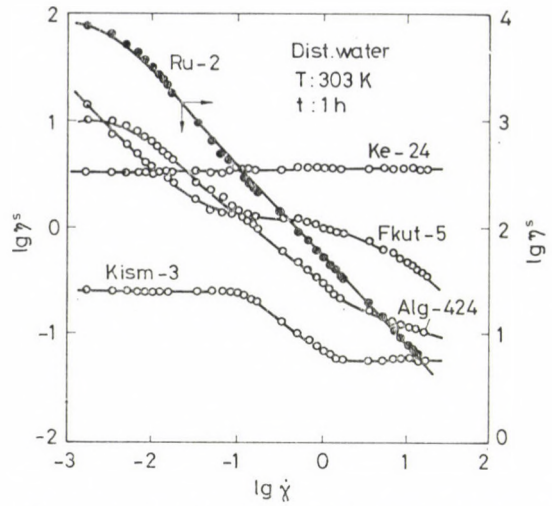

Fig. 4. Change in interfacial viscosity of different crude oil–distilled water systems as a function of shear rate

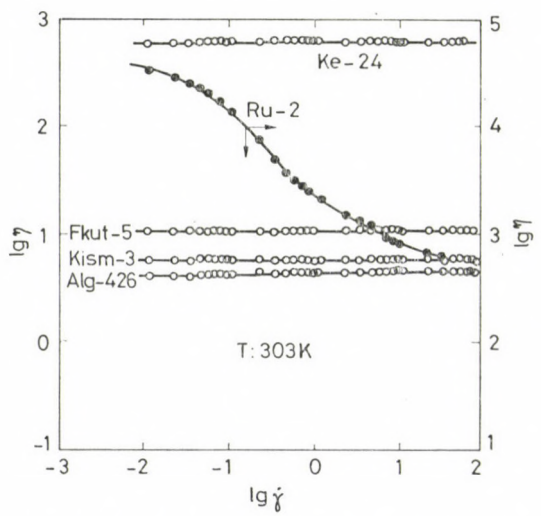

Fig. 5 Change in apparent viscosity of different crude oils as a function of shear rate

rates, respectively. The properties of the interfacial layer differ from those of the usual systems with structural viscosity. For comparison the apparent viscosities of the same crude oils under similar experimental conditions are given in Fig. 5. As will be noted, bulk phases are characterized by Newtonian flow, with the exception of a single oil (Ru-2).

The non-Newtonian character of the interface of oil–water systems can be interpreted by the intermolecular interaction of molecules in the boundary

layer. The structure does not change at low shear rate, therefore, the interfacial layer is characterized by high viscosity and Newtonian flow. However, with increasing shear force the interaction gradually diminishes and, consequently, interfacial viscosity decreases with the increase of shear rate. In the range of high rates the interfacial layer is already characterized by low viscosity and again by Newtonian flow, which indicate that the structure causing high viscosity in the layer is completely disintegrated.

It follows from the dependence of interfacial viscosity on shear rate that crude oil–water systems cannot be characterized by a single interfacial viscosity. Oils can be arranged in very different orders according to the shear rate at which interfacial viscosity is determined. From this point of view the fact deserves special attention that in the range of low shear rate paraffinic oils have a characteristically high interfacial viscosity. On the other hand, at high shear rate the naphthenic oil Ke-24 with Newtonian flow properties proved to have a high interfacial viscosity. Presumably, the presence of microcrystalline paraffines plays a role in the non-Newtonian behaviour of the interfacial layer, which is also partly responsible for the non-Newtonian flow characteristics of the bulk phase of crude oils. The so-called grid shell theory elaborated by Szilas [14, 15] is based on the development of a paraffin skeleton structure, and it proved to be suitable for the description of the non-Newtonian flow of crude oils from both theoretical and the practical viewpoints. The role of microcrystalline paraffins is indicated by the fact that paraffinic oils are characterized by a higher interfacial viscosity than naphthenic oils and, on the other hand, deviation from Newtonian flow behaviour is the greatest for those oils whose bulk phase viscosity proves to be also non-Newtonian. While a paraffinic grid structure is easily sheared, the structure of an interfacial layer formed by naphthene-aromatic compounds is essentially not influenced by the shear forces generated in the interface and, therefore, the viscosity of the layer preserves its Newtonian flow behaviour.

In practice, Ostwald's relationship proved suitable for the empirical description of yield curves

$$\dot{\gamma} = k\tau^n,$$

the exponent n of which was used for the characterization of the deviation from Newtonian flow properties. Figure 6 shows the yield curves of systems of strongly non-Newtonian character, while Fig. 7 yield curves obtained for films of Newtonian or only slightly differing rheological properties. Table III contains the values of the constants of Ostwald's relationship. For oils Fkút-5 and Kism-3 three (a, b, c) data are given, as yield curves were approximated with three straight lines.

The behaviour of constant k was not studied, since its magnitude is in relationship with the reciprocal of viscosity. As concerns the value of exponent

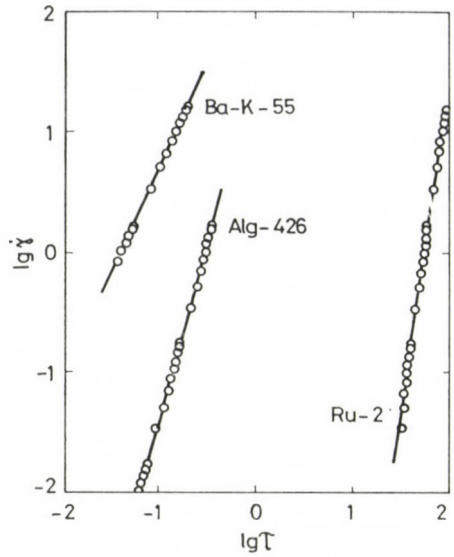

Fig. 6. lg $\dot{\gamma}$ vs. lg τ relationships obtained for interfacial layers of strongly non-Newtonian flow behaviour

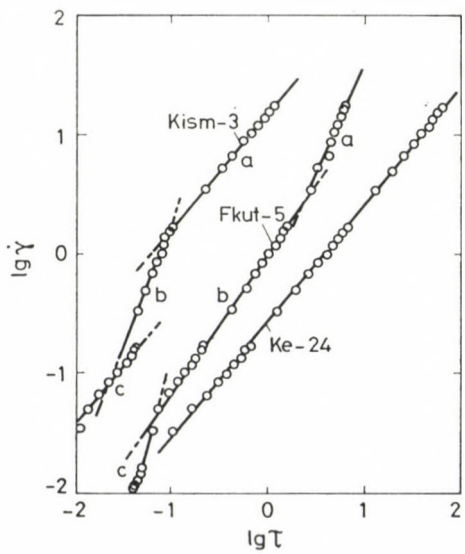

Fig. 7. lg $\dot{\gamma}$ vs. lg τ relationships obtained for interfacial layers of Newtonian (Ke-24) and of slightly non-Newtonian flow behaviour

Table III

Constants of Ostwald's relationship in various crude oil–water systems

Symbol of the oil	k	n
Alg-426	1.49	2.96
Ba-K-55	2.47	1.62
Ba-K-65	2.06	1.96
Fkút-5		
a	−0.23	1.77
b	−0.02	1.14
c	−1.99	2.86
Ke-24	0.55	0.98
Kism-3		
a	1.18	0.96
b	2.26	1.99
c	0.57	0.98
Ru-2	−9.33	5.32

$T = 303$ K
$t = 1$ h

n, it can be seen that data obtained for the crude oils investigated are between $n \sim 1$, characteristic of Newtonian flow, and $n = 5.317$, considered as characteristic of high structural viscosity. According to expectation, the two limiting cases are represented by oils Ke-24 and Ru-2. Eventually, on the basis of exponent n, crude oils can be arranged in an order with respect to the degree of non-Newtonian flow behaviour.

Preceding data presented for the non-Newtonian behaviour of crude oil–water interfacial layers belonged to a contact time of one hour. However, it was mentioned earlier that the formation of the interfacial layer is by far not terminated during this time. Curves in Fig. 8 show that, besides interfacial viscosity, the extent of deviation from Newtonian flow characteristics increases also with increasing contact time. It will be noted from data in Table IV that,

Table IV

Change with time of the constants of Ostwald's relationship in different crude oil–water system

Time h	Alg-426		Ba-K-55		Ba-K-65		Ru-2	
	k	n	k	n	k	n	k	n
0	1.23	1.48	2.48	1.04	2.08	0.97	−6.11	4.03
1	1.49	2.96	2.47	1.76	2.06	1.96	−9.33	5.32
2	1.01	2.75	2.41	2.24	1.91	2.40	−8.53	4.71
4	0.75	2.87	2.25	2.60	1.88	2.90	−8.16	4.39
6	0.01	3.54	2.13	2.83	1.84	3.38	−9.45	5.06
24	—	—	1.70	3.63	1.62	4.80	−9.23	5.11

$T = 303$ K

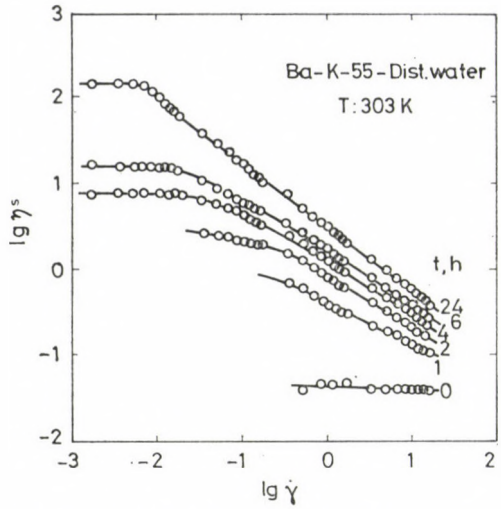

Fig. 8. Dependence of the interfacial viscosity of the system Ba-K-55 crude oil–distilled water system upon shear rate and time

e.g. in the case of oil Ba-K-55, the value of exponent n gradually increases to 3.628 with increasing time. This tendency is manifested more or less by all the oils, with the exception of the originally Newtonian interfacial layers or those of initially very strong non-Newtonian character. The two oils from the field Battonya-Kelet differ not only with respect to the inrease of interfacial viscosity, but also with respect to the strengthening of the non-Newtonian character, namely on increasing contact time the interfacial layer of the system Ba-K-65 oil–water is characterized by higher n values, than the Ba-K-55 oil–water system.

In the production history of hydrocarbon reservoirs, the time inevitably comes, when water has to be injected into the reservoir to maintain formation energy. In these cases the quality of water is of crucial importance, because the unbalancing of natural ion equilibrium may cause severe formation damage. The effect of salt content (and within this, the quality and quantity of inorganic electrolytes) of the water to be injected was investigated from several aspects (swelling of clay minerals, degree of spontaneous emulsification, the behaviour of interfacial tension), but the literature does not contain data definitely relevant to the effect of inorganic salts on the interfacial viscosity of crude oil–water systems.

In Fig. 9 the interfacial viscosity is plotted as a function of shear rate for the system Ba-K-55 oil–distilled water and formation water, respectively. It can be seen that on using formation water, the interfacial viscosity is lower by almost an order of magnitude than on using deionized water. At the same time, there is no substantial difference in the non-Newtonian character of the

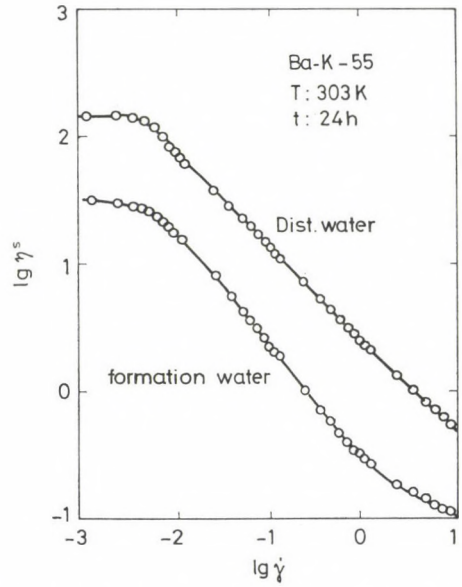

Fig. 9. Dependence of the interfacial viscosity of the crude oil Ba-K-55 upon shear rate in distilled water and formation water systems

interfacial layer. The effect of water quality can be evidently attributed to the presence of dissolved salts in the formation water. According to data contained in Table V, the formation water Ba-K-48 belongs in Hungarian relation to those of high salt content, and has the characteristic that the predominant part of total salt content is sodium chloride. In the natural state of the formation water its carbon dioxide saturation is also considerable, and leads in the carbonaceous reservoirs to high hydrogen carbonate concentrations. However, under laboratory conditions, part of the dissolved carbon dioxide is set free, and most of the hydrocarbonate precipitates from the solution. On the basis of the composition of formation water, the salt effect can presumably be attributed mainly to monovalent inorganic electrolytes.

The other crude oils included in this work could not be studied in for-

Table V

Composition of the formation water Ba-K-48

Ion	Concentration g dm^{-3}
Na^+	6.25
K^+	0.43
Mg^{2+}	0.08
Ca^{2+}	0.04
Cl^-	8.11
HCO_3^-	4.50

mation water system. Therefore, these were measured against 5—10 g dm^{-3} NaCl solution instead of formation water. The comparison of data obtained at identical shear rates, with distilled water and solutions containing electrolytes support our finding in connection with formation water, namely that in the latter systems interfacial viscosity is generally lower.

Results of investigation of the tendency of Hungarian crude oils for emulsification proved that e.g. the oil from Algyő forms within a wide range of phase ratios stable W/O emulsions with aqueous phases of different compositions [16—18]. On the other hand, samples taken from the field of Battonya-Kelet proved that the emulsion appears already at the well bottom. This permits to conclude that the emulsification of the aqueous and oil phases, flowing together, begins already in the layer, under the action of low shear deformation, exerted on the phase interface. The emulsion formed impairs in the surrounding of the well bottom the flow conditions of the fluid, and thus the productibility of the well. Therefore, it is insufficient to investigate under steady state conditions the formation of the interfacial layer of crude oil–water systems and the behaviour of its viscosity, but interfacial rheological properties must also be studied under continuously acting shear deformation. We cannot speak in this case of the development of equilibrium interfacial layers, but data obtained in this way yield information on the emulsification process in the interfacial layer.

Figure 10 gives a real picture of the effect of constant shear deformation. The change of the interfacial viscosity of the system Ba-K-55-distilled water is plotted as a function of time at shear rate 9.77 s^{-1} and 12.21 s^{-1}. It can be noted that the viscosity of the interfacial layer increases in proportion with the time of shear deformation and with shear rate. This is in accordance with expectation and supports the experience that the size of dispersed particles

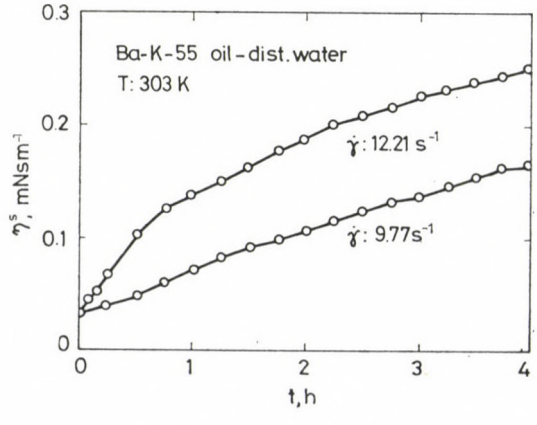

Fig. 10. Dependence of the interfacial viscosity of the system Ba-K-55 crude oil–distilled water upon shear rate and time at continuous shear

decreases and the viscosity of the emulsion increases with increasing shear forces and shear rate.

Earlier investigations showed that at identical phase ratios the stability and the dispersity of the emulsion formed depends strongly on the composition of the aqueous phase. Using deionized water, stable emulsions, difficult to break and of extremely high viscosity were always formed, while when formation water or an aqueous phase containing sodium chloride were used, either no stable emulsion formed, or the crude oil formed a rapidly demulsifying, coarsely dispersed system characterized by large drop size. This finding is fully supported by our dynamic investigations, the results of which are shown in Figs 11—13. The two oils are readily emulsified with distilled water, and as a result, interfacial viscosity steeply increases with time (Fig. 11), while in the system containing sodium chloride the change is considerably smaller (Fig. 12), or no emulsion is formed at all when formation water is used as aqueous phase (Fig. 13).

The emulsifying ability of crude oil in aqueous systems of different nature cannot be interpreted on the basis of interfacial tension. Inorganic salts usually diminish interfacial tension (Fig. 14), but this decrease is too small to bring about strong reduction of the tendency for emulsion formation and, on the other hand, the rapid demulsification of the emulsion formed. However, if the stability of emulsions formed in oil–water systems is interpreted on the basis of the action of inorganic salts on both interfacial tension and viscosity, then already an unequivocal answer can be given to the question of why emulsions formed in formation water systems have a tendency for quick demulsification. The experimental data shown support the concept that it is mainly the decrease in interfacial viscosity and the absence of formation of rigid films that play the fundamental role.

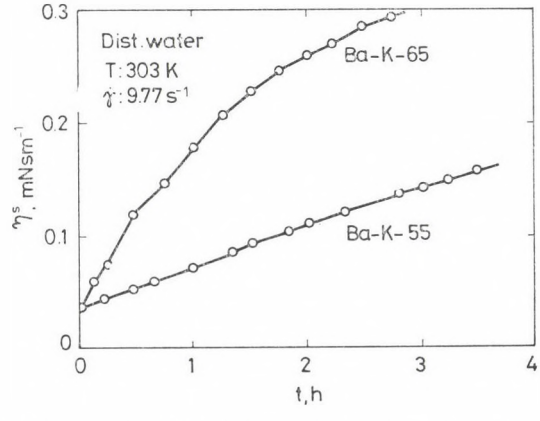

Fig. 11. Change in interfacial viscosity of the crude oils from the two wells of Battonya-Kelet field as a function of time in distilled water system at continuous shear

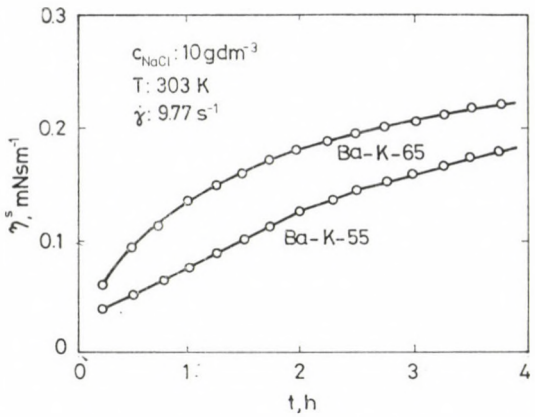

Fig. 12. Change in interfacial viscosity of the crude oils from the two wells of the Battonya-Kelet field as a function of time, at continuous shear, in a system containing 10 g dm^{-3} sodium chloride

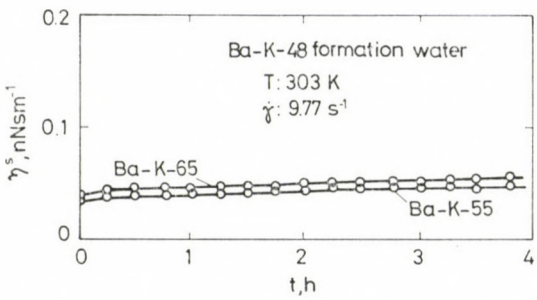

Fig. 13. Change in interfacial viscosity of the crude oils from the two wells of the Battonya-Kelet field as a function of time, at continuous shear, in formation water system

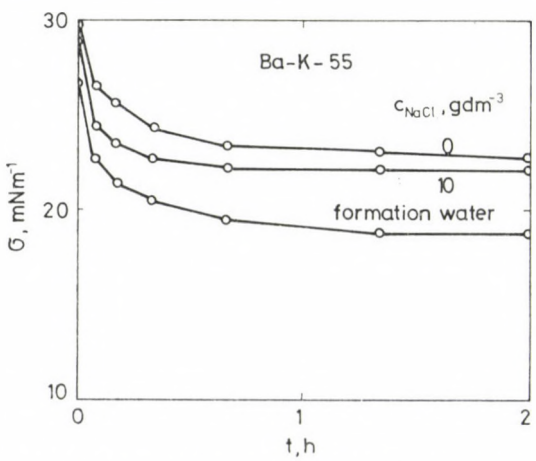

Fig. 14. Change in interfacial tension of the crude oil Ba-K-55 as a function of time, against various aqueous phases

Conclusions

Based on the measuring of the interfacial viscosity of various crude oil–water systems, the following has been established:

1) The interfacial viscosities of crude oil–water systems may differ by several orders of magnitude from one another, and may be used for the characterization and identification of crude oils.

2) The change with time of interfacial viscosity yields information on the development of the interfacial layer. Data obtained prove that at the interface of natural oil–water systems considerably longer time is needed for the attainment of equilibrium than that resulting from the measurement of interfacial tension.

3) From the rheological aspect, interfacial layers may be Newtonian, however, in most of the cases non-Newtonian flow behaviour are characteristic. The deviation from Newtonian character is of different degree for the individual oils. Interfacial viscosity can change by several orders of magnitude with the shear rate.

4) The viscosity of interfacial layers and their non-Newtonian flow behaviour increase with contact time, while inorganic electrolytes decrease interfacial viscosity.

5) According to dynamic investigations, the emulsification of the interfacial layer increases in proportion to the increase of shear rate and time, while it decreases with increasing salt content in the aqueous phase.

The interfacial rheological study of different crude oil–water systems convincingly prove that interfacial viscosity, the flow properties of films formed on the boundary of the two phases, plays the same important and decisive role in crude oil displacement processes as interfacial tension and wetting properties, and without their knowledge capillary phenomena, entrapped oil bodies, formation of oil banks, spontaneous emulsification, the coalescence of dispersed phases, etc., cannot be unequivocally interpreted.

Symbols

c	concentration, g dm^{-3}
k, n	constants of Ostwald's relationship
t	time, h
T	temperature, K
$\dot{\gamma}$	shear rate, s^{-1}
η	apparent viscosity of the bulk phase, mPa s
η^s	interfacial viscosity, mN s m^{-1}
σ	interfacial tension, mN m^{-1}
τ	shear stress, mPa

REFERENCES

[1] Reisberg, J., Doscher, T. M.: Prod. Monthly, **21,** 43 (1956)
[2] Bourgoyre, A. T., Caudle, B. M., Kimbler, O. K.: Soc. Petr. Eng. J., **12,** 60 (1972)
[3] Slattery, J. C.: AIChE J., **20,** 1145 (1974)
[4] Brown, C. E., Jones, T. J., Neustadter, E. L.: The influence of interfacial properties on immiscible displacement behaviour, in Surface Phenomena in Enhanced Oil Recovery, Ed. Shah, D. O., Plenum Press, New York 1981
[5] Strange, L. K., Talash, A. W.: SPE Paper No. 5885 (1976)
[6] Whiteley, R. C., Ware, J. W.: J. Petr. Tech., **29,** 925 (1977)
[7] Widmyer, R. J., Salter, A., Frazier, G. D., Graves, R. H.: J. Petr. Tech., **29,** 933 (1977)
[8] Wasan, D. T., McNamara, J. J., Shah, S. M., Sampath, K., Aderangi, N.: J. Rheology, **23,** 181 (1979)
[9] Wasan, D. T., Shah, S. M., Chan, M., Sampath, K., Shah, R.: Spontaneous emulsification and the effect of interfacial fluid properties on coalescence and emulsion stability in caustic flooding, in Chemistry of Oil Recovery, Ed. Johansen, R. T., Berg, R. L., Am. Chem. Soc., Washington D. C. 1979
[10] Neustadter, E. L., Wnittingham, K. P., Graham, D. E.: Interfacial rheological properties of crude oil/water systems, in Surface Phenomena in Enhanced Oil Recovery, Ed. Shah, D. O., Plenum Press, New York 1981
[11] Joly, M.: Rheological properties of monomolecular films, Part I. Basic concepts and experimental methods, in Surface and Colloid Science, Vol. **5,** Ed. Matijevic, E., Wiley-Interscience, New York 1972
[12] Denekas, M. O., Carlson, F. T., Moore, J. W., Rodd. C. G.: Ind. Eng. Chem., **43,** 1165 (1951)
[13] Joly, M.: Rheological properties of monomolecular films, Part II.: Experimental results, theoretical interpretation, applications, in Surface and Colloid Science, Vol. **5,** Ed. Matijevic, E., Wiley-Interscience, New York 1972
[14] Szilas, A. P.: Kőolaj és Földgáz, **1,** 1 (1982)
[15] Szilas, A. P.: Rheologica Acta, **23,** 70 (1984)
[16] Felián, B., Balázs, J., Lakatos, I.: Acta Phys. Chem., **29,** 223 (1983)
[17] Felián, B., Balázs, J., Lakatos-Szabó, J., Lakatos, I.: Acta Phys. Chem., **30,** 183 (1984)
[18] Felián, B., Balázs, J., Lakatos, I.: Magy. Kém. Lapja (in press)

Acta Chimica Hungarica 121 (4), pp. 363—371 (1986)

STUDIES ON SOME QUINOLINE DERIVATIVES, III*

COPPER(I) HALIDE COMPLEXES OF 3-, AND 4-QUINOLINECARBOXYLIC ACIDS AND SOME OTHER QUINOLINE DERIVATIVES

Mohamed Abdel-Rahman Sidahmed GOHER** and Afaf Kamal HAFEZ

(Chemistry Department, Faculty of Science, Alexandria University, Alexandria, Egypt)

Received February 28 1935
Accepted for publication May 29, 1935

The copper(I) halide complexes of 3-, and 4-quinolinecarboxylic acids, 2-, and 4-chloroquinoline and 4-methylquinoline have been prepared and characterized. The complexes are coloured and diamagnetic exhibiting strong MICT bands in the visible region. All ligands mentioned here act as neutral monodentate ligands in the isolated complexes. The structures of the complexes are suggested on basis of their spectral properties.

Introduction

In a previous paper [1] we described the solid copper (I) complexes of 2-quinolinecarboxylic acid, also called quinaldic acid, and its methyl and ethyl esters. Quinaldic acid was found to act as a monodentate ligand in its copper(I) chloride complex while in its iodide complex it acts as a bidentate ligand. Recently the chemistry of copper(I) complexes of pyridine derivatives has been the target of intensive studies [2—8], as they are the first intermediates in the preparation of the copper-pyridine catalysts which catalyse cleavage of aromatic ring systems [9] or used in the oxidation of phenols to polyphenyl ethers and diphenoquinones [10]. As an extension of our work mentioned earlier [1] we report here on the synthesis and characterization of copper(I) halide complexes of 3-, and 4-quinolinecarboxylic acids, 2-, and 4-chloroquinoline and 4-methylquinoline.

Experimental

3-Quinolinecarboxylic acid (3-HQA), 4-quinolinecarboxylic acid (4-HQA), 2-chloroquinoline (2-ClQ), 4-chloroquinoline (4-ClQ) and 4-methylquinoline (4-MeQ) were purchased from BDH and Aldrich companies.

Physical measurements have been carried out as described previously [1].

The complexes have been prepared and recrystallized according to the methods given earlier [1]. The copper content has been determined gravimetrically as CuSCN or by titration against disodium EDTA after degradation and oxidation of the complexes with boiling mixtures of *conc.* H_2SO_4 and 30% H_2O_2. Carbon, hydrogen and nitrogen were determined using a Perkin-Elmer 240 elemental analyzer.

* Part II: Acta Chim. Hung. (In press)
** To whom correspondence should be addressed

Results and Discussion

The isolated copper(I) halide complexes (Table I) are sufficiently stable when carefully dried. They are coloured and diamagnetic compounds. We could not isolate the 1 : 3 copper(I) chloride complexes of 4-ClQ or 4-MeQ which may be because of their sizes since 4-, and 3-methylpyridine form 1 : 3 copper(I) chloride and bromide complexes [7, 11, 12]. 4-Quinolinecarboxylic

Table I

Analytical data

Complex	Colour	M.P. °C	% Found/calculated				
			C	H	N	X	Cu
Cu(3-HQA)Cl	red brown fine crystals	265—9*	44.39 44.12	2.72 2.59	5.02 5.25	13.35 13.04	23.72 23.35
Cu(3-HQA)Br	red brown cryst. powder	240—5*	38.21 37.93	2.45 2.24	4.21 4.42	25.00 25.23	19.72 20.06
Cu(3-HQA)I	orange cryst. powder		32.45 33.03	2.31 2.04	3.72 3.83	34.57 34.90	17.82 17.47
Cu(4-HQA)Cl	red orange fine crystals		43.82 44.12	2.65 2.04	5.18 3.8	12.84 13.04	23.62 23.35
Cu(4-HQA)Br	red orange cryst. powder	255—260	38.17 37.93	2.34 2.24	4.23 4.42	25.00 25.23	20.22 20.06
Cu(4-HQA)I	orange cryst. powder		33.33 33.03	2.00 2.04	3.94 3.83	34.63 34.90	17.09 17.47
Cu(2-ClQ)Cl	yellow needles	160**	46.26 46.46	2.52 2.60	6.15 6.02	15.02 15.26	27.00 27.29
Cu(2-ClQ)Br	yellow needles	130**	38.66 39.02	2.00 2.18	4.88 5.05	28.75 28.84	22.67 22.92
Cu(2-ClQ)I	pale yellow needles		33.48 33.36	1.98 1.87	4.22 4.32	39.34 39.16	20.00 19.60
Cu(4-ClQ)Cl	yellow needles	175	46.23 46.46	2.32 2.60	6.32 6.02	15.00 15.26	27.38 27.29
$Cu(4\text{-}ClQ)_2Cl$	red fine crystals		58.78 59.02	3.20 3.30	7.56 7.64	13.23 13.00	17.17 17.34
Cu(4-ClQ)Br	yellow needles		39.15 29.02	2.32 2.18	5.25 5.05	28.92 28.84	23.13 22.92
Cu(4-ClQ)I	pale yellow needles	160	33.10 33.36	1.92 1.87	4.33 4.32	39.42 39.16	19.80 19.60
Cu(4-MeQ)Cl	yellow needles	170***	49.76 49.59	3.82 3.74	5.88 5.78	14.43 14.66	26.00 26.22
$Cu(4\text{-}MeQ)_2Cl$	red fine crystals	130	61.75 62.33	4.53 4.71	7.15 7.26	99.33 9.26	16.65 16.48
Cu(4-MeQ)Br	yellow needles	195***	42.12 41.91	3.32 3.16	5.00 4.89	27.67 27.88	22.34 22.16
Cu(4-MeQ)I	pale yellow needles	160	36.20 36.00	2.60 2.72	4.42 4.20	38.52 38.04	18.78 19.04

Abbreviation: 3-HQA = 3-quinolinecarboxylic acid,
4-HQA = 4-quinolinecarboxylic acid,
2-ClQ = 2-chloroquinoline,
4-ClQ = 4-chloroquinoline,
4-MeQ = 4-methylquinoline = lepidine
(*) change to green, (**) change to white (***) melts with decomposition

acid forms only 1 : 1 copper(I) halide complexes in a similar manner as 4-pyridinecarboxylic acid [13]. The stability of the isolated complexes depends on the nature of the halogen as suggested [14] for other copper(I) complexes. The stability increases from chloride to iodide, except for the 4-HQA-CuI complex which is the least stable in the series of halide complexes of 4-HQA.

Polymerization of the complexes derived from 4-HQA or 3-HQA may be the reason that their melting or decomposing points are indefinite and depend upon the heating rate.

X-ray powder diffraction has revealed the isomorphism of the chloride or bromide complexes of the same ligand.

The halide complexes derived from 4-HQA and 3-HQA are soluble in boiled water in the presence of ascorbic acid to prevent oxidation. The complexes of other ligands are soluble in one or the other of the polar solvents, e.g. alcohols, acetone, etc . . .

Electronic spectra

Table II summarizes the electronic spectral data of the solid complexes mulled in nujol. The absorption bands in the UV region depend only on the moiety of the ligands.

In the 21—27 kK region, a strong absorption band appears in the spectra of all complexes. These bands are due to metal-to-ligand charge transfer (MLCT) transition from copper(I) d^{10} to an empty π^*-orbital on the ligand [15].

Table II

*Electronic spectral data for the complexes**

Complex	$\pi—\pi^*$			ν_{MLCT} (kK)
Cu(3-HQA)Cl	34.5			27.0—21.0
Cu(3-HQA)Br	36.3			27.0
Cu(3-HQA)I	36.3			28.2
Cu(4-HQA)Cl	35.7	29.4	sh	22.5
Cu(4-HQA)Br	35.7	29.4	sh	23.2
Cu(4-HQA)I	35.7	29.4	sh	25.0
Cu(4-MeQ)Cl	35.7			26.3
Cu(4-MeQ)Br	35.7			27.0
Cu(4-MeQ)I	35.7			28.2
$Cu(4\text{-}MeQ)_2Cl$	35.7			27.0—22.0
Cu(4-ClQ)Cl	35.5			25.0
Cu(4-ClQ)Br	35.5			25.6
Cu(4-ClQ)I	35.5			26.3
$Cu(4\text{-}ClQ)_2Cl$	35.5			25.0—20.0
Cu(2-ClQ)Cl	36.3	30.0	sh	25.0
Cu(2-ClQ)Br	36.3	30.7	sh	26.0
Cu(2-ClQ)I	36.3	30.7	sh	26.6

* The spectra of samples mulled in nujol.

Comparison of these MLCT bands for copper(I) chloride complexes of 4-MeQ, 4-ClQ and 4-HQA (Table II) shows that the energy of such transition decreases in the order 4-MeQ > 4-ClQ > 4-HQA. This result reflects the effect of the substituent group upon the MLCT transitions. For an electron attracting group, e.g. Cl, the electron density on the nitrogen atom decreases which enhances the MLCT and hence shifts the absorption band to shorter ν_{max}. The reverse is true for electron releasing groups. Similar trends have been observed for copper(I) complexes of pyridine derivatives [7, 12].

Table II shows that the ν_{max} value of the MLCT bands decreases in the order I > Br > Cl. Since the excited states have considerable copper(II) character, we may assume that if the crystal field splitting Δ for copper(I) halide is as follows; I < Br < Cl, the most destabilized is the t_2 orbital (t_2 are the metal d orbitals in a tetrahedral field involved in MLCT) in the case of chloride. The difference in energy, $\Delta\varepsilon$, between the t_2 and the lowest vacant π^* orbital on the ligand is minimum in the case of chloride and maximum in the case of iodide. This explains the halide-ion dependence on the MLCT band. A similar situation occurs [7] in the bis(2-(phenylazo)-pyridine) copper(I) [16].

CuL_2Cl complexes of 4-ClQ and 4-MeQ exhibit MLCT bands (Table II) at lower ν_{max} than the corresponding 1 : 1 complexes. The existence of two ligand units per copper(I) atom in the complex molecule increases the acceptor properties and hence shifts the absorption to lower ν_{max} [15].

Infrared spectra

(a) Complexes of quinolinecarboxylic acids

The spectrum of 3-quinolinecarboxylic acid (Table III) exhibits a strong broad band in the range 2700—2400 cm^{-1} and another band centered around 1950 cm^{-1}. These bands are attributed [17] to a H-bond of the type N . . . H—O formed between a carboxylic group and a heterocyclic nitrogen from another molecule. This spectrum which is very similar to that of 3-pyridincarboxylic acid [17, 18], does not show the free ν_{OH} band in the vicinity of 3500 cm^{-1}. The spectrum of 4-quinolinecarboxylic acid on the other hand exhibits a strong band around 3450 cm^{-1} due to ν_{OH}. Additionally it shows medium bands around 2450 cm^{-1} and 2000 cm^{-1}. These results indicate that the acid exists almost in the free neutral form and to a lesser extent contains an intramolecular H-bonding of the type N . . . H—O. The spectra of the copper(I) halide complexes of both acids exhibit a strong broad band in the range 3500—2400 cm^{-1}. This band is attributed [19, 20] to the vibration of a H-bond of the type O—H . . . O in complexes. Thus the N . . . H—O in free acids is therefore changed to O . . . H—O type in complexes. This latter H-bonding is formed between two carboxylic groups of two different complex molecules giving rise

to a dimeric structure. The dimeric H-bonding is evidenced by the appearance of a medium broad of medium intensity around 930 cm^{-1}, due to dimeric δ OH out of plane. The ν C=O band appears around 1710 cm^{-1} in the spectra of complexes of both acids (Tables III and IV). The carbonyl groups therefore do not participate in coordination. This indicates that both acids act as monodentate neutral ligands in their copper(I) complexes, and coordinating only via their heterocyclic nitrogens. This is evidenced by the appreciable shifts of the bands related to quinoline ring [21] to higher frequencies in complexes

Table III

IR *spectra of free and coordinated* 3*-quinolinecarboxylic acid* (3-HQA)

3-HQA	Cu(3-HQA)Cl	Cu(3-HQA)Br	Cu(3-HQA)I	Assignments
	3500—2500 s	3500—2400 s	3450—2550 s	ν O—H . . . O
2700—2400 s				
1900 ms, br				ν O—H . . . N
1720 vs, br	1710 vs	1715 vs	1710 s	ν C=O
1630 s	1645 m	1645 m	1640 m	ν C—C, C—N
1610 s	1625 m	1625 m	1625 m	ν C—C, C—N
1690 s	1605 m	1600 m	1600 ms	ν C—C, C—N
1580 sh	1585 wm	1580 m	1580 wm	ν C—C, C—N
1510 vs	1515m—1505ms	1508 m	1510 m	
1465 m	1475 ms	1480 m	1480 m	ν C—C, C—N
1435 m	1432 ms	1338 ms	1435 m	ν C—C
1385 s	1410 wm	1415 m	1410 m	
	1385 ms	1380 m	1380 m	ν C—C, C—N
1370 vs	1375 ms	1370 m	1367 m	ν C—C, C—N
1340 m	1330 w	1330 w	1330 w	ν C—C, C—N
1305 vs	1295 vs	1295 vs	1300 s	ν COO
1270 s	1255 m	1255 m	1260 m	β (C—H)
1225 vs	1232 wm	1240 wm	1230 m	ν CCO
1200 vs	1208 wm	1210 wm	1205 wm	
1190 vs	1190 wm	1195 wm	1190 w	β (C—H)
1135 vs	1140 w	1140 w	1140 w	β (C—H)
1110 m	1115 w	1110 w	1115 w	β (C—H)
1028 m	1050 w	1050 w	1050 w	β (C—H)
990 ms	1025 w	1025 w	1020 w	ring breathing
972 m	990 w	985 w	990 w	
	925 m, br	930 m, br	925 m, br	δ OH out of plane
825 m	825 vw	825 m	825 wm	γ-(C—H)
790 vs	790 s	790 s	790 s	γ-(C—H)
768 vs	772 m	770 sh	770 m	
750 vs	750 m	750 m	750 m	γ-(C—H)
660 ms	660 w	660 w	660 w	
595 ms	622 w	622 w	622 w	
535 s	570 w	570 m	570 m	ring deformation
495 wm	530 w	510 m	520 m	
470 s	490 wm	490 wm	490 w	
385 s	410 m	410 m	410 m	

w = weak, m = medium, s = strong, v = very, st = stretching.

Table IV

IR *spectra of free and coordinated* 4-*quinolinecarboxylic acid* (4-HQA)

4-HQA	Cu(4-HQA)Cl	Cu(4-HQA)Br	Assignments
3450 s	3300—2500 ms	3300—2500 s	ν OH
2450 m			ν O—H . . . O
2000 m			ν O—H . . . N
1700 m, br	1700 s	1705 s	ν C=O
1630 ms	1635 wm	1640 m	ν C—C, C—N
1610 ms	1615 m	1620 wm	ν C—C, C—N
1580 m	1580 m	1585 m	ν C—C, C—N
1565 wm	1570 m	1570 m	ν C—C, C—N
1528 m	1550 w	1545 w	ν C—C, C—N
1510 m	1525 w	1525 ww	ν C—C
1465 m	1470 m	1465 m	ν C—C, C—N
1410 sh	1415 m	1415 m	ν C—C, C—N
1340 s, br	1355 ms	1355 ms	
1280 s	1280 s	1280 s	ν COO, β(C—H)
1255 ms	1255 vs	1255 s	ν CCO
1225 ms	1222 w	1220 w	β(C—H)
1200 ms	1200 m	1200 m	β(C—H)
1155 ms	1155 m	1155 m	
1090 ms	1085 m	1080 m	β(C—H)
1010 m	1050 w	1045 w	
980 m	1010 w	1010 w	ring breathing
960 m	970 w	970 w	
860 m	890 wm	885 wm	
	860 m, br	860 m, br	δ OH out of plane
800 vs	795 ms	790 ms	γ (C—H)
765 vs	770 s	770 s	γ (C—H)
750 s	755	750 s	γ (C—H)
735 s	745 m	740 m	γ (C—H)
655 ms	660 s	660 s	
595 m	630 wm	630 wm	ring deformation
545 s	590 ms	585 ms	
465 wm	495 m	495 m	
415 ms	465 m	465 m	
395 vs	410 ms	410 ms	
385 vs	398 ms	395 ms	

when compared with those of free acids. Tables III and IV show that the greatest shifts are observed for bands below 650 cm^{-1} which are due to ring deformation modes, in a similar manner as those of pyridine derivatives [22, 23].

(b) Complexes of 2-ClQ, 4-ClQ and 4-MeQ

These spectra (Table V) show that the bands above 630 cm^{-1} are slightly shifted to higher frequencies upon complexation. Those below 650 cm^{-1} experience substantial shifts to higher frequencies when compared with corresponding bands in free ligands. The spectra of the 1 : 2 copper(I) chloride

Table V

IR *spectra of free and coordinated 4-methylquinoline* (4-MeQ)

4-MeQ	Cu(4-MeQ)Cl	$Cu(4\text{-MeQ})_2Cl$	Cu(4-MeQ)I	Assignments
1622 m	1625 wm	1625 wm	1625 wm	ν (C—C, C—N)
1600 vs	1600 vs	1595 vs	1605 vs	ν (C—C, C—N)
		1575 wm		
1575 s	1580 sh		1582 m	ν (C—C, C—N)
		1565 m		
1530 sh	1550 w	1545 wm	1550 w	ν (C—C, C—N)
		1525 m		
1515 s	1520 s		1520 s	
		1515		
1460 ms	1465 m	1440 ms	1460 m	ν (C—C)
1445 m	1450 m	1440 ms	1445 m	ν CH_3, antisym. bending
1425 wm	1430 w	1425 m	1430 m	ν (C—C, C—N)
1395 w	1400 s	1395 s	1395 s	ν (C—C, C—N)
1382 wm		1385 s	1380 m	CH_3 sym. bending
	1365 m	1365 m	1365 m	
1308 s	1305 s	1305 s	1308 s	
	1270 w	1270 wm	1270 w	β (C—H)
1248 ms				
	1255 ms	1255 ms	1250 ms	β (C—H)
1220 w	1210 m	1210 m	1215 m	β (C—H)
1165 m	1160 m	1160 m	1165 m	β (C—H)
1145 m		1145 m	1150 ms	
1090 w	1100 m	1090 m	1105 m	
1065 w	1070 w	1070 w	1070 w	
1020 wm	1035 m	1030 m	1028 m	CH_3, rock
	885 m	875 m		
860 w			880 m	
	865 m	865 m		
842 vs	840 vs	840 vs	845 s	γ (C—H)
818 m	830 sh	835 vs	835 s	γ (C—H)
		820 m		
790 m	815 m		815 m	γ (C—H)
		810 m		
760 vs	778 m	775 s	768 ms	γ (C—H)
750 sh	745 vs	755 vs	755 vs	γ (C—H)
708 m	705 m	705 m	710 m	
630 w	635 wm	635 m	632 m	
568 m	585 m	580 m	590 m	
520 w	530 w	530 w	530 w	
480 wm	490 w	490 w	495 wm	ring deformation
		475 m		
455 m	472 m		475 m	
		465 ms		
		420 s	418 s	

complexes of 4-MeQ and 4-ClQ show splitting of many absorption bands when compared with those of 1 : 1 copper(I) halide complexes of the same ligand.

In the case of 4-MeQ complexes appreciable shifts are observed for bands at 568, 520, 480 and 455 cm^{-1}, particularly the first and the fourth bands. Similar shifts are observed for other metal complexes of 4-MeQ [24].

For 2-ClQ the shifts of 402, 440 and 605 cm^{-1} bands are of appreciable magnitude. These results are similar to those observed for the corresponding pyridine derivative complexes [22, 23].

Likely structures for the complexes

The IR spectra of the copper(I) halide complexes of 3-HQA and 4-HQA show that they contain a H-bonding of the type;

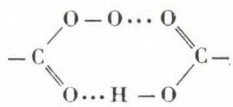

In the spectra of the copper(I) chloride complexes of both acids no bands in the region 400—200 cm^{-1} could be assignable to ν Cu—Cl stretching vibrations. This implies [25] that the halides act as bridging atoms. The spectrum of the copper(I) chloride complex of 4-HQA is very close to that of the Cu(HINA)Cl complex (HINA = isonicotinic acid) which has been studied by means of X-ray structure analysis [26]. This complex was found to exhibit a "ribbon" structure;

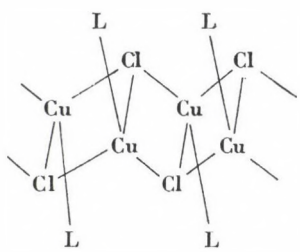

We proposed a similar structure for the 4-HQA complexes where the copper atom is attached to the organic ligand and to three chlorides in a zigzag chain having a tetrahedral geometry.

1 : 1 copper(I) halide complexes of 4-MeQ, 4-ClQ and 2-ClQ, exhibit MLCT bands in the range 370—500 nm, and their energies are influenced by the substituent group as well as the halide ion. These trends are very similar to those of pyridines [7, 12]. The far infrared spectra of the 1 : 1 copper(I) chloride complexes of the three ligands do not show any band assignable to ν Cu—Cl stretching modes, and therefore indicating bridging chloride ions. A "Cubane" like structure has been frequently revealed by the X-ray analysis of $[CuLX]_4$ (L = py for X = I [4], L = diethyl nicotinamide for X = I [3]);

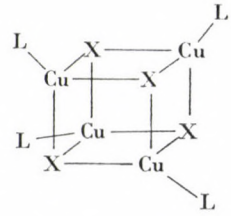

The very close similarities of such copper(I) complexes with those of 4-MeQ, 4-ClQ and 2-ClQ led us to propose tetrameric $[CuLX]_4$ with "cubane" like structures for these latter complexes.

The spectra of the 1 : 2 copper(I) chloride complexes of 4-MeQ or 4-ClQ, do not exhibit ν Cu—Cl bands in the 400—200 cm^{-1} region. These complexes are almost certainly dimers $[CuL_2Cl]_2$ with tetrahedral geometry around copper(I).

REFERENCES

[1] Goher, M. A. S., Hafez, A. K.: Bull. Soc. Chim. France, **1980,** 1—287
[2] Davies, G., El-Sayed, M. A.: Inorg. Chem., **22,** 1257 (1983)
[3] Churchill, M. R., Davies, G., El-Sayed, M. A., Hutchinson, J. P., Rupich, M. W.: Inorg. Chem., **21,** 995 (1982)
[4] Raston, C. L., White, A. H.: J. Chem. Soc. **1976,** 2153
[5] Speier, G., Tyeklar, Z.: Inorg. Chim. Acta, **66,** 169 (1982)
[6] Ainscough, E. W., Bingham, A. G., Brodie, A. M.: J. Chem. Soc. Dalton Trans., **1984,** 989
[7] Kitagawa, S., Munakata, M., Higashie, A.: Inorg. Chim. Acta, **59,** 219 (1982)
[8] Churchill, M. R., Davies, G., El-Sayed, M. A., Hutchinson, J. P.: Inorg. Chem., **21,** 1002 (1982)
[9] Ochiai, E.: Tetrahedron, **20,** 1831 (1964)
[10] Blanchard, H. S., Finkbeiner, H. L.: USP, 3219626/1965; Bodek, I., Davies, G.: Inorg. Chem., **17,** 1813 (1978)
[11] Goher, M. A. S.: Acta Chim. Acad. Sci. Hung., **99,** 307 (1979)
[12] DeAhna, H. D., Hardt, H. D.: Z. Anorg. Allg. Chem., **387,** 61 (1984)
[13] Goher, M. A. S., Drátovský, M.: J. Inorg. Nucl. Chem., **38,** 1269 (1976)
[14] Marsich, H., Camus, A., Cebulec, E.: J. Inorg. Nucl. Chem., **34,** 933 (1972) and references therein
[15] Williams, R. J. P.: J. Chem. Soc., **1955,** 137
[16] Datta, D., Chakravorty, A.: Inorg. Chem., **22,** 1085 (1983)
[17] Yoshida, S., Assai, M.: Chem. Pharm. Bull. (Japan), **7,** 162 (1957)
[18] Goher, M. A. S., Drátovský, M.: Coll. Czech., Chem. Commun., **40,** 26 (1975)
[19] Alyaviya, M. K., Rysopaeva, R. S., Kats, A. L.: Zh. Neorg. Khim., **17,** 957 (1972)
[20] Evans, R. E., Kynaston, W.: J. Chem. Soc., **1962,** 1005
[21] Katritzky, A. R., Jones, R. A.: J. Chem. Soc., **1960,** 2942
[22] Gill, N. S., Nuttall, R. H., Scaife, D. E., Sharp., R. W. A.: J. Inorg. Nucl. Chem., **18,** 79 (1961)
[23] Greenwood, N. N., Wade, K.: J. Chem. Soc., **1960,** 1130
[24] Goher, M. A. S., Hafez, A. K.: Acta Chim. Hung. (Submitted)
[25] Petillon, F., Guerchais, J. E., Goodgame, M. L.: J. Chem. Soc., **1973,** 1209
[26] Goher, M. A. S., Mak., T. C. W.: Inorg. Chim. Acta, **101,** 227 (1985)

Acta Chimica Hungarica 121 (4), pp. 373—376 (1986)

STUDIES ON METAL COMPLEXES OF 2-(*o*-HYDROXYPHENYLIMINOMETHYL) THIOPHENE AND 2-(*o*-HYDROXYPHENIL-IMINOMETHYL)PYRROLE

Fermín CAPITÁN, Francisca MOLINA, Pedro ESPINOSA and Luis Fermín CAPITÁN-VALLVEY*

(Department of Analytical Chemistry, Faculty of Sciences, University of Granada, Granada, Spain)

Received April 9, 1985
Accepted for publication May 24, 1985

The synthesis of Zn, Cd and Ni complexes of Schiff bases 2-(*o*-hydroxyphenyliminomethyl)thiophene and 2-(*o*-hydroxyphenyliminomethyl)pyrrole is described. The nature, composition and structure of the isolated solid complexes have been elucidated by elemental and thermogravimetric analysis, molar conductance, UV-VIS, IR and ^{1}H-NMR spectra, and magnetic measurements. Both reagents acts as mononegative bidentate ligands.

Introduction

Schiff bases can be considered as useful chelating agents when a suitable functional group e.g. -OH, -SH, -COOH, etc., is present sufficiently close to the azomethine group so as to form a five or six-membered chelate ring upon reaction with a metal ion. Excellent reviews are now available on the preparation, properties and structural aspects of Schiff base-metal complexes [1—5].

We are interested in the study of the complexing abilities and analytical applications of heterocyclic azomethines. Some results have been previously reported [6—8]. In the present paper we report on chelates of Schiff bases derived from the reaction of thiophene- and pyrrole-2-aldehyde with *o*-aminophenol. The study involved the synthesis and characterization of these complexes in order to establish the bonding sites on the ligands under investigation.

Experimental

Material and solutions

All the reagents used were of analytical grade. Thiophene-2-aldehyde was distilled and pyrrole-2-aldehyde was recrystallized (from petroleum ether) before use.

Schiff bases under investigation were prepared by condensing equimolar amounts of *o*-aminophenol and the corresponding aldehyde in ethanol under reflux. The products were recrystallized from ethanol-water.

* To whom correspondence should be addressed

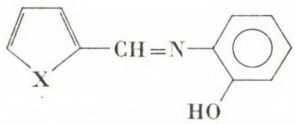

I, 2-(*o*-Hydroxyphenyliminomethyl) thiophene (X = S)
II, 2-(*o*-Hydroxyphenyliminomethyl) pyrrole (X = NH)

Synthesis and analysis of the complexes

These were synthesized by mixing hot ethanolic solutions of the ligand and the metal salts (nitrates or acetates) containing the appropriate quantities of the reactants in molar ratio (ligand : M^{2+}) 2 : 1. The reaction mixture was then refluxed on a water bath for about 30 min. The products were filtered, washed with ethanol and dried in vacuum over $CaCl_2$. (It is worthy to note that the solid complex of Ni with thiophene derivative ligand could not be isolated).

The chelates were then analyzed for their carbon, hydrogen, nitrogen and metal contents. The analytical data along with the decomposition temperatures are given in Table I. The

Table I

Properties and analytical data of Schiff base chelates

Complex	M Ω^{-1} cm^2 · mol^{-1}	Colour	Decomp. temp °C	% Found (Calcd.)			
				C	H	N	M
$Zn(C_{11}H_8NOS)_2$	2.8	reddish	277	56.45 (56.24)	3.27 (3.43)	6.01 (5.96)	14.21 (13.91)
$Cd(C_{11}H_8NOS)_2$	8.6	yellowish	285	51.82 (51.12)	3.18 (3.12)	5.53 (5.42)	21.32 (21.74)
$Zn(C_{11}H_9N_2O)_2$	1.8	yellow	260	60.42 (60.64)	4.29 (4.16)	12.74 (12.85)	15.30 (15.00)
$Cd(C_{11}H_9N_2O)_2$	6.3	yellow	290	54.64 (54.73)	3.98 (3.76)	11.32 (11.60)	24.10 (23.30)
$Ni(C_{11}H_9N_2O)_2$	6.8	yellowish	260	61.34 (61.58)	4.24 (4.23)	12.64 (13.06)	14.01 (13.71)

absence of water molecules in each chelate was confirmed by thermogravimetric analysis. All the complexes have ML_2 stoichiometry.

Physical measurements

Molar conductance in DMF solutions were carried out using a Conductivity meter Radiometer type CDM 2e at 25 °C. IR spectra were recorded on a Beckman 4240 IR Spectrophotometer in the 4000—250 cm^{-1} range using KBr pellets of the samples. ^{1}H-NMR spectra were recorded on a Bruker mod. WP80SY NMR Spectrometer in DMSO using TMS as internal reference. The electronic spectra were determined with a UV-VIS Bausch-Lomb Spectronic 2000 Spectrophotometer using 1 cm quartz cells.

Magnetic measurements for Ni complex were done in a Bruker B-M4 apparatus at room temperature by the Gouy method using mercury(II) tetrahiocyanato cobaltate(II). The value reported was measured at three field strengths and it is the average of three determinations. Diamagnetic corrections were applied to the complex before calculating the magnetic moment.

Results and Discussion

Schiff base complexes are yellowish or reddish and they have limited solubility in common organic solvents. The limited solubilities did not permit the determination of their molecular weights.

Electrical conductance measurements in DMF show these complexes to be non-electrolytes.

The assignment of characteristic infrared frequencies for ligands and their complexes are given in Table II. The high intensity band around 1615 cm^{-1} in the ligands attributable to the C=N stretching is shifted to lower frequencies in the complexes showing that the coordination has taken place through the azomethine nitrogen and as a results of this the bond order of carbon to nitrogen link is decreased [9—14].

Table II

IR and ^{1}H-NMR data

Compound	IR (cm^{-1})				^{1}H-NMR (δ, ppm)			
	ν(N—H)	ν(O—H)	ν(C=N)	ν(C—O)	Aromatic ring protons	(—CH=N)	(O—H)	(N—H)
$C_{11}H_9NOS$	—	3200—2700vb	1612 s	1260 s	5.5—6.5	7.53	7.65	—
$Zn(C_{11}H_8NOS)_2$	—	—	1597 s	1280 m	5.1—6.9	7.86	—	—
$Cd(C_{11}H_8NOS)_2$	—	—	1595 s	1280 m	5.2—6.6	7.67	—	—
$C_{11}H_{10}N_2O$	3278s,	3323s	1617 s	1240 s	6.0—7.3	8.40	b	8.6
$Zn(C_{11}H_9N_2O)_2$	3120—3048w	—	1607 s	1280 m	6.3—7.6	8.75	—	15
$Cd(C_{11}H_9N_2O)_2$	3120—3015w	—	1612 s	1275 m	a	a	a	a
$Ni(C_{11}H_9N_2O)_2$	3100—3015w	—	1608 s	1275 m	a	a	a	a

a: slightly soluble; b: included in protons aromatic multiplet

The band which appears in the region 1260—1240 cm^{-1} in the IR spectra of the Schiff bases is attributed to the phenolic C—O stretching vibration. This band is found around 1280 cm^{-1} in the IR spectra of the complexes, suggesting that the oxygen atom of the phenolic group is a bonding site of the ligands [12, 15—17]. The disappearance of the ν (O—H) band in the 3300—2700 region in the complexes confirms this fact.

Evidence for the thiophene sulfur atom being coordinated to the metal atom could not be obtained.

^{1}H—NMR spectra for ligands and their complexes were taken in DMSO. Chemical shifts for protons are given in Table II. The resonance signal due to azomethine proton shows, in the complexes, a down-field shift as compared to the corresponding Schiff base ligand indicating its deshielding as a result of coordination through the azomethine group to the metal. Furthermore, in the spectra of the complexes, the resonance signal due to *o*-OH group disappears, suggesting that the hydroxy group has taken part in the reaction. On the other

hand, the presence of a signal at 15 ppm for Zn complex of pyrrole-derivate ligand indicates that the pyrrole nitrogen is protonated and therefore it is not involved in chelation. In all cases, the integrated proton ratios correspond to the formula assigned to these complexes. These observations support the infrared conclusions.

IR and ^{1}H—NMR data provide unequivocal evidence that the ligands, potentially tridentate, function as mononegative bidentate, showing the coordination to the central metal atom through nitrogen of azomethine group and oxygen of phenolic group.

The electronic spectra of the complexes in DMSO or DMF exhibit three bands in the 250—400 nm region, which correspond to the absorption band of the ligands. Furthermore, Zn complex of I and Ni complex of II show a band at 440 and 518 nm, respectively, which may be assigned to a charge-transfer transition.

On the basis of the experimental results, a tetrahedral stereochemistry may be proposed for the complexes studied.

A further confirmation of the proposed structure is evidenced for Ni complex by: (i) the magnetic moment ($\mu_{eff} = 3.43$ BM; $\chi'_m = 4.9 \times 10^{-3}$ ucgs. mol^{-1}) fall within the range 2.97—4.1 BM reported for tetrahedral complexes of Ni [18]; (ii) the presence in the visible spectrum of a low intensity band at 578 nm, which may be assigned to a transition, $^3T_1(P) \leftarrow {}^3T_1(F)$ in a tetrahedral field [19].

REFERENCES

[1] Dwyer, F. P., Mellor, D. P.: "Chelating Agents and Metal Chelates" Academic Press. Inc., New York 1964
[2] Holm, R. H., Everett, G. W., Chakraborty, A.: Prog. Inorg. Chem., **7,** 83 (1969)
[3] Lindoy, L. F.: Quart. Rev., **25,** 379 (1971)
[4] West, B. O.: "New Pathways in Inorganic Chemistry", edited by Ebsworth, E. A. V., Maddock, A. G., Sharp, A. G., Cambridge University Press Ltd., London 1966
[5] Dey, K.: J. Scient. Ind. Res., **33,** 76 (1974)
[6] Capitán, F., Salinas, F., Capitán-Vallvey, L. F.: An. Quim., **73,** 1308 (1977); ibid., **74,** 276 (1978)
[7] Capitán, F., Salinas, F., Capitán-Vallvey, L. F.: Bull. Soc. Chim. France, **1,** 36 (1979); ibid., **5,** 185 (1979)
[8] Capitán-Vallvey, L. F., Espinosa, P.: Polyhedron, **2,** 1147 (1983)
[9] Gupta, G., Sharan, R., Kapoor, R. N.: Bull. Chem. Soc. Japan, **52,** 3088 (1979); Ind. J. Chem., **18A,** 58 (1979)
[10] Sharan, R., Gupta, G., Kapoor, R. N.: Transition Met. Chem., **3,** 282 (1978)
[11] Uttmachandami, J., Kapoor, R. N.: Transition Met. Chem., **3,** 79 (1978)
[12] Khera, B., Kaushik, N. K.: Bull. Soc. Chim. France, **11—12,** 278 (1983)
[13] Teyssie, P., Charette, J. J.: Spectrochim. Acta, **19,** 1407 (1963)
[14] Chiswell, B., Lee, K. W.: Inorg. Chim. Acta, **6,** 583 (1972)
[15] El-Haty, M. T., Adam. F. A.: Bull. Soc. Chim. France, **11—12,** 256 (1983)
[16] Biradar, N. S., Mahale, V. H., Kulkarni, V. H.: Inorg. Chim. Acta, **7,** 267 (1973)
[17] Mahmoud, M. R., El-Haty, M. T.: J. Inorg. Nucl. Chem., **42,** 349 (1980)
[18] Nicholls, D.: "Comprehensive Inorganic Chemistry", Ed. Pergamon Press, Vol. **3,** Chapter **42,** (1973)
[19] Sutton, D.: "Espectros electrónicos de los complejos de los metales de transición" (Electronic spectra of the transition metal complexes) Ed. Reverté, p. 179 (1975)

Acta Chimica Hungarica 121 (4), pp. 377—383 (1986)

HYDROGEN BONDING AND THE EFFECT OF ANION ON THE INTERNAL CONFORMATIONAL STRUCTURE OF TRIS-ETHYLENEDIAMINE NICKEL(II) COMPLEX ION

Abd El-Moneim Barakat EL-SAYED[1]*, El-Metwally Mohamed NOUR[2], Foad Abd EL-REHIM[3], Hamdi Ahmed HASSAN[1] and Wagiha Hamed MAHMOUD[1]

([1] Department of Chemistry, Faculty of Science, Ain Shams University, Abbassia, Cairo, Egypt, [2] Department of Chemistry, Faculty of Science, Zagazig University, Zagazig, Egypt, [3] National Center for Radiation Research and Technology, Nasr City, P.O. Box 29, Cairo, Egypt)

Received December 4, 1984
In revised form April 26, 1985
Accepted for publication June 13, 1985

The actual internal conformational structure of trisethylenediamine nickel(II) complex ion has been investigated and solved.

The effect of the counter ion on the complex ion was found to produce different conformational structures. Only sulphate ion was able to stabilize the complex ion in the *cis*-form via strong hydrogen bonding whereas a *gauche*-form appeared to be the common form with nitrate and chloride ions.

Introduction

Powel and Sheppard [1] made a general classification for many of the compounds of the metal ethylenediamine complex according to the degree of complexity involved in the spectral patterns of their infrared charts. Complexes of A-type include those charts which have infrared spectra similar to the spectrum of tris-ethylenediamine cobalt(III) complex ion and β-type comlpexes have charts with rather simpler spectral patterns which are similar to the spectrum corresponding to tris-ethylenediamine nickel(II) complex ion.

The internal conformational orientation of the ethylenediamine (en) chelate attached to the central metal atom was the principal basis for the classification, i.e. whether a *cis*- or *gauche*-form is produced.

As a result of the fact that both conformational structures belong to the same D_3 point group, symmetry consideration alone was not able or sufficient to discriminate between this class of complexes. A close examination of the *cis*-form has, however, revealed the existence of higher local symmetry in the chelate ring. Accordingly, it is expected for complexes belonging to this type to exhibit infrared spectra with slightly simpler patterns. This fact led Powell and Sheppard, in the first place, to classify a complex ion like tris-ethylene-

* To whom correspondences should be addressed

diamine nickel(II) as to possess a *cis*-configuration, where the two carbon atoms of the ethylenediamine molecule are in the same plane occupied by the nickel and two nitrogen atoms of the ethylenediamine molecule. Later, Watanabe and Atoje [2], on the contrary, pointed out that the results of the x-ray diffraction analysis made on the chloride salt of the same complex species has predicted a *gauche*-form. In the opposite case, both infrared and x-ray studies carried out by other investigators [3, 4] agreed to assign **A**-type complexes exemplified by the tris-ethylenediamine cobalt(III) complex to the *gauche*-form which possesses less local symmetry.

In fact, these reports appear to be highly contradictous the thing that made the authors [5] to revoke their earlied suggestion and reinvestigate the results of more spectral charts of other similar complexes. In a recent report, they concluded that the marked variations observed in the spectral patterns between **A**-type and **B**-type complexes are, in fact, caused mainly by the great changes in intensities of various bands e.g. the regions 600—800; 1000—1200 cm^{-1} showed the most distinctive differences between the two types of complexes. For example, the characteristic band at 1030 cm^{-1} is particularly very strong and can only be observed in the infrared charts of **B**-type complexes. This band was concluded by the authors [6] to be responsible for the desappearance of some vibrational bands the reason that the infrared charts of **B**-type complexes seemed to appear rather simpler in spectral patterns. Furthermore, an x-ray diffraction study was made on another complex of **B**-type brought a further confirmation for the results obtained by Powell and Sheppard.

Nakahara et al. [7] reported that in case of the $[Cu(en)_2]^{2+}$ complex ion, despite the fact that the four nitrogen atoms of both ethylenediamine molecules are equally bonded to the central copper atom, the ring formed by the ethylenediamine molecule showed an leave space appreciable dissimilarity in N—Cu bond distances while the complex was in the *gauche*-configuration of the ring [8]. This would, effectively, result in a ring distortion, thus it might account for the differences observed in the intensity of various vibrational bands of **B**-type spectra. This last fact urged Powell and Sheppard [6] to abandon their earlier suggestion and withdraw another conclusion that trisethylenediamina nickel(II) complex ion belongs to *gauche*-configuration.

In order to clarify the matter about this problem, the infrared spectrum of $[Ni(en)_3]^{2+}$ complex ion has been reinvestigated and the effect of the counter ion on the internal conformational structure of the complex species has also been examined.

Experimental

The sulphate, nitrate and chloride salts of the trisethylenediamine nickel(II) complex have been prepared according to standard methods [9]. Chemical formulas have been checked by chemical analysis. This is carried out by passing a solution containing a known weight of the

dried solid complex through a cation exchanger in the H-form. The equivalent amount of the acid liberated was titrated with a standard borax solution using methyl orange as an indicator.

A Pye Unicam SP 2000 ir spectrometer was utilized to record the infrared spectra of the different salts of the nickel complex in potassium bromide discs. The chemical formulas were found as follows:

$$Ni(en)_3SO_4;\ Ni(en)_3Cl_2 \cdot 2H_2O;\ Ni(en)_3(NO_3)_2$$

Results and Discussion

The infrared spectra of sulphate, nitrate and chloride salts of the tris-ethylenediamine nickel(II) complex are shown in Fig. 1. The important vibrational frequencies which have indicated some noticeable changes are given in Table I. The solid line represents the spectrum of the complex species as sulphate salt whereas those for the nitrate and chloride salts are represented by the broken and dotted lines, respectively.

The spectrum in its overall pattern is in close agreement with that obtained by Powell and Sheppard [6]. However, there have been some gradual

Table I

Changes in intensity of $[Ni(en)_3]^{2+}$ *complex by the counter ion*

Vibrational mode	Wave number given by reference [6]	Wave number recorded	Per cent transmittance %T		
			$Ni(en)_3SO_4$	$Ni(en)_3(NO_3)_2$	$Ni(en)_3Cl_2$
Ni—N	480.0 (s)	490.0	64.0	39.0	46.2
		505.0	57.8	49.5	—
	515.0 (s)	517.0	54.5	31.5	32.0
		532.0	44.0	—	—
NH_2 rock	617.0	613.0	30.2	—	55.1
	640.0				
	653.0	654.0	59.0	28.0	32.0
Ring skel.	867.0 (w)	706.0	51.8	59.5	—
CH_2 rock	882.0 (vw)				
	972.0 (s)	978.0	57.8	37.5	42.6
Ring skel.	1023.0 (vs)	1026.0	13.5	4.5	6.0
		1035.0	15.5	—	—
		1072.0	—	60.0	55.8
NH_2 Twist	1101.0 (m)	1095.0	8.6	52.5	45.5
		1112.0	—	52.5	43.0
NH_2 Wag	1142.0 (w)	1122.0	4.2	—	—
Ring skel.	1158.0 (w)	1150.0	—	40.5	38.2
CH_2 Twist	1282.0	1272.0	55.3	33.5	50.5
		1323.0	—	22.0	55.3
CH_2 Wag	1332.0 (s)	1336.0	64.5	—	—
	1373.0 (w)				
	1399.0 (vw)				
CH_2 Scissors	1463.0	1451.0	60.0	28.0	50.6
NH_2 Scissors	1581.0 (s)	1580.0	—	33.0	47.7
	1596.0 (s)	1598.0	48.0	31.8	49.5
$\nu\ CH_2$	2897.0	2882.0	43.0	36.4	38.0
	2947.0	2922.0	40.5	33.0	36.0
$\nu\ NH_2$	3188.0	3165.0	22.0	28.5	26.0
		3250.0	—	12.2	11.5
	3292.0 (s)	3295.0	8.0	7.5	7.5
	3342.0 (s)	3324.0	—	9.0	12.5
		3480.0	45.0	30.5	30.5

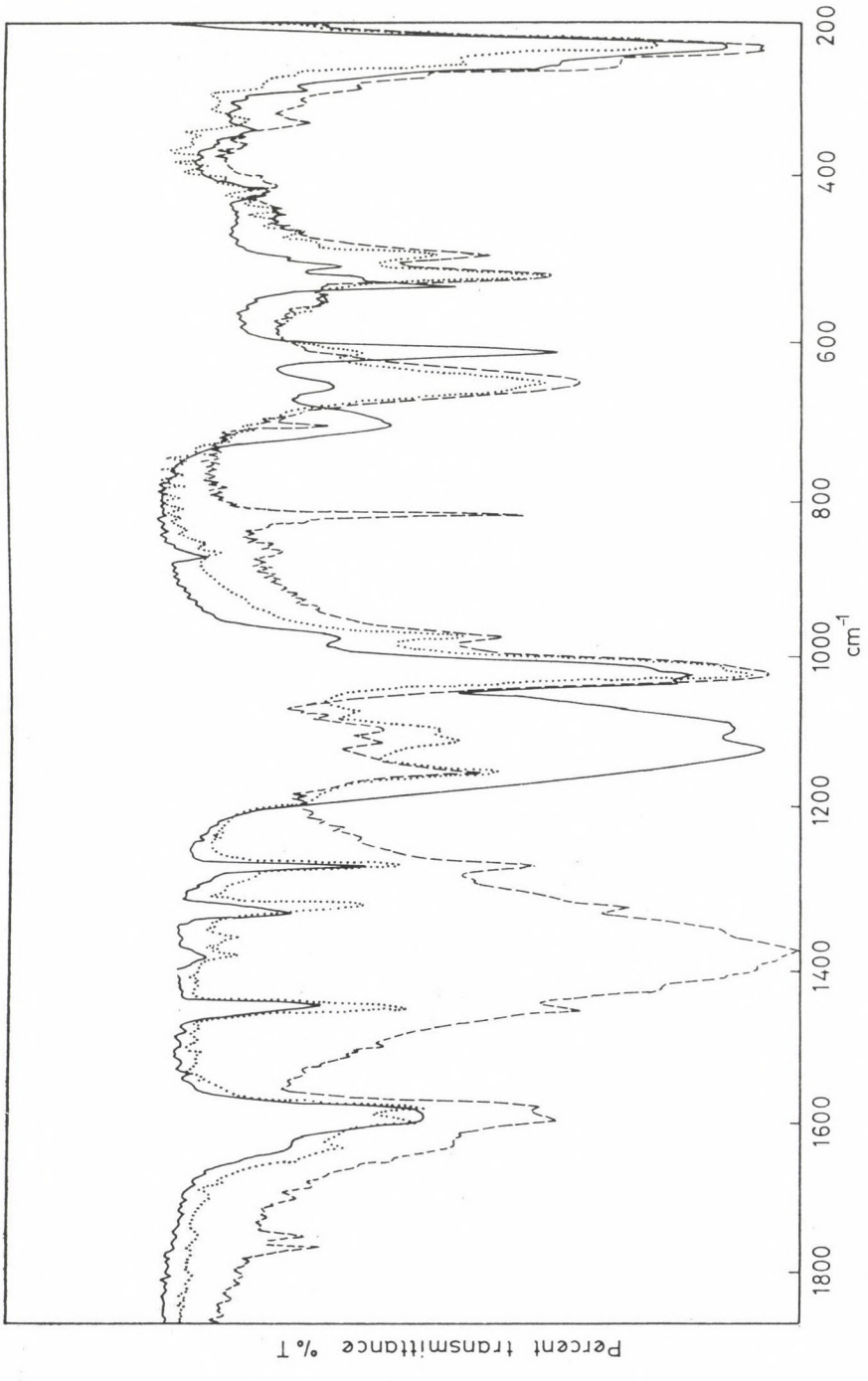

Fig. 1. Infrared spectra of the sulphate, nitrate and chloride salts of tris-ethylenediamine nickel(II) complex ion

changes observed in the intensity of various vibrational bands on going from the complex species as sulphate salt to those corresponding to nitrate and chloride salts. A number of vibrational bands were found to decrease in intensity and at the same time another set of new bands appeared at different wavelengths with different intensity. For example, in the spectrum representing the complex species in the sulphate salt, the bands at 505, 613 and 706 cm^{-1} appeared with much lower intensity in the spectra of the same complex species in the nitrate and chloride salts. Whereas, the bands at 532, 1035, 1122 and 1336 cm^{-1} did not appear space at all. On the other hand, the bands at 1072, 1112, 1150 1323, 1580, 3250 and 3285 cm^{-1} appeared with much higher intensity in the spectra representing those for nitrate and chloride salts whereas these bands disappeared completely in the spectrum corresponding to the sulphate salt.

It is interesting to note that none of these frequencies belong to the normal vibrational frequencies of the free sulphate ion [10].

The overall effect resulted on changing the anion is to cause some variations in band intensity, changes of this kind might primarily suggest that changing the anion would probably alter the overall geometry of the complex $[Ni(en)_3]^{2+}$ i.e. from octahedral to tetragonal or square planar. Such a suggestion seems to be highly improbable. This is due to the fact that the general features of the three spectral charts were found almost the same except in band intensity as explained earlier in the text. This leaves little doubt that such changes must bear a direct relevance to the internal configuration of the ethylenediamine ring attached to the central nickel atom with the same D_3 point group i.e. whether the chelated ring is going to produce a *cis-* or *gauche*-form.

The question is: exchanging the anion from sulphate to nitrate or chloride would cause a major change in the conformational structure of the basic unit $[Ni(en)_3]^{2+}$ i.e. from *cis-* to *gauche*-form or vice versa? If the answer is yes, then to what extent this conversion takes place and what is the original conformational structure in which the complex of tris-ethylenediamine nickel(II) sulphate has been crystallized?

In order to give satisfactory answers to these questions the investigation was extended to the corresponding chloride and nitrate salts of $[Ni(en)_3]^{2+}$ complex ion, as well as, also to see the effect of some bulky anions and have very little tendency for coordination to the central nickel atom e.g. perchlorate and tetra-chloroplatinate(II). The spectra of these salts showed no changes in intensity and position of the vibrational bands. This revealed that the presence of sulphate ion within the crystal lattice of the complex and at a definite position has shown to be highly important to have any changes in the intensity of various vibrational bands. This fact might provide an indirect answer to the third question. This can be seen through a closer inspection of the nature and the type of interaction that may exist between the complex species of tris-ethylenediamine nickel(II) and the counter ion.

It has been reported by Powell and Sheppard [6] that hydrogen bonds between the hydrogen atoms of the amino and methyl groups and the counter ion may play a major role in determining the general spectral patterns of the infrared charts, and hence, the overall geometry of the complex species. This effect was noticed in the case of $[Pt(en)_2]^{2+}$ and $(Pd(en)_2]^{2+}$ complex ions. The infrared spectra of both $[Cu(en)_2]^{2+}$ and the present complex $[Ni(en)_3]^{2+}$ in the chloride salt were not affected on replacing the anion by a bulky non-interacting group such as $(PtCl_4)^{2-}$ ion. This could provide a strong evidence for the absence or very weak nature of hydrogen bonding with chloride ions in the last two complexes.

Now, since the presence of sulphate ion has produced a distinct change in the infrared spectrum of the $[Ni(en)_3]SO_4$ complex only, this change may tentatively be taken as a mark for the formation of some kind of interaction between the counter ions and the complex species, i.e. the sulphate ion must have assumed the character of imposing certain restraint on the internal geometry of the ethylenediamine ring. Such a restraint may be weakened (or strengthened) on replacing the sulphate ion by any other counter ion. This effect may be determined practically by the disappearance of the bands at 532, 1035, 1122 and 1336 cm^{-1} which correspond to Ni—N, C—C ring skeletal and CH_2 wag vibrations, respectively, and the appearance of a new set of bands with comparable intensity at 1072, 1112, 1150, 1323, 1580, 3250 and 3324 cm^{-1}, these bands correspond to NH_2 twist, ring skeletal, NH_2 wag, CH_2 wag, NH_2 Scissors and NH_2 stretching vibrations, respectively.

An early reference in this connection refers to the x-ray studies made on the $[Ni(en)_3]^{2+}$ complex ion indicated that the ethylenediamine ring has been found to assume a *gauche*-configuration [2]. This investigation was applied only to the nitrate salt. Since, however, it has already been established experimentally that the three salts of the $[Ni(en)_3]^{2+}$ complex were found to have similar spectral patterns, therefore, the variation associated in band intensity of the sulphate salt can best be explained in terms of formation of hydrogen bonds.

In another x-ray diffraction analysis made on $[Co(en)_3]Cl_2$ complex a sufficient structural description was given. The complex species has been found to be surrounded by nine chloride ions, six of them are at the apices of a distorted trigonal prism at distances 3.18 and 3.26 Å apart from the nitrogen atoms, whereas the other three form equilateral triangle being at distances 3.13 and 3.41 Å. Distances of these magnitudes, in fact, seem to minimize the probability of the existence of hydrogen bonding with chloride ions or any existing molecule of water of crystallization.

There are no available data concerning the results of x-ray measurements for the same complex species in sulphate or nitrate salts.

However, if it is to suggest that ethylenediamine ring is originally assumed

to be in the *cis*-form then the sulphate ion must be present at definite position within the crystal lattice so as to produce a sufficient restraint imposed on the internal geometrical structure of the ring. Such a position may be located at a direction of the three-fold symmetry axis. In this way, the sulphate oxygen (in a staggered orientation with respect to the three ethylenediamine rings attached to the central nickel atom) can strongly interact with the hydrogen atoms of the amino groups. This interaction can best be achieved if the positions of the two carbon atoms were in the same plane occupied by the nickel and two nitrogen atoms i.e. if the ring is to assume the *cis*-form.

A close typical modelling inspection of the complex structure reveals the fact that within the crystal lattice the sulphate ions and the complex species are present in 2 : 1 ratio instead of 9 : 1 as in the case of chloride or nitrate salts, such an arrangement could lead to strong interaction with the three rings thus it might be responsible for the marked changes in the intensity of various vibrational bands.

At the present stage of investigation it is not easy to judge the relative stability for both conformational structures, it was found, however, that the sulphate salt of the complex is affected by gamma radiation. Also, it is interesting to note that the infrared spectrum of potassium bromide disc of the sulphate salt came in close agreement with the spectra of chloride and nitrate salts after a sufficient period of irradiation. This observation might suggest the possibility of existence of some kind of interconversion in the internal conformational structure from *cis*- to *gauche*-form. When the potassium bromide discs of both chloride and nitrate salts of the complex were exposed for the same period of time to gamma radiation no changes were observed in band intensity. This might suggest primarily that the *gauche*-form is slightly more stable than the *cis*-form.

*

The authors wish to express their appreciation for the facilities offered by "National Center for Radiation Research and Technology", Nasr City P.O. Box 29 Cairo—Egypt.

REFERENCES

[1] Powell, D. B., Sheppard, N.: J. Chem. Soc., **1959,** 791
[2] Watanabè, T., Atoji, M.: Science Kagaku (Japan), **21,** 301 (1951)
[3] Nakatsu, K., Saito, Y., Kuroya, H.: Bull. Chem. Soc. Japan, **29,** 428 (1956; Saito, Y., Nakatsu, K., Shiro, M. Kuroya, H.: Acta Crys., **8,** 792 (1955); Nakatsu, K., Shiro, M., Saito, Y., Kuroya, H.: Bull. Chem. Soc. Japan, **30,** 158 (1957)
[4] a) Mizushima, S., Quagliano, J. V.: J. Am. Chem. Soc., **75,** 6084 (1953); b) J. Chem. Phys., **22,** 1614 (1954); c) J. Phys. Chem., **59,** 293 (1955)
[5] Powell, D. B., Sheppard, N.: J. Chem. Soc., **1961,** 1112
[6] Powell, D. B., Sheppard, N.: Spectrochimica Acta, **17,** 68 (1961)
[7] Nakahara, A., Saito, Y., Kuroya, H.: Bull. Chem. Soc. Japan **25,** 331 (1952)
[8] Scouloudi, H.: Acta Cryst., **6,** 651 (1953)
[9] Inorganic Synthesis, Vol. **VI,** 200 (1960)
[10] Nakamoto, K.: "Infrared and Raman Spectra of Inorganic and Coordination Compounds" Wiley-Interscience, Third Edition, 142, 1978

Acta Chimica Hungarica 121 (4), pp. 385—390 (1986)

DIVALENT OXOVANADIUM, MANGANESE, IRON, NICKEL AND COPPER COMPLEXES OF TETRADENTATE N_4 MACROCYCLIC LIGANDS

Vipin Kumar CHAUHAN, Satish Kumar AGARWAL, Suraj Prakash RATRA and Vidya Bhushan RANA*

(Department of Chemistry, Meerut College, Meerut-250001, India)

Received December 14, 1984
In revised form May 27, 1985
Accepted for publication June 24, 1985

Divalent oxovanadium, manganese, iron, nickel, cobalt, and copper salts react with *m*-phenylenediamine and 2,3-butanedione to form complexes of a 14-membered N_4 tetradentate macrocyclic ligand. The complexes are characterized as distorted octahedral of the $[M(TML)X_2]$ type where M = VO(II), Mn(II), Fe(II), Co(II), Ni(II) and Cu(II); TML = tetradentate macrocyclic ligand and X = Cl, Br, NO_3 or NCS. The ligand could not be isolated in free state, however, in its complexes it coordinates through all the azomethine nitrogen atoms which are bridged by biacetyl moieties.

Itntroduction

The condensation reactions of carbonyl compounds and polyamines are primarily responsible for a major part of process leading to the formation of macrocyclic ligands. Most of the macrocycles are derived from 2,6-diacetylpyridine and polyamines [1, 2] however, very few are prepared from aromatic diamines and dicarbonyl compounds [3, 4]. In continuation to our studies on N_6, N_4 or N_2O_2 type of macrocycles [5—9] we report here on the synthesis and characterization of metal complexes of a 14-membered macrocyclic ligand.

Experimental

All the chemicals and solvents used were of reagent grade. *m*-Phenylenediamine and 2,3-butanedione were purified before use.

Preparation of complexes

m-Phenylenediamine (0.02 mol) and 2,3-butanedione (0.02 mol) each dissolved in 100 mL dry methanol were refluxed for 2h. 50 mL methanolic solution of metal salt (0.01 mol) was added followed by 2 mL glacial acetic acid and the mixture refluxed for 12 h concentrated to half of its volume and allowed to stand for 4 days. The dark crystals separated were filtered, washed with methanol, ether and acetone and dried in vacuum; yield $\sim$ 35%.

Attempts to synthesize free ligands by condensation reactions of *m*-phenylenediamine and acetylacetone in various solvents fail. However, an open chain ligand $CH_3COCH_2C(CH_3)=NC_6H_4N=C(CH_3)CH_2COCH_3$ results.

* To whom correspondence should be addressed

Table I

Analytical data of VO(II), Mn(II), Fe(II), Co(II), Ni(II) *and* Cu(II)

Complex	Colour	Found (Calcd)%					
		C	H	N	M	X	M.W
$[VO(C_{20}H_{20}N_4)Cl]Cl$	Bluish Green	52.72 (52.86)	4.45 (4.40)	12.40 (12.33)	14.90 (14.75)	15.50 (15.63)	—
$[VO(C_{20}H_{20}N_4)Br]Br$	Green	44.30 (44.19)	3.80 (3.68)	10.22 (10.31)	12.40 (13.33)	29.38 (29.46)	—
$[VO(C_{20}H_{20}N_4)NO_3]NO_3$	Bluish Green	47.20 (47.33)	3.86 (3.94)	16.62 (16.56)	13.40 (13.21)	24.60 (24.45)	—
$[Mn(C_{20}H_{20}N_4)Cl_2]$	Blackish Brown	54.00 (54.29)	4.42 (4.52)	12.70 (12.66)	12.38 (12.44)	16.00 (16.06)	—
$[Mn(C_{20}H_{20}N_4)Br_2]$	Brown	45.25 (45.19)	3.80 (3.76)	10.62 (10.54)	10.28 (10.64)	30.00 (30.13)	—
$[Fe(C_{20}H_{20}N_4)Cl_2]$	Orange	54.20 (54.17)	4.48 (4.51)	12.70 (12.64)	12.72 (12.64)	16.05 (16.02)	430 (442)
$[Fe(C_{20}H_{20}N_4)(NO_3)_2]$	Brownish Yellow	48.50 (48.38)	4.00 (4.03)	16.85 (16.93)	12.50 (11.29)	24.82 (25.00)	488 (496)
$[Co(C_{20}H_{20}N_4)Cl_2]$	Pink	54.00 (53.81)	4.54 (4.48)	12.60 (12.55)	13.12 (13.22)	16.02 (15.91)	446 (451)
$[Co(C_{20}H_{20}N_4)(NO_3)_2]$	Yellowish Brown	47.98 (48.09)	4.05 (4.00)	16.80 (16.83)	11.90 (11.82)	25.00 (24.84)	490 (499)
$[Ni(C_{20}H_{20}N_4)Cl_2]$	Light Green	54.00 (53.93)	4.85 (4.49)	12.62 (12.58)	13.00 (13.03)	16.00 (15.95)	
$[Ni(C_{20}H_{20}N_4)(NO_3)_2]$	Bluish Green	48.25 (48.19)	4.05 (4.01)	16.92 (16.86)	10.72 (11.64)	24.80 (24.89)	—
$[Ni(C_{20}H_{20}N_4)(NCS)_2]$	Green	53.80 (53.87)	4.00 (4.08)	17.22 (17.14)	12.00 (11.83)	— —	— —
$[Cu(C_{20}H_{20}N_4)Cl_2]$	Deep Blue	53.42 (53.33)	4.50 (4.44)	12.50 (12.44)	14.15 (14.00)	15.82 (15.77)	
$[Cu(C_{20}H_{20}N_4)(NO_3)_2]$	Bluish Green	47.65 (47.71)	3.91 (3.97)	16.72 (16.70)	12.56 (12.52)	24.60 (24.65)	—

The chloro and nitrato complexes were prepared using metal chlorides and nitrates, respectively. Bromo and thiocyanato complexes were prepared by stirring and adding slowly KBr and NH_4NCS solutions to ethanolic solution of metal chloride and filtering off KCl and NH_4Cl.

All the complexes are stable upto 200 °C. The vanadyl, iron and cobalt complexes are soluble in water and DMF whereas those of other metals are slightly soluble in DMF.

Physical and analytical measurements

The analysis of C, H and N were done by microanalytical techniques. Metal contents were determined by EDTA titration using Eriochrome Black-T as an indicator. Halides were determined by Volhard's method and nitrate as its nitron salt.

Magnetic moments and conductivity determinations, molecular weight and spectral measurements were made as described earlier [6].

Results and Discussion

The analytical data of all the complexes correspond to the formula $[M(C_{20}H_{20}N_4)X_2]$ where M = VO(II), Mn(II), Fe(II) Co(II), Ni(II) and Cu(II); X = Cl, Br, NO_3 or NCS. The molar conductance of vanadyl, iron, and cobalt complexes measured in DMF show that all complexes are non-electrolytes except those of oxovanadium which are 1 : 1 electrolytes. The test for anions could only be positive after decomposing the complexes with HNO_3 showing their presence in the coordination sphere. However, these tests are positive directly in case of VO(II) complexes indicating their presence also outside the coordination sphere. The molecular weights of iron and cobalt complexes, determined cryoscopically, are consistent with the proposed formulas.

Infrared spectra

Various important bands and their assignments are given in Table II. The I.R. spectra of all the complexes do not show any bands in the 3200—3400 and 1700 cm^{-1} regions indicating the absence of free carbonyl or amino groups in these complexes.

Table II

Infrared spectral data of VO(II), Mn(II), Fe(II) Co(II), Ni(II), *and* Cu(II) *complexes*

Complexes	ν CN	Phenyl	ν CH_3	Anions
$[VO(C_{20}H_{20}N_4)Cl]Cl$	1620	1615, 1600	810, 790 805, 800	375
$[VO(C_{20}H_{20}N_4)Br]Br$	1610	1605, 1595	805, 800	220
$[VO(C_{20}H_{20}N_4)NO_3]NO_3$	1615	1610, 1605	810, 800	1260, 1010, 860 1340, 1245, 830
$[VO(C_{20}H_{20}N_4)NCS]NCS$	1605	1580, 1575	800, 790	2120, 830, 485
$[Mn(C_{20}H_{20}N_4)Cl_2]$	1620	1610, 1600	790, 770	345
$[Mn(C_{20}H_{20}N_4)Br_2]$	1625	1620, 1605	795, 775	220
$[Mn(C_{20}H_{20}N_4)(NO_3)_2]$	1600	1590, 1580	800, 780	1265, 1015, 865
$[Mn(C_{20}H_{20}N_4)(NCS)_2]$	1620	1595, 1585	805, 795	2110, 825, 480
$[Fe(C_{20}H_{20}N_4)Cl_2]$	1625	1600, 1595	810, 805	[330
$[Fe(C_{20}H_{20}N_4)Br_2]$	1615	1585, 1580	810, 795	—
$[Fe(C_{20}H_{20}N_4)(NO_3)_2]$	1605	1585, 1575	815, 780	1260, 1010, 860
$[Fe(C_{20}O_{20}H_{20}N_4)(NCS)_2]$	1620	1605, 1600	795, 770	2115, 835, 480
$[Co(C_{20}H_{20}N_4)Cl_2]$	1600	1680, 1575	790, 770	310
$[Co(C_{20}H_{20}N_4)Br_2]$	1600	1590, 1585	780, 775	218
$[Co(C_{20}H_{20}N_4)(NO_3)_2]$	1625	1620, 1610	785, 780	1265, 1010, 865
$[Co(C_{20}H_{20}N_4)(NCS)_2]$	1615	1600, 1595	800, 795	2115, 830, 420
$[Ni(C_{20}H_{20}N_4)Cl_2]$	1605	1595, 1580	805, 790	285
$[Ni(C_{20}H_{20}N_4)Br_2]$	1610	1580, 1570	800, 780	215
$[Ni(C_{20}H_{20}N_4)(NO_3)_2]$	1600	1585, 1580	795, 770	1265, 1015, 860
$[Ni(C_{20}H_{20}N_4)(NCS)_2]$	1600	1590, 1575	805, 795	2120, 825, 475
$[Cu(C_{20}H_{20}N_4)Cl_2]$	1620	1600, 1590	805, 790	270
$[Cu(C_{20}H_{20}N_4)Br_2]$	1605	1585, 1580	810, 800	—
$[Cu(C_{20}H_{20}N_4)(NO_3)_2]$	1600	1585, 1580	800, 790	1265, 1010, 865
$[Cu(C_{20}H_{20}N_4)(NCS)_2]$	1615	1600, 1595	805, 770	2115, 830, 480

The absence of stretching and bending vibrations of (C—O) group at $\sim$ 1525 and 1280 cm^{-1} indicates the absence of this group in these complexes [10]. Characteristic phenyl group bands are observed in the spectra at $\sim$ 700—820 cm^{-1}. The strong bands appearing as doublets at $\sim$ 1600—1625 cm^{-1} may be assigned to (C=N) vibrations and their appearance at lower regions indicates the presence of coordinated azomethine groups [11]. Thus, it is obvious from i.r. spectra that amino groups of diamines have condensed with the carbonyl groups of 2,3-butanedione to give rise a planar arrangement of four azomethine nitrogen atoms for coordination.

The spectra of nitrato complexes show new bands at $\sim$ 1260, 1015 and 865 cm^{-1} consistent with the monodentate nature of the nitrato group in these complexes [10, 12] however, three other bands are observed in the spectra of the VO(II) complex at $\sim$ 1340, 1245 and 830 cm^{-1} and show that nitrato group is also present as an ion in this complex [10, 12].

In the spectra of thiocyanato complexes, strong bands are observed at $\sim$ 2110 ν(CN), 485 NCS bending and 830 cm^{-1} ν(CS) of NCS group, respectively, and are in accordance with monodentate *N*-bonded thiocyanate group [13]. The coordination of nitrato and thiocyanato groups are further substantiated by the appearance of new bands at $\sim$ 225—240 and 260—280 cm^{-1} assignable to ν(M—ONO_2) and ν(M—NCS), respectively [10, 14]. One weak and one strong band at $\sim$ 2375 and 2100 cm^{-1} are also observed in the thiocyanato complex of VO(II) indicating that ionic thiocyanate is also present in it.

The new bands in the spectra of VO(II) complexes at $\sim$ 960—970 cm^{-1} assignable to νVO(II) are characteristic of the terminal (V=0) group [15].

Far I.R. spectra

The new bands at $\sim$ 430—490 cm^{-1} in the far i.r. spectra originate from ν(M—N) azomethine vibrations and substantiate this coordination. The spectra of halo complexes which show new bands at $\sim$ 370—380 ν(VO—Cl) [15], 340—350 ν(Mn—Cl) [16], 330—335 ν(Fe—Cl), 300—310 ν(Co—Cl), 280—295 ν(Ni—Cl) and 270—275 ν(Cu—Cl), respectively are consistent with octahedral geometry around the metal atom [16—17]. Similar bands for bromo complexes are observed at $\sim$ 220 ν(VO—Br), 220 ν(Mn—Br), 218 ν(Co—Br) and 215 cm^{-1} ν(Ni—Br), respectively [16, 18].

Magnetic moments and electronic spectra

Magnetic moments of the complexes are given in Table III. All the values are consistent with the spin free octahedral nature of these complexes [19]. The electronic spectra of the complexes recorded in nujol mull are given

Table III

Electronic spectral and magnetic data of VO(II), Mn(II), Fe(II), Co(II), Ni(II) *and* Cu(II) *complexes*

Complexes	Spectral bands	10 Dq	μ_{eff} B.M.
[VO(TML)Cl]Cl	12750, 15800, 25850	1580	1.74
[VO(TML)Br]Br	12920, 16250, 24500	1625	1.80
[VO(TML)NO_3]NO_3	13150, 16400, 24750	1640	1.78
[VO(TML)NCS]NCS	13200, 15950, 23950	1595	1.82
[Mn(TML)Cl_2]	1774, 21450, 25250 27800, 29700	1129	5.80
[Mn(TML)Br_2]	17500, 20850, 25500 27900, 29550	1194	6.00
[Mn(TML)$(NO_3)_2$]	17820, 21200, 25300 27750, 29850	1124	5.92
[Mn(TML)$(NCS)_2$]	17500, 21350, 25350 27820, 29650	1169	5.84
[Fe(TML)Cl_2]	8500, 11450	1145	5.52
[Fe(TML)Br_2]	8920, 12300	1230	5.56
[Fe(TML)$(NO_3)_2$	8720, 11950	1195	5.36
[Fe(TML)$(NCS)_2$]	8850, 12250	12250	5.42
[Co(TML)Cl_2]	8320, 15820, 18200	1040	4.58
[Co(TML)Br_2]	8950, 15950, 18750	1118	4.70
[Co(TML)$(NO_3)_2$]	8720, 16150, 19200	1090	4.62
[Co(TML)$(NCS)_2$]	9000, 16450, 20200	1125	4.54
[Ni(TML)Cl_2]	10200, 11700, 16300 27950	1170	3.12
[Ni(TML)Br_2]	9850, 11850, 16720, 27700	1185	3.30
[Ni(TML)$(NO_3)_2$]	9950, 11450, 16800, 27800	1145	3.14
[Ni(TML)$(NCS)_2$]	9500, 11400, 16850, 27550	1140	3.20
[Cu(TML)Cl_2]	15300, 18050	1530	1.71
[Cu(TML)Br_2]	16000, 18750	1600	1.68
[Cu(TML)$(NO_3)_2$]	15850, 1900	1580	1.70
[Cu(TML)$(NCS)_2$]	16150, 18820	1610	1.69

in Table III. The spectra of the complexes resemble to those observed for octahedral complexes reported earlier [20]. The assignments of various bands can be made as, for VO; $\sim$ 13000, $d_{xy} \rightarrow d_{xz, yz}$; 15000—17000, $d_{xy} \rightarrow d_{x^2-y^2}$; 24000—25000 cm^{-1} $d_{xy} \rightarrow d_{z^2}$; for Mn; $\sim$ 17000—18000, $^6A_{1g} \rightarrow {}^4T_{1g}$ (G); $\sim$ 20000, $^6A_{1g} \rightarrow {}^4T_{2g}$ (G); 25500, $^6A_{1g} \rightarrow {}^4E_g$ (G); 27000—28000, $^6A_{1g} \rightarrow {}^4T_{2g}$ (D); and 29500 cm^{-1}, $^6A_{1g} \rightarrow {}^4E_g$ (D); for Fe; $\sim$ 8500, $^5T_{2g} \rightarrow {}^5A_{1g}$; 11000—12000 cm^{-1}, $^5T_{2g} \rightarrow {}^5B_{1g}$; for Ni; $\sim$ 10000, $^3B_{1g} \rightarrow {}^3E_g$; 12000, $^3B_{1g} \rightarrow {}^3B_{2g}$; 16000—17000, $^3B_{1g} \rightarrow {}^3A_{2g}$ (F), $^3E_g^b$; 27000—28000 cm^{-1}, $^3B_{1g} \rightarrow {}^3A_{2g}$ (P); for Co; $\sim$ 8000, $^4T_{1g} \xrightarrow{(F)} {}^4T_{2g}$ (F); 15000, $^4T_{1g} \xrightarrow{(F)} {}^4A_{2g}$ (F); 19000 cm^{-1}, $^4T_g \xrightarrow{(F)} {}^4T_{1g}$ (P); for Cu; $\sim$ 15000, $^2B_{1g} \rightarrow {}^2B_{2g}$; 18000 cm^{-1}, $^2B_{1g} \rightarrow {}^2E_g$ and $^2B_{1g} \rightarrow {}^2A_{2g}$; respectively, based on D_{4h} symmetry [20]. The true symmetry, however, would be lower than D_{4h} since the detailed crystallographic studies [21] reveal that the macrocycle obtained from *o*-phenylenediamine and acetylacetone, offers a saddle like shape from the steric interactions of benzanoid rings with the methyl substituents of the macrocyclic ring. The resulting

strain is relieved through twisting of torsional angles about the (C=N) bonds on the N_4 ring, which is the most readily deformable site. In the saddle shape the nitrogen lone pairs directed out of the N_4 plane [21, 22] so that the metal 'sits atop' and not inside the N_4 cavity [21—24]. It seems, therefore, that the macrocycle offers a planar N_4 arrangement and the metal sits atop the macrocycle incorporating anions on axial positions.

Based on analysis, conductance, magnetic, electronic and infrared spectral studies structure (1) may be proposed for these complexes.

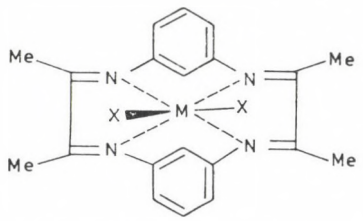

M = VO(II), Mn(II), Fe(II), Ni(II), Co(II) and Cu(II) X = Cl, Br, NO_3, or NCS

*

The authors are grateful to U.G.C. and CSIR New Delhi, for financial assistance and to RSIC, IIT, Madras for spectral measurements.

REFERENCES

[1] Busch, D. H.: Record. Chem. Prog., **25,** 107(1964)
[2] Lindoy, L. F., Busch, D. H.: in W. L. Jolly (Ed) Preparative Inorganic Reactions, **6,** 1 (1971)
[3] Malik, W. U., Bembi, R., Singh, R.: Polyhedron **2,**, 369 (1983)
[4] Goedken, V. L., Lodd, J. A.: J. Chem. Soc. Chem. Comm., **1982,** 142
[5] Rana, V. B., Singh, P., Singh, D. P., Teotia, M. P.: Polyhedron, **1,** 377 (1982)
[6] Rana, V. B., Singh, D. P., Singh, P., Teotia, M. P.: Transition Met. Chem., **6,** 36 (1981)
[7] Rana, V. B., Singh, P., Singh, D. P., Teotia, M. P.: Transition Met. Chem., **7,** 174 (1982)
[8] Rana, V. B., Teotia, M. P.: Ind. J. Chem., **19A,** 267 (1980)
[9] Chauhan, V. K., Agarwal, S. K., Singh, P., Rana, V. B.: Acta Chim. Hung., **118,** 315 (1985)
[10] Nakamoto, K.: Infrared Spectra of Inorganic and Coordination Compounds, Wiley Interscience, New York 1970
[11] Rao, C. N. R.: Chemical Applications of Infrared Spectroscopy, Academic Press, New York 1963
[12] Lever, A. B. P., Mantovani, E., Ramaswamy, B. S.: Canad. J. Chem., **49,** 1957 (1971)
[13] Burmeister, J. L.: Coord. Chem. Rev., **1,** 205 (1966); **3,** 225 (1968)
[14] Baldwin, D. A., Lever, A. B. P., Parish, R. V.: Inorg. Chem., **8,** 107 (1969)
[15] Rana, V. B., Sahni, S. K., Swami, M. P., Jain, P. C., Shrivastava, A. K.: J. Inorg. Nucl. Chem., **38,** 176 (1976)
[16] Ferraro, J. R.: Low Frequency Vibrations of Inorganic and Coordination Compounds, Plenum Press, New York 1971
[17] Beecroft, B., Campbell, M. J. M., Grazeskowiak, R.: J. Inorg. Nucl. Chem., **36,** 55 (1974)
[18] Clark, R. J. H., Williams, C. S.: Inorg. Chem., **4,** 350 (1965)
[19] Figgis, B. N., Lewis, J.: Prog. Inorg. Chem., **6,** 37 (1964)
[20] Lever, A. B. P.: Inorganic Electronic Spectroscopy, Elsevier, Amsterdam 1968
[21] Goedken, V. L., Park, Y. A.: J. Chem. Soc. Chem. Comm., **1976,** 814
[22] Weiss, M. C., Goedken, V. L.: J. Chem. Soc. Chem. Comm., **1976,** 531
[23] Weiss, M. C., Peng, S. M., Goedken, V. L.: J. Am. Chem. Soc., **98,** 839 (1976)
[24] Martin, L. Y., Dehayes, L. J., Zumpa, L. J., Busch, D. H.: J. Am. Chem., Soc., **96,** 4046 (1974)

Acta Chimica Hungarica 121 (4), pp. 391—402 (1986)

NEW METAL COMPLEXES OF SOME DIPOSITIVE METAL IONS WITH THIOSEMICARBAZIDE AND SEMICARBAZIDE DERIVATIVES

Ahmed Abdel-Hamid EL-ASMY, Magdy Mohamed BEKHEIT, Kamal Mohamed IBRAHIM and Mohsen Mahmoud MOSTAFA*

(Chemistry Department, Faculty of Science, Mansoura University, Mansoura, Egypt)

Received January 25, 1985
In revised form April 17, 1985
Accepted for publication June 24, 1985

The preparation and characterization of some dipositive metal ions with 1-acetyl-4-phenyl-3-thiosemicarbazide (ATSC) and 1-acetyl-4-phenyl-3-semicarbazide (ASC) are reported. The data of elemental analyses, molar conductivities, polarographic, magnetic measurements and spectral (i.r., n.m.r., visible) studies have been used to elucidate the structure of the metal complexes. I.r. spectra show that ATSC acts as a bidentate ligand and reacts through keto and/or enol forms while ASC behaves in a bidentate and/or tetradentate manner. Also ASC behaves as a reducing agent towards Cu^{II} chloride and bromide forming diamagnetic Cu^{I} complexes which are oxidized slowly to Cu^{II} complexes on exposure to air for about one weak. Cu^{II} sulphate and acetate are stable and show no tendency toward reduction. Different stereochemistries are proposed for Co^{II}, Ni^{II} and Cu^{II} complexes according to the data of spectral and magnetic studies. The anomalons magnetic moment for $[Cu(ATSC\text{-}H)Cl]_2$ is discussed.

Introduction

Recently, we reported [1] the characterization of some complexes of the ligands, 1-anthranyl-4-phenyl-3-thiosemicarbazide and 1-anthranyl-4-phenyl-3-semicarbazide, with some transition metal ions. In the present work, we extend our studies to 1-acetyl-4-phenyl-3-thiosemicarbazide and 1-acetyl-4-phenyl-3-semicarbazide and its metal complexes. The stereochemistry of the isolated complexes has been designated with the help of spectral and magnetic studies. The behaviour of the ligands as well as their ability to coordinate through the potential sites are discussed. The comparison of our earlier work [2], the ligands under investigation and its metal complexes have been reported.

Experimental

All the chemicals used were of BDH quality. The ligands were prepared by adding equimolar amounts of phenylisothiocyanate (27 mL, 0.2 mol) or phenylisocyanate (23.8 mL, 0.2 mol) to an alcoholic solution of acetic acid hydrazide (15 g, 0.2 mol). The mixture was refluxed for 10 min. On cooling white crystals separated. The product was filtered off, washed,

* To whom correspondence should be addressed

recrystallized from absolute ethanol and finally dried in a vacuum desiccator over anhydrous $CaCl_2$.

The Cu^I complexes with the formulae $[Cu_2(ASC)Cl_2]$ and $[Cu_2(ASC)Br_2]$ were prepared by refluxing equimolar amounts of the ligand, ASC, and the hydrated Cu^{II} salts in absolute ethanol on a water bath until the solution became colourless. On cooling pale green crystals separated. The isolated products were filtered off, washed with ethanol and diethylether, respectively. The other Cu^I complex, $[Cu^I(ASC\text{-}H)]$, was prepared by adding equimolar amounts of the ligand and copper(II) chloride dihydrate in absolute ethanol. The reflux was continued for 5 min. and the solution was allowed to cool. A pale brown precipitate separated on standing for about 2 hr. The product was filtered off, washed several times with absolute ethanol and diethylether. All the Cu^I complexes are dried in vacuum desiccator over silica gel and inert atmosphere (nitrogen).

All the other metal complexes of both ligands were prepared by heating an equimolar mixture of the ligands and the hydrated metal salts in refluxing absolute ethanol for a time (0.5—3 hr) depending on the metal salt as well as the ligand used. This method was carried out for the preparation of all complexes except Cu^{II} and Co^{II} acetate which were prepared by adding 1 mmol of the ligand in absolute ethanol and 1 mmol of the metal salt in bidistilled water and refluxed for 0.5 hr. On the other hand, the complex $[Hg(ASC\text{-}H)Cl.H_2O]$, was formed on adding sodium acetate as a buffer. In all cases the product formed was filtered off, washed several times with absolute EtOH and Et_2O and finally dried in a vacuum desiccator over anhydrous $CaCl_2$.

Elemental analyses were performed by the Microanalytical Unit at Mansoure University. The metal and chloride contents were determined by standard methods [3]. Molecular weights were estimated using camphor (172 °C) by the Rast method [4].

The infrared spectra were recorded on Pye Unicam SP 2000 and Perkin—Elmer model 557 spectrophotometers (4000—200 cm^{-1}) using Nujol mulls in CsI discs. Electronic and reflectance spectra were recorded using Unicam SP 700 C and Pye Unicam SP 1800 spectrophotometers. Magnetic measurements were carried out by the Gouy method at Alexandria University and $Hg[Co(SCN)_4]$ as a calibrant. Diamagnetic corrections were made using pascal's constants [5]. Conductance measurements were carried out at 25 °C in dimethyl formamide solution ($10^{-3}M$) with a Tacussel conductivity bridge, type CD 6NG. Polarographic studies were carried out using Metrohm polarecord E 506 and a polarography stand E505 dc polarography. Proton magnetic resonance spectra were recorded on a Perkin—Elmer R 12B (60Mz) spectrophotometer.

Results and Discussion

The experimental trial shows that 1-acetyl-4-phenyl-3-thiosemicarbazide (ATSC) forms complexes with Mn^{II}, Co^{II}, Ni^{II}, Cu^{II}, Zn^{II}, Cd^{II} and Hg^{II}, while 1-acetyl-4-phenyl-3-semicarbazide (ASC) forms complexes only with Co^{II}, Ni^{II}, Cu^{II} and Hg^{II}. The stoichiometries, colours, melting points, analytical data, molar conductivities and the magnetic susceptibilities for the isolated metal complexes are listed in Tables I and II. All the complexes are stable at room temperature, except those of Cu^I, and insoluble in most common organic solvents. Only, the complexes of ATSC are easily soluble in dimethyl formamide (DMF) and dimethyl sulphoxide (DMSO) while the complexes of ASC are insoluble except for the complexes, $[Cu_2(ASC)Cl_2]$ and $[Cu_2(ASC)Br_2]$, which are easily soluble in these solvents. The molar conductivity of ATSC complexes in DMF is considerably lower than those of uni-univalent electrolytes [6] in this solvent indicating that the complexes are covalent in nature except for $[Co(ATSC)Cl.H_2O]Cl.3H_2O$ and $[Co(ATSC)Cl.Py2H_2O]Cl.2H_2O$ which have 40 and 45 $ohm^{-1}\ cm^2\ mol^{-1}$, respectively, suggesting 1 : 1 electrolytes [7]. The insolubility and the high melting point of ASC complexes may be attributed to their polymeric character [8].

Table I

Analytical and physical data of ATSC *and its complexes*

Compound	Colour	M.P., °C	% Calc (found)				Λ_m* (DMF)	μ_{eff} (B.M.)
			C	H	M	Cl		
ATSC	white	163	51.6 (51.5)	5.3 (5.1)	—	—	—	—
$[Mn(ATSC)Cl_2]$	yellowish white	>300	39.4 (40.0)	3.3 (2.9)	16.4 (16.2)	21.2 (21.0)	10	—
$[Co(ATSC)Cl.H_2O]Cl.3H_2O$	olive green	>300	26.3 (26.5)	4.9 (5.0)	14.4 (14.7)	17.3 (17.8)	40	4.76
$[Co(ATSC)Cl.Py.2H_2O]Cl.2H_2O$	brown	>300	34.4 (34.9)	5.1 (4.7)	12.0 (12.4)	14.5 (14.9)	45	—
[Co(ATSC-H)(AC)]	greenish brown	>300	40.5 (41.0)	4.0 (4.1)	17.9 (17.2)	—	15	4.63
$[Ni(ATSC\text{-}H)_2.2H_2O]$	brown	>300	42.3 (42.7)	5.5 (4.8)	11.5 (12.1)	—	10	3.12
[Cu(ATSC-H)(AC)]	violet	>300	39.9 (40.0)	3.9 (4.0)	19.2 (19.0)	—	20	1.95
$[Cu(ATSC\text{-}H)Cl]_2$	grey	>300	35.2 (34.5)	3.3 (3.6)	20.7 (20.7)	11.5 (11.6)	23	0.73
[Cu(ATSC-H)Cl.Py]	green	>300	43.5 (43.8)	3.9 (4.1)	16.4 (16.2)	9.2 (9.5)	18	—
[Zn(ATSC-H)(AC)]	white	>300	39.7 (40.3)	3.9 (3.8)	19.6 (20.0)	—	16	Diam.
[Cd(ATSC-H)(AC)]	white	>300	33.7 (33.6)	3.8 (4.0)	28.3 (27.9)	—	24	Diam.
$[Cd(ATSC\text{-}H)_2]$	white	>300	40.9 (40.3)	3.8 (3.5)	21.2 (21.2)	—	8	Diam.
$[Hg(ATSC\text{-}H)Cl.H_2O]$	white	>300	22.5 ( )	2.3 ( )	41.7 (41.5)	7.7 (7.9)	15	Diam.

* $ohm^{-1}\ cm^2\ mol^{-1}$

Table II

Analytical and physical data of ASC *and its complexes*

Compound	Colour	M.P., °C	% Calc. (found)				μ_{eff} (B.M.)
			C	H	M	X*	
ASC	white	165	56.0 (55.7)	5.7 (5.9)	—	—	—
$[Co(ASC)Cl_2.H_2O]H_2O$	beige	>300	31.7 (31.5)	3.8 (4.6)	17.3 (16.8)	20.8 (20.6)	4.43
$[Co(ASC)(AC)_2]$	pale brown	>300	42.2 (42.3)	4.6 (4.8)	15.9 (15.7)	—	4.84
$[Ni(ASC)Cl_2]$	green	>300	33.5 (33.8)	3.4 (4.2)	18.2 (18.3)	21.9 (21.1)	3.53
[Cu(ASC-H)(AC)]	brownish green	>300	42.0 (42.8)	4.5 (4.2)	20.2 (20.6)	—	—
$[Cu^{I}(ASC\text{-}H)]$	pale brown	>300	42.1 (42.0)	3.9 (3.5)	24.7 (25.0)	—	Diam.
$[Cu^{I}_2(ASC)Cl_2]$	greenish white	265	27.6 (28.0)	2.8 (3.3)	32.5 (32.0)	18.1 (18.0)	Diam.
$[Cu^{I}_2(ASC)Br_2]$	greenish white	270	22.5 (22.3)	2.3 (2.7)	26.7 (26.5)	33.3 (33.5)	Diam.
$[Hg(ASC\text{-}H)Cl.H_2O]$	white	>300	—	—	44.9 (45.0)	7.9 (8.1)	Diam.

* X = Cl or Br

The bonding sites have been determined by comparing the spectra of the solid complexes with those of ASC and ATSC (Table III) and by considering our previous work [2, 9]. The three bands at 3320, 3300 and 3220 cm^{-1} in the spectrum of ASC and at 3380, 3270 and 3150 cm^{-1} in the spectrum of ATSC are assigned to ν(NH) vibrations $\nu(^4NH)$, $\nu(^2NH)$, $\nu(^1NH)$, respectively [9]. The spectrum of ASC shows two bands at 1680 and 1635 cm^{-1} assigned to the stretching vibrations of the carbonyl groups of the hydrazide and the urea moieties, respectively, while that of ATSC is observed at 1695 cm^{-1}. The board weak bands at $\sim$ 2100 and $\sim$ 1800 cm^{-1} are assigned to the stretching and bending vibrations of N—H . . . O [10]. This may suggest the presence of intramolecular hydrogen bonding. The thioketo group of ATSC exhibits two bands at 1220 and 780 cm^{-1}. Other bands are observed at 1520, 1490 and 1470 cm^{-1} assignable to ν(N—C=S) vibrations [11]. No bands exist above 3500 cm^{-1} or in the 2600—2500 cm^{-1} region which are due to ν(OH) and ν(SH) vibrations, respectively. The absence of these bands may suggest the presence of ASC and ATSC in the keto and thioketo forms.

The i.r. spectra of ASC complexes show that the ligand behaves as bidentate or tetradentate depending on the metal salt used, the condition of preparation and the pH of the medium.

First, the ligand acts as a bidentate coordinating via ^2NH and the carbonyl oxygen of the hydrazide moiety in the keto form. This behaviour is found in case of $[Co(ASC)Cl_2.H_2O]$, $[Co(ASC)(AC)_2]$ and $[Ni(ASC)Cl_2]$ and supported by the following evidence. The negative shifts (10—20 cm^{-1}) of the carbonyl oxygen of the hydrazide moiety (1680 cm^{-1}) and the $\nu(^2NH)$ vibration (3300 cm^{-1}). The carbonyl (C=O) band of the urea moiety remains in the same position (1635 cm^{-1}) as observed in the spectrum of the ligand. The appearance of new bands at $\sim$ 430, $\sim$ 410 and $\sim$ 270 cm^{-1} are assignable to ν(M—O) [12], ν(M—N) [13] and ν(M—Cl) [14], respectively.

Also, the ligand (ASC) reacts in the keto form in case of the diamagnetic Cu^I complexes $[Cu_2(ASC)Cl_2]$ and $[Cu_2(ASC)Br_2]$, as a tetradentate ligand. The active potential sites which participate in coordination are the two carbonyl oxygen, ^2NH and ^1NH groups. This is supported by the following evidence. Both the two carbonyl oxygen bands are shifted to lower wave numbers (10—25 cm^{-1}) together with the appearance of a new band at $\sim$ 440 cm^{-1} due to ν(M—O) [12]. The negative shifts (40—60 cm^{-1}) of ^2NH and ^1NH bands with the simultaneous positive shift (20—50 cm^{-1}) of the ν(N—N) vibration is observed at 990 cm^{-1} [15] in the spectrum of the ligand (ASC). The appearance of new bands in the low frequency region at 400 cm^{-1} and in the 270—260 cm^{-1} region are tentatively assigned to ν(M—N) [13] and ν(M—X) [16]; X = Cl or Br, respectively. The diamagnetic behaviour of the complexes $[Cu_2(ASC)Cl_2]$ and $[Cu_2(ASC)Br_2]$ supports the reduction of Cu^{II} to Cu^I as shown in structure(I). Also, the formation of a white precipitate of CuSCN of

Table III

Ir. and u.v. spectral bands for ASC *and* ATSC *and its metal complexes*

Compound	IR. bands (cm^{-1})						
	4 ν NH	2 ν NH	1 ν NH	CO+	CO*	ν(C=N)	ν (C=S)
ASC	3320	3300	3220	1680	1635	—	—
$[Co(ASC)Cl_2.H_2O]$	3315	3260	3200	1670	1635	—	—
$[Co(ASC)(AC)_2]$	3310	3240	3210	1665	1635	—	—
$[Ni(ASC)Cl_2]$	3315	3250	3210	1660	1630	—	—
$[Cu_2(ASC)Cl_2]$	3300	3260	3160	1655	1625	—	—
$[Cu_2(ASC)Br_2]$	3300	3240	3180	1660	1610	—	—
[Cu(ASC-H)]	3320	3250	—	—	1615	1590	—
[Cu(ASC-H)(AC)]	3320	3240	—	—	1615	1570	—
$[Hg(ASC-H)Cl.H_2O]$	3280	3200	—	—	1610	1585	—
ATSC	3380	3270	3150	1695	—	—	1220, 780
$[Mn(ATSC)Cl_2]$	3360	3260	3160	1650	—	—	1225, 760
$[Co(ATSC)Cl.H_2O]Cl.3H_2O$	3340	3250	3180	1660	—	—	1225, 760
$[Co(ATSC)Cl.Py(H_2O)Cl.2H_2O$	3360	3240	3160	1660	—	—	1220, 760
[Co(ATSC-H)(AC)]	3360	3250	—	—	—	1610	1225, 770
$[Ni(ATSC-H)_2(H_2O)_2]$	3365	3260	—	—	—	1595	1220, 770
$[Cu(ATSC-H)_2(AC)]$	3340	3280	—	—	—	1620	1220, 780
$[Cu(ATSC-H)Cl]_2$	3380	3270	—	—	—	1590	1230, 775
[Cu(ATSC-H)Cl.Py]	3380	3270	—	—	—	1590	1220, 780
[Zn(ATSC-H)(AC)]	3370	3260	—	—	—	1610	1220, 770
[Cd(ATSC-H)(AC)]	3380	3270	—	—	—	1610	1220, 770
$[Cd(ATSC-H)_2]$	3360	3250	—	—	—	1610	1240, 770
$[Hg(ATSC-H)Cl.H_2O]$	3380	3220	—	—	—	1610	1220, 775

* In hydrazide moiety.
\+ In urea moiety.

dissolution of these complexes in aqueous DMF followed by adding KCNS solution can be taken as an additional evidence for Cu^I.

Structure (I) exhibits a coordination number 3 for both copper(I) atoms in the complexes $[Cu_2(ASC)Cl_2]$ and $[Cu_2(ASC)Br_2]$. In spite of the unusual

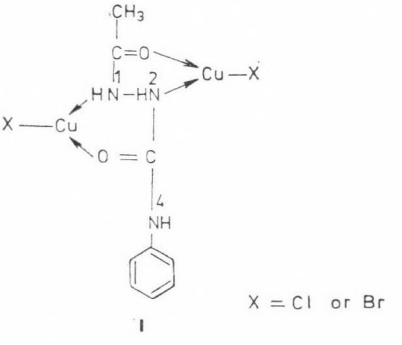

I

behaviour of the copper(I) atoms, we are convinced that structure (I) exists due to the following facts.

ν(N—C=S)	ν(C—O)	ν(N—N)	ν(M—O)	ν(M—N)	ν(M—x) X=Cl or Br	U.V. bands (cm^{-1})
—	—	990	—	—	—	—
—	—	1005	440	400	270	17540, 14410, 12600
—	—	1015	435	410	—	21740, 19600, 16260
—	—	1015	430	410	270	25150, 15570
—	—	1015	440	410	270	—
—	—	1010	430	395	260	—
—	1080	1010	430	400	—	—
—	1095	1010	420	390	—	—
—	1075	1000	440	415	260	—
520, 1490, 1470	—	1000	—	—	—	—
530, 1495, 1470	—	1010	430	360	260	—
530, 1490, 1470	—	1030	420	350	265	17000, 16600, 12100
520, 1490, 1465	—	1020	420	340	260	18800, 8330
530, 1495, 1460	1080	1010	460	410	—	17240, 16700, 12048
530, 1495, 1460	1070	1000	460	420	—	27000, 20000, 15000, 11200
520, 1495, 1460	1080	1000	460	410	—	23810, 17000
530, 1500, 1465	1070	1015	470	405	260	21270, 11000
530, 1500, 1460	1080	1015	460	410	260	—
530, 1500, 1465	1090	1015	470	390	—	—
530, 1495, 1460	1090	1015	470	395	—	—
530, 1495, 1460	1090	1010	480	385	—	—
530, 1500, 1465	1105	1010	495	385	225	—

The molecular weights as well as the low melting points suggest that the two complexes are monomers. I.r. data and chemical methods (addition of pyridine and/or triphenyl phosphine) indicate the absence of any chloride bridge. No i.r. bands or n.m.r. signals characterizing the water and/or ethanol molecules, to complete the coordination, are observed. All these observations suggest that the coordination number around the copper(I) atoms is three.

The only difference between the complex, [Cu^{I}(ASC—H)], and the afore-mentioned complexes, [Cu_2(ASC)Cl_2] and [Cu_2(ASC)Br_2], is that the ligand (ASC) coordinates in the enol form. The enolization occurs through the adjacent ^{1}NH as shown in structure (**II**) and supported by the following evidence. The disappearance of the (C=O) band of the hydrazide moiety with the negative shift of the (C=O) band of the urea moiety. The appearance of new bands at 1080 and 430 cm^{-1} assignable to ν(C—O) [16] and ν(M—O) [12] vibrations, respectively. The disappearance of the band due to $\nu(^1NH)$ with the negative shift of $\nu(^2NH)$. The appearance of new bands at 1590 and 400 cm^{-1} due to ν(C=N) [17] and ν(M—N) (the existence of the (C=N) band at lower wave number indicates the participation of the azomethine group in coordination). The positive shift of ν(N—N) [15]. The molecular weight determination shows that the complex is a polymer. Also, the diamagnetic behaviour supports the reduction process.

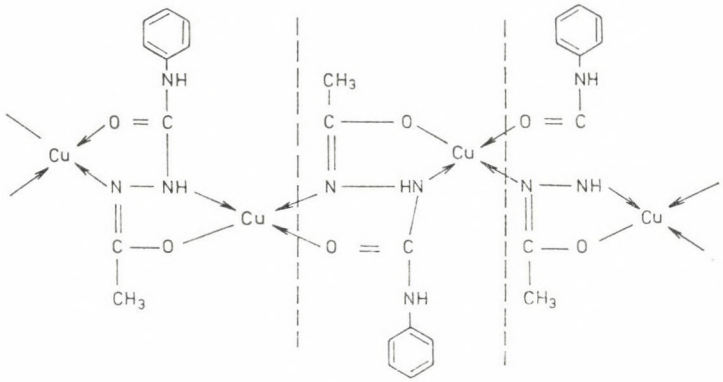

II

The reduction process of Cu^{II} salts (Cl or Br) by ASC is studied by polarographic method in 40% (*v*/*v*) ethanol-1*M* NH_4OH—NH_4Cl buffer solution. Two reduction waves are observed for Cu^{II} chloride ($5\times10^{-3}M$) with equal height (1μA). Also, the half wave potentials are found to be —0.42 V vs Ag(AgCl)KCl salt for the first and second waves, respectively. On adding excess amount of ASC, the limiting current of the first wave decreases while that of the second remains unchanged. The half wave potential of the first wave (—0.18 V) remains unchanged and the second (—0.42) shifts to —0.48 V.

The decrease in the limiting current as well as the constant value of $E_{1/2}$ for the first wave may be attributed to the reduction of Cu^{II} by means of ASC to Cu^{I} [18]. In the other hands, the shift in $E_{1/2}$ for the second wave is a good evidence for the formation of complex compounds with Cu^{I}.

Finally, the ligand (ASC) reacts in the enol form and is a bidentate in case of the paramagnetic Cu^{II} complex [Cu(ASC—H)(AC)] and [Hg(ASC—H)$Cl.H_2O$]. The ligand coordinates via ^{2}NH and the enolized carbonyl oxygen of the hydrazide moiety by the displacement of the hydrogen atom from the latter group by the metal ion. The mode of coordination is proposed on the light of the following evidence.

The disappearance of the bands due to $\nu(^1NH)$ and $\nu(C=O)$ of the hydrazide moiety with the appearance of new bands in the 1585—1570 and 1095—1075 cm^{-1} regions assigned to $\nu(C=N)$ [17] and $\nu(C—O)$ [16], respectively. The negative shift of the (^{2}NH) band together with the positive shift (10—20 cm^{-1}) of the $\nu(N—N)$vibration. The appearance of new bands in the low frequency region at 420—440 and 390—415 cm^{-1} assignable to $\nu(M—O)$ [12] and $\nu(M—N)$ [13] vibrations, respectively. The existence of the (C=O) band of the urea moiety in the same position. All these observations confirm structures (**III** and **IV**) for these complexes.

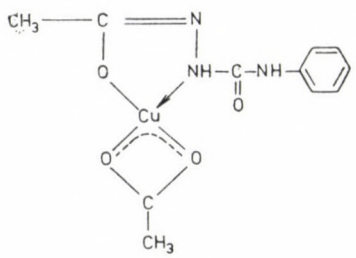

III

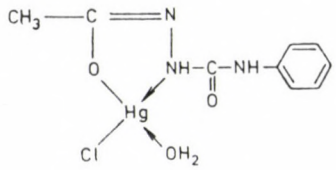

IV

The spectrum of [Hg(ASC—H)Cl.H_2O] shows bands, characteristic for coordinated water molecule [19], at 3500 (br), 1620 (sh) 880 (w) and 655 (w). The band due to ν(Hg—Cl) [20] vibration is observed at 260 cm^{-1}.

The spectra of [Cu^{II}(ASC—H)(AC)] and [Co(ASC)$(AC)_2$] show two bands at 1370 and 1560 cm^{-1} which are assigned to ν_s and ν_{as} of the acetate group. The great difference (190 cm^{-1}) between those two bands supports the bidentate nature [21] of the acetate group (structure **III**).

In contrary, ATSC acts only as a bidentate coordinating via the ^{2}NH and the carbonyl oxygen groups in either keto and/or enol forms. In all cases the ligand forms five membered ring around the metal ion.

First, the ligand coordinates in the keto form in case of [Mn(ATSC)Cl_2], [Co(ATSC)Cl.H_2O]Cl.3H_2O and [Co(ATSC)Cl.Py.2H_2O] Cl.2H_2O. The coordination is considered on the basis of the following evidence: The lower shift of the (C=O) band (1695 cm^{-1}) with the appearance of a new band in the 430—420 cm^{-1} region attributed to ν(M—O) [12]. The negative shift of the ^{2}NH band together with the positive shift of the (N—N) band. The appearance of new bands at $\sim$ 350 and $\sim$ 260 cm^{-1} due to ν(M—N) [13] and ν(M—Cl) [14], respectively. The thioketo bands remain in the same position. These observations confirm the participation of both the carbonyl oxygen and the ^{2}NH groups in coordination. The spectrum of [Co(ATSC)Cl.Py.2H_2O]Cl.2H_2O shows additional bands at 1615 and 1520 cm^{-1} which are assigned as coupled modes consisting of ν(C=C) and ν(C=N) proving the addition of pyridine molecule to this complex [22]. Also, other bands are observed in the spectra of [Co(ATSC)Cl.H_2O]Cl.3H_2O and [Co(ATSC)Cl.Py.2H_2O]Cl.2H_2O at 3480, 1625 and 670 cm^{-1} indicating the existence of coordinated water molecules [19]. Water of hydration was determined quantitatively by heating the complexes at 120 °C for 2 hr and as reported earlier [2].

On the other hand, ATSC coordinates via the ^{2}NH and the enolic carbonyl oxygen groups, with replacement of the hydrogen atom forming five membered ring including the metal atom, in case of all other complexes (Table III). The mode of coordination is suggested as a result of the following evidence: The disappearance of both ν(C=O) and ν(^{1}NH) vibrations. The appearance of

new bands in the 1620—1590 and 1105—1070 cm^{-1} regions attributable to ν(C=N) and ν(C—O) [16], respectively. The negative shift (10—50) cm^{-1} of the ν(^{2}NH) and the positive shift ($\sim$ 15 cm^{-1}) of the ν(N—N) [15]. The appearance of new bands in the 495—460 and 420—385 cm^{-1} regions assignable to ν(M—O) [12] and ν(M—N) [13] vibrations, respectively. The (C=S) bands remain unchanged. The following structures (V and VI) are suggested for the isolated complexes.

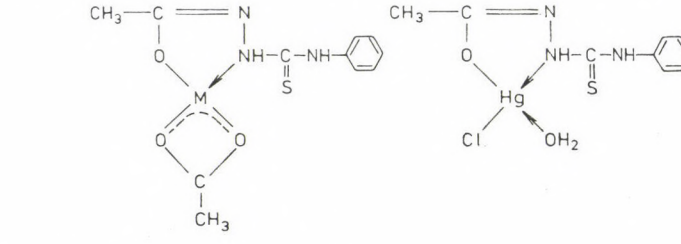

Mo=Co^{II} , Cu^{II} , Zn^{II} and Cd^{II}

V VI

Magnetic and spectral studies

Co(II) complexes

The magnetic moment of [Co(ASC)Cl_2H_2O] (4.43 B.M.) lies within the range reported for both tetrahedral or five coordinated Co^{II} complexes. The spectrum shows three bands at 17.540, 14.410 and 12.600 cm^{-1} which is in favour of the latter geometry. These bands may be due to $^4A_2(F) \rightarrow {}^4E(F)$ $^4A_2(F) \rightarrow {}^4A_2(P)$ and $^4A_2(F) \rightarrow {}^4E(F)$ transitions, respectively, in a five coordinated structure [23]. The spectrum of [Co(ASC)$(AC)_2$] is characterized by a band at 19.600 cm^{-1} which may be assigned to $^4T_{1g} \rightarrow {}^4{}_{1g}(P)(\nu_3)$ transition in octahedral environment [24]. The shoulder at 16.260 cm^{-1} may be due to $^AT_{1g} \rightarrow {}^AT_{2g}(F)$ transition, the room temperature magnetic moment for this complex (4.84 B.M.) lies within the range (4.8—5.2) reported for high-spin octahedral cobalt(II) complexes. On the other hand, the values of the magnetic susceptibility of the Co^{II} complexes, [Co(ATSC)Cl.H_2O] and [Co(ATSC—H)(AC)], derived from ATSC are 4.76 and 4.63 B.M., respectively, which may suggest a tetrahedral structure around the Co^{II} ions.

The reflectance spectra show three bands at 12.100, 16.660 and 17.000 cm^{-1}. The two bands at 12.100 and 17.000 cm^{-1} may be assigned to $^4A_2 \rightarrow {}^4T_1(P)$ and spinforbidden [25] transition, respectively, in a distorted tetrahedral environment. The addition of pyridine to [Co(ATSC)Cl.H_2O]Cl.$3H_2O$ changes the olive-green colour to brown. Also the spectrum shows bands at 18.800 and 8.330 cm^{-1} assigned to $^4T_{1g}(F) \rightarrow {}^4T_{1g}(P)(\nu_3)$ and $^4T_{1g}(F) \rightarrow {}^4T_{2g}(F)\,(\nu_1)$ transi-

tions, respectively, in an octahedral geometry [24]. Moreover, the structure of this complex [Co(ATSC)Cl.Py.$2H_2O$]Cl.$2H_2O$, is confirmed with the help of elemental analysis and molar conductance value (45 ohm^{-1} cm^2 mol^{-1}).

Ni(II) complexes

The spectrum of [Ni(ASC)Cl_2] exhibits two bands at 25.150 and 15.570 cm^{-1} assigned to $^3T_1 \rightarrow {}^3A_2$ and $^3T_1 \rightarrow {}^3T_2(P)$ transitions, respectively, in a distorted tetrahedral geometry [23]. The value of the magnetic moment (3.53 B.M.) is an evidence for the proposed structure.

The electronic spectrum (Nujol) of [Ni(ATSC—H)$_2$.$2H_2O$] shows three bands at 11.200, 20.000 and 27.000 cm^{-1} assigned to the $^3A_{2g} \rightarrow {}^3T_{2g}$, $^3A_{2g}(F) \rightarrow {}^3T_{1g}(F)$ and $^3A_{2g} \rightarrow {}^3T_{1g}(P)$ transitions, respectively. The band at 15.000 cm^{-1} may be due to the $^3A_{2g} \rightarrow {}^1E_g$ transition. The calculated values of Dq, B, β and ν_2/ν_1 1120, 813, 0.85 and 1.82, respectively, are in favour of octahedral structure around the Ni(II) ion [26]. Also, the value of magnetic moment (3.12 B.M.) can be taken as an additional evidence for the proposed structure.

Cu(II) complexes

The magnetic moment (0.73 B.M.) of [Cu(ATSC—H)Cl]$_2$ is lower than those reported for one unpaired electron (1.7—2.2 B.M.). This subnormal magnetic moment may be due to copper-copper interaction [27]. The complex has a dimeric structure with chloride bridge as shown in structure (**VII**). This

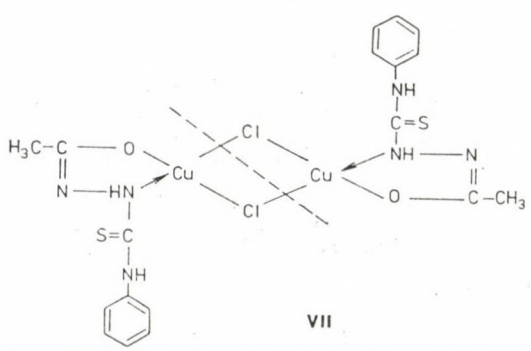

VII

structure is confirmed on the basis of the molecular weight determination (600). Also, the addition of pyridine to the dimeric complex changes the colour to green as well as the separation of a new monomer complex (**VIII**) which is characterized by elemental analysis. The spectrum of the native complex [Cu(ATSC—H)Cl]$_2$ shows an intense band at 11.000 cm^{-1} with a broad band centered at 21.27 cm^{-1}. The former band supports a tetrahedral structure around the Cu^{II} ion while the second may be assigned to a Cl → Cu charge

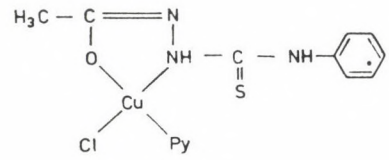

VIII

transfer [28]. The spectrum of the complex [Cu(ATSC—H)(AC)] shows a band at 17.000 cm^{-1} as those reported for square planar geometry [29]. The shoulder at 23.810 cm^{-1} may be due to M → L charge transfer [30]. The value of the magnetic moment (1.95 B.M.) lies within the range of Cu^{II} ions.

REFERENCES

[1] El-Asmy, A. A., Ibrahim, K. M., Bekheit, M. M., Mostafa, M. M.: Syn. React. Inorg. Met. Org. Chem., **15,** 287 (1985)
[2] El-Asmy, A. A., Mostafa, M. M.: J. Coord. Chem., **12,** 291 (1983)
[3] Vogel, A. I.: Quantitative Inorganic Analysis, Longmans, Green, London 1961
[4] Mann, F. G., Saunders, B. C.: Practical Organic Chemistry, Longmans, London 1960
[5] Lewis, J., Wilkins, R. G.: Modern Coordination Chemistry, Interscience, New York 1960
[6] Geary, W. J.: Coord. Chem. Rev., **7,** 81 (1971)
[7] Yordanov, N. D., Alexiev, V., Macicek, J., Glowiak, T., Garifynov, N. S., Kozirev, B. M.: Dokl, Akad Nuk SSSR, **191,** 359 (1970)
[8] Mostafa, M. M., Ibrahim, K. M., Moussa, M. N. H.: Trans. Met. Chem., **9,** 243 (1984)
[9] El-Asmy, A. A., Mostafa, M. M.: Polyhedron, A, **1983,** 491
[10] Bullock, J. I., Tajmie-Riahi, H. A.: J. Chem. Soc., Dalton Trans., **1978,** 34
[11] Rao, C. N. R., Venkataraghavan: Spectrochim. Acta, **18,** 541 (1962)
[12] Speca, A. N., Karayanis, N. M., Pytlewshki, L. L.: Inorg. Chim. Acta, **9,** 87 (1974)
[13] Beecroft, B., Campbell, M. J. M., Grzeskowiak, R.: J. Inorg. Nucl. Chem., **36,** 55 (1974)
[14] Ferraro, J. R.: Low Frequency Vibrations of Inorganic and coordination compounds, Plenum, New York 1971
[15] Braibanti, A., Delvalla, F., Pellinghelli, M. A., Leporati, E.: Inorg. Chem., **7,** 1430 (1968)
[16] Biradar, B. S., Patil, B. R., Kulkarni, V. H.: J. Inorg. Nucl. Chem., **37,** 1901 (1975)
[17] Aggarwal, R. C., Singh, N. K., Prasad, K.: Ind. J. Chem., **14A,** 325 (1976)
[18] Crow, D. R.: Polarography of Metal Complexes, London, 56 (1969)
[19] Nakamoto, N.: Infrared Spectra of Inorganic and Coordination Compounds, Wiley, New York 1970
[20] Peyronel, G., Giusti, A.: Spectrochim. Acta, **37A,** 71 (1981)
[21] Kaul, B. B., Pandeya, K. B.: J. Inorg. Nucl. Chem., **40,** 1035 (1977)
[22] Paul, R. C., Chopra, R. S., Bhambori, P. K., Singh, G.: J. Inorg. Nucl. Chem., **36,** 3703 (1974)
[23] Lever, A. B. P.: Inorganic Electronic Spectroscopy, Elsevier, Amsterdam, **318,** 321 (1968)
[24] Kondo, M., Kubo, M.: J. Phys. Chem., **62,** 1558 (1958)
[25] Faye, G. H., Horwood, J. L.: Can. J. Chem., **45,** 2335 (1967)
[26] Sacconi, L.: Transition Met. Chem., **4,** 199 (1969)
[27] Kato, M., Jonassen, H. B., Fanning, J. C.: Chem. Revs., **64,** 99 (1964)
[28] Rendell, J. C. T., Thompson, L. K.: Can. J. Chem., **1979,** 57
[29] Sacconi, L., Giampolini, M.: J. Chem. Soc. A., **1974,** 273

Acta Chimica Hungarica 121 (4), pp. 403—407 (1986)

THE INFLUENCE OF THE TIME AND ACIDIFICATION ON FORMATION AND STABILITY OF SOLID AMMONIUM MOLYBDATES

Wiesław LASOCHA and Stanisław A. HODOROWICZ*

(Faculty of Chemistry, Jagiellonian University, 30-060 Krakow, Poland)

Received May 22, 1985
Accepted for publication June 24, 1985

The transformation of fibrillar ammonium trimolybdate into other solid molybdates in aqueous solution has been observed. The pH and conductivity measurements vs time for mother solutions, and the results of chemical analysis and X-ray identifications of the solid phases are presented.

Introduction

The crystalline fraction of the fibrillar ammonium trimolybdate has recently been isolated [1]. During preparative work we have noticed that in precipitation of this compound not only acidification of the solution but the time of the condensation process is a very important factor, too. The influence of time on the condensation of isopolyacids was mentioned in the literature [2, 3] but has not yet been investigated in details. In this paper we focus our attention to the factor mentioned above and further transformations in solutions of the solid ammonium trimolybdate into other molybdates. Due to the qualitative nature of these transformations pH and conductivity measurements of solutions vs time were carried out. Additionally the obtained precipitates were identified by chemical analysis and X-ray powder diffraction method.

Experimental

Samples of ammonium heptamolybdate solutions (concentrations $c_{Mo} = 0.6$ *M*) were titrated with 1.0 *M* nitric acid to the degree of acidity $Z = 0.16$, 0.19, 0.24, 0.28, 0.33, 0.36, 0.39, 0.44 and 0.47. The pH and conductivity of the solutions had been measured at 298 $\pm$ 0.2 K for a period of 100 days with an accuracy of $\pm$ 0.01 pH and $\pm$ 0.25 mS conductivity. A digital pH-meter M517 (Poland) equipped with a complex electrode SAgP-209 W and a "Conductivity Meter" (Radelkis-Budapest) were used, respectively. The crystals precipitated were studied microscopically and then were identified with chemical and X-ray diffraction methods. Molybdenum was determined by heating the samples to constat mass in a furnace at 873 K. Ammonia was determined by the Kjeldhal method. Substracting the amount of NH_3 from the sum of NH_3 and H_2O lost by heating, percentage of H_2O could then be calculated. The X-ray powder diffraction analysis was performed on a DRON-2 diffractometer (CuK_α radiation). Calculations of the unit cells parameters were carried out on the CDC CYBER computer.

* To whom correspondence should be addressed

Results and Discussion

The influence of acidity and time on the crystallization is illustrated in Fig. 1. In the solutions at a degree of acidity $Z = 0.16$—0.28 first the fibrillar crystals of the ammonium trimolybdate form. The crystallization rate and the yield of the process are strongly influenced by the acidity. The best conditions

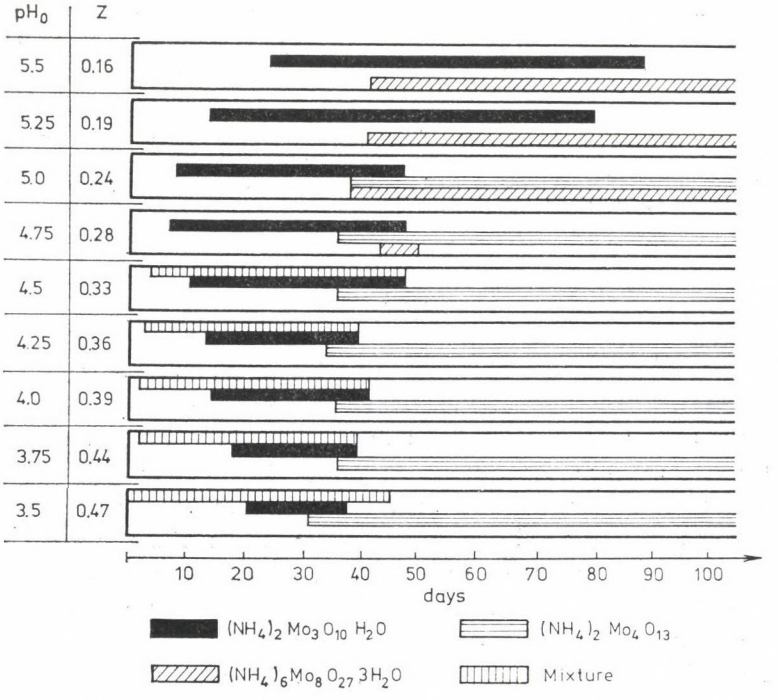

Fig. 1. The influence of acidity and time on the crystallization of solid isopolymolybdates from acidified ammonium paramolybdate solutions

for the preparation of this compound are in solutions at $Z = 0.24$ and $Z = 0.28$. After a period of about 30—40 days new phases appear and their amount increase at the sacrifice of the fibrillar form. The new phases were identified as the tetramolybdate $(NH_4)_2 0.4MoO_3$ [4] and octamolybdate $3(NH_4)_2\ 0.8\ MoO_3.4H_2O$ [5, 6] with the lattice parameters $a = 9.68$ (3), $b = 11.07$ (3), $c = 16.29$ (5) Å and $\beta = 85.4(1)°$, and $a=9.51(1)$, $b = 11.31$ (3), $c = 15.05$ (1) Å and $\beta = 109.52$ (3)°, respectively. Starting from $Z \geqslant 0.33$ the crystallization of the ammonium trimolybdate is preceded by the precipitation of a small amount of a substance which gives powder pattern typical for a "mixture" of isopolymolybdates where octamolybdate $(NH_4)_4Mo_8O_{26}.2H_2O$ reported by Ma [8] is predominant. After a few weeks all forms transform into ammonium tetramolybdate $(NH_4)_2Mo_4O_{13}$.

Changes in pH and conductivity of the solutions are presented in Figs 2 and 3. As follows from the diagrams the considerable changes in these parameters are observed even though no crystals are formed. The crystallization of the fibrillar trimolybdate and the "mixture" is connected with the

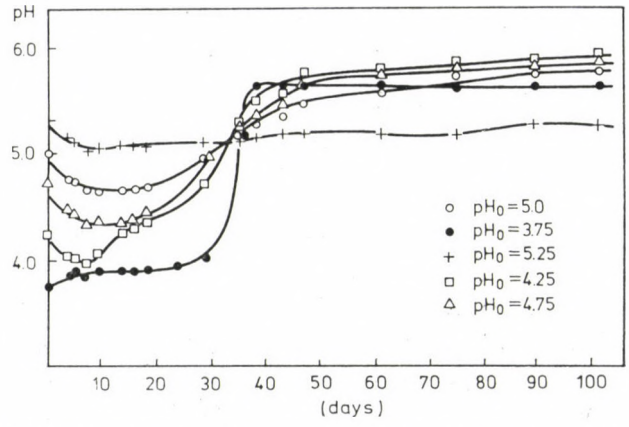

Fig. 2. pH of ammonium paramolybdate solutions vs time

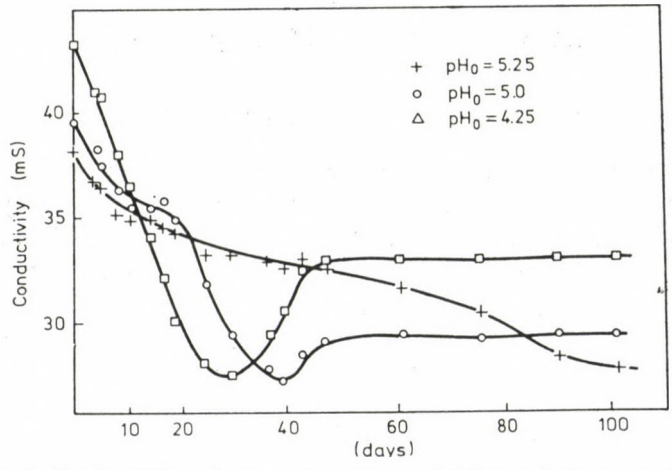

Fig. 3. Conductivity of ammonium paramolybdate solutions vs time

increase of pH while conductivity decreases. During the precipitation of the tetramolybdate the increase of these parameters occur, whereas pH keeps almost the same value and conductivity decreases when trimolybdate transforms into octamolybdate. The changes presented can be explained on the basis of theoretical considerations. The transformation of a polymolybdate $n\mathrm{Me_2O}.m\mathrm{MoO_3}$ into another one can be described by following general reaction:

$$n\mathrm{Me_2O}.m\mathrm{MoO_3} + 2k\mathrm{H^+} \rightleftharpoons (n—k)\mathrm{Me_2O}.m\mathrm{MoO_3} + 2k\mathrm{Me^+} + k\mathrm{H_2O} \quad (1)$$

According to thi reaction the acidity $Z = [H^+]/[Mo]$ is given by the ratio

$$Z = 2k/m \tag{2}$$

If we denote $s = m/n$ the reaction above is associated with following change of s:

$$\Delta s = \frac{m}{n - k} - \frac{m}{n} = \frac{km}{n(n - k)} \tag{3}$$

From (2) and (3) we obtain

$$Z = \frac{2\,n^2 \Delta s}{m\,(m + n\ \Delta s)} \tag{4}$$

The values of s for para-, tri-, tetra-, and octamolybdate are equal to 7/3, 3/1, 4/1, and 8/3, respectively. Hence according to equation (4) the theoretical acidification degree Z for the formation of these forms in paramolybdate solutions is equal to 0.19, 0.35, and 0.107. This result enables us to explain the best conditions for the paramolybdate → trimolybdate reaction and to determine forms which are present in bottoms after time long enough for the disapperance of fibrillar phase. The formation of tetra- and octamolybdate from trimolybdate can be described by the reactions:

$$4Mo_3O_{10}^{2-} + 2H^+ \rightleftarrows 3Mo_4O_{13}^{2-} + H_2O \tag{5}$$

and

$$8Mo_3O_{10}^{2-} + H_2O \rightleftarrows 3Mo_8O_{27}^{6-} + 2H^+ \tag{6}$$

The theoretical values of Z for these reactions are equal to $1/6 = 0.16$ and $-1/12 = -0.08$, respectively. Thus the formation of tetramolybdate from trimolybdate should be connected with the increase of pH, while the formation of octamolybdate should result in a slight decrease of pH. The transformation into octamolybdate is not connected with the decrease of pH. This fact suggests that a process with the consumption of protons occurs in solution. According to literature [9] it can be described by the reaction:

$$8Mo_7O_{24}^{6-} + 6H^+ \rightleftarrows 7Mo_8O_{27}^{6-} + 3H_2O$$

The formation of trimolybdate is given by the reaction:

$$3Mo_7O_{24}^{6-} + 4H^+ \rightleftarrows 7Mo_3O_{10}^{2-} + 2H_2O \tag{7}$$

The consumption of H^+ ions results in decrease in conductivity. Further changes of conductivity are probably caused by the different solubility of solid forms from the one hand and the change in NH_4^+ ion concentration in the solution [see reaction (1)] from the other.

It can be concluded that the moderate acidification of concentrated heptamolybdate solutions causes the crystallization of the fibrillar trimolybdate.

During this process the changes of pH and molybdenum concentration occur. The new conditions enable the precipitation of tetramolybdate, $(NH_4)_2O.4MoO$ or octamolybdate $3(NH_4)_2O.8MoO_3.4H_2O$. These compounds crystallize at the expense of the trimolybdate which completely disappeared. The results observed explain the origin of very different opinions about the existence of the trimolybdate and it is probably the main reason why some authors were able to point out its "double-salts character" even by X-ray method [7, 8].

REFERENCES

[1] Lasocha, W., Hodorowicz, E. K., Hodorowicz, S. A.: Polish J. Chem. (in press)
[2] Kepert, D. L.: Progress in Inorganic Chemistry, Vol. **4**, Albert Cotton 1962
[3] Chojnacka, J.: J. Inorg. Nucl. Chem., **33**, 1344 (1971)
[4] Kiss, A. B., Gado, P., Asztalos, I., Hegedűs, A. J.: Acta Chim. Acad. Sci. Hung., **66**, 235 (1970)
[5] Schwing-Weil, M. J.: Bull. Soc. Chim. France, **1967**, 3795
[6] Boschen, I., Buss, B., Krebs, B.: Acta Cryst., B, **30**, 48 (1974)
[7] Lindqvist, I.: Nova Acta Reg. Soc. Sci. Upsal., Ser IV, **15**, 7 (1950)
[8] Ma, E.: Bull. Soc. Chim. Japan, **37**, 171 (1963)
[9] Ng, K. Y. S., Gulari, E.: Polyhedron, **3**, 1001 (1984)

BOOK REVIEWS

Gyula Szekér: *Industry and Technical Development in Hungary in the Nineteen-Eighties*

(Vol. 60 of the series "Recent Results of Chemistry");
pp 205, Akadémiai Kiadó, Budapest, 1985.

Information about the actual tasks of Hungarian industry and technical development is offered in this book. Considering the changed order of values and based on a scientific analysis of world economics that creates ever more difficult conditions, the author explains how the conceptions of industrial and technical development have evolved. A review of results and errors is given; the present situation of Hungary's industry is evaluated in comparison with international achievements. Especial attention is paid to progress and to future possibilities in the domain of energy-carriers, to the pattern of export-import balance in various branches of industry and to possibilities of improvement. It is not surprising that chemical industry is treated more in detail since this is one of the most dynamically developing domains of the country's industry. Finally, the actual problems of industrial development are reviewed, including the discussion of various programmes in the 6th five-year plan, but this book also gives some directives relevant to conceptions for industrial development and progress during the 7th five-year plan period. This book is recommended reading not only for experts engaged in industry or the technical sciences but for the wide public interested in the industrial and economic aspects of national progress of this country.

Béla Csákvári

Department of General and Inorganic Chemistry, Eötvös Loránd University, Budapest

Conceptual Quantum Chemistry. Models and Applications. Special Subject Issue of Croatica Chemica Acta. Part I.

Vol. 57, No. 5, pp. 765—1030, 1984
Guest Editor: Z. B. Maksic

In the past few years the development of quantum chemistry was dominated by an extremely fast progress in the computational techniques, which made routinely accessible even the highly sophisticated ab initio calculations to chemists. In the meantime the simple conceptual models which are able to give qualitative insight into a few dominant aspects of a particular problem, albeit unable to yield precise numbers, became less and less popular. Although one cannot deny the importance of very accurate computations on molecular properties, one should not neglect the role of simple conceptual models, which bridge the gap between the fundamental laws of physics and the rules of chemistry, and form the basis of our understanding of the phenomena.

The Editorial Board of Croatica Chemica Acta recognized that the various simple conceptual models should have much more emphasis in the quantum chemical literature, and

decided to dedicate a special issue to the subject. This idea has been welcomed by the scientific society, as it was proven by the great number of interesting and good-quality papers contributed to this issue.

The issue consists of original contributions and review articles as well. The wide diversity of the topics ensures that almost everybody can find the paper he is particularly interested in. The majority of the articles deal with the analysis, further development and application of classical concepts. It is remarkable that the authors make a considerable effort to find the links between the simple concepts and the results of accurate ab initio calculations. This attitude is quite important in order to develop a fruitful symbiosis of the computational and conceptual approaches in quantum chemistry.

Several papers discuss the problem of hybrid orbitals, involving the contribution of Linus Pauling who had perhaps the greatest impact on the conceptual thinking in quantum chemistry in the past. The localized orbitals constitute another major topic. Their application for various purposes, like conformational problems, the effective treatment of correlation as well as the economic handling of large molecules is discussed by several authors. In other contributions, themes, like the VSEPR model, Koopmans' theorem, the point charge models, the concept of bond orders, the ring currents, homoconjugation, etc., are treated, in most cases by conflicting the predictions of the models with the results of semiempirical or ab initio calculations.

We think that the main goal of the editor, Z. B. Maksic, "to contribute to the further development of conceptual quantum chemistry, . . . and to a better understanding between different fields" has been excellently achieved by this first part of the special issue, and we are looking forward with excitement to the forthcoming second part. Finally we note that the special issue can be an enjoyable reading not only for theoreticians but also for experimental chemists who search for a deeper understanding of the quantum chemical concepts they are working with.

János ÁNGYÁN

CHINOIN Pharmaceutical and Chemical Works Ltd
Research Center, Budapest

Metal Ions in Biological Systems, Volume 18. Circulation of Metals in the Environment

Ed.: Helmut Sigel, Marcel Dekker Inc., New York—Basel, 1984

This series, of which this book is already the 18th volume, envisaged a very hard task, namely the complete survey of the role of metals, played in biology and in vital processes. The editor of the series emphasizes that this aim can be attained only by a far-reaching interdisciplinary approach.

Previous volumes of the series dealt with various organo-mineral complex compounds, their properties, further with the biological role of metal ions. A separate volume was dedicated to iron compounds, and to some biologically important organic substances. Volume **10** of the series discussed the carcinogenic effects of some metal ions, while Volume **11** dealt with just the opposite, topic the possible anticarcinogenic use of metal ions. Copper and zinc compounds were also treated in a separate volume, and so was calcium. Volume **19**, to be published later, will discuss the connection of metal ions with antibiotics.

Volume **18** covers a broad subject, as can be seen from its title.

The first chapter, the author of which is Peter Baccini, gives a general picture about the migration of metals in the environment, also serving as a guide to the chapters which follow. The second chapter of the book covers the analytical chemistry of metal ions occurring in the environment. This is the most extensive and perhaps the best written chapter of the book, summarizing conventional and modern processes, almost the complete analytical repertory: moreover, the limit values are given at which the various metals may be present in the environment.

The third chapter of the book deals with the role of metal ions played in the environment, but the discussion is restricted to the particular processes, such as complex formation, ion exchange, hydrolysis, redox processes, etc., without describing the concrete role of these processes in the environment. This is, of course, understandable in view of the limited extent.

The next chapter discusses in a somewhat similar approach the formation of surface complexes, including the theory of electric double-layer.

The fifth chapter deals with the relationships between chemical measurements and the uptake of biological substances, while the sixth chapter is concerned with the interactions or organic and organo-mineral compounds in aqueous medium. A logical continuation of this is the seventh chapter, discussing the evolutional aspects of the transport of metal ions through cell membranes.

An important and extensive chapter of the book is the eighth, the author of which wrote also the first chapter. Chapter 8 describes the control of trace element concentrations in fresh waters; information is given in an original approach, illustrated also by practical examples.

The problems of the other important element of the environment, of the soil, are the topics of the ninth chapter, which deals with the migration of metal ions in the earth. This chapter makes it evident that often a superficial description can only be given because of the limited extent and the multitude of the topics. The chapter is up-to-date, will approaching the subject, however, as concerns metals important in the soil, their discussion is restricted mainly to heavy metals, and almost nothing is said about alkali and alkali earth metals, playing the most important role in the soil. It should be mentioned here that it is difficult to understand why in this chapter, and in general in the book, classical geochemical findings and references to authors, such as Vernadski, are missing, the works of whom are still actual, forming the basis of modern environmental views.

The tenth chapter deals with the microbiological aspects of the toxicity of metal ions, including problems of gene engineering.

The brief closing chapter discusses, under the title "Conclusions and Outlook", some general environmental laws and global cycles. Its author is P. Baccini, who had the greatest share in writing the book.

The volume is a noteworthy summary of a wide group of problems, on which scarcely any other reference book with such an approach and manysided modern views can be found in the literature. In spite of the fact that for specialists of the particular fields the contents of certain chapters may seem superficial or insufficient, the work is a valuable contribution in the fields of information, research and tuition, and many of its useful data, theoretical and practical findings, will greatly enrich the knowledge of all those interested in environmental problems.

István Szabolcs

Research Institute of Soil Science and Agricultural Chemistry,
Hung. Acad. of Sci., Budapest

Acta Physica Hungarica

(Formerly: Acta Physica
Academiae Scientiarum Hungaricae)

Editor in Chief:
I. Kovács

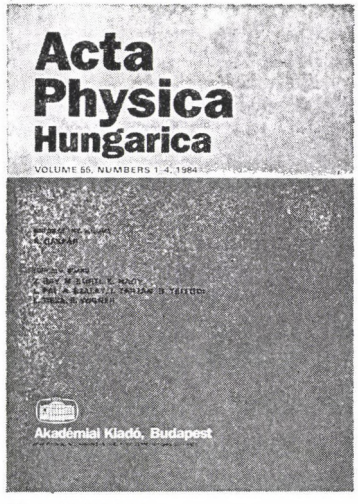

Acta Physica Hungarica publishes original papers (articles with abstracts and short communications) in the sphere of theoretical and experimental physics, including the fundamental problems and applications of classical and quantum physics, elementary particles and fields, nuclear physics, atomic and molecular physics, optics, acoustics, thermodynamics, fluids and plasmas, the properties of condensed matter, etc. It also publishes reviews on recent physical literature.

Founded 1951
Papers in English, French, German and Russian
Publication: two volumes annually — one volume contains four issues
Price per volume: $44.00; DM 99,—
Size: 17 × 25 cm
ISSN 0231–4428

Order form
to be returned to
KULTURA
Hungarian Foreign Trading Company
P.O. Box 149, H-1389 Budapest, Hungary
☐ Please enter my/our subscription for ACTA PHYSICA HUNGARICA for one year
☐ Please enter my/our standing order for ACTA PHYSICA HUNGARICA starting with

Name: _____

Address: _____

Date and signature: _____

ACTA PHYSICA HUNGARICA

Contents of Volume 54. Numbers 3–4

1828

Akadémiai Kiadó

Publishing House
of the Hungarian Academy of Sciences
Budapest

Invitation for papers

Manuscripts should be sent to
Prof. I. Kovács, Editor
Department of Atomic Physics
Technical University
1521 Budapest
Budafoki út 8.
Hungary

PRINTED IN HUNGARY

Akadémiai Kiadó és Nyomda, Budapest

Text

The text of the paper should be concise. The description of new compounds (in the Experimental) must include the complete analytical data. Special attention must be paid to structural formulas given within the text. Complicated (non-linear) formulas should be drawn on separate sheets of paper and their position in the text should be clearly marked. The numbering of formulas and equations (in parentheses on the right-hand side) is only needed if they are referred to in the text. Units should conform to the International System of Units (SI). In nomenclature the rules of the I.U.P.A.C. are accepted as standard. Symbols for physical quantities are printed in italic type and should, therefore, be underlined in the manuscript.

References

References should be numbered in order of appearance in the text (where the reference number appears in brackets) and listed at the end of the paper. The reference list, too, should by typed double-spaced. Journal titles are to be abbreviated as defined by the Chemical Abstracts Service Source Index.

Examples:

[1] Brossi, A., Lindlar, H., Walter, M., Schneider, O.: Helv. Chim. Acta, **41**, 119 (1958)
[2] Parr, R. G.: Quantum Theory of Molecular Electronic Structure, Benjamin, New York 1964
[3] Warshel, A.: in Modern Theoretical Chemistry, Vol. 7, Part A (Ed. G. A. Segal), Plenum Press, New York 1977

Tables

Each table should be given a Roman number and a brief informative title. Structural formulas should not be used in column headings or in the body of tables.

Figures

Figures should be numbered consecutively with Arabic numerals. Their approximate place should be indicated in the text on the margin. Allfigures must be identified on the back by the author's name and the figure number in pencil. Standard symbols (such as circles, triangles, squares) are to be used on line-drawings to denote the points determined experimentally. Line-drawings must not contain structural formulas and comments. Spectra or relevant segments thereof, chromatograms, and X-ray diffraction patterns will be reproduced only if concise numerical summaries are inadequate to replace them. Drawings and graphs should be prepared in black ink on good-quality white or tracing paper. Photographs should be submitted on glossy paper as high-contrast copies. Xerox or similar copies are not suitable for reproduction, but may be used for duplicate copies.

Redrawn illustrations will be sent to the authors for checking. No corrections of figures will, therefore, be accepted in the proofs.

Submission of manuscript

After having completed the corrections suggested by the referees and editors, the final manuscript should be submitted in duplicate, in a form ready for publication. If the corrected manuscript is not returned to the editots *within six weeks*, the intended publication of the paper will be regarded as withdrawn by the authors.

Page charge will not be assessed for the publication, however, authors from overseas countries must contribute to the postage of correspondence by sending, together with the manuscript, international postal coupons to the value of U.S. $ 10.—

Proofs and reprints

A set of proofs will be sent to the submitting author. The proofs must be returned within 48 hours of receipt. Late return may cause a delay in the publication of the paper. 100 reprints will be supplied to the authors free of charge.

Periodicals of the Hungarian Academy of Sciences are obtainable at the following addresses:

AUSTRALIA
C.B.D. LIBRARY AND SUBSCRIPTION SERVICE
Box 4886, G.P.O., *Sydney N.S.W. 2001*
COSMOS BOOKSHOP, 145 Ackland Street
St. Kilda (Melbourne), Victoria 3182

AUSTRIA
GLOBUS, Höchstädtplatz 3, *1206 Wien XX*

BELGIUM
OFFICE INTERNATIONAL DE LIBRAIRIE
30 Avenue Marnix, *1050 Bruxelles*
LIBRAIRIE DU MONDE ENTIER
162 rue du Midi, *1000 Bruxelles*

BULGARIA
HEMUS, Bulvar Ruszki 6, *Sofia*

CANADA
PANNONIA BOOKS, P.O. Box 1017
Postal Station "B", *Toronto, Ontario M5T 2T8*

CHINA
CNPICOR, Periodical Department, P.O. Box 50
Peking

CZECHOSLOVAKIA
MAD'ARSKÁ KULTURA, Národní třida 22
115 66 Praha
PNS DOVOZ TISKU, Vinohradská 46, *Praha 2*
PNS DOVOZ TLAČE, *Bratislava 2*

DENMARK
EJNAR MUNKSGAARD, Norregade 6
1165 Copenhagen K

FEDERAL REPUBLIC OF GERMANY
KUNST UND WISSEN ERICH BIEBER
Postfach 46, *7000 Stuttgart 1*

FINLAND
AKATEEMINEN KIRJAKAUPPA, P.O. Box 128
SF-00101 Helsinki 10

FRANCE
DAWSON-FRANCE S. A., B. P. 40, *91121 Palaiseau*
EUROPÉRIODIQUES S. A., 31 Avenue de Versailles, *78170 La Celle St. Cloud*
OFFICE INTERNATIONAL DE DOCUMENTATION ET LIBRAIRIE, 48 rue Gay-Lussac
75240 Paris Cedex 05

GERMAN DEMOCRATIC REPUBLIC
HAUS DER UNGARISCHEN KULTUR
Karl Liebknecht-Straße 9, *DDR-102 Berlin*
DEUTSCHE POST ZEITUNGSVERTRIEBSAMT
Sraße der Pariser Kommüne 3–4, *DDR-104 Berlin*

GREAT BRITAIN
BLACKWELL'S PERIODICALS DIVISION
Hythe Bridge Street, *Oxford OX1 2ET*
BUMPUS, HALDANE AND MAXWELL LTD.
Cowper Works, *Olney, Bucks MK46 4BN*
COLLET'S HOLDINGS LTD., Denington Estate
Wellingborough, Northants NN8 2QT
WM. DAWSON AND SONS LTD., Cannon House
Folkstone, Kent CT19 5EE
H. K. LEWIS AND CO., 136 Gower Street
London WC1E 6BS

GREECE
KOSTARAKIS BROTHERS INTERNATIONAL BOOKSELLERS, 2 Hippokratous Street, *Athens-143*

HOLLAND
MEULENHOFF-BRUNA B.V., Beulingstraat 2,
Amsterdam
MARTINUS NIJHOFF B.V.
Lange Voorhout 9–11, *Den Haag*
SWETS SUBSCRIPTION SERVICE
347b Heereweg, *Lisse*

INDIA
ALLIED PUBLISHING PRIVATE LTD., 13/14
Asaf Ali Road, *New Delhi 110001*
150 B-6 Mount Road, *Madras 600002*
INTERNATIONAL BOOK HOUSE PVT. LTD.
Madame Cama Road, *Bombay 400039*
THE STATE TRADING CORPORATION OF INDIA LTD., Books Import Division, Chandralok
36 Janpath, *New Delhi 110001*

ITALY
INTERSCIENTIA, Via Mazzé 28, *10149 Torino*
LIBRERIA COMMISSIONARIA SANSONI, Via Lamarmora 45, *50121 Firenze*
SANTO VANASIA, Via M. Macchi 58
20124 Milano
D. E. A., Via Lima 28, *00198 Roma*

JAPAN
KINOKUNIYA BOOK-STORE CO. LTD.
17-7 Shinjuku 3 chome, Shinjuku-ku, *Tokyo 160-91*
MARUZEN COMPANY LTD., Book Department,
P.O. Box 5050 Tokyo International, *Tokyo 100-31*
NAUKA LTD. IMPORT DEPARTMENT
2-30-19 Minami Ikebukuro, Toshima-ku, *Tokyo 171*

KOREA
CHULPANMUL, *Phenjan*

NORWAY
TANUM-TIDSKRIFT-SENTRALEN A.S., Karl Johansgatan 41–43, *1000 Oslo*

POLAND
WĘGIERSKI INSTYTUT KULTURY, Marszałkowska 80, *00-517 Warszawa*
CKP I W, ul. Towarowa 28, *00-958 Warszawa*

ROUMANIA
D. E. P., *Bucureşti*
ILEXIM, Calea Grivitei 64–66, *Bucureşti*

SOVIET UNION
SOJUZPECHAT — IMPORT, *Moscow*
and the post offices in each town
MEZHDUNARODNAYA KNIGA, *Moscow G-200*

SPAIN
DIAZ DE SANTOS, Lagasca 95, *Madrid 6*

SWEDEN
ALMQVIST AND WIKSELL, Gamla Brogatan 26
101 20 Stockholm
GUMPERTS UNIVERSITETSBOKHANDEL AB
Box 346, *401 25 Göteborg 1*

SWITZERLAND
KARGER LIBRI AG, Petersgraben 31, *4011 Basel*

USA
EBSCO SUBSCRIPTION SERVICES
P.O. Box 1943, *Birmingham, Alabama 35201*
F. W. FAXON COMPANY, INC.
15 Southwest Park, *Westwood Mass. 02090*
THE MOORE-COTTRELL SUBSCRIPTION AGENCIES, *North Cohocton, N. Y. 14868*
READ-MORE PUBLICATIONS, INC.
140 Cedar Street, *New York, N. Y. 10006*
STECHERT-MACMILLAN, INC.
7250 Westfield Avenue, *Pennsauken N. J. 08110*

YUGOSLAVIA
JUGOSLOVENSKA KNJIGA, Terazije 27, *Beograd*
FORUM, Vojvode Mišića 1, *21000 Novi Sad*

Index: 26.007